frontiers | Research Topics

Nutrient use efficiency of plants under abiotic stress

Edited by
Bowen Liang, Tuanhui Bai, Chao Li and Ping Wang

Published in
Frontiers in Plant Science

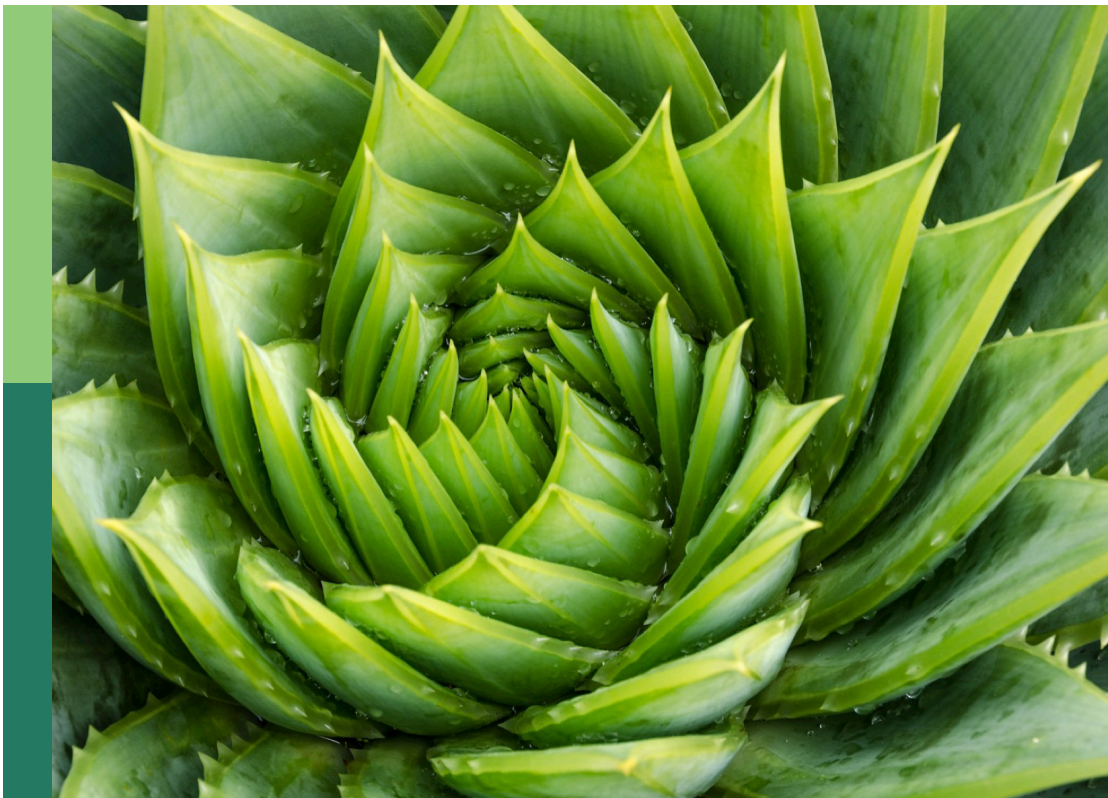

ISSN 1664-8714
ISBN 978-2-8325-2669-9
DOI 10.3389/978-2-8325-2669-9

About Frontiers

Frontiers is more than just an open access publisher of scholarly articles: it is a pioneering approach to the world of academia, radically improving the way scholarly research is managed. The grand vision of Frontiers is a world where all people have an equal opportunity to seek, share and generate knowledge. Frontiers provides immediate and permanent online open access to all its publications, but this alone is not enough to realize our grand goals.

Frontiers journal series

The Frontiers journal series is a multi-tier and interdisciplinary set of open-access, online journals, promising a paradigm shift from the current review, selection and dissemination processes in academic publishing. All Frontiers journals are driven by researchers for researchers; therefore, they constitute a service to the scholarly community. At the same time, the *Frontiers journal series* operates on a revolutionary invention, the tiered publishing system, initially addressing specific communities of scholars, and gradually climbing up to broader public understanding, thus serving the interests of the lay society, too.

Dedication to quality

Each Frontiers article is a landmark of the highest quality, thanks to genuinely collaborative interactions between authors and review editors, who include some of the world's best academicians. Research must be certified by peers before entering a stream of knowledge that may eventually reach the public - and shape society; therefore, Frontiers only applies the most rigorous and unbiased reviews. Frontiers revolutionizes research publishing by freely delivering the most outstanding research, evaluated with no bias from both the academic and social point of view. By applying the most advanced information technologies, Frontiers is catapulting scholarly publishing into a new generation.

What are Frontiers Research Topics?

Frontiers Research Topics are very popular trademarks of the *Frontiers journals series*: they are collections of at least ten articles, all centered on a particular subject. With their unique mix of varied contributions from Original Research to Review Articles, Frontiers Research Topics unify the most influential researchers, the latest key findings and historical advances in a hot research area.

Find out more on how to host your own Frontiers Research Topic or contribute to one as an author by contacting the Frontiers editorial office: frontiersin.org/about/contact

Nutrient use efficiency of plants under abiotic stress

Topic editors

Bowen Liang — Hebei Agricultural University, China
Tuanhui Bai — Henan Agricultural University, China
Chao Li — Northwest A&F University, China
Ping Wang — Iowa State University, United States

Citation

Liang, B., Bai, T., Li, C., Wang, P., eds. (2023). *Nutrient use efficiency of plants under abiotic stress*. Lausanne: Frontiers Media SA. doi: 10.3389/978-2-8325-2669-9

Table of contents

frontiers | Frontiers in Plant Science

TYPE Editorial
PUBLISHED 26 May 2023
DOI 10.3389/fpls.2023.1179842

OPEN ACCESS

EDITED AND REVIEWED BY
Baris Uzilday,
Ege University, Türkiye

*CORRESPONDENCE
Bo-Wen Liang
lbwnwsuaf@126.com
Chao Li
lc453@163.com
Tuan-Hui Bai
tuanhuibai88@163.com
Ping Wang
pingw@iastate.edu

RECEIVED 05 March 2023
ACCEPTED 02 May 2023
PUBLISHED 26 May 2023

CITATION
Liang B-W, Li C, Bai T-H and Wang P (2023) Editorial: Nutrient use efficiency of plants under abiotic stress.
Front. Plant Sci. 14:1179842.
doi: 10.3389/fpls.2023.1179842

Editorial: Nutrient use efficiency of plants under abiotic stress

Bo-Wen Liang[1]*, Chao Li[2]*, Tuan-Hui Bai[3]* and Ping Wang[4]*

[1]College of Horticulture, Hebei Agricultural University, Baoding, Hebei, China, [2]State Key Laboratory of Crop Stress Biology for Arid Areas/Shaanxi Key Laboratory of Apple, College of Horticulture, Northwest A & F University, Yangling, China, [3]College of Horticulture, Henan Agricultural University, Zhengzhou, Henan, China, [4]Department of Genetics, Development and Cell Biology, Iowa State University, Ames, IA, United States

KEYWORDS

plants, abiotic stress, nutrient use efficiency (NUE), melatonin, plant resistance

Editorial on the Research Topic
Nutrient use efficiency of plants under abiotic stress

Abiotic plant stresses such as drought, flooding, and ultraviolet (UV) radiation have intensified in recent decades due to global climate change. Abiotic stress can result in fundamental changes to cellular processes and whole-plant physiology that allow the plant to adapt to the environment (Wang et al., 2021). Mineral nutrients play electrochemical, structural, and catalytic roles in all biological organisms, and are essential for the completion of plant life cycle (Lopez et al., 2023). Abiotic stresses and nutrient deficiency severely impact the growth, development, and productivity of plants (Shikha et al., 2023). Environmental changes cause abiotic stress in plants primarily by alterations in the uptake and utilization of the nutrients. Maintaining nutrient use efficiency under abiotic stress is an effective means of increasing plant stress resistance. Thus, the intensification of abiotic stresses will require the development of plants with high nutrient use efficiency. There have been effects to increase plant abiotic stress tolerance or growth with application small molecules, melatonin is such a molecule. Exogenous melatonin application has been shown to effectively increase stress tolerance and nutrient uptake in plants, and other compounds also play key roles in nutrient uptake under abiotic stress conditions (Zhang et al., 2015; Liu et al., 2020a; Sun et al., 2021; Gao et al., 2022; Ahammed and Li, 2023)

In this Research Topic, we present 11 articles related to abiotic stress responses and nutrient use efficiency in plants, with a focus on the relevant factors that influence these processes. Although abiotic stresses and nutrient deficiency can limit plant growth and survival, plants have evolved a unique set of complex mechanisms to cope with environments under high climate variation. (Liu et al., 2022; Wang et al., 2022; Abiala et al., 2023). Therefore, research related to physiological, biochemical, and molecular responses, as well as nutrient uptake and utilization in plants, is of paramount importance to improve plant stress responses and nutrient use efficiency. Yue et al. integrated envirotyping techniques and multi-trait selection to enhance the mean performance and stability of maize genotypes, opening the door to more systematic and dynamic characterization of the environment to better understand genotype-by-environment interactions in multi-environment trials. Sun et al. provided new insights into the molecular mechanism of the iron deficiency response in *Malus baccata*. This study revealed that *MbHY5-MbYSL7* mediates chlorophyll synthesis and iron transport under iron-deficient conditions. Δ1-Pyrroline-5-carboxylate synthetase (P5CS) is

the rate-limiting enzyme in proline biosynthesis, and plays an essential role in plant responses to environmental stresses. Ma et al. identified 11 *PbP5CS* genes in pear trees, most of which exhibited distinct expression patterns in response to drought, waterlogging, salinity/alkalinity, and other abiotic stresses. These findings represent an advance in the understanding of the physiological functions of *PbP5CS* genes in the enhancement of stress tolerance in pear and other fruit trees. Song et al. performed transcriptome deep sequencing and weighted gene co-expression network analyses to explore the molecular mechanism of blueberry calli in response to UV-B radiation. They found that UV-B induced the expression of flavonoid biosynthetic pathways, and suggested that direct or indirect regulation of MYB inhibitors or activators promotes flavonoid biosynthesis under UV-B radiation. In a review article, Du et al. highlighted the structure and function of TIR1/AFB family members, with an emphasis on the potential mechanisms by which these proteins regulate abiotic stress responses at the transcriptional and post-transcriptional levels, including downstream regulation. For example, they may function in the drought tolerance, salt stress, and nitrate stress pathways. Chalcone synthase (CHS) is a key enzyme required in flavonoid synthesis. Liu et al. isolated a CHS gene from *Poncirus trifoliata* and found that relative expression of the *PtCHS* gene was regulated by soil water deficit and arbuscular mycorrhizal fungi (AMF) inoculation. Xu et al. explored the physiological roles of *CgSTPs* in pummelo, and found that *CgSTP4* plays important roles in sugar accumulation and pollen tube growth. Sun et al. compared the results of physiological, transcriptome, and metabolite analyses under different potassium conditions in apple seedlings. They found that apple seedlings regulate the carbon metabolism and flavonoid pathways in response to low and high potassium stress. This study provided new insights that may be used to improve potassium utilization efficiency in apple trees.

Melatonin is found in almost all plant tissues, and is powerful natural antioxidants that play a significant role in enhancing plant tolerance to various abiotic stressors such as drought (Muhammad et al., 2023), flooding (Moustafa-Farag et al., 2020), salt (Michard and Simon, 2020), and nutrient deficiency (Cao et al., 2022a). Exogenous application of other compounds also enhances plant abiotic stress resistance and nutrient utilization efficiency. The benefits of dopamine have been reported in previous studies on water-induced stress, which showed that exogenous dopamine enhances the tolerance of drought (Du et al., 2022a) and waterlogging (Cao et al., 2022b) by apple trees by regulating the rhizosphere microbiome. Previous studies have also reported that melatonin and dopamine significantly improve plant nutrient use efficiency (Liu et al., 2020b; Du et al., 2022b). Ionome nutrient uptake was decreased in drought-stressed plants, whereas exogenous melatonin and dopamine significantly increased the uptake of mineral elements, particularly under drought stress conditions (Liang et al., 2018a; Liang et al., 2018b). In this Research Topic, Huo et al. reported that exogenous melatonin effectively alleviated damage to kiwifruit plants in response to waterlogging stress. This study provides new insights into the links between melatonin and amino acid metabolic systems in plant stress tolerance. Xia et al. evaluated the effects of melatonin and AMF on kiwifruit seedling drought tolerance. They found that melatonin and AMF have a synergistic effect on improving drought tolerance by increasing mycorrhizal colonization and nutrient uptake. Ma et al. found that AMF (*Diversispora spurca*) promoted growth in walnut plants exposed to drought stress. Similarly, AMF increased apple tree drought resistance by regulating MAPK pathway genes (Huang et al., 2020). AMF is a useful tool for increasing plant nutrient uptake under drought stress conditions (Lotfabadi et al., 2022). Gao et al. (2020) reported that dopamine promoted AMF symbiosis by increasing carbohydrate content, and the synergistic effect of dopamine and AMF enhanced apple tree salt resistance.

Abiotic stresses are anticipated to be among the greatest challenges to future agriculture. It can diminish the uptake and utilization of elements, then influence plant nutrient status. Nutrient deficiency will continue to limit plant growth and yield. Most of the articles associated with this Research Topic increase our understanding of plant adaptive responses to abiotic stresses and nutrient use efficiency, and enrich current knowledge of the mechanisms through which melatonin and other compounds facilitate abiotic stress responses and nutrient utilization efficiency in plants, allowing them to adapt to unfavorable environmental conditions. These findings will offer new opportunities for its use in agriculture, especially in regions that are challenged by abiotic stress or nutrient deficiency condition. We hope that this Research Topic will inspire new ideas and stimulate further research in these fields.

Author contributions

All authors listed have made a substantial, direct, and intellectual contribution to the work, and approved it for publication.

Funding

Research was supported by grants from the Introduced Talents Project of Hebei Agricultural University (YJ201904) to B-WL. T-HB would like to acknowledge support from the National Natural Science Foundation of China (31872058) and the Key Technology Research and Development Program of Henan Province (222102110041).

Conflict of interest

The authors declare that the research was conducted in the absence of any commercial or financial relationships that could be construed as a potential conflict of interest.

Publisher's note

References

Abiala, M., Sadhukhan, A., Muthuvel, J., Shekhawat, R. S., Yadav, P., and Sahoo, L. (2023). Rhizosphere *Priestia* species altered cowpea root transcriptome and enhanced growth under drought and nutrient deficiency. *Planta* 257, 11. doi: 10.1007/s00425-022-04047-2

Ahammed, G. J., and Li, X. (2023). Dopamine-induced abiotic stress tolerance in horticultural plants. *Sci. Hortic.-Amsterdam* 307, 111506. doi: 10.1016/j.scienta.2022.111506

Cao, Y., Du, P. H., Ji, J. H., He, X. L., Zhang, J. R., Shang, Y. W., et al. (2022a). Ionomic combined with transcriptomic and metabolomic analyses to explore the mechanism underlying the effect of melatonin in relieving nutrient stress in apple. *Int. J. Mol. Sci.* 23, 9855. doi: 10.3390/ijms23179855

Cao, Y., Du, P. H., Yin, B. Y., Zhou, S. S., Li, Z. Y., Zhang, X. Y., et al. (2022b). Melatonin and dopamine enhance waterlogging tolerance by modulating ROS scavenging, nitrogen uptake, and the rhizosphere microbial community in *Malus hupehensis*. *Plant Soil.* 483, 475–493. doi: 10.1007/s11104-022-05759-w

Du, P. H., Cao, Y., Yin, B. Y., Zhou, S. S., Li, Z. Y., Zhang, X. Y., et al. (2022a). Improved tolerance of apple plants to drought stress and nitrogen utilization by modulating the rhizosphere microbiome *via* melatonin and dopamine. *Front. Microbiol.* 13. doi: 10.3389/fmicb.2022.980327

Du, P. H., Yin, B. Y., Cao, Y., Han, R. X., Ji, J. H., He, X. L., et al. (2022b). Beneficial effects of exogenous melatonin and dopamine on low nitrate stress in *Malus hupehensis*. *Front. Plant Sci.* 12. doi: 10.3389/fpls.2021.807472

Gao, T. T., Liu, X. M., Shan, L., Wu, Q., Liu, Y., Zhang, Z. J., et al. (2020). Dopamine and arbuscular mycorrhizal fungi act synergistically to promote apple growth under salt stress. *Environ. Exp. Bot.* 178, 104159. doi: 10.1016/j.envexpbot.2020.104159

Gao, T. T., Liu, X. M., Tan, K. X., Zhang, D. N., Zhu, B. L., Ma, F. W., et al. (2022). Introducing melatonin to the horticultural industry: physiological roles, potential applications, and challenges. *Hortic. Res.* 9, uhac094. doi: 10.1093/hr/uhac094

Huang, D., Ma, M. N., Wang, Q., Zhang, M. X., Jing, G. Q., Li, C., et al. (2020). Arbuscular mycorrhizal fungi enhanced drought resistance in apple by regulating genes in the MAPK pathway. *Plant Physiol. Bioch.* 149, 245–255. doi: 10.1016/j.plaphy.2020.02.020

Liang, B. W., Gao, T. T., Zhao, Q., Ma, C. Q., Chen, Q., Wei, Z. W., et al. (2018b). Effects of exogenous dopamine on the uptake, transport, and resorption of apple ionome under moderate drought. *Front. Plant Sci.* 9. doi: 10.3389/fpls.2018.00755

Liang, B. W., Ma, C. Q., Zhang, Z. J., Wei, Z. W., Gao, T. T., Zhao, Q., et al. (2018a). Long-term exogenous application of melatonin improves nutrient uptake fluxes in apple plants under moderate drought stress. *Environ. Exp. Bot.* 155, 650–661. doi: 10.1016/j.envexpbot.2018.08.016

Liu, Q. W., Gao, T. T., Liu, W. X., Liu, Y. S., Zhao, Y. J., Liu, Y. R., et al. (2020a). Functions of dopamine in plants: a review. *Plant Signal. Behav.* 15, 1827782. doi: 10.1080/15592324.2020.1827782

Liu, X. M., Gao, T. T., Zhang, Z. J., Tan, K. X., Jin, Y. B., Zhao, Y. J., et al. (2020b). The mitigation effects of exogenous dopamine on low nitrogen stress in *Malus hupehensis*. *J. Integr. Agr.* 19, 2709–2724. doi: 10.1016/S2095-3119(20)63344-5

Liu, Y. T., Wang, J., Liu, B., and Xu, Z. Y. (2022). Dynamic regulation of DNA methylation and histone modifications in response to abiotic stresses in plants. *J. Integr. Plant Biol.* 64, 2252–2274. doi: 10.1111/jipb.13368

Lopez, G., Ahmadi, S. H., Amelung, W., Athmann, M., Ewert, F., Gaiser, T., et al. (2023). Nutrient deficiency effects on root architecture and root-to-shoot ratio in arable crops. *Front. Plant Sci.* 13. doi: 10.3389/fpls.2022.1067498

Lotfabadi, Z. E., Weisany, W., Tahir, N. A. R., and Torkashvand, A. M. (2022). Arbuscular mycorrhizal fungi species improve the fatty acids profile and nutrients status of soybean cultivars grown under drought stress. *J. Appl. Microbiol.* 132, 2177–2188. doi: 10.1111/jam.15326

Michard, E., and Simon, A. A. (2020). Melatonin's antioxidant properties protect plants under salt stress. *Plant Cell Environ.* 43, 2587–2590. doi: 10.1111/pce.13900

Moustafa-Farag, M., Mahmoud, A., Arnao, M. B., Sheteiwy, M. S., Dafea, M., Soltan, M., et al. (2020). Melatonin-induced water stress tolerance in plants: recent advances. *Antioxidants-Basel* 9, 809. doi: 10.3390/antiox9090809

Muhammad, I., Yang, L., Ahmad, S., Farooq, S., Khan, A., Muhannad, N., et al. (2023). Melatonin priming enhances maize seedling drought tolerance by regulating the antioxidant defense system. *Plant Physiol.* 191, 2301–2315. doi: 10.1093/plphys/kiad027

Shikha, D., Jakhar, P., and Satbhai, S. B. (2023). Role of jasmonate signaling in the regulation of plant responses to nutrient deficiency. *J. Exp. Bot.* 74, 1221–1243. doi: 10.1093/jxb/erac387

Sun, C. L., Liu, L. J., Wang, L. X., Li, B. H., Jin, C. W., and Lin, X. Y. (2021). Melatonin: a master regulator of plant development and stress responses. *J. Integr. Plant Biol.* 63, 126–145. doi: 10.1111/jipb.12993

Wang, P., Clark, N. M., Nolan, T. M., Song, G. Y., Bartz, P. M., Liao, C. Y., et al. (2022). Integrated omics reveal novel functions and underlying mechanisms of the receptor kinase FERONIA in *Arabidopsis thaliana*. *Plant Cell* 34, 2594–2614. doi: 10.1093/plcell/koac111

Wang, H. T., Song, C. H., Fang, S., Wang, Z. Y., Song, S. W., Jiao, J., et al. (2021). Genome-wide identification and expression analysis of the ASMT gene family reveals their role in abiotic stress tolerance in apple. *Sci. Hortic.-Amsterdam* 293, 110683. doi: 10.1016/j.scienta.2021.110683

Zhang, N., Sun, Q. Q., Zhang, H. J., Cao, Y. Y., Weeda, S., Ren, S. X., et al. (2015). Roles of melatonin in abiotic stress resistance in plants. *J. Exp. Bot.* 66, 647–656. doi: 10.1093/jxb/eru336

frontiers | Frontiers in Plant Science

TYPE Original Research
PUBLISHED 19 October 2022
DOI 10.3389/fpls.2022.1035233

OPEN ACCESS

EDITED BY
Bowen Liang,
Hebei Agricultural University, China

REVIEWED BY
Xu Xiaozhao,
China Agricultural University, China
Jia-Yu Xue,
Nanjing Agricultural University, China

*CORRESPONDENCE
Tao Zhao
tao.zhao@nwafu.edu.cn
Fengwang Ma
fwm64@nwsuaf.edu.cn
Yangjun Zou
yangjunzou@126.com

SPECIALTY SECTION
This article was submitted to Plant Abiotic Stress, a section of the journal Frontiers in Plant Science

RECEIVED 02 September 2022
ACCEPTED 27 September 2022
PUBLISHED 19 October 2022

CITATION
Sun Y, Luo J, Feng P, Yang F, Liu Y, Liang J, Wang H, Zou Y, Ma F and Zhao T (2022) *MbHY5-MbYSL7* mediates chlorophyll synthesis and iron transport under iron deficiency in *Malus baccata*. *Front. Plant Sci.* 13:1035233. doi: 10.3389/fpls.2022.1035233

MbHY5-MbYSL7 mediates chlorophyll synthesis and iron transport under iron deficiency in *Malus baccata*

Yaqiang Sun, Jiawei Luo, Peien Feng, Fan Yang, Yunxiao Liu, Jiakai Liang, Hanyu Wang, Yangjun Zou*, Fengwang Ma* and Tao Zhao*

State Key Laboratory of Crop Stress Biology for Arid Areas/Shaanxi Key Laboratory of Apple, College of Horticulture, Northwest A&F University, Yangling, China

Iron (Fe) plays an important role in cellular respiration and catalytic reactions of metalloproteins in plants and animals. Plants maintain iron homeostasis through absorption, translocation, storage, and compartmentalization of iron *via* a cooperative regulative network. Here, we showed different physiological characteristics in the leaves and roots of *Malus baccata* under Fe sufficiency and Fe deficiency conditions and propose that *MbHY5* (elongated hypocotyl 5), an important transcription factor for its function in photomorphogenesis, participated in Fe deficiency response in both the leaves and roots of *M. baccata*. The gene co-expression network showed that *MbHY5* was involved in the regulation of chlorophyll synthesis and Fe transport pathway under Fe-limiting conditions. Specifically, we found that Fe deficiency induced the expression of *MbYSL7* in root, which was positively regulated by *MbHY5*. Overexpressing or silencing *MbYSL7* influenced the expression of *MbHY5* in *M. baccata*.

KEYWORDS

Malus baccata*, iron deficiency, chlorophyll synthesis, Fe transporter, regulatory network, *MbHY5

Introduction

Although iron content is very abundant in the earth, its main existing form is ferric iron (Fe^{3+}), which is insoluble and difficult for plants to uptake (Jeong and Guerinot, 2009). Iron (Fe) is one of the most essential micronutrients in plants and plays an important role in whole-life processes, including chlorophyll synthesis, electron transfer, and respiration (Kobayashi and Nishizawa, 2012). Also, iron can affect physiological

processes such as nitrogen metabolism, carbohydrate, and organic acid metabolism in plants (Curie and Briat, 2003; Hell and Stephan, 2003; Kobayashi and Nishizawa, 2012).

Fe deficiency can cause a series of problems in fruit production (Tagliavini et al., 1995; Alvarez-Fernandez et al., 2003; Hao et al., 2022). Therefore, revealing the sophisticated mechanism of Fe^{2+} uptake, transport, and homeostasis in fruit plants is important for fruit yield and quality. Fe deficiency affects a variety of physiological and biochemical reactions in the leaves and roots of fruit plants. One of the most prominent symptoms in plant is interveinal chlorosis, or veins yellowing, which leads to a reduced photosynthetic performance of fruit trees (Curie and Briat, 2003; Hao et al., 2022). About 80% of the total iron was stored in chloroplasts; although iron is not a component of chlorophyll, it is an indispensable catalyst for chlorophyll synthesis (Yang et al., 2022). Previous studies have shown that the number of thylakoid membranes decreased in the lamellar structure of the chloroplast under iron deficiency (TerBush et al., 2013). Roots under iron deficiency can form root tip swellings or increase lateral roots and/or root hairs (Morrissey and Guerinot, 2009).

Iron content in plants mainly depends on the uptake and transport of exogenous iron by roots. In plants, there are two distinct strategies for root iron uptaking (Ivanov et al., 2012). Plant species belonging to the dicot and non-graminaceous monocot lineages use Strategy I, which consists of three steps: first, proton efflux from plant cells was mediated by the P-type ATPase to decrease the pH of the rhizosphere soil, which leads to soil acidification and an increase of iron solubility. Meanwhile, Fe(III) is also chelated and mobilized by coumarin-family phenolics exported by an ABC transporter PDR9 from the cortex to the rhizosphere (Tsai and Schmidt, 2017). Next, Fe (III) is reduced to Fe(II) by ferric reduction oxidase 2 (FRO2) localized on the plasma membrane. Third, the divalent iron Fe (II) was taken up into epidermal cells by metal transporter IRT1 (Eide et al., 1996; Santi and Schmidt, 2009). Subsequently, nicotianamine synthase (NAS), yellow stripe-like (YSL), and other transporters helped Fe(II) transport to vacuoles, chloroplasts, and other organs and organelles for further utilization (Walker and Connolly, 2008). Strategy II plants (grasses) synthesize and secrete phytosiderophores (PS) which form chelates with Fe(III) in roots, and this complex was then transported into cells by YSL transporters (Curie et al., 2009). In either way, YSLs play key roles in iron transportation and acquisition. Multiple copies of YSL genes were found in the genomes of angiosperm and gymnosperm species (Chowdhury et al., 2022). *AtYSL1*, *AtYSL3*, *AtYSL4*, and *AtYSL6* have been demonstrated to be involved in the transportation of Fe and Zn from leaves to seeds through the phloem (Murata et al., 2006; Ishimaru et al., 2010; Kumar et al., 2019). The expression of *AtYSL2* was downregulated in response to iron deficiency (Zang et al., 2020). In addition, YSLs have been proposed as transporters of iron from xylem to phloem and then to young tissues (Le Jean et al., 2005; Morrissey and Guerinot, 2009). YSL2 and YSL7 have been found to be associated with the movement of Fe/Zn-NA complexes to maintain Fe homeostasis in *Arabidopsis* (Khan et al., 2018).

HY5 (elongated hypocotyl 5) is a member of the basic leucine zipper (bZIP) transcription factors, which is known for its key roles in light reception and transmission (Gangappa and Botto, 2016; Li et al., 2020). Moreover, HY5 has been shown to be a positive regulator in nitrate absorption, phosphate response, and copper signaling pathways (Zhang et al., 2014; Huang et al., 2015; Chen et al., 2016; Gao et al., 2021). *Arabidopsis* HY5 mutants contain less chlorophyll content (Oyama et al., 1997; Holm et al., 2002; Xiao et al., 2022). A recent study has shown that HY5 can bind the promoter of the FER gene in roots, which is required for the induction of iron mobilization genes, thus providing us a new perspective in understanding the regulatory mechanism of iron uptake in plants (Guo et al., 2021). However, few studies have reported the correlation of HY5 and chlorophyll synthesis genes under Fe-deficient conditions. Moreover, no report has yet been published on the regulative role of HY5 to YSL iron transporters in response to iron stress in *Malus*.

Malus baccata has been widely used as a cold-resistant apple rootstock, especially in Northeast China. However, *M. baccata* is sensitive to iron deficiency. In this study, we compared the physiological characteristics and the transcriptive features of *M. baccata* under Fe-sufficient/deficiency conditions in the leaves and the roots and explored the regulative role of MbHY5 to chlorophyll metabolic genes and iron transporters (*MbYSL*). Our results provide insight into the molecular mechanism of iron deficiency response in *M. baccata*.

Materials and methods

Plant material and growth conditions

M. baccata in vitro shoots were cultured on MS medium (0.5 mg/l 6-BA and 0.5 mg/l IBA) for 30 days (Hao et al., 2022). Next, seedlings (with a height ~5 cm) were transported to the rooting medium (0.5 mg/l IBA) and cultured for 30 days. Rooted seedlings were transplanted into an improved-Hoagland nutrient solution and cultured for 3 weeks. Seedlings were cultivated at 25 ± 2°C day/21 ± 1°C night with a 16-h day/8-h night photoperiod.

Measurement of chlorophyll contents and rhizosphere pH

Seedling leaves grown on Fe-sufficient (+Fe, 40 μM) and Fe-deficient (-Fe, 0 μM) for 0, 24, 72, and 144 h were sampled, respectively. Leaves were cut into pieces after cleaning and removal of the veins. Next, 0.2 g tissues was mixed with quartz

sand, calcium carbonate, and 95% ethanol. The absorbance of the filtrate was measured using a spectrophotometer (Shimadzu, Kyoto, Japan) at 663 and 645 nm. The rhizosphere pH was measured using a pH meter.

FCR activity

FCR activity was determined by the Ferrozine assay. The roots were first cultivated under +Fe and -Fe conditions for 0, 72, and 144 h and were then submerged into a chromogenic medium (0.5 mM ferrozine, 0.5 mM FeNa-EDTA, 0.5 mM $CaSO_4$, and 0.7% (w/v) agar (Schmidt et al., 2000)) and incubated in the dark for 1 h. All measurements were performed at room temperature with a Shimadzu spectrophotometer (Kyoto, Japan).

Perls staining

Fresh root, stem, and leaf tissues were collected and placed in a small box (2 cm*2 cm*2 cm), which contains an appropriate amount of OCT, with tissues submerged by an embedding agent. Next, the bottom of the box was exposed to liquid nitrogen for quick freezing. Finally, the embedded blocks were placed on a freezing microtome for slicing, with continuous slicing of 10~20 μm. Perls staining was conducted using a Prussian Blue Iron Stain Kit (Solarbio, 60533ES20). Micro-tissues were transferred into Perls solution and stained for 0.5~1 h, then they were washed with deionized water and incubated in the methanol solution (Sun et al., 2020). Imaging was performed with a volume microscope (BA210, Motic) (Jia et al., 2018).

Fe content

The roots and leaves of the *M. baccata* seedlings treated under +Fe and -Fe conditions (see above) at different times were sampled 1 g for each sample. The samples were first dried at 105° C for 30 min then were placed at 80°C for 72 h till the samples were completely dry. Inductively coupled plasma–optical emission spectrometry was used to determine the active iron contents (Zheng et al., 2021).

Quantitative real-time PCR and public RNA-seq data analysis

Total RNA was extracted from the roots of *M. baccata* seedlings and was purified using the RNAprep Pure Plant Kit (TIANGEN, Beijing, China) according to the manufacturer's instructions. cDNA was prepared from total RNA using the HiScript II 1st Strand cDNA Synthesis Kit (+gDNA wiper) (Vazyme, Nanjing, Chain). The LightCycler® 480 II system (Roche) was used for the qPCR assay, and the primers are listed in Supplementary Table 5. The relative expression of each gene was calculated based on the $2^{-\triangle\triangle Ct}$ method.

A total of 30 groups of RNA-seq data from a project (PRJNA598053) was used to analyze the expression pattern of chlorophyll synthesis and iron transporter genes under Fe sufficiency and Fe deficiency conditions (0, 24, and 72 h) (Sun et al., 2020) (https://www.ncbi.nlm.nih.gov/bioproject/PRJNA598053/). Data for the project were downloaded from the NCBI database, including roots and leaves. The expression abundance of the leaves and roots genes was calculated using the FPKM value, and the relative expression level is shown as log2 (fold change) values.

Plasmid construction and GUS histochemical staining

The full length of the *MbHY5*-coding sequence was inserted into the PRI101 (AN) vector. The promoters (upstream ~2 kb) of *MbYSL7* or *MbYSL2* were cloned respectively into the pCAMBIA1391 vector with the GUS reporter (Li et al., 2021b). Histochemical GUS staining of *Nicotiana benthamiana* leaves was conducted as previously described (Liu et al., 2002; Sun et al., 2020). The samples were incubated for 24 h at 37°C. Chlorophyll was removed by washing the samples with 70% (v/v) ethanol for 2 days. Imaging was performed with a volume microscope (MZ10F, Leica).

Transient expression

The full length of the *MbYSL7*-coding sequence was amplified without the stop codon using the specific primer pairs (Supplementary Table 5) and was inserted into the PRI101 (AN) vector with the *35S* promoter. In order to repress the expression of *MbYSL7*, the pTRV-*MbYSL7* vector was constructed as previously described (Sun et al., 2020; Hao et al., 2022). The *MbYSL7*-overexpression and VIGS vectors were transformed into *Agrobacterium tumefaciens* cells (GV3101). Infected apple seedlings were placed in a dark place for 2 days and then were transferred to normal light conditions for 1 day. Seedlings grown on Fe-sufficient and Fe-deficient conditions for 0, 24, 72, and 144 h were sampled and then stored at -80°C for RNA extraction.

Yeast one-hybrid assay

The full-length *MbHY5* CDS sequence was inserted into pB42AD (AD vector), while the MbYSL7 or MbYSL2 protein-binding sites (CACGTG) were inserted into pLacZi (BD vector).

The fusion vectors were transformed into the yeast EYG48 strain (Li et al., 2021b; Wu et al., 2021).

Phylogenetic tree

Homologous YSL gene sequences of *M. domestica*, *M. baccata*, and *Arabidopsis thaliana* were aligned using ClustalX version 2.0 (Jeanmougin et al., 1998). The phylogenetic tree was constructed in MEGA (version 11) (Tamura et al., 2021) with the Neighbor-Joining method (bootstrap replicates = 100).

Co-expression gene network analysis

In order to identify key genes involved in Fe deficiency in *M. baccata*, chlorophyll synthesis-related genes and iron homeostasis-related genes were selected, and their expression patterns under Fe deficiency were investigated based on the transcriptome data. Subsequently, their co-expressed genes were predicted using the AppleMDO database (network analysis) (http://bioinformatics.cau.edu.cn/AppleMDO/) (Da et al., 2019). Finally, these genes (503 genes in the leave samples and 693 genes in root samples) were selected to construct the co-expression network using Cytoscape 3.8.0 (Shannon et al., 2003; Zhao et al., 2017).

Statistical analysis and diagram drawing

Statistical analyses were executed using GraphPad Prism. The correlation of MbHY5 and chlorophyll synthesis- and roots iron homeostasis-related genes was calculated using the Pearson correlation (Lv et al., 2021). All statistical analyses were performed by one-way ANOVA test, with $p \leq 0.05$ considered as significantly different among different samples. Diagrams illustrating the mechanism of chlorophyll synthesis and Fe acquisition were created using BioRender (https://biorender.com/) (Therby-Vale et al., 2022).

Results

M. baccata leaves and roots are sensitive to Fe deficiency

The chlorophyll content of *M. baccata* leaves showed a continual decrease from 0 to 144 h (Figure 1A) under -Fe treatments. After 144 h, the rhizosphere pH of -Fe treatment was lower than that of +Fe treatment, but with no statistically significant differences (Figure 1B). The results indicated that iron deficiency caused lower chlorophyll content in the leaves and a decrease in rhizosphere pH. Meanwhile, as for the content of active Fe in the leaves, it decreased from 104 to 42 mg/kg·DW after 144-h Fe deficiency stress. Similarly, its content in the roots also decreased from 923 to 284 mg/kg·DW (Figures 1C, D).

We further measured the FCR activity of the roots to better understand the iron acquisition processes. Fe-deficient roots showed higher FCR activity in contrast with Fe-sufficient roots at different treatment times (Figure 1E). Moreover, Perls staining results showed that tissues (leave, stem, and root) from Fe-sufficient conditions showed stronger Fe^{3+} staining than Fe-deficient ones (Figure 1F). Interestingly, it also showed that Fe deficiency induces a sharp decrease of Fe^{3+} in xylem and phloem (Figure 1F). In conclusion, these results revealed that iron deficiency induced morphological and biochemical changes in *M. baccata*, including decreases in chlorophyll content, rhizosphere pH, and active iron content in the leaves and roots.

Iron deficiency induced the expression of chlorophyll synthesis genes in leaves

We hypothesized that the well-known light-responsive gene *HY5* or *PIF* genes may have participated in the regulation of the chlorophyll synthesis process (Figure 2A). Indeed, we detected a series of chlorophyll metabolic genes from RNA-seq analysis under Fe deficiency, including Glu-tRNA reductase (*HEMA*), Glu 1-semialdehyde (*GSA*), uroporphyrinogen III synthase (*UROS*), chlorophyll synthase (*CHLG*), GUN, Chla oxygenase (*CAO*), protochlorophyllide oxidoreductase (*PPO*), and divinyl reductase (*DVR*). The results showed that *HEMA1-1*, *HEMA1-2*, *CHLG1-1*, *CHLI*, *PPO5*, *CAO1-2*, and *CRD1* were highly expressed in all treatment times (Figure 2B). In contrast, the gene expressions of *DVR*, *CHLG1-2*, *CLH1-1*, *UROS*, and *CLH* were significantly lower in leaves (Figure 2B). Specially, the expression levels of PPO3, PPO9, CHLM1-1, CLH1, PPO8, GUN, GSA1-2, CHLM1-2, HEMA1-3, CAO1-2, CHLG1-1, and HEMA1-1 were significantly changed under Fe deficiency. We constructed a gene co-expression network to investigate the correlation of HY5 or PIF genes and the chlorophyll biosynthesis-related genes. The results showed that *HY5*, *PIF1*, *PIF3*, *HMEA*, *GSA*, and *GUN* form a complicated co-expression network in regulating chlorophyll biosynthesis (Figure 2C; Supplementary Table 1). Moreover, the expression levels of *HY5* were positively correlated with those of most chlorophyll biosynthesis-related genes, such as *HMEA*, *GSA1-2*, *CAO*, *CHLI*, *PPO*, and *GUN*. The Pearson correlation coefficients between *HY5* and these genes ranged from 0.54 to 0.78. In contrast, *UROS*, *CHLG1-2*, *DVR*, and *CLH1-1* were only slightly correlated or did not correlate with *HY5* (Figure 2D).

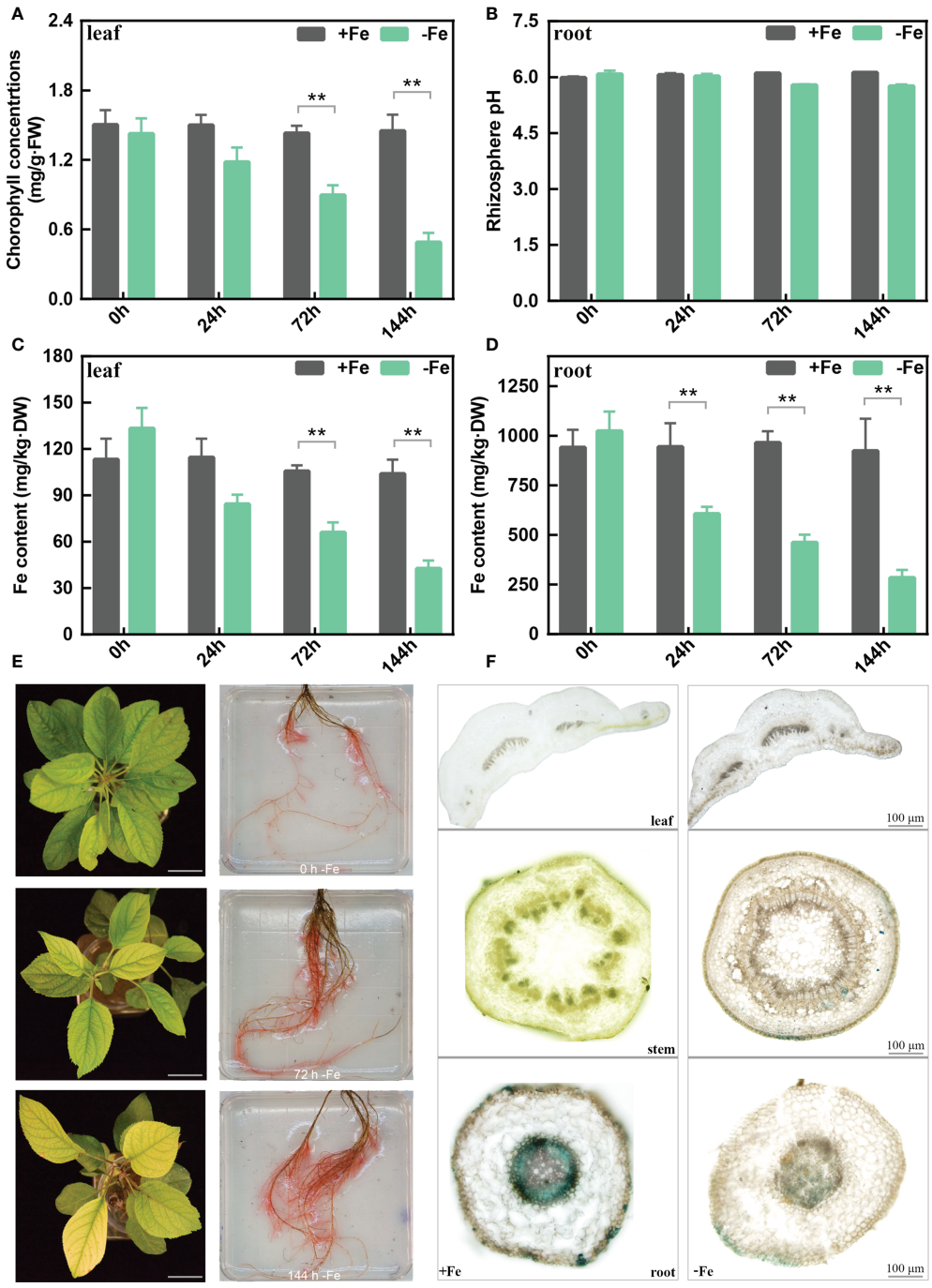

FIGURE 1
The physiological changes in the leaves and roots of *M. baccata* seedlings under Fe-deficient and Fe-sufficient conditions. **(A)** Chlorophyll concentration in leaves. **(B)** Rhizosphere pH in roots. **(C)** Fe content in leaves. **(D)** Fe content in roots. **(E)** Chlorosis extent in leaves and corresponding FCR activities in roots under 0, 72, and 144 h (scale bar: 0.5 cm). **(F)** Perls staining of different tissues, including leaf, stem, and root (scale bar: 100 μm). Asterisks indicate statistically significant differences (**p < 0.01). Error bars denote ± SD (biological replicates = 3).

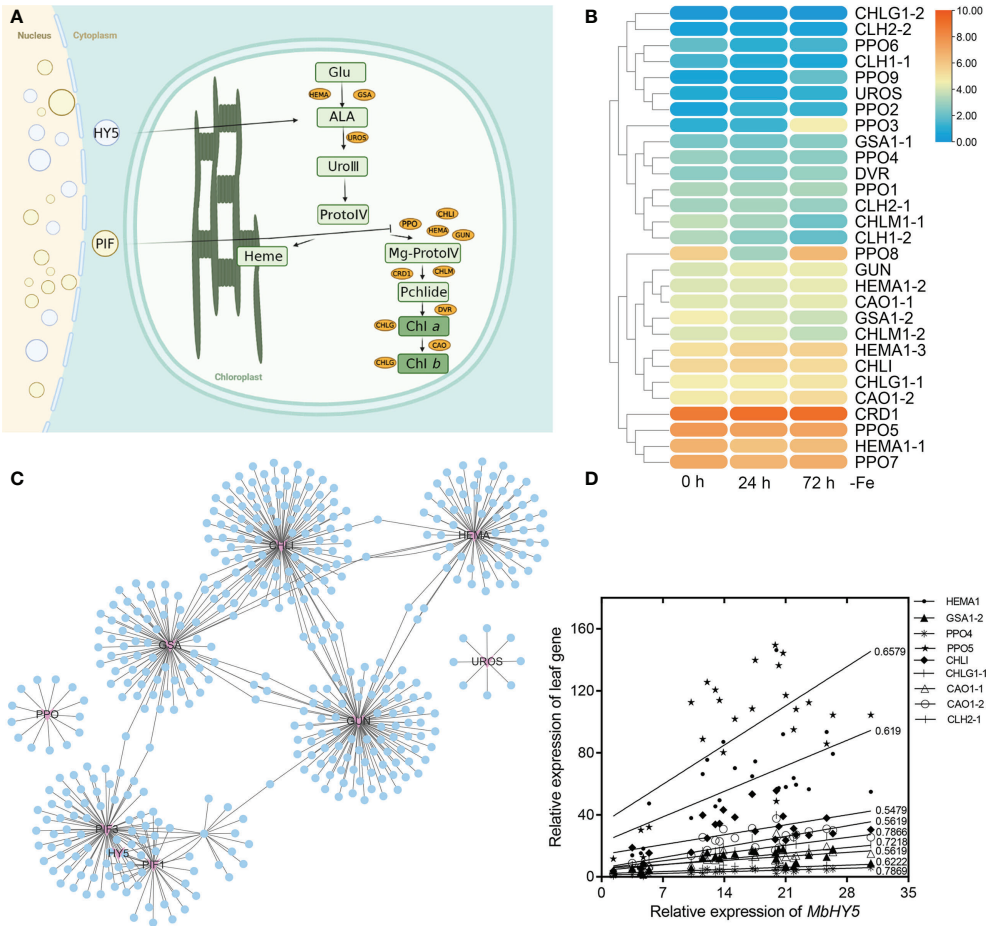

FIGURE 2
MbHY5 was associated with the chlorophyll synthesis genes in the leaves under Fe deficiency. **(A)** The assumption model of the *MbHY5* gene participating the regulation of chlorophyll synthesis. Ovals represent chlorophyll biosynthesis-related genes. HEMA: glutamyl-tRNA reductase, GSA: glutamate-1-semialdehyde 2,1-aminotransferase, CHLH, Mg-chelatase, CHLM, Mg-protoporphyrin IX methyltransferase, CRD, Mg-protoporphyrin IX monomethylester cyclase; DVR, divinyl chlorophyllide a 8-vinyl-reductase; CAO, Chla oxygenase; CHLG, chlorophyll synthase; PPO, protochlorophyllide oxidoreductase. The model was drawn by BioRender (https://biorender.com/). **(B)** The heatmap showing the expression of chlorophyll biosynthesis-related genes in Fe-deficient conditions. **(C)** The co-expression network of HY5/PIF and chlorophyll biosynthesis-related genes. **(D)** Pearson correlation coefficients between *MbHY5* and chlorophyll biosynthesis-related genes.

Analysis of the expression profiles of Strategy I-related genes under iron deficiency

Under iron deficiency conditions, *Malus baccata*, similar to other dicots, use Strategy I to acquire Fe in roots. We summarized the key genes reported in transferring and regulating Fe^{2+} transportation from the rhizosphere into root cells, including *AHA2*, *FRO2*, *PDR9*, *IRT1*, *bHLH100/101*, *OPT3*, and *FIT* (Ito and Gray, 2006; Satbhai et al., 2017; Khan et al., 2018; Lv et al., 2021; Pei et al., 2022) (Figure 3A). Under Fe deficiency, most of these genes were highly induced in roots, especially for *PDR1*, *HY5*, *YSL7*, *FDR2*, and *FER* genes (Figure 3B).

In order to analyze the regulatory network of iron homeostasis genes in roots, a total of 693 iron homeostasis-related genes in roots were selected to construct the co-expression network, and the results showed that *MbHY5–bHLH04–FIT–FRO2* constructed the biggest module, indicating that MbHY5 plays an essential role in regulation iron homeostasis in roots (Figure 3C; Supplementary Table 2). Pearson correlation analysis further showed that iron homeostasis-related genes differentially expressed in root under Fe deficiency were significantly positively related with MbHY5, including OPT3, PDR1, bHLH104, YSL, and AHA10 (Figure 3D). The correlation coefficients ranged from 0.45 to 0.78 (Figure 3D).

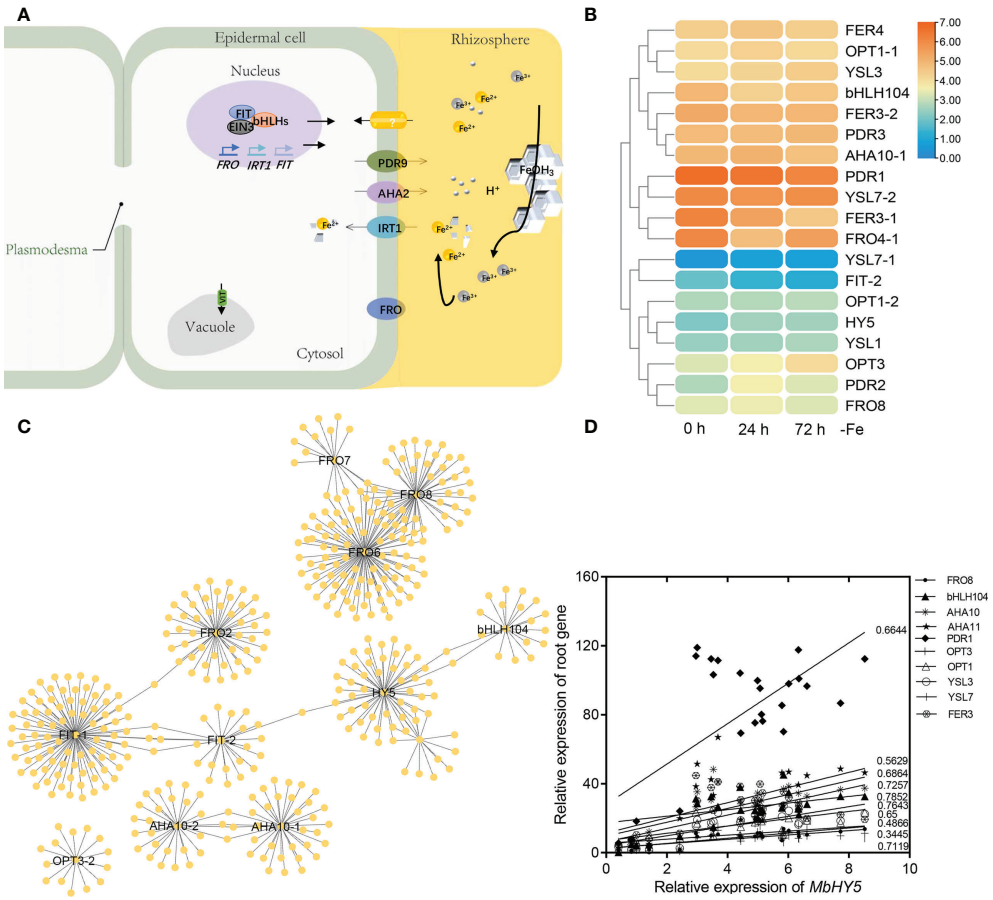

FIGURE 3
MbHY5 is related with Fe acquisition and transportation-related genes in roots in Fe-deficient conditions. **(A)** A model showing the acquisition and transportation of Fe in the roots of dicot plants under Fe deficiency. Ovals represent Fe homeostasis-related genes. **(B)** The heatmap showing the expression levels of the Fe homeostasis-related genes. **(C)** The co-expression network of HY5 and iron responsive genes in roots. **(D)** Pearson correlation coefficients between *MbHY5* and Fe homeostasis-related genes.

MbHY5 directly promotes the expression of *MbYSL7* in response to Fe deficiency

We found that the expressions of *YSL2* and *YSL7* were highly related to HY5 (r = 0.7693 and 0.7119, respectively, Pearson correlation) (Figure 4A). The phylogenetic tree showed that each of the apple YSL genes clustered with its closely related homologous genes in *Arabidopsis* (Figure 4B). Previous studies have shown that HY5 can bind to the promoters of *SlFER* and *AtBTS* and induce the expression of a series of iron-uptaken genes under iron-deficient conditions (Guo et al., 2021; Mankotia et al., 2022).

A G-box (CACGTG) element was found in each of the promoters of *MbYSL2* and *MbYSL7*, which allows HY5 binding (Figure 4C). Y1H analysis showed that MbHY5 can directly bind to the promoter of *MbYSL7*, but not that of *MbYSL2* (Figure 4D). Transient transformation of tobacco leaves with *proMbYSL7:GUS* showed lower GUS activity than co-transformation with *35S:MbHY5* (Figures 4E, F). Similarly, co-transformation of *35S:MbHY5* and *proMbYSL2:GUS* showed slightly higher GUS activity than the transformation of *proMbYSL2:GUS* only (Figures 4E, F). In conclusion, these data suggested that *MbHY5* functions as a positive and direct regulator of *MbYSL7*.

Expression of *MbYSL7* in transient transgenic apple seedlings

To further investigate whether *MbYSL7* was involved in regulating Fe deficiency responses in apple, we made transient transformed lines of apple seedlings with overexpression vector and VIGS vector, respectively. As we can see, compared with the control line, the expression levels of *MbYSL7* were highly induced

10.3389/fpls.2022.1035233

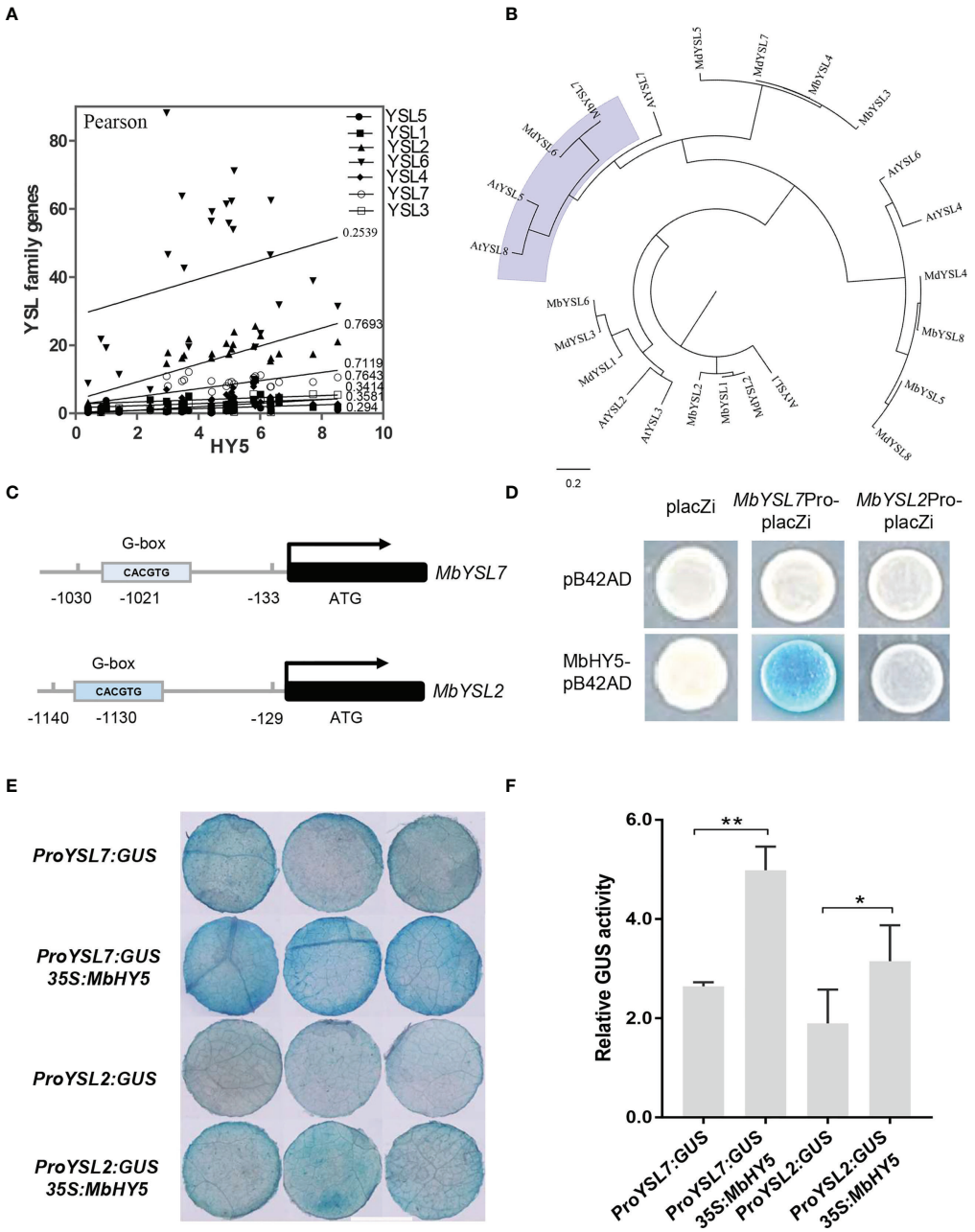

FIGURE 4
MbHY5 regulates *MbYSL7* under Fe deficiency. **(A)** Pearson correlation coefficients of *MbHY5* and YSL family genes. **(B)** The phylogenetic tree of the YSL proteins in three species, including *Arabidopsis*, *M. baccata*, and *M. domestica*. **(C)** Putative HY5-binding site (G-box) was found in the promoter region of *MbYSL7* and *MbYSL2*, respectively. **(D)** Y1H assay. Coding sequence of *MbHY5* was inserted into pB42AD while the promoter region of MbYSL7 or MbYSL2 was inserted into pLacZi, respectively. **(E, F)** GUS staining and GUS enzyme activity of transient transformations of tobacco leaves (scale bar = 1 cm); gene constructs used for the transformations were labeled. Error bars indicate SDs (biological replicates = 3), asterisks indicate statistically significant differences (*p < 0.05, **p < 0.01).

in the transient transformed apple seedling lines of *35S:MbYSL7*-1, -2, and -3 (Figure 5A). Under –Fe treatment, the expressions of *MbYSL7* and *MbHY5* were highly increased in *MbYSL7* overexpression lines, compared with the control lines (Figure 5B). The expression of *MbYSL7* was greatly reduced in *pTRV : MbYSL7*-1 (Figure 5C). Specifically, the expression of *MbYSL7* slightly increased at the 144-h -Fe treatment, compared with that of the 72-h treatment. In comparison, the expression level of *MbHY5* was lowest at the initial -Fe treatment but greatly induced from 24 h onward (Figure 5D). Similar to *MbHY5*, we

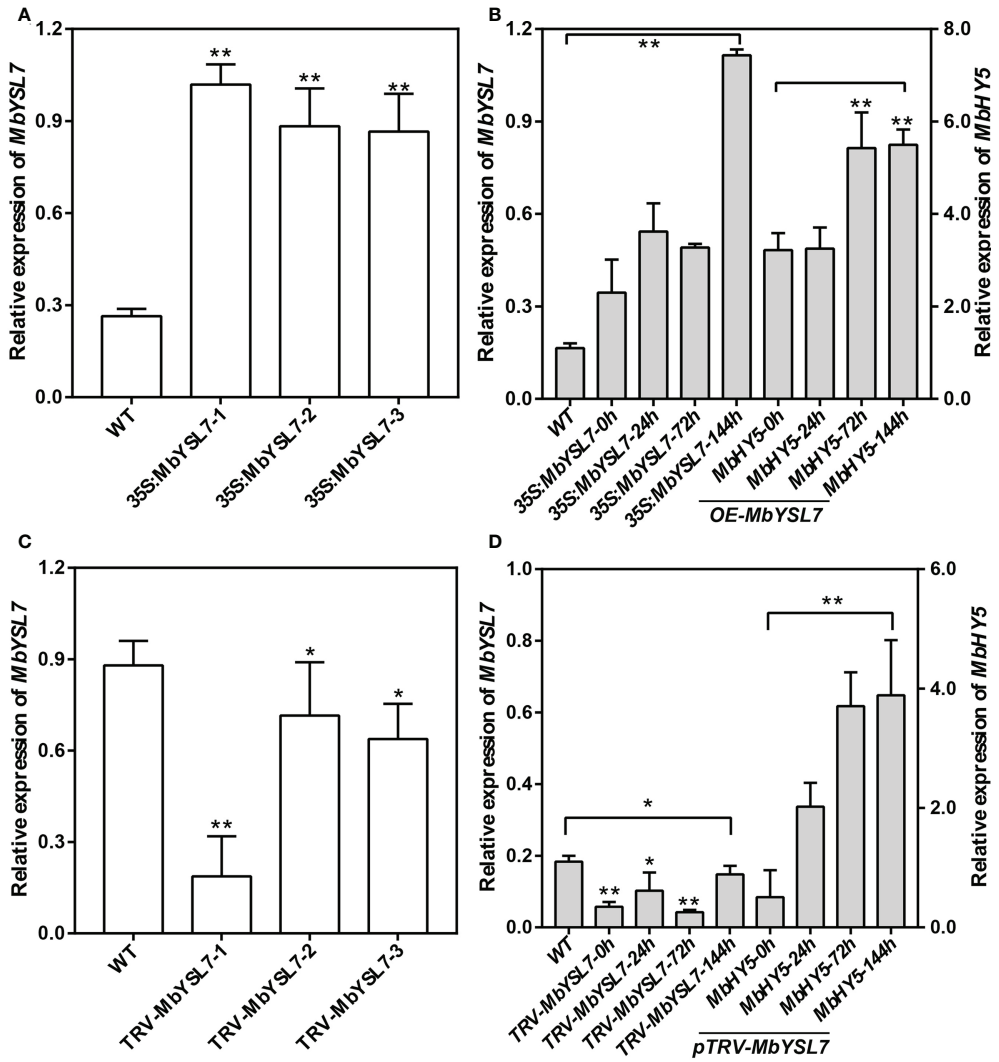

FIGURE 5
Expression of *MbHY5* in transient transgenic *M. baccata* seedlings overexpressing or silencing *MbYSL7*. **(A)** Relative expression levels of *MbYSL7* in transgenic lines overexpressing *MbYSL7*. **(B)** Relative expression levels of *MbYSL7* and *MbHY5* in the roots of the overexpression lines under Fe deficiency. **(C)** Relative expression levels of *MbYSL7* in transgenic lines silencing *MbYSL7*. **(D)** Relative expression levels of *MbYSL7* and *MbHY5* in the roots of the overexpression lines under Fe deficiency. Error bars indicate SDs (biological replicates = 3), asterisks indicate statistically significant differences (*p < 0.05, **p < 0.01).

found that *MbYSL7* was positively related with chlorophyll synthesis-related genes as well, including *PPO5*, *GSA1-2*, and *HEMA* (Supplementary Table 3). In addition, we observed that *MbYSL7* positively correlated with most of Fe homeostasis genes in root either, such as *AHA10*, *bHLH104*, and *PDR2*; the correlation coefficients ranged from 0.40 to 0.92 (Supplementary Table 4).

Discussion

In plants, iron deficiency leads to chlorosis caused by a reduced chlorophyll biosynthesis (Li et al., 2021a). Chlorophyll content decreased dramatically in chlorosis leaves under Fe deficiency (Figure 1), which is in agreement with the findings in citrus and grapes (Chen et al., 2004; Jin et al., 2017). Iron deficiency increased ferric chelate reduction (FCR) activity and decreased the rhizosphere pH of the apple roots (Figure 1). Also, we observed a reduction of active Fe content in the leaves and roots under iron deficiency. Perls staining is a reliable chemical method to stain the iron trivalent in tissues; ferric iron reacts with potassium ferrocyanide and generates blue insoluble compounds (Lv et al., 2021; Hao et al., 2022). Under Fe deficiency, a lower

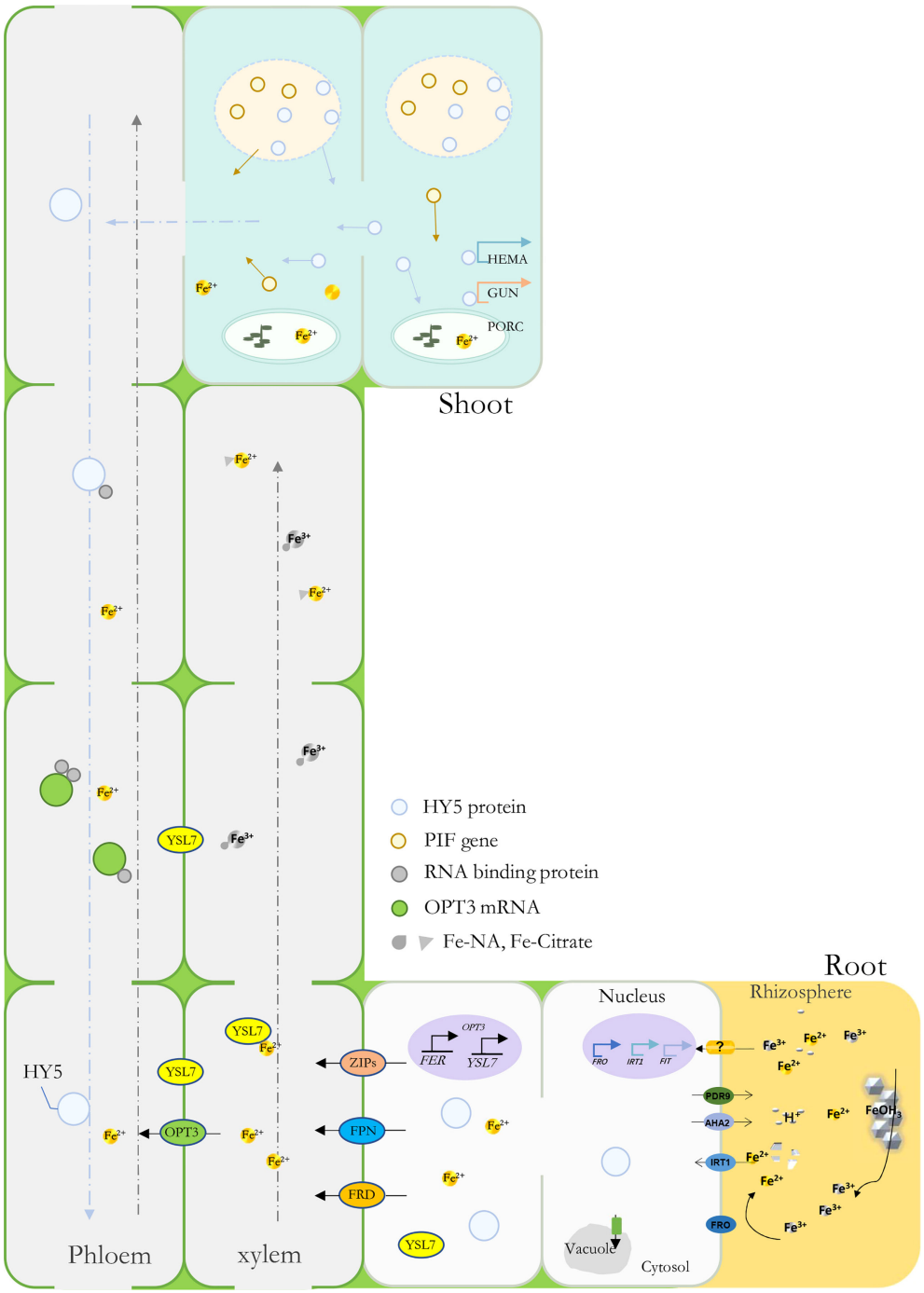

FIGURE 6
A model depicting MbHY5 as an important regulative transcription factor by regulating chlorophyll synthesis-related genes in the leaves, and Fe acquisition and transportation-related genes in the roots under Fe deficiency.

ferric iron content was observed compared to that of the Fe-sufficient treatment (Figure 1).

HY5 has been found to be involved in the metabolism of nitrogen (N), phosphorus (P), copper (Cu), sulfur (S), etc. (Zhang et al., 2014; Gangappa and Botto, 2016; Yang et al., 2020; Gao et al., 2021). In *Arabidopsis*, HY5 regulates the expression of key nitrogen signaling genes including *NIA1*, *NIR1*, *NRT1.1*, *NRT2.1*, and *AMT1;2* (Jonassen et al., 2008;

Jonassen et al., 2009; Yanagisawa, 2014; Chen et al., 2016; Xiao et al., 2022). In apple, *NIA2* and *NRT1.1* were positively regulated by HY5 in promoting nitrate assimilation (An et al., 2017). Nevertheless, few studies have reported its function in Fe uptake and homeostasis. In *Arabidopsis*, HY5 regulates *BTS* in response to Fe deficiency. Similar results were also found in tomato, in which the *HY5-FER* pathway could be involved in Fe metabolism (Guo et al., 2021; Mankotia et al., 2022). In the present study, we firstly found that *MbHY5* was significantly changed in *M. baccata* under Fe deficiency. HY5 plays essential roles in photosynthetic pigment synthesis in light responses (Liu et al., 2017; Liu et al., 2020). It regulates the expression of chlorophyll-related genes in leaves, including *HEMA1*, *GUN4*, *CAO*, *PORC*, and *CHLH* (Toledo-Ortiz et al., 2014; Job and Datta, 2021). In addition, HY5 can regulate the genes involved in maintaining iron homeostasis, such as *FRO2*, *FIT*, *IRTI*, and *PYE* in roots (Mankotia et al., 2022). Further analysis found that *MbHY5* participated in the regulation of chlorophyll synthesis in the leaves and iron acquisition in the roots under iron deficiency (Figures 2 and 3). Our results enriched the regulatory mechanism of HY5 in plants in response to Fe deficiency.

YSL genes have been found to participate in plant metal uptake, such as Cu and Fe (Ishimaru et al., 2010; Zheng et al., 2012; Dai et al., 2018). In *Arabidopsis*, *AtYSL1-3* and *AtYSL6-8* were responsive under Fe deficiency conditions; among them, some were characterized as long-distance signaling media or Fe (II)-NA transporters (Waters et al., 2006; Castro-Rodriguez et al., 2021). Previously, *MtYSL7*, *AtYSL7*, and *GmYSL7* were identified and characterized as peptide transporters without further functional annotation (Castro-Rodriguez et al., 2021; Gavrin et al., 2021). Our results suggested that *MbYSL7* plays an important role under Fe deficiency. Interestingly as evidenced by our Y1H and the transient co-transformation assays, *MbYSL7* was positively regulated by MbHY5. Overall, we propose that MbHY5-YSL7 was involved in regulating the genes involved in chlorophyll synthesis and iron transportation, in both the leaves and the roots, to alleviate iron deficiency-caused chlorosis and to promote Fe transportation (Figure 6).

Conclusion

Contrasting differences of chlorophyll content and the concentration of active iron were observed under +Fe and -Fe conditions in *M. baccata*. We propose that MbHY5 functions as a vital transcription factor in regulating chlorophyll synthesis and Fe transportation. Lastly, MbHY5 directly regulates the expression of *MbYSL7* in roots under Fe deficiency.

Data availability statement

The datasets presented in this study can be found in online repositories. The names of the repository/repositories and accession number(s) can be found in the article/Supplementary Material.

Author contributions

YS designed the experiment, analyzed the data, and drafted the manuscript. YS, JWL, and PF prepared the materials and performed the bioinformatics analysis. YL, JKL, and FY helped with the qRT-PCR analysis. YZ, FM, and TZ edited the manuscript. All authors contributed to the article and approved the submitted version.

Funding

This work was financially supported by the National Natural Science Foundation of China (32102311 and 32102338), the China Postdoctoral Science Foundation (2021M690129), the Chinese Universities Scientific Fund (2452020265 and 2452021133), and the Xinjiang Production and Construction Corps Key Laboratory of Protection and Utilization of Biological Resources in Tarim Basin (BRZD2105).

Conflict of interest

The authors declare that the research was conducted in the absence of any commercial or financial relationships that could be construed as a potential conflict of interest.

Publisher's note

Supplementary material

The Supplementary Material for this article can be found online at: https://www.frontiersin.org/articles/10.3389/fpls.2022.1035233/full#supplementary-material

References

Alvarez-Fernandez, A., Paniagua, P., Abadia, J., and Abadia, A. (2003). Effects of fe deficiency chlorosis on yield and fruit quality in peach (*Prunus persica* l. batsch). *J. Agr. Food Chem.* 51 (19), 5738–5744. doi: 10.1021/jf034402c

An, J. P., Qu, F. J., Yao, J. F., Wang, X. N., You, C. X., Wang, X. F., et al. (2017). The bZIP transcription factor MdHY5 regulates anthocyanin accumulation and nitrate assimilation in apple. *Hortic. Res-England.* 4, 17056. doi: 10.1038/hortres.2017.23

Castro-Rodriguez, R., Escudero, V., Reguera, M., Gil-Diez, P., Quintana, J., Prieto, R. I., et al. (2021). Medicago truncatula yellow stripe-Like7 encodes a peptide transporter participating in symbiotic nitrogen fixation. *Plant Cell Environ.* 44 (6), 1908–1920. doi: 10.1111/pce.14059

Chen, L. S., Smith, B. R., and Cheng, L. L. (2004). CO_2 assimilation, photosynthetic enzymes, and carbohydrates of 'Concord' grape leaves in response to iron supply. *J. Am. Soc Hortic. Sci.* 129 (5), 738–744. doi: 10.21273/JASHS.129.5.0738

Chen, X. B., Yao, Q. F., Gao, X. H., Jiang, C. F., Harberd, N. P., and Fu, X. D. (2016). Shoot-to-root mobile transcription factor HY5 coordinates plant carbon and nitrogen acquisition. *Curr. Biol.* 26 (5), 640–646. doi: 10.1016/j.cub.2015.12.066

Chowdhury, R., Nallusamy, S., Shanmugam, V., Loganathan, A., Muthurajan, R., Sivathapandian, S. K., et al. (2022). Genome-wide understanding of evolutionary and functional relationships of rice yellow stripe-like (YSL) transporter family in comparison with other plant species. *Biologia* 77 (1), 39–53. doi: 10.1007/s11756-021-00924-5

Curie, C., and Briat, J. F. (2003). Iron transport and signaling in plants. *Annu. Rev. Plant Biol.* 54, 183–206. doi: 10.1146/annurev.arplant.54.031902.135018

Curie, C., Cassin, G., Couch, D., Divol, F., Higuchi, K., Jean, M., et al. (2009). Metal movement within the plant: contribution of nicotianamine and yellow stripe 1-like transporters. *Ann. Bot-London.* 103 (1), 1–11. doi: 10.1093/aob/mcn207

Dai, J., Wang, N., Xiong, H., Qiu, W., Nakanishi, H., Kobayashi, T., et al. (2018). The yellow stripe-like (YSL) gene gunctions in internal copper transport in peanut. *Genes* 9, 635. doi: 10.3390/genes9120635

Da, L. L., Liu, Y., Yang, J. T., Tian, T., She, J. J., Ma, X. L., et al. (2019). AppleMDO: a multi-dimensional omics database for apple co-expression networks and chromatin states. *Front. Plant Sci.* 10. doi: 10.3389/fpls.2019.01333

Eide, D., Broderius, M., Fett, J., and Guerinot, M. L. (1996). A novel iron-regulated metal transporter from plants identified by functional expression in yeast. *P. Natl. Acad. Sci. U.S.A.* 93 (11), 5624–5628. doi: 10.1073/pnas.93.11.5624

Gangappa, S. N., and Botto, J. F. (2016).). the multifaceted roles of HY5 in plant growth and development. *Mol. Plant* 9 (10), 1353–1365. doi: 10.1016/j.molp.2016.07.002

Gao, Y. Q., Bu, L. H., Han, M. L., Wang, Y. L., Li, Z. Y., Liu, H. T., et al. (2021). Long-distance blue light signalling regulates phosphate deficiency-induced primary root growth inhibition. *Mol. Plant* 14 (9), 1539–1553. doi: 10.1016/j.molp.2021.06.002

Gavrin, A., Loughlin, P. C., Brear, E., Griffith, O. W., Bedon, F., Grotemeyer, M. S., et al. (2021). Soybean yellow stripe-like 7 is a symbiosome membrane peptide transporter important for nitrogen fixation. *Plant Physiol.* 186 (1), 581–598. doi: 10.1093/plphys/kiab044

Guo, Z. X., Xu, J., Wang, Y., Hu, C. Y., Shi, K., Zhou, J., et al. (2021). The phyBdependent induction of HY5 promotes iron uptake by systemically activating FER expression. *EMBO Rep.* 22 (7), e51944. doi: 10.15252/embr.202051944

Hao, P. B., Lv, X. M., Fu, M. M., Xu, Z., Tian, J., Wang, Y., et al. (2022). Long-distance mobile mRNA CAX3 modulates iron uptake and zinc compartmentalization. *EMBO Rep.* 23 (5), e53698. doi: 10.15252/embr.202153698

Hell, R., and Stephan, U. W. (2003). Iron uptake, trafficking and homeostasis in plants. *Planta* 216 (4), 541–551. doi: 10.1007/s00425-002-0920-4

Holm, M., Ma, L. G., Qu, L. J., and Deng, X. W. (2002). Two interacting bZIP proteins are direct targets of COP1-mediated control of light-dependent gene expression in *Arabidopsis*. *Gene Dev.* 16 (10), 1247–1259. doi: 10.1101/gad.969702

Huang, L. F., Zhang, H. C., Zhang, H. Y., Deng, X. W., and Wei, N. (2015). HY5 regulates nitrite reductase 1 (NIR1) and ammonium transporter1;2 (AMT1;2) in *Arabidopsis* seedlings. *Plant Sci.* 238, 330–339. doi: 10.1016/j.plantsci.2015.05.004

Ishimaru, Y., Masuda, H., Bashir, K., Inoue, H., Tsukamoto, T., Takahashi, M., et al. (2010). Rice metal-nicotianamine transporter, OsYSL2, is required for the long-distance transport of iron and manganese. *Plant J.* 62 (3), 379–390. doi: 10.1111/j.1365-313X.2010.04158.x

Ito, H., and Gray, W. M. (2006). A gain-of-function mutation in the *Arabidopsis* pleiotropic drug resistance transporter PDR9 confers resistance to auxinic herbicides. *Plant Physiol.* 142 (1), 63–74. doi: 10.1104/pp.106.084533

Ivanov, R., Brumbarova, T., and Bauer, P. (2012). Fitting into the harsh reality: regulation of iron-deficiency responses in dicotyledonous plants. *Mol. Plant* 5 (1), 27–42. doi: 10.1093/mp/ssr065

Jeanmougin, F., Thompson, J. D., Gouy, M., Higgins, D. G., and Gibson, T. J. (1998). Multiple sequence alignment with clustal x. *Trends Biochem. Sci.* 23 (10), 403–405. doi: 10.1016/s0968-0004(98)01285-7

Jeong, J., and Guerinot, M. L. (2009). Homing in on iron homeostasis in plants. *Trends Plant Sci.* 14 (5), 280–285. doi: 10.1016/j.tplants.2009.02.006

Jia, D. J., Shen, F., Wang, Y., Wu, T., Xu, X. F., Zhang, X. Z., et al. (2018). Apple fruit acidity is genetically diversified by natural variations in three hierarchical epistatic genes: *MdSAUR37*, *MdPP2CH* and *MdALMTII*. *Plant J.* 95 (3), 427–443. doi: 10.1111/tpj.13957

Jin, L. F., Liu, Y. Z., Du, W., Fu, L. N., Hussain, S. B., and Peng, S. A. (2017). Physiological and transcriptional analysis reveals pathways involved in iron deficiency chlorosis in fragrant citrus. *Tree Genet. Genomes.* 13 (3), 1104. doi: 10.1007/s11295-017-1136-x

Job, N., and Datta, S. (2021). PIF3/HY5 module regulates *BBX11* to suppress protochlorophyllide levels in dark and promote photomorphogenesis in light. *New Phytol.* 230 (1), 190–204. doi: 10.1111/nph.17149

Jonassen, E. M., Lea, U. S., and Lillo, C. (2008). HY5 and HYH are positive regulators of nitrate reductase in seedlings and rosette stage plants. *Planta* 227 (3), 559–564. doi: 10.1007/s00425-007-0638-4

Jonassen, E. M., Sevin, D. C., and Lillo, C. (2009). The bZIP transcription factors HY5 and HYH are positive regulators of the main nitrate reductase gene in *Arabidopsis* leaves, *NIA2*, but negative regulators of the nitrate uptake gene *NRT1.1*. *J. Plant Physiol.* 166 (18), 2071–2076. doi: 10.1016/j.jplph.2009.05.010

Khan, M. A., Castro-Guerrero, N. A., McInturf, S. A., Nguyen, N. T., Dame, A. N., Wang, J. J., et al. (2018). Changes in iron availability in *Arabidopsis* are rapidly sensed in the leaf vasculature and impaired sensing leads to opposite transcriptional programs in leaves and roots. *Plant Cell Environ.* 41 (10), 2263–2276. doi: 10.1111/pce.13192

Kobayashi, T., and Nishizawa, N. K. (2012). Iron uptake, translocation, and regulation in higher plants. *Annu. Rev. Plant Biol.* 63, 131–152. doi: 10.1146/annurev-arplant-042811-105522

Kumar, A., Kaur, G., Goel, P., Bhati, K. K., Kaur, M., Shukla, V., et al. (2019). Genome-wide analysis of oligopeptide transporters and detailed characterization of yellow stripe transporter genes in hexaploid wheat. *Funct. Integr. Genomic.* 19 (1), 75–90. doi: 10.1007/s10142-018-0629-5

Le Jean, M., Schikora, A., Mari, S., Briat, J. F., and Curie, C. (2005). A loss-of-function mutation in AtYSL1 reveals its role in iron and nicotianamine seed loading. *Plant J.* 44 (5), 769–782. doi: 10.1111/j.1365-313X.2005.02569.x

Li, J., Cao, X. M., Jia, X. C., Liu, L. Y., Cao, H. W., Qin, W. Q., et al. (2021a). Iron deficiency leads to chlorosis through impacting chlorophyll synthesis and nitrogen metabolism in *Areca catechu* l. *Front. Plant Sci.* 12. doi: 10.3389/fpls.2021.710093

Li, X., Shen, F., Xu, X. Z., Zheng, Q. B., Wang, Y., Wu, T., et al. (2021b). An HD-ZIP transcription factor, *MxHB13*, integrates auxin-regulated and juvenility-determined control of adventitious rooting in *Malus xiaojinensis*. *Plant J.* 107 (6), 1663–1680. doi: 10.1111/tpj.15406

Li, J., Terzaghi, W., Gong, Y. Y., Li, C. R., Ling, J. J., Fan, Y. Y., et al. (2020). Modulation of BIN2 kinase activity by HY5 controls hypocotyl elongation in the light. *Nat. Commun.* 11 (1), 1592. doi: 10.1038/s41467-020-15394-7

Liu, L. L., Lin, N., Liu, X. Y., Yang, S., Wang, W., and Wan, X. C. (2020). From chloroplast biogenesis to chlorophyll accumulation: the interplay of light and hormones on gene expression in *Camellia sinensis* cv. shuchazao leaves. *Front. Plant Sci.* 11. doi: 10.3389/fpls.2020.00256

Liu, X. Q., Li, Y., and Zhong, S. W. (2017). Interplay between light and plant hormones in the control of *Arabidopsis* seedling chlorophyll biosynthesis. *Front. Plant Sci.* 8. doi: 10.3389/fpls.2017.01433

Liu, Y. L., Schiff, M., Marathe, R., and Dinesh-Kumar, S. P. (2002). Tobacco *Rar1*, *EDS1* and *NPR1/NIM1* like genes are required for *N*-mediated resistance to tobacco mosaic virus. *Plant J.* 30 (4), 415–429. doi: 10.1046/j.1365-313x.2002.01297.x

Lv, X. M., Sun, Y. Q., Hao, P. B., Zhang, C. K., Tian, J., Fu, M. M., et al. (2021). RBP differentiation contributes to selective transmissibility of *OPT3* mRNAs. *Plant Physiol.* 187 (3), 1587–1604. doi: 10.1093/plphys/kiab366

Mankotia, S., Singh, D., Monika, K., Meena, H., Meena, V., Yadav, R. K., et al. (2022). Elongated hypocotyl 5 (HY5) regulates *BRUTUS* (*BTS*) to maintain iron homeostasis in *Arabidopsis thaliana*. *bioRxiv* 2022.04.26.489524. doi: 10.1101/2022.04.26.489524

Morrissey, J., and Guerinot, M. L. (2009). Iron uptake and transport in plants: the good, the bad, and the lonome. *Chem. Rev.* 109 (10), 4553–4567. doi: 10.1021/cr900112r

Murata, Y., Ma, J. F., Yamaji, N., Ueno, D., Nomoto, K., and Iwashita, T. (2006). A specific transporter for iron(III)-phytosiderophore in barley roots. *Plant J.* 46 (4), 563–572. doi: 10.1111/j.1365-313X.2006.02714.x

Oyama, T., Shimura, Y., and Okada, K. (1997). The *Arabidopsis* HY5 gene encodes a bZIP protein that regulates stimulus-induced development of root and hypocotyl. *Gene Dev.* 11 (22), 2983–2995. doi: 10.1101/gad.11.22.2983

Pei, D., Hua, D. P., Deng, J. P., Wang, Z. F., Song, C. P., Wang, Y., et al. (2022). Phosphorylation of the plasma membrane h^+-ATPase AHA2 by BAK1 is required for ABA-induced stomatal closure in *Arabidopsis*. *Plant Cell.* 34 (7), 2708–2729. doi: 10.1093/plcell/koac106

Santi, S., and Schmidt, W. (2009). Dissecting iron deficiency-induced proton extrusion in *Arabidopsis* roots. *New Phytol.* 183 (4), 1072–1084. doi: 10.1111/j.1469-8137.2009.02908.x

Satbhai, S. B., Setzer, C., Freynschlag, F., Slovak, R., Kerdaffrec, E., and Busch, W. (2017). Natural allelic variation of *FRO2* modulates *Arabidopsis* root growth under iron deficiency. *Nat. Commun.* 8, 15603. doi: 10.1038/ncomms15603

Schmidt, W., Tittel, J., and Schikora, A. (2000). Role of hormones in the induction of iron deficiency responses in *Arabidopsis* roots. *Plant Physiol.* 122 (4), 1109–1118. doi: 10.1104/pp.122.4.1109

Shannon, P., Markiel, A., Ozier, O., Baliga, N. S., Wang, J. T., Ramage, D., et al. (2003). Cytoscape: A software environment for integrated models of biomolecular interaction networks. *Genome Res.* 13 (11), 2498–2504. doi: 10.1101/gr.1239303

Sun, Y. Q., Hao, P. B., Lv, X. N., Tian, J., Wang, Y., Zhang, X. Z., et al. (2020). A long non-coding apple RNA, MSTRG.85814.11, acts as a transcriptional enhancer of *SAUR32* and contributes to the fe-deficiency response. *Plant J.* 103 (1), 53–67. doi: 10.1111/tpj.14706

Tagliavini, M., Rombola, A. D., and Marangoni, B. (1995). Response to iron-deficiency stress of pear and quince genotypes. *J. Plant Nutr.* 18 (11), 2465–2482. doi: 10.1080/01904169509365077

Tamura, K., Stecher, G., and Kumar, S. (2021). MEGA11 molecular evolutionary genetics analysis version 11. *Mol. Biol. Evol.* 38 (7), 3022–3027. doi: 10.1093/molbev/msab120

TerBush, A. D., Yoshida, Y., and Osteryoung, K. W. (2013). FtsZ in chloroplast division: structure, function and evolution. *Curr. Opin. Cell Biol.* 25 (4), 461–470. doi: 10.1016/j.ceb.2013.04.006

Therby-Vale, R., Lacombe, B., Rhee, S. Y., Nussaume, L., and Rouached, H. (2022). Mineral nutrient signaling controls photosynthesis: focus on iron deficiency-induced chlorosis. *Trends Plant Sci.* 27 (5), 502–509. doi: 10.1016/j.tplants.2021.11.005

Toledo-Ortiz, G., Johansson, H., Lee, K. P., Bou-Torrent, J., Stewart, K., Steel, G., et al. (2014). The HY5-PIF regulatory module coordinates light and temperature control of photosynthetic gene transcription. *PloS Genet.* 10 (6), e1004416. doi: 10.1371/journal.pgen.1004416

Tsai, H. H., and Schmidt, W. (2017). Mobilization of iron by plant-borne coumarins. *Trends Plant Sci.* 22 (6), 538–548. doi: 10.1016/j.tplants.2017.03.008

Walker, E. L., and Connolly, E. L. (2008). Time to pump iron: iron-deficiency-signaling mechanisms of higher plants. *Curr. Opin. Plant Biol.* 11 (5), 530–535. doi: 10.1016/j.pbi.2008.06.013

Waters, B. M., Chu, H. H., DiDonato, R. J., Roberts, L. A., Eisley, R. B., Lahner, B., et al. (2006). Mutations in *Arabidopsis* yellow stripe-Like1 and yellow stripe-Like3 reveal their roles in metal ion homeostasis and loading of metal ions in seeds. *Plant Physiol.* 141 (4), 1446–1458. doi: 10.1104/pp.106.082586

Wu, B., Shen, F., Wang, X., Zheng, W. Y., Xiao, C., Deng, Y., et al. (2021). Role of *MdERF3* and *MdERF118* natural variations in apple flesh firmness/crispness retainability and development of QTL-based genomics-assisted prediction. *Plant Biotechnol. J.* 19 (5), 1022–1037. doi: 10.1111/pbi.13527

Xiao, Y. T., Chu, L., Zhang, Y. M., Bian, Y. T., Xiao, J. H., and Xu, D. Q. (2022). HY5: a pivotal regulator of light-dependent development in higher plants. *Front. Plant Sci.* 12. doi: 10.3389/fpls.2021.800989

Yanagisawa, S. (2014). Transcription factors involved in controlling the expression of nitrate reductase genes in higher plants. *Plant Sci.* 229, 167–171. doi: 10.1016/j.plantsci.2014.09.006

Yang, Z. H., Chen, Z. X., He, N., Yang, D., and Liu, M. D. (2022). Effects of silicon and iron application on arsenic absorption and physiological characteristics of rice (*Oryza sativa* l.). *B. Environ. Contam. Tox.* 108 (6), 1046–1055. doi: 10.1007/s00128-022-03476-9

Yang, C., Shen, W. J., Yang, L. M., Sun, Y., Li, X. B., Lai, M. Y., et al. (2020). HY5-HDA9 module transcriptionally regulates plant autophagy in response to light-to-dark conversion and nitrogen starvation. *Mol. Plant* 13 (3), 515–531. doi: 10.1016/j.molp.2020.02.011

Zang, J., Huo, Y. Q., Liu, J., Zhang, H. R., Liu, J., and Chen, H. B. (2020). Maize *YSL2* is required for iron distribution and development in kernels. *J. Exp. Bot.* 71 (19), 5896–5910. doi: 10.1093/jxb/eraa332

Zhang, H. Y., Zhao, X., Li, J. G., Cai, H. Q., Deng, X. W., and Li, L. (2014). MicroRNA408 is critical for the HY5-SPL7 gene network that mediates the coordinated response to light and copper. *Plant Cell.* 26 (12), 4933–4953. doi: 10.1105/tpc.114.127340

Zhao, T., Holmer, R., de Bruijn, S., Angenent, G. C., van den Burg, H. A., and Schranz, M. E. (2017). Phylogenomic synteny network analysis of MADS-box transcription factor genes reveals lineage-specific transpositions, ancient tandem duplications, and deep positional conservation. *Plant Cell.* 29 (6), 1278–1292. doi: 10.1105/tpc.17.00312

Zheng, X. D., Chen, H. F., Su, Q. F., Wang, C. H., Sha, G. L., Ma, C. Q., et al. (2021). Resveratrol improves the iron deficiency adaptation of *Malus baccata* seedlings by regulating iron absorption. *BMC Plant Biol.* 21 (1), 433. doi: 10.1186/s12870-021-03215-y

Zheng, L., Yamaji, N., Yokosho, K., and Ma, J. F. (2012). YSL16 is a phloem-localized transporter of the copper-nicotianamine complex that is responsible for copper distribution in rice. *Plant Cell.* 24 (9), 3767–3782. doi: 10.1105/tpc.112.103820

frontiers | Frontiers in Plant Science

TYPE Original Research
PUBLISHED 14 November 2022
DOI 10.3389/fpls.2022.1030521

OPEN ACCESS

EDITED BY
Bowen Liang,
Hebei Agricultural University, China

REVIEWED BY
Vincent Garin,
International Crops Research Institute for the Semi-Arid Tropics (ICRISAT), India
Xiumin Fu,
South China Botanical Garden, Chinese Academy of Sciences (CAS), China
Wenxin Liu,
China Agricultural University, China
Baozhong Yin,
Agricultural University of Hebei, China

*CORRESPONDENCE
Xuwen Jiang,
Xuwen.Jiang@rhul.ac.uk

†These authors have contributed equally to this work

SPECIALTY SECTION
This article was submitted to Plant Abiotic Stress, a section of the journal Frontiers in Plant Science

RECEIVED 29 August 2022
ACCEPTED 26 October 2022
PUBLISHED 14 November 2022

CITATION
Yue H, Olivoto T, Bu J, Li J, Wei J, Xie J, Chen S, Peng H, Nardino M and Jiang X (2022) Multi-trait selection for mean performance and stability of maize hybrids in mega-environments delineated using envirotyping techniques. *Front. Plant Sci.* 13:1030521. doi: 10.3389/fpls.2022.1030521

Multi-trait selection for mean performance and stability of maize hybrids in mega-environments delineated using envirotyping techniques

Haiwang Yue[1†], Tiago Olivoto[2†], Junzhou Bu[1], Jie Li[1], Jianwei Wei[1], Junliang Xie[1], Shuping Chen[1], Haicheng Peng[1], Maicon Nardino[3†] and Xuwen Jiang[4*]

[1]Hebei Provincial Key Laboratory of Crops Drought Resistance Research, Dryland Farming Institute, Hebei Academy of Agriculture and Forestry Sciences, Hengshui, China, [2]Department of Plant Science, Center of Agrarian Sciences, Federal University of Santa Catarina, Florianópolis, SC, Brazil, [3]Department of Agronomy, Federal University of Viçosa, Viçosa, MG, Brazil, [4]Maize Research Institute, Qingdao Agricultural University, Qingdao, China

Under global climate changes, understanding climate variables that are most associated with environmental kinships can contribute to improving the success of hybrid selection, mainly in environments with high climate variations. The main goal of this study is to integrate envirotyping techniques and multi-trait selection for mean performance and the stability of maize genotypes growing in the Huanghuaihai plain in China. A panel of 26 maize hybrids growing in 10 locations in two crop seasons was evaluated for 9 traits. Considering 20 years of climate information and 19 environmental covariables, we identified four mega-environments (ME) in the Huanghuaihai plain which grouped locations that share similar long-term weather patterns. All the studied traits were significantly affected by the genotype × mega-environment × year interaction, suggesting that evaluating maize stability using single-year, multi-environment trials may provide misleading recommendations. Counterintuitively, the highest yields were not observed in the locations with higher accumulated rainfall, leading to the hypothesis that lower vapor pressure deficit, minimum temperatures, and high relative humidity are climate variables that –under no water restriction– reduce plant transpiration and consequently the yield. Utilizing the multi-trait mean performance and stability index (MTMPS) prominent hybrids with satisfactory mean performance and stability across cultivation years were identified. G23 and G25 were selected within three out of the four mega-environments, being considered the most stable and widely adapted hybrids from the panel. The G5 showed satisfactory yield and stability across contrasting years in the drier, warmer, and with higher vapor pressure deficit mega-environment, which included locations in the Hubei province. Overall, this study opens the door to a more systematic and dynamic characterization of

the environment to better understand the genotype-by-environment interaction in multi-environment trials.

KEYWORDS

maize hybrid, mega-environment delineation, genotype-environment interaction, climatic variables, MTMPS

1 Introduction

Maize *(Zea mays* L.) is an annual herb belonging to the grass family *Poaceae* in botanical classification. With its high-yielding, diverse uses, and wide adaptability, maize has surpassed rice (*Oryza sativa* L.) and wheat (*Triticum aestivum* L.) as the most important cereal crop in the world (Haarhoff and Swanepoel, 2018). If the world population grows to 10 billion, it will need 70% more food than can be accomplished today (Hickey et al., 2019). Maize is estimated to account for more than half of future cereal demand growth. Thus, there is a huge stream of innovation for maize breeders when trying to significantly increase maize productivity in an environmentally sensitive way (Yan and Tan, 2019). Since 2013, maize has become the largest crop in China in terms of planting area and production. China's maize planting area has exceeded 37 million hectares, with a total production of more than 215 million tons, accounting for one-quarter and one-fifth of the world's maize area and production, respectively (Hou et al., 2020).

Maize production is divided into spring maize, summer maize, and autumn maize according to the growth period in China. The Huanghuaihai (HHH) plain (Figure 1) is the largest concentrated summer maize planting area in China, accounting for 31.86% and 30.68% of the country's total area and yield, respectively (Zhai et al., 2022). The meteorological conditions in the HHH plain are complex, often encountering high temperatures, heat damage, cloudy rain and lack of sunshine, and the invasion of various diseases, which make maize yields vary greatly from year to year (Wang et al., 2020; Shi et al., 2021; Yue et al., 2022b). Unencouraging climate change projections suggest that the temperature increase might be a key factor affecting the drought risk in HHH (Yue et al., 2022c). This may put at risk the breeding efforts that generated maize hybrids for this area and increase the challenges of breeding programs that aim to release new hybrids (Rizzo et al., 2022). Therefore, there is an urgent need to better understand the genotype-by-environment interaction (GEI) in this region to develop and improve climate-resilient maize hybrids that are thoroughly evaluated in different locations and years/seasons before release. This can be one of the most effective ways for increasing maize production in HHH under new challenges from climate change. In this context, identifying climate-related variables that are most associated with the variations of hybrids within environments is crucial for defining management and/or selection strategies for breeding new summer maize hybrids in the HHH plain region (Yue et al., 2021).

Although the challenge of developing abiotic stress-tolerant maize hybrids has generated a large literature, most practical breeding efforts have also focused on breeding for genetic variation, heritability for grain yield progress under favorable conditions (Bänziger et al., 2006; Fischer and Edmeades, 2010). Grain yield and its components are very complex agronomic traits influenced by genotype (G), environment (E), and their interactions (GEI). The GEI makes the genotype-to-phenotype relationship environment-dependent, which makes the selection of widely adapted hybrids more difficult (Ebdon and Gauch, 2002) and occurs due to the differential response of a given genotype to a given environment stimulated by both biotic, abiotic, or an interaction between them (Nardino et al., 2022). In maize, for example, high temperatures (> 35°C) during flowering generate a cascade effect that starts with the reduction of RuBPCase activity by downregulating genes Zm0001d052595 and Zm0001d004894 which limited photosynthesis and consequently affects maize growth and development (Niu et al., 2021). As a consequence, maize grain yield (GY) is reduced mainly by reducing kernel number per ear, a process associated with carbohydrate metabolic disorders, where a lower carbohydrate availability leads to kernel abortion under post-pollination heat stress conditions (Dong et al., 2021; Niu et al., 2021). Therefore, even if the two environments are strictly similar (e.g., in terms of soil fertility, average temperatures, and rainfall precipitation), extreme events can affect the plants differently, mainly depending on the crop stage they occur.

The correct interpretation of GEI effects in multi-environment trials (METs) can help to select genotypes with high-yielding and stable under different environmental conditions, and even select special genotypes for a certain environment (Vaezi et al., 2019; Alizadeh et al., 2022). During breeding practice, breeders often measure many traits related to yield and are faced with the problem of selecting stable and superior genotypes based on multiple traits. The multi-trait stability index (MTSI) has been successfully used for selecting superior genotypes based on multiple traits (Koundinya et al., 2021; Singamsetti et al., 2021; Farhad et al., 2022; Lima et al., 2022; Padmaja et al., 2022), and has a tremendous potential to

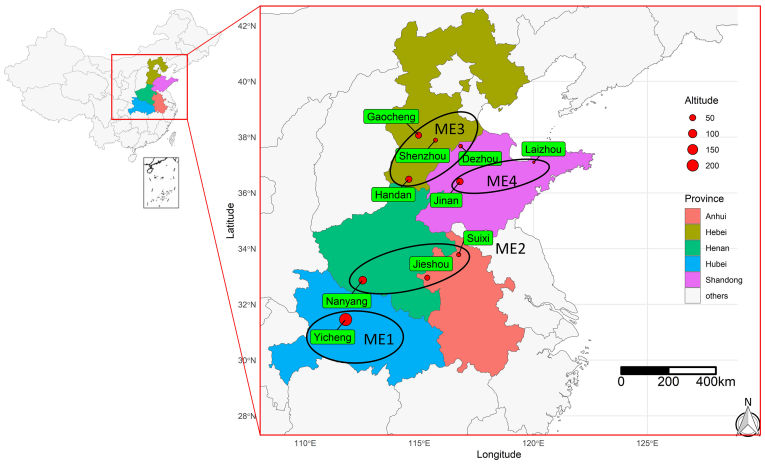

FIGURE 1
Geographical information of the 10 test locations for the trials conducted during 2019 and 2020. The ellipses show the four delineated mega-environments (ME) based on long-term (20 years) climate information.

combine morpho-physiological and yield traits aiming at selecting hybrids under optimal and stress conditions (Balbaa et al., 2022).

Identifying hybrids that rise to the top in terms of multiple criteria from a set of evaluation sites is important but does not contribute significantly to new insights into maize evaluation research. Choosing an ideal genotype (stable across all environments) may ignore specific adaptations, mainly under the climate changes in view (Lopes et al., 2015). Therefore, identifying mega-environments that include locations that share similar long-term weather patterns can be an alternative to better explore the GE interaction in favor of better selection gains, mainly in a region/environment with high variations among the locations/seasons (Costa-Neto et al., 2021a).

In this sense, the main goal of this study is to use envirotyping techniques to delineate mega-environments across the Huanghuaihai plain in China, and to select superior hybrids within each mega-environment that are stable across the cultivation years based on multi-trait. Overall, this study provides new insights into a more systematic and dynamic characterization of the test environments, helping breeders to make better strategic decisions toward an effective multivariate selection in maize breeding programs.

2 Materials and methods

2.1 Plant materials, locations, and experimental design

The experimental material consisted of 26 maize genotypes including one local check hybrid, Zhengdan 958 (Table 1). This study was carried out in ten environments (Figure 1) across five provinces ranging from middle temperate zone to the warm temperate zone, at an elevation from 18 to 235 m above mean sea level spreading across the states of Hebei, Shandong, Anhui, Henan, and Hubei during 2019-2020. The field experiment used a randomized complete block design with three replicates. The seeds of each tested genotype were provided by Dryland Farming Institute, Hebei Academy of Agriculture and Forestry Sciences, and healthy and coating seeds were selected for this study before sowing. The plot at each location was composed of 5 rows with 0.6 m spacing between rows, and the area of each plot had 20.1 m^2 in size. The planting density of each genotype was strictly controlled at 7.5 plants m^{-2}, and the field management applied during the experiment was similar to the management practiced by farmers.

2.2 Morphological data recording

A total of 9 yield-related agronomic traits were recorded in this study. Agronomic traits viz., grain yield (GY, t ha^{-1}) was manually harvested from the middle three rows, adjusting the moisture to 14% and converting the unit to tons per hectare; grain moisture content (GMC, %), measured from each plant at each plot; plant height (PH, cm), measured from the base of the root to the top of the tassel; ear height (EH, cm), measured from the base of the root to the stalk of the ear; ear length (EL, cm), measured from the line up 10 ears, and dividing the data obtained by 10; ear row (ER), counting the total number of rows in each ear; bare tip length (BTL, cm), measured from the top part with no grains (if any) to the part with grains; grain weight per ear (GWE, g) and 100-seed weight (HSW, g) (Yue et al., 2022a).

10.3389/fpls.2022.1030521

TABLE 1 Basic information of the 26 tested maize hybrids.

Code	Genotype	Parentage	Plant height (cm)	Ear height (cm)	Origin	Maturity	Input requirements
G1	Xianyu335	PH6WC×PH4CV	286	103	Liaoning	Medium	High
G2	Hengyu1702	H1027×HC705	255	98	Hebei	Medium	Medium
G3	Hengyu7182	H103×H102	245	87	Hebei	Early	Low
G4	Jiuheng517	H103×H92	243	78	Hebei	Early	Low
G5	Huanong138	B105×J66	281	102	Beijing	Medium	High
G6	Hengyu1587	H58×H59	254	101	Hebei	Medium	Medium
G7	Denongli988	Wan73-1×M518	280	120	Shandong	Late	High
G8	Xundan29	X313×X66	258	117	Henan	Medium	High
G9	Hengyu7188	HB4×H88	260	97	Hebei	Medium	Low
G10	Hengyu321	H14×H13	275	115	Hebei	Medium	Medium
G11	Hengyu1182	H11×H82	268	109	Hebei	Early	Low
G12	Heng110	H58/H59	242	82	Hebei	Early	Low
G13	Liyu16	953×L91158	264	123	Hebei	Late	High
G14	Denghai662	DH371×DH382	272	98	Shandong	Late	Medium
G15	Heng9	H1027×H765	244	79	Hebei	Early	Medium
G16	Zhengjie1	L112×Lx9801	259	92	Shandong	Medium	High
G17	Nongle988	NL278×NL167	250	113	Henan	Late	High
G18	Lianchuang5	CT07×Lx9801	270	106	Henan	Early	High
G19	Tunyu808	T88×T172	253	110	Tianjin	Medium	High
G20	Zhengdan958	Z58×C7-2	250	110	Henan	Late	Low
G21	Meiyu5	758×HC7	255	107	Henan	Early	Medium
G22	Lile66	C28×CH05	270	108	Henan	Late	High
G23	Liyu86	L5895×L5012	267	114	Hebei	Medium	High
G24	Hengdan6272	H462×H72	261	126	Hebei	Medium	Medium
G25	Weike702	WK858×WK798-2	252	107	Henan	Late	High
G26	Shengrui999	S68×S62	250	107	Henan	Medium	Medium

2.3 Statistical Analysis

2.3.1 Mega-environment delineation

Aiming at defining mega-environments with a similar long-term pattern of climate characteristics, we used the function get_wheater() function from the R package EnvRtype (Costa-Neto et al., 2021b) to download a 20-year (2001-2020), daily-basis weather data for 19 environmental covariables (EC) (Table 2). For each year, we considered the period between May and October, which cover the maize growing season in the studied locations. EnvRtype is a very practical package that downloads and processes remote weather data from "NASA's Prediction of Worldwide Energy Resources" (NASA/POWER, https://power.larc.nasa.gov/). Experimental results show that NASA/POWER can be used as a source of climatic data for agricultural activities with reasonable confidence for regional and national spatial scales (Monteiro et al., 2018). A correlation analysis between NASA/POWER data and observed data at Shenzhou location (Supplementary Figure S1) showed a high concordance for temperature variables and sunshine duration ($r > 0.91$, $P< 0.01$), and relative humidity ($r = 0.88$, $P< 0.01$). For rainfall precipitation, a lower agreement ($r > 0.54$, $P< 0.01$) was observed. For the accumulated rainfall precipitation, NASA/POWER tended to overestimate the real observed precipitation.

The 19 EC observed in each location were used to create the called envirotype covariable matrix W that was further used to compute environmental kinships using the function W_matrix() of the EnvRtype package (Costa-Neto et al., 2021b) as proposed by (Costa-Neto et al., 2021a). To better capture the temporal variation of the environmental information across months of the year, six monthly periods were considered (May-October). Therefore, each one of the 2280 variables (20 years × 19 variables × 6 periods = 2280) has become an envirotype descriptor of environmental relatedness. Finally, quality control was done by removing covariables that exceeded ±3SD, where SD is the standard deviation of the covariables across environments (Costa-Neto et al., 2021a). Then, using the W (10 rows × 2280 columns) matrix, we calculated an enviromic kernel (equivalent to a genomic relationship), using the function env kernel() of the EnvRtype package (Costa-Neto et al., 2021b), as follows:

$$K_E = \frac{\boldsymbol{W}\boldsymbol{W}'}{trace(\boldsymbol{W}\boldsymbol{W}')/nrow(\boldsymbol{W})}$$

where K_E is the enviromic-based kernel for the similarity between environments and W is the matrix of envirotype

TABLE 2 List of environmental covariables used in the study.

Source	Environmental factor	Unit
Nasa POWER[a]	Insolation Incident on a Horizontal Surface	MJ m^{-2} day^{-1}
	Downward Thermal Infrared (Longwave) Radiative Flux	MJ m^{-2} day^{-1}
	Extraterrestrial radiation	MJ m^{-2} day^{-1}
	Wind speed at 2 m above the surface of the earth	m s^{-1}
	Minimum air temperature at 2 above the surface of the earth	°C day^{-1}
	Average air temperature at 2 above the surface of the earth	°C day^{-1}
	Maximum air temperature at 2 above the surface of the earth	°C day^{-1}
	Dew-point temperature at 2 m above the surface of the earth	°C day^{-1}
	Relative air humidity at 2 above the surface of the earth	%
	Rainfall precipitation	mm day^{-1}
Calculated[b]	Temperature range	°C d^{-1}
	Potential Evapotranspiration	mm d^{-1}
	Deficit by precipitation	mm d^{-1}
	Vapor Pressure Deficit	kPa d^{-1}
	Slope of saturation vapor pressure curve	Kpa °C d^{-1}
	Effect of temperature on radiation-use efficiency	–
	Growing Degree Day	°C day^{-1}
	Actual duration of sunshine	hour
	Daylight hours	hour

[a]Estimated from NASA orbital sensors (Sparks, 2018); [b] processed using concepts from Allen et al. (1998) and Soltani and Sinclair (2012).

descriptors. To identify mega-environments, a hierarchical clustering (average method) was applied to K_E .

Finally, to visually understand the relationships between environmental variables and their association with the location study, we conducted a Principal Component Analysis (PCA) with a two-way table with the average values for the environmental variables (columns) for each location (rows). A biplot was produced with the function fviz_pca_biplot() from the R package factoextra (Kassambara and Mundt, 2020).

2.3.2 Environmental typology of the trials

To characterize the climate data observed during the experimental period, we used the function env_typing() of the R package EnvRtype to create environmental typologies based on quantilic limits of the 19 EC (Table 2) collected between the sowing and harvesting of each trial. To better capture the temporal variation of the environmental information across crop development, the crop cycles were divided into five main phenological stages in days after sowing (DAS): 0-14 (Initial growing); 15-35 DAS (leaf expansion I, V4-V8); 36-65 DAS (leaf expansion II, V8 - VT); 66-90 DAS (flowering); and 91-120 (grain filling). For each YEAR-ME-stage combination, frequency distributions were computed considering the quantiles 0.01, 0.25, 0.50, 0.75, 0.975, and 0.99; with this, extreme values (e.g., high temperatures) can be identified.

2.3.3 Variance component analysis

To estimate the effect of the respective influences of ME and year on the genotype behavior, for each trait we fitted a linear random-effects model (only intercept as fixed) was fitted using the lmer() function from the lme4 R package (Bates et al., 2015), according to the following model:

$$y_{ijkn} = \mu + G_i + M_j + Y_k + GM_{ij} + GY_{ik} + MY_{jk} + GMY_{ijk} + REP_{n(j:k)} + \epsilon_{ijkn}$$

where y_{ijkn} is the trait scores of i-th genotype observed in the n-th replicate, which is nested within the j-th mega-environment of the k-th year; μ is the grand mean; G_i , M_j , and Y_k are the main effects of genotype, mega-environment, and year; GM_{ij} is the interaction effect of genotype and mega-environment; GY_{ik} is the interaction effect of genotype and year; MY_{jk} is the interaction effect of mega-environment and year; GMY_{ijk} is the interaction of genotype, mega-environment, and year; $REP_{n(j:k)}$ is the effect of the replicate n (assumed to be the combination of location and blocks) nested within the mega-environment and year; and ϵ_{ijkn} is the random error associated to y_{ijkn} . Variance components and genetic parameters were estimated using Restricted Maximum Likelihood, REML (Dempster et al., 1977). Significance testing for random effects was done by the likelihood ratio test (LRT) comparing a complete model (with all terms) and a model without the term under test. The broad-sense heritability on a genotype-mean basis (H^2) was computed as the ratio between genotypic variance (σ^2_G) and variance of a genotype mean (σ^2_P), as follows (Yan, 2014; Schmidt et al., 2019).

$$H^2 = \frac{\sigma^2_G}{\sigma^2_P} = \frac{\sigma^2_G}{\sigma^2_G + \frac{\sigma^2_{GY}}{K} + \frac{\sigma^2_{GM}}{J} + \frac{\sigma^2_{GMY}}{JK} + \frac{\sigma^2_\epsilon}{\sum_{k=1}^{K} N}}$$

Where J, K, and N are the numbers of mega-environments, years, and combinations of location/blocks, respectively. σ^2_G, σ^2_{GY}, σ^2_{GM}, and σ^2_{GMY} are the variances of GEN, GEN×YEAR interaction, GEN×ME interaction, and the GEN×YEAR×ME interaction, respectively; σ^2_ϵ is the residual variance. An H^2 close to 1 means that any observed differences among the genotypic effects are completely due to genetic differences; On the other hand, an H^2 close to 0 means that observed genotypic differences, are due to either genotype-by-environment interactions or experimental errors (Yan, 2014). Finally, we compute the accuracy (Ac) as follows:

$$Ac = \sqrt{H^2}$$

Both the percentage of the variance of phenotypic mean values (considering each term of the random-effect model) and the percentage of the variance of a genotype mean (contribution of each component to the σ^2_P) were presented as filled bar plots.

2.3.4 Mean performance and stability of single trait

Genotype selection was performed within each delineated ME aiming at selecting genotypes that combine desired performance within the ME and are stable across years; such a genotype would be desired by both farmers and breeders. First, for each ME, the average performance of the *I* genotypes in the *K* years ($\bar{Y}_{ik}$) was computed. Then, the Wricke's Ecovalence (W_i) was used as a measure of the genotypic stability across the years and was computed as follows:

$$W_i = \sum_{k=1}^{K} (\bar{Y}_{ik} - \bar{Y}_{i.} - \bar{Y}_{.k} + \bar{Y}_{..})$$

Genotypes with low values of W_i have smaller deviations from the mean across years being then more stable. To account for both mean performance and stability (MPS_i) of genotypes, we adapted the concept of the WAASBY index, which is based on the weighted average of absolute scores from the singular value decomposition of the matrix of best linear unbiased prediction (BLUP) for the GEI effects generated by a linear mixed-effect model (LMM) and response variable (Olivoto et al., 2019a), by replacing the weighted average of absolute scores (WAASB) with W_i as stability measure, since to compute WAASB at least two Interaction Principal Component Axes are needed. The MPS_i was computed as follows:

$$MPS_i = \frac{(rY_i \times \theta_Y) + (rW_i \times \theta_s)}{\theta_Y + \theta_s}$$

where MPS_i is the superiority index for genotype *i* that weights between mean performance and stability; θ_Y and θ_s are the weights for mean performance and stability, respectively; rY_i and rW_i are the rescaled values for mean performance $\overline{Y_i}$ and stability (W_i), respectively of the genotype *i*. Here, we used θ_Y=70 and θ_s=30 to account for a higher weight for mean performance, since selecting highly stable hybrids that do not perform well is not desired. The rescaled values were computed as follows:

$$rY_i = rW_i = \frac{nma - nmi}{oma - omi} \times (o_i - oma) + nma$$

where *nma* and *nmi* are the new maximum and minimum values after rescaling; *oma* and *omi* are the original maximum and minimum value, and o_i is the original value for the response variable (or ecovalence value) for the genotype *i*. For W_i and the traits GMC, PH, EH, and BTL in which lower values are desired, we used *nma* = 0 and *nmi* = 100. So, the genotype with the lowest mean and lowest W_i would have *rYi* =100 and *rWi* =100 after rescaling. For, GY, EL, ER, GWE, and HSW in which higher values are desired, we used *nma* = 100 and *nmi* = 0. After rescaling all the traits, a two-way table $r\mathbf{M}_{qp}$ with *q* rows (genotypes) and *p* columns (traits) was created. In $r\mathbf{M}_{qp}$, each column has a 0–100 range that considers the desired sense of selection (increase or decrease) and maintains the correlation structure of the original set of variables (Olivoto and Nardino, 2021). Additionally, to show how the ranking of genotypes is altered depending on the weight for mean performance and stability, for each ME we planned 21 scenarios changing the θ_Y/θ_s ratio, as follows: 100/0, 95/5, 90/10,…, 0/100. To assist with intuitive interpretation, a heat map graph was produced. To compute these indexes we used the function mps() and wsmp() of the R package metan (Olivoto and Lúcio, 2020).

2.3.5 Mean performance and stability of multiple traits

To account for the mean performance and stability of multiple traits, we used the function mgidi() of the metan R package to compute the multi-trait mean performance and stability index (MTMPS). The MTMPS is based on the concept of the Multi-trait stability index, MTSI (Olivoto et al., 2019b). The only difference between MTMPS and the MTSI is that in this study the MTMPS was computed considering the Wricke's Ecovalence (W_i) rather than the WAASB index. First, an exploratory factor analysis was computed with rM_{qp} to group correlated variables into factors and compute the factorial scores for each genotype, as proposed by Olivoto and Nardino (2021):

$$\boldsymbol{X} = \boldsymbol{\mu} + \boldsymbol{Lf} + \boldsymbol{\epsilon}$$

where X is a $p\times1$ vector of rescaled observations; μ is a $p\times1$ vector of standardized means; L is a $p\times f$ matrix of factorial loadings; f is a $p\times1$ vector of common factors; and ε is a $p\times1$ vector of residuals, being *p* and *f* the number of traits and common factors retained, respectively. Initial loadings were obtained considering only factors with eigenvalues higher than one. After *varimax* rotation criteria (Kaiser, 1958) final loadings were obtained and were used to compute the genotype scores, as follows:

$$\boldsymbol{F} = \boldsymbol{Z}\left(A^T R^{-1}\right)^{\mathrm{T}}$$

where F is a $q \times f$ matrix with the factorial scores; Z is a $q \times p$ matrix containing the standardized (zero mean and unit variance) $r\boldsymbol{M}_{qp}$; A is a $p \times f$ matrix of canonical loadings, and R is a $p \times p$ correlation matrix between the MPS values. q , p , and f represent the number of genotypes, traits, and retained factors, respectively.

Considering the rescaled values in $r\boldsymbol{M}_{qp}$, the ideotype would be the genotype that presents 100 for all analyzed traits; in other words, is the one that has the better performance and stability for all the analyzed traits. Thus, the ideotype was defined by a $(1 \times p)$ vector $\boldsymbol{I}$ such that $\boldsymbol{I}$=[100,100,…,100] . The genotype ranking was based on the Euclidean distance computed with the scores of each genotype to the score of the ideotype, as follows:

$$MTMPS_i = \left[\sum_{j=1}^{f}(F_{ij} - F_j)^2\right]^{0.5}$$

Where $MTMPS_i$ is the multi-trait mean performance index of the ith genotype, F_{ij} represents the jth scores of the ith genotype, F_j represents the jth scores of the ideotype. The genotypes with the lowest MTMPS values were closer to the ideotypes and thus showed high mean performance and better stability in the evaluated traits.

2.3.6 Selection differentials

For each mega-environment, we assumed a selection intensity of ~23% (six selected hybrids). The selection differential in the percentage of population mean ($\Delta S\%$) was then computed for each trait as follows:

$$\Delta S\,\% = (X_s - X_o)/\ X_o \times 100$$

Where X_s and X_o are the mean phenotypic value of the selected genotypes and population mean, respectively.

2.3.7 Statistical software

All statistical analyses in this study were performed using the R software 4.1.0 (R Core Team, 2022) with the packages and functions mentioned in each method.

3 Results

3.1 Environmental kinships and typology

3.1.1 Historical data

Based on 20 years of climate information considering 19 environmental covariables, four mega-environments (ME) were delineated (Figure 2). The ME1 included only one location (Yicheng). The ME2 included Suixi, Jieshou, and Nanyang. The ME3 included Handan, Gaocheng, Shenzhou, and Dezhou; The ME4 included Jinan and Laizhou (Figure 2). The grouped ME were geographically close (Figure 1), suggesting that there is a relevant variation in the climate variables among the locations.

The extraterrestrial radiation (RTA), daylight hours (N), and deficit by precipitation (PETP) were the climate variables that most contributed to the environment scores (Supplementary Figures S2-6). The PCA biplot (Figure 3A) shows that ME1 is mainly characterized by having higher rainfall precipitation, relative humidity, and deficit by precipitation (higher deficit means more available water). The ME2 has the higher values for downward thermal infrared (Longwave) radiative flux. Contrary to ME1, ME3 has higher values for vapor pressure deficit and temperature range, meaning a drier environment (Figure 3A). The higher differences in the vapor pressure deficit of ME3 are specially observed from May to August (Supplementary Figure S6). The ME4 is mainly characterized by having a lower average temperature and consequently a small accumulation of growing degree days (Figure 3A).

The slope of the saturation vapor pressure curve, average temperature, and minimum and maximum temperature was positively associated. Temperature range and vapor pressure deficit were positively correlated but negatively correlated with relative humidity and precipitation, whereas potential evapotranspiration was strongly and positively correlated with extraterrestrial radiation (Figure 3A).

3.1.2 Two years of trials

Figure 3B and C show the PCA biplot with the climate variables and MEs for the trials conducted in 2019 and 2020, respectively. It can be seen a high temporal (seasonal) effect, with different correlation patterns between the climate variables in the two years. For example, in 2019, rainfall precipitation and vapor pressure deficit were positively correlated whereas in 2020 were negatively correlated. This suggests that the interaction genotype x ME x year would have an important contribution to the phenotypic variance. In this case, identifying superior genotypes within ME that are stable across the years would be of great interest. Overall, ME1 had higher yields and rainfall precipitation. The higher temperatures were observed in ME2 and the ME3 had the higher values for vapor pressure deficit and the lower deficits by precipitation (Figure 3D).

In ME1 during 2019, most parts of the days in the flowering and grain filling stages have vapor pressure deficit between 1.29 kPa d^{-1} and 3.33 kPa d^{-1}. In this same ME in 2020, the vapor pressure deficit was smaller, with values ranging from 0.24 kPa d^{-1} and 0.804 kPa d^{-1} during ~50% of the days in the flowering and grain filling stages. Although 2019 presented on average lower precipitation (Figure 3B), the ME1 presented the higher deficit by precipitation, with positive values for almost ⅓ of the days during leaf expansion. In grain filling, for example, ~60% of the days had deficits that ranged from−7.54 mm day^{-1} to 31.5 mm day^{-1} (Figure 4A).

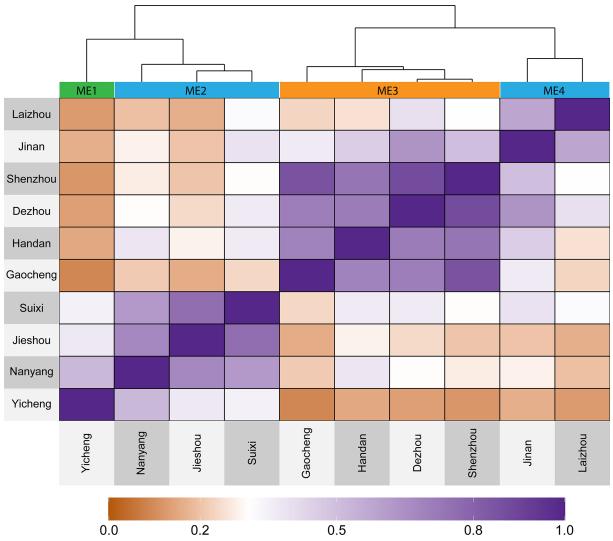

FIGURE 2
Heat map showing the delineated mega-environments considering the similarity based on 20 years of information for 19 environmental covariables.

3.2 Variance components analysis

The likelihood ratio test of the deviance analysis revealed a significant ($P \leq 0.01$) genotype effect for all the traits, except for GY and BTL (Table 3), suggesting good prospects of selection gains for most of the studied traits. The GEN × ME × YEAR interaction was significant for all the traits, with the highest contributions to the phenotypic variance of BTL, EH, ER, and PH (Figure 5A). The results suggests that those morphological traits are dependent on how the genotypes respond to different environmental stimuli. The ME × YEAR interaction was significant ($P \leq 0.01$) for GMC and GY, suggesting that the contrasting climate variables observed across the two years affected the ME differently. Thus, it is reasonable to perform the selection within each ME. Overall, the REP (ME×YEAR) effect was significant for all the traits and was the component with the highest contribution for the phenotypic variance of GY. This high contribution likely comes from the implicit effect of location, since the location and complete blocks were combined to serve as replicates within each mega-environment. Here, although showing a high contribution, the location effect is not of primary interest, since the main goal is to identify superior genotypes within each mega-environment.

The broad-sense heritability on the genotype-mean basis (H^2) ranged from 0.324 (GY) to 0.896 (ER and PH) (Table 3). For the traits GY and BTL the H^2 was less than 0.5, which means that the genotypic component accounted for less than 50% of the variance of a genotype mean (Figure 5B). For these traits, most of the variance of the genotype mean was due to both GEN × ME and GEN × ME × YEAR interactions. The greater contributions of interaction terms for these traits compared to the other ones reinforces that the phenotype-genotype relationship of this traits is strictly environment-dependent, which makes more difficult the selection of widely adapted hybrids and indicates that the selection within delineated mega-environments would provide better gains.

3.3 Correlation between traits in each mega-environment

Supplementary Figure S7 shows the phenotypic correlations among the studied traits within each mega-environment over the two years. Overall, PH and EH were positively correlated with each other across all the MEs. Negative correlations were observed between PH and HSW, suggesting that taller plants have a lower density of grains. In ME1 and ME3 a negative correlation between GY and BTL ($r = -0.13$ and $r = -0.12$, respectively) was observed. For ME2 and ME3, a positive relation between GY and BTL was observed. These changes in the relationships in the different ME resulted in a low degree of Mantel's correlation between the matrices (Supplementary Figure S8) (Guillot and Rousset, 2013). Therefore, this supports the use of a multi-trait index within each ME to take into account the different correlation structures.

3.4 Selection differentials for mean performance and stability

The selection considering the multiple traits resulted in different hybrids being selected in each ME (Figures 6 and 7).

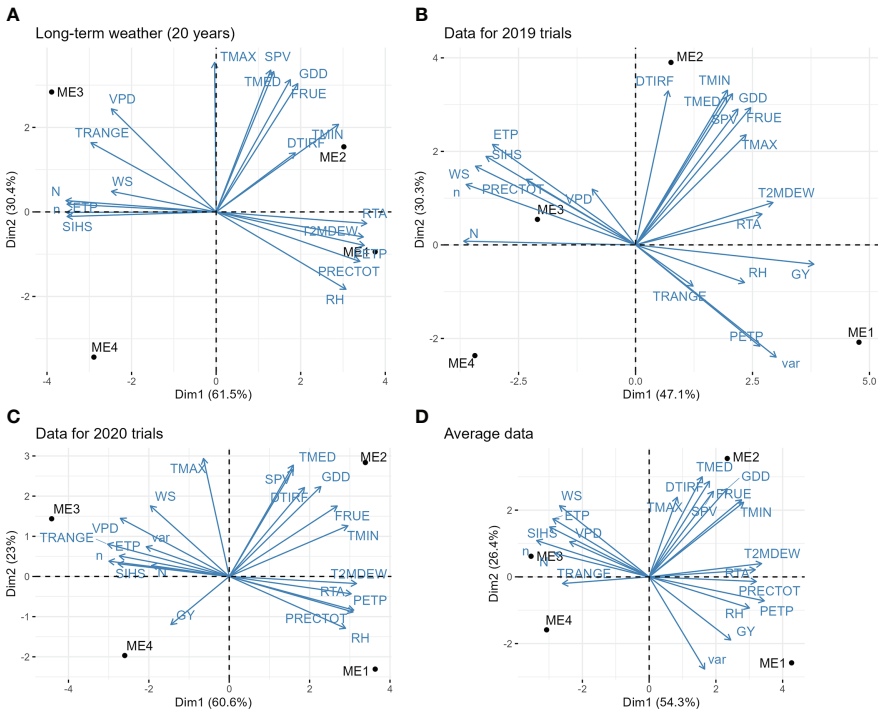

FIGURE 3
Biplot for the principal component analysis between environmental variables. **(A)** long-term pattern data (average of 20 years of climate information); **(B)** observed climate variables in the trials during 2019; **(C)** observed climate variables in the trials during 2020; **(D)** average information of the two years of trials. The variables are: grain yield (GY), genotype variance within mega-environment (var); average air temperature (TMED, °C d^{-1}); minimum air temperature (TMIN, °C d^{-1}); maximum air temperature (TMAX, °C d^{-1}); dew-point temperature (T2MDEW, °C d^{-1}) at 2 m above the surface of the earth at 2 m above the surface of the earth; total rainfall precipitation during the crop cycle (PRECTOT, mm); daily temperature range (TRANGE, °C d^{-1}), deficit by precipitation (PETP, mm d^{-1}); air relative humidity (RH, %), potential evapotranspiration (ETP, mm d^{-1}); slope of saturation vapor pressure curve (SVP, Kpa °C d^{-1}); vapor pressure deficit (VPD, kPa); Effect of temperature on radiation-use efficiency (FRUE); Growing Degree Day (GDD, °C day^{-1}); Actual duration of sunshine (n, hours); Daylight hours (N, hours); Wind speed at 2 m above the surface of the earth (WS, m s^{-1}); Extraterrestrial radiation (RTA, MJ m^{-2} day^{-1}); Downward Thermal Infrared (Longwave) Radiative Flux (DTIRF, MJ m^{-2} day^{-1}); Insolation Incident on a Horizontal Surface (SIHS, MJ m^{-2} day^{-1}).

FIGURE 4
Relative frequency for each envirotype for vapor pressure deficit **(A)** and deficit by precipitation **(B)** observed in the studied and mega-environments across distinct crop stages and years of trials.

TABLE 3 Variance components for the main effect of genotypes (σ^2_G), mega-environments (σ^2_M), cultivation year (σ^2_Y), and their interactions estimated for nine traits assessed in 26 maize hybrids.

Source of variation	BTL[a]	EH	EL	ER	GMC	GWE	GY	HSW	PH
σ^2_G	0.050^{ns}	50.028**	0.211**	0.859**	1.357**	39.221*	0.038^{ns}	1.770**	199.780**
σ^2_M	0.000^{ns}	0.000^{ns}	0.053^{ns}	0.000^{ns}	0.000^{ns}	104.484^{ns}	0.000^{ns}	0.000^{ns}	96.522^{ns}
σ^2_Y	0.000^{ns}	27.351^{ns}	0.083^{ns}	0.016^{ns}	9.488*	55.866^{ns}	0.000^{ns}	0.000^{ns}	31.061^{ns}
σ^2_{GM}	0.048^{ns}	0.000^{ns}	0.219**	0.078^{ns}	0.000^{ns}	26.481^{ns}	0.059^{ns}	0.250^{ns}	0.000^{ns}
σ^2_{GY}	0.00 ^{ns}	4.622^{ns}	0.000^{ns}	0.000^{ns}	0.000^{ns}	10.899^{ns}	0.000^{ns}	0.000^{ns}	4.833^{ns}
σ^2_{MY}	0.000^{ns}	30.248^{ns}	0.000^{ns}	0.000^{ns}	2.738**	0.000^{ns}	0.453*	0.000^{ns}	11.210^{ns}
σ^2_{GMY}	0.353**	59.987**	0.311**	0.484**	1.011**	77.715**	0.355**	0.852**	128.617**
$\sigma^2_{REP(M:Y)}$	0.135**	98.436**	0.657**	0.138**	4.033**	300.744**	1.521**	12.844**	108.140**
σ^2_e	0.472	126.749	1.337	1.194	9.136	464.349	1.185	9.817	274.329
σ^2_P	0.117	61.950	0.327	0.959	1.636	68.744	0.117	2.103	222.846
H_b^2	0.433	0.808	0.646	0.896	0.830	0.571	0.324	0.842	0.896
Ac	0.658	0.899	0.804	0.946	0.911	0.755	0.569	0.918	0.947

[a]BTL, bare tip length; EH, ear height; EL, ear length; ER, ear row; GMC, grain moisture content; GWE, grain weight per ear; GY, grain yield; HSW, 100-seed weight; and PH, plant height.
[b]Broad-sense heritability on the mean-basis.
*P ≤ 0.05; **P ≤ 0.01 (See the P-values in Supplementary Table S1); ^{ns} P > 0.05.

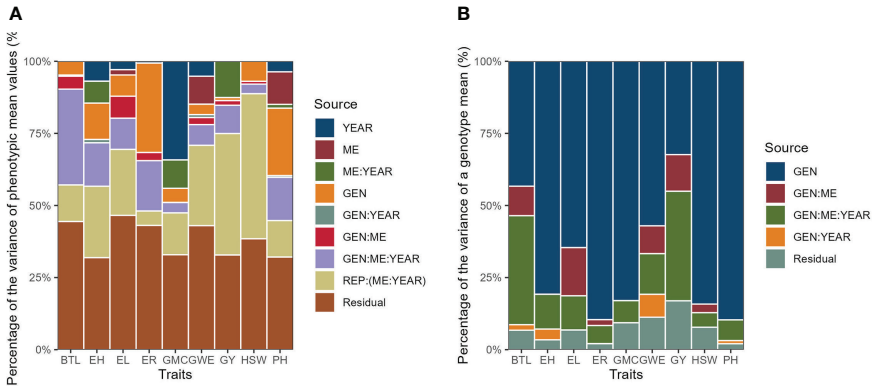

FIGURE 5
Percentage of the variance of phenotypic mean values **(A)** and percentage of the variance of a genotype mean **(B)**.

Overall, two hybrids were selected only for specific MEs, suggesting a narrow adaptation of such hybrids in such ME (Figure 7). Only two hybrids (namely, G23 and G25) were selected in three ME (ME1, ME2, and ME4). This suggests that these hybrids present a wide adaptation, performing well in different environments.

For all the MEs, four factors (FA) were retained, explaining 76.07%, 73.77%, 78.09%, and 73.64% of the total variance for ME1, ME2, ME3, and ME4, respectively (Supplementary Table S2). Given the different correlation structures (Supplementary Figure S7), different traits were included in each FA within each ME (Supplementary Table S3).

The multi-trait selection resulted in a success rate in selecting traits with desired selection differentials (SD) of ~77% (7 out of 9 traits) in ME1, ME2, and ME3, and ~44% (4 out of 9 traits) in ME4 (Figure 8). The six selected maize hybrids (ranked by MTMPS) within ME1 were G10, G23, G22, G6, G25, and G5 (Figure 6A). In ME2, the selected hybrids were G25, G4, G23, G2, G21, and G26 (Figure 6B). In ME3 the selected hybrids were G5, G11, G6, G4, G15, and G9 (Figure 6C). For ME4, G15, G25, G21, G26, G18, and G23 were selected (Figure 6D).

The SD for BTL was negative for all ME except ME1. For GY positive SD that ranged from 3.81% in ME3 to 6.17% in ME4 were observed (Figure 8; Supplementary Figures S9-12; Supplementary Table S3). Considering the stability over the two cultivation years, negative SD was observed for most of the studied traits (Figure 9). For GY, negative SDs were observed in all the ME, with lower values for ME3 and ME4. These results show that the selected hybrids stand out as having satisfactory mean performance (average GY ranging from 10.38 Mg ha^{-1} in

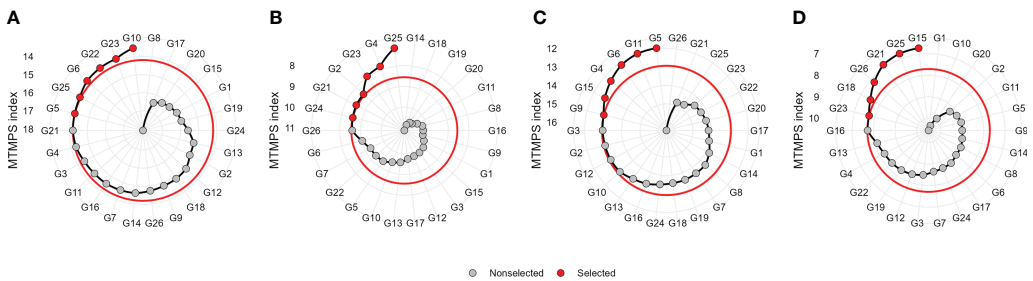

FIGURE 6
Genotype ranking and selected genotypes for the multi-trait mean performance and stability index (MTMPS) considering a selection intensity of 25% within ME1 **(A)**, ME2 **(B)**, ME3 **(C)**, and ME4 **(D)**. The red and black circles represent selected and unselected genotypes in their respective environments.

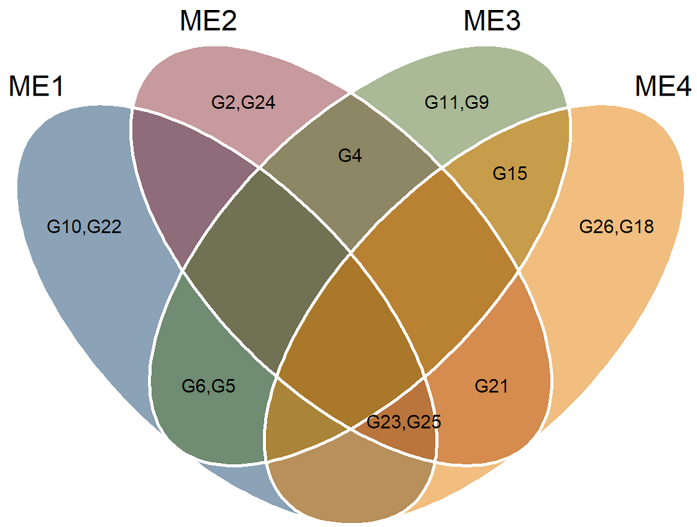

FIGURE 7
Veen plot showing the selected genotypes in each ME.

ME4 to 12.08 Mg ha-1 in ME1) with better stability across contrasting cultivation years.

3.5 Ranking the mega-environments

Figure 10 shows the genotype plus genotype-by-environment (GGE) biplot showing the ranking of the delineated mega-environments relative to an ideal mega-environment. Considering the average yield in each ME, the ME1 (which included only Yicheng) is closer to the "ideal" environment. On average, the yield in ME1 was 11.4 Mg ha^{-1} (Supplementary Figures S13-14). On the contrary, ME4 presented lower average yields (9.8 Mg ha^{-1}), appearing far from the score of the "ideal" environment (Figure 10).

4 Discussion

4.1 Seasonal effects impacted the mega-environments differently

The 10 environments included in this study were categorized into 4 mega-environments (ME) by which the similarity was assessed on an "omics" scale of 19 environmental covariables with long-term (20 years) weather data (Figure 2). These results support previous studies that also identified the complex climatic conditions in HHH (Tao et al., 2017).

The two years of trials had contrasting climate characteristics (Figures 3B, C), which may be the source of the significant ($P< 0.05$) ME×YEAR interaction for GY (Table 3; Supplementary Table S1). In ME1, for example, a highly distinct pattern of vapor pressure

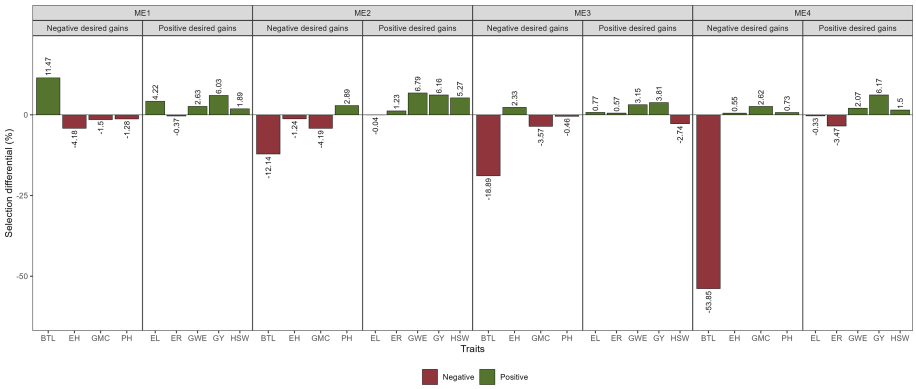

FIGURE 8
Selection gains for mean performance considering the selection within each ME.

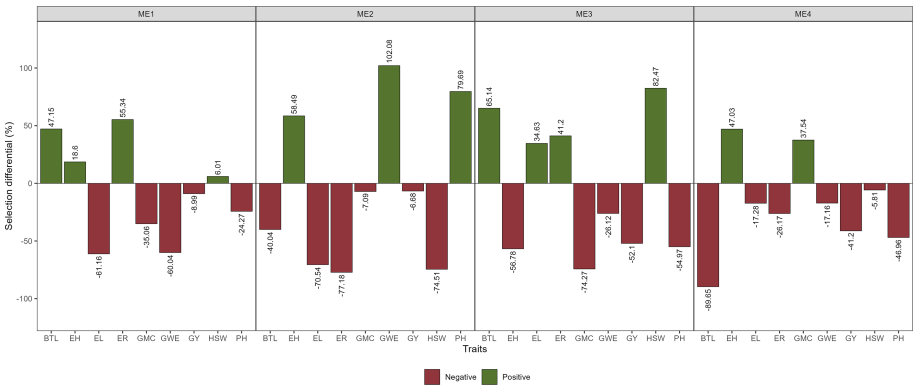

FIGURE 9
Selection gains for stability considering the selection within each ME.

deficit, minimum and maximum air temperatures across the crop cycle were observed in the two cultivation years. While in 2019 most of the flowering period in ME1 had a high vapor pressure deficit (Figure 4A) and maximum temperatures between 34.5°C and °C 39.3°C (Supplementary Figure S15A), 2020 had milder temperatures and a smaller vapor pressure deficit. This approach can leverage plant ecophysiology knowledge aiding to identify the main sources of the genotype-environment interaction to select stress-resilient hybrids (Costa-Neto and Fritsche-Neto, 2021; Resende et al., 2021; Carcedo et al., 2022).

In warm weather, the loss of water by evapotranspiration is greater than in colder weather. On average, ME1 experienced higher values of vapor pressure deficit, which by combining relative humidity and temperature into a single quantity (Penman and Keen, 1948) is an accurate measure for predicting plant transpiration (Seager et al., 2015). Surprisingly, ME1 2019 was the most productive environment with an average yield of 1.2 Mg ha^{-1} greater than the yield observed in 2020 at the same location (Supplementary Figure 13). The high yields in such environments lead to the hypothesis that the deficit by precipitation (Figure 4B), mainly during grain filling, was not sufficiently high to cause the limited transpiration rate trait, frequently expressed in some hybrids under high vapor pressure deficit and water-limited areas (Shekoofa et al., 2016). As a C4-metabolism plant, maize has a higher temperature optimum for photosynthesis than C3 plants due to the operation of a CO_2-concentrating system that inhibits Rubisco oxygenase activity (Berry and Bjorkman, 2003). Previous studies have shown that maize net photosynthesis is only inhibited at leaf temperatures above 38°C and that the maximum quantum yield of photosystem II is relatively insensitive to leaf temperatures up to 45°C (Crafts-Brandner and Salvucci, 2002). When leaf temperature is increased gradually, rubisco activation and net photosynthesis acclimate by the expression of a new activase polypeptide. This acclimation may have occurred in ME1 since maximum air temperatures > 32°C were observed for most of the days since leaf expansion and may explain why this environment

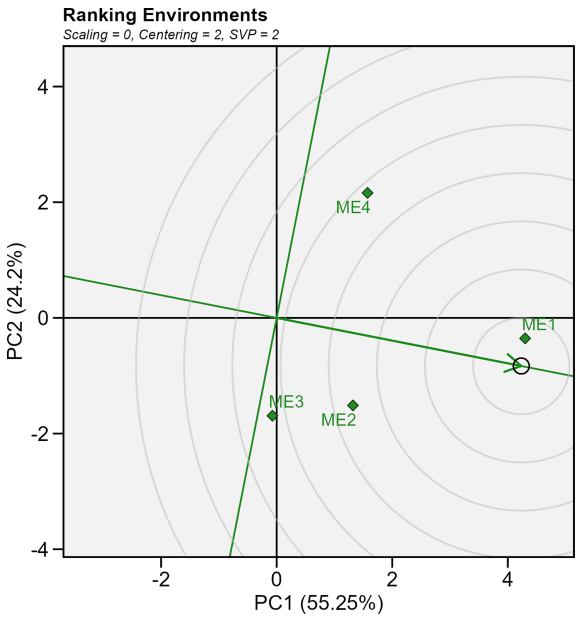

FIGURE 10
GGE biplot showing ranking of test mega-environment relative to an ideal test mega-environment.

presented a high yield even with ~75% of the flowering period experiencing temperatures > 34.5 °C (Supplementary Figure S15A).

Another climate variable that can explain the higher yield of ME1 in 2019 is the minimum temperatures. In 2020, ~75% of the days during the grain filling stage had minimum air temperatures below 19.2°C (Supplementary Figure S15B), which resulted in a negative correlation between GY and minimum temperature (Figure 3C). Previous studies have shown that temperatures below 20°C rose abruptly the redox state of the primary electron acceptor of photosystem II (QA), and increase the non-photochemical quenching of chlorophyll fluorescence, suggesting a restriction in electron transport in such conditions (Labate et al., 1990; Sowiński et al., 2020).

4.2 Higher precipitation does not ensure higher yields

Overall, the environments in 2020 presented accumulated rainfall during the experiment greater than 500 mm, researching ~920 mm in ME1 (Supplementary Figure S16). As a result, these environments showed a higher deficit by precipitation (positive deficits mean more water availability), and a lower vapor pressure deficit (Figure 4B). Unexpectedly, higher yields were not observed in such environments. In Jieshou, for example, the average yield was 2.6 t ha^{-1} smaller in 2020 compared to 2019, even with rainfall precipitation ~2.4-fold higher, with 387 mm in 2019, and 917 mm in 2020 (Supplementary Figure S16).

A possible explanation for the lower yields observed in environments with higher water availability may be related to the restricted plant transpiration in such cases. Water moves from the soil into plant roots, and by negative pressures within the xylem due to capillary forces in the cell walls, to the leaves. The water, warmed by the sun, turns into vapor passing out through stomata, at the same time that allows absorption of CO_2 to photosynthesize (Taiz and Zeiger, 2010). The propulsive force of this process is regulated by the difference in the concentration of water vapor between the intercellular spaces of the leaves and the external atmospheric mass; the energy of this process is provided by the amount of radiation available. In ME1 during 2020, for example, ~87% of the grain filling period presented relative humidity greater than 70% (Supplementary Figure S15C). In addition, the wind speed in such a location had the lowest average (0.20 m s^{-1}). The combination of high relative humidity and lower wind speed might have dramatically reduced plant transpiration. While limitation on transpiration at high vapor pressure deficit is a promising trait that could be incorporated into breeding programs to improve drought tolerance in maize (Yang et al., 2012), lower yield under elevated air relative humidity may be related to the hindered acquisition of mineral nutrients, mainly those supplied to plant roots by mass flow (NO_3^-, Ca^{+2}, and Mg^{+2}), considering the transpiration-driven mass flow concept (Cramer et al., 2009).

4.3 Envirotyping helped to better understand the genotype-environment interaction

The significant GEN×ME×YEAR interaction suggests the complex interaction of the genotypes with contrasting environments on the trait phenotypic expression. Similar reports were also observed in previous studies (Kamutando et al., 2013; Mebratu et al., 2019; Yue et al., 2020; Singamsetti et al., 2021). Along with the global changes in climatic variables over the past decades, there is a growing consensus that future food production will be threatened by environmental conditions (Ceglar and Kajfež-Bogataj, 2012; Steward et al., 2018). Therefore, knowledge about the influence of climatic variables on maize yield and genotypic variation within a certain environment is particularly necessary. Among the climatic factors investigated, temperature, vapor pressure deficit, deficit by precipitation, and relative humidity were key environmental factors to distinguish yield across different environments, which in turn affects GE interactions (de Araujo et al., 2019).

Growing resilient crops with consistent yield performance in unpredictable and complex weather changes is critical to ensuring food security. Given the large scale of production, high degree of mechanization, and developed biotechnology, coupled with measures and technical means such as reasonably dense planting, scientific fertilization, biological pest control,

and water-saving irrigation, the maize yield level of Unites States of America has long been among the highest in the world (~10.5 Mg ha^{-1}). China's maize yield in 2020 was 6.35 Mg ha^{-1} which was 60% of the US yield level (Guo et al., 2021). Given the huge difference in corn production between China and the United States, how to select and breeding excellent corn hybrids that adapt to the climate characteristics of different ecological regions is the key to ensuring the healthy and stable development of China's corn industry (Yue et al., 2022b). Since the 1960s, the Dryland Farming Institute, Hebei Academy of Agriculture and Forestry Sciences has been focusing on the breeding of new high-yield and stable maize hybrids and the multi-environment trials of summer maize in the HHH Plain, making full use of foreign germplasm resources to improve local germplasm. A series of excellent summer maize hybrids were selected and bred.

Here, we provided evidence that using envirotyping techniques to define mega-environments based on climate variables may help breeders to better understand the genotype-by-environment interaction. Several studies define mega-environments based on the genotypes' response in a single year (Singh et al., 2019; Mushayi et al., 2020; Enyew et al., 2021), but since the environmental pattern that defines the genotype response may change significantly across years (Figure 4), this may lead to mistaken recommendations. In most studies that evaluate genotypes across multiple locations and years, the average yield across years is used to fill a two-way table (genotypes x locations) that is further used in AMMI or GGE biplot analysis (Shojaei et al., 2022). Here, we have shown how integrating multi-trait selection for mean performance (within mega-environments) and stability (across years) with detailed environmental typology may be useful to identify specific adaptations (such as tolerance to warmer environments), increasing the sustainability of breed programs mainly under the climate changes in view (Lopes et al., 2015). Therefore, our results can leverage plant ecophysiology knowledge aiding in identifying the primary sources of the genotype-environment interaction in plant breeding programs (Costa-Neto and Fritsche-Neto, 2021; Resende et al., 2021). The use of this approach becomes particularly interesting due to the dynamism and exhaustivity of the data available (climate information available for all points of the globe) that make it possible to replicate the procedure anywhere, anytime, and the possibility of including additional information such as soil proprieties, crop management, companion organisms, and crop canopy (Xu, 2016).

4.4 The multi-trait selection provided desired gains for most of the studied traits

To the best of our knowledge, this is the first introduction of the term multi-trait mean performance and stability index (MTMPS). The MTMPS can be seen as an adaptation of the MTSI (Olivoto et al., 2019b) where several parametric and non-parametric stability measures (beyond the WAASB) can be used. Similar to the MTSI, genotypes that have lower values of MTMPS are assumed to have better mean performance and stability based on the set of accessed traits. Multi-trait stability index has recently been employed as a robust tool to assist the selection of elite genotypes based on the mean performance and stability of various variables. Some examples include the selection of resistant soybean genotypes to drought and salinity (Zuffo et al., 2020), bread wheat ideotypes for adaptation to early sown conditions (Farhad et al., 2022), barnyard millet lines for shoot fly resistance (Padmaja et al., 2022), drought tolerant chickpea genotypes (Hussain et al., 2021), pea lines adapted to autumn sowings in broomrape-prone Mediterranean environments (Rubiales et al., 2021), and maize inbred lines under optimal and drought stress conditions (Balbaa et al., 2022).

A key factor in using the MTMPS is choosing an adequate θ_Y/θ_s ratio for each trait, which will likely change the genotype ranking. By plotting the genotype ranks in several scenarios of θ_Y/θ_s ratio (Supplementary Figure S17) it is possible to identify groups of genotypes with similar performance regarding stability and productivity. For example, in ME1, G10 and G23 (selected by the MTMPS) remained well-ranked regardless of the θ_Y/θ_s ratio. This suggests that they have both high yield and satisfactory stability. On the other hand, G8 remained poorly ranked either considering only the mean performance or stability (Supplementary Figure S17). The poor performance for GY –and possibly for all the other traits– made this genotype the last ranked within ME1 (Figure 6A). In our case, highly stable hybrids across years could be identified as those that are better ranked when θ_Y/θ_s tends to 0. One example in ME1 would be G21, which was the top-ranked when only stability was considered in the MPS (Supplementary Figure S17).

Here, we found that the use of the MTMPS provided desired gains for the mean performance and stability for most of the studied traits (Figures 8 and 9) and that the selection within mega-environments with similar climatic patterns may provide satisfactory gains. The use of MTMPS is expected to grow rapidly among breeders helping to identify hybrids that combine desired mean performance and stability for important traits. For example, envirotyping and morpho-physiological and yield traits accessed [eg., Balbaa et al. (2022)] can be combined to identify stress-adaptive traits with a high yield and helps to better understand the genotype-by-environment interaction.

5 Conclusions

Considering 20 years of climate information and 19 environmental covariables, we identified four mega-environments (ME) for maize cultivation in the Huanghuaihai plain in China. Overall, most of the studied traits were

significantly affected by genotype × mega-environment × year interaction. The vapor pressure deficit, maximum temperature, relative humidity, and deficit by precipitation were the climate variables that most contributed to the envirotyping. This provides relevant evidence that evaluating maize stability and adaptation to mega-environments using single-year, multi-environment trials may provide misleading recommendations. Counterintuitively, higher yields were not observed in the environments with higher accumulated rainfall precipitation. We provide strong pieces of evidence that vapor pressure deficit, minimum temperatures, and relative humidity may be climate variables that –in environments with no water restriction–, have a relevant control on the plant transpiration and consequently, yield. Utilizing the MTMPS approach in this study led to identifying six different selected hybrids in each mega-environment, with higher stability and prominent mean performance for most of the studied traits. G23 and G25 were selected within three out of the four mega-environments, being identified as stable. The G5 shows satisfactory yield and stability across contrasting years in the drier, warmer, and with higher vapor pressure deficit mega-environment, which included locations in the Hubei province. To the best of our knowledge, this is the first study that integrated envirotyping techniques and multi-trait selection for mean performance and stability, opening the door to a more systematic and dynamic characterization of the environment to better understand the genotype-by-environment interaction in multi-environment trials.

Data availability statement

The source code used to produce the static website and the results in this article have been archived at https://doi.org/10.5281/zenodo.7221255 as manuscript_v3.0.0 (Olivoto, 2022).

Author contributions

HY: Conceptualization, data curation, formal analysis, funding acquisition, investigation, methodology, software, visualization, writing-original draft, writing-review & editing. TO: Conceptualization, statistical analysis, writing- review & editing. JB: Conceptualization, data curation, formal analysis. JL: Data curation, formal analysis. JW: Conceptualization, writing original draft, writing-review & editing. JX: Conceptualization, data curation, formal analysis, funding acquisition, methodology, supervision. SC: Conceptualization, data curation, formal analysis, funding acquisition, methodology, supervision, validation. HP: Conceptualization, data curation, funding acquisition, methodology, supervision. MN: Conceptualization, statistical analysis. XJ: Conceptualization, data curation, formal analysis, funding acquisition, investigation, methodology, software, visualization, writing-original draft, writing-review & editing. All authors contributed to the article and approved the submitted version.

Funding

This study was supported by the Key Research and Development Projects of Hebei Province (20326305D), Special Fund for National System (Maize) of Modern Industrial Technology (CARS-02), the Science and Technology Support Program of Hebei Province (16226323D-X), HAAFS Science and Technology Innovation Special Project, "Three-Three-Three Talent Project" Funded Project in Hebei Province (A202101056), the Agricultural Science and Technology Achievement Transformation Project of Hebei province (21626310D), the National Key Research and Development Program of China (2019YFE0120400) and Natural Science Foundation of Shandong Province, China (ZR2021MC107).

Acknowledgments

The authors are grateful to the K. M. Chen (Assistant Professor, Meteorological Bureau of Hengshui, Hebei, China) for compiling and collecting meteorological data of this research.

Conflict of interest

The authors declare that the research was conducted in the absence of any commercial or financial relationships that could be construed as a potential conflict of interest.

Publisher's note

Supplementary material

The Supplementary Material for this article can be found online at: https://www.frontiersin.org/articles/10.3389/fpls.2022.1030521/full#supplementary-material

References

Allen, R. G., Pereira, L. S., Raes, D., and Smith, M.. (1998). Crop evapotranspiration: guidelines for computing crop water requirements, FAO Drainage and Irrigation Paper 56, Food and Agriculture Organization, Rome, 1998. Available at: http://www.fao.org/docrep/X0490E/X0490E00.htm.

Alizadeh, B., Rezaizad, A., Hamedani, M. Y., Shiresmaeili, G., Nasserghadimi, F., Khademhamzeh, H. R., et al. (2022). Genotype × Environment interactions and simultaneous selection for high seed yield and stability in winter rapeseed (Brassica napus) multi-environment trials. *Agric. Res.* 11, 185–196. doi: 10.1007/s40003-021-00565-9

Balbaa, M. G., Osman, H. T., Kandil, E. E., Javed, T., Lamlom, S. F., Ali, H. M., et al. (2022). Determination of morpho-physiological and yield traits of maize inbred lines (Zea mays l.) under optimal and drought stress conditions. *Front. Plant Sci.* 13. doi: 10.3389/fpls.2022.959203

Bänziger, M., Setimela, P. S., Hodson, D., and Vivek, B. (2006). Breeding for improved abiotic stress tolerance in maize adapted to southern Africa. *Agric. Water Manage.* 80, 212–224. doi: 10.1016/j.agwat.2005.07.014

Bates, D., Mächler, M., Bolker, B., and Walker, S. (2015). Fitting linear mixed-effects models using lme4. *J. Stat. Software* 67, 1–48. doi: 10.18637/jss.v067.i01

Berry, J., and Bjorkman, O. (2003). Photosynthetic response and adaptation to temperature in higher plants. *Annu. Rev. Plant Physiol.* 31, 491–543. doi: 10.1146/annurev.pp.31.060180.002423

Carcedo, A. J. P., Mayor, L., Demarco, P., Morris, G. P., Lingenfelser, J., Messina, C. D., et al. (2022). Environment characterization in sorghum (Sorghum bicolor l.) by modeling water-deficit and heat patterns in the great plains region, united states. *Front. Plant Sci.* 13. doi: 10.3389/fpls.2022.768610

Ceglar, A., and Kajfež-Bogataj, L. (2012). Simulation of maize yield in current and changed climatic conditions: Addressing modelling uncertainties and the importance of bias correction in climate model simulations. *Eur. J. Agron.* 37, 83–95. doi: 10.1016/j.eja.2011.11.005

Costa-Neto, G., and Fritsche-Neto, R. (2021). Enviromics: bridging different sources of data, building one framework. *Crop Breed. Appl. Biotechnol.* 21, 393521-393533. doi: 10.1590/1984-70332021v21Sa25

Costa-Neto, G., Fritsche-Neto, R., and Crossa, J. (2021a). Nonlinear kernels, dominance, and envirotyping data increase the accuracy of genome-based prediction in multi-environment trials. *Heredity* 126, 92–106. doi: 10.1038/s41437-020-00353-1

Costa-Neto, G., Galli, G., Carvalho, H. F., Crossa, J., and Fritsche-Neto, R. (2021b). EnvRtype: a software to interplay enviromics and quantitative genomics in agriculture. *G3 Genes Genomes Genet.* 11, jkab040. doi: 10.1093/G3JOURNAL/JKAB040

Crafts-Brandner, S. J., and Salvucci, M. E. (2002). Sensitivity of photosynthesis in a C4 plant, maize, to heat stress. *Plant Physiol.* 129, 1773–1780. doi: 10.1104/pp.002170

Cramer, M. D., Hawkins, H.-J., and Verboom, G. A. (2009). The importance of nutritional regulation of plant water flux. *Oecologia* 161, 15–24. doi: 10.1007/s00442-009-1364-3

de Araujo, M. J., de Paula, R. C., Campoe, O. C., and Carneiro, R. L. (2019). Adaptability and stability of eucalypt clones at different ages across environmental gradients in Brazil. *For. Ecol. Manage.* 454, 117631. doi: 10.1016/j.foreco.2019.117631

Dempster, A. P., Laird, N. M., and Rubin, D. B. (1977). Maximum likelihood from incomplete data *via* the EM algorithm. *J. R. Stat. Society Ser. B.* 39, 1–38. doi: 10.1111/j.2517-6161.1977.tb01600.x

Dong, X., Guan, L., Zhang, P., Liu, X., Li, S., Fu, Z., et al. (2021). Responses of maize with different growth periods to heat stress around flowering and early grain filling. *Agric. For. Meteorology* 303, 108378. doi: 10.1016/j.agrformet.2021.108378

Ebdon, J. S., and Gauch, H. G. Jr. (2002). Additive main effect and multiplicative interaction analysis of national turfgrass performance trials: I. interpretation of genotype × environment interaction. *Crop Sci.* 42, 489–496. doi: 10.2135/cropsci2002.4890

Enyew, M., Feyissa, T., Geleta, M., Tesfaye, K., Hammenhag, C., and Carlsson, A. S. (2021). Genotype by environment interaction, correlation, AMMI, GGE biplot and cluster analysis for grain yield and other agronomic traits in sorghum (Sorghum bicolor l. moench). *PloS One* 16, e0258211. doi: 10.1371/journal.pone.0258211

Farhad, M., Tripathi, S. B., Singh, R. P., Joshi, A. K., Bhati, P. K., Vishwakarma, M. K., et al. (2022). Multi-trait selection of bread wheat ideotypes for adaptation to early sown condition. *Crop Sci.* 62, 67–82. doi: 10.1002/csc2.20628

Fischer, T., and Edmeades, G. O. (2010). Breeding and cereal yield progress. *Crop Sci.* 50, S–85-S-98. doi: 10.2135/cropsci2009.10.0564

Guillot, G., and Rousset, F. (2013). Dismantling the mantel tests. *Methods Ecol. Evol.* 4, 336–344. doi: 10.1111/2041-210x.12018

Guo, Q., Huang, G., Guo, Y., Zhang, M., Zhou, Y., and Duan, L. (2021). Optimizing irrigation and planting density of spring maize under mulch drip irrigation system in the arid region of Northwest China. *Field Crops Res.* 266, 108141. doi: 10.1016/j.fcr.2021.108141

Haarhoff, S. J., and Swanepoel, P. A. (2018). Plant population and maize grain yield: A global systematic review of rainfed trials. *Crop Sci.* 58, 1819–1829. doi: 10.2135/cropsci2018.01.0003

Hickey, L. T., Hafeez, N. A., Robinson, H., Jackson, S. A., Leal-Bertioli, S. C. M., Tester, M., et al. (2019). Breeding crops to feed 10 billion. *Nat. Biotechnol.* 37, 744–754. doi: 10.1038/s41587-019-0152-9

Hou, P., Liu, Y., Liu, W., Liu, G., Xie, R., Wang, K., et al. (2020). How to increase maize production without extra nitrogen input. *Resources Conserv. Recycling* 160, 104913. doi: 10.1016/j.resconrec.2020.104913

Hussain, T., Akram, Z., Shabbir, G., Manaf, A., and Ahmed, M. (2021). Identification of drought tolerant chickpea genotypes through multi trait stability index. *Saudi J. Biol. Sci.* 28, 6818–6828. doi: 10.1016/j.sjbs.2021.07.056

Kaiser, H. F. (1958). The varimax criterion for analytic rotation in factor analysis. *Psychometrika* 23, 187–200. doi: 10.1007/BF02289233

Kamutando, C. N., Muungani, D., Masvodza, D. R., and Gasura, E. (2013). Exploiting genotype × environment interaction in maize breeding in Zimbabwe. *Afr. J. Agric. Res.* 8, 4058–4066. Available at: https://academicjournals.org/journal/AJAR/article-full-text-pdf/E7FFE6735132.

Kassambara, A., and Mundt, F. (2020) *Factoextra: Extract and visualize the results of multivariate data analyses*. Available at: https://cran.r-project.org/package=factoextra.

Koundinya, A. V. V., Ajeesh, B. R., Hegde, V., Sheela, M. N., Mohan, C., Asha, K. I., et al. (2021). Genetic parameters, stability and selection of cassava genotypes between rainy and water stress conditions using AMMI, WAAS. *Scientia Hortic.* 281, 109949. doi: 10.1016/j.scienta.2021.109949

Labate, C. A., Adcock, M. D., and Leegood, R. C. (1990). Effects of temperature on the regulation of photosynthetic carbon assimilation in leaves of maize and barley. *Planta* 181, 547–554. doi: 10.1007/BF00193009

Lima, G. W., Silva, C. M., Mezzomo, H. C., Casagrande, C. R., Olivoto, T., Borem, A., et al. (2022). Genetic diversity in tropical wheat germplasm and selection *via* multitrait index. *Agron. J.* 114, 887–899. doi: 10.1002/AGJ2.20991

Lopes, M. S., El-Basyoni, I., Baenziger, P. S., Singh, S., Royo, C., Ozbek, K., et al. (2015). Exploiting genetic diversity from landraces in wheat breeding for adaptation to climate change. *J. Exp. Bot.* 66, 3477–3486. doi: 10.1093/jxb/erv122

Mebratu, A., Wegary, D., Mohammed, W., Teklewold, A., and Tarekegne, A. (2019). Genotype × environment interaction of quality protein maize hybrids under contrasting management conditions in Eastern and southern Africa. *Crop Sci.* 59, 1576–1589. doi: 10.2135/cropsci2018.12.0722

Monteiro, L. A., Sentelhas, P. C., and Pedra, G. U. (2018). Assessment of NASA/POWER satellite-based weather system for Brazilian conditions and its impact on sugarcane yield simulation. *Int. J. Climatology* 38, 1571–1581. doi: 10.1002/joc.5282

Mushayi, M., Shimelis, H., Derera, J., Shayanowako, A. I. T., and Mathew, I. (2020). Multi-environmental evaluation of maize hybrids developed from tropical and temperate lines. *Euphytica* 216, 1–14. doi: 10.1007/s10681-020-02618-6

Nardino, M., Perin, E. C., Aranha, B. C., Carpes, S. T., Fontoura, B. H., Sousa, D. J. P., et al. (2022). Understanding drought response mechanisms in wheat and multi-trait selection. *PloS One* 17, e0266368. doi: 10.1371/journal.pone.0266368

Niu, S., Du, X., Wei, D., Liu, S., Tang, Q., Bian, D., et al. (2021). Heat stress after pollination reduces kernel number in maize by insufficient assimilates. *Front. Genet.* 12. doi: 10.3389/fgene.2021.728166

Olivoto, T. (2022). *TiagoOlivoto/paper_maize_huanghuaihai: manuscript v3 (manuscript_v3.0.0)* (Zenodo). doi: 10.5281/zenodo.7221255

Olivoto, T., and Lúcio, A. D. (2020). Metan: An r package for multi-environment trial analysis. *Methods Ecol. Evol.* 11, 783–789. doi: 10.1111/2041-210X.13384

Olivoto, T., Lúcio, A. D. C., Silva, J. A. G., Marchioro, V. S., Souza, V. Q., and Jost, E. (2019a). Mean performance and stability in multi-environment trials I: Combining features of AMMI and BLUP techniques. *Agron. J.* 111, 2949–2960. doi: 10.2134/agronj2019.03.0220

Olivoto, T., Lúcio, A. D. C., Silva, J. A. G., Sari, B. G., and Diel, M. I. (2019b). Mean performance and stability in multi-environment trials II: Selection based on multiple traits. *Agron. J.* 111, 2961–2969. doi: 10.2134/agronj2019.03.0221

Olivoto, T., and Nardino, M. (2021). MGIDI: toward an effective multivariate selection in biological experiments. *Bioinformatics* 37, 1383–1389. doi: 10.1093/bioinformatics/btaa981

Padmaja, P. G., Kalaisekar, A., Tonapi, V. A., and Madhusudhana, R. (2022). A multi-season analysis of barnyard millet (Echinochloa frumentacea) germplasm lines for shoot fly resistance and multi-trait stability. *Plant Breed.* 141, 399–407. doi: 10.1111/pbr.13011

Penman, H. L., and Keen, B. A. (1948). Natural evaporation from open water, bare soil and grass. *Proc. R. Soc. London. Ser. A. Math. Phys. Sci.* 193, 120–145. doi: 10.1098/rspa.1948.0037

R Core Team (2022) *R: a language and environment for statistical computing*. Available at: https://www.r-project.org/.

Resende, R. T., Piepho, H.-P., Rosa, G. J. M., Silva-Junior, O. B., e Silva, F. F., de Resende, M. D. V., et al. (2021). Enviromics in breeding: applications and perspectives on envirotypic-assisted selection. *Theor. Appl. Genet.* 134, 95–112. doi: 10.1007/s00122-020-03684-z

Rizzo, G., Monzon, J. P., Tenorio, F. A., Howard, R., Cassman, K. G., and Grassini, P. (2022). Climate and agronomy, not genetics, underpin recent maize yield gains in favorable environments. *P. Natl. A. Sci.* 119 (4), e2113629119. doi: 10.1073/pnas.2113629119

Rubiales, D., Osuna-Caballero, S., González-Bernal, M. J., Cobos, M. J., and Flores, F. (2021). Pea breeding lines adapted to autumn sowings in broomrape prone Mediterranean environments. *Agronomy* 11, 769. doi: 10.3390/agronomy11040769

Schmidt, P., Hartung, J., Bennewitz, J., and Piepho, H.-P. (2019). Heritability in plant breeding on a genotype-difference basis. *Genetics* 212, 991–1008. doi: 10.1534/genetics.119.302134

Seager, R., Hooks, A., Williams, A. P., Cook, B., Nakamura, J., and Henderson, N. (2015). Climatology, variability, and trends in the U.S. vapor pressure deficit, an important fire-related meteorological quantity. *J. Appl. Meteorology Climatology* 54, 1121–1141. doi: 10.1175/JAMC-D-14-0321.1

Shekoofa, A., Sinclair, T. R., Messina, C. D., and Cooper, M. (2016). Variation among maize hybrids in response to high vapor pressure deficit at high temperatures. *Crop Sci.* 56, 392–396. doi: 10.2135/cropsci2015.02.0134

Shi, W., Wang, M., and Liu, Y. (2021). Crop yield and production responses to climate disasters in China. *Sci. Total Environ.* 750, 141147. doi: 10.1016/j.scitotenv.2020.141147

Shojaei, S. H., Mostafavi, K., Bihamta, M. R., Omrani, A., Mousavi, S. M. N., Illés, Á., et al. (2022). Stability on maize hybrids based on GGE biplot graphical technique. *Agronomy* 12, 394. doi: 10.3390/agronomy12020394

Singamsetti, A., Shahi, J. P., Zaidi, P. H., Seetharam, K., Vinayan, M. T., Kumar, M., et al. (2021). Genotype × environment interaction and selection of maize (Zea mays l.) hybrids across moisture regimes. *Field Crops Res.* 270, 108224. doi: 10.1016/J.FCR.2021.108224

Singh, C., Gupta, A., Gupta, V., Kumar, P., Sendhil, R., Tyagi, B. S., et al. (2019). Genotype x environment interaction analysis of multi-environment wheat trials in India using AMMI and GGE biplot models. *Crop Breed. Appl. Biotechnol.* 19, 309–318. doi: 10.1590/1984-70332019v19n3a43

Soltani, A., and Sinclair, T. R. (2012). Modeling Physiology of Crop Development, Growth and Yield Wallingford, CA: CAB International. pp 322.

Sowiński, P., Fronk, J., Jończyk, M., Grzybowski, M., Kowalec, P., and Sobkowiak, A. (2020). Maize response to low temperatures at the gene expression level: A critical survey of transcriptomic studies. *Front. Plant Sci.* 11. doi: 10.3389/fpls.2020.576941

Sparks, A. H. (2018). Nasapower: A NASA POWER global meteorology, surface solar energy and climatology data client for r. *J. Open Source Software* 3, 1035. doi: 10.21105/joss.01035

Steward, P. R., Dougill, A. J., Thierfelder, C., Pittelkow, C. M., Stringer, L. C., Kudzala, M., et al. (2018). The adaptive capacity of maize-based conservation agriculture systems to climate stress in tropical and subtropical environments: A meta-regression of yields. *Agriculture Ecosyst. Environ.* 251, 194–202. doi: 10.1016/j.agee.2017.09.019

Taiz, L., and Zeiger, E. (2010). *Plant physiology* (Massachusetts: Sinauer Associates Inc).

Tao, F., Xiao, D., Zhang, S., Zhang, Z., and Rötter, R. P. (2017). Wheat yield benefited from increases in minimum temperature in the Huang-Huai-Hai plain of China in the past three decades. *Agric. For. Meteorology* 239, 1–14. doi: 10.1016/j.agrformet.2017.02.033

Vaezi, B., Pour-Aboughadareh, A., Mohammadi, R., Mehraban, A., Hossein-Pour, T., Koohkan, E., et al. (2019). Integrating different stability models to investigate genotype × environment interactions and identify stable and high-yielding barley genotypes. *Euphytica* 215, 63. doi: 10.1007/s10681-019-2386-5

Wang, P., Wu, D., Yang, J., Ma, Y., Feng, R., and Huo, Z. (2020). Summer maize growth under different precipitation years in the Huang-Huai-Hai plain of China. *Agric. For. Meteorology* 285–286, 107927. doi: 10.1016/j.agrformet.2020.107927

Xu, Y. (2016). Envirotyping for deciphering environmental impacts on crop plants. *Theor. Appl. Genet.* 129, 653–673. doi: 10.1007/s00122-016-2691-5

Yan, W. (2014). *Crop variety trials: Data management and analysis* (New York: John Wiley & Sons Inc.). doi: 10.1002/9781118688571

Yang, Z., Sinclair, T. R., Zhu, M., Messina, C. D., Cooper, M., and Hammer, G. L. (2012). Temperature effect on transpiration response of maize plants to vapour pressure deficit. *Environ. Exp. Bot.* 78, 157–162. doi: 10.1016/j.envexpbot.2011.12.034

Yan, J., and Tan, B.-C. (2019). Maize biology: From functional genomics to breeding application. *J. Integr. Plant Biol.* 61, 654–657. doi: 10.1111/jipb.12819

Yue, H., Gauch, H. G., Wei, J., Xie, J., Chen, S., Peng, H., et al. (2022a). Genotype by environment interaction analysis for grain yield and yield components of summer maize hybrids across the huanghuaihai region in China. *Agriculture* 12, 602. doi: 10.3390/agriculture12050602

Yue, H. W., Wang, Y. B., Wei, J. W., Meng, Q. M., Yang, B. L., Chen, S. P., et al. (2020). Effects of genotype-by-environment interaction on the main agronomic traits of maize hybrids. *Appl. Ecol. Env. Res.* 18, 1437–1458. doi: 10.15666/aeer/1801_14371458

Yue, H., Wei, J., Xie, J., Chen, S., Peng, H., Cao, H., et al. (2022b). A study on genotype-by-Environment interaction analysis for agronomic traits of maize genotypes across Huang-Huai-Hai region in China. *Phyton* 91, 57–81. doi: 10.32604/PHYTON.2022.017308

Yue, Y., Yang, W., and Wang, L. (2022c). Assessment of drought risk for winter wheat on the huanghuaihai plain under climate change using an EPIC model-based approach. *Int. J. Digital Earth* 15, 690–711. doi: 10.1080/17538947.2022.2055174

Yue, H., Jiang, X., Wei, J., Xie, J., Chen, S., Peng, H., and Bu, J. (2021). A study on genotype× environment interactions for the multiple traits of maize hybrids in China. *Agron. J* 113, 4889–4899. doi: 10.1002/agj2.20907

Zhai, J., Zhang, Y., Zhang, G., Tian, M., Xie, R., Ming, B., and Hou, P. (2022). Effects of nitrogen fertilizer management on stalk lodging resistance traits in summer maize. *Agriculture* 12, 162. doi: 10.3390/agriculture12020162

Zuffo, A. M., Steiner, F., Aguilera, J. G., Teodoro, P. E., Teodoro, L. P. R., and Busch, A. (2020). Multi-trait stability index: A tool for simultaneous selection of soya bean genotypes in drought and saline stress. *J. Agron. Crop Sci.* 206, 815–822. doi: 10.1111/jac.12409

frontiers | Frontiers in Plant Science

TYPE Original Research
PUBLISHED 22 November 2022
DOI 10.3389/fpls.2022.1079087

OPEN ACCESS

EDITED BY
Chao Li,
Northwest A&F University, China

REVIEWED BY
Zhaohe Yuan,
Nanjing Forestry University, China
Ke Mao,
Northwest A&F University, China
Mengxia Zhang,
Cornell University, United States

*CORRESPONDENCE
Chunyu Zhang
cy_zhang@jlu.edu.cn

SPECIALTY SECTION
This article was submitted to Plant Abiotic Stress, a section of the journal Frontiers in Plant Science

RECEIVED 25 October 2022
ACCEPTED 08 November 2022
PUBLISHED 22 November 2022

CITATION
Song Y, Ma B, Guo Q, Zhou L, Lv C, Liu X, Wang J, Zhou X and Zhang C (2022) UV-B induces the expression of flavonoid biosynthetic pathways in blueberry (*Vaccinium corymbosum*) calli.
Front. Plant Sci. 13:1079087.
doi: 10.3389/fpls.2022.1079087

UV-B induces the expression of flavonoid biosynthetic pathways in blueberry (*Vaccinium corymbosum*) calli

Yan Song, Bin Ma, Qingxun Guo, Lianxia Zhou, Changyi Lv, Xiaoming Liu, Jianlei Wang, Xintong Zhou and Chunyu Zhang*

Department of Horticulture, College of Plant Science, Jilin University, Changchun, China

Ultraviolet-B (UV-B) radiation is an environmental signal that affects the accumulation of secondary metabolites in plants. In particular, UV-B promotes flavonoid biosynthesis, leading to improved fruit quality. To explore the underlying molecular mechanism, we exposed blueberry (*Vaccinium corymbosum*) calli to UV-B radiation and performed a transcriptome deep sequencing (RNA-seq) analysis to identify differentially expressed genes (DEGs). We detected 16,899 DEGs among different treatments, with the largest number seen after 24 h of UV-B exposure relative to controls. Functional annotation and enrichment analysis showed a significant enrichment for DEGs in pathways related to plant hormone signal transduction and phenylpropanoid and flavonoid biosynthesis. In agreement with the transcriptome data, flavonol, anthocyanin and proanthocyanidin accumulated upon UV-B radiation, and most DEGs mapping to the phenylpropanoid and flavonoid biosynthetic pathways using the KEGG mapper tool were upregulated under UV-B radiation. We also performed a weighted gene co-expression network analysis (WGCNA) to explore the relationship among genes involved in plant hormone signal transduction, encoding transcription factors or participating in flavonoid biosynthesis. The transcription factors VcMYBPA1, MYBPA2.1, MYB114, MYBA2, MYBF, and MYB102 are likely activators, whereas MYB20, VcMYB14, MYB44, and VcMYB4a are inhibitors of the flavonoid biosynthetic pathway, as evidenced by the direction of correlation between the expression of these MYBs and flavonoid biosynthesis-related genes. The transcription factors bHLH74 and bHLH25 might interact with MYB repressors or directly inhibited the expression of flavonoid biosynthetic genes to control flavonoid accumulation. We also observed the downregulation of several genes belonging to the auxin, gibberellin and brassinosteroid biosynthetic pathways, suggesting that MYB inhibitors or activators are directly or indirectly regulated to promote flavonoid biosynthesis under UV-B radiation.

KEYWORDS

RNA sequencing, UV-B radiation, flavonoid, blueberry, transcription, plant hormone signal transduction

Introduction

Plants are constantly exposed to changing environmental conditions, among which ultraviolet-B (UV-B) radiation (280–315 nm) is an important factor that limits plant growth and development (Dotto and Casati, 2017). Plants accumulate flavonoids that protect against potential damage caused by UV exposure; importantly, flavonoids are also economically important compounds in fruits, as they possess nutritional benefits for human health (Norberto et al., 2013). Thus, despite the possible damage it can induce, the controlled application of UV-B radiation of fruits and other crops has been proposed as a means to improve fruit quality and their antioxidant contents (Henry-Kirk et al., 2018; González-Villagra et al., 2020).

Flavonoid compounds (flavonol, anthocyanin, and proanthocyanidin) are synthesized by the general phenylpropanoid biosynthetic pathway; the expression of the structural genes encoding the corresponding enzymes is upregulated by UV-B radiation and stimulates the accumulation of flavonoid compounds (Xie et al., 2011; Martínez-Lüscher et al., 2014). The UV-B-induced signaling pathway involves the UV-B photoreceptor UV resistance locus 8 (UVR8), the E3 ubiquitin ligase constitutively photomorphogenic 1 (COP1) and the basic zipper (bZIP) TF elongated hypocotyle (HY5) and zinc finger TF B-box domain containing protein (BBX) (Rizzini et al., 2011). These proteins direct or indirect regulate the transcription levels of regulators and flavonoid biosynthetic genes to affect flavonoid accumulation (Qiu et al., 2018; Bai et al., 2019). Among these regulators, four subgroups (4, 5, 6, and 7) from the 22 existing R2R3-MYB transcription factor gene family subgroups play regulatory roles in the biosynthesis of flavonoid compounds. More specifically, subgroup 4 encodes suppressors of flavonoid biosynthesis, while subgroups 5, 6, and 7 encode positive regulators of flavonoid biosynthesis (Kranz et al., 1998; Plunkett et al., 2018; Zhang et al., 2021). For example, the subgroup 4 *FaMYB1* from strawberry (*Fragaria ananassa*) suppressed anthocyanin and flavonol accumulation and *VvMYBC2-L1* from grapevine (*Vitis vinifera*) suppressed proanthocyanidin biosynthesis (Aharoni et al., 2001; Cavallini et al., 2015). At the same time bHLH transcription factor also effected flavonoid biosynthesis by interacting with MYB TFs or regulating structural genes of flavonoid biosynthesis (Matus et al., 2010; Zhu et al., 2020). UV-B also affects the expression of MYB transcription factor genes. For example, in Arabidopsis (*Arabidopsis thaliana*), the expression of *MYB111*, *MYB12*, and *production of anthocyanin pigment 1* (*PAP1*) is upregulated in response to UV-B radiation (Heijde and Ulm, 2018). In grapevine berries, UV-B triggers the upregulation of *flavonol synthase 1* (*VvFLS1*) *via* VvMYBF1 from subgroup 7, leading to a strong increase in flavonol concentration (Martínez-Lüscher et al., 2014). In apple (*Malus domestica*), the expression of *MdMYB10* from subgroup 6 and *MdMYB22* from subgroup 7 is downregulated throughout fruit development under reduced UV radiation and influences anthocyanin and flavonol production (Henry-Kirk et al., 2018). Thus, transcription factors have important roles in accumulating of UV-B-induced flavonoids.

Plant hormones also play critical parts in helping plants adapt to adverse environmental conditions (Yu et al., 2020). The growth-promoting hormones auxin, gibberellins, and brassinosteroids negatively regulate UV-B stress tolerance (Hectors et al., 2012; Roro et al., 2017; Liang et al., 2020) and inhibit flavonoid accumulation *via* direct interaction of some constituent proteins of their signalling pathway with MYBs or by binding to the promoters of *MYB* or structural genes involved in flavonoid biosynthesis to modulate their expression (Zhang Y. et al., 2017; Tan et al., 2019; Liang et al., 2020). However, it is unclear which genes related to plant hormone signalling participate in UV-B-induced flavonoid biosynthesis.

Blueberries (*Vaccinium corymbosum*) are often referred to as a "superfood" due to the health benefits associated with the phenylpropanoid compounds they contain, particularly anthocyanins, proanthocyanidins and flavonols (Ribera et al., 2010; Norberto et al., 2013). In recent years, several structural genes involved in flavonoid biosynthesis have been cloned and characterized in blueberry (Zhang et al., 2016; Zhang C. et al., 2017). Regulatory genes involved in this process have also been described, such as VcMYBA and VcMYBPA1, which regulate anthocyanin and proanthocyanidin biosynthesis, respectively (Zifkin et al., 2012; Plunkett et al., 2018). UV-B induces anthocyanin biosynthesis in the peel of harvested blueberry fruits by upregulating the expression of the structural and regulatory genes *VcMYB21* and *VcR2R3MYB*. UV-B radiation also increases flavonoid accumulation and promotes *VcMYBPA1* expression, but the underlying mechanism is unknown (Nguyen et al., 2017; González-Villagra et al., 2020).

In this study, we identified genes that are differentially expressed in blueberry calli in response to UV-B irradiation through transcriptome deep sequencing (RNA-seq) analysis and functional annotation of these differentially expressed genes (DEGs). To elucidate the mechanism driving flavonoid biosynthesis in blueberry fruits, we also assembled a regulatory network encompassing the plant hormone signal transduction pathways, transcription factor genes, and the flavonoid biosynthesis pathway by deploying weighted gene co-expression network analysis (WGCNA). The results presented here will broaden our understanding of UV-B-induced flavonoid biosynthesis and provide basic information on how to improve blueberry quality *via* simple exposure to UV-B light.

Materials and methods

Plant materials and stress treatments

White loose blueberry (*Vaccinium corymbosum*) calli were obtained from the cultivar 'Northland', which was cultured on a

modified woody plant medium with Murashige and Skoog vitamins containing 3.0 mg/L 2,4-dichlorophenoxyacetic acid (2,4-D), 30 g/L sucrose, and 7 g/L agar, pH 5.4 ± 0.2. All calli were cultured under a 16-h light/8-h dark photoperiod at 25°C and subcultured every 21 days. UV-B was applied by means of narrow band lamps (TL20/01; 311-nm Philips, Netherlands) positioned above the calli at the height of about 10 cm. The calli were harvested right before (0 h) and after treatment consisting of 1, 3, 6, 12, and 24 h of UV-B radiation, frozen in liquid nitrogen and stored at −80°C. All samples were collected as three independent biological replicates and were labeled 0h_1, 0h_2, 0h_3, 1h_1, 1h_2, 0h_3, 3h_1, 3h_2, 3h_3, 6h_1, 6h_2, 6h_3, 12h_1, 12h_2, 12h_3, 24h_1, 24h_2, and 24h_3, respectively, for RNA-seq analysis. For reverse transcription quantitative PCR (RT-qPCR) and measurements of flavonol, anthocyanin, and proanthocyanidin contents (using the 0 h and 24 h samples), each biological replicate was assessed as three technical replicates.

Transcriptome sequencing

Total RNAs were extracted with TRIzol reagent (Invitrogen, USA) and RNA concentration and purity was measured using a NanoDrop 2000 (Thermo Fisher Scientific, Wilmington, DE). RNA integrity was assessed using an RNA Nano 6000 Assay Kit for the Agilent Bioanalyzer 2100 system (Agilent Technologies, CA, USA). Sequencing libraries were generated using a NEBNext UltraTM RNA Library Prep Kit for Illumina (NEB, USA). The libraries were sequenced on an Illumina HiSeq 2500 platform, and 150 bp paired-end reads were generated. Raw reads in fastq format were processed through in-house perl scripts to obtain clean data. Q20, Q30, GC-content, and the sequence duplication level of the clean reads were calculated. The clean reads were mapped to the reference *Vaccinium corymbosum* cv. Draper V1.0 genome sequence (https://www.vaccinium.org/genomes) using Hisat2 software.

Differential expression analysis and functional annotation

Gene expression levels were quantified as fragments per kilobase of transcript per million fragments mapped (FPKM) values. Differentially expressed genes (DEGs) resulting from the comparison of the 0 h sample to the 1, 3, 6, 12, and 24 h samples were identified using the criteria of absolute $\log_2$(fold change) ≥1 and a false discovery rate (FDR) < 0.01 by DEGSeq2. Gene function was annotated based on the following databases: Clusters of Orthologous Groups (COG) (Tatusov et al., 2000), Gene Ontology (GO) (Ashburner et al., 2000), Kyoto Encyclopedia of Genes and Genomes (KEGG) (Kanehisa et al., 2004), Eukaryotic Orthologous Groups (KOG) (Koonin et al., 2004), NCBI non-redundant protein sequences (NR) (Deng et al., 2006), Protein family (Pfam) (Finn et al., 2014), Swiss-Prot (A manually annotated and reviewed protein sequence database) (Apweiler et al., 2004) and evolutionary genealogy of genes: Non-supervised Orthologous Groups (eggNOG) (Huerta-Cepas et al., 2017). KEGG pathway enrichment analysis of DEGs was implemented with KOBAS software (Mao et al., 2005). The phenylpropanoid and flavonoid biosynthetic pathways were mapped against the phenylpropanoid, flavonoid, flavonol, and anthocyanin KEGG pathways using the DEGs identified above. Heatmap representations of gene expression levels were drawn using $\log_{10}$(FPKM) with the Tbtools (v1.098761) software (Chen et al., 2020).

Weighted gene co-expression network analysis

WGCNA was performed with the WGCNA package in R (Langfelder and Horvath, 2008). First, the WGCNA algorithm assumes that the gene network follows a scale-free distribution, defines the gene co-expression correlation matrix and the adjacency function formed by the gene network, and then calculates the correlation coefficients of different nodes, based on which WGCNA builds a hierarchical clustering tree. The different branches of the clustering tree represent different gene modules. The co-expression degree of genes in significant individual modules is high, while the co-expression degree of genes belonging to different modules is low. Genes with different expression levels were assigned to various modules *via* a dynamic tree cut. There were at least 30 genes per co-expression module. Correlations among various modules were calculated using 0.25 as the similarity threshold. For genes in each module, KEGG pathway enrichment analysis was conducted to reveal the biological functions of each module. The genes within the WGCNA kMEblue module were selected to screen for enrichment of the plant hormone signal transduction pathway, transcription factor genes, and flavonoid biosynthetic pathway genes, and to draw the corresponding expression heatmap and regulatory network of the flavonoid pathway. Pearson's correlation coefficients were compared using SPSS 19.0 software.

RNA-Seq data validation

Total RNA was extracted from each sample using an RNA Extraction Kit (Sangon Biotech, Shanghai, China). RT-qPCR was performed on an ABI 7900HT real-time PCR system. Ten genes of interest (*4CL2*, *VcCHI3*, *DFR*, *VcF3'5'H*, *VcF3H-2*, *VcLAR*, *MYB44*, *MYB114*, *VcMYBPA1*, and *ARF18*) involved in flavonoid biosynthesis and belonging to the WGCNA kMEblue module were selected for analysis, using *GAPDH* (AY123769) as the reference transcript. Primer sequences are

shown in Table S1. The relative expression levels of each gene were calculated using the $2^{-\Delta\Delta Ct}$ method.

Measurement of flavonoid contents

The contents of flavonoid compounds including flavonols, anthocyanins, and proanthocyanidins for calli at 0 h and 24 h UV-B treatment were determined as described by Yang et al. (2022a). Each sample was ground to a powder and 0.5 g was extracted in 5 mL 80% (v/v) methanol at 4°C for 2 h to isolate the flavonols. The mixtures were centrifuged (8,000 g, 10 min, 4°C), 1 mL of the supernatant was removed and mixed with 1 mL methanol, and then 0.1 mL of 10% (w/v) aluminum chloride, 0.1 mL 1 M KOAc, and 2.8 mL water were added and the mixtures was incubated for 30 min at 25°C. Rutin was used as a master standard and the absorbance at 415 nm was measured. To measure total anthocyanin contents, samples (0.5 g) were extracted in 3 mL of 1% HCl in methanol and incubated at 4°C for 16 h. After centrifugation (8,000 g, 10 min, 4°C), a 2-mL supernatant was diluted with 2 mL water and the absorbance was measured at 530 nm and 650 nm. Total anthocyanin content was calculated using a previously published formula (Rabino and Mancinelli, 1986). Proanthocyanidin was detected using the DMACA method. Briefly, samples (0.5 g) were extracted in 5 mL of 70% (v/v) acetone containing 0.1% (w/v) ascorbic acid at 4°C for 30 min. After centrifugation (8,000 *g*, 10 min, 4°C), a 3-mL supernatant aliquot was extracted with 3 mL of ether at −20°C for 1 h. Then, 2 mL of the lower phase of the extracted liquid was removed and mixed with 1 mL of methanol and 0.5 mL 2% (w/v) DMACA solution. The mixture was incubated for 20 min at 25°C, and the absorbance was then measured at 643 nm. Catechin was used as the master standard (Wang et al., 2017).

Results

Transcriptome sequencing analysis

To reveal the regulatory network underlying the blueberry response to UV-B radiation, we performed an RNA-seq analysis using total RNA extracted from blueberry calli exposed to UV-B radiation for 1, 3, 6, 12, or 24 h. Table 1 summarizes the details of all RNA-seq samples; we obtained 5.85–8.66 Gb of clean bases for each sample, with a Q30 ranging from 93.70 to 94.97% and a GC content ranging from 46.35 to 46.90%. We successfully mapped approximately 90.88 to 91.90% of all clean reads per sample to the blueberry reference genome.

Differential expression gene analysis

To investigate changes in gene expression under UV-B radiation, we identified differentially expressed genes (DEGs) between the control samples (0 h) and each time point of the UV-B treatment, which returned a total of 16,899 DEGs (Table S2). We detected 2,706 DEGs in 0h_vs_1h, of which 2,428 were upregulated and only 278 were downregulated. The number of DEGs increased gradually with longer UV-B exposure of up to 6 h, with downregulated DEGs remaining scarcer than

TABLE 1 Summary of sequencing data.

Samples	Clean reads	Clean bases	GC Content	≥ Q30	Mapped reads
0h_1	2.78×10^7	8.26×10^9	46.4%	94.2%	91.1%
0h_2	2.70×10^7	8.06×10^9	46.6%	94.0%	91.2%
0h_3	2.23×10^7	6.64×10^9	46.5%	94.9%	91.3%
1h_1	2.76×10^7	8.19×10^9	46.8%	94.2%	90.9%
1h_2	1.99×10^7	5.92×10^9	46.8%	94.5%	90.9%
1h_3	2.60×10^7	7.75×10^9	46.9%	94.2%	91.0%
3h_1	2.60×10^7	7.76×10^9	46.9%	94.2%	91.1%
3h_2	2.65×10^7	7.90×10^9	46.9%	93.7%	91.1%
3h_3	2.69×10^7	8.04×10^9	46.8%	94.2%	91.3%
6h_1	2.90×10^7	$8,66 \times 10^9$	46.6%	94.1%	91.6%
6h_2	2.43×10^7	7.22×10^9	46.9%	95.0%	91.7%
6h_3	2.15×10^7	6.39×10^9	46.8%	94.4%	91.5%
12h_1	2.48×10^7	7.38×10^9	46.9%	94.5%	91.7%
12h_2	2.09×10^7	6.21×10^9	46.9%	94.7%	91.3%
12h_3	1.96×10^7	5.85×10^9	46.5%	94.6%	91.6%
24h_1	2.52×10^7	7.52×10^9	46.65%	94.6%	91.9%
24h_2	2.06×10^7	6.10×10^9	46.7%	94.8%	91.8%
24h_3	2.59×10^7	7.71×10^9	46.8%	94.5%	91.9%

upregulated DEGs. The number of DEGs further increased to 10,146 in 0h_vs_12h and to 10,718 in 0h_vs_24h, respectively, but now with more downregulated DEGs than upregulated DEGs (Figure 1A). A Venn diagram comparing all the lists of DEGs shows that 806 DEGs are shared by all pairwise comparisons (Figure 1B). These results indicate that the number of DEGs increases with the duration of UV-B radiation treatment.

Functional annotation and enrichment analysis of DEGs

We annotated the function of DEGs in response to UV-B radiation with the COG, GO, KEGG, KOG, NR, Pfam, Swiss-Prot, and eggNOG databases (Table S3). During UV-B treatment, the number of annotated DEGs increased, starting at 2,596 annotated DEGs out of 2,706 after 1 h, and rising to 9,953 annotated DEGs out of 10,718 after 24 h. The number of annotated DEGs also differed by database, with the highest number obtained with the NR database and the lowest with the COG database.

We then undertook a functional classification of DEGs that were annotated in the COG, eggNOG, and KOG databases (Table S4). We observed that DEGs are most enriched in terms related to signal transduction mechanisms, secondary metabolite biosynthesis, transport and catabolism, as well as transcription, especially in the eggNOG and KOG functional annotations. Furthermore, we performed a GO classification of shared annotated DEGs for the three categories biological process, cellular component, and molecular function (Figure S1; Table S5). In the biological process category, cellular processes and metabolic processes were the most enriched; in the cellular components category, cell and cell part were the most enriched; and in the molecular functions category, binding and catalytic activity were the most enriched.

To further elucidate the biological functions of the DEGs, we carried out a KEGG pathway enrichment analysis. We identified 136 KEGG pathways whose encoded proteins are affected during UV-B treatment in blueberry calli (Table S6). Using a *Q*-value < 0.01 as cutoff, we determined that the KEGG pathway circadian rhythm-plant pathway was significantly affected at all time points of UV-B treatment (Figure 2). Similarly, the plant hormone signal transduction pathway was significantly enriched at almost all stages, suggesting that plant hormones are involved in the response to UV-B stress. We also established that many DEGs are involved in the biosynthesis of phenylpropanoid-derived compounds. Among them, genes participating in the isoflavonoid biosynthetic pathway were induced after 1 and 3 h UV-B treatment (Figures 2A, B). Likewise, genes from the phenylpropanoid biosynthetic pathway began to be enriched after 3 h of UV-B treatment (Figures 2B–E), followed by genes from the anthocyanin and flavonoid biosynthetic pathways, starting at 6 h of UV-B treatment (Figures 2C–E). We conclude that genes involved in the biosynthesis of phenylpropanoid-derived compounds exhibit a precise spatial pattern: the expression of isoflavonoid biosynthetic genes is induced first, followed by genes involved in the phenylpropanoid pathway, and finally genes involved in the anthocyanin and flavonoid biosynthetic pathways. In agreement with this result, the top 20 enriched pathways identified when comparing the control samples (0 h) to any sample exposed to UV-B included anthocyanin biosynthesis, phenylpropanoid biosynthesis, and flavonoid biosynthesis (Figure 2F).

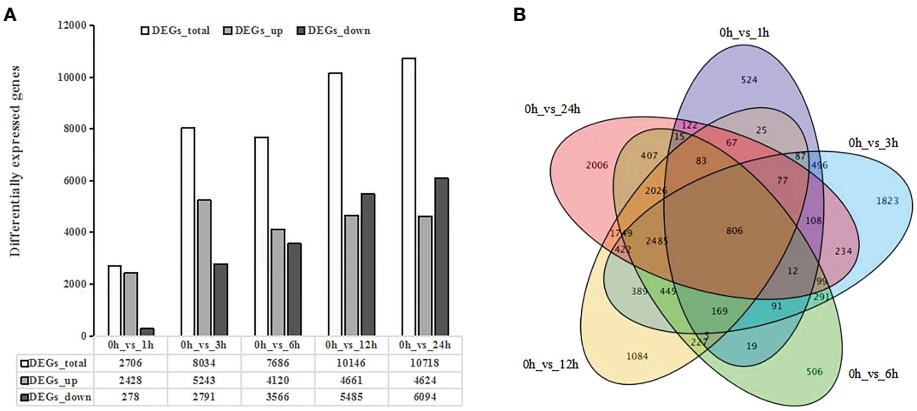

FIGURE 1
Differentially expressed genes (DEGs) in response to UV-B treatment in blueberry revealed by transcriptome deep sequencing (RNA-seq). **(A)** Number of DEGs in response to UV-B. DEGs_up, upregulated DEGs; DEGs_down, downregulated DEGs. **(B)** Venn diagrams showing the extent of overlaps between DEGs across pairwise comparisons. Purple, DEGs for 0 h vs 1 h; blue, DEGs for 0 h vs 3 h; green, DEGs for 0 h vs 6 h; yellow, DEGs for 0 h vs 12 h; and pink, DEGs for 0 h vs 24 h Q-value < 0.01.

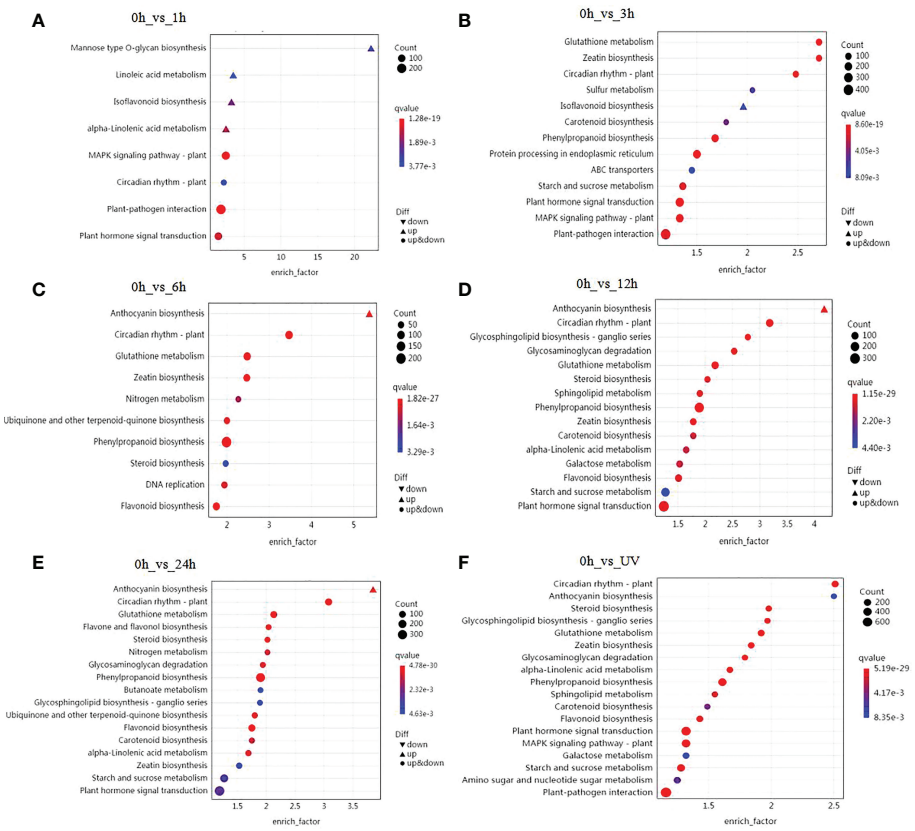

FIGURE 2
Summary of KEGG pathway enrichment analysis. Analysis of significantly enriched DEGs after 1 h **(A)**, 3 h **(B)**, 6 h **(C)**, 12 h **(D)**, or 24 h **(E)** of UV-B radiation compared to 0 h The number of DEGs is indicated by the size of the circle, and the solid upper triangle and inverted triangle represent upregulated and downregulated DEGs, respectively. **(F)** Analysis of significantly enriched DEGs comparing the control samples (0 h) to all samples exposed to UV-B.

UV-B radiation induces flavonoid accumulation

To elucidate the effects of UV-B radiation on the biosynthesis of flavonoid compounds, we measured the flavonoid contents of blueberry calli treated by UV-B radiation for 24 h (Figure 3A). The contents of flavonols, proanthocyanidins, and anthocyanins increased 3.1-, 7.0-, and 2.1-fold, respectively, after 24 h of UV-B irradiation relative to the control samples (Figures 3B–D). Thus, UV-B radiation promotes the accumulation of flavonoid compounds.

The phenylpropanoid and flavonoid biosynthetic KEGG pathways under UV-B radiation

We screened for genes involved in the phenylpropanoid, flavonoid, flavonol, and anthocyanin KEGG pathways among the DEGs. We identified 73 genes encoding 32 types of enzymes, based on Enzyme Commission (EC) annotated data (Table 2). We then plotted the expression levels of these genes as a heatmap. Again, the genes selected here clustered as a function of the duration of UV-B exposure, with the 0, 1, and 3 h treatments forming one group and the 6, 12, and 24 h treatments forming another (Figure S2). Notably, the later induction of these DEGs suggested that the accumulation of phenylpropanoid metabolites mainly occurs after a longer UV-B exposure.

We mapped the 73 DEGs identified above onto the KEGG phenylpropanoid and flavonoid biosynthetic pathways (Figure 4). Among them, only three genes were induced after 1 h of UV-B radiation, and many genes were induced after 3 h. Most of the genes, including *phenylalanine ammonia lyase* (*PAL1*), *PAL3*, *4-coumarate CoA ligase* (*4CL2*), *chalcone synthase synthase* (*CHS*), *chalcone isomerase* (*CHI3*), *VcFLS*, and *VcUFGT*, were induced under UV-B radiation, and their expression reached the highest levels at 24 h (Table 2). Most genes involved in the phenylpropanoid biosynthetic pathway

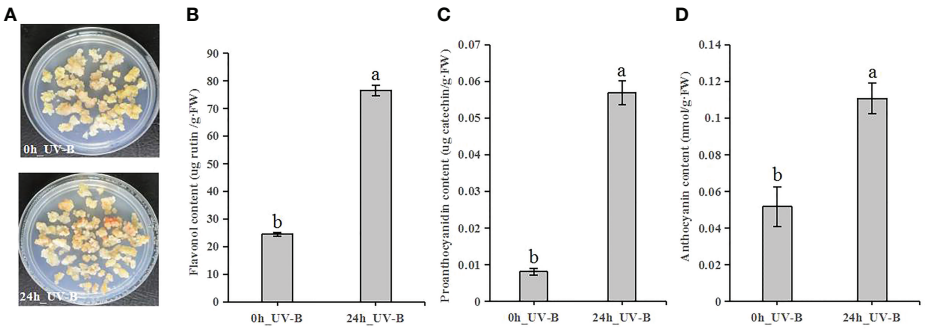

FIGURE 3
UV-B exposure induces flavonoid accumulation in blueberry calli. **(A)** Representative blueberry calli before (0 h) and after (24 h). **(B-D)** Contents of flavonol **(B)**, proanthocyanidin **(C)** and anthocyanin **(D)** after UV-B radiation for 0 h or 24 h Error bars indicate ± SD of the mean of three independent biological replicates. Different letters indicate significant differences ($p < 0.05$) among samples by Tukey's test.

were rapidly upregulated, especially *PAL1* and *4CL2* from 6 h of UV-B radiation treatment onwards. By contrast, *4CL6* was rapidly downregulated from 3 h of UV-B radiation onwards. Most genes involved in the flavonoid biosynthetic pathway were upregulated; *CHS* expression was induced from 3 h of UV-B radiation treatment onwards, reaching a $\log_2$(FC) value of 6.33 at 24 h. The expression of *F3'5'H*, *F3'H*, and *FLS*, which are involved in the flavonol biosynthetic pathway, was upregulated under UV-B radiation. Among genes involved in the anthocyanin biosynthetic pathway, *VcUFGT* expression was induced from 1 h of UV-B exposure onwards, and then rapidly upregulated from 3 h onwards, reaching the highest level at 24 h (7.86 for $\log_2$(FC) value). *VcLAR*, which is involved in the proanthocyanin biosynthesis pathway, was also upregulated from 6 h onwards, reaching a $\log_2$(FC) value of 2.13 at 24 h (Table 2). These results indicate that the expression of most genes involved in phenylpropanoid metabolite biosynthesis is induced under UV-B radiation and that *PAl1*, *4CL2*, *CHS*, *VcFLS*, *VcUFGT*, and *VcLAR* play important roles in UV-B-induced flavonoid accumulation.

Weighted gene co-expression network analysis identifies gene modules associated with flavonoid metabolism under UV radiation

To reveal the regulatory network underlying flavonoid metabolism under UV radiation, we conducted a weighted gene co-expression network analysis (WGCNA) using the DEGs defined above. WGCNA clustered the DEGs into three modules, namely, kMEblue, kMEbrown, and kMEturquoise, which contained 2,174, 783, and 2,171 genes, respectively (Figures 5A, B). KEGG enrichment analysis showed that the kMEblue module comprises many of the genes involved in the phenylpropanoid, flavonoid, and anthocyanin metabolism pathways (Figure S3). We thus characterized the connection between these genes and those associated with plant hormone signal transduction, or encoding transcription factors by looking for their annotations in the KEGG, Swiss-Prot, and NR databases (Table S7). We identified 37 genes fulfilling the above criteria, and their expression levels fell into two groups, as evidenced by a heatmap (Figure 5C). Genes from group I were downregulated, whereas genes from group II were upregulated under UV-B radiation; the latter group included all flavonoid metabolism genes. We also identified ten MYB transcription factor genes in the kMEblue module; these genes belonged to subgroups 4 (*VcMYB4a*), 11 (*MYB102*), 8 (*MYB20*), 5 (*MYBA2.1* and *VcMYBPA*), 2 (*VcMYB14*), 7 (*MYBF*), 6 (*MYBA2* and *VcMYB144*), and 22 (*MYB44*) (Figure S4).

To investigate the functions of these MYB transcription factor genes in the flavonoid pathway, we calculated the Pearson's correlation coefficients (r) between their expression levels and those of genes involved in flavonoid biosynthesis during UV-B radiation (Table 3). We observed that the expression of *MYBA2*, *MYBF*, *MYB102*, *MYBPA1*, *MYBPA2.1*, and *MYB114* is positively correlated with that of most genes involved in the flavonoid pathway. Conversely, the expression levels of *MYB20*, *VcMYB14*, *MYB44*, and *VcMYB4a* were negatively correlated with those of most flavonoid metabolism genes. We also observed a positive correlation between the expression levels of *bHLH74*, *VcMYB20*, and *VcMYB44* and between *bHLH25* and *VcMYB4a*, and a negative correlation between the expression levels of *bHLH74* and *MYB114*, and between the expression levels of *bHLH25* and those of *MYB114*, *MYBA2*, and *MYBF*. The expression of *bHLH74* and *bHLH25* was also negatively correlated with the expression levels of genes involved in flavonoid metabolism.

To elucidate the roles of plant hormones in regulating the flavonoid biosynthesis pathway, we calculated the correlation

TABLE 2 The regulation of DEGs involved in flavonoid biosynthesis under UV-B radiation.

Enzymes	Gene orhomologue name	Gene ID	0h_vs_1h		0h_vs_3h		0h_vs_6h		0h_vs_12		0h_vs_24h	
			log_2 (FC)[a]	regulated[b]	log_2 (FC)	regulated	log_2 (FC)	regulated	log_2 (FC)	regulated	log_2 (FC)	regulated
PAL [EC:4.3.1.24]	*PAL1*	VaccDscaff24-augustus-gene-101.15	-0.69	normal	-0.13	normal	2.04	up	2.28	up	2.87	up
	PAL3	VaccDscaff10-augustus-gene-222.29	-0.49	normal	0.13	normal	1.76	up	1.75	up	1.82	up
C4H [EC:1.14.14.91]	*C4H*	VaccDscaff11-augustus-gene-343.38	0.57	normal	1.16	up	1.03	up	1.34	up	1.31	up
4CL [EC:6.2.1.12]	*4CL2*	VaccDscaff34-processed-gene-57.9	-0.47	normal	0.03	normal	1.72	up	1.72	up	2.06	up
	4CL2-like	VaccDscaff28-augustus-gene-349.38	–[c]	–	–	–	–	–	0.58	normal	1.28	up
	4CL6	VaccDscaff47-augustus-gene-2.17	-0.23	normal	-1.68	down	-1.79	down	-2.25	down	-2.82	down
HCT [EC:2.3.1.133]	*HST*	VaccDscaff17-processed-gene-329.4	1.02	up	1.00	up	0.20	normal	-0.10	normal	0.22	normal
	SHT	VaccDscaff38-augustus-gene-0.16	-0.15	normal	1.00	normal	1.89	up	0.99	normal	0.85	normal
C3'H [EC:1.14.14.96]	*C3'H*	VaccDscaff10-snap-gene-65.38	–	–	–	–	1.22	up	1.18	up	1.55	up
F5H [EC:1.14.-.-]	*F5H*	VaccDscaff123-augustus-gene-2.26	0.62	normal	1.80	up	1.09	normal	1.09	normal	0.85	normal
COMT [EC:2.1.1.68]	*COMT-like*	VaccDscaff19-augustus-gene-150.25	-0.44	normal	-0.63	normal	-0.88	normal	-1.81	down	-2.47	down
	COMT1	VaccDscaff40-augustus-gene-215.28	-0.42	normal	-0.55	normal	-0.39	normal	-1.56	down	-1.51	down
CCoAOMT [EC:2.1.1.104]	*CCoAOMT*	VaccDscaff45-snap-gene-216.26	0.27	normal	0.58	normal	-0.19	normal	-0.86	normal	-1.08	down
CCR [EC:1.2.1.44]	*VcCCR*	VaccDscaff4-processed-gene-398.7	-0.04	normal	-0.18	normal	0.82	normal	0.24	normal	1.13	up
	CCR1-like	VaccDscaff6-augustus-gene-409.27	-0.88	normal	-1.09	normal	0.50	normal	0.82	normal	1.52	up
	CCR	VaccDscaff12-processed-gene-15.8	0.44	normal	1.58	up	1.12	up	1.12	up	0.79	normal
	CCR2-like	VaccDscaff7-processed-gene-8.8	-0.17	normal	-0.84	normal	-0.06	normal	-0.86	normal	-1.04	down
	CCR2	VaccDscaff23-snap-gene-364.44	0.62	normal	2.06	up	1.63	up	1.82	up	1.43	up

(Continued)

TABLE 2 Continued

Enzymes	Gene orhomologue name	Gene ID	0h_vs_1h		0h_vs_3h		0h_vs_6h		0h_vs_12		0h_vs_24h	
			log_2 (FC)[a]	regulated[b]	log_2 (FC)	regulated	log_2 (FC)	regulated	log_2 (FC)	regulated	log_2 (FC)	regulated
	CCR-like	VaccDscaff2-augustus-gene-63.19	-0.41	normal	-0.88	normal	1.12	up	0.88	normal	1.93	up
	CCR1	VaccDscaff3-processed-gene-55.9	-0.16	normal	-0.77	normal	-0.71	normal	-1.04	down	-1.03	down
CAD [EC:1.1.1.195]	*CAD1*	VaccDscaff14-snap-gene-183.27	0.53	normal	2.52	up	2.72	up	2.73	up	2.38	up
	CAD6	VaccDscaff12-snap-gene-1.33	-0.54	normal	-1.52	down	-0.97	normal	-1.66	down	-1.66	down
	CAD9	VaccDscaff13-augustus-gene-6.23	-0.72	normal	0.28	normal	0.62	normal	0.67	normal	1.03	up
CHS [EC:2.3.1.74]	*CHS*	VaccDscaff42-augustus-gene-14.30	-0.90	normal	1.40	up	5.28	up	5.35	up	6.33	up
	CHS1	VaccDscaff3-augustus-gene-334.17	-0.70	normal	-0.74	normal	0.98	normal	1.04	up	1.14	up
CHI [EC:5.5.1.6]	*CHI*	VaccDscaff21-processed-gene-199.1	-0.44	normal	-0.29	normal	1.31	up	1.02	normal	-0.02	normal
	CHI3	VaccDscaff21-augustus-gene-108.29	-0.42	normal	-0.68	normal	1.63	up	2.25	up	2.57	up
DFR [EC:1.1.1.219 1.1.1.234]	*VcDFR*	VaccDscaff13-processed-gene-166.8	-0.79	normal	-0.64	normal	0.70	normal	1.00	up	1.27	up
	DFR	VaccDscaff1613-processed-gene-0.0	0.09	normal	1.02	up	1.19	up	0.61	normal	0.56	normal
F3H [EC:1.14.11.9]	*VcF3H2*	VaccDscaff16-augustus-gene-381.32	-0.71	normal	-0.63	normal	1.80	up	2.03	up	2.74	up
	VcF3H1	VaccDscaff13-augustus-gene-41.36	-0.48	normal	-0.67	normal	0.64	normal	1.16	up	1.33	up
F3'5'H [EC:1.14.14.81]	*F3'5'H2*	VaccDscaff29-augustus-gene-305.28	-0.93	normal	0.03	normal	1.09	up	1.83	up	1.50	up
	VcF3'5'H	VaccDscaff10-augustus-gene-348.25	0.07	normal	-0.96	normal	1.13	up	0.72	normal	2.67	up
F3'H [EC:1.14.14.82]	*F3'H1*	VaccDscaff32-augustus-gene-159.26	-0.46	normal	-0.88	normal	1.24	up	1.57	up	2.03	up
	F3'H	VaccDscaff43-snap-gene-241.31	0.09	normal	-0.41	normal	-1.02	down	-0.98	normal	-0.96	normal
FLS [EC:1.14.20.6]	*FLS1*	VaccDscaff6-augustus-gene-163.26	-0.49	normal	-0.74	normal	-0.25	normal	0.70	normal	1.06	up

(Continued)

TABLE 2 Continued

Enzymes	Gene orhomologue name	Gene ID	0h_vs_1h		0h_vs_3h		0h_vs_6h		0h_vs_12		0h_vs_24h	
			log_2 (FC)[a]	regulated[b]	log_2 (FC)	regulated	log_2 (FC)	regulated	log_2 (FC)	regulated	log_2 (FC)	regulated
	VcFLS	VaccDscaff25-augustus-gene-225.24	–	–	1.29	normal	2.99	up	4.08	up	4.53	up
LDOX [EC:1.14.20.4]	*VcLDOX*	VaccDscaff43-augustus-gene-236.29	-0.41	normal	-0.79	normal	0.24	normal	0.63	normal	1.04	up
	LDOX-like	VaccDscaff33-processed-gene-213.10	0.31	normal	1.52	up	0.46	normal	–	–	-0.50	normal
UFGT [EC:2.4.1.115]	*VcUFGT*	VaccDscaff20-augustus-gene-68.33	1.10	up	4.39	up	6.85	up	7.33	up	7.86	up
UGT75 [EC:2.4.1.298]	*UGT75C1*	VaccDscaff4-processed-gene-124.9	0.44	normal	1.30	up	1.26	up	1.11	up	1.43	up
LAR [EC:1.17.1.3]	*LAR-like*	VaccDscaff35-augustus-gene-247.32	-0.56	normal	-1.52	down	-0.96	normal	-1.73	down	-1.09	down
	VcLAR	VaccDscaff2-augustus-gene-298.20	-0.94	normal	0.55	normal	1.69	up	1.82	up	2.13	up
ANR [EC:1.3.1.77]	*ANR*	VaccDscaff15-augustus-gene-178.21	-0.55	normal	-1.26	down	-0.28	normal	0.20	normal	0.32	normal
	ANR-like	VaccDscaff44-augustus-gene-19.33	0.42	normal	1.24	up	1.09	up	0.81	normal	0.62	normal
F6H [EC:1.14.11.61]	*F6H1-2*	VaccDscaff21-augustus-gene-269.37	-0.07	normal	1.18	up	0.52	normal	0.88	normal	0.47	normal
FGGT1 [EC:2.4.1.239 2.4.1.-]	*GT1*	VaccDscaff38-processed-gene-219.4	–	–	–	–	3.86	up	2.81	up	3.28	up
POD [EC:1.11.1.7]	*PERP7*	VaccDscaff8-processed-gene-129.6	0.87	normal	1.35	up	-0.01	normal	-1.09	down	-2.42	down
	PER15	VaccDscaff44-augustus-gene-228.32	-0.13	normal	-0.74	normal	-1.87	down	-1.36	down	0.66	normal
	PERP7-like	VaccDscaff88-snap-gene-4.29	0.52	normal	1.32	up	-0.55	normal	-0.29	normal	-2.12	down
PS [EC:2.4.1.357]	*UGT88A1-like*	VaccDscaff21-snap-gene-49.64	0.17	normal	-1.82	down	-1.28	down	-1.52	down	-1.05	down
	UGT88B1-like	VaccDscaff21-processed-gene-49.13	-0.85	normal	-1.22	down	-0.41	normal	-0.55	normal	-0.80	normal
SGT [EC:2.4.1.128]	*SGT*	VaccDscaff14-processed-gene-356.18	0.38	normal	2.80	up	2.87	up	3.10	up	1.27	up
UGT29 [EC:2.4.1.236]	*UGT29-like1*	VaccDscaff1-processed-gene-272.1	-0.62	normal	-0.80	normal	-1.10	down	-1.92	down	-2.48	down
	UGT29		0.51	normal	2.28	up	0.95	normal	1.67	up	1.17	up

(Continued)

TABLE 2 Continued

Enzymes	Gene orhomologue name	Gene ID	0h_vs_1h		0h_vs_3h		0h_vs_6h		0h_vs_12		0h_vs_24h	
			log_2 (FC)[a]	regulated[b]	log_2 (FC)	regulated	log_2 (FC)	regulated	log_2 (FC)	regulated	log_2 (FC)	regulated
		VaccDscaff29-augustus-gene-198.28										
	UGT94-like2	VaccDscaff21-processed-gene-210.10	–	–	3.22	up	3.22	up	3.77	up	4.40	up
	UGT94-like3	VaccDscaff28-snap-gene-281.34	-0.10	normal	1.29	up	1.67	up	1.25	up	1.41	up
	UGT94-like4	VaccDscaff28-augustus-gene-280.39	0.39	normal	1.29	up	1.09	up	0.99	normal	1.19	up
UGT73 [EC:2.4.1.-]	*UGT73C6*	VaccDscaff33-processed-gene-116.6	0.25	normal	0.60	normal	1.21	up	1.27	up	1.78	up
ALDH2 [EC:1.2.1.68]	*ALDH2C4*	VaccDscaff69-augustus-gene-3.25	0.32	normal	0.61	normal	-0.53	normal	-0.69	normal	-2.49	down
BGLU [EC:3.2.1.21]	*GH3BG3*	VaccDscaff10-snap-gene-111.37	-0.41	normal	-0.33	normal	-0.49	normal	-1.07	down	-1.07	down
	GH3B	VaccDscaff21-snap-gene-299.24	0.49	normal	0.80	normal	0.40	normal	-0.66	normal	-1.00	down
	GH3BG1	VaccDscaff33-augustus-gene-101.21	0.26	normal	0.79	normal	-0.53	normal	-1.49	down	-1.93	down
	GH3BG5	VaccDscaff15-augustus-gene-315.29	0.57	normal	1.61	up	1.49	up	1.33	up	1.04	up
	BGLU41	VaccDscaff1-snap-gene-432.37	1.14	up	0.60	normal	0.77	normal	0.87	normal	0.72	normal
	BGLU11-like	VaccDscaff46-snap-gene-198.38	0.07	normal	-0.60	normal	-0.17	normal	-0.97	normal	-1.17	down
	BGLU40-like	VaccDscaff35-processed-gene-230.7	0.13	normal	-0.83	normal	-1.09	down	-2.11	down	-1.21	down
	BGLU42	VaccDscaff17-snap-gene-224.18	-0.21	normal	-0.78	normal	-0.90	normal	-1.07	down	-0.87	normal
	BGLU42-like	VaccDscaff27-augustus-gene-205.16	-0.19	normal	-0.56	normal	-0.67	normal	-1.27	down	-0.67	normal
	BGLU44	VaccDscaff27-processed-gene-4.10	0.50	normal	0.61	normal	0.57	normal	0.69	normal	1.80	up
	GH3BG5	VaccDscaff221-processed-gene-1.6	0.55	normal	-0.51	normal	-0.48	normal	-0.28	normal	-1.24	down

(Continued)

TABLE 2 Continued

Enzymes	Gene orhomologue name	Gene ID	0h_vs_1h		0h_vs_3h		0h_vs_6h		0h_vs_12		0h_vs_24h	
			log_2 (FC)[a]	regulated[b]	log_2 (FC)	regulated	log_2 (FC)	regulated	log_2 (FC)	regulated	log_2 (FC)	regulated
CSE [EC:3.1.1.-]	*CSE*	VaccDscaff42-augustus-gene-210.23	0.76	normal	1.01	up	0.11	normal	0.44	normal	0.25	normal
	CSE-like	VaccDscaff27-augustus-gene-309.30	0.51	normal	0.49	normal	1.05	up	0.89	normal	1.15	up

[a]log_2(fold change).
[b]upregulation or downregulation.
[c]No expression.

between *MYB* expression levels and the expression of plant-hormone-related genes (Table 3). In the auxin biosynthetic pathway, the expression levels of *indole-3-acetic acid inducible 14* (*IAA14*) and *auxin-response factor 18* (*ARF18*) were negatively correlated with those of *MYB114* and positively correlated with those of *MYB20* and *MYB44*. In the gibberellic acid biosynthetic pathway, *chitin-inducible gibberellin-responsive protein 1* (*CIGR1*) expression was positively correlated with that of *MYB20* and *MYB44* and negatively correlated with that of *MYB114*. Scarecrow-like transcription factor (*PAT1*) expression was positively correlated with that of *MYB20*, *MYB44*, and *VcMYB14* and negatively correlated with that of *VcMYBPA1*. The expression level of *Ga insensitive dwarf 2* (*GID2*) was positively correlated with those of *CIGR1* and *PAT1*. However, among genes involved in the brassinosteroid biosynthetic pathway, only *brassinosteroid-signaling kinase KINASE 7* (*BSK7*) expression levels appeared to be positively correlated with *MYB20* and *MYB44* expression and negatively correlated with *MYB114* expression (Table 3). Figure 6 summarizes the regulatory network of UV-B-induced flavonoid biosynthetic pathway through hormone signal transduction and transcriptional regulation pathways based on DEGs identified from the WGCNA kMEblue module in this study.

To validate the accuracy and reliability of the RNA-seq data, we selected ten genes of interest involved in flavonoid

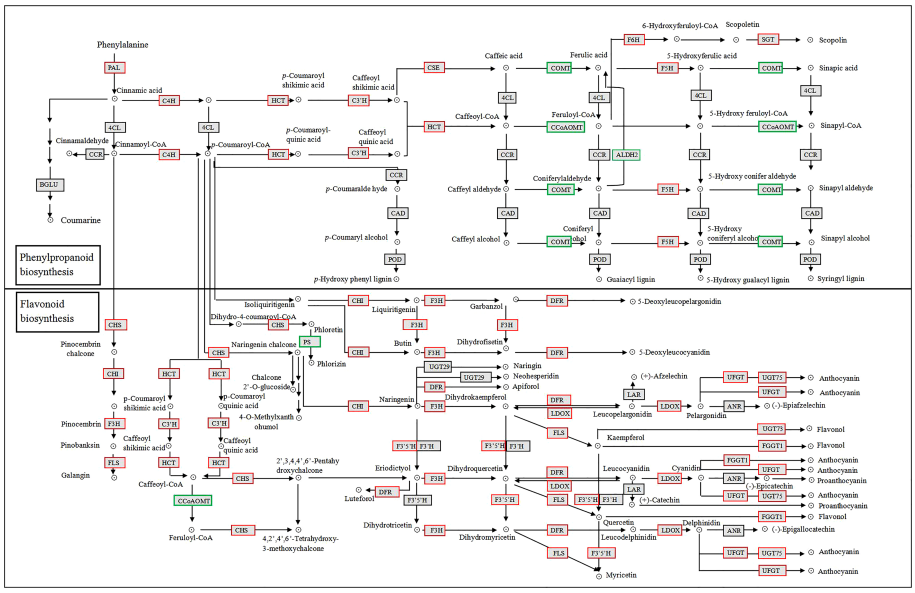

FIGURE 4
Phenylpropanoid and flavonoid KEGG biosynthetic pathways in blueberry calli under UV-B radiation. Red and green boxes represent upregulated and downregulated DEGs, respectively.

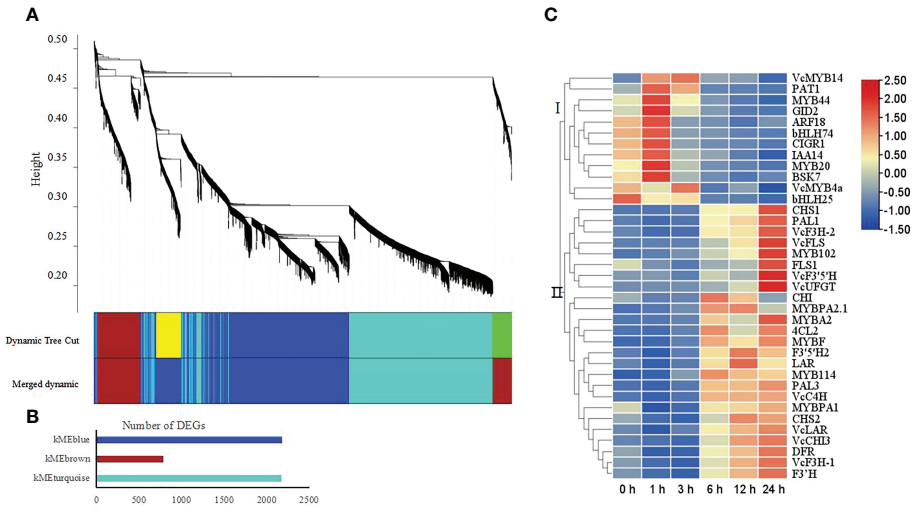

FIGURE 5
Weighted gene co-expression network analysis (WGCNA) of DEGs obtained from all pairwise comparisons. **(A)** Hierarchical clustering tree showing the co-expression modules identified by WGCNA. Different modules are marked with different colors. Each leaf of the cluster tree represents a gene. **(B)** Number of assigned DEGs to the different modules. **(C)** Heatmap representation of hierarchical clustering analysis of identified genes involved in the phenylpropanoid, flavonoid, and anthocyanin metabolic pathways, in the plant hormone signal transduction pathway, and encoding transcription factors in the kMEblue module. Blue, low expression; red, high expression, based on $\log_2$(FPKM).

biosynthesis from the WGCNA kMEblue module for RT-qPCR analysis (Figure S5). A linear regression analysis showed a positive correlation between the RNA-seq and RT-qPCR results, with correlation coefficients (R^2) of 0.8926 (0 h vs 1 h), 0.8338 (0 h vs 3 h), 0.8849 (0 h vs 6 h), 0.8856 (0 h vs 12 h), and 0.8336 (0 h vs 24 h). This observation confirmed that the RNA-seq data in this study are accurate and reliable.

Discussion

UV-B radiation is a major abiotic stress that triggers a variety of plant responses with consequences for plant growth, development, and accumulation of secondary metabolites that involve the actions of many genes (Dotto and Casati, 2017; Gupta et al., 2018; González-Villagra et al., 2020; Ding et al., 2021). For example, transcriptome profiling and DEG analysis have shown that UV-B radiation influences secondary metabolite biosynthesis, plant–pathogen interaction, and plant hormone signal transduction pathways in lettuce (*Lactuca sativa*) (Zhang et al., 2019) and plant hormone signal transduction pathways in horseweed (*Conyza lini*) (Zhan et al., 2021). In our study, functional annotation showed that genes from plant hormone signal transduction pathways and secondary metabolism biosynthetic pathways (including phenylpropanoid, flavonoid, and anthocyanin) were the most enriched among DEGs (Table S4; Figure 2). The timing of DEG appearance is important, as DEGs involved in plant hormone signal transduction pathways were significantly enriched after 1 h of UV-B exposure, followed by genes involved in the phenylpropanoid biosynthetic pathway after 3 h, and by genes involved in the flavonoid and anthocyanin biosynthetic pathways after 6 h of UV-B treatment. These results indicated that phytohormone-related genes may constitute the first response to UV-B radiation.

UV-B radiation affects the phenylpropanoid biosynthetic pathway and influences the accumulation of flavonoid compounds, especially flavonols, proanthocyanidins, and anthocyanins (Berli et al., 2011; Henry-Kirk et al., 2018). In this study, we showed that the flavonol, proanthocyanidin, and anthocyanin contents of blueberry calli significantly increased after 24 h of UV-B radiation, indicating that UV-B radiation promotes the accumulation of flavonoid compounds (Figure 3). In grapevine berries, the expression of *FLS1* and *UFGT* is induced by UV-B, leading to increased flavonol and anthocyanin concentration (González-Villagra et al., 2020). In lettuce, transcriptome analysis showed that the transcriptional upregulation of *C4H*, *4CL*, *CHS*, *FLS*, and *DFR* promoted anthocyanin biosynthesis in response to UV-B radiation (Zhang et al., 2019). Our study demonstrated that the expression of most genes involved in flavonoid biosynthesis was upregulated, especially *PAl1*, *4CL2*, *CHS*, *VcFLS*, *VcUFGT*, and *VcLAR* genes (Figure 4; Table 2). These genes are involved in the biosynthesis of flavonol, proanthocyanidin, or anthocyanin and may be the key genes for UV-B-induced flavonoid biosynthesis.

WGCNA has been widely used to identify gene regulatory networks from different KEGG pathways (Zhu et al., 2019; Li

TABLE 3 Pearson's correlation coefficients (*r*) between the transcription factor genes and DEGs from the phenylpropanoid metabolite pathway DEGs, plant hormone signal transduction pathway in the kMEblue module.

Genes	*PAL1*	*PAL3*	*VcC4H*	*4CL2*	*CHS1*	*CHS2*	*CHI*	*VcCHI3*	*VcF3H-1*	*VcF3H-2*	*F3'H*	*VcF3'5'H*	*F3'5'H*	*FLS1*	*VcFLS*	*DFR*	*VcUFGT*	*VcLAR*	*LAR*	*bHLH74*	*bHLH25*	*IAA14*	*ARF18*	*GID2*	*CIGR1*	*PAT1*	*BSK7*
MYBPA1	0.88*	0.88*	0.89*	0.80	0.83*	0.91*	0.61	0.88*	0.89*	0.92**	0.92*	0.69	0.86*	0.73	0.79	0.96**	0.69	0.92*	0.83*	-0.65	-0.62	-0.76	-0.64	-0.87*	-0.68	-0.99**	-0.75
MYBPA2.1	0.65	0.83*	0.87*	0.71	0.59	0.71	0.91*	0.70	0.63	0.66	0.68	0.22	0.89*	0.08	0.47	0.67	0.26	0.75	0.92**	-0.70	-0.80	-0.68	-0.74	-0.67	-0.70	-0.70	-0.74
MYB114	0.83*	0.95**	0.96**	0.90*	0.80	0.75	0.78	0.81	0.82*	0.77	0.20	0.51	0.92**	0.33	0.69	0.80	0.53	0.88*	0.89*	-0.84*	-0.91*	-0.84*	-0.84*	-0.78	-0.85*	-0.76	-0.85*
MYBA2	0.96**	0.92**	0.88*	0.97**	0.98**	0.75	0.41	0.86*	0.97**	0.87*	0.89*	0.91*	0.77	0.77	0.92*	0.89*	0.88*	0.90*	0.68	-0.70	-0.85*	-0.79	-0.63	-0.70	-0.72	-0.73	-0.68
MYBF	0.95**	0.99**	0.97**	0.98**	0.95**	0.81*	0.62	0.90*	0.95**	0.89*	0.91*	0.76	0.90*	0.61	0.86*	0.91*	0.76	0.95**	0.84*	-0.79	-0.92**	-0.85*	-0.75	-0.77	-0.80	-0.80	-0.79
MYB102	0.97**	0.87*	0.82*	0.84*	0.98**	0.81	0.19	0.91*	0.96**	0.91*	0.92*	0.94**	0.77	0.84*	0.99*	0.90*	0.97**	0.91*	0.68	-0.69	-0.82*	-0.81*	-0.61	-0.68	-0.70	-0.66	-0.65
MYB20	-0.78	-0.83*	-0.82*	-0.75	-0.74	-0.73	-0.56	-0.75	-0.76	-0.75	-0.75	-0.51	-0.84*	-0.47	-0.68	-0.79	-0.57	-0.86*	-0.79	0.96**	0.64	0.97**	0.96**	0.99**	0.97**	0.84*	0.99**
VcMYB14	-0.72	-0.69	-0.70	-0.63	-0.68	-0.81	-0.48	-0.73	-0.75	-0.81*	-0.80	-0.63	-0.67	-0.76	-0.66	-0.85*	-0.60	-0.74	-0.64	0.37	0.37	0.52	0.36	0.71	0.41	0.92**	0.52
MYB44	-0.86*	-0.89*	-0.89*	-0.80	-0.82*	-0.85*	-0.58	-0.85	-0.85*	-0.86*	-0.86*	-0.61	-0.89*	-0.60	-0.77	-0.90*	-0.66	-0.93*	-0.86*	0.88*	0.66	0.94**	0.88*	0.99**	0.90*	0.94**	0.94**
VcMYB4a	-0.88*	-0.89*	-0.88*	-0.89*	-0.89*	-0.78	-0.54	-0.85	-0.89*	-0.85*	-0.87*	-0.77	-0.78	-0.64	-0.82*	-0.85*	-0.73	-0.83*	-0.73	0.45	0.87*	0.56	0.40	0.48	0.47	0.67	0.46
bHLH74	-0.74	-0.80	-0.79	-0.73	-0.71	-0.64	-0.49	-0.70	-0.71	-0.66	-0.67	-0.46	-0.80	-0.34	-0.66	-0.70	-0.55	-0.81*	-0.76	—	—	—	—	—	—	—	—
bHLH25	-0.86*	-0.91*	-0.90*	-0.86*	-0.86*	-0.73	-0.54	-0.84*	-0.85*	-0.79	-0.81*	-0.64	-0.85*	-0.42	-0.80	-0.77	-0.67	-0.85*	-0.81	—	—	—	—	—	—	—	—
IAA14	—	—	—	—	—	—	—	—	—	—	—	—	—	—	—	—	—	—	—	—	—	—	0.95*	—	—	—	—
GID2	—	—	—	—	—	—	—	—	—	—	—	—	—	—	—	—	—	—	—	—	—	—	—	—	0.91*	0.91*	—

*Correlation significant at the 0.05 level. **Correlation significant at the 0.01 level. — Correlation analysis was not conducted.

et al., 2022). The biosynthesis of flavonoid compounds is co-regulated by multiple genes (e.g., *PAL*, *4CL*, *CHI*, and *FLS*) during half-high blueberry fruit development (Yang et al., 2022b). In the current study, we assembled the regulatory network of the phenylpropanoid biosynthesis pathway under UV radiation using WGCNA. The transcriptome analysis showed that 19 genes encoding flavonoid biosynthetic enzymes are co-regulated to promote the accumulation of flavonols, proanthocyanidins, and anthocyanins (Figure 6).

R2R3-MYB transcription factors control the transcriptional regulation of flavonoid structural genes in various horticultural plants including blueberry (Zifkin et al., 2012; Plunkett et al., 2018). In this study, we systematically compared the expression levels of ten MYB transcription factor genes against those of structural genes from the flavonoid biosynthetic pathway. Among the encoded transcription factors, VcMYBPA1 and MYBPA2.1 (subgroup 5), MYB114 and MYBA2 (subgroup 6), and MYBF (subgroup 7) promoted the expression of genes involved in flavonoid biosynthesis. Subgroups 5, 6, and 7 positively regulate anthocyanin, proanthocyanidin, or flavonol biosynthesis (Bogs et al., 2007; Czemmel et al., 2009; Zifkin et al., 2012; An et al., 2015; Plunkett et al., 2018; Karppinen et al., 2021; Zhang et al., 2021). Thus, these MYBs may activate UV-B-induced flavonoid biosynthesis. MYB102 belongs to subgroup 11, which contributes to plant resistance against stress (Denekamp and Smeekens, 2003; Xu et al., 2015). The co-expression analysis showed that *VcMYB102* expression was positively correlated with that of genes involved in flavonoid biosynthesis. VcMYBPA1, MYBPA2.1, MYB114, MYBA2, MYBF, and MYB102 may activate the UV-B-induced flavonoid pathway.

VcMYB4a belongs to subgroup 4 and inhibits lignin biosynthesis (Yang et al., 2022a). In this study, *VcMYB4a* expression was also negatively correlated with that of genes from the flavonoid biosynthetic pathway and *VcMYB4a* likely encodes an inhibitor. Subgroups 22, 8, and 2 play important roles in plant responses to abiotic stresses. For example, AtMYB73 from subgroup 22 negatively regulates responses to salt stress, AtMYB20 from subgroup 8 negatively regulates plant response to drought stress; and AtMYB15 from subgroup 2 decreases tolerance to freezing stress (Agarwal et al., 2006; Kim et al., 2013; Gao et al., 2014). Thus, some MYB transcription factors from these subgroups function as negative regulators of abiotic stresses. Transcriptome analysis showed that the expression of *MYB44* (subgroup 22), *MYB20* (subgroup 8), and *VcMYB14* (subgroup 2) was negatively correlated with the expression of genes involved in flavonoid biosynthesis under UV-B radiation in blueberry calli (Table 3). Furthermore, MYB44, MYB20, and VcMYB14 inhibit the flavonoid pathway in response to UV-B radiation.

Basic helix-loop-helix (bHLH) family members also regulate flavonoid biosynthesis (Matus et al., 2010; Zhu et al., 2020). bHLH proteins directly regulate the expression of structural

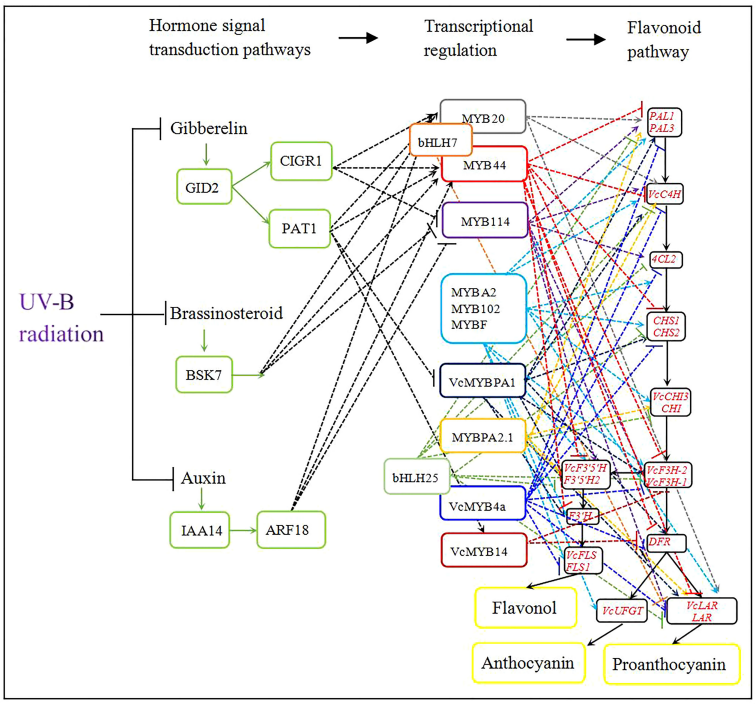

FIGURE 6
Model of the integration of UV-B-induced flavonoid accumulation with plant hormone signal transduction pathways. Black solid lines represent the flavonoid metabolic pathway and colored dashed lines represent regulatory pathways emanating from each transcription factor gene. In particular, green solid lines represent plant hormone signal transduction pathways and black dashed lines indicate MYB transcription factor genes that are regulated by a phytohormone. Arrows indicate activation; short lines indicate inhibition.

genes or interact with MYB proteins to regulate flavonoid accumulation (Hartmann et al., 2005; An et al., 2012). In Arabidopsis, bHLH74 regulates root growth and bHLH25 influences cyst nematode parasitism (Jin et al., 2011; Bao et al., 2014). In this study, the expression of *bHLHL74* homologs was positively correlated with that of *MYB20* and *MYB44*, while the expression of a *bHLH25* homolog was also positively correlated with that of *VcMYB4a* in blueberry calli under UV-B radiation. Importantly, *bHLHL74* and *bHLH25* expression levels were negatively correlated with those of genes involved in flavonoid biosynthesis (Figure 6; Table 3). Thus, the bHLHL74 and bHLH25 transcription factors may negatively regulate flavonoid biosynthesis by repressing the expression of genes involved in the flavonoid biosynthetic pathway or by interacting with MYB proteins under UV-B irradiation.

Plant hormones, including auxin, gibberellins, and brassinosteroids, play important roles in flavonoid biosynthesis (Jeong et al., 2004; Loreti et al., 2008; Peng et al., 2011). In Arabidopsis, gibberellins negatively regulate low temperature- or sucrose-induced anthocyanin accumulation and inhibit flavonol biosynthesis (Loreti et al., 2008; Zhang et al., 2011; Tan et al., 2019). The F-box protein, GID2 (also named SLEEPY1) positively regulates gibberellin signaling by promoting the polyubiquitination of DELLA proteins, subsequently leading to their degradation by the 26S proteasome. (Sasaki et al., 2003; McGinnis et al., 2003). DELLA, PAT1, and CIGR1 all belong to the GRAS family of transcriptional regulators. PAT1 is involved in phytochrome A signal transduction in Arabidopsis, while *OsCIGR1* expression is induced by exogenous gibberellins in rice (*Oryza sativa*) (Bolle et al., 2000; Day et al., 2004). DELLA proteins are repressors of gibberellin signaling. In the absence of GA, DELLA proteins accumulate and interact with MYB proteins to promote flavonol biosynthesis. In the presence of GA, the GA-dependent complex GA-GID1-DELLA promotes DELLA degradation *via* the 26S proteasome and then reduces the transcriptional activity of MYBs to inhibit flavonol biosynthesis (Tan et al., 2019). DELLA proteins also positively regulate nitrogen-deficiency-induced anthocyanin accumulation by directly interacting with PAP1 (Zhang Y. et al., 2017). Our study showed that the expression of *GID2*, *PAT1*, and *CIGR1* is downregulated under UV-B radiation; moreover, correlation analysis showed that *GID2* expression is positively correlated with those of *PAT1* and *CIGR1*, which are themselves positively correlated with the expression of *MYB20* and *MYB44* (Figure 6; Table 3). UV-B results in a decrease in endogenous gibberellin concentration (Roro et al., 2017), such that in the absence of

gibberellin under UV-B exposure, the GA-GID2-PAT1 and GA-GID2-CIGR1 complexes are less abundant and can no longer repress MYB114 and VcMYBPA1 function, leading to the induction of *MYB20*, *MYB44*, and *VcMYB14* expression, and thus to flavonoid accumulation.

The phytohormone auxin inhibits anthocyanin biosynthesis and controls UV-mediated accumulation of flavonoids (Hectors et al., 2012; Ji et al., 2015). In apple, auxin regulates anthocyanin biosynthesis through the Aux/IAA-ARF signaling pathway. MdARF13 interacts with MdIAA121 and directly binds to the promoter of *MdDRF* to inhibit anthocyanin biosynthesis. MdARF13 also interacts with MdMYB10 to repress anthocyanin accumulation by downregulating *MdMYB10* expression (Wang et al., 2018). In Arabidopsis, ARF17 directly binds to the *MYB108* promoter to regulate anther dehiscence (Xu et al., 2019). In this study, *ARF18* and *IAA14* expression were repressed by UV-B radiation; we observed that *ARF18* expression was positively correlated with that of *IAA14*, *MYB20*, and *MYB44* and negatively correlated with that of *MYB114* under UV-B irradiation (Figure 6; Table 3). Thus, it is possible that UV-B radiation reduces endogenous auxin concentrations and diminishes the expression levels of *ARF18* and *IAA*, resulting in higher *MYB114* expression or lower *MYB20* and *MYB44* expression to induce flavonoid biosynthesis.

Brassinosteroids negatively affect plant tolerance of UV-B stress. BRI1-EMS-Suppressor 1 (BES1) acts downstream of brassinosteroid-insensitive 1 (BRI1) to promote UV-B-induced flavonol biosynthesis by binding to the promoters of *MYB11*, *MYB12*, and *MYB111* (Liang et al., 2020). BSK is a critical family of receptor-like cytoplasmic kinases acting in BR signal transduction, of which BSK3, BSK4, BSK7, and BSK8 belong to the same clade and functionally overlap (Tang et al., 2008; Sreeramulu et al., 2013). AtBSK3 interacts with BRI1, the phosphatase BRI1 suppressor 1 (BSU1), and the kinase brassinosteroid-insensitive 2 (BIN2) to regulate the BR signaling pathway; BSK8 interacts with the Kelch-type phosphatase BSL2 to regulate the activity of sucrose-phosphate synthase enzyme (Wu et al., 2014; Ren et al., 2019). However, the function of BSKs in the regulation UV-B-induced flavonoid biosynthesis is unclear. We used the WGCNA method to determine the role of *BSK7*. *BSK7* expression was downregulated and showed a significant association with the expression levels of genes encoding MYB proteins involved in flavonoid biosynthesis under UV-B radiation (Figure 6; Table 3). Therefore, BSK7 may negatively regulate UV-B-induced flavonoid biosynthesis; however, it is unclear whether BSKs regulate flavonoid biosynthesis by regulating MYB transcription factors or other pathways.

Data availability statement

The original contributions presented in the study are publicly available. This data can be found here: NCBI, PRJNA892908.

Author contributions

CZ conceived and designed the project. YS, BM, QG, LZ, CL, XL, JW and XZ participated in the experiments and analyzed the data. YS and BM drafted the manuscript. CZ modified the manuscript. All authors read and approved the final manuscript. All authors contributed to the article and approved the submitted version.

Funding

This study was supported by the National Natural Science Foundation of China (grant number 31700260).

Conflict of interest

The authors declare that the research was conducted in the absence of any commercial or financial relationships that could be construed as a potential conflict of interest.

Publisher's note

Supplementary material

The Supplementary Material for this article can be found online at: https://www.frontiersin.org/articles/10.3389/fpls.2022.1079087/full#supplementary-material

References

Agarwal, M., Hao, Y., Kapoor, A., Dong, C., Fujii, H., Zheng, X., et al. (2006). A R2R3 type MYB transcription factor is involved in the cold regulation of CBF genes and in acquired freezing tolerance. *J. Biol. Chem.* 281, 37636–37645. doi: 10.1074/jbc.M605895200

Aharoni, A., De Vos, C., Wein, M., Sun, Z., Greco, R., and Kroon, A. (2001). The strawberry FaMYB1 transcription factor suppresses anthocyanin and flavonol accumulation in transgenic tobacco. *Plant J.* 28, 319–332. doi: 10.1046/j.1365-313X.2001.01154.x

An, X., Tian, Y., Chen, K., Liu, X., Liu, D., Xie, X., et al. (2015). MdMYB9 and MdMYB11 are involved in the regulation of the JA-induced biosynthesis of anthocyanin and proanthocyanidin in apples. *Plant Cell Physiol.* 56, 650–662. doi: 10.1093/pcp/pcu205

An, X., Tian, Y., Chen, K., Wang, X., and Hao, Y. (2012). The apple WD40 protein MdTTG1 interacts with bHLH but not MYB proteins to regulate anthocyanin accumulation. *J. Plant Physiol.* 169, 710–717. doi: 10.1016/j.jplph.2012.01.015

Apweiler, R., Bairoch, A., Wu, C. H., Barker, W. C., Boeckmann, B., Ferro, S., et al. (2004). UniProt: the universal protein knowledgebase. *Nucleic Acids Res.* 32, D115–D119. doi: 10.1093/nar/gkh131

Ashburner, M., Ball, C. A., Blake, J. A., Botstein, D., Butler, H., Cherry, J. M., et al. (2000). Gene ontology: tool for the unification of biology. *Nat. Genet.* 25, 25–29. doi: 10.1038/75556

Bai, S., Tao, R., Tang, Y., Yin, L., Ma, Y., Ni, J., et al. (2019). BBX16, a b-box protein, positively regulates light-induced anthocyanin accumulation by activating MYB10 in red pear. *Plant Biotechnol. J.* 19, 1985–1997. doi: 10.1111/pbi.13114

Bao, M., Bian, H., Zha, Y., Li, F., Sun, Y., Bai, B., et al. (2014). miR369a-mediated basic helix-loop-helix transcription factor bHLH74 repression acts as a regulator for root growth in arabidopsis seedlings. *Plant Cell Physiol.* 55, 1343–1353. doi: 10.1093/pcp/pcu058

Berli, F. J., Fanzone, M., Piccoli, P., and Bottini, R. (2011). Solar UV-b and ABA are involved in phenol metabolism of vitis vinifera l. increasing biosynthesis of berry skin polyphenols. *J. Agric. Food Chem.* 59, 4874–4884. doi: 10.1021/jf200040z

Bogs, J., Faffé, F. W., Takos, A. M., Walker, A. R., and Robinson, S. P. (2007). The grapevine transcription factor VvMYBPA1 regulates proanthocyanidin synthesis during fruit development. *Plant Physiol.* 143, 1347–1361. doi: 10.1104/pp.106.093203

Bolle, C., Koncz, C., and Chua, N. H. (2000). PAT1, a new member of the GRAS family, is involved in phytochrome a signal transduction. *Gene. Dev.* 14, 1269–1278. doi: 10.1101/gad.14.10.1269

Cavallini, E., Matus, J. T., Finezzo, L., Zenoni, S., Loyola, R., Guzzo, F., et al. (2015). The phenylpropanoid pathway is controlled at different branches by a set of R2R3-MYB C2 repressors in grapevine. *Plant Physiol.* 167, 1448–1470. doi: 10.1104/pp.114.256172

Chen, C., Chen, H., Zhang, Y., Thomas, H. R., Frank, M. H., He, Y., et al. (2020). TBtools: an integrative toolkit developed for interactive analyses of big biological data. *Mol. Plant* 13, 1194–1202. doi: 10.1016/j.molp.2020.06.009

Czemmel, S., Stracke, R., Weissharr, B., Cordon, N., Harris, N. N., Walker, A. R., et al. (2009). The grapevine R2R3-MYB transcription factor VvMYBF1 regulates flavonol synthesis in developing grape berries. *Plant Physiol.* 151, 1513–1530. doi: 10.1104/pp.109.142059

Day, R. B., Tanabe, S., Koshioka, M., Mitsui, T., Itoh, H., Ueguchi-Tanaka, M., et al. (2004). Two rice GRAS family genes responsive to n-acetylchitooligosaccharide elicitor are induced by phytoactive gibberellins: evidence for cross-talk between elicitor and gibberellin signaling in rice cells. *Plant Mol. Biol.* 54, 261–272. doi: 10.1023/B:PLAN.0000028792.72343.ee

Denekamp, M., and Smeekens, S. C. (2003). Integration of wounding and osmotic stress signals determines the expression of the AtMYB102 transcription factor gene. *Plant Physiol.* 132, 1415–1423. doi: 10.1104/pp.102.019273

Deng, Y., Li., J., Wu, S., Zhu, Y., Chen, Y., and Fuchu, H. E. (2006). Integrated nr database in protein annotation system and its localization. *Comput. Eng.* 32, 71–74. doi: 10.1109/INFOCOM.2006.241

Ding, R., Che, X., Shen, Z., and Zhang, Y. (2021). Metabolome and transcriptome profiling provide insights into green apple peel reveals light- and UV-b-responsive pathway in anthocyanins accumulation. *BMC Plant Biol.* 21, 351. doi: 10.1186/s12870-021-03121-3

Dotto, M., and Casati, P. (2017). Developmental reprogramming by UV-b radiation in plants. *Plant Sci.* 264, 96–101. doi: 10.1016/j.plantsci.2017.09.006

Finn, R. D., Bateman, A., Clements, J., Coggill, P., Eberhardt, R. Y., Eddy, S. R., et al. (2014). Pfam: the protein families database. *Nucleic Acids Res.* 42, D222–D230. doi: 10.1093/nar/gkt1223

Gao, S., Zhang, Y. L., Yang, L., Song, J. B., and Yang, Z. M. (2014). AtMYB20 is negatively involved in plant adaptive response to drought stress. *Plant Soil* 376, 433–443. doi: 10.1007/s11104-013-1992-6

González-Villagra, J., Marjorie, R., Alberdi, M., Acevedod, P., Loyolae, R., Tighe-Neira, R., et al. (2020). Solar UV irradiation effects on photosynthetic performance, biochemical markers, and gene expression in highbush blueberry (Vaccinium corymbosum l.) cultivars. *Sci. Hortic.* 259, 108816. doi: 10.1016/j.scienta.2019.108816

Gupta, S., Gupta, V., Singh, V., and Varadwaj, P. K. (2018). Extrapolation of significant genes and transcriptional regulatory networks involved in zea mays in response in UV-b stress. *Genes Genom.* 40, 973–990. doi: 10.1007/s13258-018-0705-1

Hartmann, U., Sagasser, M., Mehrtens, F., Stracke, R., and Weisshaar, B. (2005). Differential combinatorial interactions of cis-acting elements recognized by R2R3-MYB, BZIP, and BHLH facotors control light-responsive and tissue-specific activation of phenylpropanoid biosynthesis genes. *Plant Mol. Biol.* 57, 155–171. doi: 10.1007/s11103-004-6910-0

Hectors, K., Oevelen, S. V., Guisez, Y., Prinsen, E., and Jansen, M. A. K. (2012). The phytohormone auxin is a component of the regulatory system that controls UV-mediated accumulation of flavonoids and UV-induced morphogenesis. *Physiol. Plant.* 145, 594–603. doi: 10.1111/j.1399-3054.2012.01590.x

Heijde, M., and Ulm, R. (2018). UV-B photoreceptor-mediated signalling in plants. *Trends Plant Sci.* 17, 230–237. doi: 10.1016/j.tplants.2012.01.007

Henry-Kirk, R. A., Plunkett, B., Hall, M., McGhie, T., Alla, A. C., Wargent, J. J., et al. (2018). Solar UV light regulates flavonoid metabolism in apple (Malus × domestica). *Plant Cell Enviro.* 41, 675–688. doi: 10.1111/pce.13125

Huerta-Cepas, J., Forslund, K., Coelho, L. P., Szklarczyk, D., Jensen, L. J., Mering, C. V., et al. (2017). Fast genome-wide functional annotation through orthology assignment by eggNOG-mapper. *Mol. Biol. Evol.* 34, 2115–2122. doi: 10.1093/MOLBEV/MSX148

Jeong, S. T., Goto-Yamamoto, N., Kobayashi, S., and Esaka, M. (2004). Effects of plant hormones and shading on the accumulation of anthocyanins and the expression of anthocyanin biosynthetic genes in grape berry skins. *Plant Sci.* 167, 247–252. doi: 10.1016/j.plantsci.2004.03.021

Jin, J., Hewezi, T., and Baum, T. J. (2011). The arabidopsis bHLH25 and bHLH27 transcription factors contribute to susceptibility to the cyst nematode heterodera schachtii. *Plant J.* 65, 319–328. doi: 10.1111/j.1365-313X.2010.04424.x

Ji, X., Zhang, R., Wang, N., Yang, L., and Chen, X. (2015). Transcriptome profiling reveals auxin suppressed anthocyanin biosynthesis in red-fleshed apple callus (Malus sieversii f. niedzwetzkyana). *Plant Cell Tiss. Organ. Cult.* 123, 389–404. doi: 10.1007/s11240-015-0843-y

Kanehisa, M., Goto, S., Kawashima, S., Okuno, Y., and Hattori, M. (2004). The KEGG resource for deciphering the genome. *Nucleic Acids Res.* 32, D277–D280. doi: 10.1093/nar/gkh063

Karppinen, K., Lafferty, D. J., Albert, N. W., Mikkola, N., McGhie, T., Allan, A. C., et al. (2021). MYBA and MYBPA transcription factors co-regulate anthocyanin biosynthesis in blue-coloured berries. *New Phytol.* 232, 1350–1367. doi: 10.1111/nph.17669

Kim, J. H., Nguyen, N. H., Jeong, C. Y., Nguyen, N. T., Hong, S., and Lee, H. (2013). Loss of the R2R3 MYB, AtMyb73, causes hyper-induction of the SOS1 and SOS3 genes in response to high salinity in arabidopsis. *J. Plant Physiol.* 170, 1461–1465. doi: 10.1016/j.jplph.2013.05.011

Koonin, E. V., Fedorova, N. D., Jackson, J. D., Jacobs, A. R., Krylov, D. M., Makarova, K. S., et al. (2004). A comprehensive evolutionary classification of proteins encoded in complete eukaryotic genomes. *Genome Biol.* 5, R7. doi: 10.1186/gb-2004-5-2-r7

Kranz, H. D., Denekamp, M., Greco, R., Jin, H., Leyva, A., Meissner, R. C., et al. (1998). Towards functional characterisation of the members of the R2R3-MYB gene family from arabidopsis thaliana. *Plant J.* 16, 263–276. doi: 10.1046/j.1365-313x.1998.00278.x

Langfelder, P., and Horvath, S. (2008). WGCNA: an r package for weighted correlation network analysis. *BMC Bioinf.* 9, 559. doi: 10.1186/1417-2105-9-559

Liang, T., Shi, C., Peng, Y., Tan, H., Xin, P., Yang, Y., et al. (2020). Brassinosteroid-activated BRI1-MES-SUPPRESSOR 1 inhibits flavonoid biosynthesis and coordinates growth and UV-b stress responses in plants. *Plant Cell* 32, 3224–3239. doi: 10.1105/tpc.20.00048

Li, Z., Zhang, W., Jue, D., Liu, X., Jiang, Y., and Tang, J. (2022). Transcriptome changes induced by botrytis cinerea stress and weighted gene co-expression network analysis (WGCNA) in actinidia chinensis. *Plant Mol. Biol. Rep.* 40, 389–401. doi: 10.1007/s11105-021-01325-3

Loreti, E., Povero, G., Novi, G., Solfanelli, C., Alpi, A., and Perata, P. (2008). Gibberellins, jasmonate and abscisic acid modulate the sucrose-induced expression of anthocyanin biosynthetic genes in arabidopsis. *New Phytol.* 179, 1004–1016. doi: 10.1111/j.1469-8137.2008.02511.x

Mao, X., Cai, T., Olyarchuk, J. G., and Wei, L. (2005). Automated genome annotation and pathway identification using the KEGG orthology (KO) as a controlled vocabulary. *Bioinformatics* 21, 3787–3793. doi: 10.2307/1592215

Martínez-Lüscher, J., Sánchez-Díaz, M., Delrot, S., Aguirreolea, J., Pascual, I., and Gomès, E. (2014). Ultraviolet-b radiation and water deficit interact to alter flavonol and anthocyanin profiles in grapevine berries through transcriptomic regulation. *Plant Cell Physiol.* 55, 1925–1936. doi: 10.1093/pcp/pcu121

Matus, J. T., Poupin, M. J., Cañón, P., Bordeu, E., Alcalde, J. A., and Arce-Johnson, P. (2010). Isolation of WDR and bHLH genes related to flavonoid synthesis in grapevine (Vitis vinifera l.). *Plant Mol. Biol.* 72, 607–620. doi: 10.1007/s11103-010-9597-4

McGinnis, K. M., Thomas, S. G., Soule, J. D., Strader, L. C., Zale, J. M., Sun, T., et al. (2003). The arabidopsis SLEEPY1 gene encodes a putative f-box subunit of an SCF E3 ubiquitin ligase. *Plant Cell* 15, 1120–1130. doi: 10.1105/tpc.010827

Nguyen, C. T. T., Lim, S., Lee, J. G., and Lee, E. J. (2017). VcBBX, VcMYB21, VcR2R3 MYB transcription factors are involved in UV-b induced anthocyanin biosynthesis in the peel of harvested blueberry fruit. *J. Agric. Food Chem.* 65, 2066–2073. doi: 10.1021/acs.jafc.6b05253

Norberto, S., Silva, S., Meireles, M., Faria, A., Pintado, M., and Calhau, C. (2013). Blueberry anthocyanins in health promotion: a metabolic overview. *J. Funct. Foods.* 5, 1518–1528. doi: 10.1016/j.jfff.2013.08.015

Peng, Z., Han, C., Yuan, L., Zhang, K., Huang, H., and Ren, C. (2011). Brassinosteroid enhances jasmonate-induced anthocyanin accumulation in arabidopsis seedlings. *J. Integr. Plant Biol.* 53, 632–640. doi: 10.1111/j.1744-7909.2011.01042.x

Plunkett, B. J., Espley, R. V., Dare, A. P., Warren, B. A. W., Grierson, E. R. P., Cordiner, S., et al. (2018). MYBA from blueberry (Vaccinium section cyanococcus) is a subgroup 6 type R2R3MYB transcription factor that activates anthocyanin production. *Front. Plant Sci.* 9. doi: 10.3389/fpls.2018.01300

Qiu, Z., Wang, H., Li, D., Yu, B., Hui, Q., Yan, S., et al. (2018). Identification of candidate HY5-dependent and -independent regulators of anthocyanin biosynthesis in tomato. *Plant Cell Physiol.* 60, 643–656. doi: 10.1093/pcp/pcy236

Rabino, I., and Mancinelli, A. L. (1986). Light, temperature, and anthocyanin production. *Plant Physiol.* 81, 922–924. doi: 10.2307/4270070

Ren, H., Willige, B., Jaillais, Y., Geng, S., Park, M. Y., Gray, W. M., et al. (2019). BRASSINOSTEROID-SIGNALING KINASE 3, a plasma membrane-associated scaffold protein involved in early brassinosteroid signaling. *PloS Genet.* 15, e1007904. doi: 10.1371/journal.pgen.1007904

Ribera, A. E., Reyes-Díaz, M., Alberdi, M., Zuniga, G. E., and Mora, M. L. (2010). Antioxidant compounds in skin and pulp of fruits change among genotypes and maturity stages in highbush blueberry (Vaccinium corymbosum l.) grown in southern Chile. *J. Soil Sci. Plant Nutr.* 10, 509–536. doi: 10.4067/S0718-95162010000200010

Rizzini, L., Favory, J. J., Cloix, C., Faggionato, D., O'Hara, A., Kaiserli, E., et al. (2011). Perception of UV-B by the Arabidopsis UVR8 protein. *Science* 332, 103–106. doi: 10.1126/science.1200660

Roro, A. G., Dukker, S. A. F., Melby, T. I., Solhaug, K. A., Torre, S., and Olesn, J. E. (2017). UV-B-induced inhibition of stem elongation and leaf expansion in pea depends on modulation of gibberellin metabolism and intact gibberellin signalling. *J. Plant Growth Regul.* 36, 680–690. doi: 10.1007/s00344-017-9671-0

Sasaki, A., Itoh, H., Gomi, K., Ueguchi-Tanaka, M., Ishiyama, K., Jeong, D., et al. (2003). Accumulation of phosphorylated repressor for gibberellin signaling in an f-box mutant. *Science* 299, 1896–1898. doi: 10.1126/science.1081077

Sreeramulu, S., Mostizky, Y., Sunitha, S., Shani, E., Nahum, H., Salomon, D., et al. (2013). BSKs are partially redundant positive regulators of brassinosteroid signaling in arabidopsis. *Plant J.* 74, 905–919. doi: 10.1111/tpj.12175

Tang, W., Kim, T. W., Oses-Prieto, J. A., Sun, Y., Deng, Z., Zhu, S., et al. (2008). BSKs mediate signal transduction from the receptor kinase BRI1 in arabidopsis. *Science* 321, 557–560. doi: 10.1126/science.1156973

Tan, H., Man, C., Xie, Y., Yan, J., Chun, J., and Huang, J. (2019). A crucial role of GA-regulated flavonol biosynthesis in root growth of arabidopsis. *Mol. Plant* 12, 521–537. doi: 10.1016/j.molp.2018.12.021

Tatusov, R. L., Galperin, M. Y., Natale, D. A., and Koonin, E. V. (2000). The COG database: a tool for genome-scale analysis of protein functions and evolution. *Nucleic Acids Res.* 28, 33–36. doi: 10.1093/nar/28.1.33

Wang, Y. C., Wang, N., Xu, H. F., Jiang, S. H., Fang, H. C., Su, M. Y., et al. (2018). Auxin regulated anthocyanin biosynthesis throuth the Aux/IAA-ARF signaling pathway in apple. *Hortic. Res.* 5, 59. doi: 10.1038/s41438-018-0068-4

Wang, N., Xu, H., Jiang, S., Zhang, Z., Lu, N., Qiu, H., et al. (2017). MYB12 and MYB22 play essential roles in proanthocyanidin and flavonol synthesis in red-fleshed apple (Malus sieversii f. niedzwetzkyana). *Plant J.* 90, 276–292. doi: 10.1111/tpj.13489

Wu, X. N., Sklodowski, K., Encke, B., and Schulze, W. X. (2014). A kinase-phosphatase signaling module with BSK8 and BSL2 involved in regulation of sucrose-phosphate synthase. *J. Proteome Res.* 13, 3397–3409. doi: 10.1021/pr5003164

Xie, R., Zheng, L., He, S., Zheng, Y., Yi, S., and Deng, L. (2011). Anthocyanin biosynthesis in fruit tree crops: Genes and their regulation. *Afr. J. Biotechnol.* 10, 19890–19897. doi: 10.5897/AJBX11.028

Xu, X., Wang, B., Feng, Y., Xue, J., Qian, X., Liu, S., et al. (2019). AUXIN RESPONSE FACTOR17 directly regulates MYB108 for anther dehiscence. *Plant Physiol.* 181, 645–655. doi: 10.1104/pp.19.00576

Xu, R., Wang, Y., Zheng, H., Lu, W., Wu, C., Huang, J., et al. (2015). Salt-induced transcription factor MYB74 is regulated by the RNA-directed DNA methylation pathway in arabidopsis. *J. Exp. Bot.* 66, 5997–6008. doi: 10.1093/jxb/erv312

Yang, B., Li, Y., Song, Y., Wang, X., Guo, Q., Zhou, L., et al. (2022a). The R2R3-MYB transcription factor VcMYB4 inhibits lignin biosynthesis in blueberry (Vaccinium corymbosum). *Tree Genet. Genomes* 18, 27. doi: 10.1007/s11295-022-01560-z

Yang, B., Song, Y., Li, Y., Wang, X., Guo, Q., Zhou, L., et al. (2022b). Key genes for phenylpropanoid metabolite biosynthesis during half-highbush blueberry (Vaccinium angustifolium × vaccinium corymbosum) fruit development. *J. Berry. Res.* 12, 297–311. doi: 10.3233/JBR-211554

Yu, Z., Duan, X., Luo, L., Dai, S., Ding, Z., and Xia, G. (2020). How plant hormones mediate salt stress responses. *Trends Plant Sci.* 25, 1117–1130. doi: 10.1016/j.tplants.2020.06.008

Zhang, L., Gong, F., Song, Y., Liu, K., and Wan, Y. (2019). *De novo* transcriptome analysis of lettuce (Lactuca sativa l.) and the identification of structural genes involved in anthocyanin biosynthesis in response to UV-b radiation. *Acta Physiol. Plant* 41, 148. doi: 10.1007/s11738-019-2941-7

Zhang, C., Guo, Q., Liu, Y., Liu, H., Wang, F., and Jia, C. (2017). Molecular cloning and functional analysis of a flavanone 3-hydroxylase gene from blueberry. *J. Hortic. Sci. Biotech.* 92, 57–64. doi: 10.1080/14620316.2016.1224604

Zhang, C., Liu, H., Jia, C., Liu, Y., Wang, F., and Wang, J. (2016). Cloning, characterization and functional analysis of a flavonol synthase from vaccinium corymbosum. *Trees* 30, 1595–1605. doi: 10.1007/s00468-016-1393-6

Zhang, Y., Liu, Z., Liu, R., Hao, H., and Bi, Y. (2011). Gibberellins negatively regulate low temperature-induced anthocyanin accumulation in a HY5/HYH-dependent manner. *Plant Signal. Behav.* 6, 632–634. doi: 10.4161/psb.6.5.14343

Zhang, Y., Liu, Z., Liu, J., Lin, S., Wang, J., Lin, W., et al. (2017). GA-DELLA pathway is involved in regulation of nitrogen deficiency-induced anthocyanin accumulation. *Plant Cell Rep.* 36, 557–569. doi: 10.1007/s00299-017-2102-7

Zhang, Y., Wang, K., Albert, N. W., Elborough, C., Espley, R. V., Andre, C. M., et al. (2021). Identification of a strong anthocyanin activator, VbMYBA, from berries of vaccinium bracteatum thunb. *Front. Plant Sci.* 12. doi: 10.3389/fpls.2021.697212

Zhan, J., Yang, Q., Lin, Z., Zheng, T., Wang, M., Sun, W., et al. (2021). Enhanced antioxidant capacity and upregulated transporter genes contribute to the UV-b-induced increase in blinin in conyza blinii. *Environ. Sci. Pollut. R.* 28, 13275–13287. doi: 10.1007/s11356-020-11502-8

Zhu, J., Xia, D., Xu, J., Guo, D., Li, H., Wang, Y., et al. (2020). Idenfification of the bHLH gene family in dracaena cambodiana reveals candidate genes involved in flavonoid biosynthesis. *Ind. Crop Prod.* 150, 112407. doi: 10.1016/j.indcrop.2020.112407

Zhu, Q., Xu, Y., Yang, Y., Guang, C., Zhang, Q., Huang, J., et al. (2019). The persimmon (Diospyro oleifera Cheng) genome provides new insights into the inheritance of astringency and ancestral evolution. *Hortic. Res.* 6, 138. doi: 10.1038/s41438-019-0227-2

Zifkin, M., Jin, A., Ozga, J. A., Zaharia, L. I., Schernthaner, J. P., Gesell, A., et al. (2012). Gene expression and metabolite profiling of developing highbush blueberry fruit indicates transcriptional regulation of flavonoid metabolis and activation of abscisic acid metabolism. *Plant Physiol.* 158, 200–224. doi: 10.1104/pp.111.180950

frontiers | Frontiers in Plant Science

TYPE Original Research
PUBLISHED 24 November 2022
DOI 10.3389/fpls.2022.1066765

OPEN ACCESS

EDITED BY
Tuanhui Bai,
Henan Agricultural University, China

REVIEWED BY
Changhai Liu,
Northwest A&F University, China
Qinglong Dong,
Agricultural University of Hebei, China

*CORRESPONDENCE
Caihong Wang
chw6068@126.com

†These authors have contributed equally to this work

SPECIALTY SECTION
This article was submitted to Plant Abiotic Stress, a section of the journal Frontiers in Plant Science

RECEIVED 11 October 2022
ACCEPTED 07 November 2022
PUBLISHED 24 November 2022

CITATION
Ma C, Wang M, Zhao M, Yu M, Zheng X, Tian Y, Sun Z, Liu X and Wang C (2022) The Δ1-pyrroline-5-carboxylate synthetase family performs diverse physiological functions in stress responses in pear (*Pyrus betulifolia*). *Front. Plant Sci.* 13:1066765. doi: 10.3389/fpls.2022.1066765

The Δ1-pyrroline-5-carboxylate synthetase family performs diverse physiological functions in stress responses in pear (*Pyrus betulifolia*)

Changqing Ma[1,2†], Mengqi Wang[1,2†], Mingrui Zhao[1,2], Mengyuan Yu[1,2], Xiaodong Zheng[1,2], Yike Tian[1,2], Zhijuan Sun[3], Xiaoli Liu[1,2] and Caihong Wang[1,2*]

[1]College of Horticulture, Qingdao Agricultural University, Qingdao, China, [2]Qingdao Key Laboratory of Genetic Improvement and Breeding in Horticulture Plants, Qingdao, China, [3]College of Life Science, Qingdao Agricultural University, Qingdao, China

Δ1-Pyrroline-5-carboxylate synthetase (P5CS) acts as the rate-limiting enzyme in the biosynthesis of proline in plants. Although P5CS plays an essential role in plant responses to environmental stresses, its biological functions remain largely unclear in pear (*Pyrus betulifolia*). In the present study, 11 putative pear *P5CSs* (*PbP5CSs*) were identified by comprehensive bioinformatics analysis and classified into five subfamilies. Segmental and tandem duplications contributed to the expansion and evolution of the *PbP5CS* gene family. Various cis-acting elements associated with plant development, hormone responses, and/or stress responses were identified in the promoters of *PbP5CS* genes. To investigate the regulatory roles of *PbP5CS* genes in response to abiotic and biotic stresses, gene expression patterns in publicly available data were explored. The tissue-specific expressional dynamics of *PbP5CS* genes indicate potentially important roles in pear growth and development. Their spatiotemporal expression patterns suggest key functions in multiple environmental stress responses. Transcriptome and real-time quantitative PCR analyses revealed that most *PbP5CS* genes exhibited distinct expression patterns in response to drought, waterlogging, salinity-alkalinity, heat, cold, and infection by *Alternaria alternate* and *Gymnosporangium haraeanum*. The results provide insight into the versatile functions of the *PbP5CS* gene family in stress responses. The findings may assist further exploration of the physiological functions of *PbP5CS* genes for the development and enhancement of stress tolerance in pear and other fruits.

KEYWORDS

P5CS, *Pyrus betulifolia*, transcriptome, stress response, biotic stress

Introduction

It is well known that abiotic stresses impose severe restrictions on plant growth. These environmental constraints restrict cultivation sites, and diminish agricultural productivity worldwide (Zhu, 2001). To cope with different stresses, plants have evolved multiple mechanisms from physiological, morphological, and molecular perspectives (Tan et al., 2013). Proline plays an essential role in plant growth, development, and stress responses (Anton et al., 2020). It is a compatible solute and a scavenger of reactive oxygen species that provides protection against oxidative damage in plants (Szabados and Savouré, 2010). Free proline is rapidly accumulated in plant cells for adaptation to drought, cold and salinity (Hayat et al., 2012).

Proline biosynthesis involves evolutionarily conserved metabolic pathways in bacteria and higher organisms (Rai and Penna, 2013). Proline biosynthesis uses ornithine or glutamic acid as the substrate, with glutamic acid being preferred under stress conditions (Delauney and Verma, 1993). Δ1-Pyrroline-5-carboxylate synthetase (P5CS) is a key enzyme in the biosynthesis of proline in plants, and it regulates proline content by catalyzing the rate-limiting step in the glutamate pathway (Chen et al., 2013). An increase in P5CS activity can stimulate accumulation of proline to improve osmotic adjustment in plants under environmental stresses (Guan et al., 2014; Anton et al., 2020). P5CS can control proline biosynthesis by transcriptional regulation (Yoshiba et al., 1995). There are two isoforms of P5CS in *Arabidopsis thaliana*, P5CS1 and P5CS2 (Turchetto-Zolet et al., 2009; Funck et al., 2020). Both P5CS isoforms are mainly present in the cytosol, but may be localized in plastids under stress conditions (Székely et al., 2008). However, other P5CS homologues should exist in the plant genome, some of which may be highly stress-induced and essential for proline accumulation.

Since P5CS plays a crucial role in proline biosynthesis, many attempts have been made to enhance proline accumulation by manipulating the *P5CS* gene in order to improve plant stress tolerance. Studies have shown that an increase in P5CS enzyme can induce the accumulation of proline in plants, favoring osmotic adjustment under environmental stresses (Peng et al., 1996; Anton et al., 2020). Over-expression of *P5CS* increased proline content and oxidative stress tolerance in several plants, such as rice (*Oryza sativa*), *A. thaliana*, switchgrass (*Panicum virgatum*), and *Stipa purpurea* under salt and drought stresses (Kumar et al., 2010; Chen et al., 2013; Guan et al., 2020; Yang D. et al., 2021). Moreover, in oriental hybrid lily (*Lilium* spp.), *LhSorP5CS* expression was up-regulated by mannitol and abscisic acid treatments, accompanied by increased proline accumulation (Wang et al., 2017). In addition to abiotic stress, biotic stress also leads to alterations in proline metabolism. For example, *P5CS2* expression was up-regulated in response to infection by *Pseudomonas syringae* in *A. thaliana* (Fabro et al., 2004).

Pear (*Pyrus* spp.) fruits have high nutritional value and are popular among consumers. Pears are reproduced primarily through grafting, with *Pyrus betulifolia* as one of the major rootstocks used in China. Although *P5CS* genes have been identified in *Eugenia uniflora*, *S. purpurea*, rice, and lily (Kumar et al., 2010; Wang et al., 2017; Anton et al., 2020; Yang D. et al., 2021), no comprehensive study of the pear *P5CS* (*PbP5CS*) gene family has been reported. Following the release of the pear genome (Dong et al., 2020), we can now systematically analyze the putative functions of *PbP5CS* genes. In the present study, 11 members of the *PbP5CS* gene family were identified. The *PbP5CS* genes were characterized in terms of gene structures and phylogenetic relationships. Their tissue expression profiles and the expression patterns under different stress conditions were analyzed. The results of *PbP5CS* gene analysis provide insight into the functional role of this gene family in pear.

Materials and methods

Identification of *P5CS* genes in the pear genome

Amino acid sequences of the model plant *A. thaliana* P5CS were obtained from the *Arabidopsis* Information Resource database (https://www.arabidopsis.org/). Using these sequences as queries, the pear genome database was screened by BLASTp (E-value <$1e^{-5}$). The complete genome assembly of pear (*Pyrus betulifolia* Bunge.) and the complete proteome sequence file were obtained from the Genome Database for Rosaceae (https://www.rosaceae.org/). Putative *P5CS* genes were confirmed by BLASTp searches of the National Center for Biotechnology Information database (https://www.ncbi.nlm.nih.gov/). Other information obtained from this database included chromosome number, gene accession numbers, predicted masses of proteins encoded by *P5CS* genes, and genomic information. The isoelectric point, grand average of hydropathicity (GRAVY), and molecular weight of P5CS proteins were calculated *via* the ExPasy website (Duvaud et al., 2021). Subcellular locations of pear P5CS proteins were predicted using WoLF PSORT II (Horton et al., 2007).

Construction of P5CS phylogenetic trees

P5CS amino acid sequences from apple (*Malus domestica*), peach (*Prunus persica*), poplar (*Populus trichocarpa*), and *A. thaliana* were downloaded from Ensembl (https://plants.ensembl.org/index.html). ClustalW v1.83 (Hung et al., 2015) was used for multiple sequence alignments of P5CS proteins.

The Muscle module within MEGA 7.0 (Kumar et al., 2016) was used to align the sequences of full-length proteins. Construction of phylogenetic trees based on PbP5CS protein sequences was performed using the neighbor-joining approach with Poisson model, pairwise deletion, and 1000 bootstrap replicates.

Analysis of conserved motifs, conserved domains, and gene structure

Conserved motifs of all P5CS proteins were identified using the online MEME analysis tool (Bailey et al., 2015) with the maximum number of motifs set at 10, and default values for all other parameters. The NCBI CDD database (https://www.ncbi.nlm.nih.gov/Structure/bwrpsb/bwrpsb.cgi/) was used to analyze the conserved domains of 11 PbP5CS protein sequences, and *P5CS* genes' domain information data were retained. The information of exon (coding sequence), intron, and untranslated region for 11 *PbP5CS* genes was determined according to the alignments of their sequences in the *P. betulifolia* genome database (https://www.rosaceae.org/species/pyrus_betulifolia/genome_v1.0/). To compare conserved motifs, conserved domains, and gene structures of different groups, TBtools software (Chen et al., 2020) was used for clustering, drawing phylogenetic trees, and mapping conserved motifs of PbP5CS. Exon-intron structures were visualized using Gene Structure Display Server 2.0 (Hu et al., 2014).

Chromosomal localization and duplication analysis

The chromosomal localization of each *PbP5CS* gene was determined based on physical location information obtained from the pear genome database (https://www.rosaceae.org/species/pyrus_betulifolia/genome_v1.0/). Then, a gene localization and distribution map was drawn using TBtools. Pear genome proteins data were self-compared by BLASTp, and fragment replication type and tandem repeat replication type of *PbP5CSs* were analyzed by MCScanX (Wang et al., 2012). Tandem duplicated genes were identified by analyzing physical locations on specific chromosomes. MCScanX was used to assess syntenic blocks for *PbP5CS* genes, as well as those between pear and *A. thaliana*, between pear and apple, between pear and peach, and between pear and poplar

Cis-element analysis of *PbP5CS* gene promoters

The promoter sequences of 2000 bp regions upstream of each *PbP5CS* gene-coding region were retrieved from the pear genome database. PlantCARE (Lescot et al., 2002) was then used to annotate elements, and elements related to hormones, stress, growth, and development were selected for location distribution mapping.

Expression profiles of *PbP5CSs* in various tissues

Expression patterns of *PbP5CS* genes in various tissues were acquired from RNA sequencing (RNA-seq) data available in the NCBI database (https://www.ncbi.nlm.nih.gov/sra/?term=SRP230672/; SRA accession no.: SRP230672). Fragments per kilobase of exon per million mapped reads (FPKM) values were used to estimate gene expression levels. Multi Experiment Viewer (Saeed et al., 2006) was used to evaluate and graphically characterize means of expression values for each gene in all tissues. A heatmap of *PbP5CS* genes was generated using the OmicShare Tool (https://www.omicshare.com/tools/).

Plant growth conditions and different stress treatments

Pear seeds after vernalization were sown in nutritive soil (65% fertile garden soil, 25% burning soil, 10% fine sand, 0.4% calcium-magnesium-phosphate fertilizer). All materials were kept in a plant incubator. When seedlings grew to the five-leaf stage, they were transplanted into wet vermiculite in pots (7 cm × 7 cm × 10 cm) and kept in an artificial climate room. Pear seedlings received Hoagland solution every 3 days and were grown at 23 ± 2°C with a light intensity of 800 μmol m^{-2}·s^{-1}. Two-month-old seedlings were used to measure mRNA expression levels of *PbP5CSs* under biotic and abiotic stress conditions. Drought stress of potted pear plants was inflicted by withholding water for 20 days (Yang S. et al., 2021); waterlogging stress was inflicted by submerging plants in water (Yu et al., 2019); salinity-alkalinity stress was performed at a ratio of 1:1.4 NaCl and $NaHCO_3$ (Zhang et al., 2020); cold stress was simulated at 4°C (Xi et al., 2011); heat stress was simulated at 40°C (Liu et al., 2013). Pear rust was applied by infecting leaves with *Gymnosporangium haraeanum* Syd. (Li et al., 2006). Pear leaves were taken at 0, 1, 3, and 6 days after abiotic stresses, and at 0, 6, 12, and 24 hours after biotic stress. The samples (with three independent biological replications) were immediately frozen in liquid nitrogen and stored at -80°C until analysis. To explore the gene expression profiles of *PbP5CSs* in response to salt, cold, drought, and *Alternaria alternate* infection, pear RNA-seq datasets were retrieved from published supplemental datasets (SRA accession nos.: SRP077703, SRP287704, SRP148620, and SRP276846).

Measurements of P5CS enzyme activities

P5CS enzyme activities were measured using a commercial kit (Suzhou Geruisi Biotechnology, Suzhou, China) following the

manufacturer's instructions. Each experiment was independently repeated three times.

Real-time quantitative PCR analysis

Total RNA extraction from leaf samples was performed using the method of Ma et al. (2022). First-strand cDNA was prepared using PrimeScript RTase (TaKaRa Biotechnology, Dalian, China). Primers for qPCR were designed using Primer Premier 5.0 (Premier Biosoft International, Silicon Valley, CA, USA). Primer sequences are detailed in Supplementary Table S1. A LightCycler R 480 SYBR Green Master (Roche, Mannheim, Germany) was used for qPCR assays with a LightCycler R 480 II system (Roche, Rotkreuz, Switzerland). Relative expression levels of the target genes were calculated using the $2^{-\Delta\Delta CT}$ method (Livak and Schmittgen, 2001) and normalized against the *Actin* gene (GenBank: AB190176).

Results

Identification of *P5CS* genes in pear

Based on the conserved domains of protein sequences, 11 P5CS protein sequences were screened and named PbP5CS1 –PbP5CS11 according to their chromosomal sequences and positions. Detailed physical and chemical characterizations of PbP5CS proteins are listed in Table 1. The 11 PbP5CS proteins have different numbers of amino acids; PbP5CS7 is the shortest (276 amino acids), while PbP5CS4 is the longest (755 amino acids). The molecular weight of PbP5CSs ranged from 31.16 kDa (PbP5CS7) to 82.67 kDa (PbP5CS4). The isoelectric point values of PbP5CS proteins ranged from 6.06 (PbP5CS9) to 8.95 (PbP5CS2). Except for PbP5CS9 and PbP5CS11, the GRAVY values of other PbP5CSs were less than zero. The predicted subcellular localizations were cytoplasm for PbP5CS2, PbP5CS5, and PbP5CS9, endoplasmic reticulum for PbP5CS1 and PbP5CS4, chloroplast for PbP5CS3 and PbP5CS11, and nucleus for the other PbP5CSs.

Phylogenetic relationships of PbP5CS members

To explore the evolutionary relationships of PbP5CS members, a phylogenetic tree was built using 50 conserved domain sequences of P5CS proteins from pear (11), apple (8), peach (14), poplar (13), and *A. thaliana* (4; Figure 1). In the tree, PbP5CS, MdP5CS, PpP5CS, PtP5CS, and AtP5CS were classified into five groups (Groups I, II, III, IV, and V). Notably, *P5CS* genes of woody plants (pear, apple, peach, and poplar) clustered together. Most of the pear P5CSs also clustered together with proteins from *A. thaliana*, consistent with the closer relationship of pear to eudicots. The distribution of pear P5CSs was uneven in these groups. Group I was the largest with 24 members, including nearly half of all pear P5CSs (PbP5CS1, PbP5CS3, PbP5CS4, PbP5CS5, and PbP5CS8). PbP5CS9 and PbP5CS11 were in both Groups II and IV, PbP5CS6 and PbP5CS7 were in Group III, and PbP5CS2 and PbP5CS10 were in Group V.

Conserved protein motifs and exon-intron structures of *PbP5CS* genes

A total of 10 conserved motifs were predicted in PbP5CSs (Figure 2B; Supplementary Table S2), ranging from 21 to 100 amino acids in length. Interestingly, we observed that Motifs 1, 2,

TABLE 1 General information on *Pyrus betulifolia P5CS* genes.

Gene Name	Gene ID Number[1]	Chr	Start Site	Termination Site	Length (aa)	MW (Da)	PI	GRAVY	Subcellular Localization[2]
PbP5CS1	GWHGAAYT001370	1	12601277	12607167	717	77547.02	6.61	-0.052	Endoplasmic reticulum lumen
PbP5CS2	GWHGAAYT033428	2	20298570	20301019	338	35870.92	8.95	-0.093	Cytoplasmic
PbP5CS3	GWHGAAYT039316	4	20355850	20361403	727	78451.63	6.11	-0.085	Chloroplast
PbP5CS4	GWHGAAYT049560	7	21713305	21719297	755	82665.04	6.74	-0.095	Endoplasmic reticulum lumen
PbP5CS5	GWHGAAYT011709	12	19348694	19354150	733	79442.93	6.26	-0.051	Cytoplasmic
PbP5CS6	GWHGAAYT011728	12	19492870	19502013	450	50284.14	6.72	-0.356	Nuclear
PbP5CS7	GWHGAAYT011735	12	19539554	19546307	276	31162.25	6.62	-0.496	Nuclear
PbP5CS8	GWHGAAYT011744	12	19602037	19605102	280	31803.65	8.82	-0.329	Nuclear
PbP5CS9	GWHGAAYT013594	13	3796252	3799633	338	35712.85	6.06	0.095	Cytoplasmic
PbP5CS10	GWHGAAYT017700	14	11096882	11101455	521	56854.74	6.57	-0.493	Nuclear
PbP5CS11	GWHGAAYT022995	15	28622901	28626996	335	35632.72	8.83	0.001	Chloroplast

[1]From Pyrus betulifolia Genome Sequence Consortium database. [2]Predicted using WoLFPSORT (https://www.genscript.com/psort/wolf_psort.).
MW, molecular weight; pI, theoretical isoelectric point; GRAVY, Grand Average of Hydropathicity.

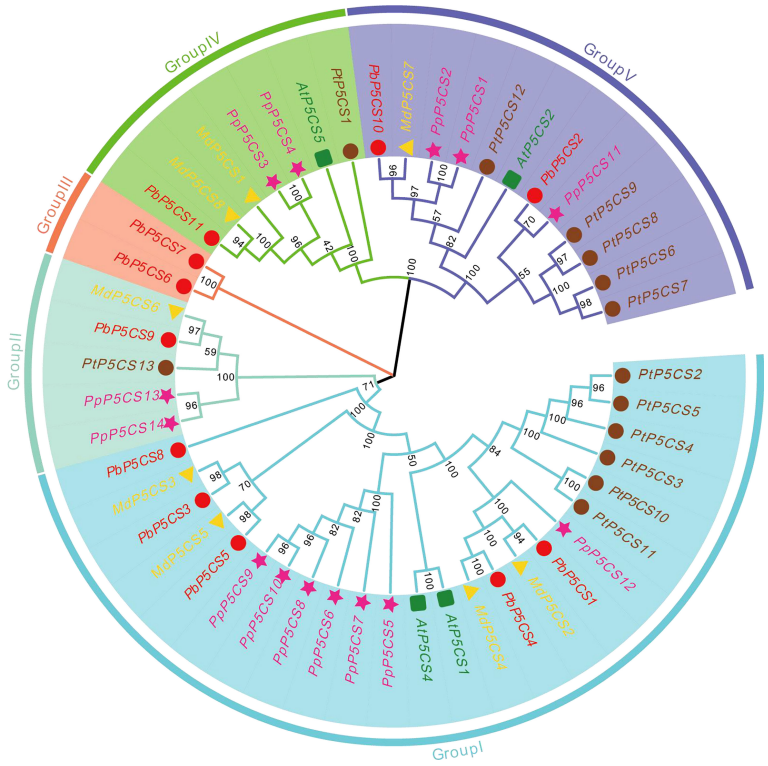

FIGURE 1
Phylogenetic tree of P5CS proteins constructed using the neighbor-joining method with P5CS domains from pear *Pyrus betulifolia* (red circles), *Malus domestica* (yellow triangles), *Populus trichocarpa* (pink pentagons), *Prunus persica* (brown circles), and *Arabidopsis thaliana* (green squares). Members are divided into Groups I, II, III, IV, and V.

3, 6, 7, 9, and 10 were present only in Group I members, which might contribute to the functional divergence of *P5CS* genes. Motif 5 was found not only in all members of Group I, but also in PbP5CS6 and PbP5CS7 in Group III, this suggests that PbP5CS6 and PbP5CS7 may have evolved from Group I. Group II only comprised Motif 4, Group IV only contained Motif 8. As Motifs 4 and 8 were found in PbP5CS2 and PbP5CS10 in Group V, PbP5CS2 and PbP5CS10 may have evolved from Groups II and IV (Figures 2A, B). We also found that four genes in Group I (*PbP5CS1*, *PbP5CS3*,

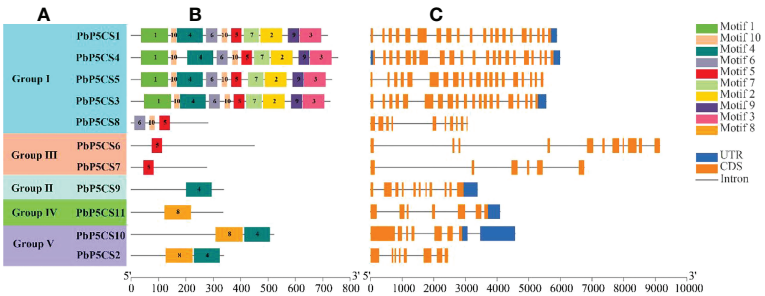

FIGURE 2
Schematic representation of protein and gene structures of pear *P5CS* (*PbP5Cs*) genes. **(A)** Phylogenetic relationships. **(B)** Motif composition. **(C)** Gene structure. Motifs 1–8 identified using the MEME search tool are marked on protein sequences in each clade (I–V). The length and order of each motif corresponds to the actual length and position in the protein sequences. Coding sequence and untranslated regions are represented by filled orange and dark blue boxes, respectively.

PbP5CS4, and *PbP5CS5*) had more than 20 exons, while all others carried between six and 11 exons (Figure 2C).

Chromosomal locations and homologous genotypes of *PbP5CS* genes

According to their annotated genomic locations, we found that the 11 *PbP5CSs* were widely distributed among the pear chromosomes. Chromosome 12 contained four *PbP5CS* genes, whereas Chromosomes 1, 2, 4, 7, 13, 14, and 15 had only one gene (Figure 3). PbP5CS1, PbP5CS3, PbP5CS4, and PbP5CS5 (six pairs) were segmental (Figure 4A). In order to further explore the homologous gene relationships of *PbP5CSs*, we compared the physical locations of *P5CS* genes among the genomes of pear, apple, peach, poplar, and *A. thaliana* (Figure 4B). *P5CS* genes showed intimate collinear relationships in these five species. *P5CSs* in pear and apple showed the closest collinear relationship, with seven *P5CS* genes in apple sharing a close evolutionary relationship with *PbP5CS* genes. Moreover, six *P5CS* genes in each of peach and poplar, as well as two *P5CS* genes in *A. thaliana*, shared close evolutionary relationships with *PbP5CS* genes (Supplementary Table S3).

Promoter cis-regulatory elements of *PbP5CS* genes

To better understand the gene functions and transcriptional regulation of *PbP5CSs*, we analyzed cis-elements in the promoter regions of *PbP5CSs* (Figure 5). The conventional promoter element CAAT-box was found in all *PbP5CS* promoters. Various cis-elements related to plant growth, development, and responses to stresses and phytohormones were also identified (Supplementary Table S4). Additionally, the conventional promoter element GC-motif was present in *PbP5CS2*, the seed-specific regulation element (RY-element) was found in the promoter of *PbP5CS7*, and the endosperm expression regulation element (GCN4_motif) was observed in the promoters of *PbP5CS1* and *PbP5CS8*. The zein metabolism regulation element (O_2-site) was identified in the promoters of seven *PbP5CS* genes.

Among the cis-elements that respond to plant hormones, the abscisic acid responsive element (ABRE) was present in the promoter of all *PbP5CS* genes, methyl jasmonate responsive elements (TGACG-motif and CGTCA-motif) were observed in the promoters of all *PbP5CS* genes excluding *PbP5CS8*, and salicylic acid-responsive element (TCA-element) was found in eight *PbP5CS* genes. Gibberellin responsive elements (GARE-motif, P-box, and TATC-box) and auxin responsive elements (AUXRR-core and TGA) were identified in six *PbP5CS* genes. We also found the stress-related cis-acting element (ARE) involved in anaerobic induction in all *PbP5CS* genes. Furthermore, defense and stress response element (TC-rich repeat), drought-inducible response element (MBS), low temperature responsiveness (LTR), and circadian features were identified in the promoters of *PbP5CS* genes (Figure 5; Supplementary Table S4).

Tissue-specific expression patterns of *PbP5CS* genes

To investigate the putative roles of the *PbP5CS* genes in pear development, we analyzed organic-specific expression patterns of *PbP5CSs*. Expression patterns of *PbP5CS* genes in five different tissues (petal, stigma, leaf, ovary, and shoot) were analyzed using publicly available gene expression data (SRP230672). Some *PbP5CSs* were expressed at considerably high levels in specific tissues (Figure 6). For example, three

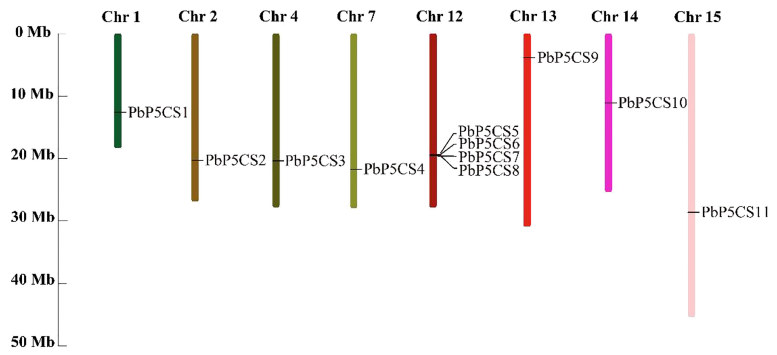

FIGURE 3
Chromosomal distribution of *PbP5CS* genes. Chromosomal mapping was based on the physical position (Mb) in 17 pear chromosomes. The scale on the left is in megabases (Mb). Chromosome numbers are indicated at the top of each bar.

10.3389/fpls.2022.1066765

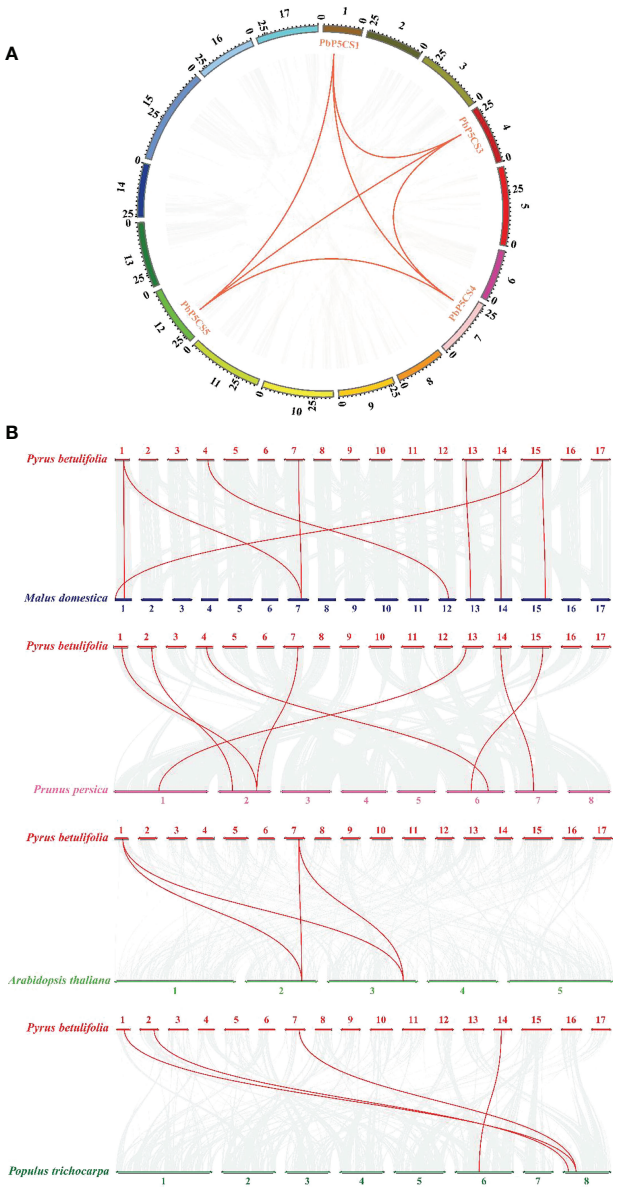

FIGURE 4
Synteny analysis of *P5CS* genes. **(A)** Synteny analysis of *PbP5CS* genes in pear. Gray lines indicate collinear blocks in the whole *Pyrus betulifolia* genome, and red lines indicate duplicated *PbP5CS* gene pairs. **(B)** Synteny analysis of *P5CS* genes in the *P. betulifolia*, *Populus trichocarpa*, *Arabidopsis thaliana*, *Malus domestica*, and *Prunus persica* genomes. Red lines highlight syntenic *P5CS* gene pairs.

PbP5CSs (*PbP5CS1*, *PbP5CS5*, and *PbP5CS8*) displayed higher expression levels in the petal than other tissues, implying that they play important roles in pear petal growth and development.

PbP5CS1, *PbP5CS2*, and *PbP5CS4* exhibited high levels of expression in the stigma, which suggests that they may play roles in stigma growth and development. *PbP5CS4*, *PbP5CS6*, and *PbP5CS9* were preferentially expressed in the ovary, which suggests that they may take part in in ovary growth and development. *PbP5CS3*, *PbP5CS5*, *PbP5CS10*, and *PbP5CS11* showed relatively high expression levels in the leaf, which means that they could participate in leaf development. *PbP5CS7* showed higher expression in the shoot than other tissues, which reflects its possible role in shoot growth (Supplementary Table S5). These results suggest that *PbP5CS* genes have different expression patterns, and may play diverse roles in pear during growth and development of different tissues.

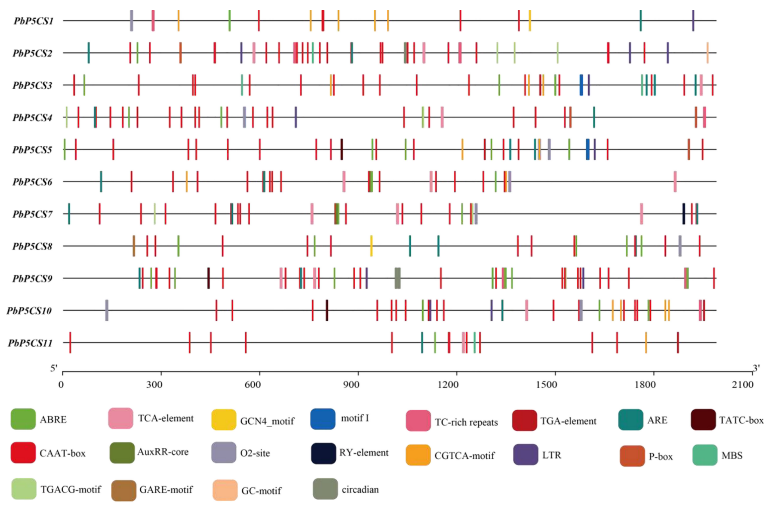

FIGURE 5
Promoter cis-regulatory element analysis of *PbP5CS* genes. Different colors indicate various promoter elements in *PbP5CS* genes.

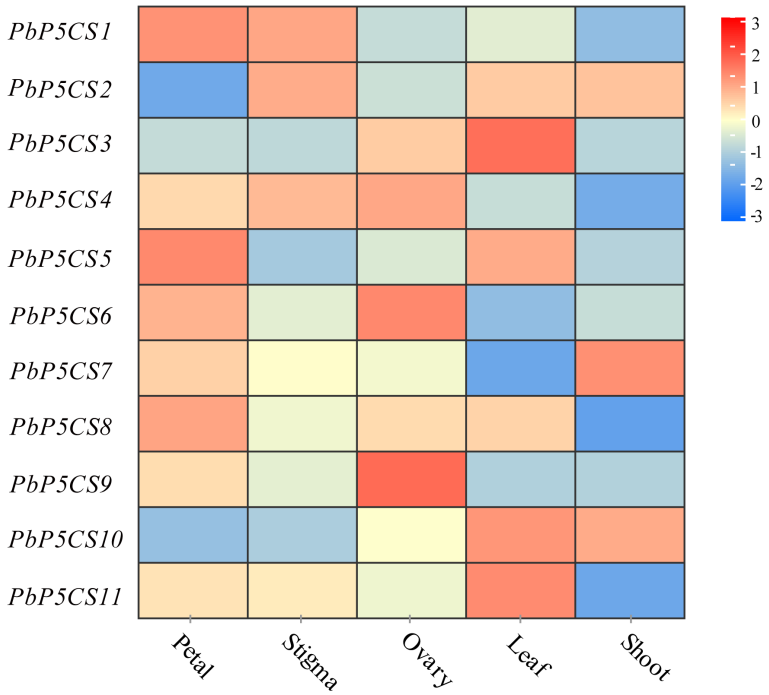

FIGURE 6
Expression patterns of *PbP5CS* genes in different tissues of pear. Microarray analysis results of *PbP5CS* genes in *Pyrus bretschneideri* 'Yali' were downloaded from NCBI GEO DataSets (SRP230672). Red and blue boxes indicate high and low expression levels, respectively, for each gene.

Expression patterns of *PbP5CS* genes under abiotic and biotic stresses

To explore whether the P5CS enzyme plays an essential role under biotic and abiotic stresses, we measured the enzyme activities of P5CS under drought, waterlogging, salinity-alkalinity, cold, heat, and *G. haraeanum* infection (Supplementary Figure S1). The enzyme activities of P5CS gradually increased under the different stresses. We then investigated expression patterns of *PbP5CS* genes in response to different stresses. With regard to abiotic stresses, RNA-seq datasets for pear subjected to drought (SRP148620), salt (SRP077703), and cold (SRP287704) were explored. In general, expression levels of *PbP5CS1*, *PbP5CS3*, *PbP5CS4*, *PbP5CS5*, *PbP5CS6*, and *PbP5CS11* were up-regulated by all abiotic stress treatments, indicating potential roles of these *PbP5CSs* in abiotic stress responses (Figure 7; Supplementary Table S6). Under drought treatment, *PbP5CS1*, *PbP5CS2*, *PbP5CS3*, *PbP5CS4*, *PbP5CS5*, *PbP5CS6*, *PbP5CS7*, *PbP5CS9*, and *PbP5CS11* were up-regulated, but *PbP5CS8* and *PbP5CS10* were repressed in response to short-term drought stress (Figure 7A). Furthermore, *PbP5CS2*, *PbP5CS3*, *PbP5CS5*, and *PbP5CS8* were significantly up-regulated at 72 hours of NaCl treatment (Figure 7B). *PbP5CS6* and *PbP5CS9* were significantly induced at 50 days of cold treatment (Figure 7C). These results indicate that the responsive *PbP5CSs* may be involved in plant defense mechanisms under both short- and long-term abiotic stress.

To explore the potential roles of *PbP5CS* genes in responses to biotic stresses, we investigated RNA-seq datasets from the infection experiment of pear with *A. alternate* (SRP276846). *PbP5CS1* and *PbP5CS2* were significantly up-regulated at 24 and 8 hours post-infection, respectively. *PbP5CS3*, *PbP5CS9*, and *PbP5CS11* showed significant up-regulation at 16 hours post-infection. *PbP5CS4*, *PbP5CS5*, and *PbP5CS8* were markedly induced at 48 hours post-infection. However, *PbP5CS6* and *PbP5CS10* were distinctively repressed following *A. alternate* infection, whereas *PbP5CS7* did not respond to infection (Figure 7D).

To validate previous RNA-seq data and reveal more details of *PbP5CSs* in stress responses, we investigated the transcription levels of *PbP5CS* genes under different environmental stresses, including drought, waterlogging, salinity-alkalinity, cold, heat, and *G. haraeanum* infection. Under drought stress, nine (*PbP5CS1, PbP5CS2, PbP5CS3, PbP5CS4, PbP5CS5, PbP5CS6, PbP5CS7, PbP5CS9*, and *PbP5CS11*) and two (*PbP5CS8* and *PbP5CS10*) *PbP5CSs* were up-regulated and down-regulated, respectively (Figure 8A). Moreover, seven (*PbP5CS2, PbP5CS3, PbP5CS4, PbP5CS5, PbP5CS7, PbP5CS9*, and *PbP5CS11*) and four (*PbP5CS3, PbP5CS8, PbP5CS9*, and *PbP5CS10*) *PbP5CS* genes were respectively up-regulated and down-regulated under waterlogging treatment (Figure 8B). Similarly, eight *PbP5CS* genes (*PbP5CS1, PbP5CS2, PbP5CS3, PbP5CS4, PbP5CS7, PbP5CS9, PbP5CS10*, and *PbP5CS11*) showed increased expression levels and three *PbP5CSs* (*PbP5CS5, PbP5CS6*, and *PbP5CS8*) were down-regulated by salinity-alkalinity treatment (Figure 8C). Additionally, the transcription levels of seven *PbP5CS* genes (*PbP5CS1, PbP5CS3, PbP5CS4, PbP5CS5, PbP5CS9, PbP5CS10*, and *PbP5CS11*) were increased under cold stress (Figure 8D). Under heat stress, seven *PbP5CS* genes (*PbP5CS1, PbP5CS2, PbP5CS4, PbP5CS5, PbP5CS6, PbP5CS7*, and *PbP5CS11*) were up-regulated, and the remaining four

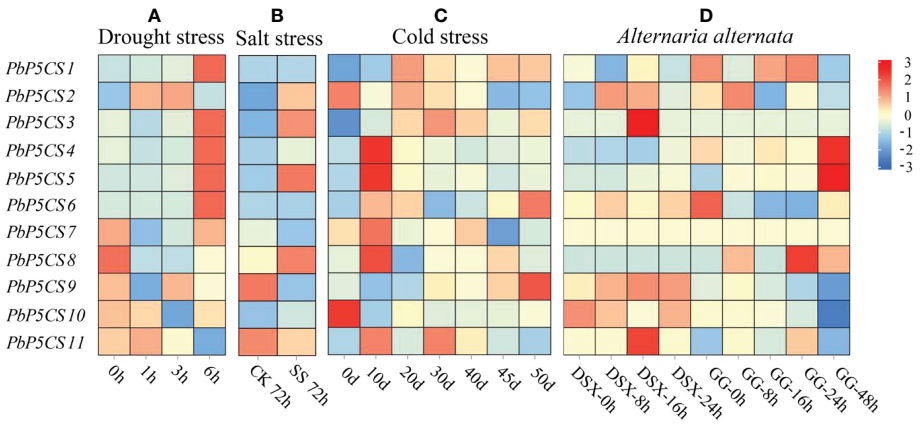

FIGURE 7
Expression patterns of *PbP5CS* genes in response to abiotic and biotic stresses. **(A)** Gene expression patterns in *Pyrus bretschneideri* at 1, 3, and 6 hours of drought treatment (GEO series SRP148620). **(B)** Gene expression patterns in *Pyrus betulifolia* at 72 hours of salt stress treatment (GEO series SRP077703). CK, control; SS, salt stress treatment. **(C)** Gene expression patterns in *Pyrus bretschneideri* 'Suli' at 0, 10, 20, 30, 40, 45, and 50 days of cold treatment (GEO series SRP287704). **(D)** Gene expression patterns in *Pyrus pyrifolia* 'Deshengxiang' (DSX) and *Pyrus pyrifolia* 'Guiguan' (GG) at 0, 8, 12,16, 24, and 48 hours post-infection by *Alternaria alternate* (GEO series SRP276846). Data are expressed as fragments per kilobase of exon per million mapped reads. Blue and red blocks indicate decreased and increased transcription levels, respectively.

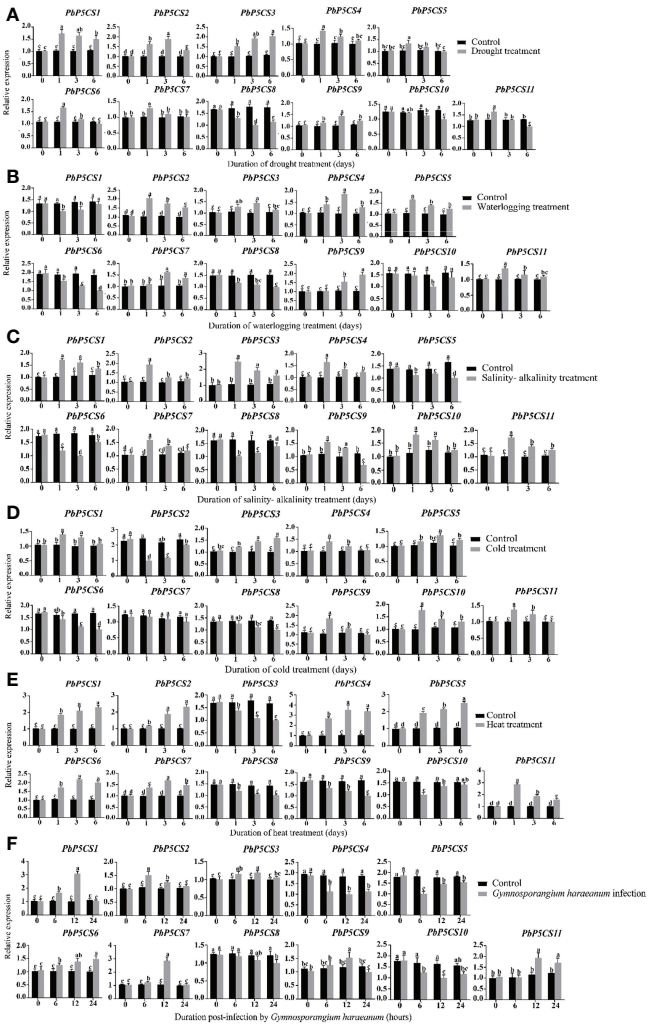

FIGURE 8
Real-time quantitative PCR (qPCR) analysis of pear *P5CS* genes in response to **(A)** drought, **(B)** waterlogging, **(C)** salinity-alkalinity, **(D)** cold, **(E)** heat, and **(F)** *Gymnosporangium haraeanum* infection stresses. Data were normalized against expression levels of the *Actin* gene. Mean values were calculated from three independent replicates. Vertical bars indicate standard error of the mean. Different lowercase letters indicate significant differences between treatments according to Fisher's least significant difference ($P < 0.05$).

PbP5CSs (*PbP5CS3, PbP5CS8, PbP5CS9*, and *PbP5CS10*) were down-regulated (Figure 8E).

Pear rust caused by *G. haraeanum* is one of the main diseases affecting pear production. To understand the potential functions of *PbP5CS* genes in response to biotic stress, transcript levels of 11 *PbP5CSs* were measured by qPCR in pear subjected to *G. haraeanum* infection. Seven (*PbP5CS1, PbP5CS2, PbP5CS3, PbP5CS6, PbP5CS7, PbP5CS9*, and *PbP5CS11*) and four (*PbP5CS4, PbP5CS5, PbP5CS8*, and *PbP5CS10*) *PbP5CS* genes were up-regulated and down-regulated, respectively (Figure 8F). Interestingly, *PbP5CS4* and *PbP5CS11* were also strongly induced by drought, waterlogging, salinity-alkalinity, cold, and heat, suggesting that these two genes might be candidate genes for mitigating abiotic stresses. In particular, *PbP5CS11* was induced dramatically by various abiotic and biotic stresses (Figure 8).

Discussion

P5CS genes play key roles in biochemical and physiological processes in response to various stressors in plants (Chen et al., 2013; Yang D. et al., 2021). Therefore, studying the functions of *P5CS* gene families in inhospitable environments can provide valuable information on the mechanisms underlying plant adaptation. In the current work, we performed a genome-wide analysis of *P5CSs* in pear by considering their gene structures, phylogenetic relationships, cis-acting elements, linkage group

organization, and duplication events. We also explored their possible roles in plant tissues and responses to stress. The genome-wide results for *PbP5CS* genes not only provides novel insights into their physiological functions, but also a foundation for functional research on these genes during pear growth and development.

The expansion of gene family members is driven by gene duplication events, either segmental or tandem duplications, during plant evolution (Guo et al., 2014; Wang et al., 2022). Most plants have two *P5CS* isoforms, as demonstrated for *Phaseolus vulgaris*, *Lotus japonicus*, and *Brassica napus* (Xue et al., 2009; Chen et al., 2013; Signorelli and Monza, 2017). In the present work, 11 *P5CS* genes were identified in the pear genome (Table 1; Figure 1), more than apple (8) and *A. thaliana* (4), but fewer than poplar (13) and peach (14). The variation might be due to gene duplication differences, considered a fundamental driving force in the evolution of genomes (Kong et al., 2007). Gene duplications can provide raw materials for new genes, leading to the emergence of new functions.

Our phylogenetic analysis of P5CS proteins among pear, apple, peach, poplar, and *A. thaliana* showed that the proteins formed species-specific clusters (Figure 1). This result indicates that P5CS proteins have been highly conserved during evolution. Furthermore, there were six segmental duplication pairs (*PbP5CS1*/*PbP5CS3*, *PbP5CS1*/*PbP5CS4*, *PbP5CS1*/*PbP5CS5*, *PbP5CS3*/*PbP5CS4*, *PbP5CS3*/*PbP5CS5*, and *PbP5CS4*/*PbP5CS5*) in pear (Figure 4A). These results demonstrate that segmental duplication plays a vital role in driving the expansion of the pear *PbP5CS* gene family. The synteny analysis of *P5CS* genes in pear, apple, peach, poplar, and *A. thaliana* showed that *PbP5CS* genes shared higher homology with *P5CS* genes in apple than in peach, poplar, and *A. thaliana* (Figure 4B; Supplementary Table S3). However, *PbP5CS1* and *PbP5CS4* were collinear with the *P5CS* genes of the other four species (Supplementary Table S3), indicating that *PbP5CS1* and *PbP5CS4* in different plants may have evolved from a common ancestor.

Variation in introns and exons plays is essential for the evolution of different genes (Mustafin and Khusnutdinova, 2015; Rogers, 1990). Introns play major roles in gene evolution (Rose, 2008). Our analysis of *P5CS* gene structure revealed that all *PbP5CS* genes contained different numbers of exons and introns (Figure 2C), indicating functional diversity among *PbP5CS* genes. In addition, cis-regulatory element analysis revealed the presence of a series of abiotic/biotic stress responsive cis-acting elements, such as ARE, ABRE, MBS, LTR, and AuxRR-core, in the promoter regions of *PbP5CS* genes (Figure 5; Supplementary Table S4). This implies that the *PbP5CS* genes perform potential functions in response to abiotic and biotic stresses. The different cis-regulatory elements in *P5CS* genes presumably allows them to exert diverse effects on plant growth and development, including under different stress conditions.

Proline has been shown to be critically involved in a number of plant developmental processes, such as pollen fertility, root elongation, embryo development, and floral transition (Trovato et al., 2018). P5CS1 predominantly contributes to stress-induced proline accumulation, and P5CS2 is mainly involved in plant growth and development (Funck et al., 2020). For example, an increase in proline content was accompanied by markedly high expression of *BnP5CS* in flowers of *B. napus*, suggesting possible contribution of proline to flower development (Xue et al., 2009). In pear, eight *PbP5CS* genes (*PbP5CS1*, *PbP5CS4*, *PbP5CS5*, *PbP5CS6*, *PbP5CS7*, *PbP5CS8*, *PbP5CS9*, and *PbP5CS11*) displayed high expression levels in the petal (Figure 6), which further indicates that proline is a key factor in floral development (Trovato et al., 2018). Furthermore, *PbP5CS1*, *PbP5CS2*, and *PbP5CS4* were highly expressed in the stigma, *PbP5CS4*, *PbP5CS6*, and *PbP5CS9* showed relatively high expression levels in the ovary, and *PbP5CS3*, *PbP5CS10*, and *PbP5CS11* were predominantly expressed in the leaf (Figure 6). All these *PbP5CS* members likely function in the particular pear tissues.

Proline accumulation is mainly regulated by the P5CS enzyme in plant cells under stress conditions (Yang D. et al., 2021). Increasing evidence demonstrates that *P5CS* genes participate in plant development, biological regulation, and stress responses, and they play an essential role in plant resistance to different abiotic stresses (Zhang et al., 1995; Parida et al., 2008; Bandurska et al., 2017). P5CS is a key enzyme enhancing oxidative stress tolerance in plants under salt and drought stresses (Kumar et al., 2010; Rai and Penna, 2013). P5CS activity and expression levels were up-regulated in barley (*Hordeum vulgare*), cotton (*Gossypium hirsutum*), and *S. purpurea* under drought stress conditions (Parida et al., 2008; Bandurska et al., 2017; Yang D. et al., 2021). In pear, P5CS enzyme activity was induced under six different stresses (Supplementary Figure S1). The expression of *PbP5CS1, PbP5CS2, PbP5CS3, PbP5CS4, PbP5CS5, PbP5CS6*, and *PbP5CS11* was significantly induced in response to drought stress according to RNA-seq and qPCR data (Figures 7, 8), indicating roles for these genes in drought stress tolerance by regulating P5CS enzyme activities. Moreover, most pear P5CSs (PbP5CS1, PbP5CS2, PbP5CS3, PbP5CS4, PbP5CS5, PbP5CS6, PbP5CS8, PbP5CS10, and PbP5CS11) clustered together with proteins from *A. thaliana* (Figure 1). The *AtP5CS* gene was induced by high salt treatment in *A. thaliana* (Yoshiba et al., 1995). Similarly, *PbP5CS2*, *PbP5CS4*, and *PbP5CS10* expression was induced in response to salt and salinity-alkalinity stresses, according to RNA-seq and qPCR data (Figures 7, 8C), indicating putative functions for these genes in pear salt or salinity-alkalinity stress tolerance. Furthermore, *AmP5CS* was rapidly initiated by heat stress in grey mangrove (*Avicennia marina*) (Liu and Wang, 2020). *PvP5CS* was prominently up-regulated in common bean (*Phaseolus vulgaris*), which enhanced tolerance under cold stress (Atienza et al., 2004; Chen et al.,

2009; Chen et al., 2013). *CpP5CS* can be induced by both heat and cold stress in papaya (*Carica papaya*) (Zhu et al., 2012). In the current work, P5CS enzyme activity was gradually increased, and the expression of *PbP5CS1*, *PbP5CS4*, *PbP5CS5*, and *PbP5CS11* was significantly induced by heat and cold. Additionally, the enzyme activity of P5CS was induced, and *PbP5CS2*, *PbP5CS3*, *PbP5CS4*, *PbP5CS5*, *PbP5CS7*, *PbP5CS9*, and *PbP5CS11* were up-regulated by waterlogging stress (Supplementary Figure S1; Figure 8). The collective results indicate that these *PbP5CS* genes also regulate P5CS enzyme activities to mitigate various abiotic stresses.

Regarding biotic stresses, *AtP5CS2* participates in the *A. thaliana* hypersensitive response induced by avirulent *Pseudomonas* spp. (Fabro et al., 2004). Herein, *PbP5CS1*, *PbP5CS2*, *PbP5CS3*, *PbP5CS6*, *PbP5CS7*, *PbP5CS9*, and *PbP5CS11* were up-regulated in response to *G. haraeanum* infection (Figure 8). Accordingly, these *PbP5CSs* might participate in the pathogen response pathway. However, *PbP5CS4*, *PbP5CS5*, *PbP5CS8*, and *PbP5CS10* were down-regulated in response to *G. haraeanum* infection, suggesting that the four genes may function through different mechanisms to protect against biotic stimuli. All identified *PbP5CS* members were differentially regulated by both biotic and abiotic stresses, indicating that these genes are likely to mediate plant defense mechanisms in pear. Currently, the biological functions of most *PbP5CS* genes in plant developmental and defense processes remain unknown. The present bioinformatic and expression analyses of *PbP5CS* genes provide valuable information for screening candidate genes, and the results are helpful to further investigate the functions of this gene family in pear.

Conclusions

Eleven *PbP5CS* genes were identified in pear, and a systematic study of the *PbP5CS* gene family was carried out. The comprehensive analyses encompassed conserved domains, gene structures, and phylogenetic relationships, in addition to gene duplications, chromosome locations, cis-acting elements, and expression patterns. There were various cis-acting elements in the *PbP5CS* promoter sequences, suggesting that *PbP5CSs* act in complex networks regulating plant development and responses to stresses. Transcriptome and qPCR analyses revealed that *PbP5CS* genes are likely to take part in plant response to biotic and abiotic stresses. Our genome-wide analysis of *PbP5CSs* provides evidence for the functions of this gene family in pear. Further studies on *PbP5CS* genes are underway to verify their functions in stressed environments.

Data availability statement

The datasets presented in this study can be found in online repositories. The names of the repository/repositories and accession number(s) can be found in the article/Supplementary Material.

Author contributions

CM and CW conceived and designed the research. MW, MZ, MY, XZ, YT, ZS, and XL performed the experiments, conducted the field work, and analyzed the data. MC and MW wrote the manuscript. All authors contributed to the article and approved the submitted version.

Funding

This study was supported by the Funds for Modern Agricultural Industry Technology System in Shandong Province (SDAIT-06-06), the Shandong Provincial Natural Science Foundation (ZR2019BC038), and the High-level Scientific Research Foundation of Qingdao Agricultural University (Grant 663/1121043), China.

Conflict of interest

The authors declare that the research was conducted in the absence of any commercial or financial relationships that could be construed as a potential conflict of interest.

Publisher's note

Supplementary material

The Supplementary Material for this article can be found online at: https://www.frontiersin.org/articles/10.3389/fpls.2022.1066765/full#supplementary-material

References

Anton, D. B., Guzman, F. L., Vetö, N. M., Krause, F. A., Kulcheski, F. R., Coelho, A. P. D., et al. (2020). Characterization and expression analysis of P5CS (Δ1-pyrroline-5-carboxylate synthase) gene in two distinct populations of the Atlantic forest native species *Eugenia uniflora* l. *Mol. Biol. Rep.* 47, 1033–1043. doi: 10.1007/s11033-019-05195-7

Atienza, S. G., Faccioli, P., Perrotta, G., Dalfino, G., Zschiesche, W., Humbeck, K., et al. (2004). Large Scale analysis of transcripts abundance in barley subjected to several single and combined abiotic stress conditions. *Plant Sci.* 167, 1359–1365. doi: 10.1016/j.plantsci.2004.07.006

Bailey, T. L., Johnson, J., Grant, C. E., and Noble, W. S. (2015). MEME SUITE: tools for motif discovery and searching. *Nucleic Acids Res.* 37, W202–W208. doi: 10.1093/nar/gkp335

Bandurska, H., Niedziela, J., Pietrowska-Borek, M., Nuc, K., Chadzinikolau, T., and Radzikowska, D. (2017). Regulation of proline biosynthesis and resistance to drought stress in two barley (*Hordeum vulgare* l.) genotypes of different origin. *Plant Physiol. Biochem.* 118, 427–437. doi: 10.1016/j.plaphy.2017.07.006

Chen, C., Chen, H., Zhang, Y., Thomas, H. R., and Xia, R. (2020). TBtools: an integrative toolkit developed for interactive analyses of big biological data. *Mol. Plant* 13 (8), 1194–1202. doi: 10.1016/j.molp.2020.06.009

Chen, J. B., Wang, S. M., Jing, R. L., and Mao, X. G. (2009). Cloning the *PvP5CS* gene from common bean (*Phaseolus vulgaris*) and its expression patterns under abiotic stresses. *J. Plant Physiol.* 166 (1), 12–19. doi: 10.1016/j.jplph.2008.02.010

Chen, J. B., Yang, J. W., Zhang, Z. Y., Feng, X. F., and Wang, S. M. (2013). Two *P5CS* genes from common bean exhibiting different tolerance to salt stress in transgenic *Arabidopsis*. *J. Genet.* 92 (3), 461–469. doi: 10.1007/s12041-013-0292-5

Delauney, A. J., and Verma, D. P. S. (1993). Proline biosynthesis and osmoregulation in plants. *Plant J.* 4, 215–223. doi: 10.1046/j.1365-313X.1993.04020215.x

Dong, X., Wang, Z., Tian, L., Zhang, Y., Qi, D., Huo, H., et al. (2020). *De novo* assembly of a wild pear (*Pyrus betuleafolia*) genome. *Plant Biotechnol. J.* 18 (2), 581–595. doi: 10.1111/pbi.13226

Duvaud, S., Gabella, C., Lisacek, F., Stockinger, H., Ioannidis, V., and Durinx, C. (2021). Expasy, the Swiss bioinformatics resource portal, as designed by its users. *Nucleic Acids Res.* 49, 216–227. doi: 10.1093/nar/gkab225

Fabro, G., Kovács, I., Pavet, V., Szabados, L., and Alvarez, M. E. (2004). Proline accumulation and *AtP5CS2* gene activation are induced by plant-pathogen incompatible interactions in *Arabidopsis*. *Mol. Plant Microbe Interact.* 17 (4), 343–350. doi: 10.1094/MPMI.2004.17.4.343

Funck, D., Baumgarten, L., Stift, M., von Wirén, N., and Schönemann, L. (2020). Differential contribution of P5CS isoforms to stress tolerance in *Arabidopsis*. *Front. Plant Sci.* 11. doi: 10.3389/fpls.2020.565134

Guan, C., Cui, X., Liu, H. Y., Li, X., Li, M. Q., and Zhang, Y. W. (2020). Proline biosynthesis enzyme genes confer salt tolerance to switchgrass (*Panicum virgatum* l.) in cooperation with polyamines metabolism. *Front. Plant Sci.* 11. doi: 10.3389/fpls.2020.00046

Guan, C., Ji, J., Guan, W., Feng, Y., Li, X., Jin, C., et al. (2014). A *Lycium chinense*-derived P5CS-like gene is regulated by water defcit-induced endogenous abscisic acid and overexpression of this gene enhances tolerance to water defcit stress in *Arabidopsis*. *Mol. Breed.* 34, 1109–1124. doi: 10.1007/s11032-014-0103-6

Guo, Z., Jiang, W., Lages, N., Borcherds, W., and Wang, D. (2014). Relationship between gene duplicability and diversifiability in the topology of biochemical networks. *BMC Genomics* 15 (1), 577. doi: 10.1186/1471-2164-15-577

Hayat, S., Hayat, Q., Alyemeni, M. N., Wani, A. S., Pichtel, J., and Ahmad, A. (2012). Role of proline under changing environments: a review. *Plant Signal Behav.* 7 (11), 1456–1466. doi: 10.4161/psb.21949

Horton, P., Park, K. J., Obayashi, T., Fujita, N., Harada, H., Adams-Collier, C. J., et al. (2007). WoLF PSORT: protein localization predictor. *Nucleic Acids Res.* 35, 585–587. doi: 10.1093/nar/gkm259

Hu, B., Jin, J., Guo, A. Y., Zhang, H., Luo, J., and Gao, G. (2014). GSDS 2.0: An upgraded gene feature visualization server. *Bioinformatics.* 31 (8), 1296–1297. doi: 10.1093/bioinformatics/btu817

Hung, C. L., Lin, Y. S., Lin, C. Y., Chung, Y. C., and Chung, Y. F. (2015). CUDA ClustalW: An efficient parallel algorithm for progressive multiple sequence alignment on multi-GPUs. *Comput. Biol. Chem.* 58, 62–68. doi: 10.1016/j.compbiolchem.2015.05.004

Kong, H., Landherr, L. L., Frohlich, M. W., Leebens-Mack, J., Ma, H., and DePamphilis, C. W. (2007). Patterns of gene duplication in the plant *SKP1* gene family in angiosperms: Evidence for multiple mechanisms of rapid gene birth. *Plant J.* 50, 873–885. doi: 10.1111/j.1365-313X.2007.03097.x

Kumar, V., Shriram, V., Kishor, P., Jawali, N., and Shitole, M. (2010). Enhanced proline accumulation and salt stress tolerance of transgenic *indica* rice by over-expressing *P5CSF129A* gene. *Plant Biotechnol. Rep.* 4, 37–48. doi: 10.1007/s11816-009-0118-3

Kumar, S., Stecher, G., and Tamura, K. (2016). MEGA7: Molecular evolutionary genetics analysis version 7.0 for bigger datasets. *Mol. Biol. Evol.* 33, 1870–1874. doi: 10.1093/molbev/msw054

Lescot, M., Déhais, P., Thijs, G., Marchal, K., Moreau, Y., Van de Peer, Y., et al. (2002). PlantCARE, a database of plant cis-acting regulatory elements and a portal to tools for in silico analysis of promoter sequences. *Nucleic Acids Res.* 30, 325–327. doi: 10.1093/nar/30.1.325

Li, B., Dong, X., Zhang, Z., Zhao, H., Lian, S., and Li, B. (2006) *Optimum time for control of pear rust (Gymnosporangium haraeanum syd.) with fungicides in laiyang plant protection*. Available at: https://en.cnki.com.cn/Article_en/CJFDTOTAL-ZWBH200601020.htm.

Liu, J., and Wang, Y. S. (2020). Proline metabolism and molecular cloning of *AmP5CS* in the mangrove *Avicennia marina* under heat stress. *Ecotoxicol.* 29 (6), 698–706. doi: 10.1007/s10646-020-02198-0

Liu, D. F., Zhang, D., Liu, G. Q., Hussain, S., and Teng, Y. W. (2013). Influence of heat stress on leaf ultrastructure, photosynthetic performance, and ascorbate peroxidase gene expression of two pear cultivars (*Pyrus pyrifolia*). *J. Zhejiang Univ. Sci. B.* 14 (12), 1070–1083. doi: 10.1631/jzus.B1300094

Livak, K. J., and Schmittgen, T. D. (2001). Analysis of relative gene expression data using real-time quantitative PCR and the $2^{-\Delta\Delta CT}$ method. *Methods.* 25 (4), 402–408. doi: 10.1006/meth.2001.1262

Ma, C., Bian, C., Liu, W., Sun, Z., Xi, X., Guo, D., et al. (2022). Strigolactone alleviates the salinity-alkalinity stress of *Malus hupehensis* seedlings. *Front. Plant Sci.* 13. doi: 10.3389/fpls.2022.901782

Parida, A. K., Dagaonkar, V. S., Phalak, M. S., and Aurangabadkar, L. P. (2008). Differential responses of the enzymes involved in proline biosynthesis and degradation in drought tolerant and sensitive cotton genotypes during drought stress and recovery. *Acta Physiol. Plant* 30, 619–627. doi: 10.1007/s11738-008-0157-3

Peng, Z., Lu, Q., and Verma, D. P. (1996). Reciprocal regulation of delta 1-pyrroline-5-carboxylate synthetase and proline dehydrogenase genes controls proline levels during and after osmotic stress in plants. *Mol. Gen. Genet.* 253 (3), 334–341. doi: 10.1007/pl00008600

Rai, A. N., and Penna, S. (2013). Molecular evolution of plant *P5CS* gene involved in proline biosynthesis. *Mol. Biol. Rep.* 40 (11), 6429–6435. doi: 10.1007/s11033-013-2757-2

Rogers, J. H. (1990). The role of introns in evolution. *FEBS Lett.* 268(2):339–43. doi: 10.1016/0014-5793(90)81282-s

Rose, A. B.. (2008). Intron-mediated regulation of gene expression. *Curr. Top. Microbiol. Immunol.* 326 (2), 277–290. doi: 10.1007/978-3-540-76776-3_15

Saeed, A. I., Bhagabati, N. K., Braisted, J. C., Sharov, V., Howe, E. A., Li, J. W., et al. (2006) TM4 microarray software suite. *Methods Enzymol.* 411, 134–193. doi: 10.1016/S0076-6879(06)11009-5

Signorelli, S., and Monza, J. (2017). Identification of Δ1-pyrroline 5-carboxylate synthase (*P5CS*) genes involved in the synthesis of proline in *Lotus japonicus*. *Plant Signal Behav.* 12 (11), e1367464. doi: 10.1080/15592324.2017.1367464

Szabados, L., and Savouré, A. (2010). Proline: A multifunctional amino acid. *Trends Plant Sci.* 15, 89–97. doi: 10.1016/j.tplants.2009.11.009

Székely, G., Abrahám, E., Cséplo, A., Rigó, G., Zsigmond, L., Csiszár, J., et al. (2008). Duplicated *P5CS* genes of *Arabidopsis* play distinct roles in stress regulation and developmental control of proline biosynthesis. *Plant J.* 53 (1), 11–28. doi: 10.1111/j.1365-313X.2007.03318.x

Tan, C. M., Chen, R. J., Zhang, J. H., Gao, X. L., Li, L. H., Wang, P. R., et al. (2013). *OsPOP5*, a prolyl oligopeptidase family gene from rice confers abiotic stress tolerance in *Escherichia coli*. *Int. J. Mol. Sci.* 14, 20204–20219. doi: 10.3390/ijms141020204

Trovato, M., Mattioli, R., and Costantino, P. (2018). From a. rhizogenes RolD to plant P5CS: Exploiting proline to control plant development. *Plants (Basel).* 7 (4), 108. doi: 10.3390/plants7040108

Turchetto-Zolet, A. C., Margis-Pinheiro, M., and Margis, R. (2009). The evolution of pyrroline-5-carboxylate synthase in plants: a key enzyme in proline synthesis. *Mol. Genet. Genomics* 281 (1), 87–97. doi: 10.1007/s00438-008-0396-4

Wang, L., Guo, Z., Zhang, Y., Wang, Y., Yang, G., Yang, L., et al. (2017). Characterization of *LhSorP5CS*, a gene catalyzing proline synthesis in oriental hybrid lily Sorbonne: molecular modelling and expression analysis. *Bot. Stud.* 58 (1), 10. doi: 10.1186/s40529-017-0163-0

Wang, Y., Tang, H., DeBarry, J. D., Tan, X., Li, J., Wang, X., et al. (2012). MCScanX: a toolkit for detection and evolutionary analysis of gene synteny and collinearity. *Nucleic Acids Res.* 40 (7), e49. doi: 10.1093/nar/gkr1293

Wang, P., Wang, Z., Guan, L., Muhammad, S. H., Maazullah, N., Yuan, Y., et al. (2022). Versatile physiological functions of the nudix hydrolase family in berry

development and stress response in grapevine. *J. Integr. Agriculture.* 21, 91–112. doi: 10.1016/S2095-3119(20)63490-6

Xi, L., Xu, K., Qiao, Y., Qu, S., Zhang, Z., and Dai, W. (2011). Differential expression of ferritin genes in response to abiotic stresses and hormones in pear (*Pyrus pyrifolia*). *Mol. Biol. Rep.* 38, 4405–4413. doi: 10.1007/s11033-010-0568-2

Xue, X., Liu, A., and Hua, X. (2009). Proline accumulation and transcriptional regulation of proline biosynthesis and degradation in *Brassica napus*. *BMB Rep.* 42, 28–34. doi: 10.5483/bmbrep.2009.42.1.028

Yang, S., Bai, M., Hao, G., Zhang, X., Guo, H., and Fu, B. (2021b). Transcriptome survey and expression analysis reveals the adaptive mechanism of 'Yulu xiang' pear in response to long-term drought stress. *PloS One* 16, e0246070. doi: 10.1371/journal.pone.0246070

Yang, D., Ni, R., Yang, S., Pu, Y., Qian, M., Yang, Y., et al. (2021a). Functional characterization of the *Stipa purpurea P5CS* gene under drought stress conditions. *Int. J. Mol. Sci.* 22, 9599. doi: 10.3390/ijms22179599

Yoshiba, Y., Kiyosue, T., Katagiri, T., Ueda, H., Mizoguchi, T., Yamaguchi-Shinozaki, K., et al. (1995). Correlation between the induction of a gene for delta 1-pyrroline-5-carboxylate synthetase and the accumulation of proline in *Arabidopsis thaliana* under osmotic stress. *Plant J.* 7, 751–760. doi: 10.1046/j.1365-313x.1995.07050751.x

Yu, F., Liang, K., Fang, T., Zhao, H., Han, X., Cai, M., et al. (2019). A group VII ethylene response factor gene, *ZmEREB180*, coordinates waterlogging tolerance in maize seedlings. *Plant Biotechnol. J.* 17 (12), 2286–2298. doi: 10.1111/pbi.13140

Zhang, H., Huo, Y., Xu, Z., Guo, K., Wang, Y., Zhang, X., et al. (2020). Physiological and proteomics responses of nitrogen assimilation and glutamine/glutamine family of amino acids metabolism in mulberry (*Morus alba* l.) leaves to NaCl and $NaHCO_3$ stress. *Plant Signal Behav.* 15 (10), 1798108. doi: 10.1080/15592324.2020.1798108

Zhang, C. S., Lu, Q., and Verma, D. P. S. (1995). Removal of feedback inhibition of Δ1-pyrroline-5-carboxylate synthetase, a bifunctional enzyme catalyzing the first two steps of proline biosynthesis in plants. *J. Biol. Chem.* 270, 20491–20496. doi: 10.1074/jbc.270.35.20491

Zhu, J. K. (2001). Plant salt tolerance. *Trends Plant Sci.* 6, 66–71. doi: 10.1016/S1360-1385(00)01838-0

Zhu, X. Y., Li, X. P., Zou, Y., Chen, W. X., and Lu, W. J. (2012). Cloning, characterization and expression analysis of Δ1-pyrroline-5-carboxylate synthetase (P5CS) gene in harvested papaya (*Carica papaya*) fruit under temperature stress. *Food Res. Int.* 49 (1), 272–279. doi: 10.1016/j.foodres.2012.08.003

frontiers | Frontiers in Plant Science

TYPE Original Research
PUBLISHED 29 November 2022
DOI 10.3389/fpls.2022.1089420

OPEN ACCESS

EDITED BY
Chao Li,
Northwest A&F University, China

REVIEWED BY
Jiadong He,
Université Catholique de Louvain, Belgium
Yuejun He,
Guizhou University, China

*CORRESPONDENCE
Qiang-Sheng Wu
wuqiangsh@163.com
Yong-Jie Xu
498674563@qq.com

SPECIALTY SECTION
This article was submitted to Plant Abiotic Stress, a section of the journal Frontiers in Plant Science

RECEIVED 04 November 2022
ACCEPTED 16 November 2022
PUBLISHED 29 November 2022

CITATION
Ma W-Y, Qin Q-Y, Zou Y-N, Kuča K, Giri B, Wu Q-S, Hashem A, Al-Arjani A-BF, Almutairi KF, Abd_Allah EF and Xu Y-J (2022) Arbuscular mycorrhiza induces low oxidative burst in drought-stressed walnut through activating antioxidant defense systems and heat shock transcription factor expression. *Front. Plant Sci.* 13:1089420. doi: 10.3389/fpls.2022.1089420

Arbuscular mycorrhiza induces low oxidative burst in drought-stressed walnut through activating antioxidant defense systems and heat shock transcription factor expression

Wen-Ya Ma[1], Qiu-Yun Qin[1], Ying-Ning Zou[1], Kamil Kuča[2], Bhoopander Giri[3], Qiang-Sheng Wu[1,2]*, Abeer Hashem[4], Al-Bandari Fahad Al-Arjani[4], Khalid F. Almutairi[5], Elsayed Fathi Abd_Allah[5] and Yong-Jie Xu[6,7]*

[1]Tibet Plateau Walnut Industry Research Institute/College of Horticulture and Gardening, Yangtze University, Jingzhou, Hubei, China, [2]Department of Chemistry, Faculty of Science, University of Hradec Kralove, Hradec Kralove, Czechia, [3]Department of Botany, Swami Shraddhanand College, University of Delhi, New Delhi, India, [4]Botany and Microbiology Department, College of Science, King Saud University, Riyadh, Saudi Arabia, [5]Plant Production Department, College of Food and Agricultural Sciences, King Saud University, Riyadh, Saudi Arabia, [6]Hubei Key Laboratory of Economic Forest Germplasm Improvement and Resources Comprehensive Utilization, Hubei Collaborative Innovation Center for the Characteristic Resources Exploitation of Dabie Mountains, Huanggang Normal University, Huanggang, China, [7]Hubei Academy of Forestry, Wuhan, China

Arbuscular mycorrhizal fungi (AMF) have important roles in enhancing drought tolerance of host plants, but it is not clear whether and how AMF increase drought tolerance in walnut (*Juglans regia*). We hypothesized that AMF could activate antioxidant defense systems and heat shock transcription factors (*Hsfs*) transcription levels to alleviate oxidative damage caused by drought. The walnut variety 'Liaohe No. 1' was inoculated with *Diversispora spurca* and exposed to well-watered (WW, 75% of the maximum soil water capacity) and drought stress (DS, 50% of the maximum soil water capacity) for 6 weeks. Plant growth, antioxidant defense systems, and expressions of five *JrHsfs* in leaves were studied. Such drought treatment inhibited root mycorrhizal colonization, while plant growth performance was still improved by AMF inoculation. Mycorrhizal fungal inoculation triggered the increase in soluble protein, glutathione (GSH), ascorbic acid (ASC), and total ASC contents and ascorbic peroxidase and glutathione reductase activities, along with lower hydrogen peroxide (H_2O_2), superoxide anion radical ($O_2^{\bullet-}$), and malondialdehyde (MDA) levels, compared with non-inoculation under drought. Mycorrhizal plants also recorded higher peroxidase, catalase, and superoxide dismutase activities than non-mycorrhizal plants under drought. The expression of *JrHsf03*, *JrHsf05*, *JrHsf20*, *JrHsf22*, and *JrHsf24* was up-regulated under WW by AMF, while the

expression of *JrHsf03*, *JrHsf22*, and *JrHsf24* were up-regulated only under drought by AMF. It is concluded that *D. spurca* induced low oxidative burst in drought-stressed walnut through activating antioxidant defense systems and part *Hsfs* expressions.

KEYWORDS

arbuscular mycorrhiza, heat shock transcription factor, reactive oxygen species, symbiosis, water stress

Introduction

Walnuts (*Juglans regia* L.) are an important nut crop in the world, with the second highest yield of nut crops (Behrooz et al., 2019). Walnut kernels can not only be consumed directly, but also include a large amount of unsaturated fatty acids and a variety of active ingredients (Luca et al., 2018). Among them, the high content of polyphenols in walnuts makes them effective as antioxidants and free radical scavengers (Ebrahimzadeh et al., 2013). Walnut trees are influenced by soil drought stress (DS) because of their high water demand (Vahdati et al., 2009).

Arbuscular mycorrhizal fungi (AMF) establish symbiotic associations with various plants (Wu et al., 2013). AMF can help the host to acquire nutrients from the soil, especially difficult-to-move elements, and thus increase plant growth (Ho-Plágaro et al., 2021). Studies indicated that AMF inoculation enhanced drought tolerance of host plants through various underlying mechanisms, as outlined by Cheng et al. (2021). One important mechanism is the ability of AMF to mitigate oxidative burst by enhancing antioxidant defense systems of the host (Zou et al., 2021). The population of AMF has been observed in rhizosphere of walnuts (Ma et al., 2021), and AMF inoculation contributed to walnut growth (Wang, 2015; Huang et al., 2020). Combining AMF (*Glomus fasciculatus*) inoculation with foliar fertilization would increase plant growth as well as the survival of walnuts (Ponder, 1984). In addition, AMF (*Diversispora spurca*) inoculation accelerated nutrient uptake of walnuts such as P and K (Huang et al., 2020; Thioye et al., 2022). Potted studies had shown the role of AMF in drought tolerance of walnut plants. Behrooz et al. (2019) reported that AMF (*G. mosseae* and *G. etunicatum*) significantly increased contents of some metabolites (e.g., total phenols and proline) in walnut plants under DS. Moreover, AMF also promoted plant growth and nutrient acquisition in walnut plants (Thioye et al., 2022), and thereby improved the adaption of walnut plants in response to DS. The study of Liu et al. (2021) showed the an endophytic fungus (*Serendipita indica*) triggered the enhancement in superoxide dismutase (SOD), catalase (CAT), and peroxidase (POD) activities in walnut plants under soil water deficit, accompanied by the reduction of superoxide anion free radical ($O_2^{\bullet-}$) and hydrogen peroxide (H_2O_2) levels, thus alleviating drought-induced oxidative burst. These results suggested that symbiotic fungi can alleviate oxidative burst in walnut under drought by activating antioxidant defense systems. However, it is unclear whether the dominant AMF strain, *D. spurca* (Huang et al., 2020), has similar functions in response to drought as *S. indica*.

Heat shock transcription factors (*Hsfs*) are key components of signal transduction and also regulate the response of genes to stress (Si et al., 2021). Moreover, *Hsfs* members such as *SPL7*, *HsfA1b*, *HsfA4a*, and *HsfA8* are involved in the homeostasis of reactive oxygen species (ROS) under DS conditions (Hoang et al., 2019). In addition, *Hsfs* can sense ROS in plant cells, and *Hsfs* are an important regulator to control oxidative burst under stress (Miller et al., 2008).

Although AMF has been shown to enhance drought tolerance in many plants, it is not clear whether and how a dominant strain, *D. spurca*, enhances drought tolerance in walnuts. We hypothesized that AMF could activate antioxidant defense systems and *Hsfs* transcription levels to alleviate oxidative damage caused by drought. Hence, the present study was performed to analyze effects of *D. spurca* on plant growth, antioxidant enzyme activities, antioxidant concentrations, transcription levels of *Hsfs*, ROS levels, and degree of membrane lipid peroxidation in leaves of walnuts subjected to DS.

Materials and methods

Plant culture, mycorrhizal inoculation, and soil water regimes

Walnut seeds of 'Liaohe No. 1' variety were pre-disinfected with 75% ethanol and germinated in autoclaved sands at room temperature. Subsequently, the seedlings having four leaves were transplanted into 2.4-L plastic pots containing 2.05 kg autoclaved mixture of sand and soil in the volume ratio of 1:

3. Mycorrhizal fungal inoculums were applied to the rhizosphere of walnut seedlings at the time of plant transplanting. The AMF-inoculated treatment (+AMF) received 150 g inoculum (23 spores/g) of *D. spurca* per pot, and the non-AMF-inoculated treatment (-AMF) received both 2 mL of 25 μm of inoculum filtrates and 150 g of autoclaved mycorrhizal inoculum per pot. The origin and propagation of the *D. spurca* strain were described in detail by Huang et al. (2020).

After plant transplanting, two soil moisture regimes (75% and 50% of the maximum soil water capacity) were performed according to the result of Li et al. (2020). The water content of potted soil was controlled at 75% of the maximum soil water capacity (well-watered, WW). After 7 weeks, half of the treated plants continued to maintain under WW conditions, and the other half of the treated plants was adjusted to 50% of the maximum soil water capacity (DS). The soil moisture was monitored by daily weighing, and the reduced water was supplemented immediately, so as to maintain the designed soil moisture condition. Such DS treatment was maintained for 6 weeks, and the seedlings were harvested. All the plants were grown in a greenhouse with a light density of 1360 lux, a relative air humidity of 66%, and a temperature of 28°C/22°C (day/night).

Experimental design

The experiment was a completely randomized block design consisting of two factors: (i) *D. spurca* inoculation (+AMF) and non-inoculation (-AMF); and (ii) soil moisture regimes with WW and DS. A total of four treatments in the experiment were arranged, coupled with five replicates (two pots as a replicate) per treatment.

Measurements of mycorrhizal development and plant growth

Stem diameter, plant height, and leaf number per plant were measured before harvesting. Shoot and root biomass was weighed after the harvest. Root mycorrhizas were stained using the trypan blue described by Phillips and Hayman (1970). Mycorrhizal fungal colonization degree (%) = (mycorrhizal colonized root length/total length of root segments examined) × 100. Hyphal length in the soil was determined as per the method of Bethlenfalvay and Ames (1987).

Measurements of ROS levels and degree of membrane lipid peroxidation in leaves

Malondialdehyde (MDA, an indicator of the degree of membrane lipid peroxidation) concentrations in leaves were assayed by the thiobarbituric acid colorimetry (Sudhakar et al., 2001). H_2O_2 and $O_2^{\bullet-}$ levels were assayed by the 1 mol/L KI colorimetric method and the hydroxylamine reaction, respectively (Li et al., 2022).

Measurements of non-enzymatic antioxidant concentrations in leaves

Soluble protein concentrations in leaves were measured as per the protocol described by Bradford (1976). Ascorbic acid (ASC) and glutathione (GSH) in leaves were extracted by grinding 0.15 g of leaf samples with 6 mL of 5% trichloroacetic acid into a homogenate and centrifuging at 15,000×*g* for 10 min (Wu et al., 2006). ASC and GSH concentrations in the supernatant were measured according to the method described by Li (2009). In addition, the 1 mL supernatant was incubated with 0.5 mL of 60 mmol/L dithiothreitol for 10 min to reduce the dehydroascorbic acid (DHA). The reaction solution was then incubated with 5% trichloroacetic acid, 0.4% phosphoric acid, 0.5% bathophenanthroline, and 0.03% $FeCl_3$, and the absorbance at 534 nm was measured for total ascorbic acid (TASC) concentrations. The DHA content was obtained by subtracting ASC from TASC.

Measurements of antioxidant enzyme activities in leaves

Extraction and activity of CAT were carried out by UV spectrophotometry (Li et al., 2022). POD activity was determined using the guaiacol (0.05 mol/L) method (Li et al., 2022). Ascorbate peroxidase (APX) and glutathione reductase (GR) activities were assayed by the protocol outlined by Wu et al. (2006). Fe-SOD, Mn-SOD, and Cu/Zn-SOD activities were measured by the Enzyme-Linked Immunosorbent assay using the corresponding kit (ml902210, mll614100, and ml201168) (Shanghai Enzyme-link Biotechnology Co., Ltd., Shanghai, China), on the basis of the user manual.

Measurements of expression levels of *JrHsfs* in leaves

Based on the identification of *Hsfs* in walnuts by Liu et al. (2020), the sequence of walnut *Hsfs* genes (*JrHsf03*, *JrHsf05*, *JrHsf20*, *JrHsf22*, and *JrHsf24*) was extracted from the walnut genome (https://www.ncbi.nlm.nih.gov/genome/?term=txid2249226 [orgn]). Primer sequences (Table 1) were designed using Primer premier 5.0. The TaKaRa MiniBEST plant RNA kits (9769; Takara, Dalian, China) were used to extract leaf total RNA according to the user manual. After

TABLE 1 Specific primer sequences of genes used for qRT-PCR.

Gene name	Gene ID	Primer sequences (5'→3')
JrHsf03	LOC109009449	F: TGCTTATGATGTCATGGCAGAGA
		R: TCCTCCTCTAAATCCACCCAAA
JrHsf05	LOC108997276	F: AGACTCCCCAATCAAGAGGAAAG
		R: CCGCAGCAAGGTTTTAGCA
JrHsf20	LOC108992254	F: AGGTTGTTCTTGAGCTTTCGATG
		R: GGTAGGTTTTGGTGAGGAATGG
JrHsf22	LOC109011524	F: GAACGGGGTTTGTAGTATGGTCTC
		R: GACACTTGGCTCGCACTTCTT
JrHsf24	LOC108989320	F: GAAGACGTACATGCTGGTGGAG
		R: TATGCTTGAAAAGTGTAGGGAGGAG
18S-rRNA	LIHL01052714.1_7	F: GGTCAATCTTCTCGTTCCCTT
		R: TCGCATTTCGCTACGTTCTT

checking the integrity and concentration, the RNA was reversely transcribed into cDNA using the PrimeScript™ RT reagent kits with gDNA Eraser (RR047A; Takara, Dalian, China). The cDNA was used as a template for qRT-PCR amplification using 18S-rRNA as a house-keeping gene. Prior to performing qRT-PCR, the selected primers and melting curves had been checked to determine the reliability of the relative quantification results. Real-time fluorescence quantitative expression analysis was performed using a fluorescent dye method with three biological replicates of each treatment, and relative expression of genes was calculated using the $2^{-\Delta\Delta Ct}$ method (Livak and Schmittgen, 2001).

Data analysis

Statistical analysis was performed with two-factor analysis of variance, based on the SAS software 8.1v (SAS Institute Inc., Cary, NC, USA). The Duncan's multiple range test at the 0.05% level was used to compare the significant difference among treatments.

Results

Root mycorrhizal colonization

No mycorrhiza was observed in the roots of walnut inoculated without *D. spurca*, and the degree of mycorrhizal colonization on the roots of walnut inoculated with *D. spurca* ranged from 62.9% to 73.5% (Table 2). Soil water deficit significantly inhibited the degree of root mycorrhizal colonization by 14.4%, compared to WW treatment. Soil drought treatment and AMF inoculation significantly interacted on root mycorrhizal colonization.

Plant growth responses

Drought treatment obviously inhibited the growth of walnut seedlings, while mycorrhizal introduction improved plant growth (Table 2). *D. spurca* inoculation only significantly increased plant height under WW by 29.3%, whereas it increased plant height, stem diameter, and leaf number per plant under DS significantly by 36.1%, 47.2%, and 14.4%, respectively. AMF-inoculated seedlings exhibited 25.2% significantly higher biomass under WW and 29.4% higher biomass under DS, compared with non-inoculated seedlings. A significant interaction between drought treatment and mycorrhizal inoculation occurred on biomass production.

ROS levels

Drought treatment significantly induced an increase in leaf H_2O_2 and $O_2^{\bullet-}$ concentrations by 20.3% and 152.6% in

TABLE 2 Effects of AMF (*Diversispora spurca*) on root mycorrhizal colonization and plant growth performance of walnut under well-watered (WW) and drought stress (DS).

Treatments	Root mycorrhizal colonization (%)	Plant height(cm)	Stem diameter(mm)	Leaf number per plant	Biomass (g/plant)
WW+AMF	73.5 ± 3.8a	47.2 ± 4.8a	6.7 ± 0.4a	36.6 ± 3.2a	34.8 ± 1.6a
WW-AMF	0.0 ± 0.0c	36.5 ± 5.6b	6.0 ± 0.9ab	34.6 ± 3.0a	27.8 ± 2.0b
DS+AMF	62.9 ± 4.1b	36.2 ± 2.2b	5.3 ± 0.4b	33.4 ± 2.8a	27.7 ± 4.3b
DS-AMF	0.0 ± 0.0c	26.6 ± 7.8c	3.6 ± 0.8c	29.2 ± 2.6b	21.4 ± 1.7c
Significance					
DS	**	**	**	**	**
AMF	**	**	**	*	**
DS×AMF	**	NS	NS	NS	*

Data (means ± SD, n = 4) followed by different letters among treatments indicate significant differences at the 5% level. * $P < 0.05$; ** $P < 0.01$; NS, not significant at the 0.05 level.

uninoculated plants and by 32.2% and 98.7% in inoculated plants (Figures 1A, B). However, the inoculated plants with *D. spurca* recorded significantly lower leaf H_2O_2 and $O_2^{\bullet-}$ concentrations by 44. 5% and 41.7% under WW and by 27.7% and 80.2% under DS, respectively, compared with the uninoculated plants. A significant interaction between drought treatment and AMF inoculation occurred on $O_2^{\bullet-}$ concentrations (Table 3).

Degree of membrane lipid peroxidation

The DS treatment significantly promoted MDA levels in both inoculated and uninoculated plants by 29.7% and 157.6%, respectively, relative to the WW (Figure 2). On the other hand, inoculated walnut plants showed significantly lower MDA levels by 13.8% under WW and 126.1% under DS. There was a significant interaction between drought treatment and AMF inoculation for MDA levels (Table 3).

Non-enzymatic antioxidant concentrations

Compared to the WW treatment, the DS treatment triggered a distinct decrease in soluble protein and DHA concentrations in inoculated and uninoculated plants, but induced an increase in GSH, ASC and TASC concentrations in inoculated and uninoculated plants (Figures 3A–E). Under WW conditions, soluble protein, ASC and TASC concentrations were increased by 40.54%, 141.57% and 3.79% in inoculated plants, compared to uninoculated plants (Figures 3A, C, E). Under DS conditions, soluble protein, GSH, ASC and TASC concentrations of inoculated plants were increased by 112.50%, 9.52%, 91.89% and 4.17%, compared to that of uninoculated plants (Figures 3A, B, C, E). AMF inoculation caused the decrease in DHA concentrations by 52.46% and 110.78% under WW and DS, respectively, compared with non-AMF inoculation (Figure 3D). No significant interaction between drought treatment and AMF inoculation occurred on non-enzymatic antioxidants (Table 3).

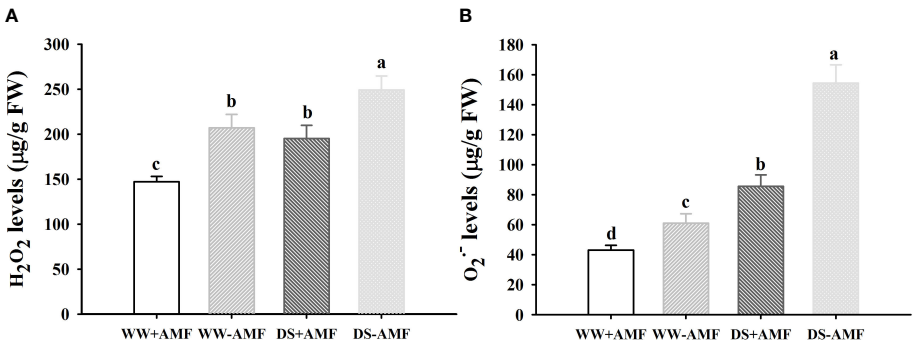

FIGURE 1
Effect of AMF (*Diversispora spurca*) on leaf H_2O_2 **(A)** and $O_2^{\bullet-}$ **(B)** concentrations of walnut under well-watered (WW) and drought stress (DS). Data (means ± SD, n = 4) are significantly different ($P < 0.05$) if followed by different letters above the bars.

TABLE 3 Significance of variables between AMF and non-AMF colonized walnut seedlings grown in well-watered (WW) and drought stress (DS).

Variables	DS	AMF	DS×AMF	Variables	DS	AMF	DS×AMF
H_2O_2	**	**	NS	Cu/Zn-SOD	**	**	NS
$O_2^{\bullet-}$	**	**	**	CAT	**	**	**
MDA	**	**f	**	POD	**	**	NS
Soluble protein	**	**	NS	APX	**	**	*
GSH	**	**	NS	GR	**	**	NS
ASC	**	**	NS	*JrHsf03*	**	**	NS
DHA	**	**	NS	*JrHsf05*	NS	**	**
TASC	**	**	NS	*JrHsf20*	**	**	NS
Mn-SOD	**	**	NS	*JrHsf22*	**	**	**
Fe-SOD	**	**	**	*JrHsf24*	**	**	NS

NS, not significant at the 0.05 level. *, P <0.05; **, P <0.01.

10.3389/fpls.2022.1089420

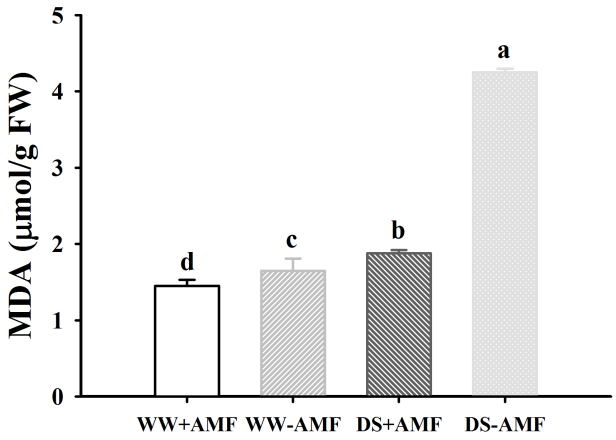

FIGURE 2
Effect of AMF (*Diversispora spurca*) on leaf malondialdehyde (MDA) concentrations of walnut under well-watered (WW) and drought stress (DS). Data (means ± SD, n = 4) are significantly different ($P < 0.05$), if followed by different letters above the bars.

Antioxidant enzyme activities

The DS treatment significantly increased various antioxidant enzyme activities compared to WW treatment, independent of AMF inoculation or not (Figures 4A–E). In addition, under WW, Mn-SOD, Fe-SOD, CAT, POD, APX and GR activities were increased by 8.8%, 8.9%, 570.2%, 142.3%, 98.7% and 76.0% in inoculated plants compared to uninoculated plants, respectively; under DS, Mn-SOD, Cu/Zn-SOD, CAT, POD, APX and GR activities were increased by 13.8%, 1.7%, 340.4%, 80.5%, 106.3% and 77.2% in inoculated plants compared to uninoculated plants, respectively. A significant interaction between DS and AMF treatment occurred on Fe-SOD, CAT, and APX activities (Table 3).

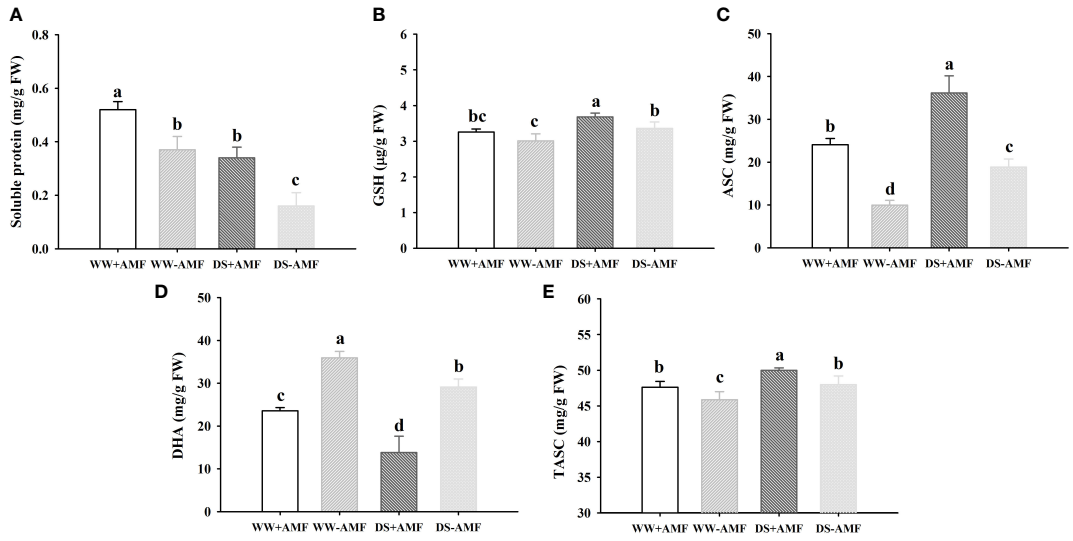

FIGURE 3
Effect of AMF (*Diversispora spurca*) on leaf soluble protein **(A)**, GSH **(B)**, ASC **(C)**, DHA **(D)**, and TASC **(E)** concentrations of walnut under well-watered (WW) and drought stress (DS). Data (means ± SD, n = 4) are significantly different ($P < 0.05$), if followed by different letters above the bars.

10.3389/fpls.2022.1089420

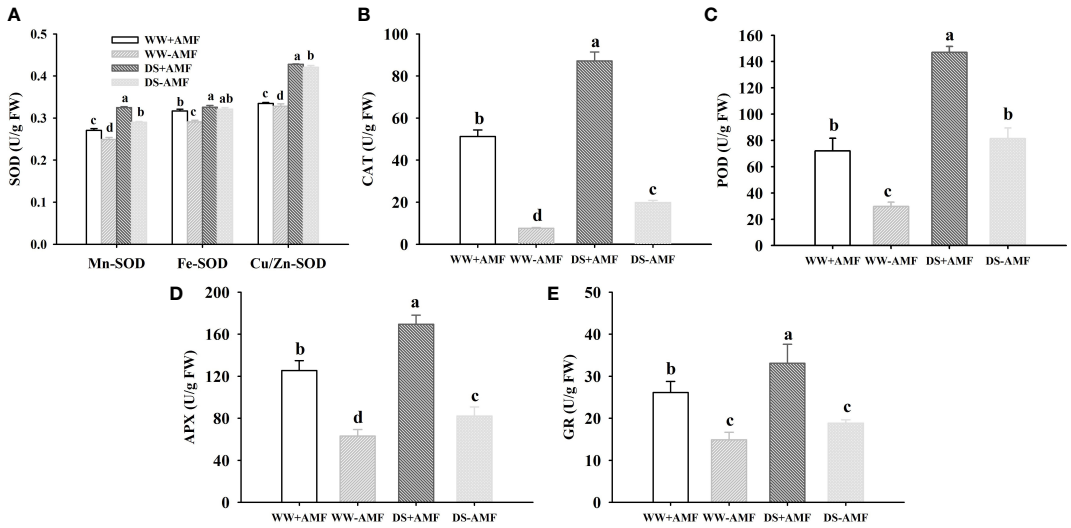

FIGURE 4
Effect of AMF (*Diversispora spurca*) on leaf superoxide dismutase (SOD) **(A)**, catalase (CAT) **(B)**, peroxidase (POD) **(C)**, ascorbate peroxidase (APX) **(D)**, and glutathione reductase (GR) **(E)** activities of walnut under well-watered (WW) and drought stress (DS). Data (means ± SD, $n = 4$) are significantly different ($P < 0.05$), if followed by different letters above the bars.

Hsfs expression levels in leaves

Drought treatment up-regulated expressions of *JrHsf03*, *JrHsf20*, *Jrhsf22* and *JrHsf24* in inoculated and uninoculated walnut plants, compared to WW treatment (Figure 5). However, DS also induced *JrHsf05* expressions in uninoculated plants, but down-regulated *JrHsf05* expressions in inoculated plants. AMF inoculation significantly up-regulated expressions of *JrHsf03*, *JrHsf05*, *JrHsf20*, *JrHsf22*, and *JrHsf24* under WW by 4.42-fold, 2.57-fold, 3.15-fold, 2.60-fold, and 1.95-fold, respectively, compared to non-AMF treatment; under DS, AMF up-regulated expressions of *JrHsf03*, *Jrhsf22*, and *JrHsf24* by 1.32-

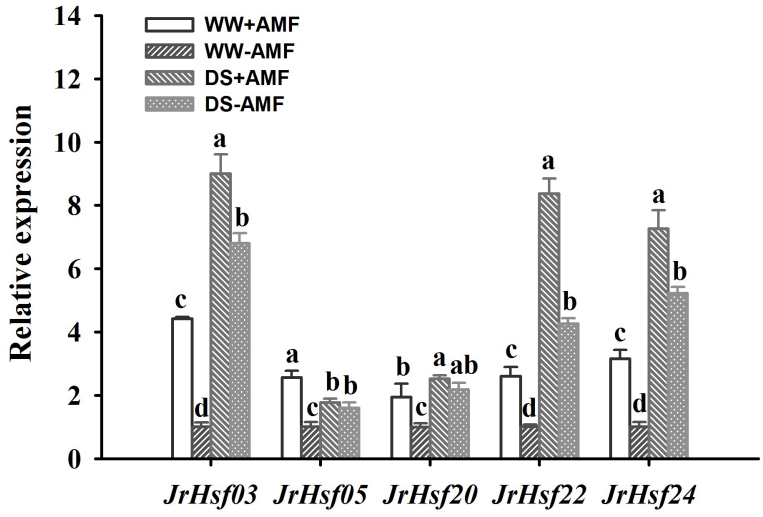

FIGURE 5
Effect of AMF (*Diversispora spurca*) on *Hsfs* gene expression levels in leaves of walnut under well-watered (WW) and drought stress (DS). Data (means ± SD, $n = 3$) are significantly different ($P < 0.05$), if followed by different letters above the bars.

fold, 1.96-fold, and 1.39-fold, respectively, compared to non-AMF inoculation, with no effect on the expression of *JrHsf05* and *JrHsf20*. A significant interaction between drought treatment and AMF inoculation occurred on *JrHsf05* and *JrHsf22* expression (Table 3).

Discussion

Soil drought inhibited mycorrhizal colonization, while AMF still promoted walnut growth under drought

Our study indicated that the DS treatment reduced the degree of root colonization by *D. spurca* in walnut seedlings. Similar result was reported in trifoliate orange (Liang et al., 2021) and peanut (Bi et al., 2021). Such reduction of mycorrhizal colonization under DS is due to the decrease in roots, host's carbohydrates, and root exudates by DS, thus inhibiting spore germination and mycorrhizal colonization (Tyagi et al., 2017). Inoculation with *D. spurca* significantly promoted plant growth performance of walnut seedlings, which is attributed to the fact that AMF enhanced the uptake of mineral nutrients such as P, Zn and Cu, along with water absorption by mycorrhizal extraradical hyphae (Cheng et al., 2021).

AMF activated enzymatic and non-enzymatic antioxidant defense systems to mitigate oxidative burst under drought

Under stress, plants produce electron overflow in chloroplasts, mitochondria, peroxisomes, and plasma membranes, and thus lead to excess accumulation of ROS such as H_2O_2 and $O_2^{\bullet-}$, which thus triggers oxidative damage (Cao et al., 2022). This study showed that the soil drought triggered oxidative burst (H_2O_2 and $O_2^{\bullet-}$) in leaves of mycorrhizal and non-mycorrhizal walnut plants, thus increasing the degree of membrane lipid peroxidation, in accordance with increased MDA levels. However, *D. spurca*-inoculated walnut plants presented significantly lower ROS and MDA levels than uninoculated plants, suggesting that inoculated plants suffered relatively lower oxidative damage than uninoculated plants (Abd_Allah et al., 2015). This finding is consistent with that on trifoliate orange (Zhang et al., 2020) and lettuce (Kohler et al., 2009).

Soil drought causes oxidative damage to plants, while plants also have enzymatic (e.g., SOD, POD, and CAT) and non-enzymatic (e.g., soluble protein, ASC, and GSH) antioxidant defense systems to reduce ROS levels (Verma et al., 2019). Soluble proteins are involved in the metabolic process and are related to the water holding capacity of cells and the protective role in cell membranes (Lu et al., 2012). Our study showed that soil drought treatment inhibited soluble protein concentrations in walnut leaves, while AMF inoculation promoted soluble protein concentrations, suggesting that the inoculated plants had stronger water retention of cells and protective effect on cell membranes than uninoculated plants. Cao et al. (2022) found that *Piriformospora indica*, but not *G. versiforme*, also significantly increased leaf and root soluble protein concentrations in Satsuma mandarin, under cold temperature, but not favorable temperature conditions, implying that AMF-mediated changes in soluble protein depend on AMF species, host genotypes, and environmental stresses.

ASC-GSH cycle regulates the balance of redox state of plant cells and is an important pathway for ROS removal (Miller et al., 2010). Meanwhile, GSH maintains cell function and regulates the state of sulfhydryl groups, and ASC as an electron donor participates in substance transformation (Noctor, 2006). In this cycle, ASC is first oxidized to monohydroascorbic acid (MDHA), in which APX utilizes ASC as an electron donor to remove H_2O_2 (Wang et al., 2012). In our study, inoculated walnut plants under two soil moisture conditions showed significantly higher ASC and TASC concentrations and stronger APX activities than uninoculated plants, implying that AMF activates ASC to scavenge more H_2O_2 of the host caused by drought. In addition, AMF inoculation also increased GSH concentrations of walnut plants while decreased DHA concentrations under DS. It is known that MDHA can undergo disproportionation reaction to produce ASC and DHA (Qadir et al., 2022). DHA uses GSH as the substrate to generate GSSG and ASC under the action of dehydroascorbate reductase, and GSSG further combines with NAD(P)H as an electron donor to generate GSH under the action of GR (Li et al., 2010). Lower DHA levels and higher GSH levels and GR activity in mycorrhizal plants under DS mean that mycorrhizal plants convert more DHA to ASC and modulate more accumulation of GSH under the action of GR, as compared with non-mycorrhizal plants. Al-Arjani et al. (2020) also reported the elevation in GR and APX activities in *Ephedra foliata* plants after inoculated with AMF under DS. Saroy and Garg (2021) also observed that *Rhizoglomus intraradices* distinctly increased APX and GR activities and GSH, TASC, ASC, and GSSH concentrations in two pigeon pea genotypes under Ni stress. *Glomus viscosum*-inoculated *Cynara scolymus* plants also exhibited higher ASC and GSH concentrations than non-inoculated plants, along with elevated APX activities, for resisting the fungal pathogen *Verticillium dahliae* (Villani et al., 2021). These results indicate that mycorrhizal plants have a stronger ASC-GSH cycle to remove more H_2O_2 induced by stresses than non-mycorrhizal plants, thus maintaining lower oxidative damage.

In ROS scavenging enzymes, SOD catalyzes $O_2^{\bullet-}$ to H_2O_2; generated H_2O_2 is then removed by POD and CAT (Qadir et al., 2022). In our study, three SODs, CAT, and POD activities were enhanced by DS, indicating that the enzymatic antioxidant defense system in walnut plants was activated in response to drought. Additionally, mycorrhizal walnut plants recorded higher POD, CAT, Mn-SOD, and Zn-SOD activities than non-mycorrhizal plants under two soil moisture regime conditions. Similar results were reported in *Citrus sinensis* inoculated with three different AMF species (Li et al., 2022). He et al. (2020) further found the induced expression of *PtMn-SOD*, *PtCAT1*, and *PtPOD* genes in trifoliate orange by *F. mosseae* under DS. These results suggest that AMF enhanced enzymatic antioxidant defense system to mitigate oxidative burst in response to DS.

AMF activated expressions of some Hsfs members such as *JrHsf03*, *JrHsf22*, and *JrHsf24* under drought

Our study revealed that soil drought induced transcriptional levels of *JrHsf03*, *JrHsf20*, *Jrhsf22*, and *JrHsf24* in walnut plants, independent on mycorrhizal presence. It suggests that *Hsfs* of walnut can respond to DS, not limited to heat stress, which is consistent with the results of Liu et al. (2020) in *Hsfs* of walnut under DS, heat stress, and salt stress. Similar responses of *Hsfs* to DS were also observed in mulberry (Zhai and Zhu, 2021) and arabidopsis (Tan et al., 2015). Moreover, We also firstly observed that *JrHsf03*, *JrHsf05*, *JrHsf20*, *JrHsf22*, and *JrHsf24* were up-regulated by AMF inoculation under WW, while only *JrHsf03*, *JrHsf22*, and *JrHsf24* were induced by AMF inoculation under DS, indicating that AMF-mediated response of *JrHsfs* depends on *Hsfs* types. It is not clear whether *JrHsf03*, *JrHsf22*, and *JrHsf24* are specifically induced by AMF, which needs to be confirmed by additional studies. However, Gaude et al. (2012) reported the inhibited expression of *HsfB3* in arbuscule-containing cortical cells of mycorrhizal roots versus cortical cells of non-mycorrhizal roots with 3.2-fold after three weeks of inoculation in roots of *Medicago truncatula* plants. These heat shock factors were suppressed during the initial mycorrhizal colonization (Gaude et al., 2012). Nevertheless, our study was performed for 13 weeks along with soil drought, mycorrhizal colonization had already been established, and thus this suppression may be relieved. In addition, *Hsfs* members are redox-sensitive transcription factors sensing ROS, transducing and amplifying the ROS signal by various proteins and transcription factors (e.g., WRKY) (Miller et al., 2008). In walnut plants, *Hsfs* may be associated with the signaling pathways of abscisic acid and Ca^{2+} that regulate ROS production (Mohanta et al., 2018; Liu et al., 2020). Hence, it is concluded that AMF activated some *Hsfs* members such as *JrHsf03*, *JrHsf22*, and *JrHsf24* to regulate ROS production, but additional evidence needs to be presented. In addition, most of *Hsfs* members are expressed highly in roots than other tissues (Dossa et al., 2016), and mycorrhizal colonization firstly occurs in roots. More work needs to focus on the responsive pattern of root *Hsfs* to AMF colonization under drought, how AMF-initiated *Hsfs* trigger the antioxidant defense system, and whether AMF's *Hsfs* are also involved in this response.

Conclusion

In short, our study confirmed that an arbuscular mycorrhizal fungus, *D. spurca*, could promote growth performance of walnut plants exposed to DS. In the meantime, *D. spurca* activated antioxidant defense systems (e.g., enzymatic defense system and ASC-GSH cycle) and transcription levels of three *Hsfs* to alleviate oxidative burst. This study firstly provides insights into the role of AMF-regulated responses of *Hsfs* in possibly mitigating ROS burst. However, future work needs to focus on how mycorrhizal fungi initiate host or fungal *Hsfs* to mitigate oxidative burst under drought.

Data availability statement

The original contributions presented in the study are included in the article/supplementary material. Further inquiries can be directed to the corresponding authors.

Author contributions

W-YM, Y-JX, and Q-SW designed the experiment. W-YM, Q-YQ, and Y-NZ prepared the materials for the experiment. W-YM, Q-YQ, Y-JX, and Y-NZ conducted the experiment. W-YM and Q-YQ analyzed the data. W-YM wrote the manuscript. KK, BG, AH, A-BA-A, KA, EA, and Q-SW revised the manuscript. All authors contributed to the article and approved the submitted version.

Funding

This work was supported by the Open Fund in Hubei Key Laboratory of Economic Forest Germplasm Improvement and Resources Comprehensive Utilization, Hubei Collaborative Innovation Center for the Characteristic Resources Exploitation of Dabie Mountains, Huanggang Normal University (202019604),

the Hubei Province '14th Five-Year' Major Science and Technology Aid Tibet project (SCXX-XZCG-22016), and 2021 Undergraduate Innovation and Entrepreneurship Training Program of Yangtze University (Yz2021328). The authors are grateful to their sincere appreciation to the Researchers Supporting Project Number (RSP-2021/134), King Saud University, Riyadh, Saudi Arabia.

Acknowledgement

This work was supported by the Open Fund in Hubei Key Laboratory of Economic Forest Germplasm Improvement and Resources Comprehensive Utilization, Hubei Collaborative Innovation Center for the Characteristic Resources Exploitation of Dabie Mountains, Huanggang Normal University (202019604), the Hubei Province '14th Five-Year' Major Science and Technology Aid Tibet project (SCXX-XZCG-22016), and 2021 Undergraduate Innovation and Entrepreneurship Training Program of Yangtze University (Yz2021328). The authors are grateful to their sincere appreciation to the Researchers Supporting Project Number (RSP-2021/134), King Saud University, Riyadh, Saudi Arabia.

Conflict of interest

The authors declare that the research was conducted in the absence of any commercial or financial relationships that could be construed as a potential conflict of interest.

Publisher's note

All claims expressed in this article are solely those of the authors and do not necessarily represent those of their affiliated organizations, or those of the publisher, the editors and the reviewers. Any product that may be evaluated in this article, or claim that may be made by its manufacturer, is not guaranteed or endorsed by the publisher.

References

Abd_Allah, E. F., Hashem, A., Alqarawi, A. A., Bahkali, A. H., and Alwhibi, M. S. (2015). Enhancing growth performance and systemic acquired resistance of medicinal plant *Sesbania sesban* (L.) merr using arbuscular mycorrhizal fungi under salt stress. *Saudi J. Biol. Sci.* 22, 274–283. doi: 10.1016/j.sjbs.2015.03.004

Al-Arjani, A. B. F., Hashem, A., and Abd_Allah, E. F. (2020). Arbuscular mycorrhizal fungi modulates dynamics tolerance expression to mitigate drought stress in *Ephedra faliata* boiss. *Saudi J. Biol. Sci.* 27, 380–394. doi: 10.1016/j.sjbs.2019.10.008

Behrooz, A., Vahdati, K., Rejali, F., Lotfi, M., Sarikhani, S., and Leslie, C. (2019). Arbuscular mycorrhiza and plant growth-promoting bacteria alleviate drought stress in walnut. *HortScience.* 54, 1087–1092. doi: 10.21273/HORTSCI13961-19

Bethlenfalvay, G. J., and Ames, R. N. (1987). Comparison of two methods for quantifying extraradical mycelium of vesicular-arbuscular mycorrhizal fungi. *Soil Sci. Soc Am. J.* 51, 834–837. doi: 10.2136/sssaj1987.03615995005100030049x

Bi, Y. L., Zhou, H. L., Ma, S. P., and Gao, Y. K. (2021). Effects of bacterial inoculation on drought tolerance and phenotypic structure of peanut: Take coal mining area of northern shaanxi as example. *J. China Coal Soc.* 46, 1936–1944. doi: 10.13225/j.cnki.jccs.ST21.0499

Bradford, M. M. (1976). A rapid and sensitive method for the quantitation of microgram quantities of protein utilizing the principle of protein-dye binding. *Anal. Biochem.* 72, 248–254. doi: 10.1016/0003-2697(76)90527-3

Cao, M. A., Zhang, F., Abd_Allah, E. F., and Wu, Q. S. (2022). Mycorrhiza improves cold tolerance of Satsuma orange by inducing antioxidant enzyme gene expression. *Biocell.* 46, 1959–1966. doi: 10.32604/biocell.2022.020391

Cheng, S., Zou, Y. N., Kuča, K., Hashem, A., Abd_Allah, E. F., and Wu, Q. S. (2021). Elucidating the mechanisms underlying enhanced drought tolerance in plants mediated by arbuscular mycorrhizal fungi. *Front. Microbiol.* 12, 809473. doi: 10.3389/fmicb.2021.809473

Dossa, K., Diouf, D., and Cissé, N. (2016). Genome-wide investigation of hsf genes in sesame reveals their segmental duplication expansion and their active role in drought stress response. *Front. Plant Sci.* 7, 1522. doi: 10.3389/fpls.2016.01522

Ebrahimzadeh, M. A., Nabavi, S. F., and Nabavi, S. M. (2013). Antihemolytic activity and mineral contents of *Juglans regia* L. flowers. *Eur. Rev. Med. Pharmaco.* 17, 1881–1883.

Gaude, N., Bortfeld, S., Duensing, N., Lohse, M., and Krajinski, F. (2012). Arbuscule-containing and non-colonized cortical cells of mycorrhizal roots undergo extensive and specific reprogramming during arbuscular mycorrhizal development. *Plant J.* 69, 510–528. doi: 10.1111/j.1365-313X.2011.04810.x

He, J. D., Zou, Y. N., Wu, Q. S., and Kuča, K. (2020). Mycorrhizas enhance drought tolerance of trifoliate orange by enhancing activities and gene expression of antioxidant enzymes. *Sci. Hortic.* 262, 108745. doi: 10.1016/j.scienta.2018.08.010

Hoang, T. V., Vo, K. T. X., Rahman, M. M., Choi, S. H., and Jeon, J. S. (2019). Heat stress transcription factor OsSPL7 plays a critical role in reactive oxygen species balance and stress responses in rice. *Plant Sci.* 289, 110273. doi: 10.1016/j.plantsci.2019.110273

Ho-Plágaro, T., Huertas, R. L., Tamayo-Navarrete, M. A. I., Blancaflor, E., Gavara, N., and GarcA-Garrido, J. M. (2021). A novel putative microtubule-associated protein is involved in arbuscule development during arbuscular mycorrhiza formation. *Plant Cell Physiol.* 62, 306–320. doi: 10.1016/j.plantsci.2019.110273

Huang, G. M., Zou, Y. N., Wu, Q. S., and Xu, Y. J. (2020). Mycorrhizal roles in plant growth, gas exchange, root morphology, and nutrient uptake of walnuts. *Plant Soil Environ.* 66, 295–302. doi: 10.17221/240/2020-PSE

Kohler, J., Hernández, J. A., Caravaca, F., and Roldán, A. (2009). Induction of antioxidant enzymes is involved in the greater effectiveness of a PGPR versus AM fungi with respect to increasing the tolerance of lettuce to severe salt stress. *Environ. Exp. Bot.* 65, 245–252. doi: 10.1016/j.envexpbot.2008.09.008

Li, L. (2009). *Experimental guidance of the plant physiology module.* (Beijing, China: Science Press).

Liang, S. M., Zhang, F., Zou, Y. N., Kuča, K., and Wu, Q. S. (2021). Metabolomics analysis reveals drought responses of trifoliate orange by arbuscular mycorrhizal fungi with a focus on terpenoid profile. *Front. Plant Sci.* 12, 740524. doi: 10.3389/fpls.2021.740524

Li, Y.L., Liu, Y. F., and Zhang, J. G. (2010). Advances in the research on the AsA-GSH cycle in horticultural crops. *Front. Agric. China.* 4, 84–90. doi: 10.1007/s11703-009-0089-8

Liu, B., Jing, D., Liu, F., Ma, H., Liu, X., and Peng, L. (2021). *Serendipita indica* alleviates drought stress responses in walnut (*Juglans regia* L.) seedlings by stimulating osmotic adjustment and antioxidant defense system. *Appl. Microbiol. Biotechnol.* 105, 8951–8968. doi: 10.1007/s00253-021-11653-9

Liu, X., Meng, P., Yang, G., Zhang, M., Peng, S., and Zhai, M. Z. (2020). Genome-wide identification and transcript profiles of walnut heat stress transcription factor involved in abiotic stress. *BMC Genomics.* 21, 474. doi: 10.1186/s12864-020-06879-2

Livak, K. J., and Schmittgen, T. D. (2001). Analysis of relative gene expression data using real-time quantitative PCR and $2^{-\Delta\Delta Ct}$ method. *Methods.* 25, 402–408. doi: 10.1006/meth.2001.1262

Li, Q. S., Xie, Y. C., Rahman, M. M., Hashem, A., Abd_Allah, E. F., and Wu, Q. S. (2022). Arbuscular mycorrhizal fungi and endophytic fungi activate leaf antioxidant defense system of lane late navel orange. *J. Fungi.* 8, 282. doi: 10.3390/jof8030282

Li, J. W., Yan, S. L., Huang, Y. C., Xia, X. X., Chu, L. F., Li, C. Y., et al. (2020). Physiological and biochemical responses of pecan seedlings to drought stress. *J. Nucl. Agric. Sci.* 34, 2326–2334. doi: 10.11869/j.issn.100-8551.2020.10.2326

Luca, P., Claudio, F., Cristina, C., Raffaele, T., and Mario, B. (2018). Kernel oil content and oil composition in walnut (*Juglans regia* l.) accessions from north-Eastern Italy. *J. Sci. Food Agric.* 98, 955–962. doi: 10.1002/jsfa.8542

Lu, Q. Q., Song, X. S., and Yan, D. H. (2012). Effects of drought stress on photosynthetic physiological characteristics in soybean seeding. *Chin. Agric. Sci. Bull.* 28, 42–47.

Ma, W. Y., Wu, Q. S., Xu, Y. J., and Kuča, K. (2021). Exploring mycorrhizal fungi in walnut with a focus on physiological roles. *Not. Bot. Horti Agrobo.* 49, 12363. doi: 10.15835/nbha49212363

Miller, G., Shulaev, V., and Mittler, R. (2008). Reactive oxygen signaling and abiotic stress. *Physiol. Plant.* 133, 481–489. doi: 10.1111/j.1399-3054.2008.01090.x

Miller, G., Suzuki, N., Ciftci-Yilmaz, S., and Mittlerl, R. (2010). Reactive oxygen species homeostasis and signalling during drought and salinity stresses. *Plant Cell Environ.* 33, 453–467. doi: 10.1111/j.1365-3040.2009.02041.x

Mohanta, T. K., Bashir, T., Hashem, A., Abd_Allah, E. F., Khan, A. L., and Al-Harrasi, A. S. (2018). Early events in plant abiotic stress signaling: interplay between calcium, reactive oxygen species and phytohormones. *Plant Growth Regul.* 37, 1033–1049. doi: 10.1007/s00344-018-9833-8

Noctor, G. (2006). Metabolic signalling in defence and stress: The central roles of soluble redox couples. *Plant Cell Environ.* 29, 409–425. doi: 10.1111/j.1365-3040.2005.01476.x

Phillips, J. M., and Hayman, D. S. (1970). Improved procedures for clearing roots and staining parasitic and vesicular-arbuscular mycorrhizal fungi for rapid assessment of infection. *Trans. Br. Mycol. Soc.* 55, 158–161. doi: 10.1016/S0007-1536(70)80110-3

Ponder, F. (1984). Growth and mycorrhizal development of potted white ash and black walnut fertilized by two methods. *Can. J. Bot.* 62, 509–512. doi: 10.1139/B84-075

Qadir, S. U., Raja, V., Siddiqui, W. A., Shah, T., Alansi, S., and El-Sheikh, M. A. (2022). Ascorbate glutathione antioxidant system alleviates fly ash stress by modulating growth physiology and biochemical responses in *Solanum lycopersicum*. *Saudi J. Biol. Sci.* 29, 1322–1336. doi: 10.1016/j.sjbs.2021.12.013

Saroy, K., and Garg, N. (2021). Relative effectiveness of arbuscular mycorrhiza and polyamines in modulating ROS generation and ascorbate-glutathione cycle in *Cajanus cajan* under nickel stress. *Environ. Sci. Poll. Res.* 28, 48872–48889. doi: 10.1007/s11356-021-13878-7

Si, W. N., Liang, Q. Z., Chen, L., Song, F. Y., Chen, Y., and Jiang, H. (2021). Ectopic overexpression of maize heat stress transcription factor *ZmHSf05* confers drought tolerance in transgenic rice. *Genes.* 12, 1568. doi: 10.3390/genes12101568

Sudhakar, C., Lakshmi, A., and Giridarakumar, S. (2001). Changes in the antioxidant enzymes efficacy in two high yielding genotypes of mulberry (*Morus alba* l.) under NaCl salinity. *Plant Sci.* 161, 613–619. doi: 10.1016/S0168-9452(01)00450-2

Tan, Y., He, C. Z., and Guo, L. H. (2015). Effect of heat shock factor *AtHsfAla* on physiological indexes in *Arabidopsis thaliana* seedlings in drought. *J. Kunming Univ.* 37, 64–68. doi: 10.14091/j.cnki.kmxyxb.2015.03.015

Thioye, B., Legras, M., Castel, L., Hirissou, F., and Trinsoutrot-Gattin, I. (2022). Understanding arbuscular mycorrhizal colonization in walnut plantations: The contribution of cover crops and soil microbial communities. *Agriculture.* 12, 1. doi: 10.3390/agriculture12010001

Tyagi, J., Varma, A., and Pudake, R. N. (2017). Evaluation of comparative effects of arbuscular mycorrhiza (*Rhizophagus intraradices*) and endophyte (*Piriformospora indica*) association with finger millet (*Eleusine coracana*) under drought stress. *Eur. J. Soil Biol.* 81, 1–10. doi: 10.1016/j.ejsobi.2017.05.007

Vahdati, K., Lotfi, N., Kholdebarin, B., Hassani, D., Amiri, R., Mozaffari, M. R., et al. (2009). Screening for drought-tolerant genotypes of persian walnuts (*Juglans regia* l.) during seed germination. *HortScience.* 44, 1815–1819. doi: 10.21273/HORTSCI.44.7.1815

Verma, G., Srivastava, D., Tiwari, P., and Chakrabarty, D. (2019). "ROS modulation in crop plants under drought stress," in *Reactive oxygen, nitrogen and sulfur species in plants: Production, metabolism, signaling and defense mechanisms.*. Eds. M. Hasanuzzaman, V. Fotopoulos, K. Nahar and M. Fujita (West Sussex, UK: John Wiley & Sons Ltd.), 311–336. doi: 10.1002/9781119468677.ch13

Villani, A., Tommasi, F., and Paciolla, C. (2021). The arbuscular mycorrhizal fungus *Glomus viscosum* improves the tolerance to verticillium wilt in *Artichoke artichoke* by modulating the antioxidant defense systems. *Cells.* 10, 1944. doi: 10.3390/cells10081944

Wang, J. (2015). Master's thesis. (Jingzhou, China: Yangtze University).

Wang, P., Yin, L., Liang, D., Li, C., Ma, F. W., and Yue, Z. (2012). Delayed senescence of apple leaves by exogenous melatonin treatment: Toward regulating the ascorbate-glutathione cycle. *J. Pineal Res.* 53, 11–20. doi: 10.1111/j.1600-079X.2011.00966.x

Wu, Q. S., Srivastava, A. K., and Zou, Y. N. (2013). AMF-induced tolerance to drought stress in citrus: A review. *Sci. Hortic.* 164, 77–87. doi: 10.1016/j.scienta.2013.09.010

Wu, Q. S., Xia, R. X., and Zou, Y. N. (2006). Reactive oxygen metabolism in mycorrhizal and non-mycorrhizal citrus (*Poncirus trifoliata*) seedlings subjected to water stress. *J. Plant Physiol.* 163, 1101–1110. doi: 10.1016/j.jplph.2005.09.001

Zhai, R. B., and Zhu, J. H. (2021). Identification and function anlysis of mulberry heat stess trascription factor gene *HSF10-2*. *Sci. Sericult.* 47, 111–118. doi: 10.13441/j.cnki.cykx.2021.02.002

Zhang, F., Zou, Y. N., Wu, Q. S., and Kuča, K. (2020). Arbuscular mycorrhizas modulate root polyamine metabolism to enhance drought tolerance of trifoliate orange. *Environ. Exp. Bot.* 171, 103962. doi: 10.1016/j.envexpbot.2019.103926

Zou, Y. N., Wu, Q. S., and Kuča, K. (2021). Unravelling the role of arbuscular mycorrhizal fungi in mitigating the oxidative burst of plants under drought stress. *Plant Biol.* 23, 50–57. doi: 10.1111/plb.13161

frontiers | Frontiers in Plant Science

TYPE Review
PUBLISHED 29 November 2022
DOI 10.3389/fpls.2022.1083409

OPEN ACCESS

EDITED BY
Chao Li,
Northwest A&F University, China

REVIEWED BY
Zhilong Bao,
Shandong Agricultural University, China
Dongfeng Jia,
Jiangxi Agricultural University, China

*CORRESPONDENCE
Na Li
yyln@hebau.edu.cn
Xueping Chen
chenxueping@hebau.edu.cn

†These authors have contributed equally to this work

SPECIALTY SECTION
This article was submitted to Plant Abiotic Stress, a section of the journal Frontiers in Plant Science

RECEIVED 29 October 2022
ACCEPTED 16 November 2022
PUBLISHED 29 November 2022

CITATION
Du W, Lu Y, Li Q, Luo S, Shen S, Li N and Chen X (2022) TIR1/AFB proteins: Active players in abiotic and biotic stress signaling. *Front. Plant Sci.* 13:1083409. doi: 10.3389/fpls.2022.1083409

TIR1/AFB proteins: Active players in abiotic and biotic stress signaling

Wenchao Du[1†], Yang Lu[2†], Qiang Li[1], Shuangxia Luo[1], Shuxing Shen[1], Na Li[1*] and Xueping Chen[1*]

[1]Key Laboratory for Vegetable Germplasm Enhancement and Utilization of Hebei, Collaborative Innovation Center of Vegetable Industry in Hebei, College of Horticulture, Hebei Agricultural University, Baoding, China, [2]Hebei University Characteristic sericulture Application Technology Research and Development Center, Institute of Sericulture, Chengde Medical University, Chengde, China

The TIR1/AFB family of proteins is a group of functionally diverse auxin receptors that are only found in plants. TIR1/AFB family members are characterized by a conserved N-terminal F-box domain followed by 18 leucine-rich repeats. In the past few decades, extensive research has been conducted on the role of these proteins in regulating plant development, metabolism, and responses to abiotic and biotic stress. In this review, we focus on TIR1/AFB proteins that play crucial roles in plant responses to diverse abiotic and biotic stress. We highlight studies that have shed light on the mechanisms by which TIR1/AFB proteins are regulated at the transcriptional and post-transcriptional as well as the downstream in abiotic or biotic stress pathways regulated by the TIR1/AFB family.

KEYWORDS

TIR1/AFB, abiotic stress, biotic stress, structural and functional specialization, transcription

Introduction

Transport Inhibitor Response 1 and Auxin-Signaling F-box (TIR1/AFB) proteins are plant-specific receptors that mediate diverse responses to the plant hormone auxin (Dharmasiri et al., 2005; Parry et al., 2009). Upon binding indole-3-acetic acid (IAA), or other hormones in the auxin class, TIR1/AFB proteins form a co-receptor complex with Auxin/IAA (Aux/IAA) proteins (Salehin et al., 2015). Formation of this co-receptor complex results in ubiquitination and degradation of Aux/IAA proteins *via* the 26S proteasome (Pan et al., 2009; Salehin et al., 2015; Todd et al., 2020). Degradation of Aux/IAA proteins releases their inhibition of auxin response factors (ARFs), which are transcriptional regulators of auxin-responsive genes such as *Aux/IAA* (Strader and Zhao, 2016; Yu et al., 2022). In this way, TIR1/AFB proteins serve as positive regulators of downstream auxin-responsive pathways upon the perception of auxin (Quint and Gray, 2006; Dezfulian et al., 2016; Takato et al., 2017).

The first *TIR1/AFB* gene identified and shown to play an important role in auxin-regulated processes, such as hypocotyl elongation and lateral root formation, was *TIR1* in *Arabidopsis* (Ruegger et al., 1998). Subsequent studies identified *TIR1/AFB* family members encoded in the genomes of algae, mosses, and spermatophytes in addition to all land plants (Parry et al., 2009). The large number of *TIR1/AFB* genes encoded in plant genomes has allowed for functional redundancy and neofunctionalization to evolve (Prigge et al., 2020). It is now clear that TIR1/AFB proteins contribute to biological processes including regulation of primary and secondary metabolism (Gomes and Scortecci, 2021), seed and root development (Pan et al., 2009; Ozga et al., 2022), cell proliferation (Rast-Somssich et al., 2017), immunity and stress responses in plants (Iglesias et al., 2010). In this review, we highlight our current understanding of the structure and function of TIR1/AFB family members with an emphasis on possible mechanisms by which these proteins regulate abiotic and biotic stress responses.

Structural and functional specialization of TIR1/AFB family members in *Arabidopsis*

Based on comparisons of land plant genomes sequenced to-date, TIR1/AFB proteins can be divided into four phylogenetic clades: TIR1/AFB1, AFB2/3, AFB4/5, and AFB6. *Arabidopsis* contains six TIR1/AFB proteins from three out of the four clades: TIR1, AFB1, AFB2, AFB3, AFB4, and AFB5 (Shimizu-Mitao and Kakimoto, 2014). AFB6 orthologs are noticeably absent in the core Brassicales species such as *Arabidopsis* as well as Poaceae species such as rice and maize (Prigge et al., 2020).

The specific functions of TIR1/AFB family members vary considerably across and within clades. For instance, AFB4 and AFB5 are in the same clade yet exhibit distinct specificities for auxin (Prigge et al., 2016). Yeast two-hybrid and immunoblot assays demonstrated that IAA3 binds TIR1, AFB1, and AFB2 with different affinities but binds AFB5 very poorly at 0.1 μM IAA. Distinct motifs are necessary for the assembly of TIR1/AFB-IAA coreceptor complexes (Villalobos et al., 2012). Here, we generated a phylogenetic tree containing all TIR1/AFB family members from *Arabidopsis* and used Motif ENRichment Analysis (MEME) to identify conserved protein motifs (Figure 1). We believe the unique motifs present in TIR1/AFB proteins may explain their preferential binding of certain IAA proteins over others.

Our analysis showed that *Arabidopsis* TIR1/AFB proteins contain different conserved motifs. These proteins consist of a single F-box domain and eighteen LRR repeats (Prigge et al., 2020). F-box domains are critical for the regulated degradation of cellular proteins (Jain et al., 2007) while LRRs belong to an archaic procaryal protein architecture that is widely involved in protein-protein interactions (Martin et al., 2020). We found that different TIR1/AFB family members contain unique motifs. Motifs 1 and 12 are only present in AFB4 and AFB5, motifs 11 and 20 are only present in AFB2 and AFB3, motif 14 is only present in AFB3, and motif 9 is only found in AFB4. The presence and absence of certain motifs indicates that TIR1/AFBs may have different functions.

Synthetic auxin herbicides are one of the most potent man-made abiotic stresses that plants are subjected to (Gorina et al., 2022). Picloram, 2,4-dichlorophenoxy acetic acid (2,4-D), and dicamba are three of the most widely used chemical classes of auxin. These herbicides function by binding to a hydrophobic pocket within TIR1/AFB proteins (Meng et al., 2008; Guo et al., 2021). Auxin binding TIR1 by filling in the bottom of TIR1 pocket, which floor is made up of several key residues containing His 78, Arg 403, Ser 438, Ser 462, and Glu 487 as shown in (Figure 2) (Guo et al., 2021). Distinct amino acid residues exist in the AFB4/5 clade

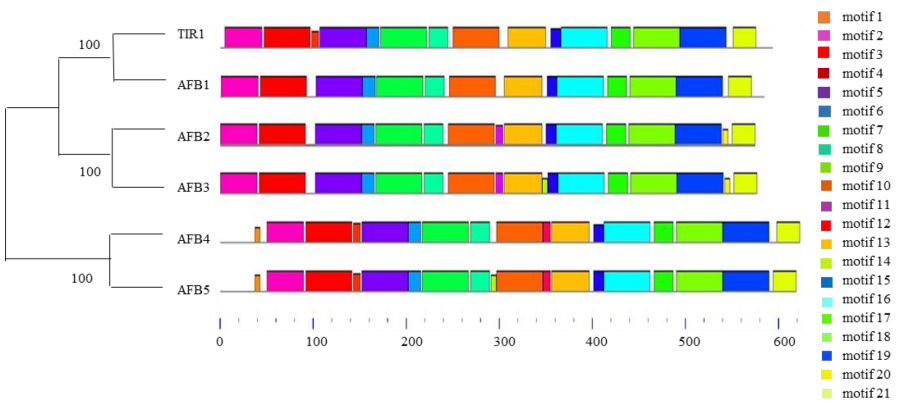

FIGURE 1
Neighbor-joining phylogenetic tree (left) and conserved motif (right) analysis of TIR1/AFBs in *Arabidopsis*.

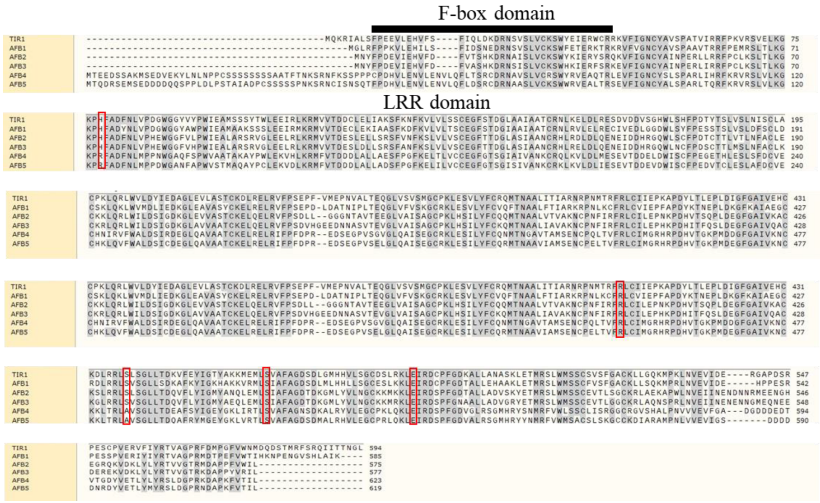

FIGURE 2
Multiple alignment of TIR1/AFB proteins in *Arabidopsis* adapted from Fu Guo et al. (Guo et al., 2021). Residues highlighted in gray are present in more than 50% of aligned sequences. The key residues making up the active site of the TIR1 pocket are highlighted by red boxes. Accession numbers of the genes encoding the proteins for the sequence alignment are as follows: TIR1 (*At3g62980*), AFB1 (*At4g03190*), AFB2 (*At3g26810*), AFB3 (*At1g12820*), AFB4 (*At4g24390*), and AFB5 (*At5g49980*).

compared with the TIR1/AFB1 and AFB2/3 clades at His 78 and Ser 438: histidine is replaced by arginine and serine is replaced by alanine. These differences demonstrate the diversity of TIR1/AFB members and suggest a structural reason for their specialized responses to different synthetic auxin herbicides.

Studies on *Arabidopsis* mutants have demonstrated that some members of the TIR1/AFB family are responsible for the recognition of specific auxin herbicides (Grossmann et al., 1996). For instance, the *Arabidopsis afb4/5* mutant is resistant to picloram whereas other *tir1/afb* mutants are still susceptible (Walsh et al., 2006). The AFB4 protein itself was shown to be a target of picloram based on *in vitro* binding assays (Prigge et al., 2016). TIR1 has been shown to be a receptor for 2,4-D and induces changes in gene expression when plants are treated with low concentrations of 2,4-D (Sheedy et al., 2006; Walsh et al., 2006). As anticipated, the *Arabidopsis tir1* mutant is resistant to 2,4-D whereas AFB1, a member of the same clade as TIR1, has not been implicated in 2,4-D resistance (Gleason et al., 2011).

In vitro assays demonstrated that TIR1 and AFB5 can bind to dicamba (de Figueiredo et al., 2022). Of all the *TIR1/AFB* family members in *Arabidopsis*, only the *tir1-1* and *afb5* mutants were shown to be resistant to dicamba (Gleason et al., 2011). No studies have yet implicated the AFB2/3 subgroup in auxin herbicide sensitivity, which further demonstrates the structural and functional specialization that exists in the TIR1/AFB family. However, studies on the rice mutants *Osabf2* and *Osabf3* showed *OsAFB2/3* genes are involved in the response to 2,4-D resistance (Guo et al., 2021). These results suggest that more studies should focus on the function of the AFB2/3 subgroup in herbicide susceptibility.

The role of TIR1/AFB family members in abiotic and biotic stress responses

Plants are sessile organisms challenged by a variety of abiotic and biotic stresses from which they cannot escape. Abiotic stresses are caused by environmental conditions such as drought, high salinity, heat, and cold whereas biotic stresses are caused by living organisms such as bacteria, fungi, viruses, nematodes, and insects (Verma et al., 2016; Burns et al., 2018). Both abiotic and biotic stress induce reactive oxygen species (ROS) production in the form of hydroxyl radicals, hydrogen peroxide, and superoxide anions (Singh et al., 2020). At low concentrations, many ROS species function as signaling molecules in stress tolerance pathways. However, elevated and sustained levels of ROS can become toxic and lead to nutrient loss, resulting in metabolic disruption, abnormal hormone metabolism (Rejeb et al., 2014; Muchate et al., 2016), and growth inhibition (Gimenez et al., 2018). Auxin plays an indispensable role in how plants rapidly adapt to abiotic and biotic stress. As key auxin receptors in plants, the TIR1/AFB family has been shown to be essential for abiotic and biotic stress responses mediated by auxin.

Drought stress

Drought is an important abiotic stress that negatively impacts plant development and results in reduced crop yield and quality. The expression of many *TIR1/AFB* genes is

influenced by drought stress, which suggests the *TIR1/AFB* family may function in the drought tolerance pathway (Shu et al., 2015; Sharma et al., 2018; Benny et al., 2019). Over-expression and transcriptomic studies in *Populus trichocarpa*, *Arabidopsis thaliana*, *Oryza sativa*, *Zea mays*, *Solanum tuberosum*, *Triticum aestivum*, and *Agrostis stolonifera* have demonstrated that many *TIR1/AFB* genes are responsive to drought (Chen et al., 2012; Shu et al., 2015; Dalal et al., 2018; Sharma et al., 2018; Benny et al., 2019; Zhao et al., 2019). Relative water content (RWC) is used as a measure of plant water status and is a meaningful index of water stress tolerance (Lo Gullo and Salleo, 1988). *PtrFBL1* is a *TIR1* homolog in *Populus trichocarpa*. Overexpression of *PtrFBL1* in *P. trichocarpa* resulted in higher plant RWC values upon drought stress compared with non-transgenic plants (Shu et al., 2015).

Gene expression analyses suggest that some TIR1/AFB family members participate in drought responses in *Arabidopsis*. For example, TIR1 and AFB2 are required for the inhibition of lateral root growth by ABA or osmotic stress under drought stress (Chen et al., 2012). In seedling studies, *TIR1* was up-regulated under drought stress as determined by RNA-Seq (Benny et al., 2019). In addition to the well-studied *Arabidopsis* TIR1/AFB family, several TIR1/AFB proteins have also been implicated in drought responses in other species by transcriptional analysis. In rice, *TIR1* and *AFB2* expression levels were significantly downregulated in spikelets upon drought stress (Sharma et al., 2018). In maize and the Solanaceous crops tomato and potato, RNA-Seq results demonstrated that *TIR1* expression increased in seedlings exposed to drought stress (Benny et al., 2019). Drought-stressed roots of the wheat genotype viz. Raj3765 had increased expression of *AFB2*, suggesting *AFB2* may play a key role in response to drought (Dalal et al., 2018). Creeping bentgrass (*Agrostis stolonifera* L.) overexpressing the rice pri-miR393a exhibited improved tolerance to drought stress due to targeting and suppression of *AsAFB2* and *AsTIR1* expression (Zhao et al., 2019).

Salt stress

Salt stress is a major environmental factor limiting plant growth and productivity. Salt stress can lead to ionic stress, osmotic stress, and secondary stresses such as oxidative stress (Yang and Guo, 2018). Mutant, overexpression, and ectopic expression studies of *TIR1/AFB* genes in *Arabidopsis* have uncovered a key role for some of these genes in salt stress tolerance. Expression of *AtNAC2*, which is typically induced by salt stress, is unresponsive to salt stress in the *tir1-1* mutant (He et al., 2005). An *Arabidopsis tir1afb2* double mutant exhibited enhanced tolerance against salt stress compared with wild-type plants as determined by a higher germination rate, greater root elongation, and higher chlorophyll content (Iglesias et al., 2010). The cucumber (*Cucumis sativus* L.) CsTIR1 and CsAFB1 proteins share 78% and 76% amino acid identity with their *Arabidopsis* homologs, respectively. However, ectopic overexpression of *CsTIR1* and *CsAFB1* in *Arabidopsis* led to higher germination and plant survival rates under salt stress (Chen et al., 2017). Over-expression of the *Arabidopsis AFB3* in *Arabidopsis* resulted in better primary and lateral root development and higher germination rates upon salt stress compared with the wild type (Garrido-Vargas et al., 2020).

It certainly seems contradictory that a *tir1afb2* double mutant and overexpression of *AFB3* or *CsTIR1/CsAFB1* both enhance salt stress resistance in *Arabidopsis*. This may be explained by increased activity of antioxidant enzymes in the *tir1afb2* mutant under salt stress. Higher levels of ABA are also detected in *tir1afb2* compared with wild-type plants (Iglesias et al., 2010) while more lateral roots are found in Arabidopsis transgenic lines overexpressing *AFB3*, *CsTIR1*, or *CsAFB1* (Chen et al., 2017; Garrido-Vargas et al., 2020). This may contribute to differential participation of TIR1/AFB family members and their tissue-specific functions (Iglesias et al., 2010; Garrido-Vargas et al., 2020).

In addition to numerous studies in *Arabidopsis*, TIR1/AFB proteins have also been implicated in salt stress responses in other plant species. Overexpression of maize *ZmAFB2* in tobacco led to enhanced salt tolerance (Yang et al., 2013). Eighteen *TIR1/AFB* genes have been identified in *Brassica juncea* var. tumida with qPCR analysis, which showed that some *BjuTIR1/AFB* genes are repressed by salt treatment (Cai et al., 2019). Degradome and miRNA sequencing analysis between salt-tolerant and salt-sensitive *Fraxinus velutina* Torr. tree cuttings demonstrated that reduced expression of *TIR1* by miR393a explains the enhanced salt stress tolerance of this tree species (Liu JN et al., 2022). Interestingly, AsAFB2 and AsTIR1 from creeping bentgrass may serve as a link between drought and salt stress response pathways, both pathways rely on ionic and osmotic homeostasis signaling (Zhu, 2002; Zhao et al., 2019), and AsAFB2 and AsTIR1 have been implicated involving in this process (Zhao et al., 2019). It is thus plausible that some TIR1/AFB family members may serve as key regulators of plant responses to multiple abiotic stresses.

Temperature stress

Temperature is one of the most important environmental signals for plants. High and low temperatures have a variety of effects that affect plant growth and development profoundly (Sakamoto and Kimura, 2018). Expression data from different plant species indicates that members of the TIR1/AFB family participate in plant responses to temperature stress. For example, the *Arabidopsis tir1-1* mutant displays defective hypocotyl elongation at elevated temperatures (Gray et al., 2003). Expression of *TIR1/AFB2* in rice spikelets was significantly downregulated by heat stress, and the rice protein OsAFB6 can suppress flowering, which is thought to be a temperature sensor (He et al., 2018; Sharma et al., 2018). Finally, repression of *TIR1*

expression in wheat impairs pollen exine formation in male sterility under cold stress (Liu YJ et al., 2022).

Phosphorus and nitrate stress

Phosphorus (Pi) and nitrate (a main source of inorganic nitrogen) are crucial nutrients for crop growth and development that are mainly absorbed from soil by roots. Phosphorous deficiency and excessive nitrate result in retardation of plant growth, development, and productivity (Koide et al., 1999; Zhang et al., 2017). The first TIR1/AFB protein found to be involved in Pi and nitrate availability is TIR1 from *Arabidopsis*, which was shown to be involved in pattern alterations of lateral root formation and emergence in response to phosphate availability (Perez-Torres et al., 2008). The expression level of *TIR1* is also induced under low Pi conditions (Mayzlish-Gat et al., 2012).

Regulation of root system architecture by external nitrate is mediated by AFB3 in *Arabidopsis* as demonstrated by *afb3* insertional mutants (Vidal et al., 2010). Integrated genomics, bioinformatics, and molecular genetics revealed that the expression of genes downstream of *AFB3* are influenced by external nitrate with the NAC4 transcription factor serving as a key regulator of this network (Vidal et al., 2013). AFB3-mediated activation of the two independent pathways in response to nitrate suggests that AFB3 is a unique nitrate response factor in *Arabidopsis* (Vidal et al., 2010). TIR1/AFB family members were also found to be key players in response to nitrate in other plant species. In *Lotus japonicus*, expression of *LjAFB6* is induced in response to exogenous nitrate (Rogato et al., 2021). These studies indicate that AFB3 in *Arabidopsis* and LjAFB6 in *L. japonicus* are potentially involved in plant responses to stress caused by excessive nitrate.

Herbicide stress

Herbicides are small molecules that inhibit specific molecular target sites within plant biochemical pathways to affect physiological processes. Inhibition of these sites often has catastrophic consequences that are lethal to the plant (Dayan et al., 2010). Synthetic auxin, triazine, and organophosphorus herbicides are commonly used in agriculture to control weeds (Todd et al., 2020; Bigner et al., 2021; Striegel et al., 2021). Multiple members of the TIR1/AFB family are involved in susceptibility to synthetic auxin herbicides. Studies on *Arabidopsis TIR1/AFB* mutants have revealed a role for these genes in response to classical auxin herbicides. Recently, the *afb5* mutant was found to be resistant to a new auxin herbicide, halauxifen-methyl, which preferentially binds to AFB5 (Xu et al., 2022).

TIR1/AFB proteins also play a key role in the response to auxin herbicides in other plant species. In rice, CRISPR/Cas9 genome editing was used to generate *Ostir1/Osafb2/Osafb3/Osafb4/Osafb5* mutants that was resistant to 2,4-D. *Osafb4* mutants are highly resistant to the herbicide picloram (Guo et al., 2021). Expression of *TIR1* in wheat is clearly higher in *Triticum aestivum* than in *Aegilops tauschii*, resulting in less sensitive to the herbicide 2,4-D (Yu et al., 2021).

Emerging evidence implicates TIR1/AFB proteins in metal stress tolerance and boron deficiency

In addition to the stresses described above, emerging evidence suggests that TIR1/AFB proteins may be involved in plant responses to metal, and boron deficiency. Aluminum toxicity inhibits plant growth and development (Liu HB et al., 2022). Inhibition of root morphogenesis under aluminum stress decreased in *Arabidopsis tir1* single and *tir1 afb2 afb3* triple mutants. Other genes in the auxin signaling pathway, such as ARFs, were also shown to be involved in aluminum sensitivity (Ruiz-Herrera and Lopez-Bucio, 2013). MicroRNAs targeting and mediating the cleavage of *TIR1/AFB* transcripts were shown to be essential for the aluminum stress response in *Arabidopsis* (Mendoza-Soto et al., 2012). These results suggest *TIR1*, *AFB2*, *AFB3*, and downstream auxin-responsive genes play an important role in aluminum sensitivity in *Arabidopsis*.

Boron is an abundant and essential micronutrient required by plants with deficiencies causing impaired plant growth (Park et al., 2005; Duran et al., 2018). Boron deficiency is positively correlated with the expression of many miRNAs. Gene expression analysis indicates that a subgroup of miRNAs regulate *TIR1/AFB* expression in Arabidopsis when boron is limited. This leads to decreased expression of *TIR1*, *AFB1*, and *AFB2* but increased expression of *AFB3* (Lu et al., 2015). Other reports have demonstrated that application of α-(phenylethyl-2-oxo)-indole-3-acetic acid (PEO-IAA), a synthetic antagonist of TIR1, could partially or fully restore cell elongation in boron deficient roots (Camacho-Cristobal et al., 2015).

Biotic stress from pathogenic bacteria, fungi, viruses, nematodes, and phytophagous insects

Biotic stresses are mainly caused by pathogenic species of bacteria, fungi, viruses, nematodes, and insects that seek to acquire nutrients from their plant hosts (Jagdale and Joshi, 2019; Bhar et al., 2022). Damages caused by diseases and herbivory reduce crop yield and quality by affecting photosynthesis and secondary metabolite production in the host plant (Vo et al., 2021). Plants have evolved numerous strategies to defend themselves against these pathogens. These strategies rely on coordinated gene, protein, and hormone regulation to allow plants to sense and adapt to biotic

stresses (Atkinson and Urwin, 2012). Auxin is a critical signaling component of the plant response to biotic stress, which suggests that TIR1/AFB proteins have a role to play as well (Ghanashyam and Jain, 2009; Bouzroud et al., 2018; Gidhi et al., 2022).

Plant pathogenic bacteria cause symptoms such as spots with yellow halos or mucus-like materials, which negatively impact agricultural production in many important crops (Zimaro et al., 2011). The tomato bacterial pathogen *Pseudomonas syringae* DC3000 (PtoDC3000) produces IAA to promote PtoDC3000 growth in plant tissues through suppression of SA-mediated host defenses (Wildermuth et al., 2001; McClerklin et al., 2018; Djami-Tchatchou et al., 2020). An *Arabidopsis tir1afb1 afb4 afb5* quadruple-mutant exhibited elevated IAA levels and reduced SA levels compared with WT (Djami-Tchatchou et al., 2020). An analysis of a *tir1* single mutant and *tir1 afb2 afb3* triple mutant revealed that these TIR1/AFB family members are targeted by diketopiperazines derived from *Pseudomonas aeruginosa* during colonization of *Arabidopsis* (Ortiz-Castro et al., 2011). The planar structure of diketopiperazines likely fits into the same pocket of TIR1 that synthetic auxins bind (Ortiz-Castro et al., 2011).

Fungal plant pathogens are ubiquitous, highly diverse, and can cause severe damage to many important crops (Termorshuizen, 2016). The *Arabidopsis afb1* and *afb3* mutants are partially resistant to the soilborne root pathogen *Verticillium dahlia*. Up-regulation of *pathogen-related gene 1* (*PR1*) in *afb1* and *pathogen defense factor 1.2* (*PDF1.2*) in *afb3* may be responsible for *afb1*- and *afb3*-mediated resistance, respectively (Fousia et al., 2018). Fusarium head blight (FHB) of wheat, caused by *Fusarium graminearum* Schwabe, results in large annual yield losses in wheat production regions. RNAi-mediated knockdown of the *TaTIR1* gene led to increased FHB resistance (Su et al., 2021). Gene expression studies also revealed that *TaTIR1* expression is highest at 24 and 48 h post-inoculation with the leaf rust pathogen *Puccinia triticina* Eriks (Gidhi et al., 2022). A maize *TIR1*-like gene is involved in the Zma-miR393b-mediated response to *Rhizoctonia solani* infection of leaf sheaths (Luo et al., 2014). Eighteen *TIR1/AFB* genes have been identified in *Brassica juncea* var. tumida using genome-wide analysis. qPCR analysis demonstrated that the expression of some *BjuTIR1/AFB* genes is influenced by *Plasmodiophora brassicae* infection (Cai et al., 2019).

Although no involvement in biotic stress has been reported for soybean TIR1/AFB proteins, TIR1/AFB proteins have been implicated in root nodulation induced by the nitrogen-fixing bacterium *Bradyrhizobium japonicum* (Cai et al., 2017). Overexpression of *GmTIR1* in soybean significantly increased the number of inflection foci and nodules while *GmAFB3A* may also play a minor role in this process (Cai et al., 2017).

Few studies to-date have implicated the TIR1/AFB family in plant defense responses against viruses. However, one study has shown that the rice dwarf virus (RDV) capsid protein P2 binds OsIAA10 and blocks the interaction between OsIAA10 and OsTIR1. This prevents 26S proteasome-mediated degradation of OsIAA10, resulting in plant dwarfism, increased tiller number, and short crown roots in infected plants (Jin et al., 2016).

Nematodes are pathogens of *Arabidopsis* (Moradi et al., 2021), apple (Fallahi et al., 1998), tomato (Khan and Khan, 1995), and wheat (Cortese et al., 2003), these species could move through roots and be vector of some virus, caused root damage, yield loss. The tomato *Mi-1* gene confers isolate-specific resistance against root-knot nematodes (Seah et al., 2007). Co-localization of TIR1-like proteins with the Mi-1 protein was observed (Seifi et al., 2011). *TIR1*-like transcript abundance in roots and leaves of nematode-resistant tomato lines was lower than in susceptible tomato lines, suggesting a possible role for *TIR1*-like genes in nematode resistance (Seifi et al., 2011).

Feeding by phytophagous insects such as aphids leads to reduced plant growth, reduced yield, water stress, dwarfism, wilting, and transmission of economically important plant viruses. In melon, genes like *TIR1* and *AFB2* are down-regulated in response to aphid herbivory. Application of the TIR1 inhibitor PEO-IAA to leaf discs resulted in significantly decreased feeding by aphids, providing *in vivo* support for TIR1/AFB in response to aphids (Sattar et al., 2016), suggested that TIR1 may play a role in aphid resistance.

TIR1/AFB-regulated gene networks in abiotic and biotic stress responses

In addition to the regulation of *Aux/IAA* genes, many other proteins and genes regulated by TIR1/AFB family members have been identified that act downstream of auxin perception. These studies have contributed to our understanding of the mechanisms underlying the function of TIR1/AFB proteins in abiotic and biotic stress. These downstream genes and proteins include *nascent polypeptide-associated complex* (*NAC*) family members, SA synthesis proteins, PR proteins, PDF proteins and phosphorus transporters,

Auxin/indoleacetic acid (Aux/IAA) proteins play an important regulatory role in plant development and stress responses. TIR1/AFB proteins are essential regulators of the expression of a large number of *Aux/IAA* genes (Gray, 2003). For example, the rice Aux/IAA protein OsIAA20 mediates abiotic stress tolerance in rice through the ABA pathway (Zhang et al., 2021). Constitutive expression of *OsIAA18* in *Arabidopsis* led to improved salt and osmotic tolerance through enhanced ABA biosynthesis and ROS scavenging (Wang et al., 2021). The homeostatic expression of *Aux/IAA* is thought to be one of the most important resistance mechanisms to auxin herbicides mediated by TIR1/AFB proteins (Todd et al., 2020).

Aux/IAA proteins also play essential roles in response to biotic stress. Silencing of *GhIAA43* in cotton enhanced wilt resistance and activated the expression of SA-related defense genes (Su et al., 2022). Tobacco mosaic virus (TMV) replicase proteins negatively regulate IAA26 through a ubiquitin-mediated destabilization process to reduce TMV infection

(Padmanabhan et al., 2005). The RDV capsid protein P2 can bind OsIAA10 directly, which implicates OsIAA10 in the defense response against RDV (Jin et al., 2016).

In addition to the *Aux/IAA* genes, many other stress-related genes are also regulated by TIR1/AFB proteins in response to abiotic and biotic stress. For example, the transcription factor NAC4 is an important positive regulator downstream of the AFB3 regulatory network, which plays an important role in the regulation of nitrate uptake in *Arabidopsis* (Vidal et al., 2013). The presence of a functional copy of *NAC1* is required by the fungal pathogen *Alternaria alternata* for full virulence in *Arabidopsis* (Wang et al., 2020). *NAC1* overexpression can restore lateral root formation in the *Arabidopsis tir1* mutant, whereas *TIR1* overexpression results in increased *NAC1* expression. These results demonstrate that NAC1 acts downstream of and can be positively regulated by TIR1 in *Arabidopsis* (Xie et al., 2000).

The SA-related genes *PR1* and *PDF1.2* are positive regulators of plant disease resistance that are negatively regulated by TIR1/AFB. A transcriptomic study in cotton demonstrated that knockdown of *GhTIR1* leads to a significant increase in the expression of SA-related genes in response to *Verticillium dahliae* infection (Shi et al., 2022). The *Arabidopsis* mutants *afb1* and *afb3* exhibit significantly higher expression of both *PR1* and *PDF1.2* in response to *Verticillium dahliae* infection (Fousia et al., 2018).

TIR1/AFB proteins act as mediators of low Pi uptake in *Arabidopsis* (Perez-Torres et al., 2008; Perez Torres et al., 2009). Pi deprivation increases the expression of *TIR1* in *Arabidopsis* seedlings (Perez-Torres et al., 2008). *ARF* was regulated by TIR1/AFB as described above. Knockout of *OsARF12* enhanced the expression of *PHOSPHATE TRANSPORTER1*(*PHT1*) genes such as *OsPHR2* in rice, suggesting that OsARF negatively regulates the *PHT1* gene family in rice (Wang et al., 2014).

Regulation of TIR1/AFB expression and protein activity in response to abiotic and biotic stress

Many *TIR1/AFB* genes are differentially expressed in response to diverse abiotic or biotic stresses. Yet the underlying mechanism of *TIR1/AFB* gene regulation remains unknown.

TIR1 expression is up-regulated or down-regulated in *Arabidopsis* upon infection by plant pathogens such as *Verticillium dahlia* and *Botrytis cinerea* (Llorente et al., 2008; Fousia et al., 2018). Many plant pathogens manipulate host auxin biosynthesis, inducing the degradation of AUX/IAA proteins through TIR1-mediated ubiquitination to enable greater infection (Wang et al., 2007). The *Arabidopsis* mutants *afb1* and *afb3* have enhanced plant resistance against *Verticillium dahlia*. However, the *tir1-1* mutant exhibits no increase in susceptibility to *Botrytis cinerea* compared to wild-type *Arabidopsis*. These studies indicate that TIR1/AFBs may be targeted by some pathogens.

Plant-produced small molecules are key systemic modulators of numerous biological pathways. Nitric oxide (NO) is an important signaling molecule involved in establishing resistance to plant stress. External NO represses *TIR1* expression and decreases *Arabidopsis* susceptibility to *Pseudomonas. syringae pv.* tomato: a process believed to be mediated by SA (Vitor et al., 2013). Hydrogen sulfide (H_2S) is a gaseous molecule involved in various responses to stress. H_2S negatively regulates the expression of *TIR1*, *AFB1*, *AFB2*, and *AFB3* in antibacterial resistance in *Arabidopsis* through a miR393a/b-regulated mechanism (Shi et al., 2015).

While most abiotic and biotic stresses suppress the expression of *TIR1/AFB* family members, some stresses can induce their expression. In *L. japonicus*, *LjAFB6* expression increased by 2.5-fold after nitrate treatment (Rogato et al., 2021). *Arabidopsis AFB3* was also found to be positively regulated by nitrate addition (Vidal et al., 2010; Vidal et al., 2013). Infections of *Plasmodiophora brassicae* in *Brassica juncea* var. tumida also induce the expression of *BjuTIR1/AFB* and *BjuTIR1* (Cai et al., 2019), but the mechanism by which this process occurs is not yet clear.

Some members of the *TIR1/AFB* family involved in abiotic or biotic stress responses are known targets of small RNAs. One of the most well-studied small RNAs shown to target and repress *TIR1/AFB* transcripts is MicroRNA393 (miR393) (Navarro et al., 2006). In *Arabidopsis*, miR393 directly targets *TIR1*, *AFB1*, *AFB2*, and *AFB2* transcripts in response to abiotic stress (Vidal et al., 2010; Chen et al., 2012; Iglesias et al., 2014). Regulation of *AFB3* by miR393 represents a unique nitrate-responsive module that is induced by nitrate and repressed by nitrogen metabolites in *Arabidopsis* (Vidal et al., 2010). Studies also indicate that miR393 negatively regulates *TIR1*, *AFB2*, and *AFB3* in response to pathogen challenge in several plant species (Navarro et al., 2006; Zhang et al., 2019; Shi et al., 2022). Though studies indicate that miR393 negatively regulates *TIR1* expression at the posttranscriptional level (Parry et al., 2009), the relationship between miR393 and *TIR1/AFB* transcripts needs to be investigated further.

In addition to regulated gene expression or posttranscriptional level, TIR1/AFB proteins are also regulated post-translationally by other proteins. The *Arabidopsis* TIR1 protein is stabilized by a complex consisting of heat shock protein 90 (HSP90) and Suppressor of G2 allele of skp1 (SGT1b), which itself is an HSP90 co-chaperone, co-immunoprecipitation analyses further validated that HSP90 interacted with TIR1 (Watanabe et al., 2016; Munoz et al., 2022). So far, no other factors were found to positively or negatively regulate TIR1/AFB proteins at post-translational level under stress. Therefore, future study should explore factors that regulate or interact with TIR1/AFB proteins.

Conclusions and perspectives

Phylogenetic, structural, and functional studies have revealed that there are many homologs of TIR1/AFB proteins

10.3389/fpls.2022.1083409

TABLE 1 TIR1/AFB proteins involved in abiotic and biotic stress in plants.

Plant species	Name	Subfamily	stress	reference
Arabidopsis (*Arabidopsis thaliana*)	AtTIR1	TIR1/AFB1	salt	(Chen et al., 2015)
	AtAFB2	AFB2/3	Salt	(Iglesias et al., 2010)
	AtAFB3	AFB2/3	Salt	(Iglesias et al., 2010)
	AtTIR1	TIR1/AFB1	Temperature	(Wang et al., 2016)
	AtTIR1	TIR1/AFB1	Drought	(Chen et al., 2012)
	AtAFB2	AFB2/3	Drought	(Benny et al., 2019)
	AtTIR1	TIR1/AFB1	Low Pi	(Perez-Torres et al., 2008; Mayzlish-Gat et al., 2012)
	AtAFB3	AFB2/3	Nitrate	(Vidal et al., 2010; Vidal et al., 2013)
	AtTIR1	TIR1/AFB1	Herbicide	(Sheedy et al., 2006; Walsh et al., 2006; Gleason et al., 2011)
	AtAFB4	AFB4/5	Herbicide	(Gleason et al., 2011)
	AtAFB5	AFB4/5	Herbicide	(Gleason et al., 2011; Xu et al., 2022)
	AtTIR1	TIR1/AFB1	Aluminum	(Ruiz-Herrera and Lopez-Bucio, 2013)
	AtAFB2	AFB2/3	Aluminum	(Ruiz-Herrera and Lopez-Bucio, 2013)
	AtAFB3	AFB2/3	Aluminum	(Ruiz-Herrera and Lopez-Bucio, 2013)
	At TIR1	TIR1/AFB1	Boron deficiency	(Camacho-Cristobal et al., 2015; Lu et al., 2015)
	AtTIR1/AFB1/AFB4/AFB5	TIR1/AFB1, AFB4/5	bacterium	(Djami-Tchatchou et al., 2020)
	AtAFB1	TIR1/AFB1	Fungi	(Fousia et al., 2018)
	AtAFB3	AFB2/3	Fungi	(Fousia et al., 2018)
	AtTIR1	TIR1/AFB1	Fungi	(Ortiz-Castro et al., 2011)
	AtTIR1/AFB2/AFB3	TIR1/AFB	Fungi	(Ortiz-Castro et al., 2011)
Rice (*Oryza sativa*)	OsTIR1	TIR1/AFB1	Salt	(Xia et al., 2012)
	OsAFB2	AFB2/3	Salt	(Xia et al., 2012)
	OsAFB2	AFB2/3	Drought	(Xia et al., 2012; Sharma et al., 2018)
	OsTIR1	TIR1/AFB1	Drought	(Xia et al., 2012; Sharma et al., 2018)
	OsTIR1	TIR1/AFB1	Temperature	(Sharma et al., 2018)
	OsAFB2	AFB2/3	Temperature	(Sharma et al., 2018)
	OsAFB6	AFB6	Temperature	(He et al., 2018)
	OsTIR1	TIR1/AFB1	Herbicide	(Guo et al., 2021)
	OsAFB2	AFB2/3	Herbicide	(Guo et al., 2021)
	OsAFB3	AFB2/3	Herbicide	(Guo et al., 2021)
	OsAFB4	AFB4/5	Herbicide	(Guo et al., 2021)
	OsAFB5	AFB4/5	Herbicide	(Guo et al., 2021)
	OsTIR1	TIR1/AFB1	Virus	(Jin et al., 2016)
Wheat (*Triticum aestivum*)	TaAFB2	AFB2/3	Drought	(Dalal et al., 2018)
	TaTIR1	TIR1/AFB1	Temperature	(Liu Y. J. et al., 2022)
	TaTIR1	TIR1/AFB1	Herbicide	(Yu et al., 2021)
	TaTIR1	TIR1/AFB1	Fungi	(Su et al., 2021)
	TaTIR1	TIR1/AFB1	Fungi	(Gidhi et al., 2022)
Maize (*Zea mays*)	ZmAFB2	AFB2/3	Salt	(Yang et al., 2013)
	ZmTIR1	TIR1/AFB1	Drought	(Benny et al., 2019)
	ZmTIR-like	TIR1/AFB1	Fungi	(Luo et al., 2014)
Soybean (*Glycine max L.*)	GmTIR1	TIR1/AFB1	Fungi	(Cai et al., 2017)
	GmAFB3	AFB2/3	Fungi	(Cai et al., 2017)
Melon (*Cucumis melo L.*)	CmTIR1	TIR1/AFB1	Aphid	(Sattar et al., 2016)
	CmAFB2	AFB2/3	Aphid	(Sattar et al., 2016)
Cucumber (*Cucumis sativus L.*)	CSTIR1	TIR1/AFB1	Salt	(Chen et al., 2017)

(Continued)

TABLE 1 Continued

Plant species	Name	Subfamily	stress	reference
	CsAFB2	AFB2/3	Salt	(Chen et al., 2017)
Tomato (*Solanum lycopersicum*)	SlTIR1	TIR1/AFB1	Drought	(Benny et al., 2019)
	SlTIR1	TIR1/AFB1	Nematode	(Seah et al., 2007; Seifi et al., 2011)
Potato (*Solanum tuberosum*)	StTIR1	TIR1/AFB1	Drought	(Benny et al., 2019)
Mustard (*Brassica juncea* var. *tumida)*	BjuTIR1	TIR1/AFB1	Salt	(Cai et al., 2019)
	BjuAFB3		Salt	(Cai et al., 2019)
	BjuTIR1	TIR1/AFB1	Fungi	(Cai et al., 2019)
Crowtoe (*Lotus corniculatus* L.)	LjAFB6	AFB6	nitrate	(Rogato et al., 2021)
Creeping bentgrass (*Agrostis stolonifera L.)*	AsTIR1	TIR1/AFB1	Salt	(Zhao et al., 2019)
	AsAFB2	AFB2/3	Salt	(Zhao et al., 2019)
Fraxinus tomentosa (*Fraxinus velutina* Torr.)	FvTIR1	TIR1/AFB1	Salt	(Liu J. N. et al., 2022)

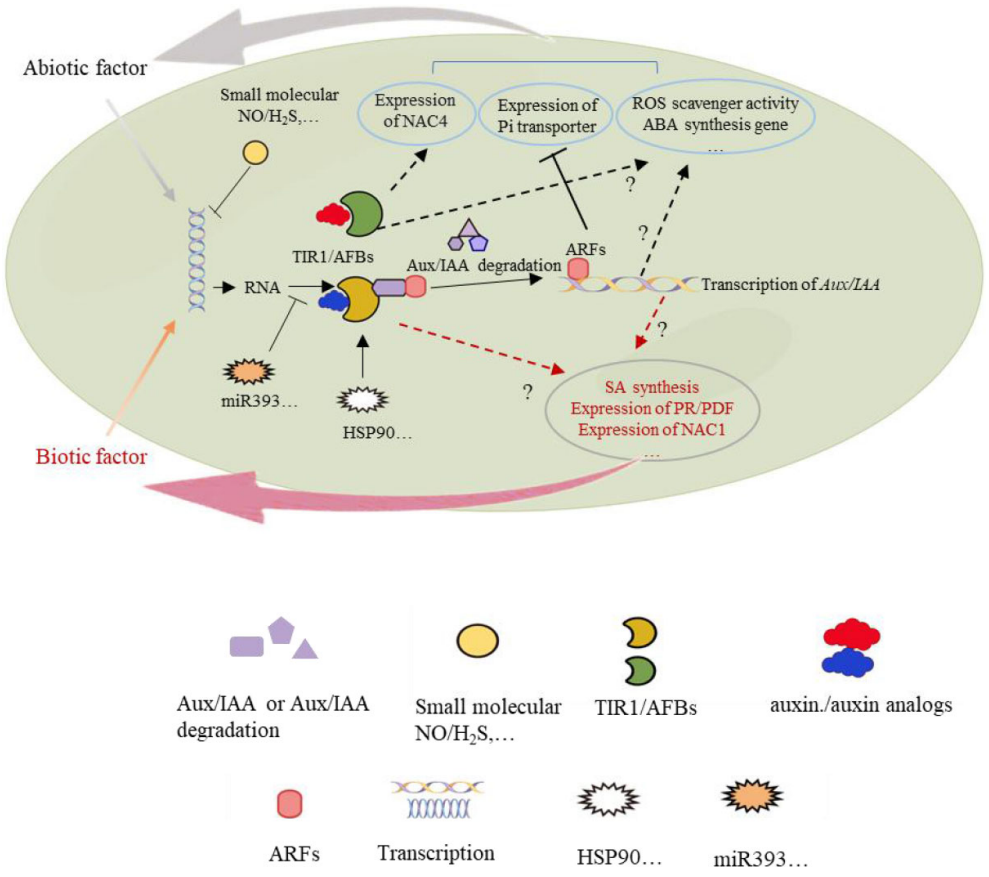

FIGURE 3
TIR1/AFB regulatory network in response to abiotic and biotic stress. TIR1/AFBs response to abiotic or biotic factors in different signal transduction pathways.

with conserved domains. Many *TIR1/AFB* genes are differentially expressed in response to diverse abiotic and biotic stress (Table 1). Small molecules such as NO and H_2S regulate *TIR1/AFB* gene expression, MicroRNAs, such as miR393, are some of the most well-studied regulators of *TIR1/AFB* transcripts. The regulation of some TIR1/AFB family members through protein-protein interactions and small molecules is also indispensable (Figure 3). Future studies should focus on identifying more factors that can regulate TIR1/AFB family members at the transcriptional, post-transcriptional, and protein levels. These studies will shed light on the evolution of the TIR1/AFB family and identify new roles for these proteins in plant abiotic and biotic stress responses.

TIR1/AFB proteins are known regulators of numerous stress-related genes. The most well-studied examples of gene regulation by TIR1/AFB proteins are the *Aux/IAA* genes. Expression of many *Aux/IAA* genes in response to abiotic and biotic stress is both directly and indirectly controlled by TIR1/AFB proteins. Expression of *NAC4* is also regulated by TIR1/AFB proteins in response to nitrate uptake.

The general mechanism by which TIR1/AFB proteins enhance abiotic stress tolerance is by reducing ABA accumulation, increasing the abundance of ROS scavengers, and affecting the activity of other factors such as Pi transporters. In response to biotic stress, TIR1/AFB proteins promote the expression of SA biosynthesis genes, *PR* genes, and *PDF* genes. However, more studies need to be performed to determine the role of specific TIR1/AFB members in the signaling and metabolic pathways that modulate disease resistance. As the studies highlighted in this review demonstrate, much knowledge about the role of TIR1/AFB proteins in abiotic and biotic stress responses has been generated. The next challenge for the field will be deciphering the upstream and downstream events to draw a more complete picture of TIR1/AFB-mediated regulation of plant abiotic and biotic stress responses.

Author contributions

XC and NL concepted the topic of this manuscript and revised the manuscript, WD drafted this manuscript with YL. QL, SL and SS revised the manuscript. All authors contributed to the article and approved the submitted version.

Funding

This work was supported by the National Natural Science Foundation of China (grant no. 32172567), Vegetable Innovation Team Project of Hebei Modern Agricultural Industrial Technology System (grant no. HBCT2018030203), Key Research & Development Project of Hebei Province (grant no. 21326309D), The Innovation Ability Training Project for Graduate Student of Hebei Province (grant no. CXZZBS2018114), and the grant from 'Giant Plan' of Hebei Province.

Acknowledgments

We thank A&L Scientific Editing (www.alpublish.com) for its linguistic assistance during the preparation of this manuscript. We also thank Ma Wei, Lisong Ma, Lijun Song and Shiyao You in the preparation of the pictures in this manuscript.

Conflict of interest

The authors declare that the research was conducted in the absence of any commercial or financial relationships that could be construed as a potential conflict of interest.

Publisher's note

All claims expressed in this article are solely those of the authors and do not necessarily represent those of their affiliated organizations, or those of the publisher, the editors and the reviewers. Any product that may be evaluated in this article, or claim that may be made by its manufacturer, is not guaranteed or endorsed by the publisher.

References

Atkinson, N. J., and Urwin, P. E. (2012). The interaction of plant biotic and abiotic stresses: From genes to the field. *J. Exp. Bot.* 63, 3523–3543. doi: 10.1093/jxb/ers100

Benny, J., Pisciotta, A., Caruso, T., and Martinelli, F. (2019). Identification of key genes and its chromosome regions linked to drought responses in leaves across different crops through meta-analysis of RNA-seq data. *BMC Plant Biol.* 19, 1–18. doi: 10.1186/s12870-019-1794-y

Bhar, A., Chakraborty, A., and Roy, A. (2022). Plant responses to biotic stress: Old memories matter. *Plants-Basel* 11, 84. doi: 10.3390/plants11010084

Bigner, J. A., Fiester, S. E., Fulcher, J. W., Schammel, C. M. G., Ward, M. E., Burney, H. E., et al. (2021). Glyphosate and polyoxyethyleneamine ingestion leading to renal, hepatic, and pulmonary failure. *Am. J. Foren. Med. Path.* 42, 282–285. doi: 10.1097/PAF.0000000000000660

Bouzroud, S., Gouiaa, S., Hu, N., Bernadac, A., Mila, I., Bendaou, N., et al. (2018). Auxin response factors (ARFs) are potential mediators of auxin action in tomato response to biotic and abiotic stress (*Solanum lycopersicum*). *PloS One* 13, 1–20. doi: 10.1371/journal.pone.0193517

Burns, E. E., Keith, B. K., Refai, M. Y., Bothner, B., and Dyer, W. E. (2018). Constitutive redox and phosphoproteome changes in multiple herbicide resistant *Avena fatua* l. are similar to those of systemic acquired resistance and systemic acquired acclimation. *J. Plant Physiol.* 220, 105–114. doi: 10.1016/j.jplph.2017.11.004

Cai, Z. M., Wang, Y. N., Zhu, L., Tian, Y. P., Chen, L., Sun, Z. X., et al. (2017). GmTIR1/GmAFB3-based auxin perception regulated by miR393 modulates soybean nodulation. *New Phytol.* 215, 672–686. doi: 10.1111/nph.14632

Cai, Z. M., Zeng, D. E., Liao, J. J., Cheng, C. H., Sahito, Z. A., Xiang, M. Q., et al. (2019). Genome-wide analysis of auxin receptor family genes in *brassica juncea* var. tumida. *Genes* 10, 165. doi: 10.3390/genes10020165

Camacho-Cristobal, J. J., Martin-Rejano, E. M., Herrera-Rodriguez, M. B., Navarro-Gochicoa, M. T., Rexach, J., and Gonzalez-Fontes, A. (2015). Boron deficiency inhibits root cell elongation *via* an ethylene/auxin/ROS-dependent pathway in arabidopsis seedlings. *J. Exp. Bot.* 66, 3831–3840. doi: 10.1093/jxb/erv186

Chen, Z., Hu, L., Han, N., Hu, J., Yang, Y., Xiang, T., et al. (2015). Overexpression of a miR393-resistant form of transport inhibitor response protein 1 (mTIR1) enhances salt tolerance by increased osmoregulation and na^+ exclusion in arabidopsis thaliana. *Plant Cell Physiol.* 56, 73–83. doi: 10.1093/pcp/pcu149

Chen, H., Li, Z., and Xiong, L. (2012). A plant microRNA regulates the adaptation of roots to drought stress. *FEBS Lett.* 586, 1742–1747. doi: 10.1016/j.febslet.2012.05.013

Chen, Z. H., Li, M. T., Yuan, Y., Hu, J. Q., Yang, Y. J., Pang, J. L., et al. (2017). Ectopic expression of cucumber (*Cucumis sativus* l.) CsTIR/AFB genes enhance salt tolerance in transgenic arabidopsis. *Plant Cell Tiss. Org.* 131, 107–118. doi: 10.1007/s11240-017-1267-7

Cortese, M. R., Fanelli, E., and De Giorgi, C. (2003). Characterization of nematode resistance gene analogs in tetraploid wheat. *Plant Sci.* 164, 71–75. doi: 10.1016/S0168-9452(02)00336-9

Dalal, M., Sahu, S., Tiwari, S., Rao, A. R., and Gaikwad, K. (2018). Transcriptome analysis reveals interplay between hormones, ROS metabolism and cell wall biosynthesis for drought-induced root growth in wheat. *Plant Physiol. Bioch.* 130, 482–492. doi: 10.1016/j.plaphy.2018.07.035

Dayan, F. E., Duke, S. O., and Grossmann, K. (2010). Herbicides as probes in plant biology. *Weed Sci.* 58, 340–350. doi: 10.1614/WS-09-092.1

de Figueiredo, M. R. A., Kupper, A., Malone, J. M., Petrovic, T., de Figueiredo, , A.B.T.B., Campagnola, G., et al. (2022). An in-frame deletion mutation in the degron tail of auxin coreceptor IAA2 confers resistance to the herbicide 2,4-d in sisymbrium orientale. *PNAS* 119, e2105819119. doi: 10.1073/pnas.2105819119

Dezfulian, M. H., Jalili, E., Roberto, D. K. A., Moss, B. L., Khoo, K., Nemhauser, J. L., et al. (2016). Oligomerization of SCF^{TIR1} is essential for Aux/IAA degradation and auxin signaling in arabidopsis. *PloS Genet.* 12, e1006301. doi: 10.1371/journal.pgen.1006301

Dharmasiri, N., Dharmasiri, S., and Estelle, M. (2005). The f-box protein TIR1 is an auxin receptor. *Nature* 435, 441–445. doi: 10.1038/nature03543

Djami-Tchatchou, A. T., Harrison, G. A., Harper, C. P., Wang, R. H., Prigge, M. J., Estelle, M., et al. (2020). Dual role of auxin in regulating plant defense and bacterial virulence gene expression during *Pseudomonas syringae* PtoDC3000 pathogenesis. *Mol. Plant Microbe In.* 33, 1059–1071. doi: 10.1094/MPMI-02-20-0047-R

Duran, C., Arce-Johnson, P., and Aquea, F. (2018). Methylboronic acid fertilization alleviates boron deficiency symptoms in arabidopsis thaliana. *Planta* 248, 221–229. doi: 10.1007/s00425-018-2903-0

Fallahi, E., Hafez, S. L., Colt, W. M., and Seyedbagheri, M. M. (1998). Effects of metam sodium and rootstock on plant-parasitic nematodes, tree growth, meld, fruit quality, and leaf minerals in 'braeburn' apple. *Nematropica* 28, 71–79.

Fousia, S., Tsafouros, A., Roussos, P. A., and Tjamos, S. E. (2018). Increased resistance to *Verticillium dahliae* in arabidopsis plants defective in auxin signalling. *Plant Pathol.* 67, 1749–1757. doi: 10.1111/ppa.12881

Garrido-Vargas, F., Godoy, T., Tejos, R., and O'Brien, J. A. (2020). Overexpression of the auxin receptor AFB3 in arabidopsis results in salt stress resistance and the modulation of NAC4 and SZF1. *Int. J. Mol. Sci.* 21, 9528. doi: 10.3390/ijms21249528

Ghanashyam, C., and Jain, M. (2009). Role of auxin-responsive genes in biotic stress responses. *Plant Signal. Behav.* 4, 846–848. doi: 10.4161/psb.4.9.9376

Gidhi, A., Mohapatra, A., Fatima, M., Jha, S. K., Kumar, M., and Mukhopadhyay, K. (2022). Insights of auxin signaling f-box genes in wheat (Triticum aestivum l.) and their dynamic expression during the leaf rust infection. *Protoplasma.* 1–17. doi: 10.1007/s00709-022-01808-4

Gimenez, E., Salinas, M., and Manzano Agugliaro, F. (2018). Worldwide research on plant defense against biotic stresses as improvement for sustainable agriculture. *Sustainability* 10, 391. doi: 10.3390/su10020391

Gleason, C., Foley, R. C., and Singh, K. B. (2011). Mutant analysis in arabidopsis provides insight into the molecular mode of action of the auxinic herbicide dicamba. *PloS One* 6, e17245. doi: 10.1371/journal.pone.0017245

Gomes, G. L. B., and Scortecci, K. C. (2021). Auxin and its role in plant development: Structure, signalling, regulation and response mechanisms. *Plant Biol.* 23, 894–904. doi: 10.1111/plb.13303

Gorina, S., Ogorodnikova, A., Mukhtarova, L., and Toporkova, Y. (2022). Gene expression analysis of potato (*Solanum tuberosum* l.) lipoxygenase cascade and oxylipin signature under abiotic stress. *Plants-Basel* 11, 683. doi: 10.3390/plants11050683

Gray, W. M., Muskett, P. R., Chuang, H. W., and Parker, J. E. (2003). Arabidopsis SGT1b is required for SCF^{TIR1}-mediated auxin response. *Plant Cell* 15, 1310–1319. doi: 10.1105/tpc.010884

Grossmann, K., Scheltrup, F., Kwiatkowski, J., and Caspar, G. (1996). Induction of abscisic acid is a common effect of auxin herbicides in susceptible plants. *J. Plant Physiol.* 149, 475–478. doi: 10.1016/S0176-1617(96)80153-2

Guo, F., Huang, Y., Qi, P., Lian, G., Hu, X., Han, N., et al. (2021). Functional analysis of auxin receptor OsTIR1/OsAFB family members in rice grain yield, tillering, plant height, root system, germination, and auxinic herbicide resistance. *New Phytol.* 229, 2676–2692. doi: 10.1111/nph.17061

He, X. J., Mu, R. L., Cao, W. H., Zhang, Z. G., Zhang, J. S., and Chen, S. Y. (2005). AtNAC2, a transcription factor downstream of ethylene and auxin signaling pathways, is involved in salt stress response and lateral root development. *Plant J.* 44, 903–916. doi: 10.1111/j.1365-313X.2005.02575.x

He, Q., Yang, L., Hu, W., Zhang, J., and Xing, Y. (2018). Overexpression of an auxin receptor OsAFB6 significantly enhanced grain yield by increasing cytokinin and decreasing auxin concentrations in rice panicle. *Sci. Rep.* 8, 14051. doi: 10.1038/s41598-018-32450-x

Iglesias, M. J., Terrile, M. C., Bartoli, C. G., D'Ippolito, S., and Casalongue, C. A. (2010). Auxin signaling participates in the adaptative response against oxidative stress and salinity by interacting with redox metabolism in arabidopsis. *Plant Mol. Biol.* 74, 215–222. doi: 10.1007/s11103-010-9667-7

Iglesias, M. J., Terrile, M. C., Windels, D., Lombardo, M. C., Bartoli, C. G., Vazquez, F., et al. (2014). MiR393 regulation of auxin signaling and redox-related components during acclimation to salinity in arabidopsis. *PloS One* 9, e107678. doi: 10.1371/journal.pone.0107678

Jagdale, S. S., and Joshi, R. S. (2019). Facilitator roles of viruses in enhanced insect resistance to biotic stress. *Curr. Opin. Insect Sci.* 33, 111–116. doi: 10.1016/j.cois.2019.05.008

Jain, M., Nijhawan, A., Arora, R., Agarwal, P., Ray, S., Sharma, P., et al. (2007). F-box proteins in rice. genome-wide analysis, classification, temporal and spatial gene expression during panicle and seed development, and regulation by light and abiotic stress. *Plant Physiol.* 143, 1467–1483. doi: 10.1104/pp.106.091900

Jin, L., Qin, Q. Q., Wang, Y., Pu, Y. Y., Liu, L. F., Wen, X., et al. (2016). Rice dwarf virus P2 protein hijacks auxin signaling by directly targeting the rice OsIAA10 protein, enhancing viral infection and disease development. *PloS Pathog.* 12, e1005847. doi: 10.1371/journal.ppat.1005847

Khan, M. R., and Khan, M. W. (1995). Effects of ammonia and root-knot nematode on tomato. *Agr. Ecosyst. Environ.* 53, 71–81. doi: 10.1016/0167-8809(94)00553-Q

Koide, R. T., Dickie, I. A., and Goff, M. D. (1999). Phosphorus deficiency, plant growth and the phosphorus efficiency index. *Funct. Ecol.* 13, 733–736. doi: 10.1046/j.1365-2435.1999.00363.x

Liu, Y. J., Li, D., Zhang, S. Q., Zhang, L. P., Gong, J., Li, Y. H., et al. (2022). Integrated analysis of microarray, small RNA, and degradome datasets uncovers the role of MicroRNAs in temperature-sensitive genic male sterility in wheat. *Int. J. Mol. Sci.* 23, 8057. doi: 10.3390/ijms23158057

Liu, J. N., Ma, X. M., Yan, L. P., Liang, Q., Fang, H. C., Wang, C. X., et al. (2022). MicroRNA and degradome profiling uncover defense response of *fraxinus velutina* torr. to salt stress. *Front. Plant Sci.* 13, 847853. doi: 10.3389/fpls.2022.847853

Liu, H. B., Zhu, R., Shu, K., Lv, W. X., Wang, S., and Wang, C. L. (2022). Aluminum stress signaling, response, and adaptive mechanisms in plants. *Plant Signal. Behav.* 17, 2057060. doi: 10.1080/15592324.2022.2057060

Llorente, F., Muskett,, ,Sanchez-Vallet, P., ,Lopez, A., ,Ramos, G., ,Sanchez-Rodriguez, B., et al. (2008). Repression of the auxin response pathway increases arabidopsis susceptibility to necrotrophic fungi. *Mol. Plant* 1, 496–509. doi: 10.1093/mp/ssn025

Lo Gullo, M. A., and Salleo, S. (1988). Different strategies of drought resistance in three mediterranean sclerophyllous trees growing in the same environmental conditions. *New Phytol.* 108, 267–276. doi: 10.1111/j.1469-8137.1988.tb04162.x

Luo, M., Gao, J., Peng, H., Pan, G. T., and Zhang, Z. M. (2014). MiR393-targeted TIR1-like (F-box) gene in response to inoculation to R.Solani in zea mays. *Acta Physiol. Plant* 36, 1283–1291. doi: 10.1007/s11738-014-1509-9

Lu, Y. B., Qi, Y. P., Yang, L. T., Guo, P., Li, Y., and Chen, L. S. (2015). Boron-deficiency-responsive microrna and their targets in citrus sinensis leaves. *BMC Plant Biol.* 15, 271. doi: 10.1186/s12870-015-0642-y

Martin, E. C., Sukarta, O. C. A., Spiridon, L., Grigore, L. G., Constantinescu, V., Tacutu, R., et al. (2020). LRRpredictor-a new LRR motif detection method for irregular motifs of plant NLR proteins using an ensemble of classifiers. *Genes* 11, 286. doi: 10.3390/genes11030286

Mayzlish-Gat, i., De-Cuyper, C., Goormachtig, S., Beeckman, T., Vuylsteke, M., Brewer, P. B., et al. (2012). Strigolactones are involved in root response to low phosphate conditions in arabidopsis. *Plant Physiol.* 160, 1329–1341. doi: 10.1104/pp.112.202358

McClerklin, S. A., Lee, S. G., Harper, C. P., Nwumeh, R., Jez, J. M., and Kunkel., B. N. (2018). Indole-3-acetaldehyde dehydrogenase-dependent auxin synthesis contributes to virulence of pseudomonas syringae strain DC3000. *PloS Pathog.* 14, e1006811. doi: 10.1371/journal.ppat.1006811

Mendoza-Soto, A. B., Sanchez, F., and Hernandez, G. (2012). MicroRNAs as regulators in plant metal toxicity response. *Front. Plant Sci.* 3, 105. doi: 10.3389/fpls.2012.00105

Meng, N., Tan, X., Caldeon-Villalobos, L. I. A., and Estelle, M. (2008). Mechanism of auxin perception by the SCF-TIR1 ubiquitin ligase. *FASEB J.* 22, 640–645.

Moradi, A., El-Shetehy, M., Gamir, J., Austerlitz, T., Dahlin, P., Wieczorek, K., et al. (2021). Expression of a fungal lectin in arabidopsis enhances plant growth and resistance toward microbial pathogens and a plant-parasitic nematode. *Front. Plant Sci.* 12, 657451. doi: 10.3389/fpls.2021.657451

Muchate, N. S., Nikalje, G. C., Rajurkar, N. S., Suprasanna, P., and Nikam, T. D. (2016). Plant salt stress: Adaptive responses, tolerance mechanism and bioengineering for salt tolerance. *Bot. Rev.* 82, 371–406. doi: 10.1007/s12229-016-9173-y

Munoz, A., Mangano, S., Toribio, R., Fernandez-Calvino, L., del Pozo, J. C., and Mar Castellano, M. (2022). The co-chaperone hop participates in TIR1 stabilisation and in auxin response in plants. *Plant Cell Environ.* 45, 2508–2519. doi: 10.1111/pce.14366

Navarro, L., Dunoyer, P., Jay, F., Arnold, B., Dharmasiri, N., Estelle, M., et al. (2006). A plant miRNA contributes to antibacterial resistance by repressing auxin signaling. *Science* 312, 436–439. doi: 10.1126/science.1126088

Ortiz-Castro, R., Diaz-Perez, C., Martinez-Trujillo, M., del Rio, R. E., Campos-Garcia, J., and Lopez-Bucio, J. (2011). Transkingdom signaling based on bacterial cyclodipeptides with auxin activity in plants. *PNAS* 108, 7253–7258. doi: 10.1073/pnas.1006740108

Ozga, J. A., Jayasinghege, C. P. A., Kaur, H., Gao, L. C., Nadeau, C. D, Reinecke, D. M., et al. (2022). Auxin receptors as integrators of developmental and hormonal signals during reproductive development in pea. *J. Exp. Bot.* 73, 4094–4112. doi: 10.1093/jxb/erac152

Padmanabhan, M. S., Gorepoker, S. P., Golem, S., Shiferaw, H., and and Culver, J. N. (2005). Interaction of the tobacco mosaic virus replicase protein with the Aux/IAA protein PAPI/IAA26 is associated with disease development. *J. Virol.* 79, 2549–2558. doi: 10.1128/JVI.79.4.2549-2558.2005

Pan, J., Fujioka, S., Peng, J., Chen, J., Li, G., and Chen, R. (2009). The E3 ubiquitin ligase $SCF^{TIR1/AFB}$ and membrane sterols play key roles in auxin regulation of endocytosis, recycling, and plasma membrane accumulation of the auxin efflux transporter PIN2 in arabidopsis thaliana. *Plant Cell* 21, 568–580. doi: 10.1105/tpc.108.061465

Park, M., Li, Q., Shcheynikov, N., Muallem, S., and Zeng, W. Z. (2005). Borate transport and cell growth and proliferation - not only in plants. *Cell Cycle* 4, 24–26. doi: 10.4161/cc.4.1.1394

Parry, G., Calderon-Villalobos, L. I., Prigge, M., Peret, B., Dharmasiri, S., Itoh, H., et al. (2009). Complex regulation of the TIR1/AFB family of auxin receptors. *PNAS* 106, 22540–22545. doi: 10.1073/pnas.0911967106

Perez-Torres, C., ,Lopez-Bucio, A., ,Cruz-Ramirez, J., ,Ibarra-Laclette, A., , Dharmasiri, E., ,Estelle, S., et al. (2008). Phosphate availability alters lateral root development in arabidopsis by modulating auxin sensitivity *via* a mechanism involving the TIR1 auxin receptor. *Plant Cell* 20, 3258–3272. doi: 10.1105/tpc.108.058719

Perez Torres, C. A., Lopez Bucio, J., and Herrera Estrella, L. (2009). Low phosphate signaling induces changes in cell cycle gene expression by increasing auxin sensitivity in the arabidopsis root system. *Plant Signal. Behav.* 4, 781–783. doi: 10.4161/psb.4.8.9230

Prigge, M. J., Greenham, K., Zhang, Y., Santner, A., Castillejo, C., Mutka, A. M., et al. (2016). The arabidopsis auxin receptor f-box proteins AFB4 and AFB5 are required for response to the synthetic auxin picloram. *Genes Genom. Genet.* 6, 1383–1390. doi: 10.1534/g3.115.025585

Prigge, M. J., Platre, M., Kadakia, N., Zhang, Y., Greenham, K., Szutu, W., et al. (2020). Genetic analysis of the arabidopsis TIR1/AFB auxin receptors reveals both overlapping and specialized functions. *Elife* 9, e54740. doi: 10.7554/eLife.54740.sa2

Quint, M., and Gray, W. M. (2006). Auxin signaling. *Curr. Opin. Plant Biol.* 9, 448–453. doi: 10.1016/j.pbi.2006.07.006

Rast-Somssich, M. I., Zadnikova, P., Schmid, S., Kieffer, M., Kepinski, S., and Simon, R. (2017). The arabidopsis JAGGED LATERAL ORGANS (JLO) gene sensitizes plants to auxin. *J. Exp. Bot.* 68, 2741–2755. doi: 10.1093/jxb/erx131

Rejeb, I. B., Pastor, V., and Mauch Mani, B. (2014). Plant responses to simultaneous biotic and abiotic stress: Molecular mechanisms. *Plants-Basel* 3, 458–475. doi: 10.3390/plants3040458

Rogato, A., Valkov, V. T., Nadzieja, M., Stougaard, J., and Chiurazzi, M. (2021). The lotus japonicus AFB6 gene is involved in the auxin dependent root developmental program. *Int. J. Mol. Sci.* 22, 8495. doi: 10.3390/ijms22168495

Ruegger, M., Dewey, E., Gray, W. M., Hobbie, L., Turner, J., and Estelle, M. (1998). The TIR1 protein of arabidopsis functions in auxin response and is related to human SKP2 and yeast Grr1p. *Gene Dev.* 12, 198–207. doi: 10.1101/gad.12.2.198

Ruiz-Herrera, L. F., and Lopez-Bucio, J. (2013). Aluminum induces low phosphate adaptive responses and modulates primary and lateral root growth by differentially affecting auxin signaling in arabidopsis seedlings. *Plant Soil* 371, 593–609. doi: 10.1007/s11104-013-1722-0

Sakamoto, T., and Kimura, S. (2018). Plant temperature sensors. *Sensors* 18, 4365. doi: 10.3390/s18124365

Salehin, M., Bagchi, R., and Estelle, M. (2015). $SCF^{TIR1/AFB}$-based auxin perception: Mechanism and role in plant growth and development. *Plant Cell* 27, 9–19. doi: 10.1105/tpc.114.133744

Sattar, S., Addo-Quaye, C., and Thompson, G. A. (2016). miRNA-mediated auxin signalling repression during vat-mediated aphid resistance in cucumis melo. *Plant Cell Environ.* 39, 1216–1227. doi: 10.1111/pce.12645

Seah, S., Telleen, A. C., and Williamson, V. M. (2007). Introgressed and endogenous mi-1 gene clusters in tomato differ by complex rearrangements in flanking sequences and show sequence exchange and diversifying selection among homologues. *Theor. Appl. Genet.* 114, 1289–1302. doi: 10.1007/s00122-007-0519-z

Seifi, A., Visser, R. G. F., and Bai, Y. (2011). Differential expression of TIR-like genes embedded in the mi-1 gene cluster in nematode-resistant and -susceptible tomato roots. *J. Plant Pathol.* 93, 701–706.

Sharma, L., Dalal, M., Verma, R. K., Kumar, S. V. V., Yadav, S. K., Pushkar, S., et al. (2018). Auxin protects spikelet fertility and grain yield under drought and heat stresses in rice. *Environ. Exp. Bot.* 150, 9–24. doi: 10.1016/j.envexpbot.2018.02.013

Sheedy, C., Yau, K. Y. F., Hirama, T., MacKenzie, C. R., and Hall, J. C. (2006). Selection, characterization, and CDR shuffling of naive llama single-domain antibodies selected against auxin and their cross-reactivity with auxinic herbicides from four chemical families. *J. Agr. Food Chem.* 54, 3668–3678. doi: 10.1021/jf060219i

Shimizu-Mitao, Y., and Kakimoto, T. (2014). Auxin sensitivities of all arabidopsis Aux/IAAs for degradation in the presence of every TIR1/AFB. *Plant Cell Physiol.* 55, 1450–1459. doi: 10.1093/pcp/pcu077

Shi, G. G., Wang, S. S., Wang, P., Zhan, J. J., Tang, Y., Zhao, G., et al. (2022). Cotton miR393-TIR1 module regulates plant defense against verticillium dahliae via auxin perception and signaling. *Front. Plant Sci.* 13, 888703. doi: 10.3389/fpls.2022.888703

Shi, H., Ye, T., Han, N., Bian, H., Liu, X., and Chan, Z. (2015). Hydrogen sulfide regulates abiotic stress tolerance and biotic stress resistance in arabidopsis. *J. Integr. Plant Biol.* 57, 628–640. doi: 10.1111/jipb.12302

Shu, W., Liu, Y., Guo, Y., Zhou,, ,Zhang, H., ,Zhao, J., et al. (2015). A populus TIR1 gene family survey reveals differential expression patterns and responses to 1-naphthaleneacetic acid and stress treatments. *Front. Plant Sci.* 6, 719. doi: 10.3389/fpls.2015.00719

Singh, S., Kumar, V., Kapoor, D., Kumar, S., Singh, S., Dhanjal, D. S., et al. (2020). Revealing on hydrogen sulfide and nitric oxide signals co-ordination for plant growth under stress conditions. *Physiol. Plantarum* 168, 301–317. doi: 10.1111/ppl.13066

Strader, L. C., and Zhao, Y. (2016). Auxin perception and downstream events. *Curr. Opin. Plant Biol.* 33, 8–14. doi: 10.1016/j.pbi.2016.04.004

Striegel, S., Oliveira, M. C., Arneson, N., Conley, S. P., Stoltenberg, D. E., and Werle, R. (2021). Spray solution pH and soybean injury as influenced by synthetic auxin formulation and spray additives. *Weed Technol.* 35, 113–127. doi: 10.1017/wet.2020.89

Su, Y. X., Wang, G. L., Huang, Z. Y., Hu, L. L., Fu, T., Wang, X. Y., et al. (2022). Silencing GhIAA43, a member of cotton AUX/IAA genes, enhances wilt resistance *via* activation of salicylic acid-mediated defenses. *Plant Sci.* 314, 111126. doi: 10.1016/j.plantsci.2021.111126

Su, P., Zhao, L., Li, W., Zhao, J., Yan, J., Ma, X., et al. (2021). Integrated metabolo-transcriptomics and functional characterization reveals that the wheat auxin receptor TIR1 negatively regulates defense againstfusarium graminearum. *J. Integr. Plant Biol.* 63, 340–352. doi: 10.1111/jipb.12992

Takato, S., Kakei, Y., Mitsui, M., Ishida, Y., Suzuki, M., Yamazaki, C., et al. (2017). Auxin signaling through $SCF^{TIR1/AFBs}$ mediates feedback regulation of IAA

biosynthesis. *Biosci. Biotech. Bioch.* 81, 1320–1326. doi: 10.1080/09168451.2017.1313694

Termorshuizen, A. J. (2016). Ecology of fungal plant pathogens. *Microbiol. Spectr.* 4. doi: 10.1128/microbiolspec.FUNK-0013-2016

Todd, O. E., Figueiredo, M. R. A., Morran, S., Soni, N., Preston, C., Kubes, M. F., et al. (2020). Synthetic auxin herbicides: Finding the lock and key to weed resistance. *Plant Sci.* 300, 110631. doi: 10.1016/j.plantsci.2020.110631

Verma, V., Ravindran, P., and Kumar, P. P. (2016). Plant hormone-mediated regulation of stress responses. *BMC Plant Biol.* 16, 86. doi: 10.1186/s12870-016-0771-y

Vidal, E. A., Araus, V., Lu, C., Parry, G., Green, P. J., Coruzzi, G. M., et al. (2010). Nitrate-responsive miR393/AFB3 regulatory module controls root system architecture in arabidopsis thaliana. *PNAS* 107, 4477–4482. doi: 10.1073/pnas.0909571107

Vidal, E. A., Moyano, T. C., Riveras, E., Contreras-Lopez, O., and Gutierrez, R. A. (2013). Systems approaches map regulatory networks downstream of the auxin receptor AFB3 in the nitrate response of arabidopsis thaliana roots. *PNAS* 110, 12840–12845. doi: 10.1073/pnas.1310937110

Villalobos, L., Lee, S., De Oliveira, C., Ivetac, A., Brandt, W., Armitage, L., et al. (2012). A combinatorial TIR1/AFB-Aux/IAA co-receptor system for differential sensing of auxin. *Nat. Chem. Biol.* 8, 477–485. doi: 10.1038/nchembio.926

Vitor, S. C., Duarte, G. T., Saviani, E. E., Vincentz, M. G. A., Oliveira, H. C., and Salgado, I. (2013). Nitrate reductase is required for the transcriptional modulation and bactericidal activity of nitric oxide during the defense response of arabidopsis thaliana against pseudomonas syringae. *Planta* 238, 475–486. doi: 10.1007/s00425-013-1906-0

Vo, K. T. X., Rahman, M. M., Rahman, M. M., Trinh, K. T. T., Kim, S. T., and Jeon, J. S. (2021). Proteomics and metabolomics studies on the biotic stress responses of rice: An update. *Rice* 14, 30. doi: 10.1186/s12284-021-00461-4

Walsh, T. A., Neal, R., Merlo, A. O., Honma, M., Hicks, G. R., Wolff, K., et al. (2006). Mutations in an auxin receptor homolog AFB5 and in SGT1b confer resistance to synthetic picolinate auxins and not to 2,4-dichlorophenoxyacetic acid or indole-3-acetic acid in arabidopsis. *Plant Physiol.* 142, 542–552. doi: 10.1104/pp.106.085969

Wang, F., Niu, H., Xin, D., Long, Y., Wang, G., Liu, Z., et al. (2021). OsIAA18, an Aux/IAA transcription factor gene, is involved in salt and drought tolerance in rice. *Front. Plant Sci.* 12, 738660. doi: 10.3389/fpls.2021.738660

Wang, D., Pajerowska-Mukhtar, K., Culler, A. H., and Dong, X. N. (2007). Salicylic acid inhibits pathogen growth in plants through repression of the auxin signaling pathway. *Curr. Biol.* 17, 1784–1790. doi: 10.1016/j.cub.2007.09.025

Wang, P. H., Wu, P. C., Huang, R. C., and Chung, K. R. (2020). The role of a nascent polypeptide-associated complex subunit alpha in siderophore biosynthesis, oxidative stress response, and virulence in *Alternaria alternata*. *Mol. Plant Microbe In.* 33, 668–679. doi: 10.1094/MPMI-11-19-0315-R

Wang, R., Zhang, Y., Kieffer, M., Yu, H., Kepinski, S., and Estelle, M. (2016). HSP90 regulates temperature-dependent seedling growth in arabidopsis by stabilizing the auxin co-receptor f-box protein TIR1. *Nat. Commun.* 7, 1026. doi: 10.1038/ncomms10269

Wang, S. K., Zhang, S. N., Sun, C. D., Xu, Y. X., Chen, Y., Yu, C. L., et al. (2014). Auxin response factor (OsARF12), a novel regulator for phosphate homeostasis in rice (*oryza sativa*). *New Phytol.* 201, 91–103. doi: 10.1111/nph.12499

Watanabe, E., Mano, S., Nomoto, M., Tada, Y., Hara-Nishimura, I., Nishimura, M., et al. (2016). HSP90 stabilizes auxin-responsive phenotypes by masking a mutation in the auxin receptor TIR1. *Plant Cell Physiol.* 57, 2245–2254. doi: 10.1093/pcp/pcw170

Wildermuth, M. C., Dewdney, J., Wu, G., and Ausubel, F. M. (2001). Isochorismate synthase is required to synthesize salicylic acid for plant defence. *Nature* 414, 562–565. doi: 10.1038/35107108

Xia, K., Wang, R., Ou, X., Fang, Z., Tian, C., Duan, J., et al. (2012). OsTIR1 and OsAFB2 downregulation *via* OsmiR393 overexpression leads to more tillers, early flowering and less tolerance to salt and drought in rice. *PloS One* 7, 364–373. doi: 10.1371/journal.pone.0030039

Xie, Q., Frugis, G., Colgan, D., and Chua, N. H. (2000). Arabidopsis NAC1 transduces auxin signal downstream of TIR1 to promote lateral root development. *Gene Dev.* 14, 3024–3036. doi: 10.1101/gad.852200

Xu, J. Q., Liu, X. D., Napier, R., Dong, L. Y., and Li, J. (2022). Mode of action of a novel synthetic auxin herbicide halauxifen-methyl. *Agronomy-Basel* 12, 1659. doi: 10.3390/agronomy12071659

Yang, C. W., Deng, W., Tang, N., Wang, X. M., Yan, F., Lin, D. B., et al. (2013). Overexpression of ZmAFB2, the maize homologue of AFB2 gene, enhances salt tolerance in transgenic tobacco. *Plant Cell Tiss. Org.* 112, 171–179. doi: 10.1007/s11240-012-0219-5

Yang, Y., and Guo, Y. (2018). Unraveling salt stress signaling in plants. *J. Integr. Plant Biol.* 60, 796–804. doi: 10.1111/jipb.12689

Yu, H. Y., Huang, S. T., Chen, P. P., Ji, M. J., Cui, H. L., Chen, J. C., et al. (2021). Different leaf-mediated deposition, absorbed and metabolism behaviors of 2,4-d isooctyl ester between Triticum aestivum and *Aegilops tauschii* coss. *Pestic. Biochem. Phys.* 175, 104848. doi: 10.1016/j.pestbp.2021.104848

Yu, Z., Zhang, F., Friml, J., and Ding, Z. (2022). Auxin signaling: Research advances over the past 30 years. *J. Integr. Plant Biol.* 64, 371–392. doi: 10.1111/jipb.13225

Zhang, R. M., Sun, Y. K., Liu, Z. Y., Jin, W., and Sun, Y. (2017). Effects of melatonin on seedling growth, mineral nutrition, and nitrogen metabolism in cucumber under nitrate stress. *J. Pineal. Res.* 62, e12403. doi: 10.1111/jpi.12403

Zhang, H. H., Tan, X. X., Li, L. L., He, Y. Q., Hong, G. J., Li, J. M., et al. (2019). Suppression of auxin signalling promotes rice susceptibility to rice black streaked dwarf virus infection. *Mol. Plant Pathol.* 20, 1093–1104. doi: 10.1111/mpp.12814

Zhang, A. Y., Yang, X., Lu, J., Song, F. Y., Sun, J. H., Wang, C., et al. (2021). OsIAA20, an Aux/IAA protein, mediates abiotic stress tolerance in rice through an ABA pathway. *Plant Sci.* 308, 110903. doi: 10.1016/j.plantsci.2021.110903

Zhao, J., Yuan, S., Zhou, M., Yuan, N., Li, Z., Hu, Q., et al. (2019). Transgenic creeping bentgrass overexpressing osa-mir393a exhibits altered plant development and improved multiple stress tolerance. *Plant Biotechnol. J.* 17, 233–251. doi: 10.1111/pbi.12960

Zhu, J. K. (2002). Salt and drought stress signal transduction in plants. *Annu. Rev. Plant Biol.* 53, 247–273. doi: 10.1146/annurev.arplant.53.091401.143329

Zimaro, T., Gottig, N., Garavaglia, B. S., Gehring, C., and Ottado, J. (2011). Unraveling plant responses to bacterial pathogens through proteomics. *J. Biomed. Biotechnol.* 2011, 354801. doi: 10.1155/2011/354801

frontiers | Frontiers in Plant Science

TYPE Original Research
PUBLISHED 01 December 2022
DOI 10.3389/fpls.2022.1073917

OPEN ACCESS

EDITED BY
Chao Li,
Northwest AF University, China

REVIEWED BY
Qiang-Sheng Wu,
Yangtze University, China
Cuiying Li,
Northwest AF University, China

*CORRESPONDENCE
Dong Liang
liangeast@sicau.edu.cn

†These authors contributed equally to this work

SPECIALTY SECTION
This article was submitted to Plant Abiotic Stress, a section of the journal Frontiers in Plant Science

RECEIVED 19 October 2022
ACCEPTED 17 November 2022
PUBLISHED 01 December 2022

CITATION
Xia H, Yang C, Liang Y, He Z, Guo Y, Lang Y, Wei J, Tian X, Lin L, Deng H, Wang J, Lv X and Liang D (2022) Melatonin and arbuscular mycorrhizal fungi synergistically improve drought toleration in kiwifruit seedlings by increasing mycorrhizal colonization and nutrient uptake. *Front. Plant Sci.* 13:1073917. doi: 10.3389/fpls.2022.1073917

Melatonin and arbuscular mycorrhizal fungi synergistically improve drought toleration in kiwifruit seedlings by increasing mycorrhizal colonization and nutrient uptake

Hui Xia[1†], Chunguo Yang[1†], Yan Liang[1], Zunzhen He[1], Yuqi Guo[1], Yuxuan Lang[1], Jie Wei[2], Xinbo Tian[1], Lijin Lin[1], Honghong Deng[1], Jin Wang[1], Xiulan Lv[1] and Dong Liang[1*]

[1]College of Horticulture, Sichuan Agricultural University, Chengdu, China, [2]College of Life Sciences, Inner Mongolia University, Hohhot, China

Kiwifruit is a vine fruit tree that is vulnerable to water deficiency due to its shallow root system and large leaves. Although mycorrhizal inoculation and melatonin application has been proved to improve plants drought tolerance, their interaction effects are still unclear. In this study, arbuscular mycorrhizal (AM) fungi incubation and melatonin (MT) irrigation were applied to kiwifruit seedlings alone or in combination to investigate their effect on drought tolerance. The results revealed that AM had more effect on promoting root biomass, water use efficiency, and uptake of nitrogen, phosphorus and iron. While MT was more effective in promoting shoot biomass and antioxidant enzyme activities to remove reactive oxygen species accumulation. Moreover, MT supplementary significantly increased the AM colonization, spore density and hyphal length density in roots. Therefore, combined application of AM fungi and MT had additive effects on improvement biomass accumulation, increasing chlorophyll content, photosynthetic efficiency, catalase activity, and decreasing malondialdehyde accumulation under drought stress, thus promoting plant growth and alleviating the drought damage to plant. These results provide guidance for AM and MT combined application to improve abiotic resistance in plants.

KEYWORDS

arbuscular mycorrhizal fungi, melatonin, kiwifruit, drought tolerance, biomass, nutrient uptake

Introduction

Water scarcity caused by global warming is becoming more common, posing a huge challenge to agricultural production, and resulting in large-scale crop losses and food shortages for mankind (Zhang et al., 2018; Rivero et al., 2022). Plants have evolved a series of mechanisms to cope with drought stress, such as prolonged root growth, regulating stomata movement, and maintaining the osmotic balance of cells (Mathur and Roy, 2021). In addition, plants also use a variety of enzymatic and non-enzymatic antioxidants to efficiently and rapidly remove reactive oxygen species (ROS) (Fang and Xiong, 2015; Khan et al., 2021).

Plant growth-promoting rhizobacteria, such as arbuscular mycorrhizal (AM) fungi, play an important role in alleviating drought stress in plants (Vurukonda et al., 2016; Porter et al., 2020; Abdelaal et al., 2021). AM, act as an extension of the plant root system, provide their host plants with access to soil water and nutrients through far-reaching extra radical hyphae, while fungi are provided with carbon from host plants (Gutjahr and Paszkowski, 2013; Frew et al., 2022). Most importantly, this symbiosis relationship creates a functionally active ecosystem that influence nutrient cycling, decomposition, soil aggregation, belowground biodiversity, and plant community ecology (Kaushal, 2019; Zhang et al., 2020). Under drought stress, AM reduced the damage of free radicals by promoting nutrient absorption capacity, improving root function, maintaining leaf photosynthetic efficiency (Lenoir et al., 2016). In addition, extrapular-root mycelium formed a huge mycelium network in the soil, increasing root xylem conductance and improving the adaptability of water transport (Abdelaal et al., 2021; Sun et al., 2022). Meanwhile, the polysaccharides produced by fungi also have the ability to increase mineral strength and retain water (Hooker et al., 2007).

Melatonin (N-acetyl-5-methoxy-tryptamine), as a master regulator, participant in plant development and protects plant against almost all abiotic stresses, such as drought, salt damage, heavy metals, UV radiation, high temperature, cold damage, etc. (Arnao and Hernández-Ruiz, 2019; Sun et al., 2021). Melatonin ameliorates the adverse effects of drought by regulating morphological, physiological and redox regulatory processes, and a variety of regulatory mechanisms have been explored in recent years (Tiwari et al., 2021). Most fundamentally, melatonin has the strong antioxidant activity to remove ROS and free radicals caused by stress, by improving antioxidant enzymes activities, such as ascorbic acid, ascorbate peroxidase, superoxide dismutase (SOD), catalase (CAT) and peroxidase (POD), and the content of antioxidants such as flavonoids (Huang et al., 2019). Melatonin also affects the nutrients absorption from soil by regulating the activity and expression of nutrient transporters (Xia et al., 2021; Arnao et al., 2022; Du et al., 2022; Sun et al., 2022). Melatonin was also found can solve the replant problem by altering the composition of bacterial and fungal communities (Li et al., 2018), and promoted the primary root growth in *Arabidopsis* (Yang et al., 2021).

Kiwifruit (*Actinidia chinensis* Planch.) is an emerging fruit tree grown worldwide, but it is more vulnerable to drought than other fruit trees because of its shallow, fleshy root system and large, hairy leaves (Liang et al., 2019). It has been confirmed that melatonin pretreatment can increase the biomass of kiwifruit seedlings by improving leaf photosynthetic capacity and carbon fixation, and improve the drought tolerance of kiwifruit seedlings by promoting root elongation and growth and increasing antioxidant content (Liang et al., 2019; Xia et al., 2020). However, whether melatonin and AM have synergistic effects on drought resistance in plants is still unknown. In this study, AM fungi and melatonin were applied to kiwifruit seedlings alone or in combination to investigate the effect on plant growth, photosynthesis, antioxidant enzyme activity, nutrient absorption, in order to further find a better scheme to improve the drought tolerance of kiwifruit for field cultivation.

Materials and methods

Plant materials preparation and treatment

Kiwifruit seeds (*Actinidia chinensis*) were planted in a tray containing mixed matrix and grown in a light incubator after germination treatment according to the method of Liang et al. (2019). When grow to 6-true leaves, the seedlings were then transformed into pots (18*20*20 cm) containing 1.5 kg mixed soil (garden soil: peat soil: perlite = 2:1:1, V/V/V), and placed in a greenhouse at Chengdu Campus of Sichuan Agricultural University (103°51′ E, 30°42′ N) under natural light and temperature conditions. Each pot planted 2 seedlings. After two weeks of cultivation for adaption, 96 pots of uniform seedlings were selected and evenly divided into two groups for normal watering treatment and drought treatment, and each contained four treatments, including 1) the control (CK), treated with water; 2) inoculated AM fungi in soil (AM); 3) root irrigation with melatonin solution (MT); and 4) combination treatment with melatonin and AM (AM+MT) under drought or normal watering condition. First, 10.0 g sterilized or non-sterilized mycorrhizal (*Rhizophagus intraradices*), purchased from Nanjing Cuijingyuan Biotechnology Co., Ltd. was inoculated in the soil for 4 weeks to form mycorrhizas. Then seedings were irrigated with 200 mL water or 100 μM melatonin solution for twice at three-day intervals at nightfall, followed by water control treatment. The melatonin concentration was chosen based on our previous study (Xia et al., 2020). Soil moisture content was maintained at 50~55% of maximum water holding capacity for drought treatment using soil weighing method, while 80~85% of maximum water holding capacity for watering treatment. Each treatment included 12 pots (24 seedlings), seedlings in two pots were collected as a repeat and, repeated 6 times. Samples were collected at 12 d of drought

treatment. The mature leaves (from 3rd to 5th) were sampled and frozen with liquid nitrogen and stored at -80°C for physiological index determination. Then the whole plants were removed from the soil and cleaned for biomass determination.

The arbuscular mycorrhizal fungi tested

The harvested fresh seedling roots were cleaned and stained with 0.05% trypan blue, followed by washing and decolorization with lactic acid glycerol solution (lactic acid, glycerol, distilled water = 1:1:1 (v/v/v), and then the roots were observed under a microscope (50 per plant, 5 per treatment). AM colonization was calculated according to the method of Biermann and Linderman (1981). The grid line intersection method of Yang et al. (2020) was used to determine spore density and hyphal length density.

Plant growth parameters determination

After being removed from the soil and cleaned, the plant height, root length, and stem diameter were determined with a meter ruler or vernier caliper. The dry weight of the shoot and root were weighed after drying in an oven at 105°C, then baked at 80°C until constant weight. all data contained three biological repeats.

Pigment content determination

The determination of chlorophyll content was improved according to the method of Liang et al. (2019). The 0.1 g fresh leaves were cut into pieces and put into a centrifuge tube containing 8 mL 80% acetone, and kept in dark for 48 h, shacked 3-4 times. The absorbance values of the supernatant at 663, 645 and 470 nm were determined by UV/V spectrophotometer (UV-2550). The content of total chlorophyll, chlorophyll a, and chlorophyll b was calculated.

Determination of gas exchange parameters

A portable gas exchange system (LI-6400, Li-Cor Inc., USA) was used to determine photosynthetic gas exchange parameters between 9:00 am and 11:00 am, including net photosynthetic rate (Pn), transpiration rate (Tr), intercellular CO_2 concentration (Ci), stomatal conductance (Gs) and water use efficiency (WUE). A red/blue LED light source, a constant flow rate of 500 mL·min^{-1} and CO^2 concentration of ca. 400 μmol·mol^{-1} under a PAR of 1000 μmol·m^{-2}s^{-1} were used. At least 3 seedlings were measured in each treatment.

Determination of physiological indexes

The relative electrical conductivity (REL) and the content of malondialdehyde (MDA), proline, soluble protein and soluble sugar were determined according to the methods of Liu et al. (2020). Regards to antioxidant enzyme activity, the frozen leaf samples were homogenized in liquid nitrogen and extracted with an extraction buffer composed of 100 mM potassium phosphate buffer (pH 7.8), 0.1 mM EDTA and 10 mM ascorbic acid. The supernatant after centrifugation was used to determine the activities of superoxide dismutase (SOD), catalase (CAT) and peroxidase (POD) (Cakmak and Marschner, 1992).

Determination of nutrients content

0.2 g of dry leaves were digested with 10 mL nitric acid and 2 mL perchloric acid, and boiled until white crystal appeared in graphite digestion machine (Xiyang Instrument Co., Ltd., Shanghai, China) (about 2 h). After cooling, the volume was fixed to 25 mL with ultrapure water for the determination of the content of each element. The content of nitrogen (N), phosphorus (P) and potassium (K) was determined by Kjeldahl nitrogen analyzer (KDN-04C Tuopuyunnong Technology Co., Ltd., Zhejiang, China), molybdenum-antimony resistance colorimetry, and flame photometer (INESA Scientific Instrument Co., Ltd, Shanghai, China), respectively. The content of iron (Fe), manganese (Mn), copper (Cu) and zinc (Zn) were determined by atomic absorption spectrophotometry using inductively coupled plasma emission spectrometry (ICP-OES, Optima 8000, PerkinElmer, USA).

Gene expression assay

Total RNA was extracted using the Mini RNA Isolation I Kit (Beijing Tianmo Sci & Tech Development Co., Ltd, China) according to the manufacturer's instructions. The first strand cDNA was obtained by reverse transcribing RNA with PrimeScript™ RT reagent Kit with gDNA eraser (Perfect Real Time) (Takara, Japan). The gene-specific primers were designed using Primer Premier5 and synthesized by Tsingke Biotechnology Co., Ltd (Beijing, China). *Actin* was used as the reference (Xia et al., 2020). Quantitative Realtime PCR was performed on the CFX96 Real-Time System C1000 Thermal Cycler (Bio-RAD, Hercules, CA, USA) using an SYBR® Premix Ex Taq™ II (Tli RnaseH Plus) kit (TaKaRa, Japan). The reaction conditions were as follows: 95 °C for 30 s, followed by 40 cycles of 95 °C for 5 s, and at 52 °C to 55 °C for 30 s. Each sample was subjected to three replicates. The $2^{-\Delta\Delta CT}$ method was used to calculate the relative mRNA expression level.

Statistical analysis

Data were expressed as mean ± standard deviation (SD). One-way analysis of variance (ANOVA) and Tukey's *Post Hoc* test ($p < 0.05$) was used to test the difference between the treatments using SPSS.

Results

AM fungal growth and mycorrhizal colonization

The infection of AM fungi with or without MT on the root system of kiwifruit seedlings was observed by trypan blue staining (Figure 1) The results showed that the roots of uninoculated seedlings were not infected by AM fungi, while the roots of seedlings inoculated with AM fungi for 50 d showed plenty of mycelia, vesicles and typical arbuscule structures after inoculation with AM fungi. This indicated that AM fungi and kiwifruit seedling roots established a good symbiotic relationship.

Encouragingly, melatonin treatment effectively increased root infection by inoculating AM fungi. The infection rate increased by 14.6% under normal watering condition and 37.4% under drought condition. In addition, the spore density and hyphal length density increased by 40.6% and 40.7% under drought, respectively (Table 1). The results suggest that melatonin played a role to promote the colonization of *R. intraradices* in the root, thus forming a symbiotic relationship.

Effect of treatments on plant growth and biomass

After 12 d of drought treatment, the seedling leaves were seriously dehydrated and wilted, and roots, especially lateral roots, were significantly reduced and shortened (Figures 2A, B). AM, MT and AM+MT treatments apparently alleviated the morphological damage caused by drought, exhibited reduced leaf wilting and increased root length and abundance compared with CK.

Accordingly, the application of AM and MT improved seedling growth under drought stress. AM and AM+MT treatments significantly increased shoot length, stem diameter, leaf area, root length, and shoot and root dry mass under well-watering condition, while MT alone application only increased the leaf area and shoot dry mass (Figure 3). AM+MT treatment had best effect in increase shoot and root dry mass by 25% and 41.18%, respectively, compared with CK (Figures 3E, F).

Effect of treatments on photosynthetic pigments and gas exchange parameters

Under drought stress, the content of chlorophyll a, b and total chlorophyll decreased greatly (Figures 4A-C). Application

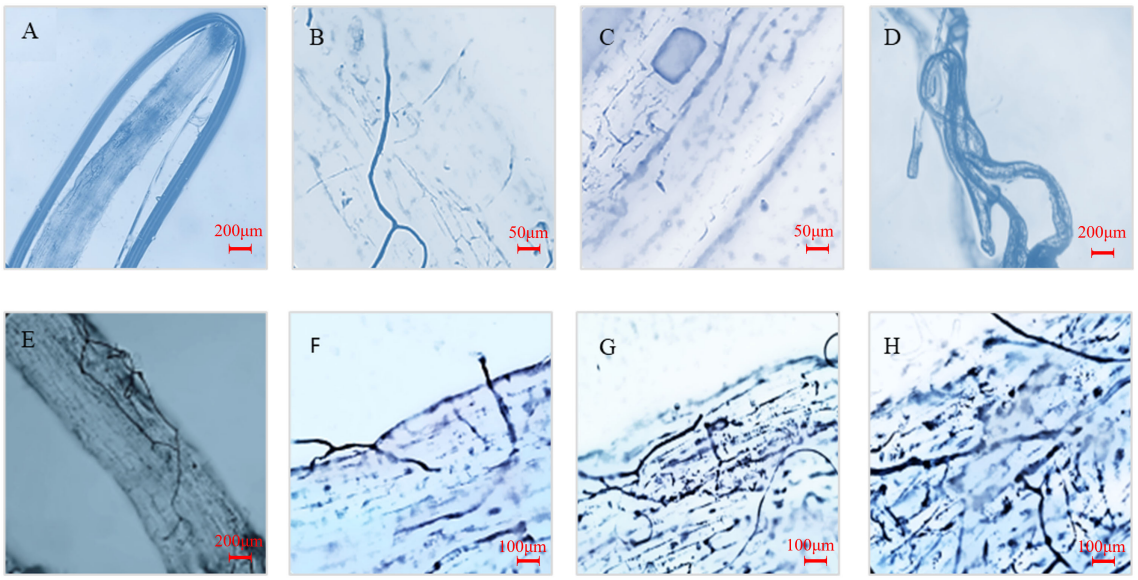

FIGURE 1
Mycorrhizal phenotype of seedling roots inoculated with *R. intraradices* after 12 d of drought treatment. **(A)** Roots of seedlings not inoculated with AM fungi; **(B–D)** Hyphae, vesicles and arbuscules in roots after mycorrhizal infection; **(E, F)**: Mycorrhizal infection of roots without external melatonin treatment; **(G, H)** Mycorrhizal infection of roots treated with external melatonin.

10.3389/fpls.2022.1073917

TABLE 1 Effects melatonin application on AM colonization, spore density and hyphal length density in seedling roots inoculated with *R. intraradices*.

Treatments		AM fungal status		
		MC (%)	SPD (number/g)	HLD (m/g)
WW	-MT	65.7 ± 0.76b	6.27 ± 0.27c	2.34 ± 0.08b
	+MT	75.3 ± 2.33a	7.58 ± 0.09b	3.77 ± 0.17a
DR	-MT	52.9 ± 1.66c	6.50 ± 0.13c	1.62 ± 0.03c
	+MT	72.7 ± 2.99a	9.14 ± 0.16a	2.28 ± 0.04b

The values (means ± SD, n = 6) followed by different letters in the same column reprensent significant difference at $p < 0.05$ assayed by Tukey's Post Hoc test. MC, AM colonization; SPD, spore density; HLD, hyphal length density; WW, well-watering; DR, drought stress; -MT, non-melatonin application; +MT, melatonin application.

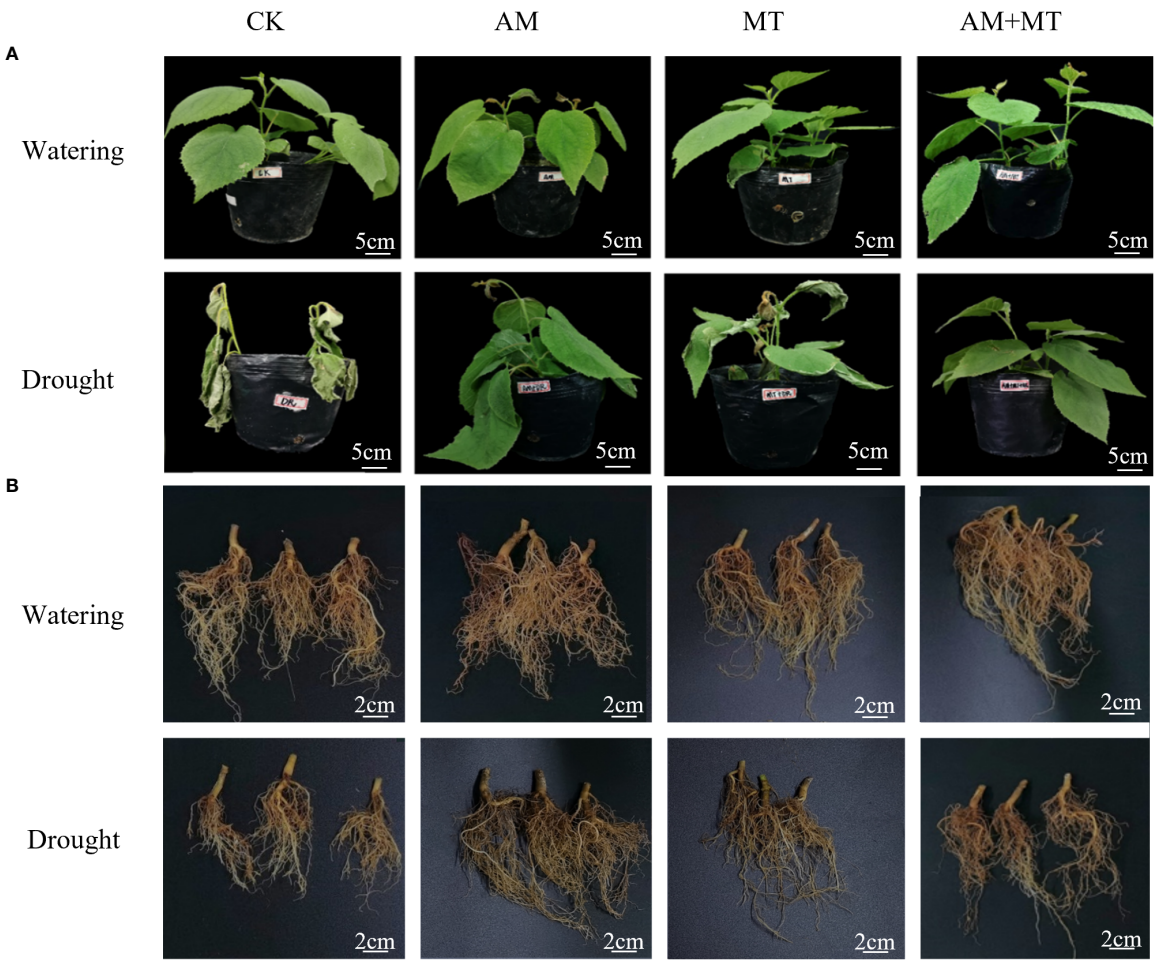

FIGURE 2
Effect of treatment on plant growth of above-ground **(A)** and under-ground **(B)** parts under well watering and drought condition. Treatments included CK (the control), AM (inoculated with arbuscular mycorrhiza), MT (irrigated with 100 μM melatonin), and AM+MT (treated with melatonin and arbuscular mycorrhiza).

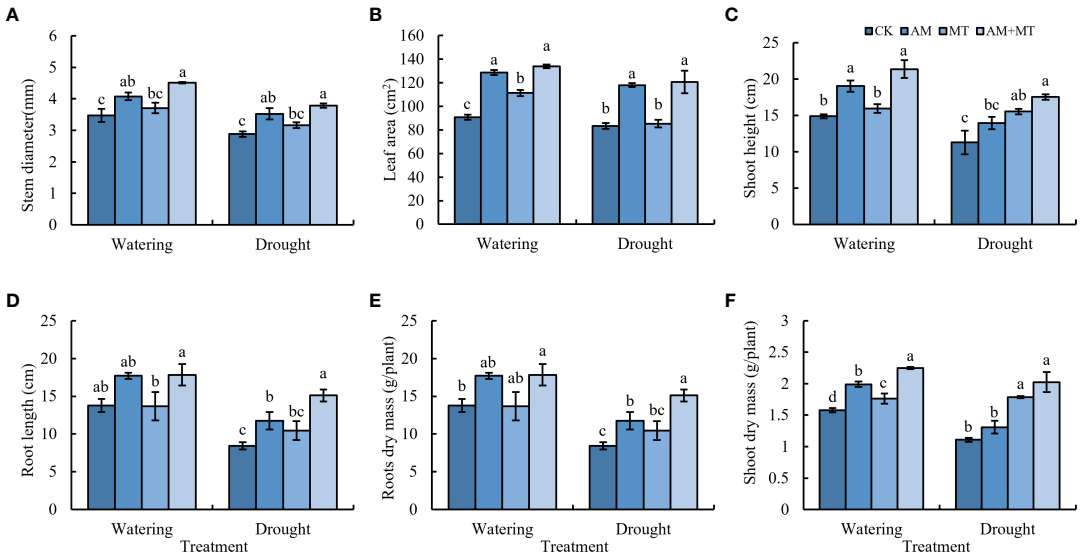

FIGURE 3
Effect of treatments on plant growth, including stem diameter **(A)**, leaf area **(B)**, shoot length **(C)**, root length **(D)**, root dry mass **(E)**, shoot dry mass **(F)**. Data are presented as meant ± SD (n = 6), different letters indicate significant differences between treatments at $p < 0.05$ by Tukey's *Post Hoc* test. Treatments included CK (the control), AM (inoculated with arbuscular mycorrhiza), MT (irrigated with 100 μM melatonin), and AM +MT (treated with melatonin and arbuscular mycorrhiza).

of AM fungi, MT alone or combined significantly increased the content of chlorophyll a, b and total chlorophyll by 25.93%, 11.11% and 35.19%, respectively, compared with CK. Results suggested that AM+MT had the best effect on the enhancement of chlorophyll content under drought condition.

Gas exchange parameters, Pn, Gs, Tr, Ci, and WUE were determined. Values of all parameters were significantly lower under drought stress than under well watering. Application of AM and MT alone didn't have significant effect on Pn, Gs, Tr and Ci. While when combined AM and MT applied together, values of Pn, Gs, Ci and Tr were increased by 180.96%, 168.72%, 38.55% and 218.99% compared with CK, respectively (Figure 5). AM treatment significantly improved the WUE value compared with other treatments.

Effect of treatments on MDA, REL and osmotic substances

MDA and REL are important indexes to reflect the damage degree of plant cell membrane caused by stress. Under well-watering condition, inoculation of AM fungi, MT application and their combination decreased MDA content, while maintained the relative electronic leakage (REL) in leaves. Water deficit dramatically increased MDA content and REL in leaves, suggestion seedlings were seriously stressed. Pretreatment of AM fungus, MT and their combined significantly reduced the increase of MDA content and REL value compared with the control. In addition, combined application of AM and MT had the best alleviating effect on drought stress than alone (Figures 6A, B).

The contents of proline, soluble sugar and soluble protein in leaves decreased due to drought stress (Figure 6C). After treatment with AM, MT and AM+MT, they all increased. Soluble sugar content increased most with more 9%, especially in treatment with MT, and proline content increased most in AM+MT groups by 28.8% (Figures 6D, E).

Effect of treatments on antioxidant enzyme activities and gene expression

Treatments of AM, MT and AM+MT significantly increased the activities of SOD and POD in kiwifruit seedling leaves under well-watering condition. Drought stress increased the activity of antioxidant enzymes. Under drought stress, AM, MT and AM +MT treatments increased SOD activity by 12.91%, 12.03% and 19.53%, and improved POD activity by 7.96%, 8.13% and 11.41% compared with CK. AM and MT alone had little effect on CAT activity, while AM+MT increased CAT activity by 13.18%. The results showed that the combined application of AM and MT had the strongest effect on improving the activities of SOD, POD and CAT (Figures 7A-C).

After 12 d of drought stress, the expression of all antioxidant enzyme genes (*SOD*, *SOD[Cu-Zn]*, *POD12*, *POD42*, *CAT1* and *CAT6*) in mycorrhizal plants was higher than that in non-

10.3389/fpls.2022.1073917

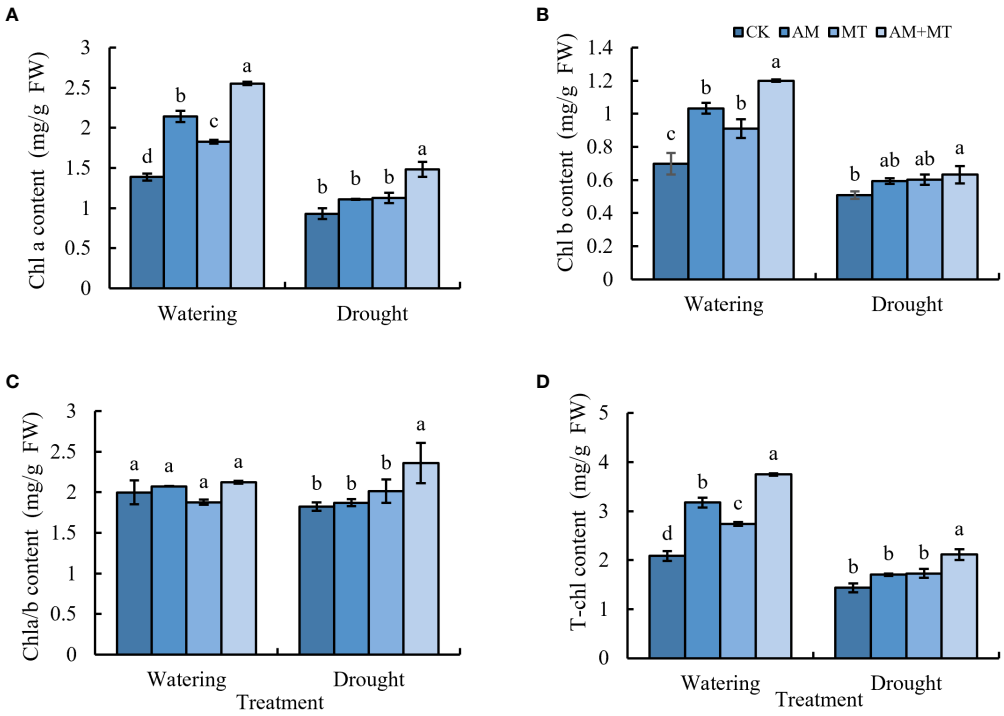

FIGURE 4
The content of chlorophyll a **(A)**, chlorophyll b **(B)**, total chlorophyll **(C)**, and chlorophyll a/b **(D)** in kiwifruit seedlings under well-watering or drought condition. Data are presented as meant ± SD (n = 6), different letters indicate significant differences between treatments at $p < 0.05$ by Tukey's *Post Hoc* test. Treatments included CK (the control), AM (inoculated with arbuscular mycorrhiza), MT (irrigated with 100 μM melatonin), and AM+MT (treated with melatonin and arbuscular mycorrhiza).

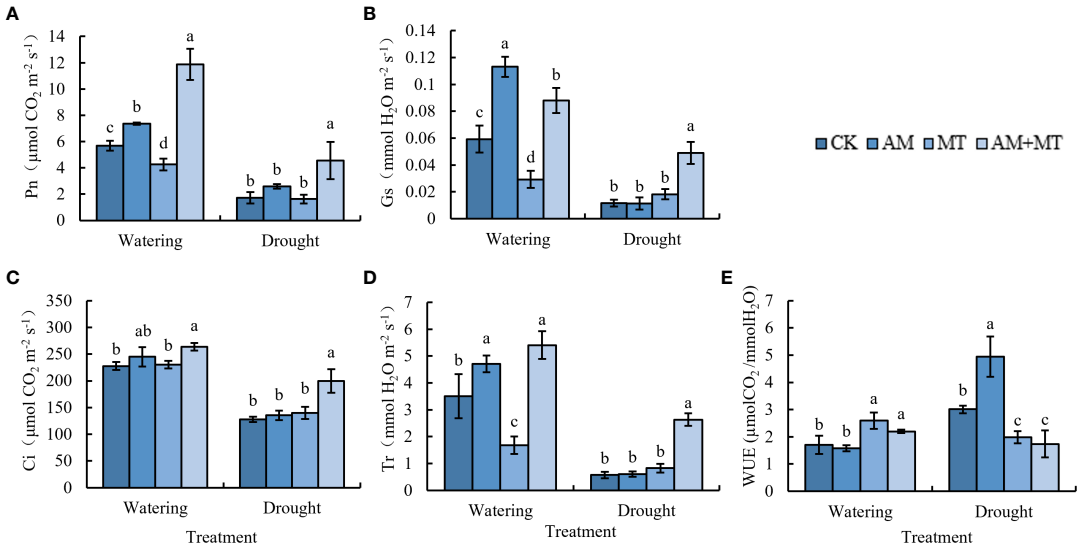

FIGURE 5
Effect of treatments on gas exchange parameters in kiwifruit seedlings under well-watering or drought stress, including net photosynthetic rate **(A)**, stomatal conductance **(B)**, intercellular CO_2 concentration **(C)**, transpiration rate **(D)** and water use efficiency **(E)**. Data are presented as meant ± SD (n = 6), different letters indicate significant differences between treatments at $p < 0.05$ (Tukey's *Post Hoc* test). Treatments included CK (the control), AM (inoculated with arbuscular mycorrhiza), MT (irrigated with 100 μM melatonin), and AM+MT (treated with melatonin and arbuscular mycorrhiza).

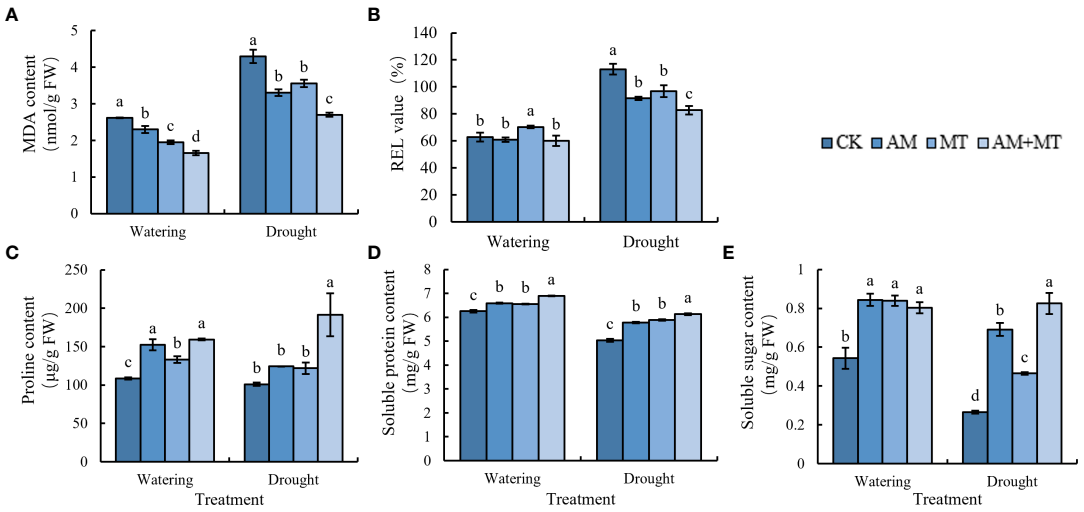

FIGURE 6
Changes of MDA **(A)**, REL **(B)**, proline **(C)**, soluble protein **(D)**, and soluble sugar **(E)** in kiwifruit seedlings under well watering and drought stress. Data are presented as meant ± SD (n = 6), different letters indicate significant differences between treatments at $p < 0.05$ by Tukey's *Post Hoc* test. Treatments included CK (the control), AM (inoculated with arbuscular mycorrhiza), MT (irrigated with 100 μM melatonin), and AM+MT (treated with melatonin and arbuscular mycorrhiza).

mycorrhizal plants. AM+MT treatments significantly affected the expression of *SOD* and *POD12* in leaves, while had no significant effect on the expression of *Cu/Zn-SOD* and *CAT1* in leaves (Figures 7D-I).

Effect of treatments on nutrient absorption

Under watering condition, AM and AM+MT treatments significantly increased the content of N and P in kiwifruit seedling leaves, while the content of K was not significantly changed (Figures 8A-C). Under drought stress, the content of N and P in CK decreased significantly, AM and AM+MT treatments significantly increased the contents of N and P. The effect of AM on N content is greater than that of MT, and MT on P content is greater than that of AM.

For mineral nutrients, AM increased the content of Cu, but decreased the absorption of Mn and Zn, while MT increased the content of Zn under well-watering condition. Under drought stress, AM and MT treatment alone increased the content of Fe and Zn, but decreased Cu content (Figures 8D-G).

Effect of treatments on expression of PHT1 genes

Phosphorous transporter class 1 (PHT1) serves as the primary transporters involved in phosphorous uptake from the rhizosphere (Sun et al., 2012). A total of 11 PHT1 genes were identified in *Actindia* using transcriptome data previously obtained by our team. Six PHT1s were detected expression during drought treatment. MT and AMF inoculation significantly induced the expression of the predicted six PHT1s under drought conditions. Both AMF and MT treatments up-regulated the expression of *AcPHT1;1*, *AcPHT1;2, and AcPHT1;6*. Furthermore, the combined treatment of MT and AMF significantly up-regulated the expression of all six genes, and the effect was significant than that of treatment alone (Figures 9A-F).

Discussion

Improving crop drought resistance and reducing yield loss have always been the focus of global agricultural production (Zhang et al., 2021). In addition to breeding resistant varieties and mining resistance genes afford by scientists, improving plant water use efficiency and resistance by use of exogenous stimulants or bacterial agents seems to be more effective way to conquer abiotic stresses brought about by climate change and thus is favored by farmers (Farooq et al., 2019).

Increasing evidence studies have demonstrated that MT application and AM fungi inoculation have positive effects on plant growth under drought conditions (Liu et al., 2020; Bolin et al., 2022). AM fungi alleviate drought stress through several mechanisms (Abdel-Salam et al., 2017). One most important is that AM fungi induce changes in plant root structure, especially

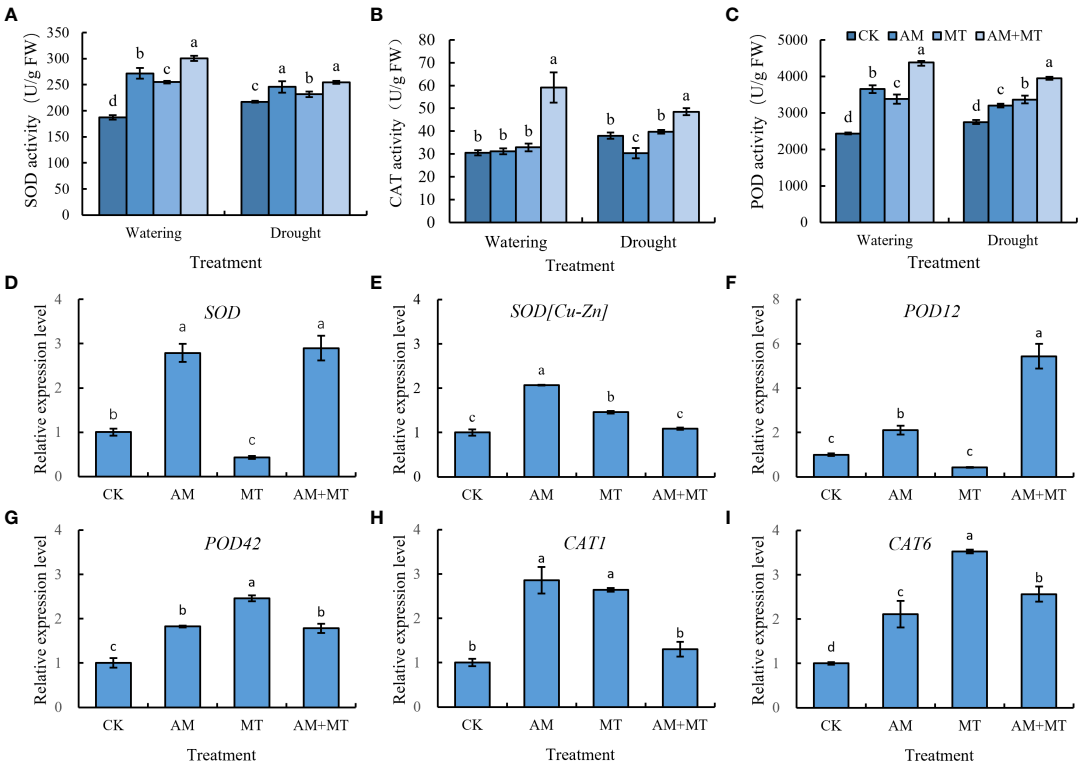

FIGURE 7
Changes of antioxidant activity of SOD **(A)**, CAT **(B)**, and POD **(C)**, and gene expression **(D–I)** in kiwifruit seedlings under well watering and drought stress. Data are presented as meant ± SD (n = 3), different letters indicate significant differences between treatments at $p < 0.05$ by Tukey's *Post Hoc* test. Treatments included CK (the control), AM (inoculated with arbuscular mycorrhiza), MT (irrigated with 100 μM melatonin), and AM+MT (treated with melatonin and arbuscular mycorrhiza).

the increase of root length, root surface area, root volume and root tip number. Improvements in the root structure of mycorrhizal plants allows extraparal hyphae to extend beyond the barren areas of the plant rhizosphere, thus more efficiently absorbing water and low-mobility mineral nutrients under water scarcity conditions (Müller, 2021; Persi and Maherali, 2021). Melatonin, on the other hand, promotes the growth of lateral root (Bian et al., 2021). In this study, both melatonin and AM application alone reduced the decline of dry biomass (Figure 2). However, inoculation with AM fungi had a greater effect on increasing root biomass than melatonin, melatonin increased shoot biomass significantly, and their combination had the strongest effect, which was consistent with previous study (Liu et al., 2020). These results indicated that AM fungi and melatonin may drive different mechanisms to alleviate drought stress (Yang et al., 2020).

Plants rely on chlorophyll for photosynthesis to accumulate biomass (Nozue et al., 2016). Under drought stress, their cells undergo plasmid lysis, chloroplast membrane rupture, ultrastructural damage, and chlorophyll synthesis decreases and degradation accelerates, leading to the reduction of its content and photosynthetic capacity, which further affects plant growth and yield (Tambussi et al., 2000; Munné-Bosch et al., 2001). In this study, melatonin treatment and AM fungi inoculation increased the content of chlorophyll a, and b in kiwifruit seedlings under drought stress (Figure 4), which was inconsistent with previous studies (Liang et al., 2019; Xia et al., 2020).

Under drought stress, plants increase water use efficiency mainly by closing stomata to reduce transpiration, but preventing carbon dioxide from entering mesophyll cells leads to a decrease in photosynthetic rate Pn, which is known as a stomatal limiting strategy (Du et al., 2018). Our results also confirmed a synchronously decline of Pn, Gs, Tr, and Ci under drought stress. However, the application of melatonin and AM did not significantly promote Pn, Gs, Tr, and Ci under drought stress, which was different from previous results (Liang et al., 2019), possibly because the weakened effect due to prolonged treatment time. Interestingly, the combined application of MT and AM had a greater effect on increasing Pn, Gs, Tr, and Ci, indicating an obvious superposition effect, as in study of tobacco (Liu et al., 2020).

Recent studies have found that melatonin enhances plant uptake of nutrients. For example, the concentrations of nitrogen,

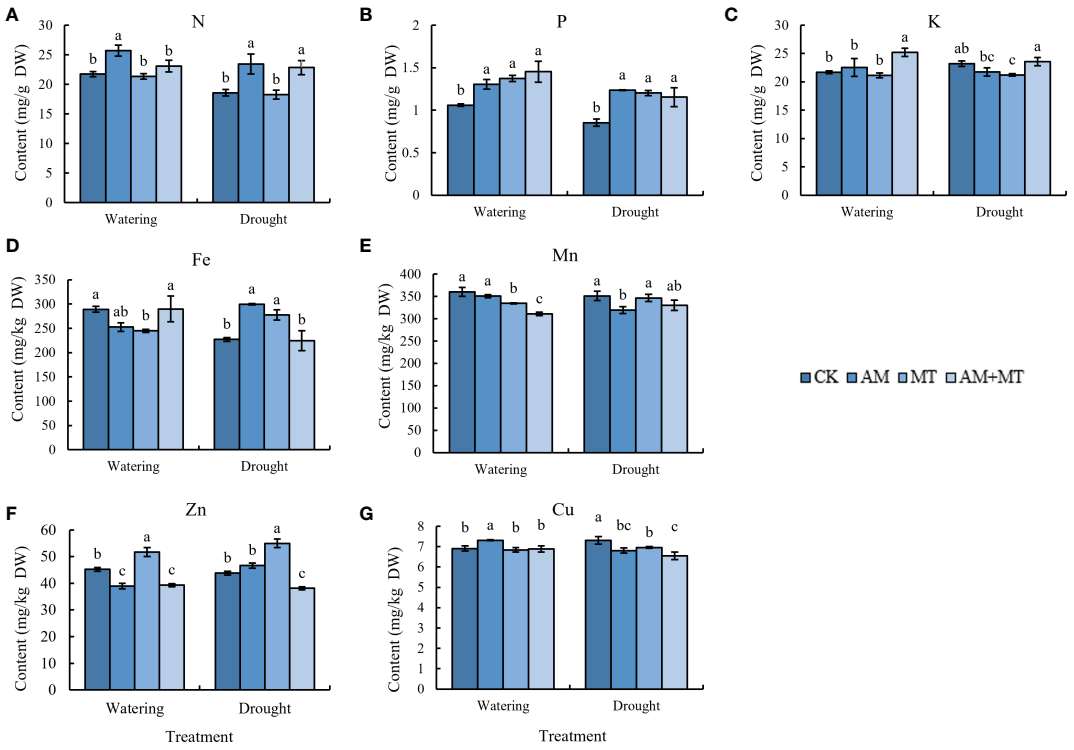

FIGURE 8
Content of N **(A)**, P **(B)**, K **(C)**, Fe **(D)**, Mn **(E)**, Zn **(F)**, and Cu **(G)** in leaves of kiwifruit seedling under well-watering or drought stress. Data are presented as meant ± SD (n = 6), different letters indicate significant differences between treatments at $p < 0.05$ by Tukey's *Post Hoc* test. Treatments included CK (the control), AM (inoculated with arbuscular mycorrhiza), MT (irrigated with 100 μM melatonin), and AM+MT (treated with melatonin and arbuscular mycorrhiza).

potassium, copper, iron, and zinc in grape fruits were improved by MT supplemental (Xia et al., 2021). Mycorrhiza can obviously promote the absorption of N, P and Fe, make the seedlings more conducive to nutrient growth and alleviate the damage caused by stress to plants (Chandrasekaran, 2022). In this study MT and AM both increased significantly the concentration of P in seedling leaves under watering and drought condition, importantly, which contributed to drought tolerance enhancement (Begum et al., 2020; Bechtaoui et al., 2021). PHT1 (phosphate transporter 1) family genes play an important role in regulating plant growth and coping with stress (Cao et al., 2020). Our results showed that the expression of all six PHT1 genes significantly increased after MT and AM induction. It was speculated that MT and AMF treatment can alleviate drought damage by inducing high expression of *PHT1*s to improve P uptake.

In addition to promoting plant uptake of nutrients in plants, melatonin supplementation also altered the composition of bacterial and fungal communities in the soil, alleviating the effect of apple diseases (Li et al., 2018). Herein, we further confirmed that melatonin could not only promote the uptake of soil nutrients by itself, but also expand plant uptake of distal soil nutrients by strengthening the symbiosis between arbuscular mycorrhizal fungi and roots and increasing colonization. However, different from the previous study on tobacco (Liu et al., 2020), melatonin and mycorrhizal seem to have no additive effect on nutrient absorption, especially in the mineral elements Fe, Zn and Cu, whose contents in the mixed treatment group decreased instead. It is speculated that they may have some competitive or antagonistic mechanism in their nutrient absorption to avoid metal poisoning.

In our study, melatonin and mycorrhiza have additive effect on improving plant growth under drought, and increasing antioxidant enzyme activity, chlorophyll content, osmotic regulating substance, photosynthetic capacity, and reducing MDA and REL. This is largely due to their different mechanisms for performing functions. As a broad-spectrum antioxidant, melatonin itself has the ability to remove ROS and prevent its accumulation in cells (Yu et al., 2018; Arnao and Hernández-Ruiz, 2019). At the same time, it can improve the activity of antioxidant enzymes and the content of antioxidant substances under adversity conditions, thus greatly reducing the damage caused by drought stress (Xia et al., 2020). On the

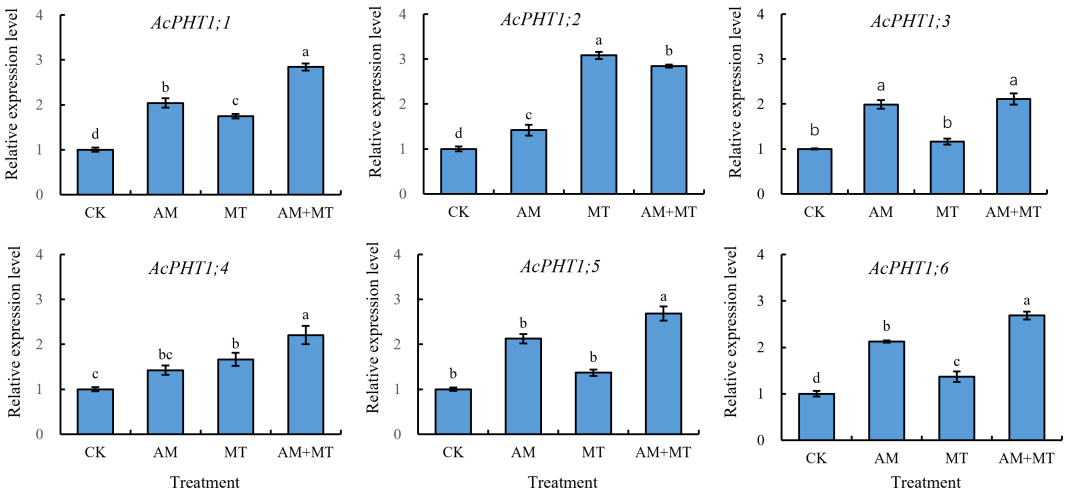

FIGURE 9
The relative expression profiles of phosphorus transport genes in the kiwifruit seedling under drought stress. Data are presented as meant ± SD (n = 6), different letters indicate significant differences between treatments at $p < 0.05$ by Tukey's *Post Hoc* test. Treatments included CK (the control), AM (inoculated with arbuscular mycorrhiza), MT (irrigated with 100 μM melatonin), and AM+MT (treated with melatonin and arbuscular mycorrhiza).

other hand, melatonin, as an auxin precursor, has a similar function of promoting plant growth (Hernandez-Ruiz et al., 2005; Szafrańska et al., 2013). While mycorrhiza reduced the stress damage mainly by promoting nutrient absorption capacity, improving root function (Lenoir et al., 2016). Because extrapular-root mycelium formed a huge mycelium network in the soil, increasing root xylem conductance and improving the adaptability of water transport (Abdalla and Ahmed, 2021; Sun et al., 2022). Most important, in this study, melatonin was found to promote the establishment of a symbiotic relationship between arbuscular mycorrhizal fungi and roots.

Conclusion

Under drought conditions, AM inoculation was more effective than MT in promoting root biomass, soluble sugar content, and absorption of N and Fe nutrients. MT has a better effect in improving shoot biomass and the activity of antioxidant enzymes to remove ROS accumulation. Moreover, combination of mycorrhizal and MT promotes the root systems to form a symbiotic relationship. In addition, the combination of AM and MT treatment had an additive effect on improving plant growth, antioxidant enzyme activity, chlorophyll content, osmotic regulating substance, photosynthetic capacity, and reducing MDA and REL. Our results indicated that MT and AM fungi have a synergistic effect on improving drought tolerance, which provides a new strategy for the widespread application of biological modulators to improve crop drought tolerance.

Data availability statement

The original contributions presented in the study are included in the article/supplementary material, further inquiries can be directed to the corresponding author/s.

Author contributions

HX and DL conceived the idea and designed the research; CY, YL, ZH and YG performed the experiments with the help of YL, HD and XT; CY, JW and XL analyzed the data; CY and HX drafted the manuscript; YuL and DL revised the manuscript, other authors provided suggestions for the revision of the manuscript. All authors contributed to the article and approved the submitted version.

Acknowledgments

This work was supported by fund received from the Sichuan Science and Technology Program (2022YFH0049 and 2022-YF05-00655-SN). We also thank the fund support from the Engineering Technology Research Center of Biological Resources Conservation and Utilization of Inner Mongolia (21400-222526).

Conflict of interest

The authors declare that the research was conducted in the absence of any commercial or financial relationships that could be construed as a potential conflict of interest.

Publisher's note

All claims expressed in this article are solely those of the authors and do not necessarily represent those of their affiliated organizations, or those of the publisher, the editors and the reviewers. Any product that may be evaluated in this article, or claim that may be made by its manufacturer, is not guaranteed or endorsed by the publisher.

Supplementary material

The Supplementary Material for this article can be found online at: https://www.frontiersin.org/articles/10.3389/fpls.2022.1073917/full#supplementary-material

References

Abdalla, M., and Ahmed, M. A. (2021). Arbuscular mycorrhiza symbiosis enhances water status and soil-plant hydraulic conductance under drought. *Front. Plant Sci.* 12. doi: 10.3389/fpls.2021.722954

Abdelaal, K., AlKahtani, M., Attia, K., Hafez, Y., Király, L., and Künstler, A. (2021). The role of plant growth-promoting bacteria in alleviating the adverse effects of drought on plants. *Biology.* 10 (6), 520. doi: 10.3390/biology10060520

Abdel-Salam, E., Alatar, A., and El-Sheikh, M. A. (2017). Inoculation with arbuscular mycorrhizal fungi alleviates harmful effects of drought stress on damask rose. *Saudi J. Biol. Sci.* 25 (8), 1772–1780. doi: 10.1016/j.sjbs.2017.10.015

Arnao, M. B., Cano, A., and Hernández-Ruiz, J. (2022). Phytomelatonin: an unexpected molecule with amazing performances in plants. *J. Exp. Bot.* 73 (17), 5779–5800. doi: 10.1093/jxb/erac009

Arnao, M. B., and Hernández-Ruiz, J. (2019). Melatonin: A new plant hormone and/or a plant master regulator? *Trends Plant Sci.* 24 (1), 38–48. doi: 10.1016/j.tplants.2018.10.010

Bechtaoui, N., Rabiu, M. K., Raklami, A., Oufdou, K., Hafidi, M., and Jemo, M. (2021). Phosphate-dependent regulation of growth and stresses management in plants. *Front. Plant Sci.* 12. doi: 10.3389/fpls.2021.679916

Begum, N., Ahanger, M. A., and Zhang, L. (2020). AMF inoculation and phosphorus supplementation alleviates drought induced growth and photosynthetic decline in nicotiana tabacum by up-regulating antioxidant metabolism and osmolyte accumulation. *Environ. Exp. Bot.* 176, 104088. doi: 10.1016/j.envexpbot.2020.104088

Bian, L., Wang, Y., Bai, H., Li, H., Zhang, C., Chen, J., et al. (2021). Melatonin-ROS signal module regulates plant lateral root development. *Plant Signal Behav.* 16 (5), 1901447. doi: 10.1080/15592324.2021.1901447

Biermann, B., and Linderman, (1981). Quantifying vesicular-arbuscular mycorrhizae: a proposed method towards standardization. *New Phytol.* 87 (1), 63–67. doi: 10.2307/2485121

Bolin, Z., Tengteng, G., Danni, Z., Ke, D., Chao, L., and Fengwang, M. (2022). Functions of arbuscular mycorrhizal fungi in horticultural crops. *Sci. Hortic.* 303, 111219. doi: 10.1016/j.scienta.2022.111219

Cakmak, I., and Marschner, H. (1992). Magnesium deficiency and high light intensity enhance activities of superoxide dismutase, ascorbate peroxidase, and glutathione reductase in bean leaves. *Plant Physiol.* 98 (4), 1222–1227. doi: 10.1104/pp.98.4.1222

Cao, M., Liu, H., Zhang, C., Wang, D., Liu, X., and Chen, Q. (2020). Functional analysis of StPHT1;7, a solanum tuberosum l. phosphate transporter gene, in growth and drought tolerance. *Plants.* 9 (10), 1384. doi: 10.3390/plants9101384

Chandrasekaran, M. (2022). Arbuscular mycorrhizal fungi mediated enhanced biomass, root morphological traits and nutrient uptake under drought stress: a meta-analysis. *J. Fungi.* 8 (7), 660. doi: 10.3390/jof8070660

Du, Q., Xing, G., Jiao, X., Song, X., and Li, J. (2018). Stomatal responses to long-term high vapor pressure deficits mediated most limitation of photosynthesis in tomatoes. *Acta Physiol. Plant* 40 (8), 149. doi: 10.1007/s11738-018-2723-7

Du, P., Yin, B., Zhou, S., Li, Z., Zhang, X., Cao, Y., et al. (2022). Melatonin and dopamine mediate the regulation of nitrogen uptake and metabolism at low ammonium levels in malus hupehensis. *Plant Physiol. Biochem.* 171, 182–190. doi: 10.1016/j.plaphy.2022.01.004

Fang, Y., and Xiong, L. (2015). General mechanisms of drought response and their application in drought resistance improvement in plants. *Cell Mol. Life Sci.* 72 (4), 673–689. doi: 10.1007/s00018-014-1767-0

Farooq, M., Hussain, M., Ul-Allah, S., and Siddique, K. (2019). Physiological and agronomic approaches for improving water-use efficiency in crop plants. *Agr Water Manage.* 219, 95–108. doi: 10.1016/j.agwat.2019.04.010

Frew, A., Antunes, P. M., Cameron, D. D., Hartley, S. E., Johnson, S. N., Rillig, M. C., et al. (2022). Plant herbivore protection by arbuscular mycorrhizas: a role for fungal diversity? *New Phytol.* 233 (3), 1022–1031. doi: 10.1111/nph.17781

Gutjahr, C., and Paszkowski, U. (2013). Multiple control levels of root system remodeling in arbuscular mycorrhizal symbiosis. *Front. Plant Sci.* 4. doi: 10.3389/fpls.2013.00204

Hernández-Ruiz, J., Cano, A., and Arnao, M. B. (2005). Melatonin acts as a growth-stimulating compound in some monocot species. *J. Pineal Res.* 39 (2), 137–142. doi: 10.1111/j.1600-079X.2005.00226.x

Hooker, J. E., Piatti, P., Cheshire, M. V., and Watson, C. A. (2007). Polysaccharides and monosaccharides in the hyphosphere of the arbuscular mycorrhizal fungi glomus E3 and glomus tenue. *Soil Biol. Biochem.* 39 (2), 680–683. doi: 10.1016/j.soilbio.2006.08.019

Huang, B., Chen, Y., Zhao, Y., Ding, C., Liao, J., Hu, C., et al. (2019). Exogenous melatonin alleviates oxidative damages and protects photosystem II in maize seedlings under drought stress. *Front. Plant Sci.* 10. doi: 10.3389/fpls.2019.00677

Kaushal, M. (2019). Microbes in cahoots with plants: MIST to hit the jackpot of agricultural productivity during drought. *Int. J. Mol. Sci.* 20 (7), 1769. doi: 10.3390/ijms20071769

Khan, R., Ma, X., Zhang, J., Wu, X., Iqbal, A., Wu, Y., et al. (2021). Circular drought-hardening confers drought tolerance *via* modulation of the antioxidant defense system, osmoregulation, and gene expression in tobacco. *Physiol. Plant* 172 (2), 1073–1088. doi: 10.1111/ppl.13402

Lenoir, I., Fontaine, J., and Lounès-Hadj Sahraoui, A. (2016). Arbuscular mycorrhizal fungal responses to abiotic stresses: A review. *Phytochemistry.* 123, 4–15. doi: 10.1016/j.phytochem.2016.01.002

Liang, D., Ni, Z., Xia, H., Xie, Y., Lv, X., Wang, J., et al. (2019). Exogenous melatonin promotes biomass accumulation and photosynthesis of kiwifruit seedlings under drought stress. *Sci. Hortic.* 246, 34–43. doi: 10.1016/j.scienta.2018.10.058

Liu, L., Li, D., Ma, Y., Shen, H., Zhao, S., and Wang, Y. (2020). Combined application of arbuscular mycorrhizal fungi and exogenous melatonin alleviates drought stress and improves plant growth in tobacco seedlings. *J. Plant Growth Regul.* 40 (3), 1074–1087. doi: 10.1007/s00344-020-10165-6

Li, C., Zhao, Q., Gao, T., Wang, H., Zhang, Z., Liang, B., et al. (2018). The mitigation effects of exogenous melatonin on replant disease in apple. *J. Pineal Res.* 65, 4. doi: 10.1111/jpi.12523

Mathur, P., and Roy., S. (2021). Insights into the plant responses to drought and decoding the potential of root associated microbiome for inducing drought tolerance. *Physiol. Plant* 172 (2), 1016–1029. doi: 10.1111/ppl.13338

Müller, L. M. (2021). Underground connections: arbuscular mycorrhizal fungi influence on interspecific plant-plant interactions. *Plant Physiol.* 187 (3), 1270–1272. doi: 10.1093/plphys/kiab397

Munné-Bosch, S., Jubany-Marí, T., and Alegre, L. (2001). Drought-induced senescence is characterized by a loss of antioxidant defences in chloroplasts. *Plant Cell Environ.* 24 (12), 1319–1327. doi: 10.1046/j.1365-3040.2001.00794.x

Nozue, H., Oono, K., Ichikawa, Y., Tanimura, S., Shirai, K., Sonoike, K., et al. (2016). Significance of structural variation in thylakoid membranes in maintaining functional photosystems during reproductive growth. *Physiol. Plant* 160 (1), 111–123. doi: 10.1111/ppl.12528

Persi, J., and Maherali, H. (2021). Influence of arbuscular mycorrhizal fungi on root allocation and morphology in two medicago species. *Int. J. Plant Sci.* 183 (1), 1–9. doi: 10.1086/716783

Porter, S. S., Bantay, R., Friel, C. A., Garoutte, A., Gdanetz, K., Ibarreta, K., et al. (2020). Beneficial microbes ameliorate abiotic and biotic sources of stress on plants. *Funct. Ecol.* 34 (10), 2075–2086. doi: 10.1111/1365-2435.13499

Rivero, R. M., Mittler, R., Blumwald, E., and Zandalinas, S. I. (2022). Developing climate-resilient crops: improving plant tolerance to stress combination. *Plant J.* 109 (2), 373–389. doi: 10.1111/tpj.15483

Sun, S., Gu, M., Cao, Y., Huang, X., Zhang, X., Ai, P., et al. (2012). A constitutive expressed phosphate transporter, OsPht1;1, modulates phosphate uptake and translocation in phosphate-replete rice. *Plant Physiol.* 159 (4), 1571–1581. doi: 10.1104/pp.112.196345

Sun, C., Liu, L., Wang, L., Li, B., Jin, C., and Lin, X. (2021). Melatonin: A master regulator of plant development and stress responses. *J. Integr. Plant Biol.* 63 (1), 126–145. doi: 10.1111/jipb.12993

Sun, C., Sun, N., Ou, Y., Gong, B., Jin, C., Shi, Q., et al. (2022). Phytomelatonin and plant mineral nutrition. *J. Exp. Bot.* 73 (17), 5903–5917. doi: 10.1093/jxb/erac289

Szafrańska, K., Glińska, S., and Janas, K. M. (2013). Ameliorative effect of melatonin on meristematic cells of chilled and re-warmed vigna radiata roots. *Bio. Plantarum* 57, 91–96. doi: 10.1007/s10535-012-0253-5

Tambussi, E. A., Bartoli, C. G., Beltrano, J., Guiamet, J. J., and Araus, J. L. (2000). Oxidative damage to thylakoid proteins in water-stressed leaves of wheat (Triticum aestivum). *Physiol. Plant* 161 (3), 400–413. doi: 10.1111/ppl.12601

Tiwari, R. K., Lal, M. K., Kumar, R., Chourasia, K. N., Naga, K. C., Kumar, D., et al. (2021). Mechanistic insights on melatonin-mediated drought stress mitigation in plants. *Physiol. Plant* 172 (2), 1212–1226. doi: 10.1111/ppl.13307

Vurukonda, S. S., Vardharajula, S., and Shrivastava, M. (2016). Enhancement of drought stress tolerance in crops by plant growth promoting rhizobacteria. *Microbiol. Res.* 184, 13–24. doi: 10.1016/j.micres.2015.12.003

Xia, H., Ni, Z., Hu, R., Lin, L., Deng, H., Wang, J., et al. (2020). Melatonin alleviates drought stress by a non-enzymatic and enzymatic antioxidative system in kiwifruit seedlings. *Int. J. Mol. Sci.* 21 (3), 852. doi: 10.3390/ijms21030852

Xia, H., Shen, Y., Deng, H., Wang, J., Lin, L., Deng, Q., et al. (2021). Melatonin application improves berry coloration, sucrose synthesis, and nutrient absorption in 'Summer black' grape. *Food Chem.* 356, 129713. doi: 10.1016/j.foodchem.2021.129713

Yang, Y., Cao, Y., Li, Z., Zhukova, A., Yang, S., Wang, J., et al. (2020). Interactive effects of exogenous melatonin and rhizophagus intraradices on saline-alkaline stress tolerance in leymus chinensis. *Mycorrhiza.* 30 (2-3), 357–371. doi: 10.1007/s00572-020-00942-2

Yang, L., You, J., Li, J., Wang, Y., and Chan, Z. (2021). Melatonin promotes arabidopsis primary root growth in an IAA-dependent manner. *J. Exp. Bot.* 72 (15), 5599–5611. doi: 10.1093/jxb/erab196

Yu, Y., Lv, Y., Shi, Y., Li, T., Chen, Y., Zhao, D., et al. (2018). The role of phyto-melatonin and related metabolites in response to stress. *Molecules.* 23 (8), 1887. doi: 10.3390/molecules23081887

Zhang, H., Sun, X., and Dai, M. (2021). Improving crop drought resistance with plant growth regulators and rhizobacteria: Mechanisms, applications, and perspectives. *Plant Commun.* 3 (1), 100228. doi: 10.1016/j.xplc.2021.100228

Zhang, Y., Wang, Y., and Niu, H. (2018). Effects of temperature, precipitation and carbon dioxide concentrations on the requirements for crop irrigation water in China under future climate scenarios. *Sci. Total Environ.* 656, 373–387. doi: 10.1016/j.scitotenv.2018.11.362

Zhang, F., Zou, Y. N., Wu, Q. S., and Kuca, K. (2020). Arbuscular mycorrhizas modulate root polyamine metabolism to enhance drought tolerance of trifoliate orange. *Environ. Exp. Botany.* 171, 103926. doi: 10.1016/j.envexpbot.2019.103926

frontiers | Frontiers in Plant Science

TYPE Original Research
PUBLISHED 09 December 2022
DOI 10.3389/fpls.2022.1081787

OPEN ACCESS

EDITED BY
Bowen Liang,
Hebei Agricultural University, China

REVIEWED BY
Guang Chen,
Zhejiang Academy of Agricultural Sciences, China
Gao Tengteng,
Northwest A and F University, China
Qiuyan Ban,
Jinling Institute of Technology, China

*CORRESPONDENCE
Kai Xu
xukai@zafu.edu.cn
Liuqing Huo
liuqings@zafu.edu.cn

†These authors have contributed equally to this work

SPECIALTY SECTION
This article was submitted to Plant Abiotic Stress, a section of the journal Frontiers in Plant Science

RECEIVED 27 October 2022
ACCEPTED 25 November 2022
PUBLISHED 09 December 2022

CITATION
Huo L, Wang H, Wang Q, Gao Y, Xu K and Sun X (2022) Exogenous treatment with melatonin enhances waterlogging tolerance of kiwifruit plants. *Front. Plant Sci.* 13:1081787. doi: 10.3389/fpls.2022.1081787

Exogenous treatment with melatonin enhances waterlogging tolerance of kiwifruit plants

Liuqing Huo*†, Hujing Wang†, Qi Wang, Yongbin Gao, Kai Xu* and Xuepeng Sun

Collaborative Innovation Center for Efficient and Green Production of Agriculture in Mountainous Areas of Zhejiang Province, Key Laboratory of Quality and Safety Control for Subtropical Fruit and Vegetable, Ministry of Agriculture and Rural Affairs, College of Horticulture Science, Zhejiang A&F University, Hangzhou, Zhejiang, China

Waterlogging stress has an enormous negative impact on the kiwifruit yield and quality. The protective role of exogenous melatonin on water stress has been widely studied, especially in drought stress. However, the research on melatonin-induced waterlogging tolerance is scarce. Here, we found that treatment with exogenous melatonin could effectively alleviate the damage on kiwifruit plants in response to waterlogging treatment. This was accompanied by higher antioxidant activity and lower ROS accumulation in kiwifruit roots during stress period. The detection of changes in amino acid levels of kiwifruit roots during waterlogging stress showed a possible interaction between melatonin and amino acid metabolism, which promoted the tolerance of kiwifruit plants to waterlogging. The higher levels of GABA and Pro in the roots of melatonin-treated kiwifruit plants partly contributed to their improved waterlogging tolerance. In addition, some plant hormones were also involved in the melatonin-mediated waterlogging tolerance, such as the enhancement of ACC accumulation. This study discussed the melatonin-mediated water stress tolerance of plants from the perspective of amino acid metabolism for the first time.

KEYWORDS

waterlogging, kiwifruit, melatonin, amino acid, GABA

Introduction

Water stress (waterlogging and drought) is becoming one of the most common abiotic stresses in the agriculture system, mainly due to the frequent occurrence of global warming, rainfall disparity, and poor drainage (Stuart et al., 2011; Hussain et al., 2018). Waterlogging stress often takes place in tropical and subtropical regions, especially

during the rain seasons (Phukan et al., 2016). It was estimated that over 10% of the agricultural land is under the threat of waterlogging stress, and in severe cases waterlogging can result in nearly 40-80% of the crop yield losses (Kreuzwieser and Rennenberg, 2014; Shabala et al., 2014). With the increased duration and intensity of extreme precipitation, waterlogging stress may be more severe in the future, which seriously threatens global food security (Li et al., 2022).

The excessive waterlogging blocked air exchange between soil and atmosphere, resulting in restricted oxygen availability for plant roots, thereby suppressing roots respiration, decreasing root activity, and causing root damage (Pan et al., 2021; van Veen et al., 2014). Another key impact of waterlogging stress is the excessive generation of reactive oxygen species (ROS), which directly and indirectly damages the cell membrane, proteins, and macromolecules (Zhang et al., 2017). These unproperly disposed ROS finally cause oxidative damage to roots and leaves, impairing the water uptake of plants, accompanied by leaf chlorosis and wilting (Hossain et al., 2009). In addition, during waterlogging stress, the leaf stomata closure is generally observed in plants, whereas chlorophyll degradation and leaf senescence adversely affect gas exchange and photosynthetic rate, which ultimately lead to a decline in the quantity and quality of crops (Arbona et al., 2010; Nguyen et al., 2012).

Indeed, plants have evolved various strategies to defend themselves against waterlogging stress. Some plants showed adaptive responses such as altering their morphologies, including aerenchyma formation, stem elongation, and the formation of adventitious roots, which is known as the low oxygen escape syndrome (Kuroh et al., 2018; Qi et al., 2020). Moreover, some plants use the quiescence strategy to alleviate the adverse effect of waterlogging stress, including the down-regulation of a suite of metabolic pathways, low growth rate, and protection against oxidative stress (Geigenberger, 2003; Garssen et al., 2015). A series of antioxidant mechanisms are activated to help plants to maintain proper cellular ROS levels under waterlogging stress. These include antioxidant enzymes, such as superoxide dismutase (SOD) and peroxidase (POD), and small molecule antioxidants (Mittler et al., 2011). In particular, as a unique antioxidant, melatonin (N-acetyl-5-methoxytryptamine) is proved to be a potent free radical scavenger and regulate various plant responses to environmental disorders (Back et al., 2016; Arnao and Hernández-Ruiz, 2019). Melatonin has been widely proved to be protective in diverse plant species under a variety of abiotic and biotic stresses (Gao et al., 2022), such as cold stress (Bajwa et al., 2014), oxidative stress (Wang et al., 2015), drought stress (Liang et al., 2019) and et al. However, studies on the roles of melatonin in waterlogging tolerance of plants are rare (Moustafa-Farag et al., 2020).

The metabolic acclimation to waterlogging stress has also been widely studied on whole seedlings or roots of plants, in which the primary nitrogen metabolism is proved to be one of the important adaptive responses in plants (Bailey-Serres et al., 2012; Oliveira and Sodek, 2013). As the important basis for synthesis of nitrogenous substances, amino acid metabolism is an important adjustment strategy of plants in responding to waterlogging stress (Batista-Silva et al., 2019). For example, an increase in the accumulation of γ-aminobutyrate (GABA) and alanine (Ala) was always observed in plants under waterlogging stress (Drew, 1997). Recent research found that roots responded more strongly to waterlogging stress while high amounts of GABA and lactate accumulation were detected in roots other than shoots; Moreover, the Ala accumulation was detected in both organs (Mustroph et al., 2014). Change in the level of plant hormones is another important strategy for plants to adapt to waterlogging stress (Dat et al., 2004). For example, previous researches found that waterlogging stress induced a significant depletion in the endogenous ABA levels in submerged tissues of various plant species, such as the model plant *Arabidopsis thaliana* (Liu et al., 2005) and the important perennial fruit tree citrus (Arbona et al., 2017). In addition, a fast cellular accumulation of the gaseous plant hormone ethylene has been reported in submerged plants, which act as a reliable component of the waterlogging sensing mechanism and crosstalk with other hormones for surviving (Kreuzwieser and Rennenberg, 2014). Particularly, endogenous ethylene production is at the basis of the induction and formation of aerenchyma cells (Fukao and Bailey-Serres, 2008).

Kiwifruits are popular for its unique flavor and high vitamin C content; however, the waterlogging problem severely decreased the annual yield of kiwifruit plants in their main planting areas (Fukao and Bailey-Serres, 2008). The use of melatonin in various field trials has validated that as an eco-friendly agrochemical, it has great potential for applying in horticultural industry to solve agricultural challenges (Gao et al., 2022). To date, the application of melatonin in agriculture systems to deal with waterlogging problems has been understudied. Here, we found that the pre-irrigation of 100 μM melatonin in kiwifruit plants could effectively alleviate the waterlogging damage on them. In addition to the antioxidant system, the amino acid metabolic pathways are also involved in the melatonin-mediated waterlogging tolerance of kiwifruit plants. Particularly, the GABA and proline (Pro) synthesis in kiwifruit roots was enhanced by melatonin treatment to encounter waterlogging stress. The 1-aminocyclopropane-1-carboxylate (ACC) accumulation in kiwifruit roots might also participate in the melatonin-mediated waterlogging tolerance. This study provides the evidence for the links between melatonin and amino acid metabolic systems in the stress tolerance of plants.

Materials and methods

Plant materials and treatments

Tissue-cultured plants of Actinidia chinensis var. deliciosa cv. Qinmei were initially grown on MS agar media containing

2.0 mg/L ZT and 0.1 mg/L IBA. They were cultured under conditions of 25°C, 60 μmol/m^2/s and a 14-h photoperiod. After rooting on 1/2 MS agar media containing 0.5 mg/L IBA for 40 days, the plantlets were transferred to black plastic pots (8 × 8 cm) containing a mixture of loam/perlite (1:1, v:v). After 40 d of adaptation in the growth chamber, the plants were moved to larger plastic pots (30 × 18 cm) filled with a mixture of soil/sand/organic matter (5:1:1, v:v:v) and grown in the glasshouse. They were watered with tap water or 1/2 Hoagland nutrient solution (Huo et al., 2021) alternately every three days.

After two months of growth under above conditions, healthy and uniformly sized plants were chosen for screening the optimal concentration of melatonin treatment: plants were fully irrigated with 300 ml 0, 10, 50, 100, 200, or 300 μM melatonin solution to the roots for 2 times in a three-day interval and then were waterlogged. After 9 days of waterlogging treatment, the plant roots were collected to measure root activity. Finally, we selected 100 μM as the melatonin concentration for downstream experiments.

The treatments were subdivided into four groups as follows: (1) control (CK), plants were well-watered during the whole experimental time; (2) melatonin treatment (MT): plants were treated with 100 μM melatonin solution for 2 times in a three-day interval, then been well-watered for 9 days; (3) waterlogging treatment (WL): plants were well-watered for 6 days, and subsequently been waterlogged for 9 days; and (4) melatonin and waterlogging treatment (MT+WL): plants were treated with 100 μM melatonin solution for 2 times in a three-day interval, and then been waterlogged for 9 days. Each treatment included 20 pots of plants and was repeated three times. To apply waterlogging treatments, three potted plants were placed in a plastic container (100 × 35 × 30 cm) filled with tap water, and the water level was continuously maintained at 4-5 cm above the soil surface. The day before waterlogging was designed as 0 day, and the third through fifth fully matured leaves from the base of the stems and the roots were sampled from all groups at 0, 3, 6, and 9 days of the experiment. For samples mentioned above, three biological replicates were prepared with each collected from three plants. The samples were stored at −80°C after being frozen quickly in liquid nitrogen until use.

Evaluation of stress tolerance

The relative electrolyte leakage of the leaves and roots was determined and calculated according to a previously described method with a minor modification (Dionisio-Sese and Tobita, 1998). Briefly, 100 mg fresh plant tissue samples were cut into 5 mm length and placed in test tubes containing 10 ml distilled deionized water. The tubes were covered with plastic caps and placed in a water bath maintained at the constant temperature of 25 °C. 4 h later, the initial electrical conductivity of the distilled deionized water and the medium in test tubes was measured using an electrical conductivity meter (CM-115, Kyoto Electronics, Kyoto, Japan). Then, the samples were autoclaved at 100°C for 15 min to completely kill the tissues and release all electrolytes. Afterwards, they were cooled for 4 h to 25°C and the final electrical conductivity was measured.

Levels of malondialdehyde (MDA), H_2O_2, and superoxide radical (O_2^-) and the activities of superoxide dismutase (SOD) and peroxidase (POD) were determined using detection kits (Suzhou Comin Biotechnology Co., Ltd, Suzhou, China) following the manufacturer's instructions. The triphenyl tetrazolium chloride method was applied to monitor root activity, which was defined as the reductive intensity.

Evaluation of photosynthetic characteristics

The net photosynthesis rate (Pn), intercellular CO_2 concentration (Ci), and stomatal conductance (Gs) were monitored by a LI-6400XT portable photosynthesis system (LI-COR, Huntington Beach, CA, USA). All measurements were taken between 9:00 and 11:00 a.m. at 1000 μmol photons m^{-2} s^{-1} and a constant airflow rate of 500 μmol s^{-1}. The concentration of cuvette CO_2 was set at 400 ± 5 cm^3 m^{-3}, and the temperature was 28 ± 2°C. Data were collected from the fully expanded, fully light-exposed leaves at the same position of three plants.

Measurement of amino acids

Amino acids (AAs), such as GABA and Pro, were extracted and measured as described previously (Huo et al., 2020), with a minor modification. Briefly, 100 mg of frozen root sample was extracted in 1 ml 50% ethanol (including 0.1 M HCl). After centrifuging at 13,000 g for 10 min, the liquid supernatant was filtered through a 0.22-μm filter and the filtered supernatant was diluted 20 times using methanol to analyze the metabolites. The liquid chromatography-mass spectrometry system (LC-MS, LC: AC, ExionLC; MS: Q-trap5500, AB Sciex Pret. Ltd., Washington, USA) equipped with an Inertsil ODS-4 C18 column (4.6 × 250 mm, 5 mm) was used at a flow rate of 0.3 ml/min, and 10 μL was used as sample injection volume. The solvent system consisted of water containing 0.1% (v/v) formic acid (A) and acetonitrile (B). Data were quantified by comparing the peak surface areas with those obtained using standard AAs (Sigma, St. Louis, MO, USA).

Measurement of phytohormones

ABA, ACC and SA were extracted as described previously (Huo et al., 2020) and measured using the LC-MS system.

Briefly, 200 mg of frozen root sample was extracted in 1 ml solvent (methanol: isopropanol: acetic acid= 20: 79: 1; v: v: v). After shaking for 1 h at 4°C and centrifugation, the supernatant was filtered through a 0.22-μm filter for analysis using the same system described above but equipped with the InertSustain AQ-C18 column (4.6 × 150 mm, 5 μm) at a flow rate of 0.5 ml/min. The solvent system consisted of methanol (A) and water containing 0.1% (v/v) formic acid (B).

Melatonin was quantified as described by Zhou et al. (2022), with some modifications. Briefly, 500 mg of frozen root sample was suspended in 5 ml methanol. After shaking overnight at −20°C and centrifugation, the supernatants were collected for drying under nitrogen gas. Then, the dried extracts were dissolved in 200 μl 80% methanol and filtered through a 0.22-μm filter membrane. The analysis system was the same as described above.

Statistical analysis

SPSS 22.0 software was used for statistical data analysis. All experimental data were subjected to one-way analysis of variance, and the statistical differences were calculated by Tukey's multiple range test ($p < 0.05$). Values were presented as means ± SEs (standard errors) of at least three biological replicates.

Results

Exogenous melatonin improves the waterlogging tolerance of kiwifruit plants

To investigate the possible effect of exogenous melatonin on kiwifruit plants in response to waterlogging stress, we first pretreated the plants with different concentrations of melatonin, and then measured their root activity after waterlogging treatment. The results showed that melatonin treatment effectively alleviated waterlogging damage on root activity of kiwifruit plants (Table 1). According to our evaluation, the 100 μM melatonin pretreatment performed better than 10 or 50 μM, meanwhile it was more economical than 200 or 300 μM on the basis of similar effect on waterlogging tolerance of kiwifruit plants. Then we applied 100 μM melatonin solution to irrigate designated plants before inducing waterlogging stress. Under normal-watered conditions, the root morphology did not differ apparently between kiwifruit plants treated with (MT) or without (CK) melatonin. After waterlogging stress (WL), the leaves of kiwifruit plants in both WL and MT+WL groups wilted severely and brown patches were observed. Moreover, while the lower leaves of plants in the WL group appeared serious shedding due to waterlogging stress, plants received melatonin pretreatment showed lighter stress symptoms and many mature leaves remained green and vigorous (Figure 1A).

TABLE 1 Effects of melatonin pretreatment (10~300 μM) on root activity of waterlogged kiwifruit plants.

Treatment group	TTC reductive intensity (μg g^{-1} FW h^{-1})
CK	153.08 ± 8.85 a
WL	86.05 ± 12.05 d
WL + 10 μM	100.30 ± 6.45 cd
WL + 50 μM	101.98 ± 8.34 cd
WL + 100 μM	120.81 ± 7.70 b
WL + 200 μM	115.34 ± 6.10 bc
WL + 300 μM	114.49 ± 7.84 bc

All data are means ± SE of three replicates. Values not followed by the same letter indicate significant differences between treatments, according to one-way ANOVA followed by Tukey's multiple range test ($P < 0.05$).

The relative electrolyte leakage and malondialdehyde (MDA) content are typical parameters for assessing stress tolerance of plants (Dionisio-Sese and Tobita, 1998; Huo et al., 2020). The electrolyte leakage of plant cell is a basic indicator of cell membrane permeability, for the value positively correlates with the severity of membrane destruction. There was no significant difference between the electrolyte leakage of CK and MT plants under normal-watered condition. After waterlogging treatment, while the electrolyte leakage being significantly increased by 4.3 times in WL plants compared to CK plants, the increment was only 2.9 times in MT+WL plants when compared with MT plants (Figure 1B). Moreover, the levels of MDA in plant cells can reflect the extent of lipid peroxidation, which is an indicator of cell damage. The data showed that while the MDA content was increased in waterlogging-stressed leaves when compared with the control, exogenous melatonin alleviated that increment (Figure 1C). These data demonstrated that exogenous melatonin alleviated the waterlogging damage on kiwifruit plants.

Effects of exogenous melatonin on the photosynthetic capacity of kiwifruit plants under waterlogging stress

Under waterlogging stress, the efficiency of photosynthetic system was seriously inhibited due to leaf necrosis and stomatal behavior. To examine the effect of melatonin on photosynthesis, we detected the gas exchange parameters after 6 days of waterlogging treatment. As shown in Figure 2A, Pn decreased in both WL and MT + WL group, which indicates the suppressed assimilation efficiency of CO_2, but the rates were significantly higher in melatonin-pretreated plants than in non-pretreated plants. The Gs of kiwifruit plants also decreased under waterlogging stress, and it was marginally but not significantly higher in melatonin-pretreated plants on the 6th day (Figure 2B). Moreover, there was a

10.3389/fpls.2022.1081787

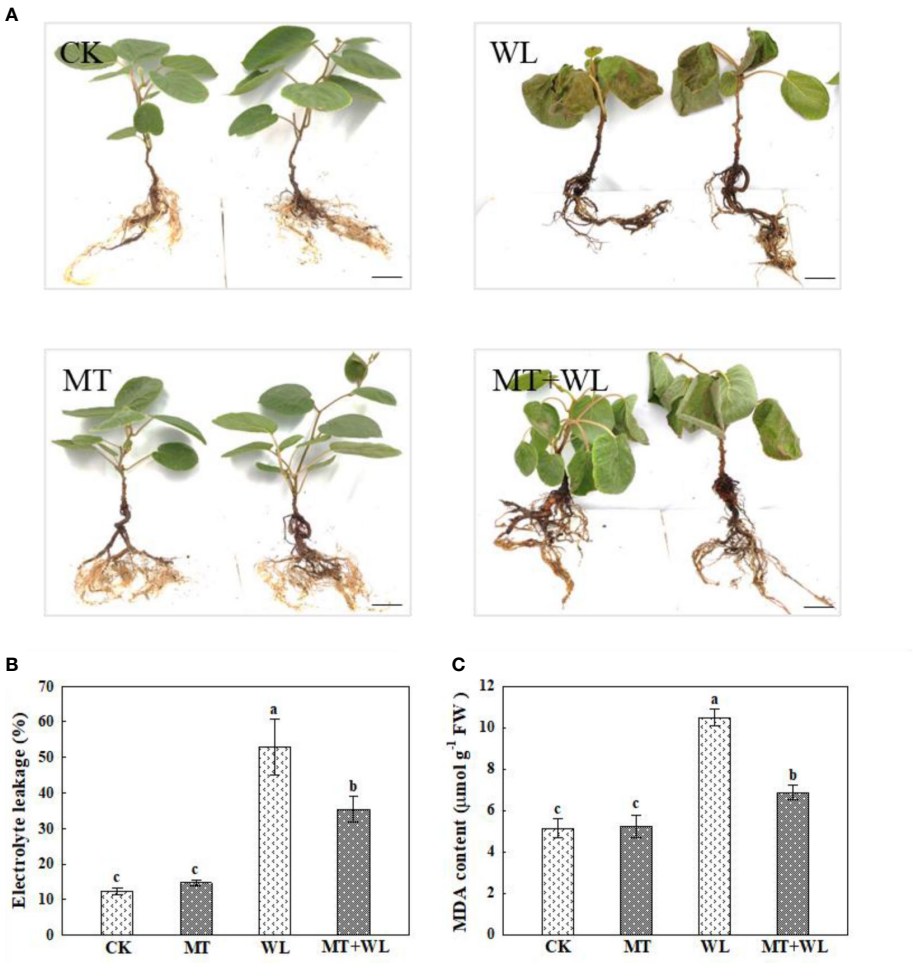

FIGURE 1
Exogenous melatonin alleviated the waterlogging damage on kiwifruit plants. **(A)** Phenotypes of kiwifruit plants in control (CK), melatonin treatment (MT), waterlogging treatment (WL), and melatonin and waterlogging treatment (MT+WL) groups, and the plants in WL and MT+WL groups were being waterlogged for 9 days. Bars: 5 cm. **(B)** Relative electrolyte leakage (REL) and **(C)** malondialdehyde (MDA) concentration of plants in CK, MT, WL, and MT+WL groups. Data are shown as the means of three replicates with SEs. Different letters indicate significant differences between treatments, according to one-way ANOVA and Tukey's multiple range test ($P < 0.05$).

substantial increase in the Ci value of non-pretreated plants after 6 d of waterlogging stress, but that increment was not presented in the melatonin-pretreated plants (Figure 2C). These results demonstrated that while the photosynthetic ability of kiwifruit plants was damaged by waterlogging stress, exogenous melatonin effectively alleviated that pressure.

Exogenous melatonin decreased ROS damage on the roots of kiwifruit plants under waterlogging stress

As shown in Figure 3A, the waterlogging damage on the roots of kiwifruit plants was remarkably relieved by melatonin treatment, represented by more vigorous and white roots on the plants in melatonin-treated groups than in non-pretreated plants after waterlogging stress. These results were further demonstrated by the relative electrolyte leakage and MDA measurements of plant roots, which were increased significantly due to the injury caused by waterlogging stress, but they were still much lower in MT+WL plants compared with that in WL plants (Figures 3B, C).

The stress-induced ROS accumulation leads to oxidative stress by disrupting cytomembranes and cell components, ultimately affecting plant growth. Here, the measurements of H_2O_2 and O_2^- levels showed that they were both increased in plant roots during the treatment (Figures 4A, B). The H_2O_2 content reached the peak after 6 d of treatment and then declined at 9 d, while the O_2^- content still showed an upward trend after 9 d of treatment. Moreover, the H_2O_2 levels were significantly higher in the roots of WL plants than in MT+WL plants from day 3 of treatment, and this difference of

10.3389/fpls.2022.1081787

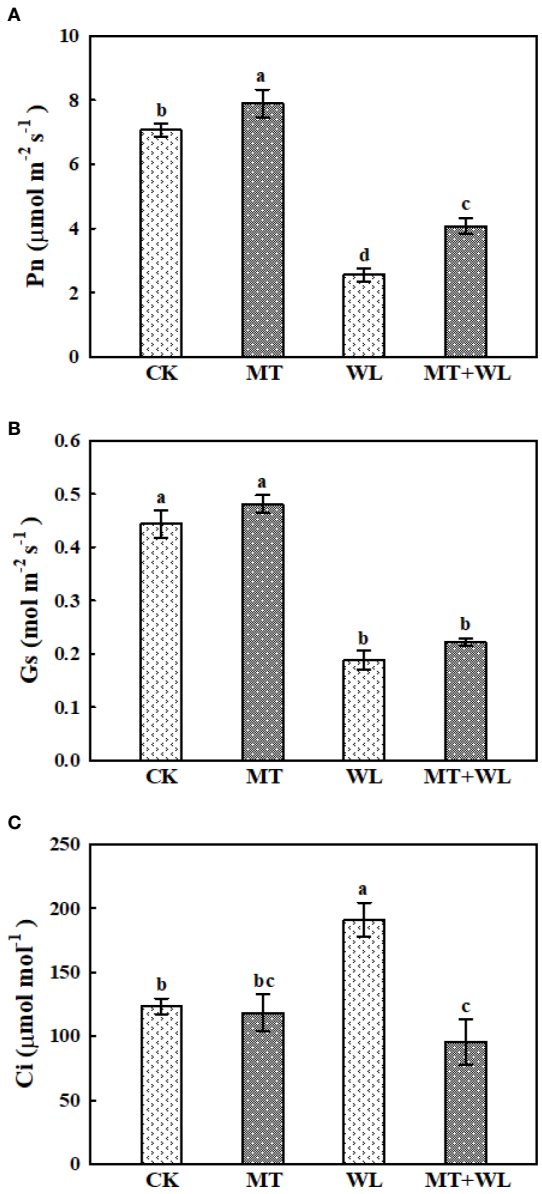

FIGURE 2
Exogenous melatonin alleviated the waterlogging damage on the photosynthetic ability of kiwifruit plants. Changes in the **(A)** net photosynthesis rate (Pn), **(B)** stomatal conductance (Gs) and **(C)** intercellular CO_2 concentration (Ci) were determined after 6 days of waterlogging treatment. Data are shown as the means of three replicates with SEs. Different letters indicate significant differences between treatments, according to one-way ANOVA and Tukey's multiple range test ($P < 0.05$).

O_2^- contents between the two groups became obviously clear after 6 d of treatment. We measured the activity of SOD and POD enzymes throughout the treatment, since SOD converts destructive O_2^- into H_2O_2 and POD can break H_2O_2 down immediately into water (Figures 4C, D). The results showed that both SOD and POD activities were induced by waterlogging stress in kiwifruit roots. The SOD activity in the roots of MT+WL plants were 1.6-times that of WL plants on day 3 and day 6 of treatment. Moreover, the POD activity in the roots of MT+WL plants was rapidly increased on day 6 of treatment, where it was 1.82-times that of WL plants. These results suggested that melatonin treatment promoted the SOD and POD activity in the roots of kiwifruit plants and thus alleviated the ROS damage under waterlogging stress.

Ala, GABA, Pro metabolism in the roots of kiwifruit plants under waterlogging stress

Previous studies have reported the accumulation of Alanine (Ala) and γ-aminobutyrate (GABA) in plant roots in response to waterlogging stress (Lothier et al., 2020), and Ala accumulation is thought to be a hypoxic biomarker in plants (Planchet et al., 2017). Here, we detected a pronounced increment in Ala and GABA concentration in the roots of kiwifruit plants in both WL and MT+WL groups under waterlogging treatment (Figures 5A, B). The Ala content was increased by 13.3 times in WL plants at 3 d of treatment compared to 0 d, and it was gradually declined afterwards, but still consistently higher than samples without waterlogging treatment. Moreover, it was lower in melatonin-treated plants than in non-pretreated plants from the day 3 of treatment (Figure 5A). The GABA content in kiwifruit roots was elevated under waterlogging stress throughout the treatments, and it was significantly higher in melatonin-treated plants than in non-pretreated plants from the day 3 (Figure 5B). The Pro content followed the same trend as GABA under waterlogging stress. More specifically, in non-pretreated plants, it was 2.54-, 3.58- and 4.01-times that of 0 d on 3, 6 and 9 d of waterlogging treatment, while it was 4.45-, 4.82- and 6.32-times that of 0 d on 3, 6 and 9 d in melatonin-treated plants (Figure 5C). These results suggested that melatonin treatment altered the Ala, GABA and Pro metabolism in the roots of kiwifruit plants in response to waterlogging stress.

Asp, Glu, Arg metabolism in the roots of kiwifruit plants under waterlogging stress

Aspartate (Asp), glutamate (Glu), and arginine (Arg) are commonly used as nitrogen storage and transport compounds in plants (Hildebrandt, 2018). Here, we analyzed the level of these three amino acids in the roots of kiwifruit plants under waterlogging stress (Figures 6A–C). At 3 d of the treatment, there was an obvious decrease of Asp concentration in kiwifruit roots, and the Asp content remained almost unchanged after 3 d. Interestingly, the Asp content was always lower in

10.3389/fpls.2022.1081787

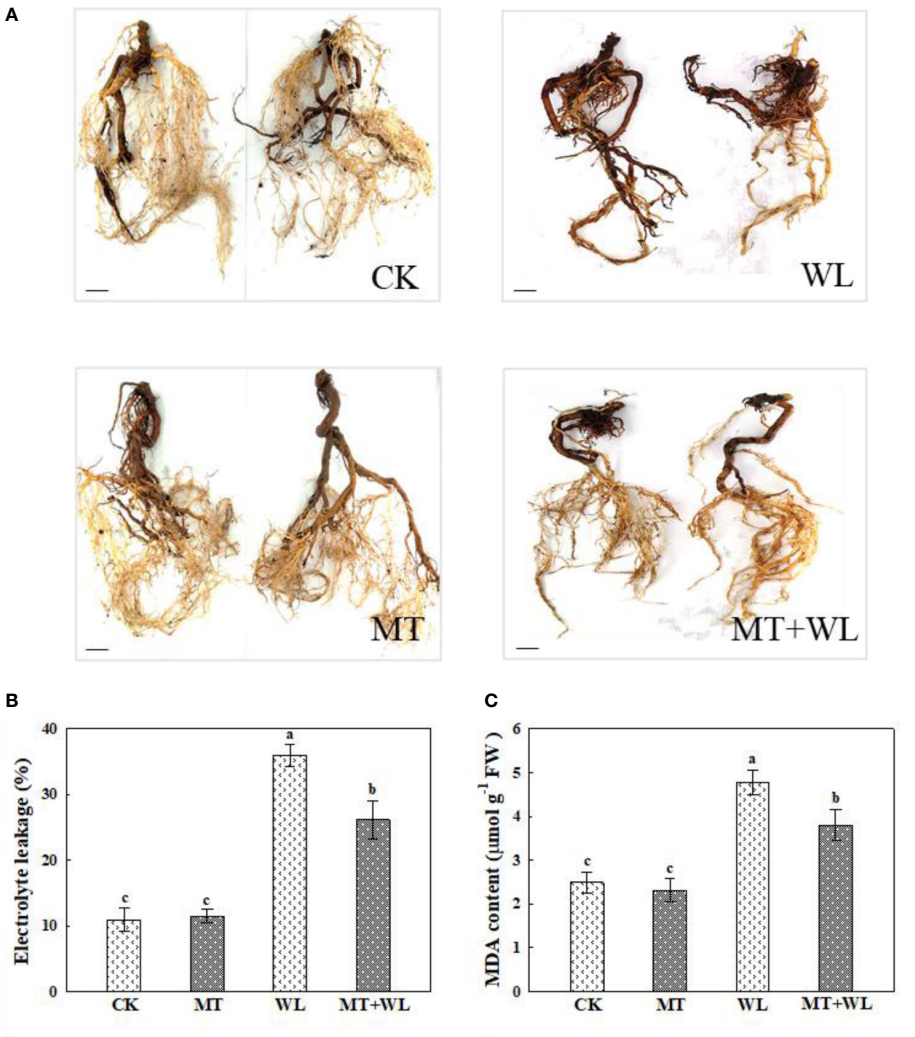

FIGURE 3
Exogenous melatonin alleviated the waterlogging damage on the roots of kiwifruit plants. **(A)** Phenotypes of the roots of kiwifruit plants in CK, MT, WL, and MT+WL groups, and the plants in WL and MT+WL groups were being waterlogged for 9 days. Bars: 5 cm. **(B)** Relative electrolyte leakage (REL) and **(C)** malondialdehyde (MDA) concentration in the roots of CK, MT, WL, and MT+WL plants. Data are shown as the means of three replicates with SEs. Different letters indicate significant differences between treatments, according to one-way ANOVA and Tukey's multiple range test ($P < 0.05$).

melatonin-treated plants than in non-pretreated plants from 3 d of treatment (Figure 6A). The Glu concentration was gradually declined in the roots during the stress treatments, and it was lower in melatonin-treated plants than in non-pretreated plants from the 6 d of treatment (Figure 6B). The Arg content in the roots of WL plants was first increased at 3 d of the treatment, and then declined on 6 d and 9 d, but it was always showing a downward trend in the MT+WL group from the 3 d of the treatment (Figure 6C). These results showed that the Asp, Glu and Arg metabolism in the roots of kiwifruit plants was altered by melatonin treatment to encounter waterlogging stress.

The branched-chain amino acids metabolism in the roots of kiwifruit plants under waterlogging stress

The branched-chain amino acids (BCAAs), including leucine (Leu), isoleucine (Ile), and valine (Val) often show a higher level of accumulation in *Arabidopsis thaliana* and other plant species in response to stress conditions (Sanchez et al., 2010; Huang and Jander, 2017). Here, we detected a pronounced accumulation of these three amino acids in the roots of kiwifruit plants in response to waterlogging stress (Figures 7A–C). In non-pretreated plants, the Leu concentration was 8.56-, 9.40-

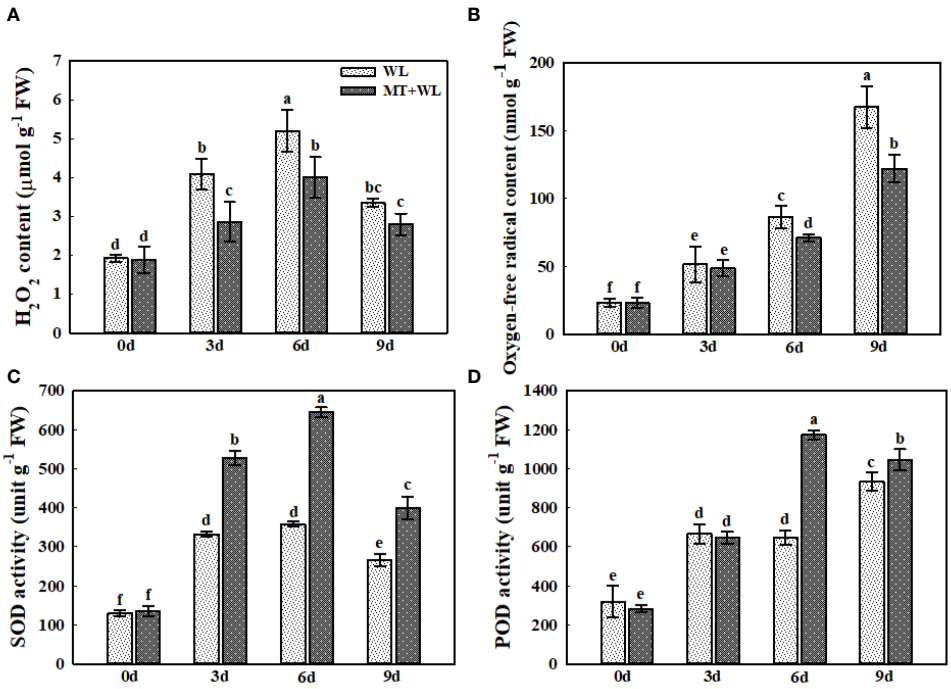

FIGURE 4
Exogenous melatonin alleviated the ROS damage in the roots of kiwifruit plants under waterlogging stress. **(A)** H_2O_2 and **(B)** O_2^- concentrations in the roots of CK, MT, WL, and MT+WL plants. Activities of **(C)** superoxide dismutase (SOD) and **(D)** peroxisome (POD) in the roots of CK, MT, WL, and MT+WL plants. Data are shown as the means of three replicates with SEs. Different letters indicate significant differences between treatments, according to one-way ANOVA and Tukey's multiple range test ($P < 0.05$).

and 14.15-times that of 0 d on 3, 6 and 9 d of waterlogging treatment, while it was 6.60-, 10.53- and 16.17-times respectively in melatonin-treated plants (Figure 7A). The levels of Ile followed the same trend, which was a bit higher in melatonin-treated plants than in non-pretreated plants from day 6 (Figure 7B). Moreover, the Val concentration was 6.60-, 6.39- and 12.00-times that of 0 d on 3, 6 and 9 d of waterlogging treatment in WL plants, while it was 6.18-, 9.71- and 19.12-times respectively in MT+WL plants (Figure 7C). These results showed that waterlogging stress caused a multiple-fold increase in the levels of BCAAs in the roots of kiwifruit plants, and melatonin treatment promoted it in the later stages of stress.

Plant hormones metabolism in the roots of kiwifruit plants under waterlogging stress

Plant hormones are involved in the regulation of waterlogging stress response *via* complex signalling pathways in plants (Benschop et al., 2006; Pan et al., 2021). Here, we analyzed the concentrations of melatonin, ACC (1-aminocyclopropane-1-carboxylate), ABA (abscisic acid), and SA (salicylic acid) in the roots of kiwifruit plants in response to waterlogging stress (Figures 8A–D). The measurements of melatonin contents showed that melatonin-treatment promoted it concentrations from 0.4 ng g^{-1} FW to 11 ng g^{-1} FW in kiwifruit roots. The melatonin concentrations in kiwifruit roots were induced by waterlogging stress, which peaked at 6 d of treatment reaching 2.21-times that of 0 d in non-pretreated plants. Interestingly, although there was already sufficiently high concentration of melatonin detected in melatonin-treated groups on 0 d, it was still induced by waterlogging stress in kiwifruit roots, which followed the same trend as in non-pretreated plants, showing 2.39-times that of 0 d at 6 d of treatment (Figure 8A). The ACC concentration in kiwifruit roots was enhanced by waterlogging stress throughout the treatment, and it was significantly higher in melatonin-treated plants than in non-pretreated plants from day 3 (Figure 8B). The ABA content in kiwifruit roots was down-regulated by waterlogging treatment, and it was lower in melatonin-treated plants than in non-pretreated plants from 0 d to 3 d. Moreover, it showed a certain degree of recovery in MT+WL plants from the day 6, but still reducing in WL group (Figure 8C). The SA content in kiwifruit roots was falling down due to the waterlogging stress, but it was always higher in MT+WL plants than in WL plants during the treatments (Figure 8D). These results suggested that the balance of plant hormones was changed in kiwifruit roots to encounter waterlogging stress.

10.3389/fpls.2022.1081787

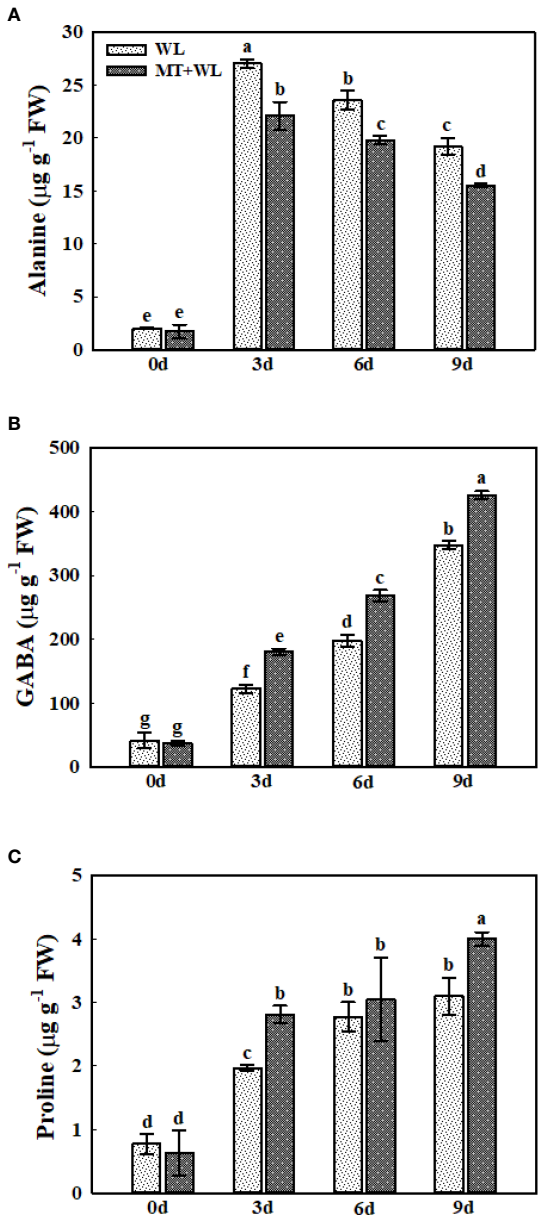

FIGURE 5
The concentrations of Ala, GABA, and Pro in the roots of kiwifruit plants under waterlogging stress, as measured by LC-MS. **(A)** Ala. **(B)** GABA. **(C)** Pro. Data are shown as the means of three replicates with SEs. Different letters indicate significant differences between treatments, according to one-way ANOVA and Tukey's multiple range test ($P < 0.05$).

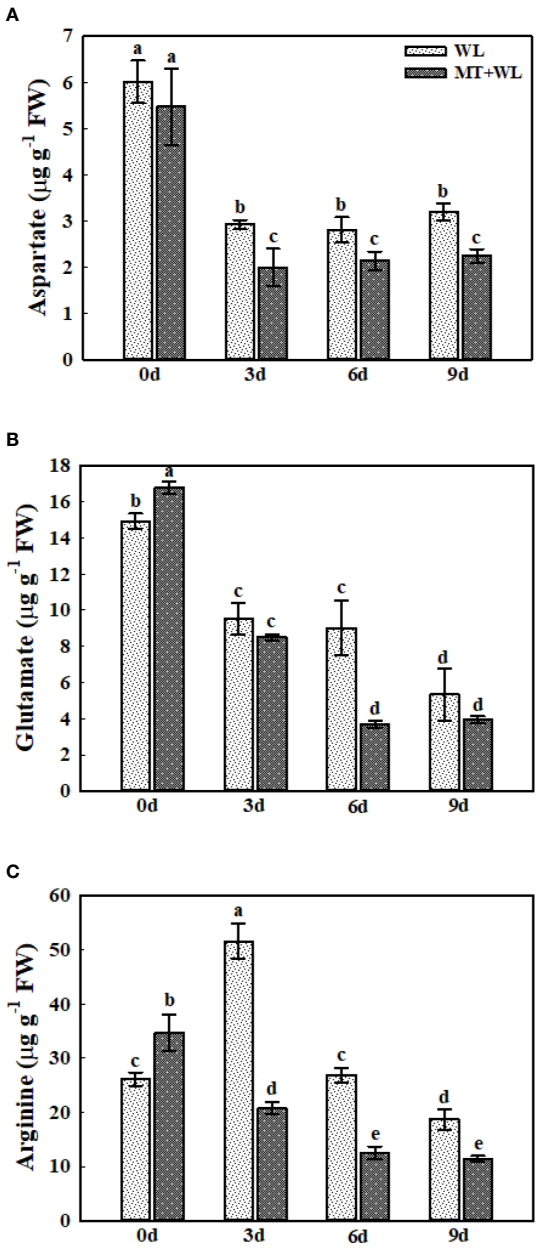

FIGURE 6
The concentrations of Asp, Glu, and Arg in the roots of kiwifruit plants under waterlogging stress, as measured by LC-MS. **(A)** Asp. **(B)** Glu. **(C)** Arg. Data are shown as the means of three replicates with SEs. Different letters indicate significant differences between treatments, according to one-way ANOVA and Tukey's multiple range test ($P < 0.05$).

Discussion

As sessile organisms, plants cannot escape from harsh environmental disorders, such as continuous oxygen shortage induced by waterlogging or submergence conditions. Despite this obvious weakness, plants are more tolerant to hypoxia stress than animals, even in species not adapted to submersed soil, which suggest that plants have evolved particular strategies to cope with waterlogging stress (Planchet et al., 2017). Recent studies found that the appropriate metabolism changes are important for plant waterlogging tolerance (Fukao and Bailey-Serres, 2004; Zheng et al., 2017). For example, after a period of waterlogging stress, the plant seedlings changed their

10.3389/fpls.2022.1081787

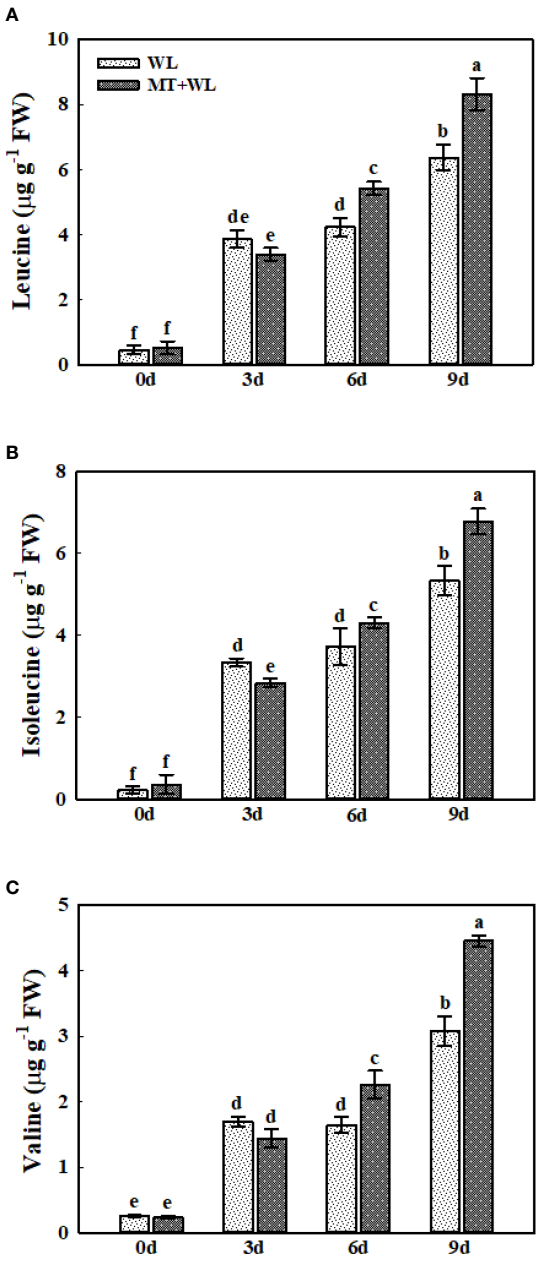

FIGURE 7
Change to "The concentrations of Leu, Ile, and Val in the roots of kiwifruit plants under waterlogging stress, as measured by LC-MS. **(A)** Leu. **(B)** Ile. **(C)** Val. Data are shown as the means of three replicates with SEs. Different letters indicate significant differences between treatments, according to one-way ANOVA and Tukey's multiple range test ($P < 0.05$).

metabolism from aerobic to anaerobic respiration, which led to a burst of reactive oxygen species (ROS) generation and resulted in oxidative damages of plant organelles (Xu et al., 2013; Takahashi et al., 2015). The excessive production of ROS in plant roots would disturb their growth and impair the uptake of water and nutrient from soil, therefore disturbing plant gas exchange and photosynthesis (Hossain et al., 2009). The proper ROS scavenging systems and the maintenance of photosynthetic ability are important for plants in response to waterlogging stress. Melatonin has been generally reported to be an effective antioxidant, with important functions in scavenging ROS and regulating plant responses to various environmental stresses (Li et al., 2018; Wu et al., 2020). However, the effects of melatonin in plant physiological and metabolic responses to waterlogging stress have yet to be elucidated (Moustafa-Farag et al., 2020).

The kiwifruit plants are always intolerant to waterlogging stress as the root system is fleshy and shallow. In many kiwifruit planting regions, especially in Southeast China, excessive rainfall in summer rainy season generally causes huge damage to kiwifruit gross yield (Liu et al., 2022). Therefore, studying the waterlogging response mechanisms of kiwifruit is urgent and has important implications for horticultural industry. Previous studies have found that exogenous melatonin could induce the tolerance of kiwifruits to drought stress and alleviate the heat-related damage, mainly through the antioxidant pathways (Liang et al., 2018; Xia et al., 2020). Here, we pre-irrigated the kiwifruit plants with melatonin solution to the roots, and found that exogenous melatonin pretreatment effectively alleviated the decline in the root activity of kiwifruit plants caused by waterlogging stress. We selected 100 μM melatonin as the exogenous concentration to investigate the potential metabolic role of exogenous melatonin on kiwifruit plants under waterlogging stress. The exogenous melatonin pretreatment did not apparently change the phenotypes of kiwifruit plants under control condition. While the waterlogging treatment resulted in visible leaf damage on kiwifruit plants in both WL and MT+WL groups, the melatonin pretreatment definitely alleviated the stress symptoms, which was indicated by decreased electrolyte leakage and MDA levels. Previous studies have reported that melatonin application could improve the photosynthesis rate and PSII efficiency in apple (Zheng et al., 2017) and alfalfa (Zhang et al., 2019) to alleviate the stress damage during waterlogging treatment. Here, the decrease in Pn of kiwifruit plants caused by waterlogging stress was also effectively lightened by melatonin pretreatment. The substantial increase in the Ci value of WL plants also indicated substantial disorders in the leaf photosynthetic structure of non-pretreated plants under waterlogging stress.

Since the plant root is the front line to continuously sense waterlogging signal, we performed further researches on kiwifruit roots. In addition to the root activity mentioned earlier in the concentration screening test, the detected relative electronic leakage and MDA concentration of the roots also showed milder increment in the kiwifruit plants with exogenous melatonin pretreatment, which indicated that exogenous melatonin could protect the integrity and vitality of the root system under waterlogging stress, thereby reducing waterlogging damage to the kiwifruit plants. Moreover, the measurements showed that both the ROS generation and antioxidant enzymes

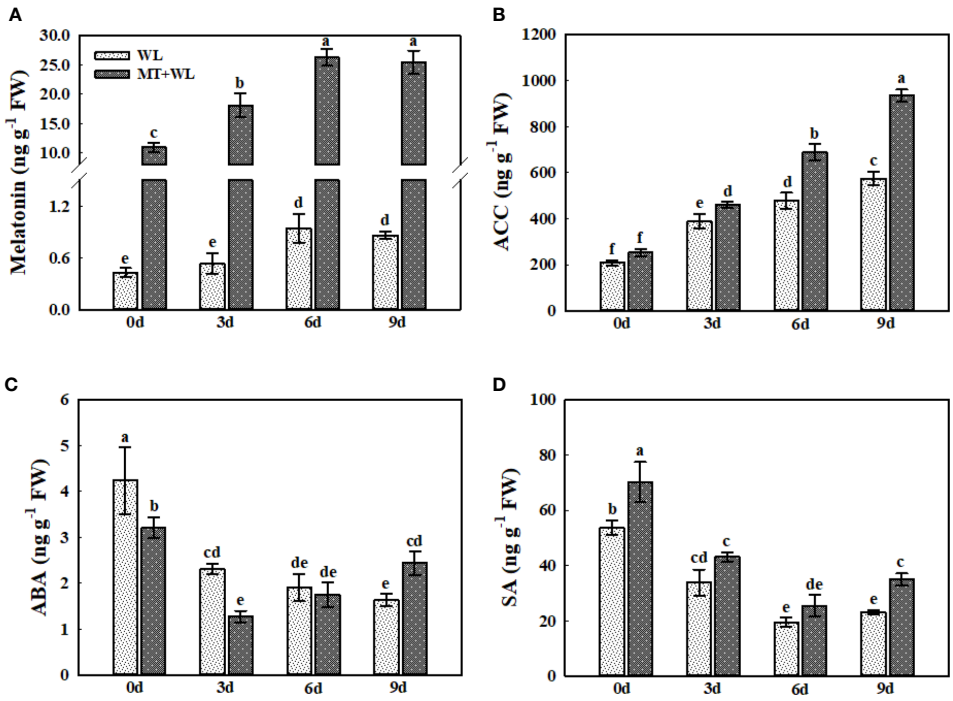

FIGURE 8
The concentrations of melatonin, ACC, ABA, and SA in the roots of kiwifruit plants under waterlogging stress, as measured by LC-MS. Data are shown as the means of three replicates with SEs. Different letters indicate significant differences between treatments, according to one-way ANOVA and Tukey's multiple range test ($P < 0.05$).

activity were induced by waterlogging stress in kiwifruit root, and the melatonin-treated plants possessed a higher antioxidant ability and lower ROS accumulation. As these results were consistent with previous researches, which reported that melatonin has important functions in scavenging ROS in different plant species in response to various biotic and abiotic stresses (Li et al., 2018; Liang et al., 2019), we believed that the melatonin treatment enhanced the waterlogging tolerance of kiwifruit plants through regulating the ROS pathway in roots.

The re-orchestration of plant primary metabolism, including the amino acid biosynthesis, plays a major role in the metabolic adjustment of plants under waterlogging stress (Batista-Silva et al., 2019; Behr et al., 2021). Moreover, previous studies have found that compared with the stronger responses of plant roots to waterlogging conditions, the hypoxic symptoms of shoots seem to be less, which probably due to the oxygen generated by leaf photosynthesis (Mustroph et al., 2014). Here, we also paid more attention on the changes in the amino acid metabolism of kiwifruit roots during waterlogging treatment. The detection showed a large increment of Ala and GABA concentrations in kiwifruit roots during waterlogging period, which were reported as a marker of hypoxic symptoms in other plant species (Rocha et al., 2010; Oliveira and Sodek, 2013), and the melatonin treatment promoted the increase of GABA while reduced the accumulation of Ala. Furthermore, we also detected a significant decrease in Asp and Glu concentrations in kiwifruit roots during waterlogging treatment, which was enhanced by melatonin treatment. The decrease in Asp and Glu levels caused by hypoxia has been reported in *Arabidopsis* and other plant species (Gibon et al., 2002; Mustroph et al., 2014), consistent with the role of these two amino acids as precursors for the synthesis of Ala and GABA. Since the reaction from Glu to GABA consumes protons, previous studies proposed the buffer role of GABA to counterbalance the detrimental effects of cellular acidification during hypoxia (Carroll et al., 1994). Here, our results showed that melatonin treatment facilitated the utilization of Asp and Glu in kiwifruit roots under waterlogging stress, and promoted the transition to GABA than to Ala. Combined with previous research which reported that the submergence intolerant variety of rice showed a higher elevation of Ala levels than tolerant variety under submerged condition (Barding et al., 2013), we believed that melatonin enhanced the waterlogging tolerance of kiwifruit plants partly through altering the Ala and GABA metabolism.

Synthesis of Pro and BCAAs and degradation of Arg in kiwifruit roots was enhanced by melatonin treatment during waterlogging stress. The Pro has been widely suggested to be indispensable for plant response to environmental stresses

(Antoniou et al., 2017; Huo et al., 2022), and it was reported to be involved in the redox buffering system of the plant cells during hypoxia (Behr et al., 2017). The high-level induction of BCAAs was reported in plants in response to various stress conditions (Huang and Jander, 2017). Here, we found that the metabolism of Pro and BCAAs in kiwifruit roots was enhanced by melatonin treatment to encounter waterlogging stress. As Arg serves as a substrate for polyamines (PAs) and nitric oxide, which was proved to be favorable in plant waterlogging tolerance (Pucciariello and Perata, 2017; Rauf et al., 2021), melatonin might promote the waterlogging resistance of kiwifruit plants by regulating the Arg transformation. Previous researches in alfalfa have reported that melatonin could modulate the nitro-oxidative homeostasis and proline metabolism to ameliorate drought damage (Antoniou et al., 2017), but the detailed interaction mechanisms between melatonin, PAs and nitric oxide in plants in response to waterlogging stress require further study. Besides the amino acid levels, we also analyzed the changes in the ACC, ABA, and SA levels in kiwifruit roots under waterlogging stress. Previous researches reported that the concentration of ABA and SA changed in soybean hypocotyls under waterlogging stress, which might contribute to the secondary aeration tissues appearing (Shimamura et al., 2014; Kim et al., 2015). Moreover, Qi et al. (2019) found that treating cucumber seedlings with exogenous ACC promoted the formation of adventitious roots under waterlogging stress. However, the relationship among melatonin and them when plants encountered waterlogging stress were rarely reported. Here, the detection showed that while the ACC concentration in kiwifruit roots was induced markedly by waterlogging stress, the ABA and SA concentrations decreased. Apparently, the melatonin treatment enhanced the ACC increment in kiwifruit roots under waterlogging stress. ACC is the direct precursor in the biosynthesis of ethylene, and the ethylene accumulation and perception are necessary for aerenchyma cells formation and adventitious root primordium generation (Yamauchi et al., 2014; Yamauchi et al., 2016). The enhanced ACC levels in kiwifruit roots under waterlogging stress might contribute, to a certain extent, in melatonin-mediated waterlogging tolerance.

Conclusion

In conclusion, our results demonstrated that pre-irrigating kiwifruit plants with 100 μM melatonin could partially alleviate the waterlogging damage on whole plant. First, the kiwifruit plants in MT+WL group maintained a better photosynthetic activity during the treatment, and they showed a less ROS accumulation in roots after waterlogging stress. Further study on kiwifruit roots showed that the levels of Ala, GABA, and Pro were increased markedly due to waterlogging stress, and melatonin treatment promoted the increment of GABA and Pro while reduced the accumulation of Ala. These responses suggested that melatonin-mediated waterlogging tolerance of kiwifruit plants was related to Ala, GABA, and Pro metabolism. Moreover, melatonin pretreatment altered the level of other plant hormones in kiwifruit roots to encounter waterlogging stress, which included the enhancement of ACC accumulation. The present study provided novel insights into the melatonin-induced waterlogging tolerance of kiwifruit plants, as well as the new and initial evidence for the effect of exogenous melatonin on plant amino acid metabolism. The specific and detailed interaction mechanisms between melatonin and metabolic pathways in the plant-water interactive system require further study.

Data availability statement

The raw data supporting the conclusions of this article will be made available by the authors, without undue reservation.

Author contributions

LH and KX designed the experiments. LH, HW, and QW performed the experiments and analyzed the data, assisted by YG. LH and XS wrote and revised the manuscript. All authors contributed to the article and approved the submitted version.

Funding

This work was supported by the National Natural Science Foundation of China (3210180210) and the Scientific Research and Development Foundation of Zhejiang A & F University (2020FR044).

Conflict of interest

The authors declare that the research was conducted in the absence of any commercial or financial relationships that could be construed as a potential conflict of interest.

Publisher's note

References

Antoniou, C., Chatzimichail, G., Xenofontos, R., Pavlou, J. J., Panagiotou, E., Christou, A., et al. (2017). Melatonin systemically ameliorates drought stress-induced damage in medicago sativa plants by modulating nitro-oxidative homeostasis and proline metabolism. *J. Pineal Res.* 62, 12401. doi: 10.1111/jpi.12401

Arbona, V., Hossain, Z., López-Climent, M., Pérez-Clemente, R., and Gómez-Cadenas, A. (2010). Antioxidant enzymatic activity is linked to waterlogging stress tolerance in citrus. *Physiol. Plant* 132, 452–466. doi: 10.1111/j.1399-3054.2007.01029.x

Arbona, V., Zandalinas, S. I., Manzi, M., Gonzalez-Guzman, M., Rodriguez, P. L., and Gomez-Cadenas, A. (2017). Depletion of abscisic acid levels in roots of flooded carrizo citrange (Poncirus trifoliata l. raf. x citrus sinensis l. osb.) plants is a stress-specific response associated to the differential expression of PYR/PYL/RCAR receptors. *Plant Mol. Biol.* 93, 623–640. doi: 10.1007/s11103-017-0587-7

Arnao, M. B., and Hernández-Ruiz, J. (2019). Melatonin: A new plant hormone and/or a plant master regulator? *Trends Plant Sci.* 24, 38–48. doi: 10.1016/j.tplants.2018.10.010

Back, K., Tan, D. X., and Reiter, R. J. (2016). Melatonin biosynthesis in plants: Multiple pathways catalyze tryptophan to melatonin in the cytoplasm or chloroplasts. *J. Pineal Res.* 61, 426–437. doi: 10.1111/jpi.12364

Bailey-Serres, J., Fukao, T., Gibbs, D. J., Holdsworth, M. J., Lee, S. C., Licausi, F., et al. (2012). Making sense of low oxygen sensing. *Trends Plant Sci.* 17, 129–138. doi: 10.1016/j.tplants.2011.12.004

Bajwa, V. S., Shukla, M. R., Sherif, S. M., Murch, S. J., and Saxena, P. K. (2014). Role of melatonin in alleviating cold stress in arabidopsis thaliana. *J. Pineal Res.* 56, 238–245. doi: 10.1111/jpi.12115

Barding, G. A., Beni, S., Fukao, T., Bailey-Serres, J., and Larive, C. K. (2013). Comparison of GC-MS and NMR for metabolite profiling of rice subjected to submergence stress. *J. Proteome Res.* 12, 898–909. doi: 10.1021/pr300953k

Batista-Silva, W., Heinemann, B., Rugen, N., Nunes-Nesi, A., Araujo, W. L., Braun, H. P., et al. (2019). The role of amino acid metabolism during abiotic stress release. *Plant Cell Environ.* 42, 1630–1644. doi: 10.1111/pce.13518

Behr, J. H., Bednarz, H., Godde, V., Niehaus, K., and Zorb, C. (2021). Metabolic responses of sugar beet to the combined effect of root hypoxia and NaCl-salinity. *J. Plant Physiol.* 267, 153545. doi: 10.1016/j.jplph.2021.153545

Behr, J. H., Bouchereau, A., Berardocco, S., Seal, C. E., Flowers, T. J., and Zorb, C. (2017). Metabolic and physiological adjustment of to combined salinity and hypoxia. *Ann. Bot.* 119, 965–976. doi: 10.1093/aob/mcw282

Benschop, J. J., Bou, J., Peeters, A. J., Wagemaker, N., Gühl, K., Ward, D., et al. (2006). Long-term submergence-induced elongation in rumex palustris requires abscisic acid-dependent biosynthesis of gibberellin1. *Plant Physiol.* 141, 1644–1652. doi: 10.1104/pp.106.082636

Carroll, A. D., Fox, G. G., Laurie, S., Phillips, R., Ratcliffe, R. G., and Stewart, G. R. (1994). Ammonium assimilation and the role of [gamma]-aminobutyric acid in pH homeostasis in carrot cell suspensions. *Plant Physiol.* 106, 513–520. doi: 10.1104/pp.106.2.513

Dat, J. F., Capelli, N., Folzer, H., Bourgeade, P., and Badot, P. M. (2004). Sensing and signalling during plant flooding. *Plant Physiol. Biochem.* 42, 273–282. doi: 10.1016/j.plaphy.2004.02.003

Dionisio-Sese, M. L., and Tobita, S. (1998). Antioxidant responses of rice seedlings to salinity stress. *Plant Sci.* 135, 1–9. doi: 10.1016/S0168-9452(98)00025-9

Drew, M. C. (1997). Oxygen deficiency and root metabolism: Injury and acclimation under hypoxia and anoxia. *Annu. Rev. Plant Physiol. Plant Mol. Biol.* 48, 223–250. doi: 10.1146/annurev.arplant.48.1.223

Fukao, T., and Bailey-Serres, J. (2004). Plant responses to hypoxia–is survival a balancing act? *Trends Plant Sci.* 9, 449–456. doi: 10.1016/j.tplants.2004.07.005

Fukao, T., and Bailey-Serres, J. (2008). Ethylene–a key regulator of submergence responses in rice. *Plant Sci.* 175, 43–51. doi: 10.1016/j.plantsci.2007.12.002

Gao, T., Liu, X., Tan, K., Zhang, D., Zhu, B., Ma, F., et al. (2022). Introducing melatonin to the horticultural industry: physiological roles, potential applications, and challenges. *Horticulture Res.*, 9, uhac094. doi: 10.1093/hr/uhac094

Garssen, A. G., Baattrup-Pedersen, A., Voesenek, L., Verhoeven, J. T. A., and Soons, M. B. (2015). Riparian plant community responses to increased flooding: a meta-analysis. *Global Change Bio.* 21, 2881–2890. doi: 10.1111/gcb.12921

Geigenberger, P. (2003). Response of plant metabolism to too little oxygen. *Curr. Opin. Plant Biol.* 6, 247–256. doi: 10.1016/S1369-5266(03)00038-4

Gibon, Y., Vigeolas, H., Tiessen, A., Geigenberger, P., and Stitt, M. (2002). Sensitive and high throughput metabolite assays for inorganic pyrophosphate, ADPGlc, nucleotide phosphates, and glycolytic intermediates based on a novel enzymic cycling system. *Plant J.* 30, 221–235. doi: 10.1046/j.1365-313X.2001.01278.x

Hildebrandt, T. M. (2018). Synthesis versus degradation: directions of amino acid metabolism during arabidopsis abiotic stress response. *Plant Mol. Biol.* 98, 121–135. doi: 10.1007/s11103-018-0767-0

Hossain, Z., López-Climent, M., Arbona, V., Pérez-Clemente, R., and Gómez-Cadenas, A. (2009). Modulation of the antioxidant system in citrus under waterlogging and subsequent drainage. *J. Plant Physiol.* 166, 1391–1404. doi: 10.1016/j.jplph.2009.02.012

Huang, T. F., and Jander, G. (2017). Abscisic acid-regulated protein degradation causes osmotic stress-induced accumulation of branched-chain amino acids in arabidopsis thaliana. *Planta* 246, 737–747. doi: 10.1007/s00425-017-2727-3

Huo, L. Q., Guo, Z. J., Wang, Q., Cheng, L., Jia, X., Wang, P., et al. (2021). Enhanced autophagic activity improved the root growth and nitrogen utilization ability of apple plants under nitrogen starvation. *Int. J. Mol. Sci.* 22, 8085. doi: 10.3390/ijms22158085

Huo, L. Q., Guo, Z. J., Wang, Q., Jia, X., Sun, X. P., and Ma, F. W. (2022). The protective role of MdATG10-mediated autophagy in apple plant under cadmium stress. *Ecotoxicol. Environ. Saf.* 234, 113398. doi: 10.1016/j.ecoenv.2022.113398

Huo, L. Q., Guo, Z. J., Wang, P., Zhang, Z. J., Jia, X., Sun, Y. M., et al. (2020). MdATG8i functions positively in apple salt tolerance by maintaining photosynthetic ability and increasing the accumulation of arginine and polyamines. *Environ. Exp. Bot.* 172, 103989. doi: 10.1016/j.envexpbot.2020.103989

Hussain, M., Farooq, S., Hasan, W., Ul-Allah, S., Tanveer, M., Farooq, M., et al. (2018). Drought stress in sunflower: Physiological effects and its management through breeding and agronomic alternatives. *Agric. Water Manage.* 201, 152–166. doi: 10.1016/j.agwat.2018.01.028

Kim, Y. H., Hwang, S. J., Waqas, M., Khan, A. L., Lee, J. H., Lee, J. D., et al. (2015). Comparative analysis of endogenous hormones level in two soybean (Glycine max l.) lines differing in waterlogging tolerance. *Front. Plant Sci.* 6, 714. doi: 10.3389/fpls.2015.00714

Kreuzwieser, J., and Rennenberg, H. (2014). Molecular and physiological responses of trees to waterlogging stress. *Plant Cell Environ.* 37, 2245–2259. doi: 10.1111/pce.12310

Kuroh, T., Nagai, K., Gamuyao, R., Wang, D. R., Furuta, T., Nakamori, M., et al. (2018). Ethylene-gibberellin signaling underlies adaptation of rice to periodic flooding. *Science* 361, 181–185. doi: 10.1126/science.aat1577

Liang, D., Fan, G. F., Ni, Z. Y., Lin, L. J., Deng, Q. X., Tang, Y., et al. (2018). Melatonin improves heat tolerance in kiwifruit seedlings through promoting antioxidant enzymatic activity and glutathione s-transferase transcription. *Molecules* 23, 584. doi: 10.3390/molecules23030584

Liang, D., Ni, Z., Xia, H., Xie, Y., Lv, X., Wang, J., et al. (2019). Exogenous melatonin promotes biomass accumulation and photosynthesis of kiwifruit seedlings under drought stress. *Sci. Hortic.* 246, 34–43. doi: 10.1016/j.scienta.2018.10.058

Li, D. D., Cisse, E. M., Guo, L. Y., Zhang, J., Miao, L. F., and Yang, F. (2022). Comparable and adaptable strategies to waterlogging stress regulated by adventitious roots between two contrasting species. *Tree Physiol.* 42, 971–988. doi: 10.1093/treephys/tpab165

Liu, J., Chen, Y., Wang, W. Q., Liu, J. H., Zhu, C. Q., Zhong, Y. P., et al. (2022). Transcription factors AcERF74/75 respond to waterlogging stress and trigger alcoholic fermentation-related genes in kiwifruit. *Plant Sci.* 314, 111115. doi: 10.1016/j.plantsci.2021.111115

Liu, F., V., T., Moy, L. P., Bock, G., Linford, L. D., and Quackenbush, J. (2005). Global transcription profiling reveals comprehensive insights into hypoxic response in arabidopsis. *Plant Physiol.* 137, 1115–1129. doi: 10.1104/pp.104.055475

Li, C., Zhao, Q., Gao, T. T., Wang, H. Y., Zhang, Z. J., Liang, B. W., et al. (2018). The mitigation effects of exogenous melatonin on replant disease in apple. *J. Pineal Res.* 65, 12523. doi: 10.1111/jpi.12523

Lothier, J., Diab, H., Cukier, C., Limami, A. M., and Tcherkez, G. (2020). Metabolic responses to waterlogging differ between roots and shoots and reflect phloem transport alteration in medicago truncatula. *Plants* 9, 1373. doi: 10.3390/plants9101373

Mittler, R., Vanderauwera, S., Suzuki, N., Miller, G., Tognetti, V. B., Vandepoele, K., et al. (2011). ROS signaling: the new wave? *Trends Plant Sci.* 16, 300–309. doi: 10.1016/j.tplants.2011.03.007

Moustafa-Farag, M., Mahmoud, A., Arnao, M. B., Sheteiwy, M. S., Dafea, M., Soltan, M., et al. (2020). Melatonin-induced water stress tolerance in plants: Recent advances. *Antioxidants* 9, 809. doi: 10.3390/antiox9090809

Mustroph, A., Barding, G. A., Kaiser, K. A., Larive, C. K., and Bailey-Serres, J. (2014). Characterization of distinct root and shoot responses to low-oxygen stress

in arabidopsis with a focus on primary c- and n-metabolism. *Plant Cell Environ.* 37, 2366–2380. doi: 10.1111/pce.12282

Nguyen, V. T., Vuong, T. D., VanToai, T., Lee, J. D., Wu, X., Mian, M. A. R., et al. (2012). Mapping of quantitative trait loci associated with resistance to phytophthora sojae and flooding tolerance in soybean. *Crop Sci.* 52, 2481–2493. doi: 10.2135/cropsci2011.09.0466

Oliveira, H. C., and Sodek, L. (2013). Effect of oxygen deficiency on nitrogen assimilation and amino acid metabolism of soybean root segments. *Amino Acids* 44, 743–755. doi: 10.1007/s00726-012-1399-3

Pan, J. W., Sharif, R., Xu, X. W., and Chen, X. H. (2021). Mechanisms of waterlogging tolerance in plants: Research progress and prospects. *Front. Plant Sci.* 11, 627331. doi: 10.3389/fpls.2020.627331

Phukan, U. J., Mishra, S., and Shukla, R. K. (2016). Waterlogging and submergence stress: affects and acclimation. *Crit. Rev. Biotechnol.* 36, 956–966. doi: 10.3109/07388551.2015.1064856

Planchet, E., Lothier, J., and Limami, A. M. (2017). "Hypoxic respiratory metabolism in plants: Reorchestration of nitrogen and carbon metabolisms," in *Plant respiration: Metabolic fluxes and carbon balance. advances in photosynthesis and respiration*. Eds. G. Tcherkez and J. Ghashghaie (Cham: Springer), 209–226.

Pucciariello, C., and Perata, P. (2017). New insights into reactive oxygen species and nitric oxide signalling under low oxygen in plants. *Plant Cell Environ.* 40, 473–482. doi: 10.1111/pce.12715

Qi, X., Li, Q., Ma, X., Qian, C., Wang, H., Ren, N., et al. (2019). Waterlogging induced adventitious root formation in cucumber is regulated by ethylene and auxin through reactive oxygen species signalling. *Plant Cell Environ.* 42, 1458–1470. doi: 10.1111/pce.13504

Qi, X. H., Li, Q. Q., Shen, J. T., Qian, C. L., Xu, X. W., Xu, Q., et al. (2020). Sugar enhances waterlogging-induced adventitious root formation in cucumber by promoting auxin transport and signalling. *Plant Cell Environ.* 43, 1545–1557. doi: 10.1111/pce.13738

Rauf, M., Awais, M., Ud-Din, A., Ali, K., Gul, H., Rahman, M. M., et al. (2021). Molecular mechanisms of the 1-Aminocyclopropane-1-Carboxylic acid (ACC) deaminase producing trichoderma asperellum MAP1 in enhancing wheat tolerance to waterlogging stress. *Front. Plant Sci.* 11, 614971. doi: 10.3389/fpls.2020.614971

Rocha, M., Licausi, F., Araujo, W. L., Nunes-Nesi, A., Sodek, L., Fernie, A. R., et al. (2010). Glycolysis and the tricarboxylic acid cycle are linked by alanine aminotransferase during hypoxia induced by waterlogging of lotus japonicus. *Plant Physiol.* 152, 1501–1513. doi: 10.1104/pp.109.150045

Sanchez, D. H., Siahpoosh, M. R., Roessner, U., Udvardi, M., and Kopka, J. (2010). Plant metabolomics reveals conserved and divergent metabolic responses to salinity. *Physiol. Plant* 132, 209–219. doi: 10.1111/j.1399-3054.2007.00993.x

Shabala, S., Shabala, L., Barcelo, J., and Poschenrieder, C. (2014). Membrane transporters mediating root signalling and adaptive responses to oxygen deprivation and soil flooding. *Plant Cell Environ.* 37, 2216–2233. doi: 10.1111/pce.12339

Shimamura, S., Yoshioka, T., Yamamoto, R., Hiraga, S., Nakamura, T., Shimada, S., et al. (2014). Role of abscisic acid in flood-induced secondary aerenchyma formation in soybean (Glycine max) hypocotyls. *Plant Prod. Sci.* 17, 131–137. doi: 10.1626/pps.17.131

Stuart, M. E., Goo Dd Y, D. C., Bloomfield, J. P., and Williams, A. T. (2011). A review of the impact of climate change on future nitrate concentrations in groundwater of the UK. *Sci. Total Environ.* 409, 2859–2873. doi: 10.1016/j.scitotenv.2011.04.016

Takahashi, H., Yamauchi, T., Rajhi, I., Nishizawa, N. K., and Nakazono, M. (2015). Transcript profiles in cortical cells of maize primary root during ethylene-induced lysigenous aerenchyma formation under aerobic conditions. *Ann. Bot.* 115, 879–894. doi: 10.1093/aob/mcv018

van Veen, H., Akman, M., Jamar, D. C. L., Vreugdenhil, D., Kooiker, M., van Tienderen, P., et al. (2014). Group VII ethylene response factor diversification and regulation in four species from flood-prone environments. *Plant Cell Environ.* 37, 2421–2432. doi: 10.1111/pce.12302

Wang, P., Sun, X., Wang, N., Tan, D. X., and Ma, F. (2015). Melatonin enhances the occurrence of autophagy induced by oxidative stress in arabidopsis seedlings. *J. Pineal Res.* 58, 479–489. doi: 10.1111/jpi.12233

Wu, Y., Wang, Y., Yan, Q., Mao, J., and Ahammed, G. J. (2020). Melatonin alleviates iron stress by improving iron homeostasis, antioxidant defense and secondary metabolism in cucumber. *Sci. Hortic.* 265, 109205. doi: 10.1016/j.scienta.2020.109205

Xia, H., Ni, Z. Y., Hu, R. P., Lin, L. J., Deng, H. H., Wang, J., et al. (2020). Melatonin alleviates drought stress by a non-enzymatic and enzymatic antioxidative system in kiwifruit seedlings. *Int. J. Mol. Sci.* 21, 030852. doi: 10.3390/ijms21030852

Xu, Q. T., Yang, L., Zhou, Z. Q., Mei, F. Z., Qu, L. H., and Zhou, G. S. (2013). Process of aerenchyma formation and reactive oxygen species induced by waterlogging in wheat seminal roots. *Planta* 238, 969–982. doi: 10.1007/s00425-013-1947-4

Yamauchi, T., Tanaka, A., Mori, H., Takamure, I., Kato, K., and Nakazono, M. (2016). Ethylene-dependent aerenchyma formation in adventitious roots is regulated differently in rice and maize. *Plant Cell Environ.* 39, 2145–2157. doi: 10.1111/pce.12766

Yamauchi, T., Watanabe, K., Fukazawa, A., Mori, H., Abe, F., Kawaguchi, K., et al. (2014). Ethylene and reactive oxygen species are involved in root aerenchyma formation and adaptation of wheat seedlings to oxygen-deficient conditions. *J. Exp. Bot.* 65, 261–273. doi: 10.1093/jxb/ert371

Zhang, Q., Liu, X., Zhang, Z., Liu, N., Li, D., and Hu, L. (2019). Melatonin improved waterlogging tolerance in alfalfa (Medicago sativa) by reprogramming polyamine and ethylene metabolism. *Front. Plant Sci.* 10, 44. doi: 10.3389/fpls.2019.00044

Zhang, P., Lyu, D. G., Jia, L. T., He, J. L., and Qin, S. J. (2017). Physiological and *de novo* transcriptome analysis of the fermentation mechanism of cerasus sachalinensis roots in response to short-term waterlogging. *BMC Genomics* 18, 649. doi: 10.1186/s12864-017-4055-1

Zheng, X. D., Zhou, J. Z., Tan, D. X., Wang, N., Wang, L., Shan, D. Q., et al. (2017). Melatonin improves waterlogging tolerance of malus baccata (Linn.) borkh. seedlings by maintaining aerobic respiration, photosynthesis and ROS migration. *Front. Plant Sci.* 8, 00483. doi: 10.3389/fpls.2017.00483

Zhou, K., Li, Y. T., Hu, L. Y., Zhang, J. Y., Yue, H., Yang, S. L., et al. (2022). Overexpression of MdASMT9, an n-acetylserotonin methyltransferase gene, increases melatonin biosynthesis and improves water-use efficiency in transgenic apple. *Tree Physiol.* 42, 1114–1126. doi: 10.1093/treephys/tpab157

frontiers | Frontiers in Plant Science

TYPE Original Research
PUBLISHED 20 December 2022
DOI 10.3389/fpls.2022.1101212

OPEN ACCESS

EDITED BY
Tuanhui Bai,
Henan Agricultural University, China

REVIEWED BY
Reetesh Kumar,
GLA University, India
Zhiyong Pan,
Huazhong Agricultural University, China

*CORRESPONDENCE
Ying-Ning Zou
zouyingning@163.com

SPECIALTY SECTION
This article was submitted to Plant Abiotic Stress, a section of the journal Frontiers in Plant Science

RECEIVED 17 November 2022
ACCEPTED 06 December 2022
PUBLISHED 20 December 2022

CITATION
Liu Z, Cheng S, Liu X-Q, Kuča K, Hashem A, Al-Arjani A-BF, Almutairi KF, Abd_Allah EF, Wu Q-S and Zou Y-N (2022) Cloning of a CHS gene of *Poncirus trifoliata* and its expression in response to soil water deficit and arbuscular mycorrhizal fungi.
Front. Plant Sci. 13:1101212.
doi: 10.3389/fpls.2022.1101212

Cloning of a CHS gene of *Poncirus trifoliata* and its expression in response to soil water deficit and arbuscular mycorrhizal fungi

Zhen Liu[1], Shen Cheng[1], Xiao-Qing Liu[1], Kamil Kuča[2], Abeer Hashem[3], Al-Bandari Fahad Al-Arjani[3], Khalid F. Almutairi[4], Elsayed Fathi Abd_Allah[4], Qiang-Sheng Wu[1,2] and Ying-Ning Zou[1]*

[1]College of Horticulture and Gardening, Yangtze University, Jingzhou, Hubei, China, [2]Department of Chemistry, Faculty of Science, University of Hradec Kralove, Hradec Kralove, Czechia, [3]Botany and Microbiology Department, College of Science, King Saud University, Riyadh, Saudi Arabia, [4]Plant Production Department, College of Food and Agricultural Sciences, King Saud University, Riyadh, Saudi Arabia

Flavonoids are secondary metabolites widely found in plants with antioxidants, of which chalcone synthase (CHS) is a key enzyme required in flavonoid synthesis pathways. The objective of this study was to clone a *CHS* gene from trifoliate orange (*Poncirus trifoliata*) and analyze its biological information and partial functions. A PtCHS gene (NCBI accession: MZ350874) was cloned from the genome-wide of trifoliate orange, which has 1156 bp in length, encoding 391 amino acids, with a predicted protein relative molecular mass of 42640.19, a theoretical isoelectric point of 6.28, and a lipid coefficient of 89.82. The protein is stable, hydrophilic, and high sequence conservation (92.49% sequence homology with CHS gene of other species). *PtCHS* was highly expressed in stems, leaves and flowers, but very low expression in roots and seeds. Soil water deficit could up-regulate expressions of *PtCHS* in leaves. An arbuscular mycorrhizal fungus, *Funneliformis mosseae*, significantly increased plant biomass production, CHS activity, expressions of *PtCHS*, and total flavonoid content in leaves and roots, independent of soil water status. Total flavonoids were significantly positively correlated with *PtCHS* expression in leaves only and also positively with root mycorrhizal colonization. Such results provide insight into the important functions of *PtCHS* in trifoliate orange.

KEYWORDS

arbuscular mycorrhiza, chalcone synthase, drought, trifoliate orange, flavonoid

Introduction

Flavonoids are important secondary metabolites of horticultural plants, which have antioxidant, antibacterial, and anti-inflammatory properties (Shen et al., 2022). In addition, flavonoids have some applications in the food industry, cosmetics, and pharmaceutical industries (Dias et al., 2021). The synthesis of flavonoids is accomplished with the joint participation of various enzymes, among which chalone synthase (CHS) is the first key enzyme in the flavonoid biosynthesis pathway (Yonekura et al., 2019). CHS is to catalyze the synthesis of naringenin chalcone from p-coumaroyl CoA and malonyl CoA, which is further derived and transformed into various flavonoid compounds under the catalysis of chalcone isomerase (CHI) (Han et al., 2016, Yahyaa et al., 2017). CHS is widely found in higher plants, and the expression of its gene family members is tissue-specific and time-specific (Chen et al., 2017; Sepiol et al., 2017). Environmental stress such as temperature stress and drought stress induces CHS expressions to promote the accumulation of flavonoids (Dao et al., 2011; Li et al., 2020; Yin et al., 2020). Hence, the gene plays an important role in plant response to stress and regulation of flavonoid synthesis (Dixon and Paiva, 1995; Gläßgen et al., 1998). CHS gene has been cloned in many crops, such as rice (Han et al., 2017), mulberry (Wang et al., 2017), and citrus (Wang et al., 2018), but there is no report in trifoliate orange (*Poncirus trifoliata*). Hu et al. (2019) reported that overexpression of a *CHS* gene from tobacco (*Nicotiana tabacum*) could mitigate drought-induced oxidative damage and thus enhanced drought tolerance. Nakabayashi et al. (2014) also observed in *Arabidopsis thaliana* that excessive accumulation of flavonoids was the key to enhance drought tolerance of plants. Therefore, up-regulated expression of flavonoid biosynthetic genes and accumulation of flavonoids are important mechanisms for drought tolerance in plants (Ma et al., 2014).

Trifoliate orange, belonging to the genus *Poncirus* in the Rutaceae family, has the advantages of resistance to root rot, tristeza virus, cold, and drought tolerance, and is the most widely used rootstock in citrus production (Wu et al., 2010). In addition, trifoliate orange is a citrus relative with abundant bioactive substances, such as flavonoids, carotenoids, and terpenoids (Gao et al., 2018; Sharma et al., 2019). All citrus plants can produce flavonoids (Ghasemi et al., 2009), such as sweet orange, pomelo, and lemon. At present, more than 60 flavonoids have been identified in citrus (Tripoli et al., 2007). Flavonoids of citrus not only have antioxidant, anti-inflammatory, anti-tumor, and other functions (Song et al., 2017; Mahato et al., 2018), but also play an important role in the coloring of flowers, fruits and leaves, abiotic and biotic tolerance, auxin transport, nutritional value, and fruit flavor (Ferreyra et al., 2012; Flamini et al., 2013; Gabriele et al., 2017).

Soil water deficit (SWD) is one of abiotic stress restricting crop growth, which can lead to reduced crop growth and yield, and even crop death in severe cases (Kunert et al., 2016). Arbuscular mycorrhizal fungi (AMF) in soil form a reciprocal symbiosis with plant roots (He et al., 2019), which can absorb water and nutrients from the soil to host plants for their growth and enhance SWD tolerance, along with high utilization value in agricultural production (Wu et al., 2013; Zou et al., 2017). Studies have shown that appropriate SWD promoted flavonoid accumulation in plants (Ma et al., 2014), and AMF promoted photosynthesis, nutrient absorption, and various secondary metabolite levels in plants under SWD (Cheng et al., 2022). We hypothesized that AMF up-regulates the expression level of *CHS* in trifoliate orange under drought and thus promotes the level of flavonoids, which is beneficial for mycorrhizal plants to tolerate SWD.

In order to confirm the above hypothesis, we cloned a CHS gene from *P. trifoliata*, analyzed the physicochemical properties of the protein, constructed an evolutionary tree, and analyzed the relative expression of *PtCHS* gene in leaves and roots under SWD and AMF inoculation.

Materials and methods

Cloning of PtCHS gene

Total RNA was extracted from leaves, stems, roots, flowers, fruits, and seeds of trifoliate orange grown in a citrus orchard of Yangtze University using the TaKaRa MiniBEST Universal RNA Extraction Kit. After checking the concentration and purity of the extracted RNA, the PrimeScript™ RT Reagent Kit with gDNA eraser was used to reverse-transcribe RNA into cDNA using a Bio Photometer Plus PCR (6132, Eppendorf, Germany).

The Arabidopsis CHS gene (NCBI accession number: AT5G13930) was used as the reference sequence, and the BLASTP of the trifoliate orange genome database was used to search CHS gene. A pair of primers (F: 5'-CCAAGCACGAG CCTCAAAAC-3'; R: 5'-ACAGCACACCCCAATCTAGC-3') was designed using Primer premier 5.0 software to amplify the full-length sequence of the gene, in which planta max super-fidelity DNA polymerase kit (Vazyme Biotech Co., Ltd, Nangjing, China) was used under the condition of 95°C for 3 min, 95°C for 15 s, 56°C for 15 s, and 72°C for 3 min with 35 cycles.

After the PCR reaction, the product fragments were recovered and the target fragments were ligated and transformed using the pEASY®-Blunt Zero Cloning Kit (Beijing TransGene Biotech Co., Ltd, Beijing, China). Positive clones were screened on LB plates coated with ampicillin, and then sequenced by Department of Qingke Biotechnology Co., LTD. (Wuhan, China). The sequencing results were spliced by DNAMAN 6.0, and the full-length sequences of the cloned genes were obtained by analysis and comparison using BLAS of NCBI.

Bioinformatics analysis of PtCHS

Multiple alignments of amino acid sequences were performed using the DNAMAN (V6.0). The amino acid sequence of PtCHS gene was constructed by Mega-X, and the neighbor-joining (NJ) method was used to generate the evolutionary tree. Bootstrap was used to validate the phylogenetic tree, and the number of replicates was defined as 1000. According to the online tool (https://swissmodel.expasy.org/) the gene structure was predicted. SOPMA (http://npsa-pbil.ibcp.fr/cgi-bin/npsa_automat.pl?page=npsa_sopma.html) and Swiss-Model (http://swissmodel.expasy.org/interactive) were used for secondary and tertiary structure prediction of the protein, respectively. The protein subcellular localization was predicted using the online WoLF PSORT (https://wolfpsort.hgc.jp/) to predict.

Plant culture and AMF inoculation

Four-leaf-old trifoliate orange seedlings grown in sterilized river sand were transplanted into a plastic pot containing 2.5 kg of autoclaved soil and sand mixture (3 : 1, v/v). At the same time, the 120 g inoculums of *Funneliformis mosseae* (BGC XZ02A) (22 spore/g) were applied near the rhizosphere. Uninoculated (-AMF) plants were treated with 120 g of autoclaved inoculums and a filtrate (25 μm filter) of 2 mL of mycorrhizal inoculums to maintain similar microbial community composition except for the *F. mosseae*. After transplantation, all treated plants maintained the soil moisture at well-watered (WW) (75% of the maximum field water capacity) for their growth. After 8 weeks, half of the inoculated and uninoculated plants were subjected to SWD (55% of the maximum field water capacity) for 10 weeks, and the other half continued to grow in the soil with WW status for another 10 weeks. Soil moisture was monitored daily by weighing method, and the loss of soil water was replenished in time. The plants were grown in a greenhouse, where the environmental conditions have been described by Zhang et al. (2020). Therefore, this experiment consisted of four treatments: the seedlings inoculated with AMF and grown in WW (WW+AMF); the seedlings inoculated without AMF and grown in WW (WW-AMF); the seedlings inoculated with AMF and grown in SWD (SWD+AMF); the seedlings inoculated without AMF and grown in SWD (SWD-AMF). Each treatment was repeated six times.

Determination of plant biomass production and root mycorrhizal colonization

At plant harvest, the biomass of the whole plant was weighted, frozen with liquid nitrogen, and immediately stored at -80°C for RNA extraction. Root mycorrhizae were stained according to the method described by Phillips and Hayman (1970). About 1-cm-long root segments were incubated in 10% KOH solution at 95°C for 100 min, rinsed with distilled water, bleached with 10% hydrogen peroxide solution for 15 min, acidified with 0.2 mol/L hydrochloric acid for 10 min, and stained with 0.05% trypan blue in lactate phenol for 1 min. The mycorrhizal colonization was observed under a microscope and calculated as the percentage of length of AMF-colonized root segments versus total length of observed root segments.

Determination of CHS activity

The 0.5 g of fresh leaf and root samples were ground in 5 mL of 0.1 mol/L phosphate buffer (pH 7.6) in an ice bath and then centrifuged at 10,000×*g* for 10 min at 4°C. The supernatant was used as the crude extract for CHS activity determination. CHS activity was determined by the Enzyme-Linked Immunosorbent Assay (ELISA) according to the user manual, where the plant CHS kit (ml036296) was provided by Shanghai Enzyme Linked Biotechnology Co., Ltd (Shanghai, China).

Relative expressions of PtCHS

Total RNA extraction from leaves and roots was performed according to the above procedure. The primer sequence of the gene was designed in Primer Premier 5.0 Software according to the full-length gene sequences obtained by sequencing, where the sequences were 5'-GTCTAAACTCGGCCTCAAAGA-3' (forward primer) and 5'-TCTCGTCAAGGATGAACAGAAC-3' (reversed primer). After reverse transcription of RNA into cDNA, the β-actin was used as the reference gene for qRT-PCR, based on the 2 × AceQ qPCR SYBR Green Master Mix (Aidlab, Beijing, China). There were three biological replicates for each treatment. The $2^{-\Delta\Delta Ct}$ method was used to calculate the relative expression of *PtCHS*, with the WW-AMF treatment as the control.

Determination of total flavonoid content of leaves and roots

Plant total flavonoid content was assayed with the protocol of Liu et al. (2022). The 0.2 powdered samples of leaves and roots were extracted with 8 mL of 70% ethanol under ultrasonic conditions for 60 min, and centrifuged at 10,000×g for 10 min at 4°C. The extraction was repeated twice, and the supernatant was concentrated, evaporated to remove the ethanol, and added with methanol. A total of 10 mL reaction solution consisted of distilled water, 5% $NaNO_2$, 10% $AlCl_3$, 1 mol/L NaOH, and 0.5 mL of the tested solution, and their absorbance was measured at 510 nm, where the rutin was used as the standard.

Data analysis

The data obtained were statistically analyzed under SAS software, where ANOVA as well as Duncan' new multiple range test at 0.05 levels were performed for significance between treatments.

Results

Physicochemical properties of PtCHS protein

Sequencing results showed that the protein had 1156 bp in length (Figure 1), contained a complete open reading frame, and encoded 391 amino acids, along with NCBI accession number MZ350874.

The information of the protein predicted by ProtParam online tool (https://www.expasy.org/resources/protscale) showed that the relative molecular mass of this protein is 42640.19, the theoretical isoelectric point is 6.28, the molecular formula is $C_{1898}H_{3037}N_{507}O_{567}S_{19}$, and the protein is not stability index of 35.00, indicating that the protein is stable. In addition, the protein had a relatively high aliphatic index of 89.82, which allows the protein to have good stability in different environments and facilitates its normal function, and a grand average hydrophilicity of -0.105. PortScale online tools (https://www.expasy.org/resources/protscale) in the prediction of protein hydrophilic/hydrophobic properties showed that amino acid sequence in the 119th and 324th position had the minimum score (-2.489) and the maximum score (2.422) (Figure 2B). Moreover, more scores fell below zero, indicating that the protein is mainly hydrophilic.

Based on the prediction of SOPMA, random coil in the secondary structure of PtCHS protein accounted for 33.25%, α-helix 44.25%, extended strand 15.6%, and β-turn 6.91%, along with irregular coils and extended chains scattered in the whole protein structure (Figure 2A). The α-helix was the main structural component of the secondary structure of PtCHS protein. The tertiary structure prediction of PtCHS protein further showed that the protein was dominated by α-helices and random coils (Figure 2C), which was consistent with our secondary structure prediction. Based on the analysis of WoLF PSORT, the sub-cellular localization of the protein was in chloroplast, cytoplasm, and nucleus.

Phylogenetic analysis of PtCHS

The alignment of the amino acid sequences of PtCHS and CHS of eight other plant species of NCBI showed that the sequence homology of *PtCHS* and *CHS* of other species was 92.49%, indicating that *PtCHS* gene has high sequence conservation. The phylogenetic tree showed that the closest homology of *PtCHS* was *MsCHS2* in *Medicago sativa* (Figure 3).

Tissue-specific expression of *PtCHS* gene

The qRT-PCR results showed that the expression of *PtCHS* gene in trifoliate orange was tissue-specific (Figure 4). *PtCHS* was expressed in the leaf, flower, stem, root, and seed. The highest expression of the gene was found in the stem, and the lowest in the root and seed, where the gene expression level of leaf was 53.2-fold higher than that of root.

Root mycorrhizal colonization and total biomass in response to soil water deficit and AMF inoculation

F. mosseae could colonize the roots of trifoliate orange seedlings, and the root mycorrhizal colonization was 38.5%–58.7%, accompanied by higher mycorrhizal colonization appearing under WW versus SWD conditions (Figure 5B). In addition, SWD significantly inhibited the growth performance of trifoliate orange seedlings, while *F. mosseae* inoculation improved plant growth response (Figure 5A). SWD treatment significantly reduced total biomass production of non-mycorrhizal and mycorrhizal plants by 18.58% and 24.48%, respectively, compared with WW treatment (Figure 5C). Nevertheless, the total biomass was increased by *F. mosseae* inoculation by 117.98% under WW and 107.64% under SWD, respectively.

Relative expressions of *PtCHS* in response to soil water deficit and AMF inoculation

SWD and AMF (*F. mosseae*) inoculation affected relative expressions of *PtCHS* in leaves and roots (Figures 6A, B). Compared with the WW treatment, the SWD only up-regulated expressions of *PtCHS* in leaves of non-AMF-inoculated plants (Figure 6A). Compared with non-AMF inoculation, AMF inoculation up-regulated expressions of *PtCHS* under both WW and SWD: 1.62- and 0.81-fold higher in leaf and 0.53- and 2.14-fold higher in root, respectively (Figures 6A, B).

CHS activity in response to soil water deficit and AMF inoculation

SWD and AMF inoculation significantly altered CHS activity in leaves and roots of trifoliate orange seedlings

10.3389/fpls.2022.1101212

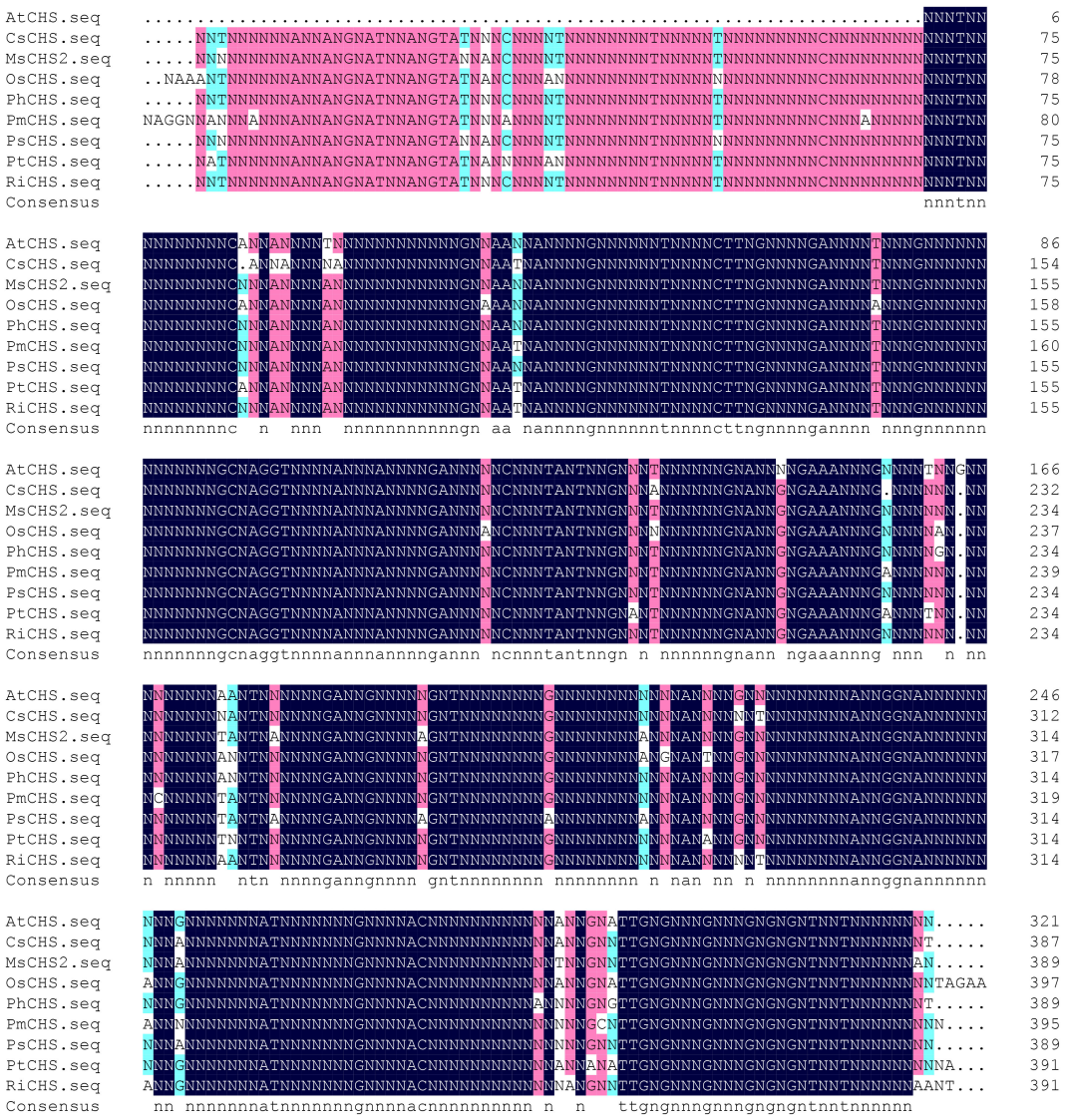

FIGURE 1
Sequence of PtCHS and its alignment with CHS gene of other plants. AtCHS, *Arabidopsis thaliana*; CsCHS, *Camellia sinensis*; MsCHS2, *Medicago sativa*; OsCHS, *Oryza sativ*; PhCHS, *Petunia* × *hybrida*; PmCHS, *Picea mariana*; PsCHS, *Pisum sativum*; PtCHS, *Poncirus trifoliata*; RiCHS, *Rubus idaeus*.

(Figures 7A, B). SWD reduced CHS activity in leaves of mycorrhizal plants by 17.76%, along with no significant effect on roots. Nevertheless, SWD reduced CHS activity in leaves and roots of non-mycorrhizal plants by 26.67% and 37.60%, respectively, compared with WW treatment. Compared with non-inoculated treatment, AMF inoculation significantly increased the CHS activity of leaves and roots by 37.69% and 45.75% under WW conditions and by 54.42% and 156.47% under SWD conditions, respectively.

Total flavonoid content and its correlation with PtCHS expressions

SWD did not significantly affect total flavonoid content in leaves and roots of plants inoculated without *F. mosseae*, but significantly reduced total flavonoid content in leaves and roots of *F. mosseae*-inoculated plants by 0.39- and 0.43-fold, respectively, compared with WW treatment (Figures 8A, B). On the other hand, inoculation with *F. mosseae* also significantly

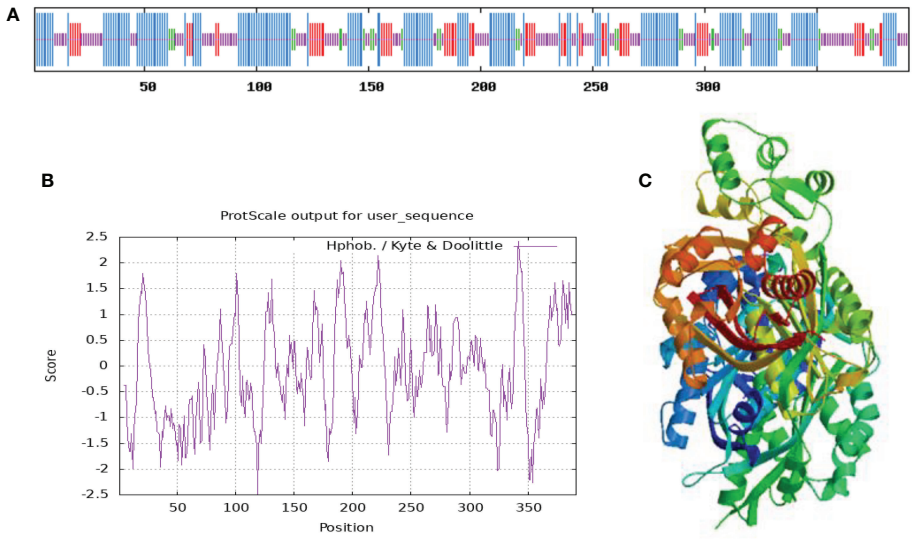

FIGURE 2
Hydrophilic and hydrophobic properties **(A)**, secondary structure **(B)**, and tertiary structure **(C)** of PtCHS protein.

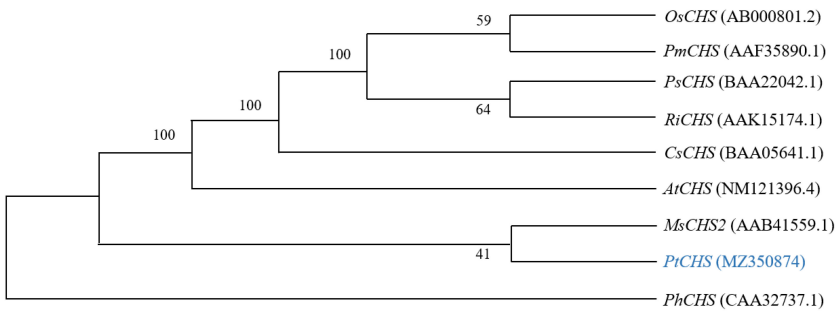

FIGURE 3
The phylogenetic tree analysis of PtCHS and CHS genes of other plants.

increased total flavonoid content of plants under both WW and SWD conditions, where it increased by 3.20- and 1.50-fold in leaves and 1.90- and 1.09-fold in roots, respectively. Correlation analysis showed that total flavonoid content was a significantly positive correlation with *PtCHS* expression in leaves (Figure 8C), along with no significant correlation in roots (Figure 8D).

Discussion

Hahlbrock and Kreuzaler (1972) firstly extracted the CHS from suspension cells of parsley. Subsequently, many scholars have carried out studies on cloning CHS gene of various plants (Liu et al., 2011; Vadivel et al., 2018). In this study, a *PtCHS* gene was cloned from trifoliate orange, with a full length of 1156 bp, encoding 391 amino acids. This gene was highly homologous to *CHS* of other plants with 92.49%, showing a high degree of conservative property and further indicating that this gene is stable, consistent with earlier results (Pang et al., 2005; Wang et al., 2017).

Earlier studies showed that most of the *CHS* genes were located in the cytoplasm at the sub-cellular level (Wang et al., 2017; Vadivel et al., 2018). This study also predicted that PtCHS protein may be located in chloroplasts, cytoplasm, and nucleus, indicating that CHS protein widely presents in cell organelles. In addition, *PtCHS* gene expression was highest in stem, followed by flower and leaf, and very low in root and seed, indicating that *PtCHS* expression is tissue-specific. Pang et al. (2005) also found

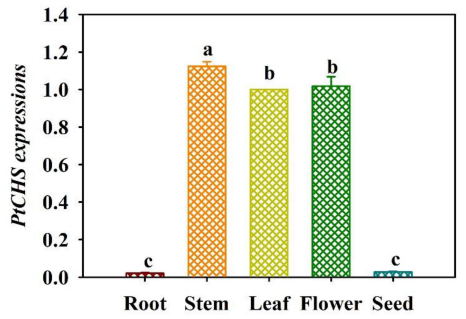

FIGURE 4
Tissue-specific expressions of *PtCHS* in trifoliate orange. Data (means ± SD, n = 4) followed by different letters above the bars indicate significant (P < 0.05) differences.

It has been shown that expression of *CHS* genes could be induced by external environments (Koes et al., 1994; Cushnie and Lamb, 2011; Singh and Kumaria, 2020). In the present study, SWD treatment increased the expression of *PtCHS* in leaves of non-mycorrhizal plants. Ahmed et al. (2021) also reported the up-regulated expression of *CHS* in leaves of poplar after SWD, and the up-regulated magnitude of the gene was increased with the extension of SWD. In addition, our study also indicated that *F. mosseae* inoculation increased expressions of *PtCHS* and CHS activity in leaves and roots regardless of soil water regimes. Moreover, the up-regulated magnitude of *PtCHS* by mycorrhization was higher under WW than under SWD, which may be due to the inhibition of root fungal colonization in SWD (Ding et al., 2022), thus reducing the efficiency of mycorrhizal fungi. Meanwhile, *PtCHS* expressions were

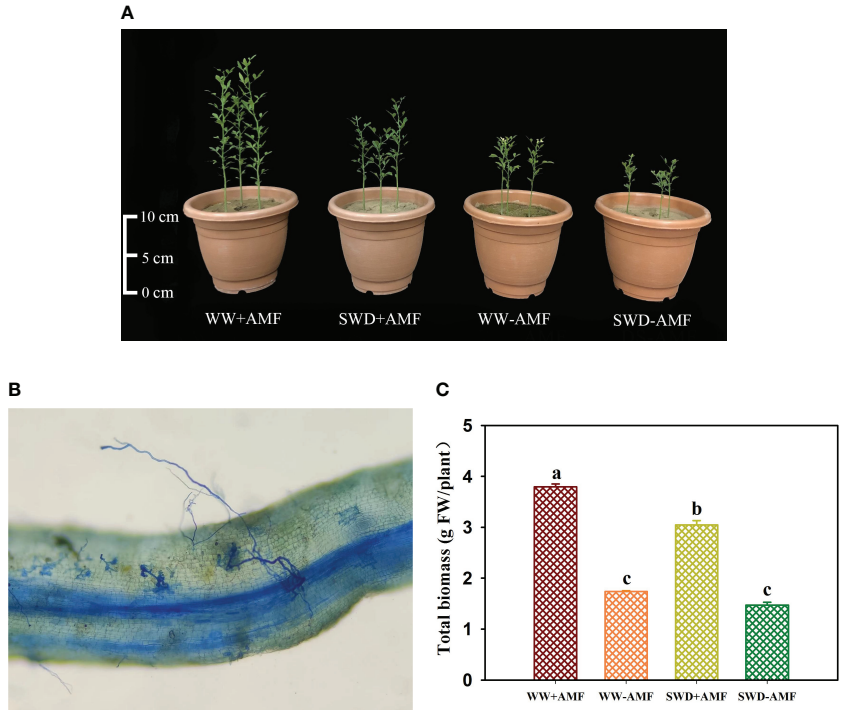

FIGURE 5
Changes in plant growth performance **(A)**, root mycorrhizal colonization **(B)**, and total biomass **(C)** of trifoliate orange in response to soil water deficit and *Funneliformis mosseae* inoculation. Abbreviations: WW+AMF, plants inoculated with *F mosseae* under well-watered; WW-AMF, plants inoculated without *F mosseae* under well-watered; SWD+AMF, plants inoculated with *F mosseae* under soil water deficit; SWD-AMF, plants inoculated without *F mosseae* under soil water deficit. Data (means ± SD, n = 4) followed by different letters above the bars indicate significant (P < 0.05) differences between treatments.

CHS expression in stem and leaf of ginkgo, and no expression was detected in roots. In addition, *CHS* expressions in plants vary in developmental periods: in early stages of plants, *CHS* expressions appear in leaves, whereas in mature plants *CHS* gene is mainly expressed in flowers, indicating that *CHS* expression in plants is mainly in aboveground parts (Knogge et al., 1986).

significantly positively correlated with leaf total flavonoid content. Wang et al. (2010) also found a significantly positive correlation between *CHS* and total flavonoid concentration in fruits of Guoqing No. 4 satsuma mandarin. In tomato, Aseel et al. (2019) reported the increase in total flavonoids in leaves after AMF inoculation and/or infection with *Tomato Mosaic*

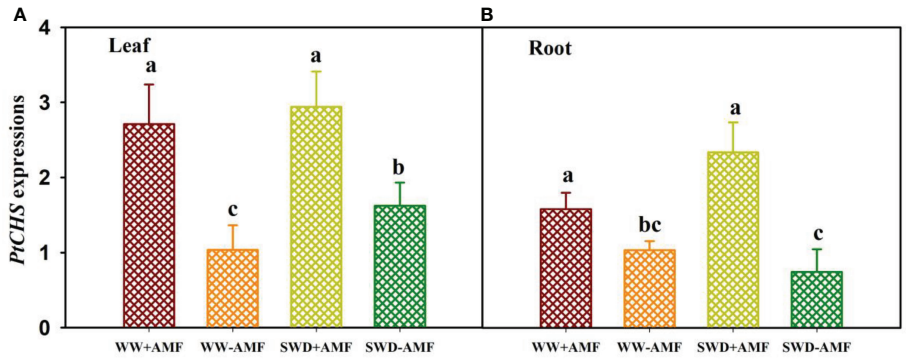

FIGURE 6
PtCHS gene expressions in leaf **(A)** and root **(B)** of trifoliate orange seedlings in response to soil water deficit and *Funneliformis mosseae* inoculation. Data (means ± SD, n = 4) followed by different letters above the bars indicate significant (P < 0.05) differences between treatments. See Figure 5 for the abbreviations.

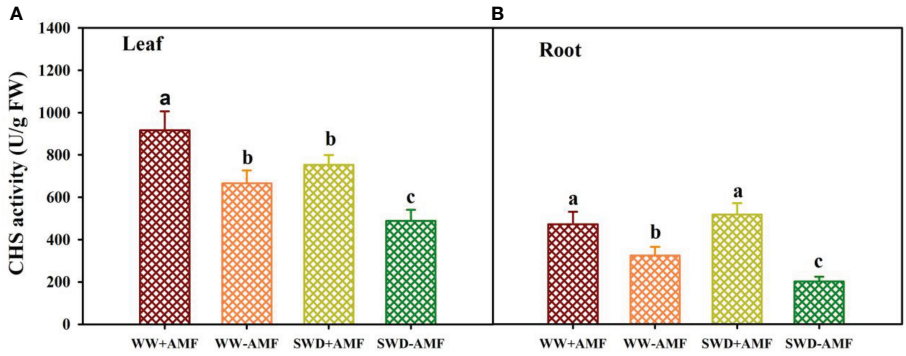

FIGURE 7
CHS activity in leaf **(A)** and root **(B)** of trifoliate orange seedlings in response to soil water deficit and *Funneliformis mosseae* inoculation. Data (means ± SD, n = 4) followed by different letters above the bars indicate significant (P < 0.05) differences between treatments. See Figure 5 for the abbreviations.

Virus. They also found that inoculation with AMF decreased the expression of *CHS*, but *Tomato Mosaic Virus* infection did not change *CHS* expression, along with induced expression of *CHS* after double inoculation of AMF and *Tomato Mosaic Virus*.

The present study also observed that SWD did not alter leaf and root total flavonoid content of non-AMF-treated plants, while it significantly reduced leaf and root total flavonoid content of AMF-treated plants. Earlier studies on alfalfa also showed that total flavonoids increased first and then decreased with the increase of PEG concentration (Li et al., 2020). In the Chuanqiao 1 variety of Tartary buckwheat, total flavonoids in leaves and grains were not changed after 7 days of drought stress, but leaf total flavonoids were decreased after 14 days of drought (Ouyang et al., 2020). This indicated that the variation of total flavonoids under SWD was affected by stress intensity, stress time, plant variety, and AMF. It is necessary to further use the targeted metabolome to determine which flavonoids in the total flavonoids can be responded to SWD in trifoliate orange. In addition, total flavonoid content was reduced in AMF-inoculated plants under SWD versus WW conditions, which may be because plants consume certain flavonoids to maintain mycorrhizal activity under SWD (Tian et al., 2021). A significantly positive correlation (r = 0.95, P < 0.01) was found between root mycorrhizal colonization and root total flavonoid content, suggesting the important role of flavonoids in mycorrhizae.

In our study, mycorrhiza-inoculated plants recorded dramatically higher total flavonoid content than mycorrhiza-uninoculated plants under both WW and SWD conditions. Similar result was observed in *Pistacia vera* inoculated with

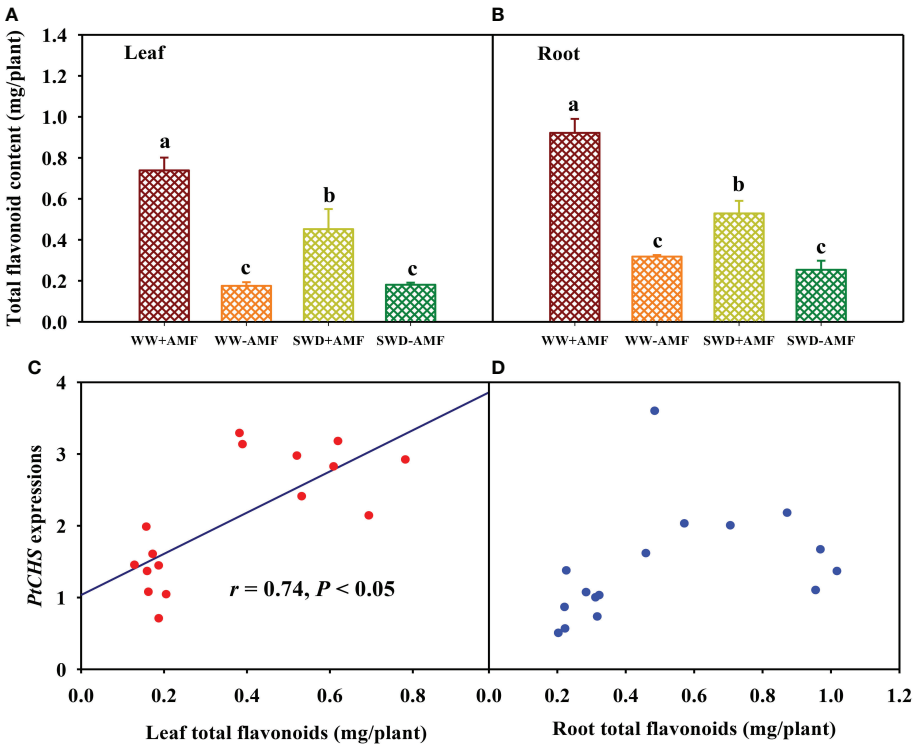

FIGURE 8
Changes in total flavonoid content in leaf **(A)** and root **(B)** of trifoliate orange in response to soil water deficit and *Funneliformis mosseae* inoculation and their correlation with *PtCHS* expressions in leaf **(C)** and root **(D)**. Data (means ± SD, n = 4) followed by different letters above the bars indicate significant (P < 0.05) differences between treatments. See Figure 5 for the abbreviations.

Glomus etunicatum and *Nicotiana tabacum* colonized by *G. versiforme* under SWD (Abbaspour et al., 2012; Begum et al., 2019). Higher total flavonoids in mycorrhizal versus non-mycorrhizal plants suggested that mycorrhizal plants under SWD have greater capacity to remove reactive oxygen species than non-mycorrhizal plants (Liu et al., 2022). Nevertheless, Amiri et al. (2017) reported a significant increase in total flavonoid levels in leaves of *Pelargonium graveolens* by *F. mosseae* under WW, but not SWD. On the other hand, the present study also showed a significantly positive correlation between total flavonoid content and *PtCHS* expression only in leaves, but not in roots, suggesting that there may be different mechanisms for mycorrhiza-induced changes in total flavonoids between leaves and roots. In addition, the up-regulated magnitude of root *PtCHS* expression levels triggered by AMF inoculation was higher under SWD conditions than under WW conditions, while the elevated magnitude of total flavonoid content in roots caused by AMF inoculation was higher under WW conditions than under SWD conditions. Therefore, *CHS* was not the most critical factor for mycorrhizal enhancement of total flavonoids under SWD conditions. Of course, the production of flavonoids depends on a number of enzymes in biological pathways of flavonoids, such as phenylalanine ammonia-lyase, 4-coumarate CoA ligase, and chalcone synthase, besides CHS (Ma et al., 2014). In wheat, *CHS* and *CHI* can be jointly regulated in response to SWD (Ma et al., 2014). Therefore, responsive patterns of more flavonoid biosynthesis genes need to be analyzed under SWD and mycorrhization conditions. It is concluded that AMF up-regulates the expression of *CHS* in the host, especially under abiotic and biotic stress conditions, thus showing the important characteristics of mycorrhizal tolerance to stress.

Conclusions

In this study, a *CHS* gene, named *PtCHS*, was cloned from the genome-wide of trifoliate orange, with 92.49% homology with other species. This gene had tissue-specific expression, along with high expression in aboveground parts such as leaf, flower, and stems. *PtCHS* was regulated by SWD and AMF inoculation, where *F. mosseae* up-regulated *PtCHS* expressions in leaves and roots, independent on soil water status, providing the support for total flavonoid production in plants, especially leaves. However, more work is needed around which flavonoid components are modulated by mycorrhizal fungi and which flavonoid synthesis genes are affected by SWD and mycorrhization.

Data availability statement

The original contributions presented in the study are included in the article/supplementary material. Further inquiries can be directed to the corresponding author.

Author contributions

Conceptualization, Q-SW and Y-NZ; data curation, ZL, SC, and X-QL; methodology, SC; resources, Q-SW; supervision, Q-SW and Y-NZ; writing—original draft, ZL; writing—review and editing, AH, A-BA-A, KK, KA, EA, Y-NZ, and Q-SW. All authors have read and agreed to the published version of the manuscript.

Funding

The authors would like to extend their sincere appreciation to the Researchers Supporting Project Number (RSP-2021/134), King Saud University, Riyadh, Saudi Arabia.

Acknowledgments

The authors would like to extend their sincere appreciation to the Researchers Supporting Project Number (RSP-2021/134), King Saud University, Riyadh, Saudi Arabia.

Conflict of interest

The authors declare that the research was conducted in the absence of any commercial or financial relationships that could be construed as a potential conflict of interest.

Publisher's note

All claims expressed in this article are solely those of the authors and do not necessarily represent those of their affiliated organizations, or those of the publisher, the editors and the reviewers. Any product that may be evaluated in this article, or claim that may be made by its manufacturer, is not guaranteed or endorsed by the publisher.

References

Abbaspour, H., Saeidi-Sar, S., Afshari, H., and Abdel-Wahhab, A. M. (2012). Tolerance of mycorrhiza infected pistachio (*Pistacia vera* l.) seedlings to drought stress under greenhouse conditions. *J. Plant Physiol.* 169, 704–709. doi: 10.1016/j.jplph.2012.01.014

Ahmed, U., Rao, M. J., Qi, C., Xie, Q., Noushahi, H. A., Yaseen, M., et al. (2021). Expression profiling of flavonoid biosynthesis genes and secondary metabolites accumulation in populus under drought stress. *Molecules* 26, 5546. doi: 10.3390/molecules26185546

Amiri, R., Nikbakht, A., Rahimmalek, M., and Hosseini, H. (2017). Variation in the essential oil composition, antioxidant capacity, and physiological characteristics of *Pelargonium graveolens* l. inoculated with two species of mycorrhizal fungi under water deficit conditions. *J. Plant Growth Regul.* 36, 502–515. doi: 10.1007/s00344-016-9659-1

Aseel, D. G., Rashad, Y. M., and Hammad, S. M. (2019). Arbuscular mycorrhizal fungi trigger transcriptional expression of flavonoid and chlorogenic acid biosynthetic pathways genes in tomato against *Tomato mosaic virus*. *Sci. Rep.* 9, 9692. doi: 10.1038/s41598-019-46281-x

Begum, N., Ahanger, M. A., Su, Y., Lei, Y., Mustafa, N. S. A., Ahmad, P., et al. (2019). Improved drought tolerance by AMF inoculation in maize (*Zea mays*) involves physiological and biochemical implications. *Plants* 8, 579. doi: 10.3390/plants8120579

Cheng, H. Q., Giri, B., Wu, Q. S., Zou, Y. N., and Kuča, K. (2022). Arbuscular mycorrhizal fungi mitigate drought stress in citrus by modulating root microenvironment. *Arch. Agron. Soil Sci.* 68, 1217–1228. doi: 10.1080/03650340.2021.1878497

Chen, S., Pan, X. H., and Li, Y. T. (2017). Identification and characterization of chalcone synthase gene family members in *Nicotiana tabacum*. *J. Plant Growth Regul.* 36, 374–384. doi: 10.1007/s00344-016-9646-6

Cushnie, T. P. T., and Lamb, A. J. (2011). Recent advances in understanding the antibacterial properties of flavonoids. *Int. J. Antimicrobe. Ag.* 38, 99–107. doi: 10.1016/j.ijantimicag.2011.02.014

Dao, T. T. H., Linthorst, H. J. M., and Verpoorte, R. (2011). Chalcone synthase and its functions in plant resistance. *Phytochem. Rev.* 10, 397–412. doi: 10.1007/s11101-011-9211-7

Dias, M. C., Pinto, D. C., and Silva, A. M. (2021). Plant flavonoids: Chemical characteristics and biological activity. *Molecules* 26, 5377. doi: 10.3390/molecules26175377

Ding, Y. E., Zou, Y. N., Wu, Q. S., and Kuča, K. (2022). Mycorrhizal fungi regulate daily rhythm of circadian clock in trifoliate orange under drought stress. *Tree Physiol.* 42, 616–628. doi: 10.1093/treephys/tpab132

Dixon, R. A., and Paiva, N. L. (1995). Stress-induced phenylpropanoid metabolism. *Plant Cell* 7, 1085. doi: 10.1105/tpc.7.7.1085

Ferreyra, M. L. F., Rius, S. P., and Casati, P. (2012). Flavonoids: biosynthesis, biological functions, and biotechnological applications. *Front. Plant Sci.* 3. doi: 10.3389/fpls.2012.00222

Flamini, R., Mattivi, F., De, Rosso, M. D., Arapitsas, P., and Bavaresco, L. (2013). Advanced knowledge of three important classes of grape phenolics: anthocyanins, stilbenes and flavonols. *Int. J. Mol. Sci.* 14, 19651–19669. doi: 10.3390/ijms141019651

Gabriele, M., Frassinetti, S., Caltavuturo, L., Montero, L., Dinelli, G., Longo, V., et al. (2017). Citrus bergamia powder: Antioxidant, antimicrobial and anti-inflammatory properties. *J. Funct. Foods* 31, 255–265. doi: 10.1016/j.jff.2017.02.007

Gao, Z., Gao, W., Zeng, S. L., Li, P., and Liu, E. H. (2018). Chemical structures, bioactivities and molecular mechanisms of citrus polymethoxyflavones. *J. Funct. Foods* 40, 498–509. doi: 10.1016/j.jff.2017.11.036

Ghasemi, K., Ghasemi, Y., and Ebrahimzadeh, M. A. (2009). Antioxidant activity, phenol and flavonoid contents of 13 citrus species peels and tissues. *Pak. J. Pharm. Sci.* 22, 277–281.

Gläßgen, W. E., Rose, A., Madlung, J., Koch, W., Gleitz, J., and Seitz, H. U. (1998). Regulation of enzymes involved in anthocyanin biosynthesis in carrot cell cultures in response to treatment with ultraviolet light and fungal elicitors. *Planta* 204, 490–498. doi: 10.1007/s004250050283

Hahlbrock, K., and Kreuzaler, F. (1972). Demonstration of two, up to now, hypothetic enzymes of flavonylglycoside biosynthesis as based on their regulation in plant cell suspension culture. *Hoppe–Seylers Z. Physiol. Chem.* 353, 1522.

Han, Y., Cao, Y., Jiang, H., and Ding, T. (2017). Genome-wide dissection of the chalcone synthase gene family in *Oryza sativa*. *Mol. Breed.* 37, 119. doi: 10.1007/s11032-017-0721-x

Han, Y. H., Ding, T., Su, B., and Jiang, H. Y. (2016). Genome-wide identification, characterization and expression analysis of the chalcone synthase family in maize. *Int. J. Mol. Sci.* 17, 161. doi: 10.3390/ijms17020161

He, J. D., Li, J. L., and Wu, Q. S. (2019). Effects of *Rhizoglomus intraradices* on plant growth and root endogenous hormones of trifoliate orange under salt stress. *J. Anim. Plant Sci.* 29, 245–250.

Hu, B., Yao, H., Gao, Y. L., Wang, R., Li, F., Guo, J. G., et al. (2019). Overexpression of chalcone synthase gene improves flavonoid accumulation and drought tolerance in tobacco. *Res. Sq.* 2019, 1–11. doi: 10.21203/rs.2.18297/v2

Knogge, W., Schmelzer, E., and Weissenböck, G. (1986). The role of chalcone synthase in the regulation of flavonoid biosynthesis in developing oat primary leaves. *Arch. Biochem. Biophysiol.* 250, 364–372. doi: 10.1016/0003-9861(86)90738-1

Koes, R. E., Quattrocchio, F., and Mol, J. N. (1994). The flavonoid biosynthetic pathway in plants: Function and evolution. *BioEssays* 16. doi: 10.3389/fpls.2020.00007

Kunert, K. J., Vorster, B. J., Fenta, B. A., Kibido, T., Dionisio, G., and Foyer, C. H. (2016). Drought stress responses in soybean roots and nodules. *Front. Plant Sci.* 7. doi: 10.3389/fpls.2016.01015

Li, D. D., Liang, Z. S., and Pu, B. (2020). Flavonoids contents and flavonoids synthetic key enzyme activities in alfalfa under drought stress. *Acta Bot. Boreali–Occidentalia. Sin.* 40, 1380–1388. doi: 10.7606/j.issn.1000-4025.2020.08.1380

Liu, X. Q., Cheng, S., Aroca, R., Zou, Y. N., and Wu, Q. S. (2022). Arbuscular mycorrhizal fungi induce flavonoid synthesis for mitigating oxidative damage of trifoliate orange under water stress. *Environ. Exp. Bot.* 204, 105089. doi: 10.1016/j.envexpbot.2022.105089

Liu, Y. L., Lou, Q., Xu, W. R., Xin, Y., Bassett, C., and Wang, Y. J. (2011). Characterization of a chalcone synthase (CHS) flower-specific promoter from *Lilium orential* 'Sorbonne'. *Plant Cell Rep.* 30, 2187–2194. doi: 10.1007/s00299-011-1124-9

Mahato, N., Sharma, K., Sinha, M., and Cho, M. H. (2018). Citrus waste derived nutra-/pharmaceuticals for health benefits: Current trends and future perspectives. *J. Funct. Foods.* 40, 307–316. doi: 10.1016/j.jff.2017.11.015

Ma, D. Y., Sun, D. X., Wang, C. Y., Li, Y. G., and Guo, T. C. (2014). Expression of flavonoid biosynthesis genes and accumulation of flavonoid in wheat leaves in response to drought stress. *Plant Physiol. Biochem.* 80, 60–66. doi: 10.1016/j.plaphy

Nakabayashi, R., Yonekura-Sakakibara, K., Urano, K., Suzuki, M., Yamada, Y., Nishizawa, T., et al. (2014). Enhancement of oxidative and drought tolerance in arabidopsis by overaccumulation of antioxidant flavonoids. *Plant J.* 77, 367–379. doi: 10.1111/tpj.12388

Ouyang, J. Y., Wan, Y., Xiang, D. B., Ma, C. R., Liu, M., Qin, M. L., et al. (2020). Effects of drought stress on agronomic traits and flavonoid compound contents of tartary buckwheat. *J. Anhui Agric. Sci.* 48 (16), 35–38. doi: 10.3969/j.issn.0517-6611.2020.16.008

Pang, Y. Z., Shen, G. A., Wu, W. S., Liu, X. F., Lin, J. A., Tan, F., et al. (2005). Characterization and expression of chalcone synthase gene from *Ginkgo biloba*. *Plant Sci.* 168, 1525–1531. doi: 10.1016/j.plantsci.2005.02.003

Phillips, J. M., and Hayman, D. S. (1970). Improved procedures for clearing roots and staining parasitic and vesicular-arbuscular mycorrhizal fungi for rapid assessment of infection. *Trans. Br. Mycol. Soc* 55, 158–161. doi: 10.1016/s0007-1536(70)80110-3

Sepiol, C. J., Yu, J., and Dhaubhadel, S. (2017). Genome-wide identification of chalcone reductase gene family in soybean: Insight into root-specific *GmCHRs* and *Phytophthora sojae* resistance. *Front. Plant Sci.* 8. doi: 10.3389/fpls.2017.02073

Sharma, K., Mahato, N., and Lee, Y. R. (2019). Extraction, characterization and biological activity of citrus flavonoids. *Rev. Chem. Eng.* 35, 265–284. doi: 10.1515/revce-2017-0027

Shen, N., Wang, T., Gan, Q., Liu, S., Wang, L., and Jin, B. (2022). Plant flavonoids: Classification, distribution, biosynthesis, and antioxidant activity. *Food Chem.* 383, 132531. doi: 10.1016/j.foodchem.2022.132531

Singh, N., and Kumaria, S. (2020). Molecular cloning and characterization of chalcone synthase gene from *Coelogyne ovalis* lindl. and its stress-dependent expression. *Gene* 762, 145104. doi: 10.1016/j.gene.2020.145104

Song, M. Y., Wu, X., Charoensinphon, N., Wang, M., Zheng, J. K., Gao, Z., et al. (2017). Dietary 5-demethylnobiletin inhibits cigarette carcinogen NNK-induced lung tumorigenesis in mice. *Food Funct.* 8, 954–963. doi: 10.1039/c6fo01367h

Tian, B., Pei, Y., Huang, W., Ding, J., and Siemann, E. (2021). Increasing flavonoid concentrations in root exudates enhance associations between arbuscular mycorrhizal fungi and an invasive plant. *ISME J.* 15, 1919–1930. doi: 10.1038/s41396-021-00894-1

Tripoli, E., La, G. M., Giammanco, S., Mijo, D. D., and Giammanco, M. (2007). Citrus flavonoids: Molecular structure, biological activity and nutritional properties: A review. *Food Chem.* 104, 466–479. doi: 10.1016/j.foodchem.2006.11.054

Vadivel, A. K. A., Krysiak, K., Tian, G., and Dhaubhadel, S. (2018). Genome-wide identification and localization of chalcone synthase family in soybean (*Glycine max* [L] merr). *BMC Plant Biol.* 18, 325. doi: 10.1186/s12870-018-1569-x

Wang, Y., Li, J., and Xia, R. X. (2010). Expression of chalcone synthase and chalcone isomerase genes and accumulation of corresponding flavonoids during fruit maturation of guoqing no. 4 satsuma mandarin (*Citrus unshiu marcow*). *Sci. Hortic.* 125, 110–116. doi: 10.1016/j.scienta.2010.02.001

Wang, Z. B., Yu, Q. B., Shen, W. X., Mohtar, C. A. E., Zhao, X. Z., and Gmitter, ,. F. G.Jr (2018). Functional study of *CHS* gene family members in citrus revealed a novel *CHS* gene affecting the production of flavonoids. *BMC Plant Biol.* 18, 189. doi: 10.1186/s12870-018-1418-y

Wang, C. H., Zhi, S., Liu, C. Y., Xu, F. X., Zhao, A., Wang, X. L., et al. (2017). Isolation and characterization of a novel chalcone synthase gene family from mulberry. *Plant Physiol. Bioch.* 115, 107–118. doi: 10.1016/j.plaphy.2017.03.014

Wu, Q. S., Srivastava, A. K., and Zou, Y. N. (2013). AMF-induced tolerance to drought stress in citrus. *Sci. Hortic.* 164, 77–87. doi: 10.1016/j.scienta.2013.09.010

Wu, Q. S., Zou, Y. N., Liu, W., Ye, X. F., Zai, H. F., and Zhao, L. J. (2010). Alleviation of salt stress in citrus seedlings inoculated with mycorrhiza: Changes in leaf antioxidant defense systems. *Plant Soil Environ.* 56, 470–475. doi: 10.1016/j.jplph.2013.06.006

Yahyaa, M., Ali, S., Rikanati, R. D., Ibdah, M., Shachtier, A., Eyal, Y., et al. (2017). Characterization of three chalcone synthase-like genes from apple (*Malus* x *domestica borkh.*). *Phytochemistry* 140, 125–133. doi: 10.1016/j.phytochem.2017.04.022

Yin, Y. C., Hou, J. M., Tian, S. K., Yang, L., Zhang, Z. X., Li, W. D., et al. (2020). Overexpressing chalcone synthase (CHS) gene enhanced flavonoids accumulation in *Glycyrrhiza uralensis* hairy roots. *Bot. Lett.* 167, 219–231. doi: 10.1080/23818107.2019.1702896

Yonekura, S. K., Higashi, Y., and Nakabayashi, R. (2019). The origin and evolution of plant flavonoid metabolism. *Front. Plant Sci.* 10. doi: 10.3389/fpls.2019.00943

Zhang, F., Zou, Y. N., Wu, Q. S., and Kuča, K. (2020). Arbuscular mycorrhizas modulate root polyamine metabolism to enhance drought tolerance of trifoliate orange. *Environ. Exp. Bot.* 171, 103962. doi: 10.1016/j.envexpbot.2019.103926

Zou, Y. N., Wang, P., Liu, C. Y., Ni, Q. D., Zhang, D. J., and Wu, Q. S. (2017). Mycorrhizal trifoliate orange has greater root adaptation of morphology and phytohormones in response to drought stress. *Sci. Rep.* 7, 41134. doi: 10.1038/srep41134

frontiers | Frontiers in Plant Science

TYPE Original Research
PUBLISHED 04 January 2023
DOI 10.3389/fpls.2022.1106219

OPEN ACCESS

EDITED BY
Chao Li,
Northwest A&F University, China

REVIEWED BY
Junhong Zhang,
Zhejiang Agriculture and Forestry University, China
Mengxia Zhang,
Cornell University, United States

*CORRESPONDENCE
Chunlong Li
cl2444@mail.hzau.edu.cn

SPECIALTY SECTION
This article was submitted to Plant Abiotic Stress, a section of the journal Frontiers in Plant Science

RECEIVED 23 November 2022
ACCEPTED 12 December 2022
PUBLISHED 04 January 2023

CITATION
Xu W, Liu Z, Zhao Z, Zhang S, Li M, Guo D, Liu J-H and Li C (2023) The functional analysis of sugar transporter proteins in sugar accumulation and pollen tube growth in pummelo (*Citrus grandis*). *Front. Plant Sci.* 13:1106219. doi: 10.3389/fpls.2022.1106219

The functional analysis of sugar transporter proteins in sugar accumulation and pollen tube growth in pummelo (*Citrus grandis*)

Weiwei Xu[1], Ziyan Liu[1], Zeqi Zhao[1], Shuhang Zhang[1], Mengdi Li[1], Dayong Guo[1], Ji-Hong Liu[1] and Chunlong Li[1,2]*

[1]Key Laboratory of Horticultural Plant Biology Ministry of Education (MOE), College of Horticulture and Forestry Science, Huazhong Agricultural University, Wuhan, China, [2]Hubei Hongshan Laboratory, Wuhan, China

Sugar transporter proteins (STPs) play vital roles in sugar transport and allocation of carbon sources in plants. However, the evolutionary dynamics of this important gene family and their functions are still largely unknown in citrus, which is the largest fruit crop in the world. In this study, fourteen non–redundant CgSTP family members were identified in pummelo (*Citrus grandis*). A comprehensive analysis based on the biochemical characteristics, the chromosomal location, the exon–intron structures and the evolutionary relationships demonstrated the conservation and the divergence of CgSTPs. Moreover, CgSTP4, 11, 13, 14 were proofed to be localized in plasma membrane and have glucose transport activity in yeast. The hexose content were significantly increased with the transient overexpression of *CgSTP11* and *CgSTP14*. In addition, antisense repression of *CgSTP4* induced the shorter pollen tube length *in vitro*, implying the potential role of CgSTP4 in pummelo pollen tube growth. Taken together, this work explored a framework for understanding the physiological role of *CgSTPs* and laid a foundation for future functional studies of these members in citrus species.

KEYWORDS

***Citrus grandis*, sugar transporter protein, gene expression, sugar accumulation, pollen tube growth**

Introduction

Soluble sugars such as sucrose, glucose and fructose are the main carbohydrates from photosynthesis of most plants (Rolland et al., 2002). These sugars are the key components of carbon and energy metabolism in plants, providing the skeleton for large molecules such as proteins and nucleic acids (Smeekens and Hellmann, 2014). Besides, sugars can

be used as signal transduction molecules regulating various metabolic pathways, biotic and abiotic stress responses, plant growth and development, and regulating the osmotic pressure of plant cells and solutions, thus affecting stomatal opening and closing and other activities (Rolland et al., 2002; Koch, 2004; Rolland et al., 2006; Radchuk et al., 2010; Smeekens and Hellmann, 2014; Huai et al., 2022). In plants, sugars need to pass through membrane several times on its way from the source cells to the sink organs. The cross boundary membrane uptake of sugars is a major event for nutrition in all eukaryotic cells (Tao et al., 2015). The carrier proteins mediating the transmembrane transport of sugars are called sugar transporters. Currently, the vast majority of identified sugar transporters belong to the major facilitator superfamily (MFS), which is usually composed of 12 transmembrane domains known as H^+/sugar or Na^+/sugar cotransporters (Yan, 2013). According to the different transport substrates, the MFS in plants is mainly divided into disaccharide transporter and monosaccharide transporters (MSTs). Among them, the main disaccharide transporter is sucrose transporters (SUTs) (Chiou and Bush, 1996), also known as sucrose carriers (SUCs), which mediate the transport of sucrose and maltose (Riesmeier et al., 1994; Kuhn and Grof, 2010). The MSTs are composed of a large gene family, which contain seven subfamilies named sugar transporters (STPs) (also known as Hexose transporters, HTs), tonoplast monosaccharide transporters (TMTs), vacuolar glucose transporters (VGTs), plastid glucose transporters (pGlcTs), early response to drought 6-like transporters (ERD6Ls), polyol/monosaccharide transporters (PMTs) and insitol transporters (INTs) (Buttner, 2007; Li et al., 2015a; Fang et al., 2020; Liu et al., 2020). In addition, there is a new class of sugar transporter, which is named as the Sugars Will Eventually be Exported Transporters (SWEETs) (Chen et al., 2010). SWEETs belong to the MtN3-Like membrane protein and have a completely different structure from the MFS sugar transporters (Gautam et al., 2022). These sugar transporters mentioned above have been reported localized in various subcellular locations such as plasma membrane, vacuolar membrane, golgi apparatus membrane, and plastid membrane (Jiu et al., 2018; Fang et al., 2020; Li et al., 2020). The diversity subcellular localization patterns confers a variety of functions for sugar transport proteins. At present, the family of sugar transporters located on the plasma membrane and vacuolar membrane are more studied.

Among the numerous sugar transporter families, the *STPs* are the most studied monosaccharides transporters, indicating the vital role of STPs in plant development or stress response. STPs are complete membrane proteins with 12 transmembrane domains and are considered to be H^+/sugar transporters located on the plasma membrane. So far, the *STPs* have been identified and studied in many plants, including *Arabidopsis thaliana* (Buttner, 2010), *Manihot esculenta* (Liu et al., 2018), *Brassica oleracea* var. *capitata L.* (Zhang et al., 2019), *Oryza sativa* (Toyofuku et al., 2000; Deng et al., 2019), *Solanum lycopersicum* (Reuscher et al., 2014), *Vitis vinifera* (Afoufa-Bastien et al., 2010), *Fragaria vesca* (Jiu et al., 2018; Liu et al., 2020), *Pyrus bretschneideri Rehd* (Li et al., 2015a), *Malus domestica* (Wei et al., 2014), *Dimocarpus longan Lour* (Fang et al., 2020). Based on previous reports, *STP* members are expressed in different tissues and participate in various metabolic pathways for specific physiological functions. The expression of *STPs* are also response to hormones, biotic and abiotic stresses, which further significantly affect plant development and stress resistance (Truernit et al., 1996; Buttner et al., 2000; Sade et al., 2013; Murcia et al., 2016; Murcia et al., 2018; Deng et al., 2019; Otori et al., 2019; Paulsen et al., 2019). A total of 14 AtSTPs have been reported in *A. thaliana* (Buttner, 2010), all of which are localized at the plasma membrane and are responsible for the transport of monosaccharides from the apoplastic space to the cytosol. For example, AtSTP1 is capable of transporting other hexose in addition to fructose, and is involved in the transport of monosaccharides in guard cells (Stadler et al., 2003). AtSTP2 is primarily responsible for absorbing glucose produced by callose degradation during the early stages of pollen maturation (Truernit et al., 1999). AtSTP4, AtSTP6, AtSTP8, AtSTP9, AtSTP10 and AtSTP11 are mainly responsible for the uptake of glucose into the pollen tube of *A. thaliana* and play a role in the supply of monosaccharides during the growth of the pollen tube (Rottmann et al., 2018). Heterologous expression of the apple hexose transporter gene *MdHT2.2* in tomato promotes sucrose, fructose, and glucose accumulation (Wang et al., 2020b) in response to tomato salt tolerance mechanism by balancing cytoplasmic to intercellular ion concentrations and scavenging reactive oxygen species (ROS) (Wang et al., 2020a). In wheat, *TaSTP3* is transcriptionally activated by the transcription factor TaWRKY19/61/82 during stripe rust, thereby increasing the sucrose concentration of host cells to guarantee carbon source supply for the fungus (Huai et al., 2022). In apple, MdSTP13a is found to absorb hexose and sucrose simultaneously in the process of sorbitol regulating pollen tube growth to promote the growth of apple pollen tubes (Li et al., 2020). These findings highlight the importance of STPs in plant growth, development, and stress tolerance *via* sugar transport and carbon source allocation.

The citrus is the largest fruit industry over the world. Studies have shown that the genus citrus originated from three ancestral species: *Citrus maxima*, *Citrus medica*, and *Citrus reticulate* (Wu et al., 2018). It has been suggested that domestication of citrus may have begun with the identification and asexual reproduction of selected, possibly hybrid or mixed individuals. For instance, the cultivation of pummelo (*Citrus grandis*) is cultivated from the ancestral *C. maxima* with the introgressions of the other citrus species (Xu et al., 2013; Wu et al., 2014). The

fruit quality of citrus is affected by flavor substances, which mainly include soluble sugars, organic acids and volatile compounds, among which the composition and content of soluble sugars is the key factor affecting taste and thus determining fruit flavor quality (Li et al., 2012; Aslam et al., 2019). There are also some reports to support that the relationship between sugar transporters and sugar accumulation in citrus (Zheng et al., 2014). For instance, the soluble sugar-related genes in 'Rongan' (RA) and its mutant 'Huapi' (HP) kumquat were analyzed, and it was found that high sugar accumulation in HP fruit was associated with up-regulation of *SUS*, *SPS*, *TST*, *STP* and *ERD6L* genes (Wei et al., 2021). In addition, artificial thinning can increase the size and sugar content of citrus fruits, affect hormone synthesis and sugar transporter activity, and significantly improve fruit quality (Liu et al., 2022a). However, these studies have only pointed out the potential role of sugar transporters in citrus, but the characteristics and functions of sugar transporters in citrus species are still confused so far.

In this study, the genes encoding *STPs* in *C. grandis* genome were identified. The phylogenetic relationships, characteristics, structure, conserved motifs, *cis*-acting elements and collinearity of CgSTP members were analyzed, revealing the conserved and correlation between homologous and near-homologous genes. Based on the expression pattern and subcellular localization assay, CgSTP4, CgSTP11, CgSTP13 and CgSTP14 were further selected and proofed to have the hexose sugar transport activity. In addition, the function of pollen-specific expression *CgSTP4* was explored to be involved in pummelo pollen tube growth *via* antisense oligonucleotide transformation. Taken together, we identified key candidate *CgSTP* genes in sugar accumulation, which will be a great scientific significance and potential application for further investigation of the physiological functions of *CgSTPs* in pummelo or other citrus species.

Materials and methods

Plant materials and growth conditions

The 'Shatian pummelo' (*Citrus grandis*) fruits, leaves, flowers and other tissues were harvested from the Centre of Citrus Plant at Huazhong Agricultural University (Wuhan, China). The pummelo trees were maintained under standard horticultural management and prevention of plant diseases and insect pests. At the popcorn stage, flowers were picked for anther collection, and the anthers were dried in a 28°C oven. The dried anthers and released pollen were collected into 1.5 or 2.0 ml centrifuge tubes sealed with silica gel and stored in -20°C refrigerator for further use. Tobacco plants (*Nicotiana benthamiana*) were grown in the growth chamber at 23-25°C with 12h light/12 h darkness.

Database searches and identification of STPs in *Citrus grandis*

In order to identify the *STP* genes in *C. grandis*, the whole-genome data of pummelo (Citrus grandis (L.) Osbeck.cv. 'Wanbaiyou' v1.0) was downloaded from the Citrus Pan-genome to Breeding Database website (http://citrus.hzau.edu.cn/index.php), which was used to obtain the gene sequences and gene annotations. The Hidden Markov Model (HMM) of the Sugar_tr domain (PF00083) from HMMER (https://www.ebi.ac.uk/Tools/hmmer/search/hmmscan) was used to search the pummelo protein database at a standard E-value < 1.0×10^{-5} (Finn et al., 2011; Chen et al., 2020; Mistry et al., 2021). A total of 53 hypothetical CgSTP proteins were identified. Furthermore, the conserved domain composition of 14 AtSTP protein sequences were analyzed by CD-search. Then, all the 53 putative protein sequences filtered to submit to the National Center for Biotechnology Information (NCBI, https://www.ncbi.nlm.nih.gov/Structure/bwrpsb/bwrpsb.cgi). Finally, 14 STP family members of *C. grandis* were screened out. They were named CgSTP1 to CgSTP14 based on their relationship with members of the STP family in *A. thaliana*.

Phylogenetic tree construction and synteny correlation analysis

To explore the evolutionary relationship of *CgSTPs* between *C. grandis* and *A. thaliana*, a phylogenetic tree was constructed by maximum likelihood (ML) method using MEGAX64 software based on the protein sequences of 14 CgSTPs from pummelo and 14 AtSTPs from *A. thaliana*. The final tree is then beautified through the ITOL website. Among them, the AtSTP protein sequences were downloaded from the The Arabidopsis Information Resource website (https://www.arabidopsis.org/). In order to better understand the conservation of *STP* genes in evolution, the collinear correlation analysis between species was carried through the MCScanX (Wang et al., 2012) of TBtools software by offering gene annotation and the whole genome sequence of *A. thaliana* and *C. grandis*.

Amino acid characteristic and gene structure prediction

The physicochemical properties of the proteins, which included amino acid number (AA), molecular weight (MW),

theoretical isoelectric point (PI), and grand average of hydropathy (GRAVY), were obtained in the ExpasyProtParam server (https://web.expasy.org/compute_pi/) (Wilkins et al., 1999). The number of transmembrane domains was predicted by the NovoPro url (https://www.novopro.cn/tools/tmhmm.html). The WoLF PSORT server (https://wolfpsort.hgc.jp/) was applied to predict protein subcellular localization. The gene structure annotation and CDS files of *C. grandis* were downloaded from the Citrus Pan-genome to Breeding Database website, and the *STP* genes information was extracted by TBtools using accession number, followed by the Gene Structure Display Server 2.0(http://gsds.gao-lab.org/)to visualize the exon–intron structure of these genes (Hu et al., 2015).

Protein motif and *cis*-acting elements analysis

To further explore the gene structure of *CgSTPs*, the MEME Suite web server (https://meme-suite.org/meme/tools/meme) (Bailey and Elkan, 1994; Bailey et al., 2009) was used to predict their protein sequences with a maximum number of motif groups of 12 for conserved motifs, any number of repeats, and an optimal width of the motif ranging from 15 to 60 amino acids. The promoter sequences (2 kb of genomic DNA sequence upstream of the translation initiation codon) of the *CgSTP* genes were obtained from *C. grandis* genome files and submitted to the PlantCARE database (http://bioinformatics.psb.ugent.be/webtools/plantcare/html/) to predict *cis*-elements in the promoter (Rombauts et al., 1999; Lescot et al., 2002).

RNA extraction, cDNA synthesis and quantitative real-time analysis

Each 0.2g pummelo tissues, including leaves, flowers and juice sac were snap frozen and ground into fine powder in liquid nitrogen with three independent repetitions. RNA from common tissues was extracted using the Ominplant RNA Kit (Cwbio. Jiangsu, China). And for polyphenol polysaccharide containing tissues, RNA was extracted using the RNAprep Pure Plant Plus Kit (TIANGEN, Wuhan, China) according to the instructions. The concentration and quality of the extracted RNA were confirmed *via* spectrophotometer and agar gel electrophoresis. Then the EasyScript One-Step gDNA Removal and cDNA Synthesis SuperMix (TransGen Biotech, Beijing, China) reverse transcribed RNA into cDNA. Finally, three technical replicates of qRT-PCR were performed using SYBR Green Supermix kit according to the manual *via* the Applied biosystem®QuantStudio™ 7 Flex Real-Time PCR System (ABI, Los Angeles, CA, USA), and $2^{-\Delta\Delta CT}$ method (Udvardi et al., 2008) was used to calculate and analyze the obtained data.

Subcellular localization of CgSTPs

The CDSs of the *CgSTP* genes were amplified using gene-specific primers without stop codons (Supplementary Table 1). The homologous recombination approach (Rozwadowski et al., 2008) was used to concatenate these target genes with the YFP101 vector, which contained a C-terminal yellow fluorescent protein (YFP) driven by 35S promoter. After the correct comparison between the sequencing results of Tsingke Biological Company (Wuhan, China) and the CDS of the genome through DNAMAN software, the recombinant plasmid was transferred into *Agrobacterium tumefaciens* GV3101 (Krenek et al., 2015) (Weidi, Wuhan, China). Then, *A. tumefaciens* containing the recombinant plasmid was injected into tobacco leaves for transient expression (Kato et al., 2002). Finally, the scanning confocal microscope (Leica TCS-SP8, Wetzlar, Germany) was used to image YFP fluorescence with an excitation wavelength of 514 nm and emission at 520-551 nm.

Functional characterization of *CgSTPs* by heterologous expression in yeast

The CDSs of the target gene were cloned with gene-specific primers containing stop codons (Supplementary Table 1). The yeast expression vector pDR196 was ligated with the gene of interest by homologous recombination, followed by transformation of the recombinant plasmids into the hexose transport deficient yeast strain *EBY.VW4000* by lithium acetate method (Soni et al., 1993). The empty vector pDR196 was used as negative control, and the recombinant vector pDR196-*AtSTP13* was served as a positive control (Riesmeier et al., 1992; Rottmann et al., 2016; Li et al., 2020). The transformed cells in *EBY.VW4000* were pre-incubated in liquid Synthesis Defect (SD)-Ura medium supplemented with 2% maltose (w/v) as the sole carbon source until the OD_{600} value reached 0.6-0.8 (Wieczorke et al., 1999). Four serial dilutions (10×) of yeast cells were then plated on solid SD-Ura medium containing 2% maltose or glucose as the sole carbon source. The samples were cultured at 30°C for 3 days and then observed and photographed.

Transient expression in tobacco leaves and sugars content analysis

The CDS(s) of *CgSTP* genes were cloned with gene-specific primers without termination codons (Supplementary Table 1) and inserted into the overexpression vector pK7WG2D with the 35S promoter (Pi et al., 2022). After that, the final recombinant plasmid was transformed into *Agrobacterium tumefaciens* GV3101, which was further used for injection of tobacco

leaves for transient overexpression. The control with empty vector and the recombinant plasmid carrying the target genes (*CgSTP(s)*-2D) were transformed into the same leaf, as control in the left and *CgSTP(s)*-2D in the right part of the leaf. Samples were taken on the third day after transformation. The relative gene expression level was determined by RT-PCR assay (the primers were listed in Supplementary Table 1). Then, the content of monosaccharides was measured by GC method as described previously (Liu et al., 2022b). Soluble sugars were extracted in 75% methanol with ribitol (0.12 mg per sample) added as an internal standard and then derivatized sequentially with methoxyamine hydrochloride and N-methyl-N-(trimethylsilyl) trifluoroacetamide (MSTFA). After derivatization, the metabolites were analyzed using a GC equipment (Fuli GC-9720 Pluse, Zhejiang, China) with a HP-FFAP column (30.00 m * 0.32 mm * 0.25 μm) and a 5 m Duraguard column (Agilent Technologies, Palo Alto, CA, USA). Sugar content was quantified based on standard curves generated for each sugar (glucose and fructose) and an internal standard. All results were determined at least three biological replicates.

In vitro pollen tube growth experiments and antisense oligonucleotide transfection

The pollen grains were cultured in liquid germination media (0.02%[w/v]$MgSO_4$, 0.01%[w/v]KNO_3, 0.03%[w/v]$Ca(NO_3)_2$, 0.01%[w/v]H_3B0_3, 15%[w/v]PEG-4000, 10%[w/v]Sucrose, and liquid NaOH to pH 6.0) (Liang et al., 2017) for pollen tube length assay. Only 1 μl of transfection agent (Biosharp, China) and 1 μl of transfection agent plus 1 μl of oligonucleotide primers (ODN concentration of 100 μM) were added as the control group, and 1 μl of transfection agent plus 1 μl of antisense oligonucleotide primers were added as the experimental group (Meng et al., 2014). Three independent experiments were performed for each treatment, and the same amount of pollen grains were added for germination culture at 25°C in a constant temperature and dark environment. At the 4 h, 6 h and 8 h of culture, the germinated pollen grains were observed and photographed by a type microscope, and then each biological replicate at least 100 germinated pollen grains were measured *via* image software. Supplementary Table 1 lists the oligonucleotide primer sequences used in this study. For gene expression assay, individual duplicate pollen tubes were collected into a 10 ml centrifuge tube and centrifuged under 12000g at 4°C for 10 min. The samples could be re-suspended once in pure water and centrifuged again to remove the supernatant under the same conditions, after that the samples were snap frozen in liquid nitrogen for RNA extraction and gene expression assay by qRT-PCR.

Result

Genome-wide identification and basic information analysis of *STP* family genes in *C. grandis*

Using the Hidden Markov Model (HMM) and the conserved domains of MSF_STP (cd17361) and Sugar_tr (pfam00083) in *STPs*, a total of 14 *STP* family members were screened in the *C. grandis* genome database *via* the HMMER and Batch CD-Search websites (Table 1; Figure 1 and Supplementary File 1). Following the distant genetic relationship with *Arabidopsis STP* family genes, the 14 pummelo *CgSTPs* were named as *CgSTP1* - *CgSTP14* (Table 1). Furthermore, the phylogenetic tree was constructed based on the protein sequences encoded by *CgSTP* genes in *C. grandis* and *AtSTP* genes in *A. thaliana via* MEGAX64 (Figure 1B). The results showed that the STP proteins could be classified into four groups (Figure 1B). Among them, tow CgSTPs (CgSTP7 and CgSTP14) together with two AtSTPs from *Arabidopsis* were attributed to Group I. Group II consisted of four CgSTPs (CgSTP2, CgSTP6, CgSTP8 and CgSTP13), and four AtSTPs. Four CgSTPs (CgSTP3, CgSTP5, CgSTP9 and CgSTP10) clustered with two AtSTPs in Group III. Group IV contained four CgSTPs (CgSTP1, CgSTP4, CgSTP11 and CgSTP12) and six AtSTPs. Furthermore, a total of two sister pairs of CgSTPs were observed in the phylogenetic tree, including CgSTP5 - CgSTP9 and CgSTP1- CgSTP12 (Figure 1B). The result indicated that the *STP* family members are closely related, which is also a good reference for renaming. Moreover, the position and evolutionary relationships of *CgSTP* members at the chromosomal level were visualized by TBtools based on the gene structure annotation file (Supplemental Figure 1). Interspecific co-linearity analysis of *STP* genes revealed that eight pairs of genes are orthologous in two species between *C. grandis* and *A. thaliana*, indicating that the STP family was widespread in higher plants and strongly conserved during the evolutionary process.

According to the genomic information of *C. grandis* chromosomes, the distribution of 14 *STP* genes on the chromosome was analyzed. It was found that all *CgSTP* members were unevenly distributed on seven chromosomes, with the most abundantly distributed 7 genes on chromosome 9 (Table 1 and Supplemental Figure 1). Protein sequence characteristics, including number of amino acids (AA), molecular weight (Mw), theoretical isoelectric point, grand average of hydropathicity (GRAVY), transmembrane domain (TMD) and subcellular localization prediction, were also analyzed. As shown in Table 1, the average STP protein length was 504 aa, with the longest 524 aa from CgSTP13 and the shortest 353 aa from CgSTP8. Accordingly, the molecular weight of these proteins ranged from 38.7 kDa (CgSTP8) to 57.9 kDa (CgSTP11). The theoretical isoelectric points ranged from 8.86

TABLE 1 The information of *CgSTP* genes.

Gene name	Accession number [1]	Chr [2]	AA [3]	Mw (Da) [4]	pl [5]	GRAVY [6]	TMD [7]	Prediction Location(s) [8]
CgSTPl	Cglg019290.l	1	522	57205.98	9.16	0.458	12	plas: 9, vacu: 3
CgSTP2	Cg8g023770. l	8	518	57190.81	9.15	0.509	11	plas: 9, vacu: 3
CgSTP3	Cg9g023330. l	9	512	55444.33	9.51	0.537	10	vacu: 8, plas: 4
CgSTP4	Cg7g013990.l	7	516	56327.43	8.89	0.596	12	plas: 6, vacu: 4
CgSTP5	Cg9g023340. l	9	511	55553.25	9.29	0.525	12	vacu: 9, plas: 4
CgSTP6	Cg9g005200. l	9	515	56567.06	8.9	0.687	12	plas: 7, vacu: 5
CgSTP7	Cg4g024730.2	4	512	55864.82	9.38	0.484	12	plas: 9, vacu: 3
CgSTP8	Cg9g0052 l 0.1	9	353	38734.75	9.33	0.567	8	vacu: 6, plas: 5
CgSTP9	Cg9g023350.2	9	511	55543.56	9.56	0.527	12	plas: 8, vacu: 3
CgSTPl0	Cg9g023370. l	9	511	55472.2	9.52	0.496	10	vacu: 10, plas: 3
CgSTPll	Cg2g041230. l	2	522	57887.94	8.86	0.472	12	plas: 6, vacu: 4
CgSTP12	Cg6g019080. l	6	522	57502.33	8.94	0.493	12	plas: 10, vacu: 2
CgSTP13	Cg9g005230. l	9	524	57802.91	9.11	0.469	12	plas: 11, vacu: 2
CgSTP14	Cglg012330. l	1	511	56065.11	9.03	0.543	12	plas: 9, vacu: 3

[1] Accession number consisted of the CPBD
[2] Chromosome location.
[3] Number of amino acids of the deduced amino acid sequence.
[4] Mw(Da) was the molecular weight.
[5] The pl was the theoretical isoelectric point.
[6] GRAVY was the grand average of hydropathicity.
[7] TMD was the number of transmembrane domains, as predicted by the NovoPro.
[8] The prediction of protein localization in cells via WoLF PSORT 11; Plas, plasma membrane; Vacu, vacuolar membrane.

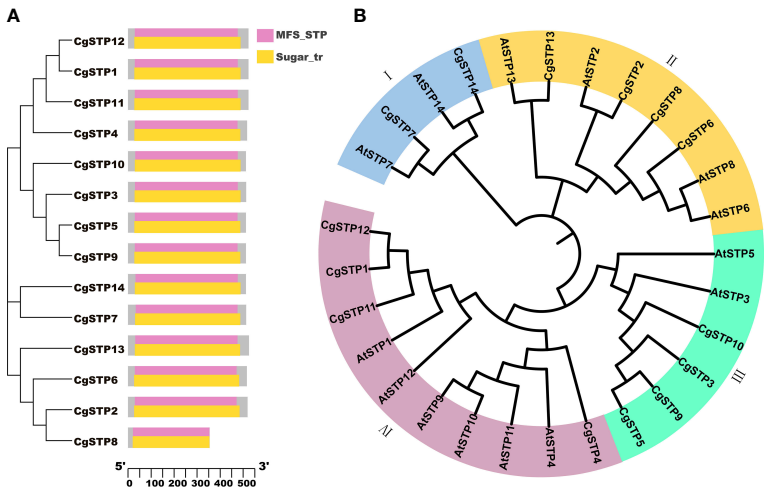

FIGURE 1
Phylogenetic analysis of STP members from *C grandis* and *A thaliana*, and conserved domain analysis of CgSTPs. **(A)** The conserved domain analysis was performed through the NCBI Batch CD-search tool. **(B)** A total of 14 STP protein sequences from *C grandis* and 14 STP protein sequences from *A thaliana* were aligned by ClustalW method. The MEGAX program was applied to construct the phylogenetic tree by the ML method in the default parameters. The beautification of the tree was carried out on the iTOL website.

(CgSTP11) to 9.56 (CgSTP9), which were all weakly basic. According to the relevant principle of grand average of hydropathicity (GRAVY), CgSTP1, CgSTP7, CgSTP10, CgSTP11, CgSTP12 and CgSTP13 were defined as amphoteric proteins with the value between -0.5 to 0.5, while the other proteins were hydrophobic proteins with more positive value (Table 1). More importantly, the number of CgSTPs transmembrane domains was presented from 8 to 12 based on the prediction by the NovoPro website. The vast majority of CgSTP members had 12 transmembrane domains, which was consistent with the characteristics of the MFS superfamily (Yan, 2013). In addition, the subcellular localization prediction of the protein sequences of *CgSTP* genes was performed *via* the WoLF PSORT (Table 1). Most of the CgSTP proteins are predicted to be plasma membrane proteins, but some are vacuolar membrane proteins, including CgSTP3, CgSTP5, CgSTP8 and CgSTP10, which are different from the localization of STP proteins in other species. These results indicate that CgSTP proteins may play different roles in sugar transport relying on their protein characterization and subcellular localization.

Gene structure, conserved motifs and promoter *cis*-acting elements analysis of the *CgSTPs*

To understand the structure of *CgSTP* genes, exons, introns, and untranslated regions were analyzed *via* GSDS2.0 and TBtools. It was found that *CgSTP1*, *CgSTP2*, *CgSTP3*, *CgSTP4*, *CgSTP6*, *CgSTP8*, and *CgSTP12* didn't have upstream and downstream UTRs. While *CgSTP5* didn't have upstream UTR, and the other six members all contained upstream and downstream UTRs (Figure 2B). Besides, all members contained exons and introns, but differed in specific numbers and locations. The exon number of the *CgSTP* genes ranged from 2 to 5 (Figure 2B). *CgSTP13* gene had five exons, whereas *CgSTP12* only had two exons. The different of gene structures might contribute to the functional diversity of closely related *STP* genes. Moreover, 12 putative conserved motifs were predicted through MEME analysis in most CgSTP proteins, and all these motifs were arranged in a stable order in the protein sequence (motif 2, motif 4, motif 10, motif 3, motif 7, motif 5, motif 6, motif 9, motif 12, motif 1, motif 8, and motif 11) (Figure 2A). The length of the conserved motifs ranges from 16 to 50 amino acids, and these 12 motifs are contained in all CgSTP proteins, except for CgSTP8 only has 8 motifs (Figure 2A; Supplementary Table 2). The high uniformity of these conserved motifs fully reflected the relatively conserved function of CgSTP proteins in the evolutionary process.

Cis-elements are important molecular switches involved in the regulation of gene transcription during plant growth and development or abiotic stress response. To detect regulatory factors and predict *cis*-elements of *CgSTPs*, each of the 2 kb promoter region (upstream of the start codon of the gene) of 13 *CgSTP* genes was retrieved from the *C. grandis* genome sequence. But for the *CgSTP2* gene, the identified sequence was shorter than 2 kb (1047bp), since the presence of another gene located less than 2 kb upstream of *CgSTP2* start codon site (Supplementary File 2). Finally, 14 *cis*-elements in the promoter region of *CgSTP* genes were predicted by PlantCARE database (Supplementary Figure 2A). A heat map was further constructed to show the frequency of different *cis*-elements (Supplementary Figure 2B). These predicted *cis*-elements respond to different phytohormones (Gibberellin, Abscisic acid, Auxin, Methyl

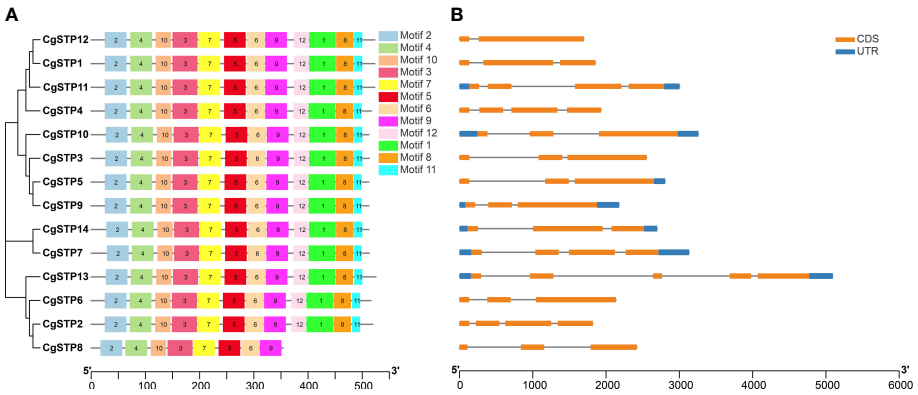

FIGURE 2
Motif, gene structure and phylogenetic relationship analysis of *CgSTP* genes. **(A)** The motif analysis was performed on the MEME. Twelve motifs were identified. The detail of motif sequence information was presented in Supplemental Table 2. **(B)** The gene exon–intron structure analysis. The blue color was the untranslated region, while the orange was the coding sequence. The line without color referred to introns. The neighbor-joining phylogenetic tree of the *CgSTP* genes sequences was constructed using 1000 bootstrap replicates by MEGAX64.

jasmonate, Salicylic acid) and various environmental factors, as well as abiotic and biotic stresses. Among them, hormone-related elements were widely presented in the promoter region of *CgSTPs*, so it was suspected that hormones play a potential role in regulating the expression of *CgSTP* genes. Besides, the anaerobic induction regulator is presented in the promoters of all genes except *CgSTP2*, which suggested that these genes might be induced by anaerobic conditions, such as waterlogging stress. In addition, some the other gene-specific *cis*-elements were also identified in the promoter region of the *CgSTP* genes, like the MYB binding site involved in drought-inducibility, low-temperature responsiveness, and the *cis*-acting element involved in defense and stress responsiveness, which provided the possibility to regulate gene expression and respond to various conditions of *CgSTPS*. Overall, *cis*-acting element analysis will provide a good reference for further studies on transcriptional regulation of *CgSTP* members.

Expression profiles of *CgSTP* Genes in different tissues

The spatiotemporal expression is a critical aspect in determining gene function. Accordingly, three different tissues of leaf, flower and juice sac of 'Shatian pummelo' were collected to perform the tissue expression pattern analysis of *STP* family members *via* qRT-PCR assay (Figure 3). The results showed that *CgSTPs* were widely expressed in leaf, flower and juice sac. Among them, *CgSTP7*, *CgSTP9*, *CgSTP11*, *CgSTP13* and *CgSTP14* had a higher expression level in two or three different tissues (Figure 3). For instance, *CgSTP13* was highly expressed in leaf and flower tissues (Figures 3A, B), while *CgSTP7* was highly expressed in leaf and juice sac tissues (Figures 3A, C). *CgSTP9*, *CgSTP11* and *CgSTP14* were highly expressed in leaf, flower and juice sac (Figure 3), implying that these members should have a universal functions in different tissues. What's more, the tissue-limited expression pattern was also presented that *CgSTP4* and *CgSTP6* were specifically expressed in flower (Figure 3B). For some other members were expressed at relatively low levels in all three tissue, such as *CgSTP1*, *CgSTP2*, *CgSTP8* and *CgSTP10*, which might be expressed at specific developmental stage or in response to certain stimuli such as abiotic and biotic stresses. Taken together, these expression patterns in different tissues suggested that *CgSTPs* should have distinct physiology functions throughout the plant.

Functional characterization of CgSTPs by heterologous expression in yeast

To investigate the transport function of *CgSTPs*, the subcellular localization was first identified. According to the expression level, the 6 higher expressed genes (*CgSTP4*, *CgSTP7*, *CgSTP9*, *CgSTP11*, *CgSTP13*, *CgSTP14*) were selected for further analysis. The cell membrane subcellular localization of CgSTPs were observed by co-expressing the YFP fusion proteins and the plasma membrane marker (PM marker) in tobacco leaves (Figure 4), which is consistent with the prediction results of the WoLF PSORT (Table 1). Based on previous reports, STPs had hexose sugar (like glucose and fructose) transport activity (Buttner et al., 2000; McCurdy et al., 2010; Liu et al., 2018; Kong et al., 2022). To characterize the transport properties of the CgSTP proteins, the monosaccharide uptake incompetent yeast mutant strain *EBY.VW4000* (only grow on maltose medium) was applied for sugar uptake assay (Wieczorke et al., 1999). For that, the yeast expression vector pDR196 containing CgSTP4, CgSTP7, CgSTP9, CgSTP11, CgSTP13, CgSTP14 were respectively transformed into the *EBY.VW4000*, and the empty vector and AtSTP13 were used as negative and hexose-uptake positive control in yeast growth assay. Glucose was added as sole carbon source to detect the sugar transport activity of CgSTPs.

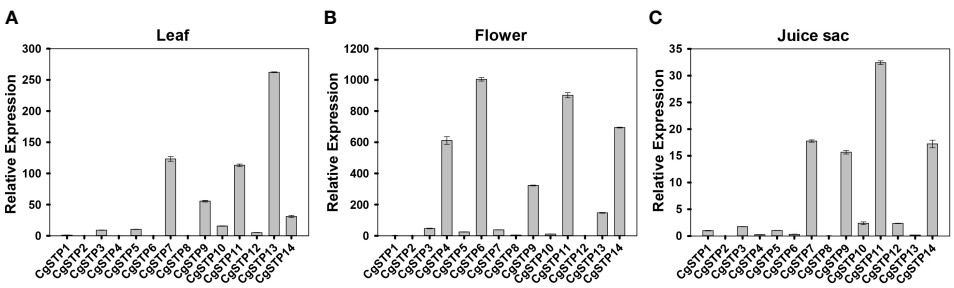

FIGURE 3
Relative expression patterns of *CgSTPs* in different tissues. **(A)** Leaf. **(B)** Flower. **(C)** Juice sac. The relative expression of all *CgSTP* members was determined by qRT-PCR assay. The *CgActin* was defined as the reference and the *CgSTP1*'s expression level was normalized as 1. Data are mean ± SE (n=3).

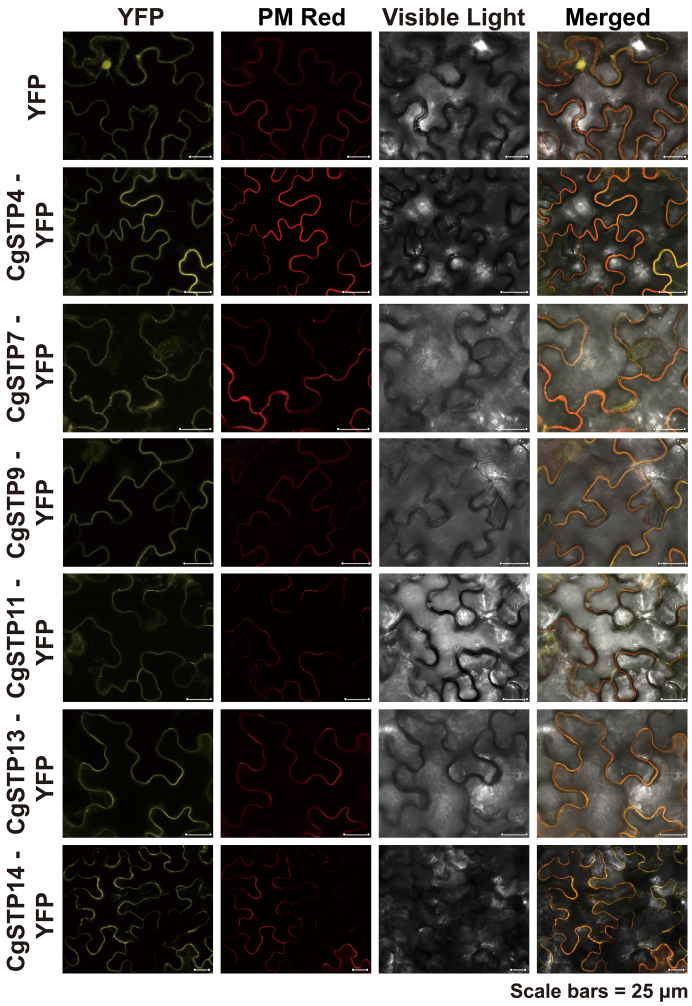

FIGURE 4
Subcellular Localization of CgSTPs. Tobacco leaves expressing 35S:YFP or 35S:CgSTP(s)-YFP, in colocalization with plasma membrane Deep Red marker, were visualized with a confocal laser microscope. Scale bars = 25 μm.

All yeast cells grew well on the synthesis deficient (SD-Ura) medium containing 2% maltose (Figure 5), indicating the successfully expression of vector in yeast. As expected, negative control yeast cells transformed with empty vector pDR196 did not grow on glucose medium, while positive control yeast cells transformed with CgSTP13-pDR196 grew normally on glucose medium (Figure 5). For yeast cells carrying CgSTP4, CgSTP11, CgSTP13, and CgSTP14 could be grown on SD medium containing glucose, suggesting that these four CgSTP proteins could have glucose transport activity. In addition, the other two CgSTP members (*CgSTP7* and *CgSTP9*) were unable to recovery yeast growth on glucose medium (Figure 5), implying that these two *CgSTP* members didn't have or had a weak hexose transport activity. The subcellular localization and the verification of the monosaccharide transport activity of *CgSTPs* would provide a foundation for further physiological function research.

Validation of sugar accumulation by transient overexpression of *CgSTPs*

To verify and analyze the sugar accumulation function of *CgSTPs*, the genes that have been confirmed to have transport activity and highly expression level in fruit or leaf tissues were selected. The overexpression vectors of pK7WG2D-*CgSTP11*, *CgSTP13*, *CgSTP14* were constructed under the 35S promoter. After that, the final expression vectors containing *CgSTP11/13/14*, and the empty vector control were transformed into tobacco leaves for transient overexpression (Supplementary Figure 3). In

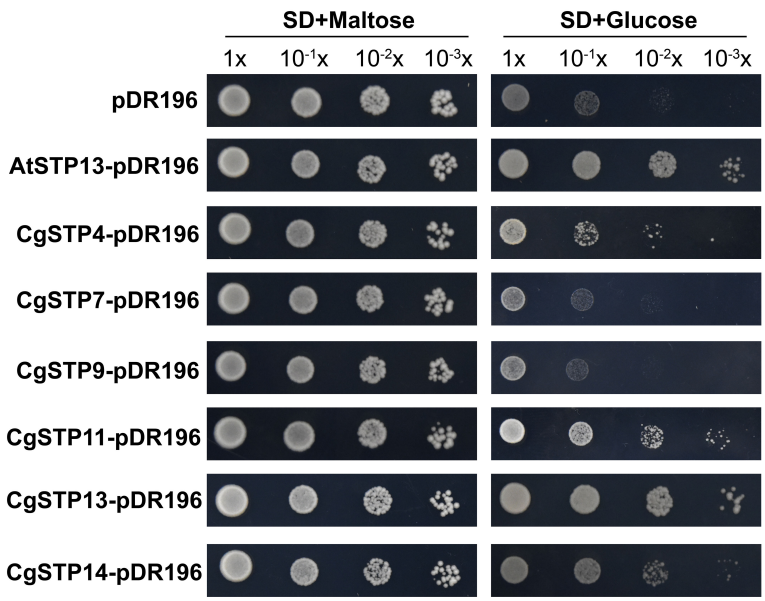

FIGURE 5
The sugar uptake assay of *CgSTPs* in Yeast (*S. cerevisiae*) Strain *EBY.VW4000*. Yeast growth assay of *EBY.VW4000* transformed with pDR196 empty vector, *AtSTP13*-pDR196 or *CgSTPs*-pDR196 alone on 2% (w/v) maltose or glucose SD-Ura medium.

consideration of the hexose transport activity, the main monosaccharides' (glucose and fructose) content were determined by GC-FID method (Li et al., 2015b). As shown in Figure 6, the glucose and fructose contents with the overexpression of target *CgSTPs* were increased in comparison with the control. For *CgSTP11* and *CgSTP14*-OE samples, both glucose and fructose had a significantly higher level, implying that they did have the function of accumulating monosaccharides in plant. Overall, the transient overexpression assay provide the important clues for further more detail research of CgSTPs in citrus species.

Antisense repression of *CgSTP4* reduces pollen tube growth

According to the previous report, sugar transport proteins were essential for pollen tube fast growth (Cheng et al., 2015; Rottmann et al., 2018; Li et al., 2020). In this study, it was found that *CgSTP4* had the specifically high expression level in flower (Figure 3). Therefore, the expression profile of *CgSTP4* in flower and various tissues of flower, including pollen, pollen tube, receptor, style, filament and petal of *C. grandis*, were further detected by qRT-PCR. The results revealed that *CgSTP4* was

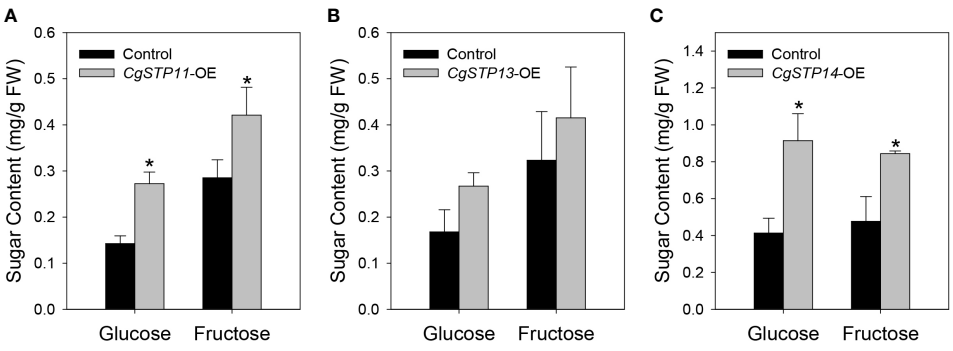

FIGURE 6
Determination of monosaccharide content in *CgSTPs* transient overexpression samples. The content of glucose and fructose in *CgSTP11* **(A)**, *CgSTP13* **(B)**, *CgSTP14* **(C)** transient overexpression tobacco leaves. Data are mean ± SE (n=3).

highly expressed in pollen grains and pollen tubes (Figure 7A). Given the importance of sugar absorption for pollen tube growth, we explored the potential role of *CgSTP4* in pollen tubes *via* the antisense oligonucleotide transfection assay (Meng et al., 2014; Meng et al., 2018). Compared with control and sense oligonucleotide transfection, the expression of *CgSTP4* can be significantly inhibited by as-ODN treatment during the germination of pollen in 'Shatian pummelo' (Figure 7B). As expected, the pollen tube length was shorter with the lower expression of *CgSTP4* (Figure 7C), indicating that *CgSTP4* plays an important potential role in the sugar uptake for the growth of pollen tubes in *C. grandis*.

Discussion

Sugar transport proteins (STPs or HTs) are mainly involved in the absorption and transport of hexose in plants. They have been reported to play a key role in plant response to biotic or abiotic stresses, growth and development (Fotopoulos et al., 2003; Buttner, 2010; Slewinski, 2011). Moreover, the sugar accumulation in plant, especially in fruit tissues, is closely related to STPs. So far, there has been no systematic study on the STPs, including their expression profile, localization, physiological functions in citrus, which is the most productive fruit in the world. The acquisition of genome sequence of citrus species provides a good opportunity to identify STP family members. Here, a total of 14 CgSTPs were identified by BLAST search and HMMER analysis of *C. grandis* genome. All selected STP proteins contained MSF_STP (cd17361) and Sugar_tr (pfam00083) conserved domains (Figure 1), which belong to the STP family of the MFS (Yan, 2013). The amino acid number of CgSTPs is between 353 aa (*CgSTP8*) and 524 aa (*CgSTP13*) (Table 1), which is similar to the other reported STP families in *Arabidopsis* (Buttner, 2010), tomato (Reuscher et al., 2014), strawberry (Jiu et al., 2018; Liu et al., 2020) and pear (Li et al., 2015a), indicating the relatively stable of STPs during the whole evolutionary process. Besides, this study was the first to

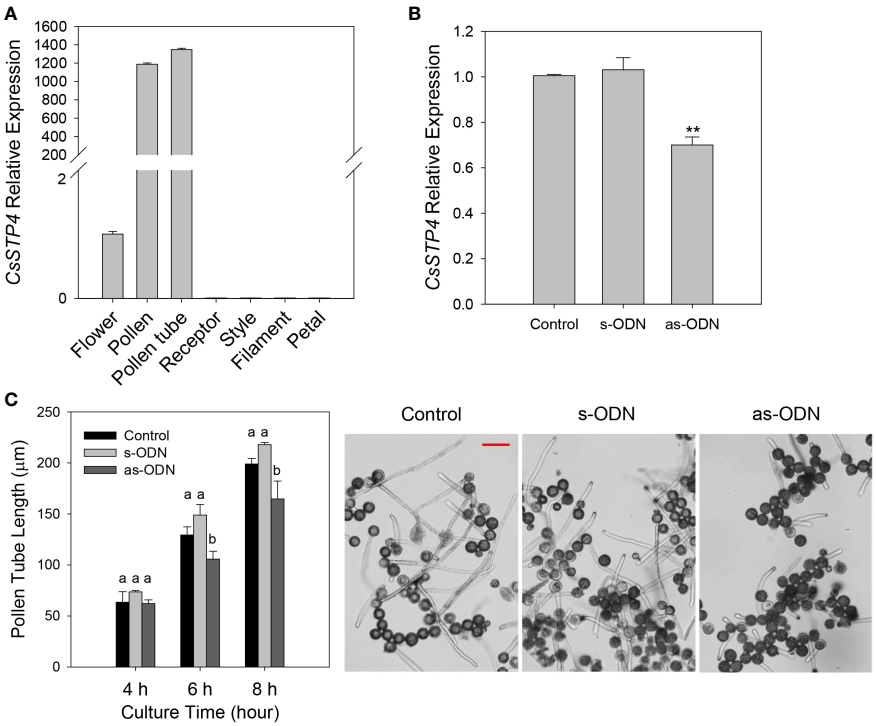

FIGURE 7
The pollen tube growth was inhibited with the lower expression of *CgSTP4*. **(A)** The expression of *CgSTP4* in different tissues of flower was determined by qRT-PCR. The *CgActin* was defined as the reference and the *CgSTP4*'s expression level in flower tissue was normalized as 1. **(B)** Expression levels of *CgSTP4* in pollen tubes transfected with antisense or sense oligonucleotide of *CgSTP4* (s-CgSTP4, as-CgSTP4), or transfection agent alone (Control). The *CgActin* was defined as the reference and the *CgSTP4*'s expression level in control condition was normalized as 1. Data are mean ± SE (n=3). * Represents significant difference in comparison with control using Student's t test at $p < 0.05$. **(C)** Pollen tube growth assay after transfection with as-CgSTP4, s-CgSTP4, or transfection agent alone (Control). Scale bar = 50 μm. Data are mean ± SE (n=3). Letters **(A–B)** indicate significant differences at each sampling point ($p < 0.05$) using Duncan's multiple range test (MRT) after ANOVA.

comprehensively analyze the gene structure, conserved motifs and *cis*-acting elements of *CgSTP* family. The expression pattern and function analysis of *CgSTP* gene were further studied.

Phylogenetic analysis presented that CgSTP proteins were classified into four groups in combination with AtSTPs in each group (Figure 1). The result of collinear correlation revealed eight pairs of homologous genes between pummelo and *Arabidopsis* (Figure S1), indicating potential similarities in evolutionary relationship and functions between the two plants. This will provide a useful reference for the future functional research of CgSTPs. It has been reported that most STP proteins have 12 transmembrane domains (TMD1-TMD12), including N-domain (TMD1-TMD6) and C-domain (TMD7-TMD12) (Hirai et al., 2002; Yan, 2013). In this study, 10 of the 14 CgSTP proteins contained the all of 12 TMDs, while CgSTP2 had 11 TMDs and 2 CgSTP had 10 TMDs (Table 1). However, CgSTP8 carries only 8 TMDs (Table 1), alone with a missing sequence in the middle of the protein. These results suggested that loss of N-terminal or C-terminal regions may have occurred in some CgSTP members during evolution. Consistent with this, similar STP protein structures have been observed in cassava (Liu et al., 2018), tomato (Reuscher et al., 2014), and grapevine (Afoufa-Bastien et al., 2010). As the transmembrane transports, most of the CgSTP were predicted to be localized in the plasma membrane, while a few be localized the vacuolar membrane based on the WoLF PSORT database (Table 1). Subcellular localization assay indicated that CgSTP4, CgSTP7, CgSTP9, CgSTP11, CgSTP13 and CgSTP14 were located to the plasma membrane (Figure 4), which was consistent with the predicted results. Accordingly, the most plasma membrane-localized members were proofed to have hexose sugar transport activity *via* the yeast mutant recovery growth assay (Figure 5).

In addition, the conserved motif analysis was carried out to further reveal the relationship between the various members and the potential roles of CgSTPs. Interestingly, the result demonstrated that CgSTPs contained all motif sequences except CgSTP8 (Figure 2A). This is similar to the characterization in *Arabidopsis* (Buttner, 2010) and cassava (Liu et al., 2018). The conservation and divergence of motifs in STP proteins may lead to functional similarities or differences among members of different STP families. We also analyzed the gene structure of *CgSTPs* and found that most *CgSTP* genes had three exons and two introns (Figure 2B). The variation in the number of exons and introns of the *STP* gene ranged from two to five, consistent with the other plant species, such as *Arabidopsis* (Buttner, 2010), cabbage (Zhang et al., 2019), grapevine (Afoufa-Bastien et al., 2010) and pear (Li et al., 2015a). The diversity of *STP* gene structures may be due to the structural differentiation formed by the insertion or deletion of exons and introns (Xu et al., 2012). Moreover, *cis*-acting element analysis was performed on the promoter sequence of *CgSTPs* (Figure S2). The predicted results indicated that *CgSTPs* may be involved in plant hormone (GA, ABA, IAA, MeJA and SA) or abiotic stress responses.

During plant growth and development, sugar accumulation and distribution has proved to be closely linked to the STP members. The most physiological functions also depend on gene expression pattern. In this study, the expression of *CgSTPs* was investigated by qRT-PCR, and it was found that *CgSTPs* had a various expression level in different pummelo tissues (Figure 3), which was consistent with the *AtSTPs* in *Arabidopsis* (Buttner, 2010). For example, *AtSTP1* is mainly expressed in the root for the hexose absorption from the extracellular (Otori et al., 2019). *AtSTP4*, *AtSTP6*, *AtSTP8*, *AtSTP9*, *AtSTP10* and *AtSTP11* are highly expressed in pollen and are mainly responsible for pollen tube growth *via* regulating glucose uptake (Rottmann et al., 2018). In here, *CgSTPs* also showed tissue-specific expression, such as *CgSTP4* was specifically expressed in pollen and pollen tubes (Figure 7). The further pollen tube growth experiment proofed that CgSTP4 was involved in regulating the pummelo pollen tube length *in vitro* (Figure 7). Given the important of sugar content for the fruit flavor quality, the *CgSTP11* and *CgSTP14*, which were highly expressed in juice sac tissue, were selected for sugar accumulation assay. The results shown that the hexose was dramatically increased with the overexpression of these two genes, implying the potential functions in improvement of the citrus fruit sweet quality. Except for these members, there are some other *CgSTP* genes that had lower expression level in detected tissues, like *CgSTP1*, *CgSTP2*, or *CgSTP8*. The more work was required in future to decipher the speculation if they were induced by special development stage or environmental conditions based on *cis*-element assay in their promoter sequence. In summary, the identification, expression pattern analysis, biological and physiological function assays of *CgSTPs* explored the functional CgSTP members in sugar accumulation and pollen tube growth, and also paved a way for further elucidating the more functions and regulatory mechanisms of sugar transport proteins in citrus species.

Data availability statement

The datasets presented in this study can be found in online repositories. The names of the repository/repositories and accession number(s) can be found in the article/Supplementary Material.

Author contributions

CL and J-HL designed the experiments. WX performed the experiments with assistance from ZL, ZZ, SZ and ML. WX, DG, J-HL, and CL analyzed and discussed the results. WX and CL finalized writing and revision of the manuscript. All authors have read and approved the final version of the manuscript. All

authors contributed to the article and approved the submitted version.

Funding

This work was supported by National Key Research and Development Program of China (2019YFD1000100), Hubei Hongshan Laboratory (2021hszd016), and the Huazhong Agricultural University (start-up funding to CL).

Conflict of interest

The authors declare that the research was conducted in the absence of any commercial or financial relationships that could be construed as a potential conflict of interest.

Publisher's note

Supplementary material

The Supplementary Material for this article can be found online at: https://www.frontiersin.org/articles/10.3389/fpls.2022.1106219/full#supplementary-material

References

Afoufa-Bastien, D., Medici, A., Jeauffre, J., Coutos-Thevenot, P., Lemoine, R., Atanassova, R., et al. (2010). The vitis vinifera sugar transporter gene family: Phylogenetic overview and macroarray expression profiling. *BMC Plant Biol.* 10, 245. doi: 10.1186/1471-2229-10-245

Aslam, M. M., Deng, L., Wang, X. B., Wang, Y., Pan, L., Liu, H., et al. (2019). Expression patterns of genes involved in sugar metabolism and accumulation during peach fruit development and ripening. *Sci. Hortic.* 257, 108633. doi: 10.3390/ijms17122112

Bailey, T. L., Boden, M., Buske, F. A., Frith, M., Grant, C. E., Clementi, L., et al. (2009). MEME SUITE: tools for motif discovery and searching. *Nucleic Acids Res.* 37, W202–W208. doi: 10.1093/nar/gkp335

Bailey, T. L., and Elkan, C. (1994). Fitting a mixture model by expectation maximization to discover motifs in biopolymers. *Proc. Int. Conf. Intell. Syst. Mol. Biol.* 2, 28–36.

Buttner, M. (2007). The monosaccharide transporter(-like) gene family in arabidopsis. *FEBS Lett.* 581, 2318–2324. doi: 10.1016/j.febslet.2007.03.016

Buttner, M. (2010). The arabidopsis sugar transporter (AtSTP) family: An update. *Plant Biol.* 12, 35–41. doi: 10.1111/j.1438-8677.2010.00383.x

Buttner, M., Truernit, E., Baier, K., Scholz-Starke, J., Sontheim, M., Lauterbach, C., et al. (2000). AtSTP3, a green leaf-specific, low affinity monosaccharide-h+ symporter of arabidopsis thaliana. *Plant Cell Environ.* 23, 175–184. doi: 10.1046/j.1365-3040.2000.00538.x

Chen, C. J., Chen, H., Zhang, Y., Thomas, H. R., Frank, M. H., He, Y. H., et al. (2020). TBtools: An integrative toolkit developed for interactive analyses of big biological data. *Mol. Plant* 13, 1194–1202. doi: 10.1016/j.molp.2020.06.009

Cheng, J. T., Wang, Z. Y., Yao, F. Z., Gao, L. H., Ma, S., Sui, X. L., et al. (2015). Down-regulating CsHT1, a cucumber pollen-specific hexose transporter, inhibits pollen germination, tube growth, and seed development. *Plant Physiol.* 168, 635–63 +. doi: 10.1104/pp.15.00290

Chen, L. Q., Hou, B. H., Lalonde, S., Takanaga, H., Hartung, M. L., Qu, X. Q., et al. (2010). Sugar transporters for intercellular exchange and nutrition of pathogens. *Nature* 468, 527–U199. doi: 10.1038/nature09606

Chiou, T. J., and Bush, D. R. (1996). Molecular cloning, immunochemical localization to the vacuole, and expression in transgenic yeast and tobacco of a putative sugar transporter from sugar beet. *Plant Physiol.* 110, 511–520. doi: 10.1104/pp.110.2.511

Deng, X. L., An, B. G., Zhong, H., Yang, J., Kong, W. L., and Li, Y. S. (2019). A novel insight into functional divergence of the MST gene family in rice based on comprehensive expression patterns. *Genes* 10, 239. doi: 10.3390/genes10030239

Fang, T., Peng, Y., Rao, Y., Li, S. H., and Zeng, L. H. (2020). Genome-wide identification and expression analysis of sugar transporter (ST) gene family in longan (Dimocarpus longan l.). *Plants-Basel* 9, 342. doi: 10.3390/plants9030342

Finn, R. D., Clements, J., and Eddy, S. R. (2011). HMMER web server: Interactive sequence similarity searching. *Nucleic Acids Res.* 39, W29–W37. doi: 10.1093/nar/gkr367

Fotopoulos, V., Gilbert, M. J., Pittman, J. K., Marvier, A. C., Buchanan, A. J., Sauer, N., et al. (2003). The monosaccharide transporter gene, AtSTP4, and the cell-wall invertase, Atbetafruct1, are induced in arabidopsis during infection with the fungal biotroph erysiphe cichoracearum. *Plant Physiol.* 132, 821–829. doi: 10.1104/pp.103.021428

Gautam, T., Dutta, M., Jaiswal, V., Zinta, G., Gahlaut, V., and Kumar, S. (2022). Emerging roles of SWEET sugar transporters in plant development and abiotic stress responses. *Cells* 11, 1303. doi: 10.3390/cells11081303

Hirai, T., Heymann, J. A., Shi, D., Sarker, R., Maloney, P. C., and Subramaniam, S. (2002). Three-dimensional structure of a bacterial oxalate transporter. *Nat. Struct. Biol.* 9, 597–600. doi: 10.1038/nsb821

Huai, B. Y., Yuan, P., Ma, X. X., Zhang, X. R., Jiang, L. H., Zheng, P. J., et al. (2022). Sugar transporter TaSTP3 activation by TaWRKY19/61/82 enhances stripe rust susceptibility in wheat. *New Phytol.* 236, 266–282. doi: 10.1111/nph.18331

Hu, B., Jin, J. P., Guo, A. Y., Zhang, H., Luo, J. C., and Gao, G. (2015). GSDS 2.0: An upgraded gene feature visualization server. *Bioinformatics* 31, 1296–1297. doi: 10.1093/bioinformatics/btu817

Jiu, S. T., Haider, M. S., Kurjogi, M. M., Zhang, K. K., Zhu, X. D., and Fang, J. G. (2018). Genome-wide characterization and expression analysis of sugar transporter family genes in woodland strawberry. *Plant Genome* 11(3). doi: 10.3835/plantgenome2017.11.0103

Kato, N., Pontier, D., and Lam, E. (2002). Spectral profiling for the simultaneous observation of four distinct fluorescent proteins and detection of protein-protein interaction *via* fluorescence resonance energy transfer in tobacco leaf nuclei. *Plant Physiol.* 129, 931–942. doi: 10.1104/pp.005496

Koch, K. (2004). Sucrose metabolism: regulatory mechanisms and pivotal roles in sugar sensing and plant development. *Curr. Opin. Plant Biol.* 7, 235–246. doi: 10.1016/j.pbi.2004.03.014

Kong, L. Y., Li, X. N., Zhan, Z. X., and Piao, Z. Y. (2022). Sugar transporters in plasmodiophora brassicae: Genome-wide identification and functional verification. *Int. J. Mol. Sci.* 23, 5264. doi: 10.3390/ijms23095264

Krenek, P., Samajova, O., Luptovciak, I., Doskocilova, A., Kornis, G., and Samaj, J. (2015). Transient plant transformation mediated by agrobacterium tumefaciens: Principles, methods and applications. *Biotechnol. Adv.* 33, 1024–1042. doi: 10.1016/j.biotechadv.2015.03.012

Kuhn, C., and Grof, C. P. (2010). Sucrose transporters of higher plants. *Curr. Opin. Plant Biol.* 13, 288–298. doi: 10.1016/j.pbi.2010.02.001

Lescot, M., Dehais, P., Thijs, G., Marchal, K., Moreau, Y., Van De Peer, Y., et al. (2002). PlantCARE, a database of plant cis-acting regulatory elements and a portal to tools for in silico analysis of promoter sequences. *Nucleic Acids Res.* 30, 325–327. doi: 10.1093/nar/30.1.325

Liang, M., Yang, W., Su, S. Y., Fu, L. L., Yi, H. L., Chen, C. W., et al. (2017). Genome-wide identification and functional analysis of s-RNase involved in the self-incompatibility of citrus. *Mol. Genet. Genomics* 292, 325–341. doi: 10.1007/s00438-016-1279-8

Li, M. J., Feng, F. J., and Cheng, L. L. (2012). Expression patterns of genes involved in sugar metabolism and accumulation during apple fruit development. *PloS One* 7 (3), e33055. doi: 10.1371/journal.pone.0033055

Li, S. J., Liu, X. J., Xie, X. L., Sun, C. D., Grierson, D., Yin, X. R., et al. (2015b). CrMYB73, a PH-like gene, contributes to citric acid accumulation in citrus fruit. *Sci. Hortic.* 197, 212–217. doi: 10.1016/j.scienta.2015.09.037

Li, C. L., Meng, D., Pineros, M. A., Mao, Y. X., Dandekar, A. M., Cheng, L. L., et al. (2020). A sugar transporter takes up both hexose and sucrose for sorbitol-modulated *In vitro* pollen tube growth in apple. *Plant Cell* 32, 449–469. doi: 10.1105/tpc.19.00638

Liu, Q., Dang, H. J., Chen, Z. J., Wu, J. Z., Chen, Y. H., Chen, S. B., et al. (2018). Genome-wide identification, expression, and functional analysis of the sugar transporter gene family in cassava (Manihot esculenta). *Int. J. Mol. Sci.* 19 (4), 987. doi: 10.3390/ijms19040987

Liu, H. T., Ji, Y., Liu, Y., Tian, S. H., Gao, Q. H., Zou, X. H., et al. (2020). The sugar transporter system of strawberry: Genome-wide identification and expression correlation with fruit soluble sugar-related traits in aFragaria x ananassagermplasm collection. *Horticult. Res.* 7, 132. doi: 10.1038/s41438-020-00359-0

Liu, C., Li, D. X., Huang, X. B., Zhang, F. Q., Xie, Z. Z., Zhang, H. Y., et al. (2022a). Manual thinning increases fruit size and sugar content of citrus reticulata blanco and affects hormone synthesis and sugar transporter activity. *J. Integr. Agric.* 21, 725–735. doi: 10.1016/S2095-3119(20)63502-x

Liu, S. C., Liu, X. C., Gou, B. R., Wang, D. L., Liu, C. R., Sun, J., et al. (2022b). The interaction between CitMYB52 and CitbHLH2 negatively regulates citrate accumulation by activating CitALMT in citrus fruit. *Front. Plant Sci.* 13. doi: 10.3389/fpls.2022.848869

Li, J. M., Zheng, D. M., Li, L. T., Qiao, X., Wei, S. W., Bai, B., et al. (2015a). Genome-wide function, evolutionary characterization and expression analysis of sugar transporter family genes in pear (Pyrus bretschneideri rehd). *Plant Cell Physiol.* 56, 1721–1737. doi: 10.1093/pcp/pcv090

McCurdy, D. W., Dibley, S., Cahyanegara, R., Martin, A., and Patrick, J. W. (2010). Functional characterization and RNAi-mediated suppression reveals roles for hexose transporters in sugar accumulation by tomato fruit. *Mol. Plant* 3, 1049–1063. doi: 10.1093/mp/ssq050

Meng, D., Gu, Z., Li, W., Wang, A., Yuan, H., Yang, Q., et al. (2014). Apple MdABCF assists in the transportation of s-RNase into pollen tubes. *Plant J.* 78, 990–1002. doi: 10.1111/tpj.12524

Meng, D., He, M., Bai, Y., Xu, H., Dandekar, A. M., Fei, Z., et al. (2018). Decreased sorbitol synthesis leads to abnormal stamen development and reduced pollen tube growth *via* an MYB transcription factor, MdMYB39L, in apple (Malus domestica). *New Phytol.* 217, 641–656. doi: 10.1111/nph.14824

Mistry, J., Chuguransky, S., Williams, L., Qureshi, M., Salazar, G. A., Sonnhammer, E. L. L., et al. (2021). Pfam: The protein families database in 2021. *Nucleic Acids Res.* 49, D412–D419. doi: 10.1093/nar/gkaa913

Murcia, G., Pontin, M., and Piccoli, P. (2018). Role of ABA and gibberellin A(3) on gene expression pattern of sugar transporters and invertases in vitis vinifera cv. Malbec during berry ripening. *Plant Growth Regul.* 84, 275–283. doi: 10.1007/s10725-017-0338-4

Murcia, G., Pontin, M., Reinoso, H., Baraldi, R., Bertazza, G., Gomez-Talquenca, S., et al. (2016). ABA and GA(3) increase carbon allocation in different organs of grapevine plants by inducing accumulation of non-structural carbohydrates in leaves, enhancement of phloem area and expression of sugar transporters. *Physiol. Plant.* 156, 323–337. doi: 10.1111/ppl.12390

Otori, K., Tanabe, N., Tamoi, M., and Shigeoka, S. (2019). Sugar transporter protein 1 (STP1) contributes to regulation of the genes involved in shoot branching *via* carbon partitioning in arabidopsis. *Biosci. Biotechnol. Biochem.* 83, 472–481. doi: 10.1080/09168451.2018.1550355

Paulsen, P. A., Custodio, T. F., and Pedersen, B. P. (2019). Crystal structure of the plant symporter STP10 illuminates sugar uptake mechanism in monosaccharide transporter superfamily. *Nat. Commun.* 10 (1), 407. doi: 10.1038/s41467-018-08176-9

Pi, M., Zhong, R., Hu, S., Cai, Z., Plunkert, M., Zhang, W., et al. (2022). A GT-1 and PKc domain-containing transcription regulator SIMPLE LEAF1 controls compound leaf development in woodland strawberry. *New Phytol.* doi: 10.1111/nph.18589

Radchuk, R., Emery, R. J., Weier, D., Vigeolas, H., Geigenberger, P., Lunn, J. E., et al. (2010). Sucrose non-fermenting kinase 1 (SnRK1) coordinates metabolic and hormonal signals during pea cotyledon growth and differentiation. *Plant J.* 61, 324–338. doi: 10.1111/j.1365-313X.2009.04057.x

Reuscher, S., Akiyama, M., Yasuda, T., Makino, H., Aoki, K., Shibata, D., et al. (2014). The sugar transporter inventory of tomato: Genome-wide identification and expression analysis. *Plant Cell Physiol.* 55, 1123–1141. doi: 10.1093/pcp/pcu052

Riesmeier, J. W., Willmitzer, L., and Frommer, W. B. (1992). Isolation and characterization of a sucrose carrier cdna from spinach by functional expression in yeast. *EMBO J.* 11, 4705–4713. doi: 10.1002/j.1460-2075.1992.tb05575.x

Riesmeier, J. W., Willmitzer, L., and Frommer, W. B. (1994). Evidence for an essential role of the sucrose transporter in phloem loading and assimilate partitioning. *EMBO J.* 13, 1–7. doi: 10.1002/j.1460-2075.1994.tb06229.x

Rolland, F., Baena-Gonzalez, E., and Sheen, J. (2006). Sugar sensing and signaling in plants: Conserved and novel mechanisms. *Annu. Rev. Plant Biol.* 57, 675–709. doi: 10.1146/annurev.arplant.57.032905.105441

Rolland, F., Moore, B., and Sheen, J. (2002). Sugar sensing and signaling in plants. *Plant Cell* 14 Suppl, S185–S205. doi: 10.1105/tpc.010455

Rombauts, S., Dehais, P., Van Montagu, M., and Rouze, P. (1999). PlantCARE, a plant cis-acting regulatory element database. *Nucleic Acids Res.* 27, 295–296. doi: 10.1093/nar/27.1.295

Rottmann, T., Klebl, F., Schneider, S., Kischka, D., Ruscher, D., Sauer, N., et al. (2018). Sugar transporter STP7 specificity for l-arabinose and d-xylose contrasts with the typical hexose transporters STP8 and STP12. *Plant Physiol.* 176, 2330–2350. doi: 10.1104/pp.17.01493

Rottmann, T., Zierer, W., Subert, C., Sauer, N., and Stadler, R. (2016). STP10 encodes a high-affinity monosaccharide transporter and is induced under low-glucose conditions in pollen tubes of arabidopsis. *J. Exp. Bot.* 67, 2387–2399. doi: 10.1093/jxb/erw048

Rozwadowski, K., Yang, W., and Kagale, S. (2008). Homologous recombination-mediated cloning and manipulation of genomic DNA regions using gateway and recombineering systems. *BMC Biotechnol.* 8, 88. doi: 10.1186/1472-6750-8-88

Sade, D., Brotman, Y., Eybishtz, A., Cuadros-Inostroza, A., Fernie, A. R., Willmitzer, L., et al. (2013). Involvement of the hexose transporter gene LeHT1 and of sugars in resistance of tomato to tomato yellow leaf curl virus. *Mol. Plant* 6, 1707–1710. doi: 10.1093/mp/sst036

Slewinski, T. L. (2011). Diverse functional roles of monosaccharide transporters and their homologs in vascular plants: A physiological perspective. *Mol. Plant* 4, 641–662. doi: 10.1093/mp/ssr051

Smeekens, S., and Hellmann, H. A. (2014). Sugar sensing and signaling in plants. *Front. Plant Sci.* 5. doi: 10.3389/fpls.2014.00113

Soni, R., Carmichael, J. P., and Murray, J. A. (1993). Parameters affecting lithium acetate-mediated transformation of saccharomyces cerevisiae and development of a rapid and simplified procedure. *Curr. Genet.* 24, 455–459. doi: 10.1007/bf00351857

Stadler, R., Buttner, M., Ache, P., Hedrich, R., Ivashikina, N., Melzer, M., et al. (2003). Diurnal and light-regulated expression of AtSTP1 in guard cells of arabidopsis. *Plant Physiol.* 133, 528–537. doi: 10.1104/pp.103.024240

Tao, Y., Cheung, L. S., Li, S., Eom, J. S., Chen, L. Q., Xu, Y., et al. (2015). Structure of a eukaryotic SWEET transporter in a homotrimeric complex. *Nature* 527, 259–263. doi: 10.1038/nature15391

Toyofuku, K., Kasahara, M., and Yamaguchi, J. (2000). Characterization and expression of monosaccharide transporters (OsMSTs) in rice. *Plant Cell Physiol.* 41, 940–947. doi: 10.1093/pcp/pcd016

Truernit, E., Schmid, J., Epple, P., Illig, J., and Sauer, N. (1996). The sink-specific and stress-regulated arabidopsis STP4 gene: Enhanced expression of a gene encoding a monosaccharide transporter by wounding, elicitors, and pathogen challenge. *Plant Cell* 8, 2169–2182. doi: 10.1105/tpc.8.12.2169

Truernit, E., Stadler, R., Baier, K., and Sauer, N. (1999). A male gametophyte-specific monosaccharide transporter in arabidopsis. *Plant J.* 17, 191–201. doi: 10.1046/j.1365-313x.1999.00372.x

Udvardi, M. K., Czechowski, T., and Scheible, W. R. (2008). Eleven golden rules of quantitative RT-PCR. *Plant Cell* 20, 1736–1737. doi: 10.1105/tpc.108.061143

Wang, Z. Y., Liang, Y. H., Jin, Y. R., Tong, X. L., Wei, X. Y., Ma, F. W., et al. (2020a). Ectopic expression of apple hexose transporter MdHT2.2 reduced the salt tolerance of tomato seedlings with decreased ROS-scavenging ability. *Plant Physiol. Biochem.* 156, 504–513. doi: 10.1016/j.plaphy.2020.10.001

Wang, Y. P., Tang, H. B., Debarry, J. D., Tan, X., Li, J. P., Wang, X. Y., et al. (2012). MCScanX: a toolkit for detection and evolutionary analysis of gene synteny and collinearity. *Nucleic Acids Res.* 40, e49. doi: 10.1093/nar/gkr1293

Wang, Z. Y., Wei, X. Y., Yang, J. J., Li, H. X., Ma, B. Q., Zhang, K. K., et al. (2020b). Heterologous expression of the apple hexose transporter MdHT2.2 altered sugar concentration with increasing cell wall invertase activity in tomato fruit. *Plant Biotechnol. J.* 18, 540–552. doi: 10.1111/pbi.13222

Wei, X. Y., Liu, F. L., Chen, C., Ma, F. W., and Li, M. J. (2014). The malus domestica sugar transporter gene family: identifications based on genome and expression prof ling related to the accumulation of fruit sugars. *Front. Plant Sci.* 5. doi: 10.3389/fpls.2014.00569

Wei, Q. J., Ma, Q. L., Zhou, G. F., Liu, X., Ma, Z. Z., and Gu, Q. Q. (2021). Identification of genes associated with soluble sugar and organic acid accumulation

in 'Huapi' kumquat (Fortunella crassifolia swingle) *via* transcriptome analysis. *J. Sci. Food Agric.* 101, 4321–4331. doi: 10.1002/jsfa.11072

Wieczorke, R., Krampe, S., Weierstall, T., Freidel, K., Hollenberg, C. P., and Boles, E. (1999). Concurrent knock-out of at least 20 transporter genes is required to block uptake of hexoses in saccharomyces cerevisiae. *FEBS Lett.* 464, 123–128. doi: 10.1016/s0014-5793(99)01698-1

Wilkins, M. R., Gasteiger, E., Bairoch, A., Sanchez, J. C., Williams, K. L., Appel, R. D., et al. (1999). Protein identification and analysis tools in the ExPASy server. *Methods Mol. Biol.* 112, 531–552. doi: 10.1385/1-59259-584-7:531

Wu, G. A., Prochnik, S., Jenkins, J., Salse, J., Hellsten, U., Murat, F., et al. (2014). Sequencing of diverse mandarin, pummelo and orange genomes reveals complex history of admixture during citrus domestication. *Nat. Biotechnol.* 32, 656–662. doi: 10.1038/nbt.2906

Wu, G. A., Terol, J., Ibanez, V., Lopez-Garcia, A., Perez-Roman, E., Borreda, C., et al. (2018). Genomics of the origin and evolution of citrus. *Nature* 554, 311–316. doi: 10.1038/nature25447

Xu, Q., Chen, L. L., Ruan, X., Chen, D., Zhu, A., Chen, C., et al. (2013). The draft genome of sweet orange (Citrus sinensis). *Nat. Genet.* 45, 59–66. doi: 10.1038/ng.2472

Xu, G., Guo, C., Shan, H., and Kong, H. (2012). Divergence of duplicate genes in exon-intron structure. *Proc. Natl. Acad. Sci. U.S.A.* 109, 1187–1192. doi: 10.1073/pnas.1109047109

Yan, N. (2013). Structural advances for the major facilitator superfamily (MFS) transporters. *Trends Biochem. Sci.* 38, 151–159. doi: 10.1016/j.tibs.2013.01.003

Zhang, W., Wang, S. Y., Yu, F. W., Tang, J., Yu, L., Wang, H., et al. (2019). Genome-wide identification and expression profiling of sugar transporter protein (STP) family genes in cabbage (Brassica oleracea var. capitata l.) reveals their involvement in clubroot disease responses. *Genes* 10 (1), 71. doi: 10.3390/genes10010071

Zheng, Q. M., Tang, Z., Xu, Q., and Deng, X. X. (2014). Isolation, phylogenetic relationship and expression profiling of sugar transporter genes in sweet orange (Citrus sinensis). *Plant Cell Tissue Organ Cult.* 119, 609–624. doi: 10.1007/s11240-014-0560-y

frontiers | Frontiers in Plant Science

TYPE Original Research
PUBLISHED 10 March 2023
DOI 10.3389/fpls.2023.1131708

OPEN ACCESS

EDITED BY
Chao Li,
Northwest A&F University, China

REVIEWED BY
Zhengyang Wang,
Northwest A&F University, China
Wang Hua,
Huazhong Agricultural University, China

*CORRESPONDENCE
Beibei Zhou
beibei_zhou@126.com
Qinping Wei
qpwei@sina.com

SPECIALTY SECTION
This article was submitted to Plant Abiotic Stress, a section of the journal Frontiers in Plant Science

RECEIVED 26 December 2022
ACCEPTED 17 February 2023
PUBLISHED 10 March 2023

CITATION
Sun T, Zhang J, Zhang Q, Li X, Li M, Yang Y, Zhou J, Wei Q and Zhou B (2023) Transcriptional and metabolic responses of apple to different potassium environments. *Front. Plant Sci.* 14:1131708. doi: 10.3389/fpls.2023.1131708

Transcriptional and metabolic responses of apple to different potassium environments

Tingting Sun[1,2], Junke Zhang[1], Qiang Zhang[1], Xingliang Li[1], Minji Li[1], Yuzhang Yang[1], Jia Zhou[1], Qinping Wei[1]* and Beibei Zhou[1]*

[1]Beijing Academy of Agriculture and Forestry Sciences, Beijing Academy of Forestry and Pomology Sciences, Beijing Engineering Research Center for Deciduous Fruit Trees, Key Laboratory of Biology and Genetic Improvement of Horticultural Crops, Ministry of Agriculture and Rural Affairs, Beijing, China, [2]College of Horticulture, China Agricultural University, Beijing, China

Potassium (K) is one of the most important macronutrients for plant development and growth. The influence mechanism of different potassium stresses on the molecular regulation and metabolites of apple remains largely unknown. In this research, physiological, transcriptome, and metabolite analyses were compared under different K conditions in apple seedlings. The results showed that K deficiency and excess conditions influenced apple phenotypic characteristics, soil plant analytical development (SPAD) values, and photosynthesis. Hydrogen peroxide (H_2O_2) content, peroxidase (POD) activity, catalase (CAT) activity, abscisic acid (ABA) content, and indoleacetic acid (IAA) content were regulated by different K stresses. Transcriptome analysis indicated that there were 2,409 and 778 differentially expressed genes (DEGs) in apple leaves and roots under K deficiency conditions in addition to 1,393 and 1,205 DEGs in apple leaves and roots under potassium excess conditions, respectively. Kyoto Encyclopedia of Genes and Genomes (KEGG) pathway enrichment showed that the DEGs were involved in flavonoid biosynthesis, photosynthesis, and plant hormone signal transduction metabolite biosynthetic processes in response to different K conditions. There were 527 and 166 differential metabolites (DMAs) in leaves and roots under low-K stress as well as 228 and 150 DMAs in apple leaves and roots under high-K stress, respectively. Apple plants regulate carbon metabolism and the flavonoid pathway to respond to low-K and high-K stresses. This study provides a basis for understanding the metabolic processes underlying different K responses and provides a foundation to improve the utilization efficiency of K in apples.

KEYWORDS

apple, potassium deficiency, potassium excess, transcriptome analysis, metabolome analysis

Introduction

Potassium (K) is one of the most essential macronutrients for plant growth and development, and it has essential physiological functions, such as plant osmoregulation, photosynthesis, protein synthesis, ion homeostasis, and enzyme activation (Kanai et al., 2011; Hafsi et al., 2014). Four forms of K exist in the soil, namely, exchangeable K, soluble K, lattice K, and fixed K. Only soluble K can be taken up by plants from the soil. The K concentration in the soil ranges from 0.1 to 6.0 mmol L^{-1} (Zeng et al., 2015). Too high or too low K concentrations in soil affect plant growth; in many regions, K concentrations are lower than 0.3 mmol L^{-1}, and K deficiency limits plant growth (Schroeder et al., 1994). Under low-K conditions, the most common phenomena include stunted growth of plants, yellowing of leaf margins, and yield reduction (Hasanuzzaman et al., 2018). Excessive use of potassium fertilizer causes high-K stress, and excessive application of potassium fertilizer in soil causes soil and water pollution, reducing the productivity of crops. However, plants initiate a series of physiological processes as well as molecular and metabolite mechanisms to adapt to different levels of K stress. K deficiency and excess conditions are typical abiotic stress forms that induce a series of biological responses. Under different K stress conditions, reactive oxygen species (ROS) and phytohormones are affected (Ashley et al., 2006; Amtmann et al., 2008). Plant responses to different K conditions are also due to various complex gene regulatory networks that cause widespread changes in gene expression and metabolite contents (Liang et al., 2013).

Transcriptomes comprehensively and efficiently reveal gene expression, thereby allowing elucidation of the plant molecular mechanism response to different K stresses. In plants, many studies have focused on K uptake, loading, and transport mechanisms. Some related genes have been studied, such as the high-affinity K transporter/uptake transporter (HAK/KUP/KT) family, including AtHAK1/5, PpHAK2, AtHAK5, HvHAK1, OsHAK1, AtKUP3, AtKUP1, and OsHKT2, as well as shaker-like K channels (AKT), including OsAKT1 and AtAKT1/5 (Kim et al., 1998; Banuelos et al., 2002; Xu et al., 2006; Fulgenzi et al., 2008; Jung et al., 2009; Pyo et al., 2010; Kim et al., 2012; Oomen et al., 2012; Wu et al., 2019; Wang et al., 2021). These genes play a vital role in plants' responses to different K conditions. Transcriptomic analysis of the response of *Arabidopsis*, rice, maize, soybean, sugarcane, and wild barley to K deficiency conditions has indicated that genes involved in metabolism, signal transduction, and ion transport are altered at the transcript level (Armengaud et al., 2004; Ma et al., 2012; Wang et al., 2012a; Zeng et al., 2014).

Metabolomics, known as qualitative and quantitative analysis of cellular metabolites, has become an important complementary tool for the study of plant functional genomics and systems biology (Weckwerth, 2003). Metabonomic analysis reflects the synthesis, decomposition, or transformation rules of some objects, all metabolites, or some metabolites in the tissue or cell (Hall, 2011). Abiotic stress causes changes in the expression of metabolic products, resulting in metabolite disorders *in vivo* (Meena et al., 2017). Many studies have reported the changes in small-molecule compounds in response to mineral nutritional stress. Sung et al. (2015) reported metabolic responses to deficiencies in nitrogen (N), phosphorus (P), and K, and they demonstrated that the lack of these elements decreases energy production and amino acid metabolism in tomato leaves and roots. Low-K stress increases monosaccharide, disaccharide, polysaccharide, and putrescine contents in barley (Zhao et al., 2021). The contents of putrescine, aconitate, citrate, malate, and fumarate increased in sunflower under low-K stress (Cui et al., 2019). Citric acid, arginine, and asparagine contents are upregulated under K deficiency in rapeseed leaves (Hu et al., 2021). The levels of glutamic acid and aspartic acid are decreased in peanut under low-K conditions, whereas the levels of histidine, lysine, and arginine are increased in peanut under low-K conditions (Patel et al., 2022). The amino acid contents are increased in both K-sensitive and K-tolerant genotypes of wheat roots under K starvation (Zhao et al., 2020).

Apple (*Malus domestica*) is one of the most important fruits in the world, and apple production and consumption are the highest in China. K fertilizer plays a key role in apple growth and ripening. When K deficiency occurs in apple trees, the middle and lower leaves of new shoots turn yellow. In severe cases, the leaves gradually show brown withered spots, resulting in a curly scorched appearance, and new shoots stop growing early, forming small flower buds and small fruits with a color difference and a decline in quality (Chang et al., 2014). High-K stress causes the occurrence of apple bitter pox, which reduces the absorption of cations, such as calcium and magnesium, by plants, thus affecting the yield of plants. Excessive application of potassium fertilizer causes soil environmental pollution and water pollution. Many studies have investigated the molecular mechanisms that occur under K deficiency in model plants, such as *Arabidopsis*, rice, and maize (Armengaud et al., 2004; Ma et al., 2012; Wang et al., 2012a). However, these mechanisms have rarely been reported in apple, especially under high-potassium stress. In the present study, we investigated the molecular response mechanism and metabolite changes of apple to low-potassium and high-potassium stresses, and we provided a theoretical basis for further study on the response mechanism of apple to potassium.

Materials and methods

Plant growth conditions

The experimental materials, namely, "CG-935" apple seedlings, were tissue cultured, after rooting, seeding, and transplantation, and the apple plants were then transported to the experimental field as previously reported by Sun et al. (2021).

Different potassium treatments

After 90 days, healthy apple seedlings of similar size (with 16–20 leaves) were transferred to a hydroponic slot (60 × 37 × 35 cm) containing 60 L of a 1/2-strength Hoagland nutrient solution (Hoagland and Arnon, 1950). Stress treatments were initiated after 10 days of precultivation. Apple seedlings were randomly divided into 3

groups with 54 plants per treatment, and there were three biological replicates for each stress treatment with 18 plants per replicate. The treatments were as follows: (1) control (CK), 1/2-strength Hoagland nutrient solution supplemented with 3 mM K_2SO_4; (2) low-K treatment (LK), 1/2-strength Hoagland nutrient solution with 50 μM K_2SO_4; and (3) high-K treatment (HK), 1/2-strength Hoagland nutrient solution with 15 mM K_2SO_4 (Chang et al., 2014). The solution was continuously aerated and refreshed every 3 days, and the experimental treatment lasted for 15 days. Plant roots and leaves were harvested for physiological, transcriptomic, and metabolomic analyses. The samples were designated as follows: the apple leaves and roots in the control condition were named CKL and CKR, respectively; the apple leaves and roots in the low-K condition were named LKL and LKR, respectively; and the apple leaves and roots in the high-K condition were named HKL and HKR, respectively.

Growth indices, photosynthetic indices, and nutrient concentration measurements

After 15 days of treatment, the plant heights, stem diameters, and dry weights (DWs) of the whole apple as well as the ratio of underground DW to aboveground DW (R/S) of the apple were calculated.

The net photosynthetic rate (Pn), transpiration rate (Tr), water use efficiency indicator (WUEi), stomatal conductance (Gs), and intercellular CO_2 concentration (Ci) values of the apple leaves were measured by an LI-6800 portable photosynthesis system (LI-COR Inc., Lincoln, NE, USA) on sunny days.

The measurements of soil plant analytical development (SPAD) of apple leaves and the concentrations of N, P, and K in apple roots, apple stems, apple leaves, and whole apple were measured according to the method of Sun et al. (2021).

Determination of H_2O_2, enzyme activities, and phytohormones

For the determination of H_2O_2, enzyme activity, and phytohormones, nine apple seedlings were selected for each experimental replicate (n = 3) to provide an adequate amount of root and leaf tissue. The levels of hydrogen peroxide (H_2O_2, SO1300), and the activities of peroxidase (POD, KT5058), catalase (CAT, KT4957), abscisic acid (ABA, KT4924), and indoleacetic acid (IAA, NR, KT4992) were determined using commercial test kits purchased from Jiangsu Kete Biotechnology Co., Ltd. (Jiangsu, China). H_2O_2 was recorded on a UV-1750 spectrometer (Shimadzu, Japan). The enzyme activities were analyzed using an ELISA reader (Multiskan MS, Labsystems 325, Helsinki, Finland).

RNA isolation, qRT-PCR analysis, and transcriptome sequencing

Total RNA of apple leaves and roots was isolated using TRIzol Reagent (Invitrogen, Carlsbad, CA, USA) for quantitative real-time PCR (qRT-PCR) analysis and RNA sequencing (RNA-seq) analysis, and three biological replicates of each sample were sequenced. Quantitative real-time PCR (qRT-PCR) analysis was conducted according to Sun et al. (2021), and the primers used for qRT-PCR are listed in Table S1. Transcriptome analysis was performed by Wuhan MetWare Biotechnology Co., Ltd. (www.metware.cn, Wuhan, China). After rapid filtering (version 0.18.0) (Chen et al., 2018), the HISAT2.2.4 and Bowtie2 tools were used to compare clean reads with the apple genome (https://iris.angers.inra.fr/gddh13/index.html) (Langmead et al., 2009; Kim et al., 2015). The RESM software was used to calculate the values of fragment per kilobase of transcript per million mapped reads (FPKM) (Li and Dewey, 2011). Differentially expressed genes (DEGs) were determined according to cutoffs of log2(fold change) ≥ 1 and $p \leq 0.05$. Kyoto Encyclopedia of Genes and Genomes (KEGG) and Gene Ontology (GO) tools were used to analyze the DEGs.

Metabolite analysis

Metabolites were extracted and analyzed at Wuhan MetWare Biotechnology Co., Ltd., Wuhan, China (www.metware.cn) (Zhang et al., 2019). The metabolite analysis was performed using a liquid chromatography–electrospray ionization–tandem mass spectrometry (LC-ESI-MS/MS) system (HPLC, Shim-pack UFLC SHIMADZU CBM30A system; MS, Applied Biosystems 6500 Q TRAP). Metabolite quantification was performed using multiple reaction monitoring (MRM) in triple quadrupole mass spectrometry (Chen et al., 2013). Metabolomic data analysis was performed according to previous methods (Zhu et al., 2018).

Statistical analysis

The statistical analysis of different plant treatments in triplicate (n = 3) was performed by one-way analysis of variance (ANOVA) using SPSS 20.0 software. A probability value of $p < 0.05$ was considered statistically significant. The data are presented as the mean ± standard deviation (SD) of three replicates.

Results

Potassium affects plant growth and mineral nutrients

After 15 days of treatment with 50 μM (LK treatment), 3 mM (CK treatment), or 15 mM (HK treatment) K_2SO_4 in hydroponic culture, the plant height, stem diameter, DW, and root/shoot ratio decreased under K stress. The plant height decreased more in LK (82.49%) than in HK (82.73%), and the stem diameter also showed a similar trend. The DW of LK-treated apple plants was 72.94% of that of CK plants, and the DW of HK-treated seedlings was 75.69% of that of CK seedlings. The root/shoot ratio significantly increased by 111.76% in LK but decreased by 65.5% in HK (Table 1).

TABLE 1 The growth indexes in apple under control (CK), low-potassium (LK), and high-potassium (HK) conditions.

Treatment	Plant height (cm)	Stem diameter (mm)	Dry weight (g/plant)	Root/Shoot
CK	18.67 ± 0.89 a	3.92 ± 0.23 a	2.18 ± 0.31 a (100)	0.34 ± 0.02 b
LK	15.40 ± 1.10 b	3.31 ± 0.16 b	1.59 ± 0.21 b (72.94)	0.38 ± 0.01 a
HK	17.50 ± 0.68 a	3.72 ± 0.15 a	1.65 ± 0.19 b (75.69)	0.28 ± 0.03 c

Data indicate means ± SE (n = 3). Different letters beside the values in the same column indicate significant difference between the treatments.

The value of SPDA is a reliable indicator that can represent the content of chlorophyll (Tan et al., 2021). The SPDA values and photosynthetic characteristics were different under LK and HK stresses. The SPAD significantly decreased under LK, but there was no difference under HK. The Pn, Tr, WUEi, and Gs were significantly reduced under LK and HK, especially under K deficiency conditions (Table 2).

Differences in K fertilization conditions were reflected in the apple root, stem, and leaf elemental N, P, and K mineral nutrients. The concentrations of K in apple trees were lower under LK stress but higher when more K was available, and the P and K concentrations were much higher in CK compared to HK and LK (Table S2).

H_2O_2 content, enzyme activities, and phytohormones

Plant biomass decreased under K stress, while root growth increased under LK stress (Figure 1A). The H_2O_2 content, superoxide dismutase (SOD) activity, and POD activity were affected by different K stresses. The H_2O_2 content increased in apple leaves and roots under the LK and HK treatments with greater increases under LK stress. Under different K conditions, the enzyme activities increased in both apple leaves and roots, but the range of increase varied. The activities of SOD and POD significantly increased under different K conditions. The ABA content increased by 1.13- and 1.29-fold in apple leaves under LK, and it increased by 1.14- and 1.25-fold in roots under HK (Figure 1E). The IAA content exhibited a similar trend (Figure 1F).

Differential gene expression analysis

To obtain a global overview of the transcriptome responses to different K treatments in apple roots and leaves, four RNA-seq libraries were prepared, namely, HKL/CKL, HKL/CKL, LKR/CKR, and HKR/CKR, according to different K stress conditions in apple roots and leaves. The transcriptome data of the 18 samples described in the study have been deposited into the National Center for Biotechnology Information (NCBI) databases, and the bioproject accession number is PRJNA895870. The sequencing data are summarized in Table S3. The average for each sample of clean reads was approximately 4.5×10^7, and the sequence alignment efficiency ranged from 82.59% to 90.04%. The FPKM of HK was higher than those of CK and LK, and FPKM > 1 was used as the threshold to determine gene expression (Figure S1A). The Pearson correlations among the LK, HK, and CK replicates ranged from 0.97 to 1 in leaves and from 0.98 to l in roots (Figure S1B). Principal component analysis (PCA) indicated that the roots and leaves of LK, HK, and CK were clustered together, indicating significant differences in gene expression profiles. The LK, HK, and CK in leaf and root replicates were not tightly clustered, showing that inoculation occurred within the replicates (Figure S1C).

According to DESeq2 analysis using cutoffs of |log 2-fold change| ≥ 1 and false discovery rate (FDR) < 0.05, a total of 2,409 transcripts were differentially expressed in apple leaves under LK with 1,412 upregulated genes and 997 downregulated genes (Figure S2A). A total of 1,393 DEGs were detected under HK conditions with 829 upregulated DEGs and 564 downregulated DEGs in apple leaves under HK (Figure S2B). These observations suggested that under different K conditions, more DEGs were found under LK conditions than under HK conditions in apple leaves. A total of 778 DEGs were differentially expressed in apple roots under LK stress with 442 upregulated genes and 336 downregulated genes (Figure S2C), and a total of 1,205 DEGs were differentially expressed in apple roots under HK with 819 upregulated DEGs and 386 downregulated DEGs (Figure S2D). In terms of fold change gene expression values, the following maximum upregulation and maximum downregulation values were observed: 8.19 $\log_2$ FC and −8.38 $\log_2$ FC in leaves under LK, respectively; 7.92 and −7.42 $\log_2$ FC in leaves under HK, respectively; 7.59 and −13.15 $\log_2$ FC in roots under LK, respectively; and 8.24 and −4.64 $\log_2$ FC in roots under HK stresses, respectively (Figure S2E).

GO annotation analysis showed enrichment classifications according to biological processes (BPs), molecular functions (MFs), and cellular components (CCs) (Figure S3). Figure 2 shows the top 20 significantly enriched pathways under different K stresses in apple leaves and roots. KEGG pathway enrichment revealed that the vital biological pathways in response to different K conditions were involved in flavonoid biosynthesis, photosynthesis, plant hormone signal transduction, and biosynthesis of various plant secondary metabolite biosynthetic processes.

The DEGs involved in potassium metabolism were then thoroughly analyzed. The DEGs associated with potassium uptake, loading, and transport processes were detected in four pairs of libraries (Table 3). Most of the potassium transporter gene family members were increased in the apple seedlings.

TABLE 2 The photosynthetic characteristics in apple under control (CK), low-potassium (LK), and high-potassium (HK) conditions.

Treatment	SPAD	Pn (μmol $CO_2/m^2/s$)	Tr (mmol $H_2O/m^2/s$)	WUEi (μmol/mmol)	Gs (mol $H_2O/m^2/s$)	Ci (μmol CO^2/mol)
CK	49.07 ± 2.74 a	12.73 ± 0.59 a	2.80 ± 0.09 a	4.55 ± 0.22 a	0.36 ± 0.01 a	282.88 ± 8.83 a
LK	43.98 ± 2.12 b	8.00 ± 0.56 c	2.24 ± 0.12 c	2.59 ± 0.25 b	0.17 ± 0.02 c	281.48 ± 12.02 a
HK	49.59 ± 2.76 a	9.75 ± 0.84 b	2.61 ± 0.07 b	2.26 ± 0.23 b	0.29 ± 0.01 b	285.44 ± 14.18 a

Data indicate means ± SE (n = 3). Different letters beside the values in the same column indicate significant difference between the treatments.

qRT-PCR validation of the DEGs

Ten apple genes were detected by qRT-PCR for expression analysis to validate the RNA-seq results. The RT-qPCR analysis results were not significantly different from the RNA-Seq data, and similar trends were found in the up- and downregulated genes (Figure S4).

Metabolomic response to different K treatments in apple

The metabolome of apple seedlings was analyzed using four different pairs of libraries, namely, LKL/CKL, HKL/CKL, LKR/CKR, and HKR/CKR. Overall, 527 DAMs were quantified and identified in

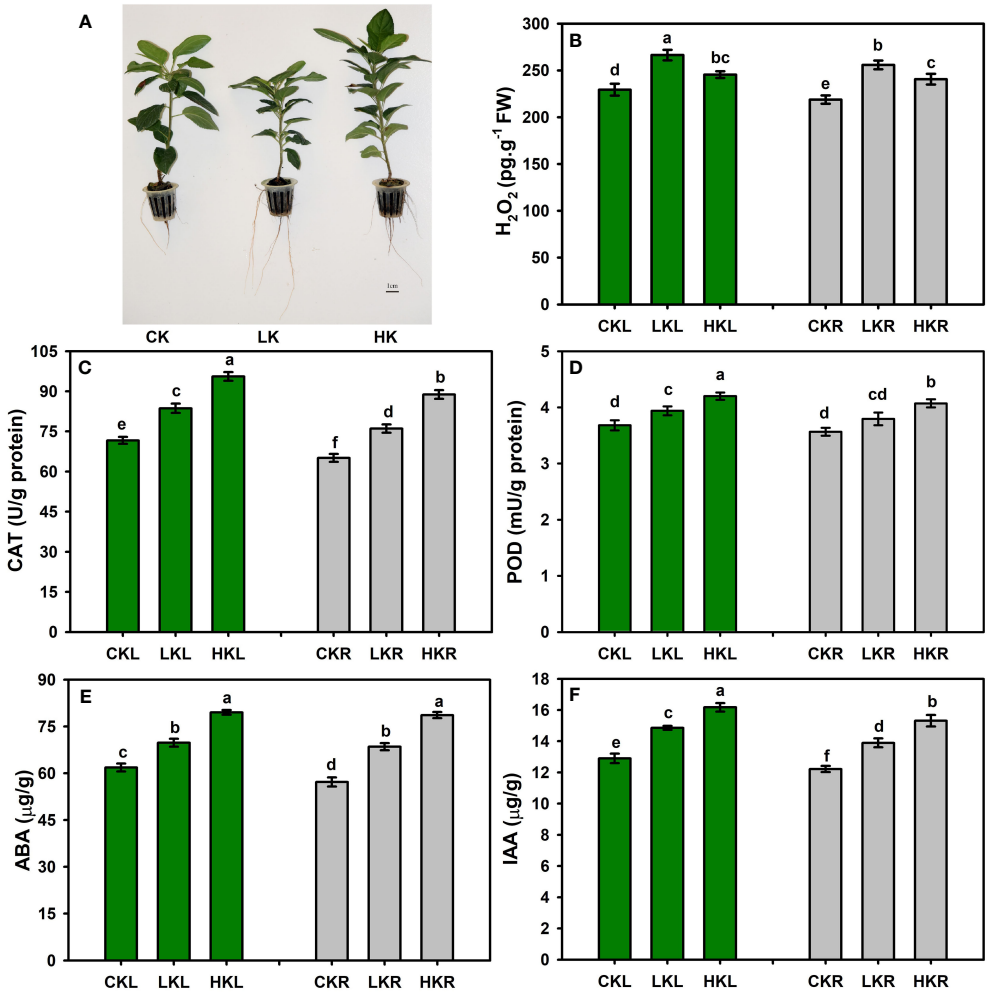

FIGURE 1
Measurement of H_2O_2, enzyme activities, and phytohormones in apple under different K treatments. **(A)** The phenotypic characteristics of apple. **(B)** The content of H_2O_2. The activities of CAT **(C)** and POD **(D)**. The contents of ABA **(E)** and IAA **(F)**. Different letters indicate significant differences according to Tukey's multiple-range tests ($p < 0.05$).

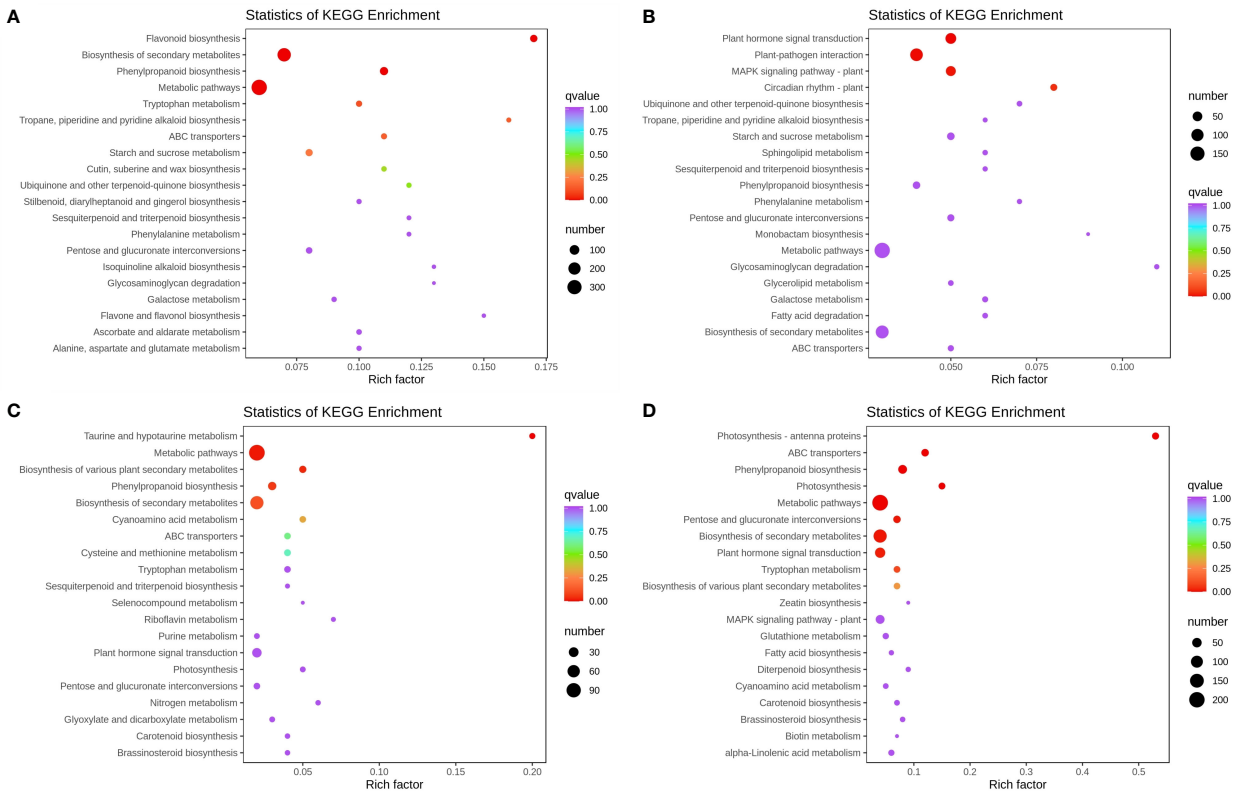

FIGURE 2
Statistics of KEGG enrichment under different K conditions in apple leaves and roots. **(A)** Statistics of KEGG enrichment under low-K conditions in apple leaves. **(B)** Statistics of KEGG enrichment under high K conditions in apple leaves. **(C)** Statistics of KEGG enrichment under low-K conditions in apple roots. **(D)** Statistics of KEGG enrichment under high K conditions in apple roots.

TABLE 3 Genes encoding transporters showed differential expression in response to different K stresses.

Gene	Seq ID	LKL	HKL	LKR	HKR
AKT	MD15G1178200			1.13	
KAT	MD05G1284400	1.18			
KUP	MD16G1089900	−1.18			
	MD01G1165900		1.04		
	MD07G1232700		1.04		
HAK	MD03G1283600				2.89
	MD10G1204500				3.37
	MD11G1302600			1.71	1.18
	MD11G1303100			1.91	1.40
	MD11G1302900			2.29	
	MD13G1133200			1.32	
	MD16G1143900			1.34	

LKL/CKL with 246 upregulated DAMs and 122 downregulated DAMs. For HKL/CKL, 228 DAMs were significantly upregulated, and 129 DAMs were downregulated. For LKR/CKR, 166 DAMs were identified with 74 upregulated DAMs and 92 downregulated DAMs. For HKR/CKR, 150 DAMs were identified with 92 upregulated DAMs and 74 downregulated DAMs (Table S4). The heatmaps of the differences in metabolites among the four combinations show the above trends (Figure 3).

Under different K stresses, the contents of amino acids, amino acid derivatives, organic acids, carbohydrates, flavonoids, and lipids changed. Under LK conditions, most lipids, flavonoids, and phenolic acids increased in apple roots. The metabolites of apple leaves and roots under different potassium stress conditions are presented in Figure 3. In apple leaves, the content of amino acids, amino acid derivatives, phenolic acids, terpenoids, and flavonoids increased under different K stresses, while nucleotides and nucleotide derivatives decreased. Under LK conditions, the content of lipids was upregulated in apple roots.

The co-joint KEGG enrichment analysis determined the co-mapped pathways in apple leaves and roots under K deficiency and excess conditions (Figures 4A, D, G, J). Of the metabolic pathways, the co-mapped pathways, namely, flavonoid biosynthesis, carbon metabolism, biosynthesis of secondary metabolites, glycerolipid biosynthesis, and phenylpropanoid biosynthesis, were the significantly enriched pathways under different K stresses. The Pearson correlation coefficients for the nine quadrants are shown in Figures 4B, E, H, K. In the third and seventh quadrants, the gene and metabolite differential expression patterns were consistent; the genes were positively correlated with the regulation of metabolites, and the changes in metabolites were positively regulated by the genes. The DEGs and DAMs with Pearson correlation coefficients (PCCs) higher than 0.8 were further selected and represented by heatmaps (Figures 4C, F, I, L).

Responses of carbon metabolite and flavonoid metabolites in apple to different potassium conditions

The concentrations of glucose, glycerate-3P, and succinate, which are involved in carbon metabolism, particularly glycolysis and the tricarboxylic acid (TCA) cycle, were increased in apple leaves under LK. The glucose content was upregulated in LKR/CKR and HKL/CKL, whereas glycerate-3P was increased in HKR/CKR (Figure 5). Under LK stress, the following changes were observed: the expression of *PFK* (MD05G13633600), *CS* (MD13G1111200), *FUM* (MD03G1292300), and *IDH* (MD09G1029200) was decreased in leaves; the expression of *PFK* (MD01G107500 and MD07G1144100) and *CS* (MD13G1153500) was increased in leaves; and the expression of *PFK* (MD 05G1363600) and *PPDK* (MD16G1179400) was decreased in roots. Under HP conditions, the expression of *PFK* (MD 05G1363600) and *PPDK* (MD16G1179400) was downregulated in leaves; the expression of *PFK* (MD05G1363600) was increased in roots; and the expression of *AD* (MD11G1038900) and *PPCK* (MD01G1046200) was decreased in roots (Figure 5).

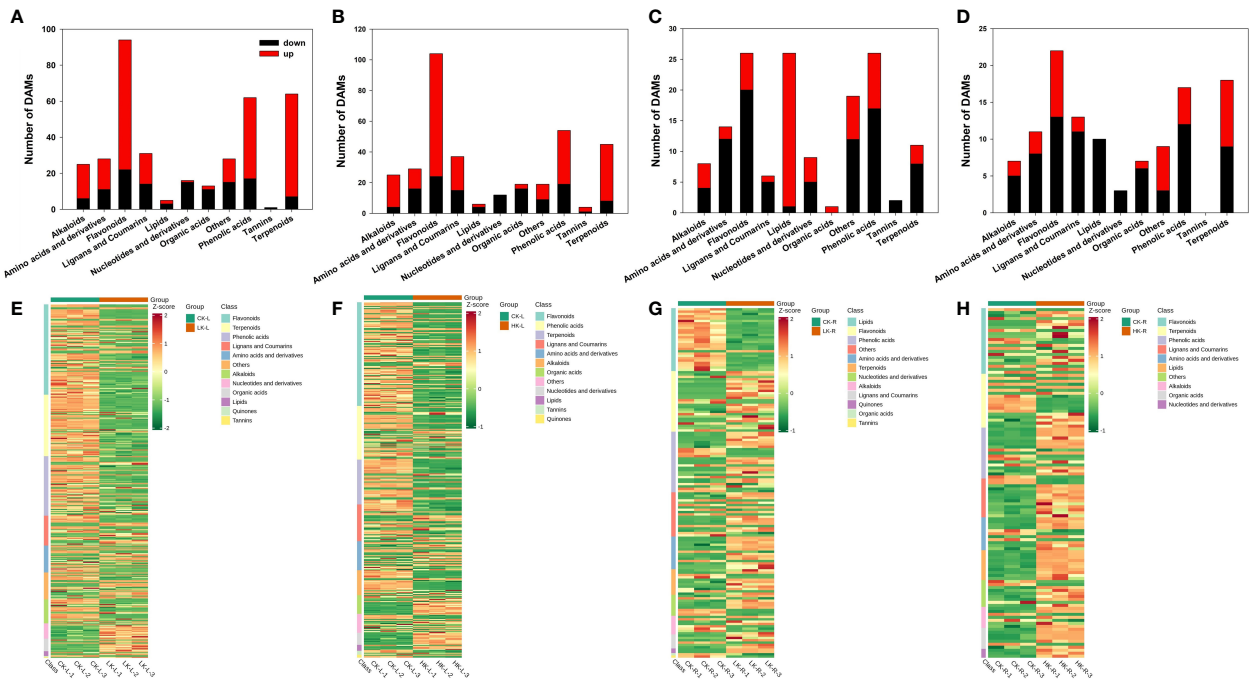

FIGURE 3
Differentially accumulated metabolites among different potassium treatments in apple. **(A, E)** Major classes of detected metabolites and heatmaps of differential metabolites between LKL/CKL. **(B, F)** Major classes of detected metabolites and heatmaps of differential metabolites between HKL/CKL. **(C, G)** Major classes of detected metabolites and heatmaps of differential metabolites between LKR/CKR. **(D, H)** Major classes of detected metabolites and heatmaps of differential metabolites between HKR/CKR. Three independent replicates of each stage are also displayed in the heatmap.

10.3389/fpls.2023.1131708

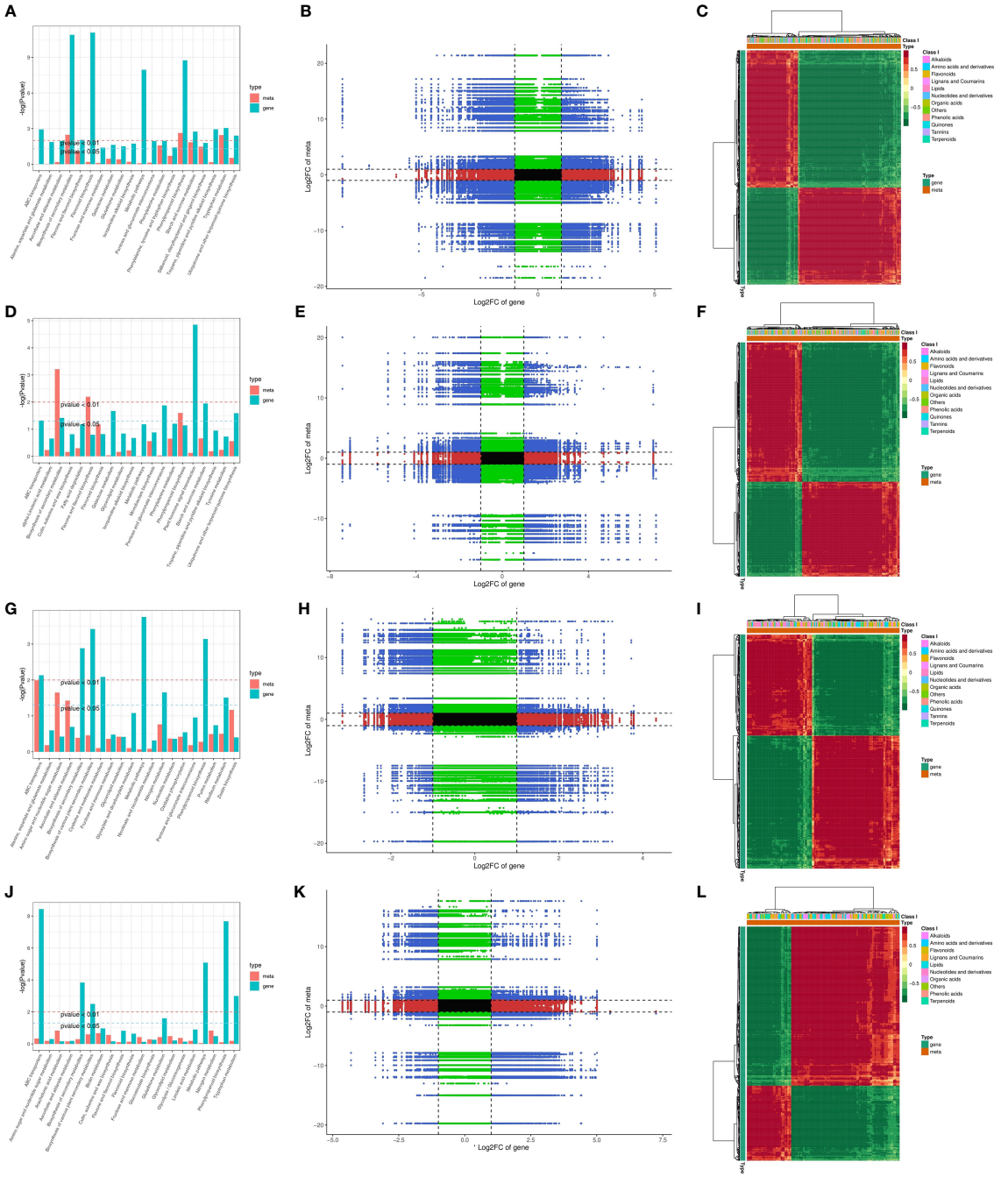

FIGURE 4
(A, D, G, J) Histograms of joint KEGG enrichment *p*-values, and **(B, E, H, K)** the associations of transcriptomic and metabolomic variation quadrant diagrams in LKL/CKL, HKL/CKL, LKR/CKR, and HKR/CKR; the black dotted lines indicate the differential thresholds. Outside the threshold lines, there were significant differences in the gene/metabolites, and within the threshold lines are shown the unchanged gene/metabolites. Each point represents a gene/metabolite. Black dots, green dots, red dots, and blue dots indicate unchanged genes/metabolites, differentially accumulated metabolites with unchanged genes, differentially expressed genes with unchanged metabolites, and both differentially expressed genes and differentially accumulated metabolites, respectively. **(C, F, I, L)** Heatmaps of the correlation coefficient clusters (>0.8), *p*-values < 0.05.

The level of naringenin chalcone, which is involved in flavonoid metabolites, was increased under LK conditions in apple leaves and roots. The phenylalanine content was decreased in apple leaves under different K conditions. The gene expression of *PAL* in leaves was increased under LK stress but decreased under HK conditions. The *C4H*, *4CL*, *CHS*, *F3H*, *ANS*, *CHI*, and *DFR* genes were upregulated under LK stress, whereas the *UGT* gene was decreased under LK stress. Under HK conditions, the *PAL*, *UGT*, *CHI* (MD01G1118300), and *DFR* (MD11G1229100) genes were downregulated in leaves (Figure 6).

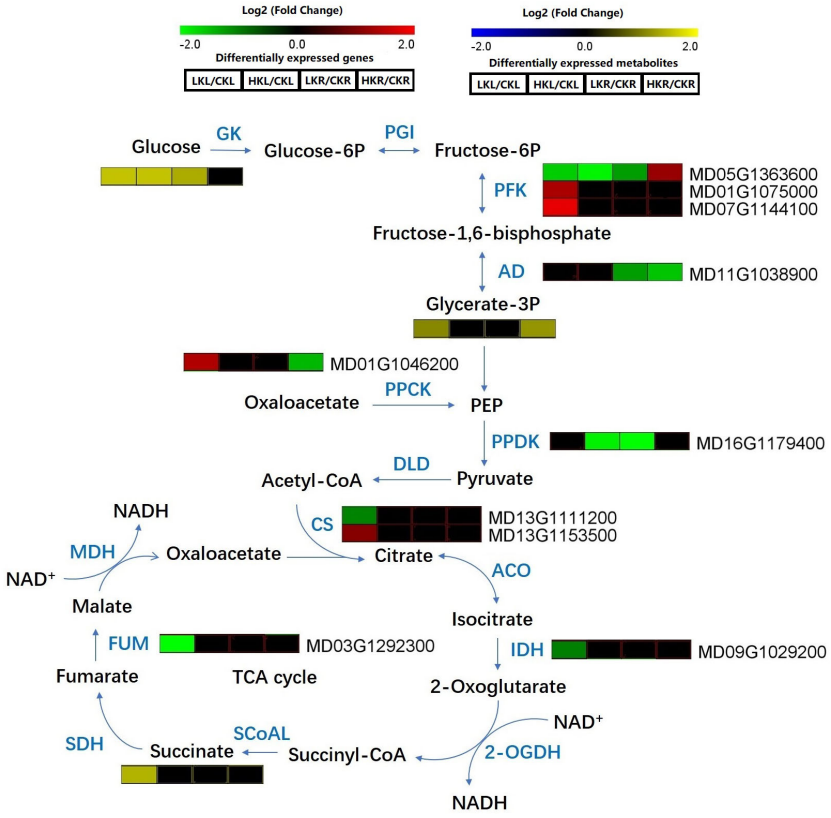

FIGURE 5
Carbon metabolites in apple leaves and roots under different K stresses. The boxes in the pathway represent DEGs or DAMs. Red and green represent upregulated and downregulated genes, respectively. Yellow and blue represent upregulated and downregulated metabolites, respectively.

Discussion

K plays essential roles in many physiological and biochemical processes in the plants, such as ion homeostasis, enzyme activation, osmoregulation, and protein synthesis (Kanai et al., 2007; Ma et al., 2020). K stress affects the normal growth of plants; the scarcity of K slows plant growth, reduces plant height, reduces stem diameter (Tester and Blatt, 1989), and decreases photosynthesis (Kanai et al., 2011). The plant height, stem diameter, plant DW, and photosynthesis were decreased under different LK and HK stresses in apple (Tables 1, 2). Trankner et al. (2018) revealed that K deficiency also reduces photosynthetic CO_2 fixation, as well as the transportation and consumption of photoassimilates, thus damaging plant membranes and chlorophyll under low-K conditions. In the present research, the SPDA value and photosynthetic characteristics decreased under LK stress in apple (Table 2). Xu et al. (2020) reported that an adequate supply of K increased the photoassimilate transportation rate from apple leaves to roots as well as increased nutrient use efficiency by influencing photosynthesis. The SPAD value of apple plants was slightly increased under HK stress, while the photosynthetic index decreased to a lesser extent under HK stress compared to LK stress (Table 2); it means that apple seedlings under low-potassium stress are more damaged than those under high-potassium stress. In the present study, RNA-Seq and KEGG enrichment analysis indicated that a different potassium environment had an effect on plant photosynthesis. Combined transcriptome metabolome analysis showed that the DEGs and DAMs were associated with biological processes, such as carbohydrate metabolism and photosynthesis. Hafsi et al. (2014) revealed that K stress limits plant leaf growth, which may be due to sugar starvation in stems and leaves. In the present study, genes involved in the TCA cycle, such as *CS*, *IDH*, and *TCA*, were downregulated in apple leaves under LK (Figure 5), which may induce apple plant growth restriction.

Plants under K stress conditions increase ROS production, resulting in oxidative stress (Hernandez et al., 2012). The accumulation of higher K in plant cells restores oxidative stress by increasing the activity of antioxidant enzymes, such as glutathione reductase (GPX), dehydroascorbate reductase (DHAR), ascorbate peroxidase (APX), CAT, SOD, and POD (García-Martí et al., 2019). The H_2O_2 content, SOD activity, and POD activity were affected by different K stresses in apple seedlings. The SOD and POD activities were significantly increased to combat different K conditions (Figures 1B–D). Under HK stress, the enzyme activities increased more significantly than under LK stress, which indicated that LK had a greater effect on apple plants. A previously metabolome analysis has revealed that the glutathione content is increased in roots in low-K-

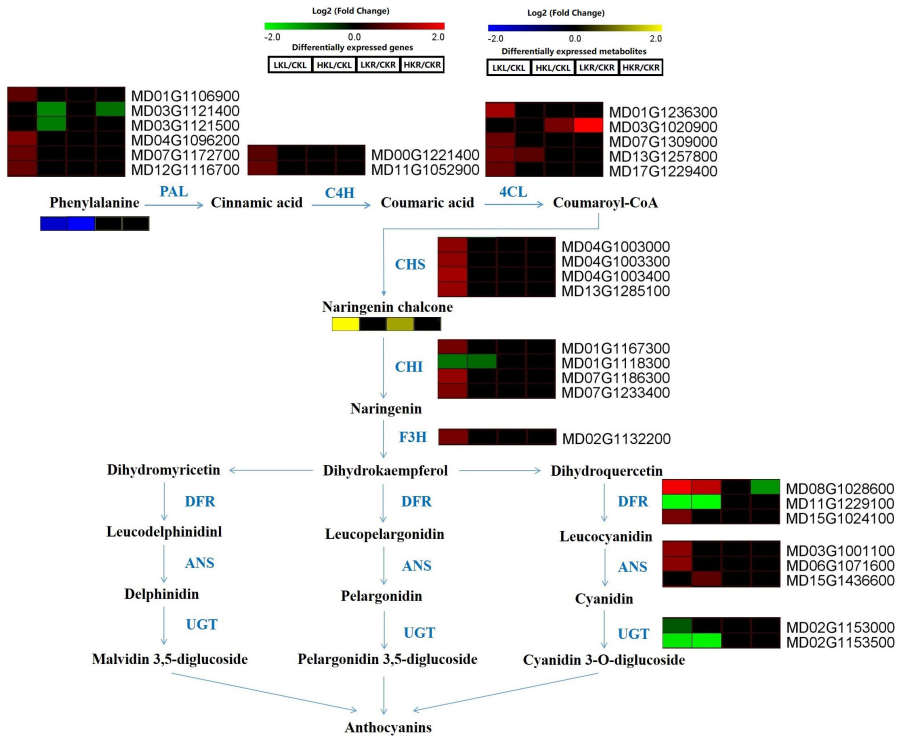

FIGURE 6
Flavonoid metabolites in apple leaves and roots under different K stresses. The boxes in the pathway represent DEGs or DAMs. Red and green represent upregulated and downregulated genes, respectively. Yellow and blue represent upregulated and downregulated metabolites, respectively.

tolerant KN9204 wheat but not in low-K-sensitive BN207 wheat (Zhao et al., 2020). Under low potassium, the content of S-(methyl) glutathione in apple leaves and roots was significantly increased in the present study (Table S4). Thus, these findings indicated that glutathione is an important metabolite for plant adaptation to K deficiency.

Phytohormones are active substances that widely exist in plants to regulate their physiological metabolism, affect plant development, affect plant growth, and play a regulatory role in stress conditions. Different potassium environments influence phytohormones in plants, such as brassinosteroids, IAA, ABA, and jasmonic acid (JA) (Ahanger et al., 2018; Ahanger et al., 2020; Yang et al., 2020). After 15 days of different K stress treatments, ABA and IAA contents increased in both apple leaves and roots (Figures 1E, F). The concentration of ABA in peanut leaves also increases under low-K stress (Patel et al., 2022). Therefore, considering the importance of phytohormones in plant growth, these findings indicated that ABA, JA, SA, and other phytohormones are important molecules in plant resistance to K stress.

Potassium uptake and absorption are mainly accomplished through potassium transporters and potassium channels in the plasma membrane (Ashley et al., 2006). K transporters and channels play vital roles in translocation and cell growth in various plants (Wang and Wu, 2013). Under the condition of K deficiency, the expression levels of *HAK1* and *HAK5* in maize are upregulated, and *AtHAK5*, *OsHAK1*, and *HvHAK1* are also induced by K-limited conditions (Santa-María et al., 1997; Banuelos et al., 2002; Ahn et al., 2004; Gierth et al., 2005; Fulgenzi et al., 2008; Qin et al., 2019). In addition, transcriptome analysis of rice roots under LK stress has revealed that the *OsHAK1*, *OsHAK7*, *OsHAK11*, and *OsHKT2;1* genes are upregulated; in addition, potassium channel genes, such as *OsAKT1*, *OsAKT2/3*, and *OsKCO1*, are also increased in response to low-K conditions (Ma et al., 2012). In tobacco seedlings, the *KUP3* K transporter and the *SKOR* K channel are increased under LK stress (Lu et al., 2015). In apple seedlings, the *AKT* (MD15G1178200) and *HAK* (MD11G1302600, MD11G1303100, MD11G1302900, MD13G1133200, and MD16G1143900) genes were upregulated in roots under KL. Moreover, the *KAT* (MD05G1284400) and *KUP* (MD01G1165900 and MD07G1232700) genes were upregulated in apple leaves, whereas *HAK* (MD03G1283600, MD10G1204500, MD11G1302600, and MD11G1303100) was increased in apple roots (Table 3). These results were consistent with previous studies, showing that a common regulatory mechanism exists across plant species whereby the transcription of genes encoding K transporters and channels increases, which may be an efficient strategy to increase potassium uptake in plants under a K-deficient environment. Therefore, these findings suggested that apple *AKT*, *HAK*, *KUP*, and *HAK* are key genes involved in potassium channels and transporters, which play an important role in coping with low- and high-potassium stresses in apple seedlings.

Under potassium-deficient conditions, the amino acid content increases in cotton (Wang et al., 2012b) and in roots of the K-tolerant genotype of wheat (Zhao et al., 2020), and lysine, histidine,

and arginine accumulated in peanut leaves and roots (Patel et al., 2022). In addition, the citric acid, arginine, and asparagine contents increase under LK in rapeseed (Hu et al., 2021), and most amino acids increase in tomato roots under LK (Sung et al., 2015). Armengaud et al. (2009) found that the selective reduction of acidic amino acids contributes to maintaining charge balance in response to potassium-deficient conditions. Under high-N conditions, most amino acids decreased in apple leaves, and under HK conditions, most amino acids decrease in apple (Sun et al., 2021). In plants, the accumulation of free amino acids has been reported under N and P deficiency conditions (Hernández et al., 2007; Pant et al., 2015; Mo et al., 2019; Ding et al., 2021). In this study, we found that the synthesis of most amino acids was increased in apple leaves under LK stress, especially in ornithine and arginine (Figure 5; Table S4). These results show that the deficiency of macronutrients affects the accumulation of amino acids in plants.

Carbohydrate metabolism plays core roles in plant metabolism, providing energy for plant growth and development, and it acts as a bridge in the communication of proteins, lipids, and metabolism (Rolland et al., 2006). The increased content of soluble sugars, including glucose, sucrose, and fructose, in plants is a typical response to different stresses (Armengaud et al., 2004; Rosa et al., 2009; Carvalhais et al., 2011; Wang et al., 2012b; Tang et al., 2015). Zeng et al. (2018) found that most sugars are significantly upregulated under a K-deficient environment in barley roots and leaves. Under LK and HK stresses, the glucose and glycerate-3P contents also increased in apple, suggesting that increased accumulation of sugar may be one of the physiological characteristics for different K stress adaptations in plants. Sugar and potassium have a common function in regulating osmotic potential. We also identified DEGs involved in carbohydrate metabolism, especially those related to glycolysis and the TCA cycle, which were differentially expressed in response to different K stresses. Glycolysis is a process of glucose breakdown to form pyruvate (Fernie et al., 2004). Changes in the levels of gene transcripts in the glycolytic pathway, such as phosphofruckinase-1 (PFK), aldolase (AD), pyruvate-phosphate kinase (PPDK), and phosphoenolpyruvate carboxylase kinase (PPCK), were found under LK and HK conditions in apple. PFK catalyzes a reversible reaction in glycolysis and regulates the glycolysis pathway (Schaeffer et al., 1996; Mustroph et al., 2013). It has been reported that the *PFK* gene is upregulated in barley under LK (Ye et al., 2022). In this study, the expression of *PFK* (MD01G107500 and MD07G1144100) was increased in apple leaves, which may have induced an increase the glycerate-3P content in apple leaves under LK (Figure 5). Li et al. (2018) revealed that the TCA cycle of two soybean genotypes is inhibited in leaves and roots under low-N stress. We have previously reported that the TCA cycle is also decreased under N-deficient stress in apple leaves (Sun et al., 2021). The DEGs involved in the TCA cycle, namely, fumarase (*FUM*), isocitrate dehydrogenase (*IDH*), and citrate synthase (*CS*), were also downregulated in apple leaves under LK (Figure 5), indicating that LK stress caused greater damage to apple leaves. Carbohydrate metabolism enzymes, particularly those involved in glycolysis and the TCA cycle, may be indispensable for plant survival under low nutrient conditions (Zeng et al., 2015).

Combined KEGG enrichment analysis of these pathways showed that the biosynthesis of flavonoids was a significantly enriched pathway under different K stresses (Figure 6). Flavonoids are secondary metabolites with low molecular weights, and they are widely found in plant communities and are closely related to the UV protection, flower color formation, plant growth regulation, and pathogen resistance. Many studies have found that flavonoids are related to macronutrients in plants, such as N, P, and K. In rapeseed, nitrogen deficiency enhances *ANS* and *DFR* gene expression (Koeslin-Findeklee et al., 2015). The expression of the *PAL5*, *CHS2*, *F3'H*, and *F3'5'H* genes is significantly increased in tomato leaves under N deficiency stress (Løvdal et al., 2010). Luo et al. (2019) reported that flavonoids are significantly decreased under low P in maize. In the present study, the DEGs and DAMs involved in the flavonoid pathway also changed in apple under different K conditions (Figure 6). The level of naringenin chalcone in apple leaves and roots was increased under LK conditions. Moreover, the phenylalanine content decreased in apple leaves under different K conditions. The *PAL* gene in apple leaves was upregulated under LK stress but downregulated under HK conditions. The *C4H*, *4CL*, *CHS*, *F3H*, *ANS*, *CHI*, and *DFR* genes were upregulated under LK stress, but the *UGT* gene was downregulated under LK stress. Under HK conditions, the *PAL*, *UGT*, *CHI* (MD01G1118300), and *DFR* (MD11G1229100) genes were downregulated in leaves. Together, these results indicated that the flavonoid pathway plays an important role in the apple response to different potassium stresses.

Data availability statement

The datasets presented in this study can be found in online repositories. The names of the repository/repositories and accession number(s) can be found in the article/Supplementary Material.

Author contributions

BZ and QW designed the experiments. TS prepared the plant samples. TS, JKZ, and QZ conducted the experiments and analyzed the data. TS, BZ, and QW wrote the manuscript, with the help of XL, ML, YY, and JZ. All authors contributed to the article and approved the submitted version.

Funding

This work was supported by the National Key Research and Development Project of China (2020YFD1000201) and the National Natural Science Foundation of China (31901965).

Conflict of interest

The authors declare that the research was conducted in the absence of any commercial or financial relationships that could be construed as a potential conflict of interest.

Publisher's note

All claims expressed in this article are solely those of the authors and do not necessarily represent those of their affiliated organizations, or those of the publisher, the editors and the reviewers. Any product that may be evaluated in this article, or claim that may be made by its manufacturer, is not guaranteed or endorsed by the publisher.

Supplementary material

The Supplementary Material for this article can be found online at: https://www.frontiersin.org/articles/10.3389/fpls.2023.1131708/full#supplementary-material

References

Ahanger, M., Ashraf, M., Bajguz, A., and Ahmad, P. (2018). Brassinosteroids regulate growth in plants under stressful environments and crosstalk with other potential phytohormones. *J. Plant Growth Regul.* 37, 1007–1024. doi: 10.1007/s00344-018-9855-2

Ahanger, M. A., Mir, R. A., Alyemeni, M. N., and Ahmad, P. (2020). Combined effects of brassinosteroid and kinetin mitigates salinity stress in tomato through the modulation of antioxidant and osmolyte metabolism. *Plant Physiol. Biochem.* 147, 31–42. doi: 10.1016/j.plaphy.2019.12.007

Ahn, S. J., Shin, R., and Schachtman, D. P. (2004). Expression of KT/KUP genes in *Arabidopsis* and the role of root hairs in k^+ uptake. *Plant Physiol.* 134, 1135–1145. doi: 10.1104/pp.103.034660

Amtmann, A., Troufflard, S., and Armengaud, P. (2008). The effect of potassium nutrition on pest and disease resistance in plants. *Physiol. Plant* 133, 682–691. doi: 10.1111/j.1399-3054.2008.01075.x

Armengaud, P., Breitling, R., and Amtmann, A. (2004). The potassium-dependent transcriptome of arabidopsis reveals a prominent role of jasmonic acid in nutrient signaling. *Plant Physiol.* 136, 2556–2576. doi: 10.1104/pp.104.046482

Armengaud, P., Sulpice, R., Miller, A. J., Stitt, M., Amtmann, A., and Gibon, Y. (2009). Multilevel analysis of primary metabolism provides new insights into the role of potassium nutrition for glycolysis and nitrogen assimilation in *Arabidopsis* roots. *Plant Physiol.* 150, 772–785. doi: 10.1104/pp.108.133629

Ashley, M. K., Grant, M., and Grabov, A. (2006). Plant responses to potassium deficiencies: A role for potassium transport proteins. *J. Exp. Bot.* 57, 425–436. doi: 10.1093/jxb/erj034

Banuelos, M. A., Garciadeblas, B., Cubero, B., and Rodriguez-Navarro, A. (2002). Inventory and functional characterization of the HAK potassium transporters of rice. *Plant Physiol.* 130, 784–795. doi: 10.1104/pp.007781

Carvalhais, L., Fedoseyenko, D., Haijirezai, M., Borriss, R., and Vonwiren, N. (2011). Root exudation of sugars, amino acids, and organic acids by maize as affected by nitrogen, phosphorous, potassium, iron deficiency. *J. Plant Nutr. Soil Sci.* 174, 3–11. doi: 10.1002/jpln.201000085

Chang, C., Li, C., Li, C. Y., Kang, X. Y., Zou, Y. J., and Ma, F. W. (2014). Differences in the efficiency of potassium (K) uptake and use in five apple rootstock genotypes. *J. Integr. Agric.* 13, 1934–1942. doi: 10.1016/S2095-3119(14)60839-X

Chen, W., Gong, L., Guo, Z., Wang, W., Zhang, H., Liu, X., et al. (2013). A novel integrated method for large-scale detection, identification, and quantification of widely targeted metabolites: application in the study of rice metabolomics. *Mol. Plant* 6, 1769–1780. doi: 10.1093/mp/sst080

Chen, S., Zhou, Y., Chen, Y., and Gu, J. (2018). Fastp: An ultra-fast all-in-one FASTQ preprocessor. *Bioinformatics* 34, i884–i890. doi: 10.1093/bioinformatics/bty560

Cui, J., Abadie, C., Carroll, A., Lamade, E., and Tcherkez, G. (2019). Responses to K deficiency and waterlogging interact *via* respiratory and nitrogen metabolism. *Plant Cell Environ.* 42, 647–658. doi: 10.1111/pce.13450

Ding, N., Huertas, R., Torres-Jerez, I., Liu, W., Watson, B., Scheible, W. R., et al. (2021). Transcriptional, metabolic, physiological and developmental responses of switchgrass to phosphorus limitation. *Plant Cell Environ.* 44, 186–202. doi: 10.1111/pce.13872

Fernie, A. R., Carrari, F., and Sweetlove, L. J. (2004). Respiratory metabolism: Glycolysis, the TCA cycle and mitochondrial electron transport. *Curr. Opin. Plant Biol.* 7, 254–261. doi: 10.1016/j.pbi.2004.03.007

Fulgenzi, F. R., Peralta, M. A. L., Mangano, S., Danna, C. H., Vallejo, A. J., Puigdomenech, P., et al. (2008). The ionic environment controls the contribution of the barley HvHAK1 transporter to potassium acquisition. *Plant Physiol.* 147, 252–262. doi: 10.1104/pp.107.114546

García-Martí, M., Piñero, M. C., García-Sanchez, F., Mestre, T. C., López-Delacalle, M., Martínez, V., et al. (2019). Amelioration of the oxidative stress generated by simple or combined abiotic stress through the K^+ and Ca^{2+} supplementation in tomato plants. *Antioxidants (Basel)* 8 (4), 81. doi: 10.3390/antiox8040081

Gierth, M., Mäser, P., and Schroeder, J. I. (2005). The potassium transporter AtHAK5 functions in k^+ deprivation-induced high-affinity k^+ uptake and AKT1 k^+ channel contribution to k^+ uptake kinetics in *Arabidopsis* roots. *Plant Physiol.* 137, 1105–1114. doi: 10.1104/pp.104.057216

Hafsi, C., Debez, A., and Abdelly, C. (2014). Potassium deficiency in plants: Effects and signaling cascades. *Acta Physiologiae Plantarum* 36, 1055–1070. doi: 10.1007/s11738-014-1491-2

Hall, R. D. (2011). Plant metabolomics in a nutshell: Potential and future challenges. *Biolioy Plant metabolomics* 43, 1–24. doi: 10.1002/9781444339956.ch1

Hasanuzzaman, M., Bhuyan, M. H. M. B., Nahar, K., Hossain, M. S., Mahmud, J. A., Hossen, M. S., et al. (2018). Potassium: A vital regulator of plant responses and tolerance to abiotic stresses. *Agronomy* 8, 31. doi: 10.3390/agronomy8030031

Hernandez, M., Fernandez-Garcia, N., Garcia-Garma, J., Rubio-Asensio, J. S., Rubio, F., and Olmos, E. (2012). Potassium starvation induces oxidative stress in *Solanum lycopersicum* l. roots. *J. Plant Physiol.* 169, 1366–1374. doi: 10.1016/j.jplph.2012.05.015

Hernández, G., Ramírez, M., Valdés-López, O., Tesfaye, M., Graham, M. A., Czechowski, T., et al. (2007). Phosphorus stress in common bean: Root transcript and metabolic responses. *Plant Physiol.* 144, 752–767. doi: 10.1104/pp.107.096958

Hoagland, D. R., and Arnon, D. I. (1950). The water-culture method for growing plants without soil. *Cal. Agric. Exp. St. Circ.* 347.

Hu, W., Lu, Z., Meng, F., Li, X., Cong, R., Ren, T., et al. (2021). Potassium modulates central carbon metabolism to participate in regulating CO_2 transport and assimilation in *Brassica napus* leaves. *Plant Sci.* 307, 110891. doi: 10.1016/j.plantsci.2021.110891

Jung, J. Y., Shin, R., and Schachtman, D. (2009). Ethylene mediates response and tolerance to potassium deprivation in *Arabidopsis*. *Plant Cell* 21, 607–621. doi: 10.1105/tpc.108.063099

Kanai, S., Moghaieb, R. E., El-Shemy, H. A., Panigrahi, R., Mohapatra, P. K., Ito, J., et al. (2011). Potassium deficiency affects water status and photosynthetic rate of the vegetative sink in green house tomato prior to its effects on source activity. *Plant Sci.* 180, 368–374. doi: 10.1016/j.plantsci.2010.10.011

Kanai, S., Ohkura, K., Adu-Gyamfi, J. J., Mohapatra, P. K., Nguyen, N. T., Saneoka, H., et al. (2007). Depression of sink activity precedes the inhibition of biomass production in tomato plants subjected to potassium deficiency stress. *J. Exp. Bot.* 58, 2917–2928. doi: 10.1093/jxb/erm149

Kim, E. J., Kwak, J. M., Uozumi, N., and Schroeder, J. I. (1998). AtKUP1: An *Arabidopsis* gene encoding high-affinity potassium transport activity. *Plant Cell* 10, 51–62. doi: 10.1105/tpc.10.1.51

Kim, D., Langmead, B., and Salzberg, S. L. (2015). HISAT: A fast spliced aligner with low memory requirements. *Nat. Methods* 12, 357–360. doi: 10.1038/nmeth.3317

Kim, M. J., Ruzicka, D., Shin, R., and Schachtman, D. P. (2012). The *Arabidopsis* AP2/ERF transcription factor RAP2.11 modulates plant response to low-potassium conditions. *Mol. Plant* 5, 1042–1057. doi: 10.1093/mp/sss003

Koeslin-Findeklee, F., Rizi, V. S., Becker, M. A., Parra-Londono, S., Arif, M., Balazadeh, S., et al. (2015). Transcriptomic analysis of nitrogen starvation- and cultivar-specific leaf senescence in winter oilseed rape (*Brassica napus* l.). *Plant Sci.* 233, 174–185. doi: 10.1016/j.plantsci.2014.11.018

Løvdal, T., Olsen, K. M., Slimestad, R., Verheul, M., and Lillo, C. (2010). Synergetic effects of nitrogen depletion, temperature, and light on the content of phenolic compounds and gene expression in leaves of tomato. *Phytochemistry* 71, 605–613. doi: 10.1016/j.phytochem.2009.12.014

Langmead, B., Trapnell, C., Pop, M., and Salzberg, S. L. (2009). Ultrafast and memory-efficient alignment of short DNA sequences to the human genome. *Genome Biol.* 10, 25. doi: 10.1186/gb-2009-10-3-r25

Li, B., and Dewey, C. N. (2011). RSEM: Accurate transcript quantification from RNA-seq data with or without a reference genome. *BMC Bioinf.* 12, 323. doi: 10.1186/1471-2105-12-323

Li, M., Xu, J., Wang, X., Fu, H., Zhao, M., Wang, H., et al. (2018). Photosynthetic characteristics and metabolic analyses of two soybean genotypes revealed adaptive strategies to low-nitrogen stress. *J. Plant Physiol.* 229, 132–141. doi: 10.1016/j.jplph.2018.07.009

Liang, C., Tian, J., and Liao, H. (2013). Proteomics dissection of plant responses to mineral nutrient deficiency. *Proteomics* 13, 624–636. doi: 10.1002/pmic.201200263

Lu, L., Chen, Y., Lu, L., Lu, Y., and Li, L. (2015). Transcriptome analysis reveals dynamic changes in the gene expression of tobacco seedlings under low potassium stress. *J. Genet.* 94, 397–406. doi: 10.1007/s12041-015-0532-y

Luo, B., Ma, P., Nie, Z., Zhang, X., He, X., Ding, X., et al. (2019). Metabolite profiling and genome-wide association studies reveal response mechanisms of phosphorus deficiency in maize seedling. *Plant J.* 97, 947–969. doi: 10.1111/tpj.14160

Ma, N., Dong, L., Lü, W., Lü, J., Meng, Q., and Liu, P. (2020). Transcriptome analysis of maize seedling roots in response to nitrogen-, phosphorus-, and potassium deficiency. *Plant Soil* 447, 637–658. doi: 10.1007/s11104-019-04385-3

Ma, T. L., Wu, W. H., and Wang, Y. (2012). Transcriptome analysis of rice root responses to potassium deficiency. *BMC Plant Biol.* 12, 161. doi: 10.1186/1471-2229-12-161

Meena, K. K., Sorty, A. M., Bitla, U. M., Choudhary, K., Gupta, P., Pareek, A., et al. (2017). Abiotic stress responses and microbe-mediated mitigation in plants: The omics strategies. *Front. Plant Sci.* 8, 172. doi: 10.3389/fpls.2017.00172

Mo, X., Zhang, M., Liang, C., Cai, L., and Tian, J. (2019). Integration of metabolome and transcriptome analyses highlights soybean roots responding to phosphorus deficiency by modulating phosphorylated metabolite processes. *Plant Physiol. Biochem.* 139, 697–706. doi: 10.1016/j.plaphy.2019.04.033

Mustroph, A., Stock, J., Hess, N., Aldous, S., Dreilich, A., and Grimm, B. (2013). Characterization of the phosphofructokinase gene family in rice and its expression under oxygen deficiency stress. *Front. Plant Sci.* 4, 125. doi: 10.3389/fpls.2013.00125

Oomen, R. J. F. J., Benito, B., Sentenac, H., Rodríguez-Navarro, A., Talón, M., Véry, A.-A., et al. (2012). HKT2;2/1, a k^+-permeable transporter identified in a salt-tolerant rice cultivar through surveys of natural genetic polymorphism. *Plant J.* 71, 750–762. doi: 10.1111/j.1365-313X.2012.05031.x

Pant, B. D., Pant, P., Erban, A., Huhman, D., Kopka, J., and Scheible, W. R. (2015). Identification of primary and secondary metabolites with phosphorus status-dependent abundance in *Arabidopsis*, and of the transcription factor PHR1 as a major regulator of metabolic changes during phosphorus limitation. *Plant Cell Environ.* 38, 172–187. doi: 10.1111/pce.12378

Patel, M., Fatnani, D., and Parida, A. K. (2022). Potassium deficiency stress tolerance in peanut (*Arachis hypogaea*) through ion homeostasis, activation of antioxidant defense, and metabolic dynamics: Alleviatory role of silicon supplementation. *Plant Physiol. Biochem.* 182, 55–75. doi: 10.1016/j.plaphy.2022.04.013

Pyo, Y. J., Gierth, M., Schroeder, J. I., and Cho, M. H. (2010). High-affinity k(+) transport in *Arabidopsis*: AtHAK5 and AKT1 are vital for seedling establishment and postgermination growth under low-potassium conditions. *Plant Physiol.* 153, 863–875. doi: 10.1104/pp.110.154369

Qin, Y. J., Wu, W. H., and Wang, Y. (2019). ZmHAK5 and ZmHAK1 function in k^+ uptake and distribution in maize under low k^+ conditions. *J. Integr. Plant Biol.* 61, 691–705. doi: 10.1111/jipb.12756

Rolland, F., Baena-Gonzalez, E., and Sheen, J. (2006). Sugar sensing and signaling in plants: Conserved and novel mechanisms. *Annu. Rev. Plant Biol.* 57, 675–709. doi: 10.1146/annurev.arplant.57.032905.105441

Rosa, M., Prado, C., Podazza, G., Interdonato, R., Gonzalez, J. A., Hilal, M., et al. (2009). Soluble sugars–metabolism, sensing and abiotic stress: A complex network in the life of plants. *Plant Signal Behav.* 4, 388–393. doi: 10.4161/psb.4.5.8294

Santa-María, G. E., Rubio, F., Dubcovsky, J., and Rodríguez-Navarro, A. (1997). The HAK1 gene of barley is a member of a large gene family and encodes a high-affinity potassium transporter. *Plant Cell* 9, 2281–2289. doi: 10.1105/tpc.9.12.2281

Schaeffer, C., Johann, P., Nehls, U., and Hampp, R. (1996). Evidence for an up-regulation of the host and a down-regulation of the fungal phosphofructokinase activity in ectomycorrhizas of Norway spruce and fly agaric. *New Phytol.* 134, 697–702. doi: 10.1111/j.1469-8137.1996.tb04935.x

Schroeder, J. I., Ward, J. M., and Gassmann, W. (1994). Perspectives on the physiology and structure of inward-rectifying k^+ channels in higher plants: Biophysical implications for k^+ uptake. *Annu. Rev. Biophys. Biomol Struct.* 23, 441–471. doi: 10.1146/annurev.bb.23.060194.002301

Sun, T., Zhang, J., Zhang, Q., Li, X., Li, M., Yang, Y., et al. (2021). Integrative physiological, transcriptome, and metabolome analysis reveals the effects of nitrogen sufficiency and deficiency conditions in apple leaves and roots. *Environ. Exp. Bot.* 192, 104633. doi: 10.1016/j.envexpbot.2021.104633

Sung, J., Lee, S., Lee, Y., Ha, S., Song, B., Kim, T., et al. (2015). Metabolomic profiling from leaves and roots of tomato (*Solanum lycopersicum* l.) plants grown under nitrogen, phosphorus or potassium-deficient condition. *Plant Sci.* 241, 55–64. doi: 10.1016/j.plantsci.2015.09.027

Tan, L., Zhou, L., Zhao, N., He, Y., and Qiu, Z. (2021). Development of a low-cost portable device for pixel-wise leaf spad estimation and blade-level SPAD distribution visualization using color sensing. *Comput. Electron. Agriculture.* 190, 106487. doi: 10.1016/j.compag.2021.106487

Tang, Z.-H., Zhang, A.-J., Wei, M., Chen, X.-G., Liu, Z.-H., Li, H.-M., et al. (2015). Physiological response to potassium deficiency in three sweet potato (*Ipomoea batatas* lam.) genotypes differing in potassium utilization efficiency. *Acta Physiol Plant* 37, 184. doi: 10.1007/s11738-015-1901-0

Tester, M., and Blatt, M. R. (1989). Direct measurement of k channels in thylakoid membranes by incorporation of vesicles into planar lipid bilayers. *Plant Physiol.* 91, 249–252. doi: 10.1104/pp.91.1.249

Trankner, M., Tavakol, E., and Jakli, B. (2018). Functioning of potassium and magnesium in photosynthesis, photosynthate translocation and photoprotection. *Physiol. Plant* 163, 3. doi: 10.1111/ppl.12747

Wang, C., Chen, H., Hao, Q., Sha, A., Shan, Z., Chen, L., et al. (2012a). Transcript profile of the response of two soybean genotypes to potassium deficiency. *PloS One* 7, e39856. doi: 10.1371/journal.pone.0039856

Wang, N., Hua, H., Eneji, A. E., Li, Z., Duan, L., and Tian, X. (2012b). Genotypic variations in photosynthetic and physiological adjustment to potassium deficiency in cotton (*Gossypium hirsutum*). *J. Photochem. Photobiol. B* 110, 1–8. doi: 10.1016/j.jphotobiol.2012.02.002

Wang, Y., and Wu, W. H. (2013). Potassium transport and signaling in higher plants. *Annu. Rev. Plant Biol.* 64, 451–476. doi: 10.1146/annurev-arplant-050312-120153

Wang, X., Zhao, J., Fang, Q., Chang, X., Sun, M., Li, W., et al. (2021). GmAKT1 is involved in k^+ uptake and Na^+/K^+ homeostasis in *Arabidopsis* and soybean plants. *Plant Sci.* 304, 110736. doi: 10.1016/j.plantsci.2020.110736

Weckwerth, W. (2003). Metabolomics in systems biology. *Annu. Rev. Plant Biol.* 54, 669–689. doi: 10.1146/annurev.arplant.54.031902.135014

Wu, L. B., Holtkamp, F., Wairich, A., and Frei, M. (2019). Potassium ion channel gene *OsAKT1* affects iron translocation in rice plants exposed to iron toxicity. *Front. Plant Sci.* 10, 579. doi: 10.3389/fpls.2019.00579

Xu, X., Du, X., Wang, F., Sha, J., Chen, Q., Tian, G., et al. (2020). Effects of potassium levels on plant growth, accumulation and distribution of carbon, and nitrate metabolism in apple dwarf rootstock seedlings. *Front. Plant Sci.* 11, 904. doi: 10.3389/fpls.2020.00904

Xu, J., Li, H. D., Chen, L. Q., Wang, Y., Liu, L. L., He, L., et al. (2006). A protein kinase, interacting with two calcineurin b-like proteins, regulates k^+ transporter AKT1 in *Arabidopsis*. *Cell* 125, 1347–1360. doi: 10.1016/j.cell.2006.06.011

Yang, T., Feng, H., Zhang, S., Xiao, H., Hu, Q., Chen, G., et al. (2020). The potassium transporter OsHAK5 alters rice architecture *via* ATP-dependent transmembrane auxin fluxes. *Plant Commun.* 1, 100052. doi: 10.1016/j.xplc.2020.100052

Ye, Z., He, X., and Liu, C. (2022). Comparative analysis of transcriptome profiles reveals the mechanisms in the difference of low potassium tolerance among cultivated and tibetan wild barleys. *Agronomy* 12, 1094. doi: 10.3390/agronomy12051094

Zeng, J., He, X., Wu, D., Zhu, B., Cai, S., Nadira, U. A., et al. (2014). Comparative transcriptome profiling of two Tibetan wild barley genotypes in responses to low potassium. *PloS One* 9, e100567. doi: 10.1371/journal.pone.0100567

Zeng, Q., Ling, Q., Fan, L., Li, Y., Hu, F., Chen, J., et al. (2015). Transcriptome profiling of sugarcane roots in response to low potassium stress. *PloS One* 10, e0126306. doi: 10.1371/journal.pone.0126306

Zeng, J., Quan, X., He, X., Cai, S., Ye, Z., Chen, G., et al. (2018). Root and leaf metabolite profiles analysis reveals the adaptive strategies to low potassium stress in barley. *BMC Plant Biol.* 18, 187. doi: 10.1186/s12870-018-1404-4

Zhang, S., Ying, H., Pingcuo, G., Wang, S., Zhao, F., Cui, Y., et al. (2019). Identification of potential metabolites mediating bird's selective feeding on *Prunus mira* flowers. *BioMed. Res. Int.* 2019, 1395480. doi: 10.1155/2019/1395480

Zhao, H., Ni, S., Cai, S., and Zhang, G. (2021). Comprehensive dissection of primary metabolites in response to diverse abiotic stress in barley at seedling stage. *Plant Physiol. Biochem.* 161, 54–64. doi: 10.1016/j.plaphy.2021.01.048

Zhao, Y., Sun, R., Liu, H., Liu, X., Xu, K., Xiao, K., et al. (2020). Multi-omics analyses reveal the molecular mechanisms underlying the adaptation of wheat (*Triticum aestivum* l.) to potassium deprivation. *Front. Plant Sci.* 11, 588994. doi: 10.3389/fpls.2020.588994

Zhu, G., Wang, S., Huang, Z., Zhang, S., Liao, Q., Zhang, C., et al. (2018). Rewiring of the fruit metabolome in tomato breeding. *Cell* 172, 249–261. doi: 10.1016/j.cell.2017.12.019

Frontiers in
Plant Science

Cultivates the science of plant biology and its applications

The most cited plant science journal, which advances our understanding of plant biology for sustainable food security, functional ecosystems and human health.

Discover the latest Research Topics

See more →

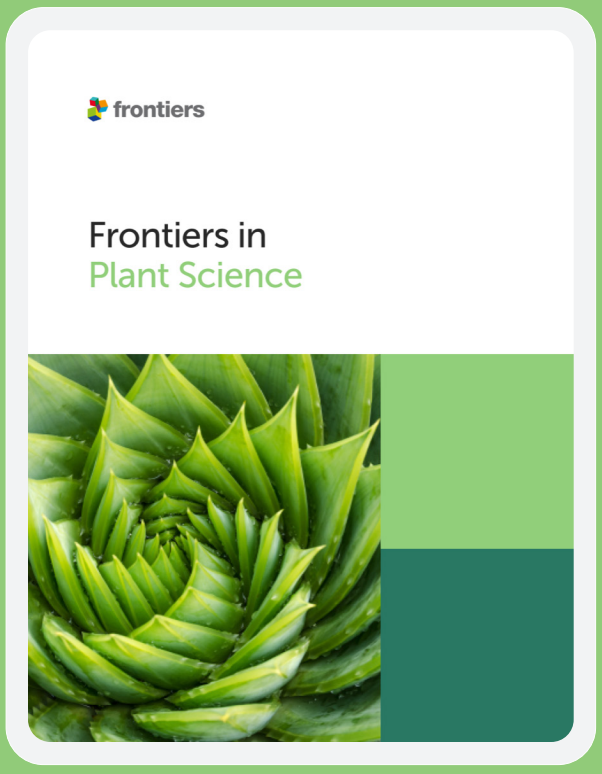

Frontiers

Avenue du Tribunal-Fédéral 34
1005 Lausanne, Switzerland
frontiersin.org

Contact us

+41 (0)21 510 17 00
frontiersin.org/about/contact